Biofunctionalization of Capillary Bioreactor with the Use of Human Hepatocyte-Derived Proliferating Cells as a Model of Bioartificial Liver

Biofunkcjonalizowany bioreaktor kapilarny wykorzystujący nową linię proliferujących komórek hepatocytarnych pochodzenia ludzkiego jako model biosztucznej wątroby

Monika Joanna Wiśniewska

Doctoral Thesis

Laboratory of Tissue Engineering, Department of Hybrid and Analytical Microbiosystems,

Nalecz Institute of Biocybernetics and Biomedical Engineering Polish Academy of Sciences

Scientific supervisor: Dorota G. Pijanowska, PhD Eng. Prof.

Auxiliary supervisor: Krzysztof D. Pluta, PhD

Warsaw 2026

Fundusze Europejskie Wiedza Edukacja Rozwój

Rzeczpospolita Polska

Unia Europejska Europejski Fundusz Społeczny

Praca nad rozprawą doktorską była jedną z najważniejszych i najbardziej wymagających dróg w moim życiu. Towarzyszyły jej chwile satysfakcji i radości, ale również trudności, niepewność i zmęczenie. Dziś, zamykając ten etap, chciałabym z całego serca podziękować wszystkim osobom, które były obok mnie i wspierały mnie na tej drodze.

Swoje podziękowania kieruję prof. Doroty Pijanowskiej za zaufanie, cierpliwość, cenne wskazówki, oraz konstruktywne uwagi, które stanowiły istotne wsparcie w realizacji niniejszej pracy doktorskiej.

Serdecznie dziękuję również dr. Krzysztofowi Plucie za pomoc merytoryczną, cenne wskazówki oraz poświęcony czas..

Słowa wdzięczności kieruję również do moich Koleżanek z zespołu. Dziękuję za pomoc w codziennych obowiązkach, za dzielenie się wiedzą i doświadczeniem, za wszystkie rozmowy – zarówno te naukowe, jak i te pozwalające nabrać dystansu do niepowodzeń. Dzięki Wam miejsce pracy było nie tylko przestrzenią rozwoju zawodowego, ale także miejscem pełnym życzliwości, wsparcia i dobrej atmosfery.

Największe podziękowania składam mojej Rodzinie. Dziękuję za bezwarunkową miłość, cierpliwość i nieustanną obecność. Dziękuję za zrozumienie podczas wielu godzin spędzonych w pracy, za wsparcie w chwilach zwątpienia i za radość dzieloną ze mną przy każdym sukcesie. To Wy byliście moją siłą i motywacją do dalszego działania, gdy pojawiały się trudności. Wasza wiara we mnie pozwalała mi iść naprzód i nie poddawać się mimo przeszkód.

Szczególne podziękowania kieruję do Kamila za wsparcie, cierpliwość i wiarę we mnie przez cały okres przygotowywania tej rozprawy. Dziękuję za motywację w chwilach zwątpienia oraz za to, że zawsze mogłam na Ciebie liczyć. Dziękuję również za stworzenie w domu stanowiska do pracy, którego nie powstydziłaby się sama NASA. Twoja pomysłowość i zaangażowanie sprawiły, że praca nad doktoratem była znacznie łatwiejsza. Przede wszystkim jednak dziękuję Ci za obecność i wsparcie każdego dnia.

Z całego serca dziękuję wszystkim, którzy byli częścią tej drogi.

Contents

Contents 1
Abbreviations 6
Abstract 11
Streszczenie 13
1 Introduction 16
1.1 Liver structure and functions 16
1.1.1 Liver main functions 17
1.1.2 Liver on the cellular level 17
1.1.3 Liver zonation 18
1.1.4 Parenchymal and non-parenchymal cells in the liver 19
1.1.5 Important Hepatocyte-Produced Proteins 22
1.2 Faulty Liver 34
1.3 Liver Transplantation 35
1.4 Liver Regeneration 37
1.4.1 Cell Dedifferentiation During Liver Regeneration 37
1.4.2 Epithelial-to-mesenchymal transition (EMT) 38
1.5 Development of Liver Cell Isolation Methods 39
1.5.1 Two-Step Collagenase Perfusion Method 39
1.5.2 Mechanical Defragmentation and Enzymatic Digestion of Tissue Method 40
1.6 Bridging Therapies to Replace or Support the Liver in Patients with Liver Failure 41
1.6.1 Liver Support Systems (LSS) 41
1.6.2 Alternative Models of Hepatocytes 48
1.7 Human Hepatocyte-Derived Proliferating Cells as a Potentially New Source of Hepatic Cells 50
Thesis Statements: 53
2 Materials 54
2.1 Cells Used in the Experiments 54
2.2 Culture Media and Supplements 55
2.3 Other Ingredients Used During Experiments 57
2.4 Antibodies and Primers Used in the Experiments 59
2.5 Buffers and Reagents Used During Experiments 62
2.5.1 Buffers and Reagents for Western Blot Analysis 62
2.5.2 Buffer and Reagents for ELISA analysis 65
2.5.3 Solutions for Immunostaining 66

2.5.4 Reagents for Liver Tissue Cell Isolation 66
2.5.5 Other Reagents and Solutions Used in Experiments 68
2.5.6 Reagents Used for the Characterization of Polysulfone Capillary Membranes 69
2.5.7 Laboratory Equipment 70
2.6 Computer Software 72
3 Methods 73
3.1 Cell Culture Methods 73
3.1.1 Culture Media Composition and Preparation 73
3.1.2 Cell Thawing 77
3.1.3 Cell Passaging 77
3.1.4 Cell Counting Using the Bürker Chamber and Trypan Blue Exclusion 78
3.1.5 Cell Freezing 78
3.1.6 Cell Doubling Time 78
3.2 Hepatocytes Isolation 79
3.2.1 Mechanical Dissociation and Enzymatic Digestion of the Liver Tissue 79
3.2.2 Determination of Yield of Cell Isolation and Cell Viability 82
3.2.3 Variants of Cultures of Isolated Cells 82
3.3 Flow Cytometry 83
3.3.1 Flow Cytometric Determination of Cell Size and Granularity 83
3.4 Immunofluorescence 83
3.5 Apical Vacuoles 84
3.6 Enzyme-linked Immunosorbent Assay (ELISA) 84
3.7 Thiazolyl Blue Tetrazolium Bromide (MTT) Assay 85
3.8 Glucose Concentration Measurements 85
3.9 Western Blot Analysis 85
3.9.1 Protein Isolation from Cells 85
3.9.2 Protein Isolation from Liver Tissue 86
3.9.3 Protein Concentration – BCA Assay 86
3.9.4 Protein Precipitation 86
3.9.5 Electrophoresis 87
3.9.6 Membrane Transfer 87
3.9.7 Antibody Labeling 87
3.9.8 Imaging 87
3.9.9 Membrane Stripping 88
3.10 Gene Expression Analysis (RT-qPCR) 88
3.10.1 RNA Isolation from Cells 88

3.10.2 RNA Isolation from Liver Tissue 89
3.10.3 Reverse Transcription and cDNA Preparation 89
3.10.4 Real-Time Detection of cDNA 90
3.11 hHDPCs Cultures Variants 90
3.11.1 Effect of Various Culture Media on hHDPCs Proliferation and Viability 90
3.11.2 Long-Term Monitoring of Morphology and Proliferation of hHDPCs 90
3.11.3 Mesenchymal Stem Cell Markers in hHDPCs 91
3.11.4 Re-differentiation of hHDPCs into Hepatocyte-like Cells Using Growth Factor-Supplemented Medium 92
3.12 Characteristics of the Polysulfone Capillary Membranes 92
3.12.1 Scanning Electron Microscopy 92
3.12.2 Wettability Angle Measurements 92
3.12.3 Ultrafiltration Measurements 93
3.12.4 Bovine Serum Albumin (BSA) Retention 93
3.12.5 Membrane Cut-Off Determination 94
3.12.6 Biocompatibility of the Polysulfone Membrane 94
3.13 Module Preparation 94
3.13.1 Dynamic System – Preparation 96
3.13.2 Dynamic System – Cell Cultures 97
3.13.3 Dynamic System – Sample Analysis 98
4 Results 99
4.1 Isolation of Human Hepatocytes from Resected Liver Fragments and Liver Lysate Culture Variants 99
4.1.1 Quantitative Analysis of Liver Cell Isolation 99
4.1.2 Cell Islands and Culture Conditions 107
4.1.3 Summary of the isolation conditions 110
4.1.4 Detection of Albumin Production by Cell Islands – Immunocytostaining 112
4.1.5 Flow Cytometric Detection of Human Hepatocytes in Isolates 113
4.1.6 Albumin Secretion – ELISA 117
4.1.7 Genes Expression in Liver Tissue Isolates – RT-qPCR 119
4.2 Human Hepatocyte-Derived Proliferating Cells (hHDPCs) as a New Model of Human Hepatocytes 129
4.2.1 hHDPCs Characteristics 129
4.2.2 Comparison of hHDPCs, HepG2, and HDFn Cultures 140
4.2.3 Effect of Various Culture Media on hHDPCs Proliferation and Viability 146
4.2.4 Effect of Hepatocyte Growth Supplement (HGS) on hHDPCs Proliferation 151

4.2.5 Protein Expression Fluctuations During hHDPCs Passaging 154
4.2.6 Long-Term Monitoring of Morphology and Proliferation of hHDPCs 165
4.2.7 Mesenchymal Stem Cell Markers in hHDPCs 171
4.2.8 Re-differentiation of hHDPCs into Hepatocyte-like Cells Using Growth Factor-Supplemented Medium 175
4.3 Human Dedifferentiated Hepatocytes (hDHes) Dividing and Retaining Hepatocyte Functions 179
4.3.1 Stage I – Proliferating Hepatocyte-Like Cells 179
4.3.2 Stage II – Proliferating Hepatocyte-Like Cells with Restored Hepatocyte Functions 186
4.4 Comparative Analysis of Tumor Models of Hepatocytes 189
4.4.1 Proliferation, Cell Doubling Time, and Morphology of Selected Liver Cancer Cell Lines 189
4.4.2 Metabolic Activity of Liver Cancer Cell Lines (MTT) 192
4.4.3 Albumin Production by Liver Cancer Cell Lines (ELISA) 193
4.4.4 Apical Vacuoles Formation 194
4.4.5 Protein Production and Gene Expression in Selected Liver Cancer Cell Lines 195
4.5 Dynamic Cell Cultures in Capillary Bioreactors 204
4.5.1 Preparation of the Hollow Fiber Bioreactor System 204
4.5.2 Dynamic Cultures 210
5 Discussion 216
5.1 Optimization of Liver Tissue Isolation Protocol and Cell Cultures 216
5.2 Albumin Secretion by Hepatocytes 224
5.3 Gene Expression in Liver Tissue Isolates 225
5.4 Human Hepatocyte-Derived Proliferating Cells (hHDPCs) as a New Model of Human Hepatocytes 232
5.4.1 hHDPCs Characteristics 232
5.4.2 Comparison of hHDPCs, HepG2, and HDFn Cultures 235
5.4.3 Optimization of hHDPCs culture conditions 240
5.4.4 Effect of Hepatocyte Growth Supplement (HGS) on hHDPCs Proliferation 242
5.4.5 Protein Expression Fluctuations During hHDPCs Passaging 244
5.4.6 Long-Term Culture of hHDPCs 247
5.4.7 Mesenchymal Stem Cell Markers in hHDPCs 249
5.4.8 Attempts to Re-differentiation of hHDPCs Into Hepatocyte-Like Cells Using Growth Factors 251
5.4.9 Human Dedifferentiated Hepatocytes (hDHes) Dividing and Retaining Hepatocyte Functions 253
5.4.10 Comparative Analysis of Tumor Models of Hepatocytes 257

5.4.11 Dynamic Culture System 260
6 Conclusions 267
Final Thoughts 275
7 References 276
List of Figures 300
List of Supplementary Figures 302
List of Tabels 303
List of Publications 304
Research Projects 305
Conferences 305
Other Scientific Activities 306
8 Supplementary 307
8.1 Comparison of hHDPCs, HepG2, and HDFn Cultures 307
8.1.1 Albumin Secretion and Glucose Consumption 307
8.2 Effect of Hepatocyte Growth Supplement (HGS) on hHDPCs Proliferation 308
8.3 Proteins Fluctuation During hHDPCs Passaging 309
8.3.1 Albumin Expression Fluctuation – IF 309
8.4 Long-Term Monitoring of Morphology and Proliferation of hHDPCs 310
8.4.1 Microscopic Observations 310
8.5 Obtaining Human Dedifferentiated Hepatocytes (hDHes) Dividing and Retaining Hepatocyte Functions 312
8.5.1 Stage I – Proliferating Hepatocytes-Like Cells 312

Abbreviations

2D – Two Dimensional
3D – Three Dimensional
A1AT – Alpha-1-Antitrypsin
ACLF – Acute on Chronic Liver Failure
ACTB – β-Actin
AdDMEM/F12 – Dulbecco's Modified Eagle Medium/Ham's F-12
AFP – Alpha-Fetoprotein
ALB; HSA – Human Serum Albumin (albumin)
ALF – Acute Liver Failure
ALSS – Artificial Liver Support Systems
AMC-BAL – Academic Medical Center-Bioartificial Liver
APC – Allophycocyanin
APS – Ammonium Persulfate
ARG1/2 – Arginase 1/2
arHMSC – Adult Rat Hepatocyte-Derived Mesenchymal-Like Stem Cells
ASL – Argininosuccinate Lyase
ASLL – Artificial Liver Support Systems
ASS – Argininosuccinate Synthetase
ATP – Adenosine Triphosphate
AV – Apical Vacuoles
BALs – Bioartificial Liver Support Systems
BCA – Bicinchoninic Acid
BECs – Biliary Epithelial Cells
BMI – Body Mass Index
BMP-7 – Bone Morphogenetic Protein 7
BSA – Bovine Serum Albumin
C3A_EGFP – Genetically Modified C3A Cells Overexpressing Enhanced Green Fluorescent Protein
CD133 – Prominin-1
CD29 – Integrin β-1; (ITGB1)
CD34 – Human Hematopoietic Progenitor Cell Antigen CD34
CD44 – Homing Cell Adhesion Molecule; HCAM
CD45 – Protein Tyrosine Phosphatase Receptor Type C; PTPRC
CD73 – Ecto-5′-Nucleotidase
cDNA – complementary/copy DNA
CIT – Cold Ischemia Time
CK18 – Cytokeratin 18
CK19 – Cytokeratin 19
CLF – Chronic Liver Failure
CO_2 – Carbon Dioxide
COPII – Coat Protein Complex I

CPS1 – Carbamoyl-Phosphate Synthetase
CYP2C8 – Cytochrome P450 family 2 subfamily C member 8
CYP2E1 – Cytochrome P450 Family 2 subfamily E member 1
CYP3A4 – Cytochrome P450 family 3 subfamily A member 4
D+H – High Glucose Dulbecco's Modified Eagle Medium Supplemented with Hepatocyte Growth Supplement
DAPI – 4′,6-diamidino-2-phenylindole
DAPT – N-[N-(3,5-Difluorophenacetyl)-L-alanyl]-S-phenylglycine t-butyl ester
DBD – DNA-Binding Domain
DBD – Donors After Brain Death
DCD – Donors After Circulatory Death
Dex – Dexamethasone
DILI – Drug-Induced Liver Injury
DM – Differentiation Medium
DMEM; D – High Glucose Dulbecco's Modified Eagle Medium
DMEM+HGS; D+H – DMEM medium Supplemented with Hepatocyte Growth Supplement
DMSO – Dimethyl Sulfoxide
DNA – Deoxyribonucleic Acid
drHDFn - Dried Human Fibroblasts
drHDFn_EGF – Dried Human Fibroblasts with overexpression of EGF
drHDFn_EGF+HGF – mix of Dried Human Fibroblasts with overexpression of EGF and HGF
drHDFn_HGF – Dried Human Fibroblasts with overexpression of HGF
DTT – Dithiothreitol
E/M – epithelial/mesenchymal
ECD – Expanded Criteria Donors
ECGS – Endothelial Cell Growth Supplements
ECL – Enhanced Chemiluminescence Substrate
ECM – Extracellular Matrix
EDTA – Ethylenediaminetetraacetic Acid
EGF – Epithelial Growth Factor
EGFP – Enhanced Green Fluorescent Protein
EGFR – Epidermal Growth Factor Receptor
ELAD – Extracorporeal Liver Assist Device
ELISA – Enzyme-Linked Immunosorbent Assay
EM – Expansion Medium
EMEM – Eagle's Minimum Essential Medium
EMT – Epithelial-to-Mesenchymal Transition
ER – Endoplasmic Reticulum
ESLD – End-Stage Liver Disease
F – Female
FA – Formaldehyde
FACS – Fluorescence-Activated Cell Sorter
FBS – Fetal Bovine Serum
FC – Flow Cytometry

FGF-10/-19/-4 –Fibroblasts Growth Factor-10/-19/-4
FITC – Fluorescein isothiocyanate
For – Forskolin
FSC – Forward Scatter
GAPDH – Glyceraldehyde-3-Phosphate Dehydrogenase
GLUL – Glutamate-Ammonia Ligasee
H_2SO_4 – Sulfuric Acid
Ham's F-12 – Nutrient Mixture F-12 Ham
HB – Hepatoblastoma
HBSS – Hanks' Balanced Salt Solution
HBV – Hepatitis B Virus
HCC – Hepatocellular Carcinoma
HCl – Hydrochloric Acid
HCM – Hepatocyte Culture Medium
HCV – Hepatitis C Virus
HDFn – Primary Dermal Fibroblast Normal; Human
hDHes – Human Dedifferentiated Hepatocytes
HepatAssist – HepatAssist Liver Support System
HepatoZYME-SFM – Hepatozyme-SFM is a serum-free medium
HF – hemofiltration
HGF – Hepatocyte Growth Factor
HGS – Hepatocyte Growth Supplement
hH_1; hH_2; hH_3; hH_4; hH_5 – Commercially Available Human Hepatocytes (from different donor)
hHDPCs – Human Hepatocyte-Derived Proliferating Cells
hHpSCs – Human Hepatic Stem Cells
hHs – Commercially Available Human Hepatocytes
HLCs – Hepatocyte-Like Cells
HLSCs – Liver Stem Cell-Derived Progenitor Cells
HM – Hepatocyte Medium
HM+HGS; H+H – Hepatocyte Medium Supplemented with Hepatocyte Growth Supplement
HNF1α – Hepatocyte Nuclear Factor 1 alpha
HNF4α – Hepatocyte Nuclear Factor 4 alpha
HOS – Human Osteosarcoma cell line
HRP – Horseradish Peroxidase
human iPS-HLCs – Human iPS Cell-Derived Hepatocyte-Like Cells
HUVECs – Human Umbilical Vein Endothelial Cells
HZ – Hepatozyme-SFM, is a serum free medium
IF – Immunocytostaining/Immunofluorescence
Il-1/-6/-8 – Interleukin-1/-6/-8
ILCs – Innate Lymphoid Cells
iPSCs – Induced Pluripotent Stem Cells
IRI – Ischemia-Reperfusion Injury
Ki67 – Marker of Proliferation Ki-67

LBD – Ligand-Binding Domain
LCI – Liver Cell Isolate
LDLT – Living Donor Liver Transplantation
LF – Liver Failure
Lib – Liberase
LPCs – Liver Progenitor Cells
LSECs – Liver Sinusoidal Endothelial Cells
LSS – Liver Support Systems
LT – Liver Transplantation
LTE IBBE PAS – Laboratory of Tissue Engineering, Nalecz Institute of Biocybernetics and Biomedical Engineering, Polish Academy of Sciences
LTI – Liver Tissue Isolate
LTM – Liver Tissue Mass
M – Male
M199 – Medium 199
MARS – Molecular Adsorbent Recirculating System
MASLD – Metabolic Dysfunction-Associated Steatotic Liver Disease
MELS – Modular Extracorporeal Liver Support
MEM – Minimum Essential Medium
MEM NEAA – Minimum Essential Medium Non-essential Amino Acids Solution
MET – Mesenchymal-to-Epithelial Transition
Mix – Collagenase Enzyme Mixture
mRNA – Messenger Ribonucleic Acid
MSCs – Mesenchymal Stem Cells
MTT – Thiazolyl Blue Tetrazolium Bromide
MWCO – Molecular Weight Cut-Off
NAC – *N*-Acetyl-L-cysteine
NaCl – Sodium Chloride
NAFLD – Non-Alcoholic Fatty Liver Disease
$NaHCO_3$ – Sodium Bicarbonate
NaN_3 – Sodium Azide
NaOH – Sodium Hydroxide
NASH – Non-alcoholic Steatohepatitis
NH_4Cl – Ammonium Chloride
Nic – Nicotinamide
NKs – Natural Killer
NKTs – Natural Killer T cells
Nog – Recombinant Human Noggin
NR – Nuclear Receptor
OTC – Ornithine Transcarbamoylase
P/S – Penicillin/Streptomycin Solution
PBS – Phosphate-Buffered Saline
PE – Phycoerythrin
PERV – Porcine Endogenous Retrovirus

Prometheus – Fractionated Plasma Separation and Adsorption system (Prometheus system)
PVDF membrane – Polyvinylidene Difluoride membrane
PXR – Pregnane X Receptor
R – Retention
RBC – Red Blood Cells
RCF – Relative Centrifugal Force
RIPA Buffer – Radioimmunoprecipitation Assay Buffer
RLC – Reactive Center Loop
RNA – Ribonucleic Acid
ROS – Reactive Oxygen Species
RPM – Revolutions Per Minute
RPS18 – Ribosomal Protein S18
RSpo1 – Recombinant Human R-Spondin-1
RT – Room Temperature
RT-qPCR – Reverse Transcription Quantitative Polymerase Chain Reaction
SB – Sample Buffer
SDS – Sodium Dodecyl Sulfate
SDS-PAGE – Sodium Dodecyl Sulfate-Polyacrylamide Gel Electrophoresis
SEM – Scanning Electron Microscope
SEPET – Selective Plasma Filtration Therapy
SLT – Split Liver Transplantation
SOTs – Solid Organ Transplants
SPAD – Single-Pass Albumin Dialysis
SSC – Side Scatter
SSM/DM – Medium Supplemented with Serum-Supplemented Medium (SSM) and Serum-Free Hormonally Defined Medium (DM)
ß-ME – Beta-Mercaptoethanol
TBST Buffer – Tris-Buffered Saline with Tween-20
TCA – Trichloroacetic Acid
TEMED – N,N,N',N'-tetramethylethane-1,2-diamine
TGF-α, TGF-β – Transforming Growth Factor α and β
TGN – *trans*-Golgi Network
TMB – 3,3',5,5'-Tetramethylbenzidine
TRITC - Tetramethylrhodamine Isothiocyanate
T_{RM} – cells memory CD8+ T
UFC – Ultrafiltration Coefficient
V – Cell Viability
VIM – Vimentin
WB – Western Blot
WEM – William's E Medium
Wnt-3a – Recombinant Human Wnt-3a Protein
WR – Working Reagent
Y – Isolation Yield
α-SMA – α-Smooth Muscle Actin

Abstract

The liver performs many important functions in the human body. Chronic liver diseases and their progression can lead to organ failure, which poses a serious threat to the patient's life. Liver transplantation remains the only effective treatment for patients with advanced liver disease. A major limitation of this therapy is the shortage of donors, resulting in many patients dying while waiting for a transplant. Therefore, alternative methods are being sought as bridge therapies to improve the patient's condition and prolong survival until liver regeneration or transplantation can occur. One of the most promising solutions is hybrid bioartificial liver support systems (BALs), which utilize liver-derived cells. The best source of biological material for BALs is highly differentiated liver parenchymal cells, namely hepatocytes. However, their use is limited because, after isolation, they rapidly lose their specialized functions and undergo dedifferentiation. Therefore, alongside the development of new therapies for liver failure, alternative cell sources for BAL systems are being explored.

The aim of this work was to obtain a new human-derived biological material for use in BAL systems. The new cell source was derived from resected human liver fragments. During culture, the cells retained some hepatocyte functions but, unlike hepatocytes in the liver, acquired the ability to proliferate. Furthermore, the newly obtained liver-derived cells demonstrated enhanced metabolic properties when cultured under dynamic conditions in a hollow-fiber flow bioreactor model.

In this work, the method for isolating liver cells from small tissue fragments was modified and developed at the Laboratory of Tissue Engineering, IBBE PAS. This method enables the efficient production of viable cells with lower complexity and cost than standard procedures. Following cell isolation, characteristic clusters known as cell islands were observed in culture. The studies confirmed that these cell islands are formed by hepatocytes.

Long-term culture of isolated hepatocytes led to the development of a new proliferating cell population (human Hepatocyte-Derived Proliferating Cells; hHDPCs), which was characterized in this study. The hHDPCs retain selected hepatocyte characteristics, such as albumin production and the expression of HNF4α, HNF1α, and CK18, although the expression levels of these proteins fluctuated during subsequent passages. This suggests a transient physiological state characteristic of liver regeneration. At the same time, the hHDPCs exhibit very low AFP expression and lack CK19 expression, indicating that these cells do not undergo the dedifferentiation typically observed in progenitor cells. The hHDPCs demonstrate a high proliferative capacity during culture, although the expression level of the Ki67 marker is low,

suggesting the simultaneous presence of synchronized and asynchronous cell-cycle states within the analyzed cell population. During 12 passages, cell numbers increased by an average of 50-fold. It was also demonstrated that both island-forming cells and individual non-island cells are capable of division. Furthermore, the studied cells expressed the mesenchymal marker VIM, indicating cellular changes associated with dedifferentiation, such as cytoskeletal remodeling and partial epithelial-to-mesenchymal transition (EMT).

Despite their advantages, the hHDPCs also have several limitations. Although they are of hepatocyte origin, they do not retain all hepatocyte functions, as evidenced by low expression of the cytochrome P450 isoform CYP3A4 and the absence of detectable expression of the key urea cycle proteins CPS1 and ARG1. Furthermore, during dedifferentiation in two-dimensional culture, the hHDPCs, similarly to freshly isolated hepatocytes, lose the ability to form apical vacuoles. This indicates a loss of cell polarization, which is essential for proper hepatocyte function. Considering all the characteristics analyzed in this study, the phenotype of the hHDPCs does not correspond to that of cancer cells or fibroblasts. However, they also do not fully represent mature hepatocytes. Nevertheless, a simplified BAL model with hHDPCs was constructed using a hollow-fiber flow culture module. This device was used to assess the suitability of the hHDPCs for culture under perfusion conditions. Dynamic cultures showed that hHDPCs secreted higher levels of albumin and urea than the other cell types studied (HepG2, LCIs, and hHs), as well as compared to conventional static culture controls. This indicates that the newly obtained cells can adapt to dynamic conditions similar to those in the liver.

The hHDPCs represent a distinct intermediate physiological state associated with functional and metabolic remodeling, similar to that observed during liver regeneration. Owing to their long-term proliferative capacity, partial retention of hepatocyte characteristics, and substantial adaptation to dynamic culture conditions, the hHDPCs represent a promising and readily available cell source for BAL systems that could effectively replace primary hepatocytes. An interesting final finding of the study was that since the hHDPC cells constitute a distinct intermediate physiological state related to their functional and metabolic remodeling, these cells may also serve as a valuable model for studies of liver regeneration, cellular plasticity, and optimization of liver cell culture procedures, as well as for in vitro assessment of the hepatotoxicity of drug candidates.

Streszczenie

Wątroba w organizmie człowieka pełni wiele istotnych funkcji. W wyniku przewlekłych chorób oraz zaostrzenia ich przebiegu dochodzi do niewydolności organu, co wiąże się z zagrożeniem życia pacjenta. Transplantacja wątroby jest nadal jedyną skuteczną metodą leczenia pacjentów z zaawansowanymi chorobami wątroby. Ograniczeniem tej terapii jest niewystarczająca liczba dawców, w wyniku czego wielu pacjentów umiera w oczekiwaniu na przeszczep. Dlatego też poszukuje się alternatywnych metod stanowiących terapie pomostowe, które poprawiają stan pacjenta oraz wydłużają jego życie do momentu regeneracji lub przeszczepu wątroby. Jednym z najbardziej obiecujących rozwiązań są hybrydowe systemy biosztucznego wspomagania wątroby (ang. *Bioartificial Liver Support Systems*; BALs), wykorzystujące komórki pochodzenia wątrobowego. Najlepszym materiałem biologicznym do BALs są skrajnie zróżnicowane komórki parenchymalne wątroby – hepatocyty. Ich zastosowanie jest jednak ograniczone, ponieważ po izolacji szybko tracą swoje wyspecjalizowane funkcje i ulegają odróżnicowaniu. Dlatego równolegle do rozwijania nowych alternatywnych metod terapii niewydolności wątroby poszukuje się nowych źródeł komórek do zastosowania w tego typu systemach.

Celem pracy było uzyskanie nowego materiału biologicznego pochodzenia ludzkiego, który będzie można wykorzystać w systemach typu BALs. Nowe źródło komórek pochodziło z resekowanych fragmentów ludzkiej wątroby. Podczas hodowli komórki zachowywały część funkcji hepatocytów, natomiast w przeciwieństwie do hepatocytów w wątrobie, nabywały zdolność do podziałów. Ponadto nowo otrzymane komórki pochodzenia wątrobowego wykazywały zwiększone właściwości metaboliczne w hodowli w warunkach dynamicznych w modelu bioreaktora przepływowego typu *hollow fiber*.

Podczas badań zmodyfikowano opracowaną w Pracowni Inżynierii Tkankowej IBIB PAN metodę izolacji komórek wątrobowych z małych fragmentów tkanki, która umożliwia efektywne otrzymywanie żywotnych komórek przy mniejszej złożoności i niższych kosztach niż w standardowych procedurach. Podczas hodowli komórek izolowanych obserwowano ich charakterystyczne skupiska, tzw. wyspy komórkowe. Przeprowadzone badania potwierdziły, że wyspy komórkowe są tworzone przez hepatocyty.

Długotrwała hodowla wyizolowanych hepatocytów doprowadziła do opracowania nowej proliferującej populacji komórek (ang. *human Hepatocyte-Derived Proliferating Cells*; hHDPCs), które scharakteryzowano w niniejszej pracy. hHDPCs zachowują wybrane cechy hepatocytów, takie jak produkcja albuminy, HNF4α, HNF1α czy CK18, przy czym poziom

ekspresji tych białek w trakcie kolejnych pasaży wykazywał charakter fluktuacyjny. To sugeruje przejściowy stan fizjologii tych komórek, charakterystyczny dla procesów regeneracji wątroby. Jednocześnie hHDPCs wykazują bardzo niski poziom ekspresji AFP oraz brak ekspresji CK19, co świadczy o tym, że te komórki nie osiągają stanu odróżnicowania typowego dla komórek progenitorowych. hHDPCs wykazują wysoki stopień proliferacji w czasie hodowli, jednak poziom ekspresji markera Ki67 jest niski, co świadczy o zachodzącej jednocześnie synchronizacji i asynchronizacji cyklu komórkowego w obrębie populacji analizowanych komórek. Komórki hHDPCs wykazują wysoki poziom proliferacji; podczas 12-stu pasaży przyrost komórek był średnio 50-krotny. Wykazano również, że podziałowi ulegają zarówno komórki tworzące wyspy jak i pojedyncze komórki niebędące częścią wysp. Co więcej, w badanych komórkach obecny jest marker komórek mezenchymalnych – VIM, który świadczy o zmianach zachodzących w odróżnicowujących się komórkach, takich jak przebudowa cytoszkieletu czy proces częściowego przejścia epitelialno-mezenchymalnego (ang. *epithelial-to-mesenchymal transition*; EMT).

Oprócz zalet hHDPCs mają one również kilka wad. Pomimo, że są pochodzenia hepatocytarnego, to nie wszystkie funkcje hepatocytów są przez nie utrzymane, jak np. niska ekspresja izoformy cytochromu P450, CYP3A4, oraz brak widocznej ekspresji ważnych białek cyklu mocznikowego CPS1 i ARG1. Dodatkowo, w trakcie odróżnicowywania się w hodowli płaskiej, podobnie jak świeżo izolowane hepatocyty, hHDPCs tracą zdolność do tworzenia wakuoli apikalnych. To dowodzi utraty polaryzacji komórek, niezbędnej do prawidłowego funkcjonowania hepatocytów. Niemniej jednak, w dalszych badaniach samodzielnie skonstruowano uproszczony model BAL, wykorzystujący przepływowy moduł hodowlany typu *hollow fiber*. Model ten wykorzystano do oceny przydatności komórek hHDPCs do hodowli w przepływie pożywki. Przeprowadzone hodowle dynamiczne wykazały, że hHDPCs wykazują większą sekrecję albuminy, a także mocznika, w porównaniu do innych badanych typów komórek (HepG2, LCIs, hHs) oraz w stosunku do klasycznych kontroli – hodowli statycznych. Może to świadczyć o zdolności adaptacji nowo otrzymanych komórek do warunków dynamicznych, przypominających te występujące w wątrobie.

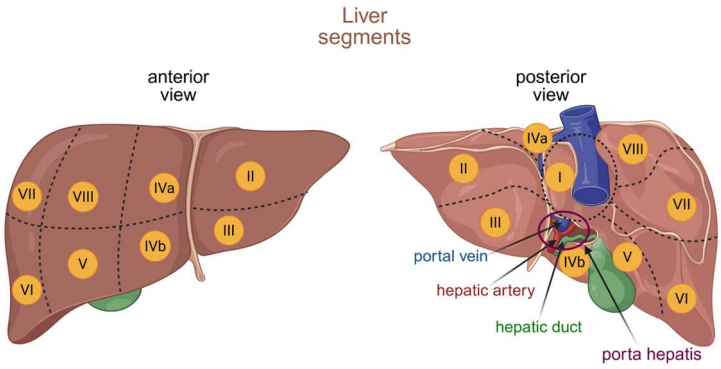
Biorąc pod uwagę wszystkie badane cechy hHDPCs, ich fenotyp nie odpowiada komórkom nowotworowym ani fibroblastom. Nie są też w pełni dojrzałymi hepatocytami ani komórkami progenitorowymi. Komórki hHDPCs stanowią odrębny pośredni stan fizjologiczny, związany z ich przebudową funkcjonalną i metaboliczną, podobny do tego obserwowanego podczas regeneracji wątroby.

Dzięki zdolności do długotrwałego wzrostu, zachowaniu istotnych właściwości hepatocytarnych oraz zdolności adaptacji do warunków hodowli dynamicznej, hHDPCs stanowią obiecujące, dostępne źródło nowych komórek w systemach BAL, które mogłyby skutecznie zastąpić hepatocyty. Ciekawym końcowym odkryciem badań było to, że ponieważ komórki hHDPCs stanowią odrębny pośredni stan fizjologiczny, związany z ich przebudową funkcjonalną i metaboliczną, to mogą być również wykorzystane jako model w badaniach nad regeneracją wątroby, plastycznością komórkową oraz optymalizacją procedur hodowli komórek wątrobowych, a także do testów *in vitro* hepatotoksyczności kandydatów na nowe leki.

1 Introduction

1.1 Liver structure and functions

The liver is the largest organ in the human body, weighing approximately 1.8-2.0 kg, and it plays a crucial role in multiple physiological processes, including digestion, metabolism, and homeostatic regulation of the organism. It is divided into two main lobes: the larger right lobe and the smaller left lobe [1]. According to the Couinaud classification, the liver consists of eight functionally independent segments (Figure 1.1) [2]. Each segment has its own portal vein, hepatic artery, and biliary drainage system, which allows for surgical removal of a single segment without impairing the blood flow or bile transport in the remaining segments [3]. The entry point for vessels into the liver is the porta hepatis, which is formed by the hepatic portal vein, hepatic artery, and hepatic duct. Approximately 25% of the liver's blood supply comes from the hepatic artery, which carries oxygen-rich blood. The remaining 75% is delivered via the hepatic portal vein, which contains deoxygenated blood enriched with nutrients, drugs, and toxins absorbed from the gastrointestinal tract [1] [4].



Segment I	Caudate lobe
Segment II	Superior lateral
Segment III	Inferior lateral
Segment IVa	Superior medial
Segment IVb	Inferior medial
Segment V	Anterior inferior
Segment VI	Anterior inferior
Segment VII	Inferior posterior
Segment VIII	Anterior superior

Figure 1.1. Liver segments. Division of the liver into eight segments according to the Couinaud classification, with the names of the liver segments shown. The posterior view demonstrates the porta hepatis, which is formed by the portal vein, hepatic artery, and hepatic duct.

1.1.1 Liver main functions

The liver performs over 500 distinct functions in the human body, which can be classified into several categories: detoxification, digestion, metabolism, synthesis, storage, and immunity.

During detoxification, the liver removes waste products, drugs, and other harmful compounds from the bloodstream. Ammonia, a particularly toxic compound, is converted into urea or glutamine for safe excretion.

In digestion, the liver produces bile and bile salts that facilitate the breakdown and absorption of fats and fat-soluble vitamins (A, D, E, and K).

Metabolically, the liver is essential for carbohydrate, lipid, and protein metabolism. It regulates blood glucose through glycolysis, gluconeogenesis, glycogenesis, and glycogenolysis. Lipid metabolism involves lipid breakdown, synthesis, and processing of various fats, while protein metabolism includes amino acid deamination, urea formation, and the synthesis of amino acid and plasma proteins. The liver synthesizes critical proteins such as clotting factors, albumin, and serine protease inhibitors like α_1-antitrypsin. It also stores glycogen, iron, copper, cholesterol, lipids, and several vitamins [5].

From an immunological perspective, Kupffer cells, resident macrophages located in the liver sinusoids, phagocytose bacteria, viruses, and other pathogens. These cells can also trigger an immune response by releasing pro-inflammatory cytokines such as interleukin-1 (IL-1), interleukin-6 (IL-6), and interleukin-8 (IL-8). Additionally, the liver produces complement proteins and C-reactive protein. Many hormones are also secreted, activated or deactivated within the liver [5].

1.1.2 Liver on the cellular level

The liver's functional units, known as hepatic lobules, typically have a hexagonal shape. At each corner of the lobule, portal triads are located. Each portal triad consists of the hepatic artery, the portal vein, and the bile duct. The central vein lies in the central structure of the lobule (Figure 1.2) [6]. Within the lobule, different types of liver cells are organized in a way that supports their specialized functions and interactions. Hepatocyte and non-parenchymal cells communicate with each other via paracrine and autocrine signaling pathways, which ensure the proper coordination of metabolic, synthetic, and immunological activities [7].

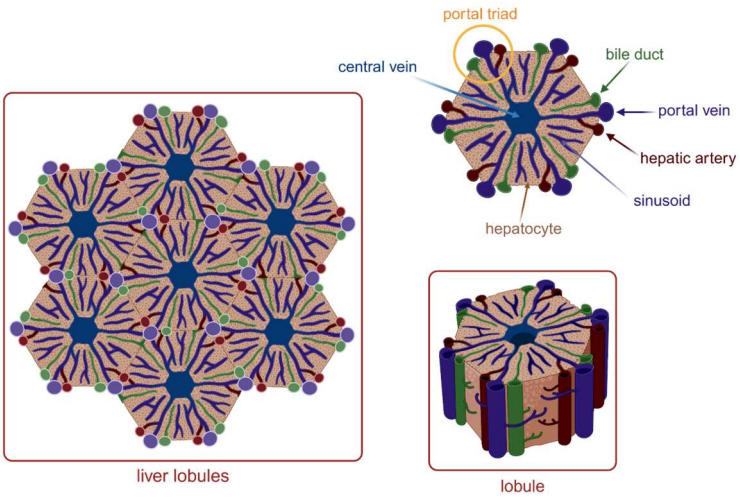


Figure 1.2. Liver lobules. Hepatocytes are arranged into hexagonal-shape structures named lobules, with a central vein in the middle of the lobule, and portal triads on the corners. The portal triad consists of the bile duct, hepatic artery, and portal vein. Between the layers of the hepatocytes are located structures called sinusoids.

1.1.3 Liver zonation

The liver lobules are divided into three metabolic zones, allowing the liver to perform multiple metabolic processes in parallel. Zone 1 (periportal) includes the portal triad, which consists of the hepatic artery, portal vein, and bile duct. Zone 2 (mid-lobular), located between zones 1 and 3, while zone 3 (perivenous), surrounds the central vein [8], [9]. The zonal organization of the liver establishes gradients of oxygen, hormones, and nutrients along the portal-central axis. As blood flows through the lobule, these substances are gradually consumed, resulting in higher concentrations in zone 1 and lower concentrations in zone 3. Hepatocytes in zone 1 are engaged in energy-demanding processes such as protein synthesis and gluconeogenesis. Cells located in zone 2 contribute to functions like the secretion of hepcidin, a hormone involved in iron regulation. Hepatocytes in zone 3 carried out processes that require less energy, including glycolysis, bile acid biosynthesis, and xenobiotic metabolism (Figure 1.3) [10].

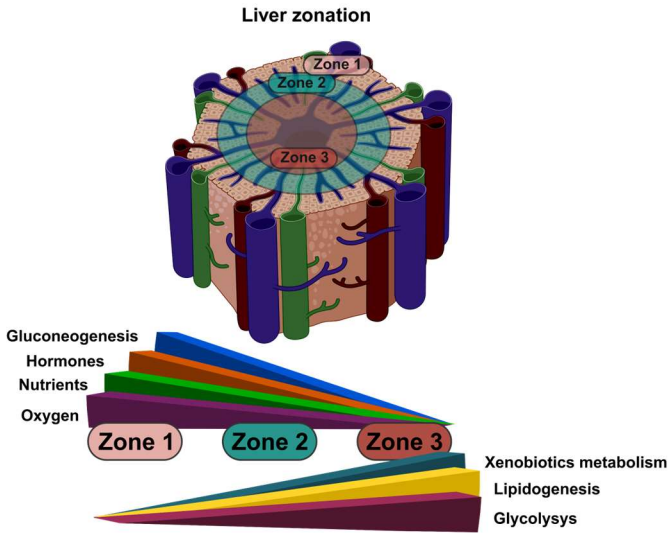


Figure 1.3. Liver zonation. Schematic representation of the hepatic lobule divided into three zones, taking into account chemical and nutritional gradients.

1.1.4 Parenchymal and non-parenchymal cells in the liver

The liver is made up of two main cell populations: parenchymal and non-parenchymal. Hepatocytes are large parenchymal cells, accounting for 60-70% of the total cell number and approximately 80% of the total liver [11], [12]. The functions of hepatocytes are supported by the non-parenchymal cells, which constitute 30-40% of all liver cells. The non-parenchymal population includes several cell types, with the following approximate composition: Kupffer Cells (KCs) – 20%, hepatic stellate cells (HSCs) – 1%, liver sinusoidal endothelial cells (LSECs) – 50%, lymphocytes – 25%, biliary cells (cholangiocytes) – 5% [11], [12], [13]. These cells play roles in supporting hepatocyte function, immune surveillance and response, regulation of the extracellular matrix, and bile formation.

1.1.4.1 Parenchymal cells - hepatocytes

Hepatocytes are polygonal-shaped cells measuring approximately 20-30 μm in diameter. They contain one or two nuclei, with polyploid nuclei being larger. In adult humans, around 40% of hepatocytes are tetraploid, and the portion of polyploid cells increases with age or during liver regeneration, oxidative stress, or metabolic overload. The presence of multinucleated cells is related to their high metabolic activity [14]. Hepatocytes, as epithelial origin cells, are highly polarized, possess the apical (canalicular) and the basolateral (sinusoidal) plasma membrane domains. The apical membrane forms networks of *bile canaliculi*, facilitating bile secretion, whereas the basal membrane is in contact with the liver

sinusoidal endothelial cells (LSECs) that form sinusoids through which blood flows. Hepatocytes are organized in two rows, separated by the hepatic sinusoid; together, these structures constitute the liver plate, aligned radially within the lobule. Blood from the portal vein and hepatic artery mixes in the hepatic sinusoids and flows toward the central vein. The portal vein delivers partially deoxygenated, nutrients-rich blood, while the hepatic artery supplies oxygen-rich blood to the liver. Through the sinusoidal blood flow, hepatocytes are exposed to a variety of molecules, including hormones, nutrients, and metabolites, which are essential for their functions [14], [15].

The urea cycle is a key metabolic pathway that occurs in liver hepatocytes. Its main function is to convert toxic ammonia into non-toxic urea, which is excreted by the kidneys. The urea cycle consists of five stages. The first two reactions occur in the mitochondria and include carbamoyl phosphate synthesis and the formation of citrulline. The remaining three stages occur in the cytoplasm and involve argininosuccinate synthesis, argininosuccinate cleavage, and urea formation (Figure 1.4) [16].

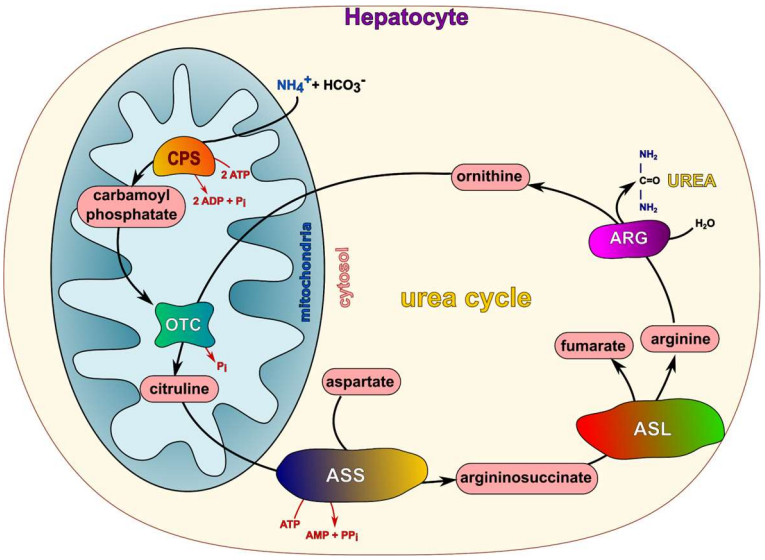


Figure 1.4. Scheme of the urea cycle occurring in a hepatocyte. The urea cycle begins in the mitochondria, where ammonia reacts with carbon dioxide in the presence of the enzyme carbamoyl phosphate synthetase I (CPS), forming carbamoyl phosphate. This process requires two ATP molecules and represents the first step in ammonia detoxification. Carbamoyl phosphate then reacts with ornithine via the enzyme ornithine transcarbamoylase (OTC), producing citrulline. Citrulline leaves the mitochondria and enters the cytosol. In the cytosol, citrulline combines with aspartate in a reaction catalyzed by argininosuccinate synthetase (ASS), forming argininosuccinate. Argininosuccinate is then cleaved by argininosuccinate lyase (ASL) into arginine and fumarate. Finally, arginase hydrolyzes arginine, producing urea, which is excreted in the urine, and ornithine, which returns to the mitochondria, completing the cycle.

1.1.4.2 Non-parenchymal cells

Between the hepatocyte layer and sinusoid lies the space of Disse, which contains hepatic stellate cells (HSCs). The walls of the sinusoids are formed by liver sinusoid endothelial cells (LSECs), while the lumen contains resident macrophages known as Kupffer Cells (KCs) (Figure 1.5) [1], [17].

KCs were first described by Carl von Kupffer in 1876 as a stellate cell. Later, in 1898, Tadeusz Browicz correctly identified them as liver macrophages [18], [19], [20]. Kupffer cells are highly specialized macrophages responsible for inflammation, hepatocytotoxicity, injury and repair. Through phagocytosis and pinocytosis, they remove senescent cells, bacteria, viruses, endotoxins, immune complexes, and other circulating particles [21], [22].

LSECs are highly specialized endothelial cells forming the permeable walls of hepatic sinusoids. They were first described at the ultrastructural level by Eddie Wisse in 1970. LSECs contain numerous fenestrations organized into structures called sieve plates. The absence of a continuous basement membrane and the presence of fenestrations place LSECs among the most permeable endothelial cell types in the human body, allowing the exchange of metabolites and macromolecules between blood and hepatocytes. Additionally, LSECs contribute to the production of extracellular matrix (ECM) components in the space of Disse, which plays a role in metabolite transport, inflammation, and angiogenesis [23], [24].

Hepatic stellate cells (HSCs), also known as fat-storing cells, were originally described by Carl von Kupffer in 1876 [18]. In a healthy liver, these cells exhibit a quiescent phenotype and severe primally as the main storage site for Vitamin A. They also contribute to the synthesis of ECM components and produce cytokines and growth factors, including hepatocyte growth factor (HGF) and transforming growth factor α and β (TGF-α, TGH-β) [21], [25]. Following liver injury, HSCs become activated and differentiated into myofibroblast-like cells that produce excessive ECM, leading to liver fibrosis [26].

Lymphocytes in the liver are highly different from lymphocytes from blood. Intrahepatic lymphocytes include natural killer (NKs), natural killer T cells (NKTs), innate lymphoid cells (ILCs), memory CD8+ T (T_{RM}) cells, and others. After activation lymphocytes play important role in the regulation of the innate and adaptive immune response, take part in the resistance in the pathogen's infections. Also, they participate in the repairing of the injure tissue and maintaining tissue homeostasis [27].

Cholangiocytes, also known as biliary epithelial cells (BECs), are epithelial cells that line the bile ducts. These cells play an important role in the regulation of bile composition by

absorbing selected molecules from bile. Cholangiocytes modify bile acid and several metabolites, including amino acids, ions, and glucose produced by hepatocytes. Through these processes, cells contribute to the transport and proper composition of bile before it reaches the intestine [4]. In addition, cholangiocytes precipitate in the liver regeneration process. Under conditions in which mature hepatocytes are damaged or unable to proliferate, cholangiocytes may differentiate toward hepatocyte-like cells [28].

Within the liver lobules, two fluid systems operate simultaneously, with blood and bile moving in opposite directions. Blood flows from the hepatic artery and portal vein toward the central vein. In contrast, bile produced by hepatocytes is secreted into bile canaliculi and transported toward the bile ducts, from where it continues to the intestine (Figure 1.5) [29], [30].

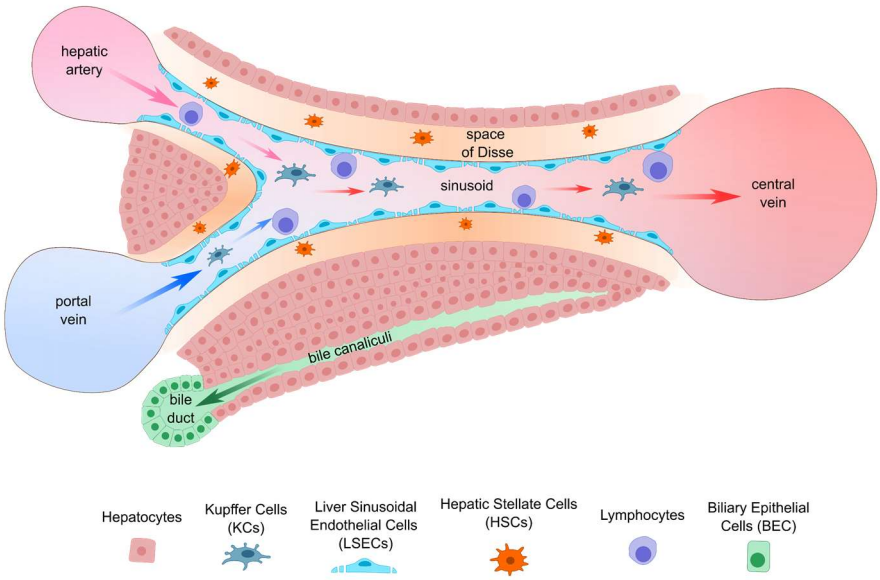


Figure 1.5. Liver structure at the cellular level. Between the layers of hepatocytes in the liver lobules, sinusoidal structures are formed in which liver sinusoidal endothelial cells (LSECs), Kupffer cells (KCs), and lymphocytes are present. Nutrient-rich blood enters the sinusoids through the hepatic artery and portal vein and subsequently reaches the central vein. The space of Disse, which containing hepatic stellate cells (HSCs), is located between hepatocytes and sinusoids. Moreover, bile produced by hepatocytes is secreted into the *bile canaliculi* and transported to the bile ducts, where it is further modified by biliary epithelial cells (BEC) before being released into the intestine. The direction of bile flow within the lobules is opposite to that of blood flow.

1.1.5 Important Hepatocyte-Produced Proteins

1.1.5.1 Human serum albumin (HSA; ALB)

Human serum albumin (HSA, also referred to as **ALB)** is a plasma protein produced by hepatocytes. It represents the most abundant protein in the blood plasma of healthy individuals, with physiological concentration typically ranging between 35 and 50 mg/mL. The

liver synthesizes approximately 10-15 g of albumin per day, what constitutes about 10% of the total protein synthesis occurring in this organ [31]. Only a small portion of newly synthetized albumin, estimated at around 2 g, is stored in the liver, whereas the majority is rapidly released into circulation [32]. In humans, albumin has a relatively long biological half-life of approximately three weeks [33]. This extended half-life contributes to the maintenance of stable plasma albumin levels even when synthesis or degradation rates fluctuate, thereby supporting several essential physiological processes [34].

ALB is a globular plasma protein with a molecular weight of approximately 67 kDa. Its primary structure consists of 585 amino acid residues, including 35 cysteine's residues. Among these, 34 cysteines form 17 disulfide bonds that stabilize the protein's secondary structure. The cysteine-34-residue (Cys-34) remains unpaired and plays an important role in ligand binding of albumin [35], [36]. The secondary structure of ALB is predominantly composed of α-helices, which constitute about 67% of the protein structure. These helices are organized into three homologous domains: domain I (residues 1-195), domain II (196-383), and domain III (384-585). Each of these domains is further divided into two subdomains, designated A and B. Structural elements such as turns represent approximately 10% of the structure, whereas random coils for around 23%. Moreover, β-sheets structures are absent in human serum albumin [37]. Crystallographic studies show that the tertiary structure of albumin adopts a characteristic heart-shaped conformation with approximate dimensions of 80 x 80 x 30 Å (8 x 8 x 3 nm) [38], [39]. Figure 1.6 illustrates the crystallographic structure of ALB.

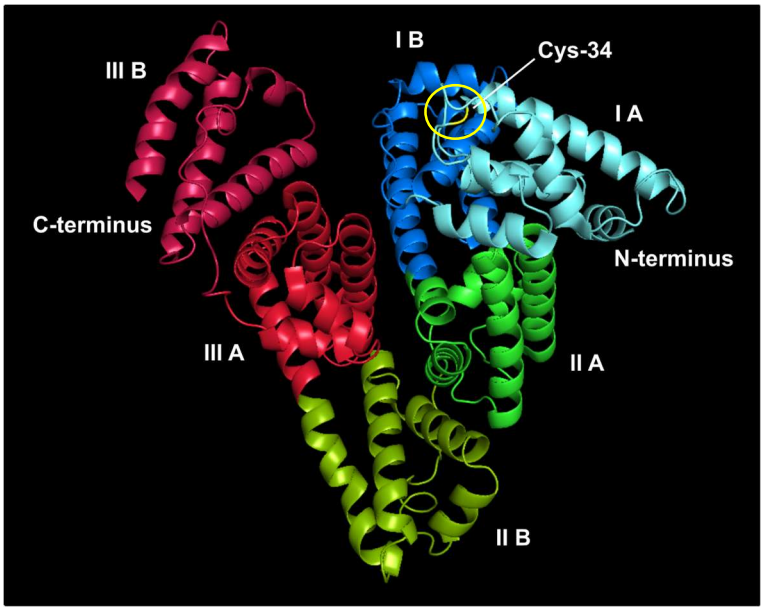


Figure 1.6. Structure of human serum albumin (ALB). Albumin primary structure is composed of 585 amino acids, whereas the tertiary structure has a heart-like shape, that consists of 3 domains (I, II, III), each of which is divided into 2 subdomains, A and B. Domain I is marked on blue (subdomain I A – light blue, subdomain I

B – blue), domain II on green (subdomain II A – lime, II B – green), domain III on red (III A – red, III B – dark pink). On the yellow color and in the yellow ring is marked cysteine 34 (Cys-34); this residue is free and available for reaction with different molecules. ALB structure purchased from RCSB Protein Data Bank (PDB ID: 1AO6).

As a multifunctional plasma protein, albumin plays several crucial physiological roles. It is responsible for maintaining oncotic pressure and contributes to the regulation of body fluid balance. In addition, albumin exhibits antioxidant properties and precipitates in the neutralization of oxidative stress. Another important function of albumin is the transport of numerous molecules, including bilirubin, fatty acids, bile acids, metal ions such as zinc and copper, vitamin D, various drugs, and divalent cations such as calcium and magnesium [40]. In recent years, there has been increased interest in albumin for its use in medicine or therapeutics. Its applications extend to multiple medical fields, including tissue engineering, intensive care medicine, drug delivery systems, and its use as a carrier for pharmaceutical compounds. Albumin is also utilizes in the infusion therapy, wound healing strategies, respiratory distress syndrome treatment, and during various surgical procedures such as cardiac or abdominal operations [41].

Albumin biosynthesis in hepatocytes begins with the formation of a precursor protein known as preproalbumin. To obtain a mature protein, this pre-protein has to be transformed several times. This precursor contains a 24-amio-acid signal peptide that directs the newly synthetized polypeptide into the endoplasmic reticulum (ER). In the ER, the signal peptide is cleaved, resulting in the formation of proalbumin. The protein is subsequently transported to the Golgi apparatus, where it is further transformed into a mature protein. Finally, the mature protein is packaged into Golgi secretory vesicles and released from the hepatocytes into the bloodstream [42], [43], [44], [45].

1.1.5.2 Alpha-fetoprotein

Human alpha-fetoprotein (AFP) is synthetized by a yolk sac and fetal liver during embryonic development. It is one of the most abundant serum proteins in the fetus; however, its concentration decreased rapidly after birth and remains very low in healthy adults, typically below 10 ng/mL [46]. Under certain physiological and pathological conditions, such as pregnancy, liver regeneration, liver diseases, or liver cancer, AFP levels may become elevated [47]. Due to its expression in fetal hepatocytes and tumor cells, AFP is widely used as a biomarker of immature liver cells as well as a tumor marker, particularly in hepatocellular carcinoma (HCC) [48], [49].

AFP is a glycoprotein belonging to the albumin family, with a molecular weight of about 70 kDa and a half-life is 3.5-4 days [50]. The amino acid sequences of AFP and ALB show approximately 40% homology, suggesting some structural similarities despite their distinct biological functions [51], [52], Similar to HAS, AFP acts as a carrier protein transporting hormones, fatty acids, and other molecules during fetal development. In addition, AFP has been implicated in the regulation of tumor growth and progression [51]. AFP plays a significant role in HCC development by promoting proliferation, migration, and metastasis, while inhibiting apoptosis. It has been shown to modulate immune responses, contributing to immunosuppression within the tumor microenvironments. Therefore, AFP is considered a potential therapeutic target in HCC [47].

AFP is composed of a single polypeptide chain consisting of 609 amino acid residues. Its secondary structure is organized into three domains, similar to ALB. Domain I (D I) comprises amino acid residues 1-210, domain II (D II) consists of residues 211-402, and domain III (D III) includes residues 403-609 [49]. Each domain is further divided into two subdomains A and B, and the overall structure is stabilized by 15 disulfide [53]. Within the AFP amino acid sequence, asparagine at position 251 (Asn-251), represents a site of N-glycosylation (Figure 1.7). This post-translational modification significantly alters the structure and physicochemical properties of the protein. Moreover, alterations in protein N-glycosylation are associated with various pathological conditions, including cancers [54].

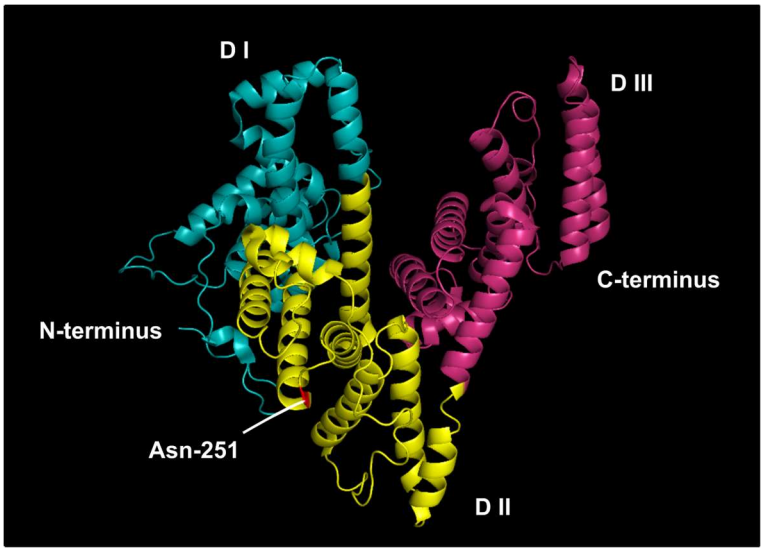


Figure 1.7. Structure of Alpha-Fetoprotein (AFP). The primary structure consists of 609 amino acid residues organized into three domains. Domain I (D I), containing the N-terminus, is shown in dark turquoise; domain II (D II) in yellow; and domain III (D III), containing the C-terminus, in dark pink. The asparagine residue at position 251 (Asn-251), which is the site of N-glycosylation, is highlighted in red. The structure was obtained from the RCSB Protein Data Bank (PDB ID: 7YIM).

1.1.5.3 Alpha -1-anty-trypsin

Alpha-1-antitrypsin (A1AT) is a protein belonging to the serine protease inhibitor (serpin) family. It is primarily synthetized by hepatocytes and subsequently released into the bloodstream. The main function of A1AT is to protect tissues from enzymatic degradation caused by proteases. A1AT is also classified as an acute-phase protein; therefore, its plasma concentration increases during inflammation or infection [55]. In healthy individuals, circulating A1AT levels range from approximately 0.9 to 1.75 mg/mL; however, during the acute-phase response, they may increase up to 4-fold [56]. Elevated A1AT levels have also been observed during pregnancy [57] and with ageing [58]. The half-life of circulating A1AT is approximately 3-5 days [59].

A1AT is a glycoprotein with a molecular weight of approximately 52 kDa, consisting of a single polypeptide chain of 394 amino acid residues. Its tertiary structure includes three β-sheets, nine α-helices, and a reactive center loop (RLC), which is essential for inhibitory activity. The inhibitory mechanism of A1AT involves the RLC, which acts as a bait for target proteases. Upon binding, A1AT undergoes a conformational change that traps the enzyme, forming a highly stable and essentially irreversible complex (Figure 1.8) [60].

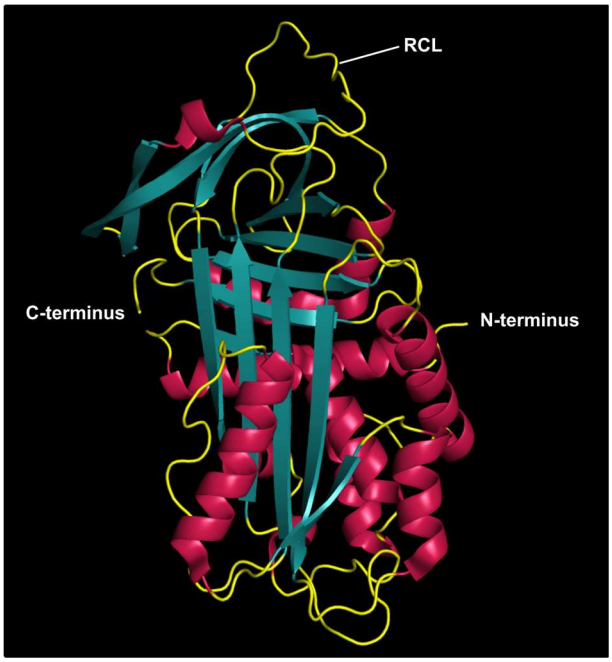


Figure 1.8. Structure of alpha-1-antitrypsin (A1AT). The primary structure consists of 394 amino acid residues. The tertiary structure includes 3 β-sheets (dark blue), nine α-helices (dark pink), and the reactive center loop (RLC; yellow). The structure was obtained from the RCSB Protein Data Bank (PDB ID: 6I7U).

1.1.5.4 Hepatocytes Nuclear Factors

Hepatocyte Nuclear Factor 4 alpha (HNF4α) belongs to the nuclear receptor (NR) superfamily of transcription factors. The highest level of expression is found in the liver, but its presence has also been reported in the kidneys, pancreas, intestines, and stomach, and lower levels of expression are found in the testes and brain. In the liver, HNF4α plays a central role in organ development and the maintenance of hepatic function by regulating the expression of genes involved in metabolism and cell proliferation. It is also essential for hepatocyte differentiation and contributes to liver regeneration processes. HNF4α controls the expression of genes associated with key metabolic pathways, including glycolysis, gluconeogenesis, bile acid synthesis, the urea cycle, fatty acid metabolism, and drug metabolism [61]. Genome-wide studies have demonstrated that HNF4α binds to regulatory regions of nearly half of actively transcribed genes in the adult liver, highlighting its role as a master regulator of hepatic gene expression. Furthermore, HNF4α is a crucial during embryonic development, where it regulates genes required for hepatocyte differentiation, and in adult organisms, it is essential for maintaining hepatocyte identity and phenotype [62].

The human *HNF4α* gene is regulated by two main promoters, P1 and P2, which generate isoforms differing in their N-terminal domains and transcriptional activities. In the adult liver, P1-derived isoforms predominate and are associated with the regulation of gene characteristics of mature hepatic genes. In contrast, P2-derived isoforms are mainly expressed during early development and in pathological conditions, including HCC [63].

HNF4α functions as a homodimer. The P1-HNF4α1 isoform consists of a polypeptide chain of 474 amino acid residues with an approximate molecular weight of 53 kDa; however, the length varies between isoforms [64]. Structurally, each HNF4α monomer contains two main functional domains: an N-terminal DNA-binding domain (DBD) and a C-terminal ligand-binding domain (LBD), connected by a flexible hinge region that enables proper DNA binding and conformational adaptability (Figure 1.9) [65].

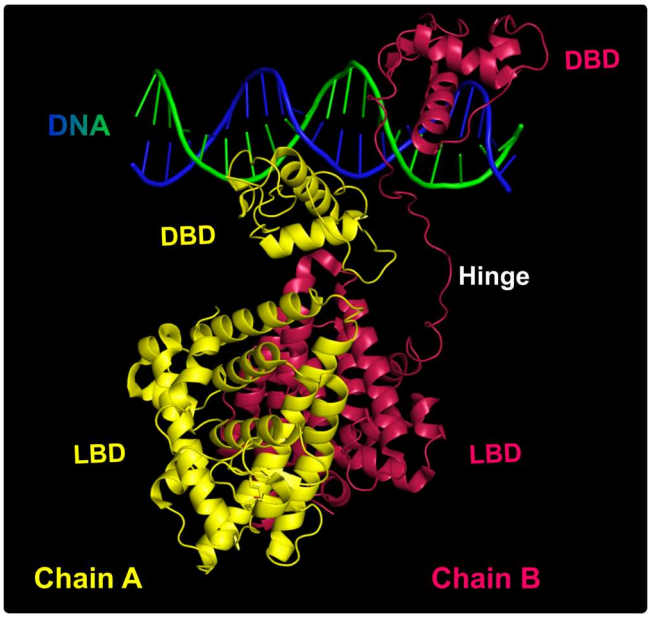


Figure 1.9. Structure of HNF4α. The HNF4α homodimer consists of two identical polypeptide chains: chain A (yellow) and chain B (magenta). Each chain contains 474 amino acid residues. The DNA-binding domain (DBD) is located at the N-terminus, whereas the ligand-binding domain (LBD) is located at the C-terminus. These two domains are connected by a hinge region. The DNA molecule is shown in blue and green. The protein structure was obtained from the RCSB Protein Data Bank (PDB ID: 4IQR).

Hepatocyte Nuclear Factor 1 alpha (HNF1α) belongs to the family of liver-enriched nuclear transcription factors and is expressed in several endoderm-derived tissues, with the highest levels observed in the liver, pancreas, and kidneys. In hepatocytes, HNF1α regulates the expression of numerous genes involved in lipid and glucose metabolism, detoxification processes, protection against cellular stress, and the maintenance of the hepatocytes-specific transcriptional program. HNF1α has been reported to exert tumor-suppressive function in the liver. Moreover, it operates within a regulatory network together with HNF4α and other transcription factors, co-regulating genes encoding metabolic enzymes and transporter proteins [66], [67]. HNF1α functions as a homodimer formed through its N-terminal dimerization [68]. The canonical human isoform consists of 631 amino acid residues and has a molecular mass of approximately 67 kDa [69].

1.1.5.5 Cytochromes P450

Cytochrome P450 3A4 (CYP3A4) is a member of cytochrome P450 enzymes family and represents the most abundant isoform in the human liver. It plays a central role in the metabolism of drugs, xenobiotics and endogenous substances, being responsible biotransformation of 30-50% of clinically used drugs [70]. CYP3A4 is a transmembrane protein localized in the membrane of the endoplasmic reticulum, which enables its interactions with a

wide range of substrates [71]. The enzyme catalyzes chemical transformations that increase the polarity of drugs, thereby preparing them for further metabolism and excretion. Importantly, CYP3A4 does not directly eliminate drugs but enables their biotransformation into more water-soluble metabolites [70].

CYP3A4 consists of a single polypeptide chain comprising 503 amino acid residues (Figure 1.10). Its secondary structure is predominantly composed of a α-helices and flexible loops, with relatively few β-sheets elements [72]. The active site of CYP3A3 is large and flexible, located in the central part of the protein, and forms a binding pocket that contains a heme group capable of interacting with various substrates [70]. The molecular weight of CYP3A4 is approximately 55 kDa [71]. The half-life of the enzyme varies widely, ranging from approximately 10 to over 100 hours, depending on the substrate it interacts with [73].

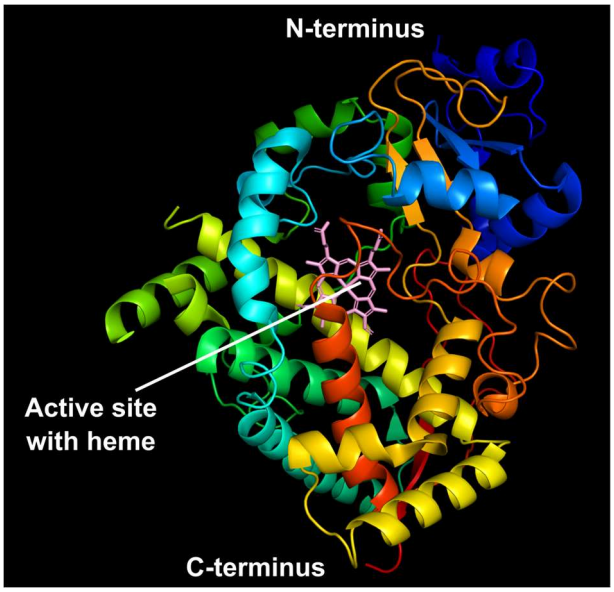


Figure 1.10. Structure of cytochrome P450 3A4 (CYP3A4). CYP3A4 consist of a single polypeptide chain composed of 503 amino acid residues. Its structure is dominated by α-helices and flexible loops, with a few β-sheet elements. The enzyme contains a heme group (shown in pink) located in the central active site, which is responsible for the metabolism of a wide range of substances. The structure was obtained from the RCSB Protein Data Bank (PDB ID: 1W0E).

Cytochrome P450 2E1 (CYP2E1) plays the key role in the metabolism of small, polar endogenous and exogenous compounds. It is primarily localized in the endoplasmic reticulum of hepatocytes, but it is also present in mitochondria and Kupffer cells [74]. CYP2E1 is involved in the metabolism of alcohols, including ethanol, as well as various toxic and carcinogenic substances such as acetone, chloroform, and benzene. It also contributes to the metabolism of small-molecule drugs, including paracetamol. The catalytic activity of CYP2E1 leads to the formation of reactive oxygen species (ROS), which can induce oxidative stress and contribute to hepatocyte damage. Additionally, CYP2E1 may convert same compounds into

toxic intermediate metabolites [75]. The active site of CYP2E1 is localized within the globular core of the enzyme and is characterized by a relatively small and hydrophobic pocket, enabling selective binding of low-molecular-weight substrates [76]. CYP2E1 is a monomeric protein consisting of a single polypeptide chain of 493 amino acids, with a molecular weight of approximately 56 kDa. Its structure is dominated by α-helices and loops, with a smaller contribution of β-sheets elements [77].

Cytochrome P450 2C8 (CYP2C8) is expressed at relatively high levels in the liver but is also present in various extrahepatic tissues, including the kidneys, adrenal glands, brain, uterus, duodenum, mammary glands, and ovaries [78]. CYP2C8 is involved in the metabolism of wide range of substances, including drugs, unsaturated fatty acids, retinoic acid, and arachidonic acid. The active site of CYP2C8 is relatively large and flexible, allowing it to accommodate bulky ligands and contributing to its distinct substrate specificity compared to CYP3A4 [79]. The active site has been described as having a trident-shaped, predominantly hydrophobic architecture, which facilitates the binding of large substrates, including those exceeding 500 Da [80]. CYP2C8 consists of approximately 490 amino acids and has a molecular weight of approximately 56 kDa. Similar to other cytochromes P450 enzymes, its structure is dominated by α-helices and loops, with relatively few β-sheets elements [81].

1.1.5.6 Other Proteins Important for Hepatocytes

Hepatocyte Growth Factor (HGF) is a pleiotropic growth factor and cytokine that plays an important role in the stimulation of cell proliferation, survival, and hepatocyte regeneration, while also protecting cells against apoptosis [82]. HGF is predominantly produced in the liver by non-parenchymal cells, including HSCs, LSECs, and KCs [83]. However, HGF is also expressed in various organs, including the kidney, lungs, heart, skin, and brain [84], [85]. Its biological effects are mediated through binding to the c-Met receptor, a receptor tyrosine kinase located on the hepatocyte membrane. Activation of c-Met triggers multiple intracellular signaling pathways that regulate hepatocyte proliferation, survival, and gene expression during liver regeneration [86].

Epidermal Growth Factor (EGF) is produced by various tissues, with the highest levels observed in Brunners's glands on the duodenum and in the salivary [87]. EGF bind to the epidermal growth factor receptor (EGFR), a tyrosine kinase receptor located in the

hepatocyte membrane. Upon activation, EGFR initiates multiple signaling pathways involved in cell proliferation, migration, angiogenesis, and apoptosis. In the liver, EGF plays an important role in tissue regeneration and repair by stimulating hepatocyte proliferation. However, dysregulation of EGFR signaling may contribute to pathological processes, including fibrosis, inflammation, and cancer development [88].

Cytokeratin 18 (CK18) is a marker of mature hepatocytes and belongs to the family of intermediate filament proteins. It plays a structural role in maintaining cell shape and provides resistance to mechanical stress. The molecular weight of CK18 is approximately 45 kDa [89], [90].

Cytokeratin 19 (CK19) is a marker of hepatic progenitor cells, early hepatoblasts, and cholangiocytes. It is not expressed in mature hepatocytes and is also considered a marker of cancer stem-like cells in liver tumors. In the liver, CK19 contributes to cytoskeletal organization, epithelial stability, and the maintenance of the biliary epithelial phenotype. Its molecular weight is approximately 40 kDa [91], [92].

Integrin β1 (CD29) is a transmembrane adhesion receptor that mediates cell attachment to the extracellular matrix (ECM) and participates in both cell–ECM and cell–cell interactions through the formation of heterodimeric integrin complexes. In hepatocytes, CD29 plays a critical role in maintaining proper liver architecture under physiological conditions as well as during liver regeneration [93]. It is also essential for preserving hepatocyte polarity and the proper organization of *bile canaliculi* [94]. At the hepatocyte surface, integrin β1 forms heterodimers with various α subunits, enabling binding to ECM components such as collagen, fibronectin, and laminin. These interactions facilitate stable cell–ECM adhesion and activate intracellular signaling pathways that regulate cytoskeletal organization, cell survival, and proliferation [95].

Pregnane X Receptor (PXR) is a nuclear receptor involved in the regulation of steroid and xenobiotic metabolism. In hepatocytes, it controls the expression of genes encoding phase I (e.g., CYP3A4), phase II enzymes (e.g., UGTs), as well as various transport proteins, thereby enhancing the metabolism and elimination of drugs and toxic compounds. In addition, PXR contributes to the regulation of bile acid homeostasis as well as lipid and glucose metabolism, and it also participates in the modulation of inflammatory responses [96].

Glutamine synthetase (GLUL) plays a crucial role in hepatocytes by detoxifying ammonia. It contributes to nitrogen metabolism by complementing the urea cycle and supports cellular metabolism by providing glutamine for nucleotide biosynthesis and energy production. GLUL expression is predominantly localized in hepatocytes of the third (perivenous) lobular zone, making it an important marker of metabolic zonation and liver [97], [98].

Carbamoyl-phosphate synthetase I (CPS1) is a mitochondrial enzyme expressed in hepatocytes that catalyzes the first and the last step of the urea cycle. It converts toxic ammonia into carbamoyl phosphate, which is subsequently processed into the urea cycle and ultimately converted into urea for excretion. CPS1 is a multidomain protein composed of approximately 1,500 amino acid residues, with a molecular mass of about 165 kDa [99].

Arginase 1 (ARG1) is a cytosolic enzyme that catalyzes the final step of the urea cycle, converting arginine into ornithine and urea. Urea is excreted by the kidneys, whereas ornithine is transported back into the mitochondria to continue the cycle. ARG1 functions as a homotrimer, and the molecular mass of each subunit is approximately 35 kDa. Each monomer consists of 322 amino acid residues [100], [101].

1.1.5.7 Proteins Not Specific to Hepatocytes

Vimentin (VIM) is an intermediate filament protein expressed in mesenchymal cells. It plays an important role in cell adhesion, proliferation, migration, and intracellular signaling [102]. VIM is not specific to hepatocytes and is typically expressed at low levels in these cells; however, in the liver, it is involved in epithelial-to-mesenchymal transitions (EMT) [103]. EMT is associated with processes such as liver regeneration, fibrosis, and carcinogenesis [104], [105]. Vimentin is also expressed in hepatic stellate cells (HSCs), where it contributes to cytoskeletal organization and regulates cell proliferation, migration, and adhesion [104].

Mesenchymal Stem Cell Markers (MSCs) are used to identify mesenchymal stem cells. These cells are characterized by a panel of surface markers with functional criteria. This approach is necessary due to the heterogeneous nature of MSCs populations and the lack of a single specific marker [106]. Table 1.1 summarizes selected positive and negative MSC markers and their biological functions.

Table 1.1. Biological functions of positive and negative MSC markers.

Marker	Function	Reference
Positive MSC markers		
CD73 (ecto-5′-nucleotidase)	A membrane-bound enzyme catalyzes the conversion of AMP to adenosine. It is involved in immunomodulation, inflammation, cell migration, and tissue regeneration.	[107]
CD44	A transmembrane glycoprotein that functions as a receptor for hyaluronic acid, a major component of the ECM. It precipitates in cell adhesion and regulates signaling pathways related to cell migration, proliferation, and differentiation. Although widely used as an MSC marker, it is not specific.	[108], [109]
CD29 (integrin β1)	A membrane protein involved in cell adhesion and signaling between cells and the ECM. It is commonly used as an auxiliary marker in MSC identification and is also present in hepatocytes.	[110]
Negative MSC markers		
CD34	A transmembrane protein involved in the regulation of cell adhesion and migration. It is typically expressed on hematopoietic stem cells and endothelial cells.	[111]
CD133 (prominin-1)	A transmembrane protein associated with the regulation of signaling pathways controlling cell proliferation, differentiation, apoptosis, and migration. It is expressed in various stem and progenitor cell populations and is widely used as a marker of cancer stem cells.	[112]
CD45 (protein tyrosine phosphatase receptor type C; PTPRC)	A transmembrane protein that regulates signaling in immune cells and is a characteristic marker of hematopoietic stem cells and mature leukocytes.	[113]

1.2 Faulty Liver

Liver disease is currently the 11th leading cause of death worldwide, accounting for approximately 2 million deaths annually, which corresponds to about 4% of all global deaths. The most common liver diseases include viral hepatitis (types A–E), fatty liver disease, cirrhosis, and liver cancer. The causes of liver disease include infections, exposure to drugs or toxins (including alcohol), autoimmune diseases, genetic defects, and physical injury [114].

Liver failure can be classified into three main types: acute liver failure (ALF), acute-on-chronic liver failure (ACLF), and chronic liver failure (CLF). ALF is characterized by rapid disease progress and typically occurs in individuals with untreated liver disease. In contrast ACLF, develops in patients with liver disease or cirrhosis following an acute hepatic insult and is frequently associated with multiorgan failure [114], [115]. CLF develops progressively over time and represents the end stage of chronic liver disease. CLF can be caused by viral infections, drug-induced liver injury (DILI), excessive alcohol consumption, or metabolic dysfunction-associated steatotic liver disease (MASLD). Chronic liver disease often progresses to cirrhosis and liver cancer [116]. The most common causes of chronic liver disease worldwide include MASLD [previously referred to as non-alcoholic fatty liver disease (NAFLD)], and alcohol-related fatty liver disease (ALD). Despite differing etiologies, both diseases follow a similar pathological progression leading to liver damage [117].

Liver damage progresses through several stages (Figure 1.11). The earliest is steatosis, characterized by excessive lipid accumulation in hepatocytes, commonly associated with obesity, diabetes, or alcohol abuse. Steatosis is generally asymptomatic and potentially reversible with appropriate intervention. Persistent lipid accumulation may lead to inflammation, known as hepatitis. Hepatitis can result from various causes, including infections, toxins, and metabolic disorders. While acute inflammation is part of a normal immune response, chronic inflammation contributes to ongoing liver injury and disease progression. In many cases, there are no clinical symptoms in the early stages of hepatitis, but with longer-lasting inflammation, symptoms may include jaundice (yellow skin or white eyes), vomiting blood, altered consciousness, fever, loss of appetite, weight loss, and more advanced cases. This stage of the disease is also reversible with proper care of the organ [116]. The next stage is liver fibrosis (scarring), which is characterized by excessive deposition of ECM components, particularly collagen. This process results from chronic inflammation and activation of hepatic stellate cells, leading to progressive scarring and disruption of normal liver architecture. The disease may produce no symptoms or symptoms similar to those of hepatitis.

In the very early stages of the disease, this process can be reversed; however, persistent injury promotes its progression [118]. Advanced fibrosis leads to cirrhosis, an irreversible stage marked by extensive scarring and architectural distortion of the liver. Cirrhosis may remain asymptomatic for a prolonged period but eventually leads to liver dysfunction and severe clinical complications. At this stage, treatment focused on symptom management and prevention of further damage [116], [119]. Chronic liver disease may ultimately progress to hepatocellular carcinoma (HCC), the most common type of primary liver cancer, which accounted for approximately 8.3% of cancer related deaths worldwide in 2020 [116]. Although cirrhosis is a major risk factor, liver cancer may also develop in its absence. Both cirrhosis and liver cancer are considered end-stage liver disease (ESLD), which is irreversible and often requires liver transplantation as the only definitive treatment option [116].

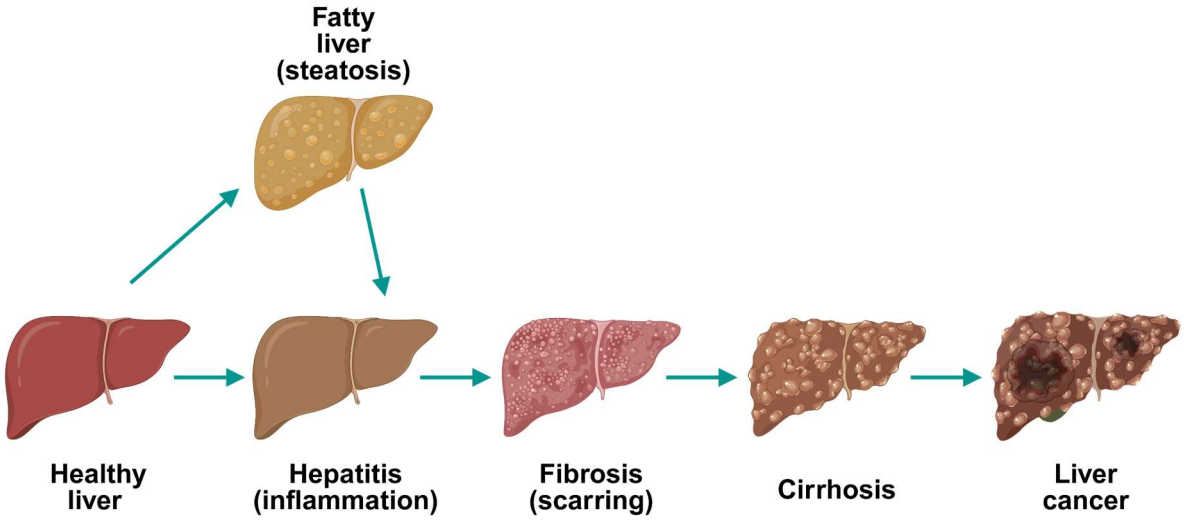


Figure 1.11. Stages of liver disease progression. The figure illustrates the progression from healthy liver to steatosis and inflammation (early damage), followed by fibrosis and cirrhosis, with liver cancer as a potential complication of advanced disease.

1.3 Liver Transplantation

Liver transplantation (LT) is considered the gold standard for the treatment of end-stage liver disease; however, the shortage of donor organs remains a major limitation of this approach. According to the Global Observatory on Donation and Transplantation, 173,727 solid organ transplants (SOTs) were performed worldwide in 2024, of which liver transplants accounted for 24.5% (42,497). This represents a 5% increase compared with 2023. The majority of transplanted organs (approximately 77%) were obtained from deceased donors, whereas 23% originated from living donors. By the end of 2024, 40,612 patients were registered on the transplant waiting list across 66 countries, and 8,895 patients did not receive a transplant [120].

The first successful liver transplant was performed in the 1960s by Thomas Starzl, marking the beginning of modern transplant surgery [121]. Since then, significant advances have been made in surgical procedures and immunosuppressive therapy, substantially improving patient outcomes. Nevertheless, LT remains a highly complex procedure due to the intricate vascular and biliary anatomy of the liver, which requires precise surgical reconstruction to restore normal hemodynamics and bile flow.

The liver performs over 500 essential physiological functions; therefore, rapid restoration of graft function after transplantation is critical. Even transient dysfunction of the transplanted organ may result in severe complications, including multiple organ failure. During transplantation, the graft remains outside the body for a certain period, leading to cold ischemia. Subsequent restoration of blood flow results in reperfusion, which induces oxidative stress and a strong inflammatory response. This process, known as ischemia-reperfusion injury (IRI), is one of the major causes of early graft dysfunction [122]. Following transplantation, immunosuppressive therapy is required to prevent graft rejection. However, these treatments are associated with significant adverse effects, including increased susceptibility to infections and malignancies, kidney damage, and metabolic complications [123]. Due to limited donor organ availability, expanded criteria donors (ECD) are increasingly used. This includes organs from older donors (e. g., >60 years), donors with hepatic steatosis (>30%) or obesity (body mass index; BMI >35 kg/m^2), and donors after circulatory death (DCD), in addition to donors after brain death (DBD) [124]. While this strategy increases organ availability, it is associated with a higher risk of early allograft dysfunction. Other factors, such as prolonged cold ischemia time (CIT; often exceeding 12 hours), elevated liver enzymes, or bilirubin level in donors, are also considered in donor selection [125], [126]. In selected cases, organs from HBV- or HCV-positive donors may also be used [127].

Another strategy to expand the donor pool is the partial liver transplantation technique, including living donor liver transplantation (LDLT) and split liver transplantation (SLT). These techniques allow transplantation of a liver segment from a living donor or division of a deceased donor liver into two grafts for transplantation, particularly for pediatric patients and smaller adult recipients [128]. A key advantage of this procedure is the liver's remarkable regenerative capacity, which enables rapid restoration of organ volume and functions after transplantation [129].

Machine perfusion techniques have emerged as an important tool for improving graft preservation, particularly for marginal organs from ECD. These methods use specialized devices to perfuse the liver *ex vivo* with oxygenated solutions, maintaining metabolic activity

and reducing ischemia-related injury. In addition to preservation, machine perfusion allows functional assessment of the organ prior to transplantation and may extend preservation time. It is also offering an opportunity for therapeutic interventions, and graft recondition, potentially increasing the number of transplantable organs [130].

1.4 Liver Regeneration

The liver possesses a unique regenerative capacity, that involves a highly complex and multistep process. Liver regeneration aims to restore both organ mass and function, minimizing tissue damage through coordinated cell proliferation and tissue remodeling. This process can be divided into three phases.

The first phase, known as the initiation phase, is triggered by liver injury and involves activation of cytokines and growth factors produced by immune cells and non-parenchymal liver cells. During this stage, hepatocytes exit the quiescent G0 phase and re-enter the cell cycle. The second phase is characterized by intensive hepatocyte proliferation, which is essential to restoring lost liver mass. This phase involves activation of multiple signaling pathways regulating cell growth, proliferation, and differentiation, including Wnt/β-catenin, Hippo, Notch, TGF-β pathways, and growth factors such as HGF and EGF [131].
The final phase of liver regeneration involves termination of proliferation once the liver has regained its appropriate size and function. During this stage, inhibitory signals suppress further cell divisions, the cell cycle is silenced, and tissue homeostasis is restored [131].

In addition to hepatocytes, non-parenchymal liver cells play a crucial role in the regenerative process. The LSECs modulate hepatocyte proliferation [132]. The HSCs contribute to the regeneration process by remodeling the ECM and secreting cytokines and growth factors [133]. The KSc, the resident macrophages of the liver, produce inflammatory mediators that stimulate hepatocyte [134]. Furthermore, liver progenitor cells (LPCs) may contribute to regeneration, particularly under conditions of chronic injury, where they can differentiate into hepatocytes [135].

1.4.1 Cell Dedifferentiation During Liver Regeneration

Cell dedifferentiation is a process in which cells undergo changes in morphology and function in response to various stimuli. In the liver, this phenomenon plays an important role in regeneration. Following liver injury, damaged or dead hepatocytes must be replaced to restore tissue integrity.

Hepatocytes exhibit remarkable cellular plasticity, allowing them to alter their phenotype in response to stress, injury, or changes in the microenvironments. Under pathological conditions, hepatocytes may undergo dedifferentiation or transdifferentiation, including conversion into LPCs or cholangiocytes [135]. The mechanism of dedifferentiation depends on the type and severity of liver injury. For example, following partial hepatectomy, mature hepatocytes and cholangiocytes proliferate to restore liver mass. In such cases, gene expression shifts from genes responsible for specialized cellular functions toward those promoting proliferation and cell adhesion [136].

In chronic liver injuries, where hepatocytes proliferation is insufficient, an alternative regenerative mechanism is activated, leading to the formation of LPCs. These bipotent cells may originate from both hepatocytes and cholangiocytes. This process typically occurs in advanced stages of liver damage, when hepatocytes lose characteristic markers, including ALB and HNF1α, while beginning to express progenitor markers, such as CK19 and Sox9. These changes are accompanied by alternation in cell morphology and increased proliferation capacity, resulting in a transitional progenitor-like state. Upon resolution of injury, LPCs can differentiate back into hepatocytes or cholangiocytes, contributing to tissue repair [135], [137].

In cases of severe liver injury, cholangiocytes may also contribute to regeneration through transdifferentiation. During this process, cholangiocytes acquire hepatocyte-like characteristics, including albumin expression, while gradually losing cholangiocyte markers such as CK19. Conversely, in biliary injury, hepatocytes may transdifferentiate into cholangiocytes to compensate for the loss of the bile duct [136].

1.4.2 Epithelial-to-mesenchymal transition (EMT)

Epithelial-to-mesenchymal transition (EMT) is a biological process in which epithelial cells lose their characteristic features, such as cell polarity and adhesion, and acquire characteristics specific to mesenchymal properties, including increased migratory and invasive capacity. This process is reversible and can be reversed through mesenchymal-to-epithelial transition (MET) [138]. During EMT, hepatocytes undergo morphological and functional changes, adopting a spindle-like shape morphology and becoming more mobile, resembling fibroblast-like cells [139]. Cells throughout the EMT exhibit increased expression of mesenchymal markers, including vimentin, α-smooth muscle actin (α-SMA), and collagen type I, as well as enhanced production of ECM components [138]. EMT plays an important role in embryonic development and tissue regeneration, including liver regeneration. However, it is

also implicated in the progression of pathological conditions, particularly liver fibrosis and HCC [138], [139].

1.5 Development of Liver Cell Isolation Methods

Attempts to isolate whole cells from liver tissue date back to the 1940s. Early techniques, such as pressing liver tissue through gauze, shaking thin slices of tissue with glass beads, or homogenization, resulted in low isolation efficiency (5-10%) and caused substantial cellular damage [140].

A major advancement in hepatocyte isolation method was the discovery and characterization of collagenase from *Clostridium histolyticum* by Mandl's and colleagues in 1953 [141]. This enzyme was later applied by Lasfargues to dissociate cells from the mammary epithelium, demonstrating its utility in tissue dissociation [142]. In 1967, Howard and colleagues reported the isolation of intact hepatocytes from rat liver using a collagenase-based method involving perfusion, tissue slicing, and enzymatic digestion, although the yield remained relatively low (3-5%) [143]. A significant breakthrough occurred in 1969, when Berry and Friend introduced a liver perfusion technique that enabled more uniform delivery of collagenase, significantly improving cell yield [144]. Further refinements led to the development of the two-step collagenase-perfusion method by Seglen in 1976, which became the foundation of the modern hepatocyte isolation protocol.

1.5.1 Two-Step Collagenase Perfusion Method

The two-step collagenase perfusion method remains the gold standard for hepatocyte isolation [145]. This technique, developed by Seglen, involves sequential perfusion of the rat liver with two distinct solutions designed to disrupt cell-cell and cell-ECM interactions [146].

In the first step, a calcium-free (Ca^{2+}-free) solution is used to weaken intercellular junctions. In the second step, the liver is perfused with a solution supplemented with Ca^{2+} ions and collagenase. Calcium ions play a dual role in this process as they stabilize cell-cell interactions, and they are also essential for collagenase activity. Therefore, the initial calcium depletion is limited to a short period (typically less than 10 minutes) to avoid irreversible hepatocyte damage. Subsequent reintroduction of calcium enables efficient enzymatic digestion while preserving cell viability. This two-step approach minimizes cellular damage and enhances the efficiency of tissue digestion [145] [147].

Over time, this method has been adapted for the isolation of human hepatocytes, particularly from surgical resections or donor organs unsuitable to transplantation. Modified protocols include partial perfusion techniques and enzymatic digestion of tissue fragments without full vascular perfusion [148].

Further optimization of hepatocyte isolation has involved refinement of enzymatic mixtures, including the use of different collagenase types, reduces enzyme concentrations, and the addition of DNase and auxiliary proteases. Techniques such as density gradient centrifugation (e. g., using Percoll) have also been implemented to separate viable hepatocytes from non-parenchymal and dead cells [149].

In parallel, methods for assessing hepatocytes quality have improved, focusing on parameters such as cell viability, metabolic activity, and cytochrome P450 [150]. More recently, efforts have been made to automate the isolation process, leading to the development of semi-automated perfusion systems that improve reproducibility. Additionally, isolated hepatocytes are increasingly used in advanced *in vitro* models, including three-dimensional cultures, organoids, and liver-on-the-chip platforms [151], [152].

Despite these advantages, there are still important limitations. In particular, variability in biological material and the rapid loss of hepatocyte-specific function *in vitro* continue to present significant challenges.

1.5.2 Mechanical Defragmentation and Enzymatic Digestion of Tissue Method

An alternative approach to hepatocyte isolation involves mechanical defragmentation and enzymatic digestion of liver tissue. This method was developed at the Laboratory of Tissue Engineering, Nalecz Institute of Biocybernetics and Biomedical Engineering, Polish Academy of Sciences (LTE IBBE PAS) [153].

Unlike the perfusion-based method, this approach does not require vascular cannulation. Instead, the enzymatic solution is directly injected into the liver parenchyma, allowing improved penetration compared to passive diffusion. Mechanical fragmentation, combined with enzymatic digestion, facilitates efficient degradation of the ECM and promotes release of cells into suspension. Compared with the two-step perfusion method, this technique is faster, technically less demanding, and suitable for both large and small, non-perfusable tissue samples. These advantages make it particularly useful for clinical and experimental applications where perfusion is not feasible.

1.6 Bridging Therapies to Replace or Support the Liver in Patients with Liver Failure

A dysfunctional liver is unable to perform its essential physiological functions, which can lead to organ failure. For patients with liver failure (LF), liver transplantation (LT) remains the only definitive treatment; however, the shortage of donor organs limits its availability. The insufficient number of donors is the reason for searching for an alternative method to extend the patients' life until the transplantation time or until the liver is regenerated. These approaches are collectively referred to as bridging methods (Figure 1.12). They include artificial liver support systems (ASLL), bioartificial liver support systems (BALs), hepatocyte transplantation, liver decellularization techniques, three-dimensional (3D) bioprinting, and lab-on-the-chip technologies [154].

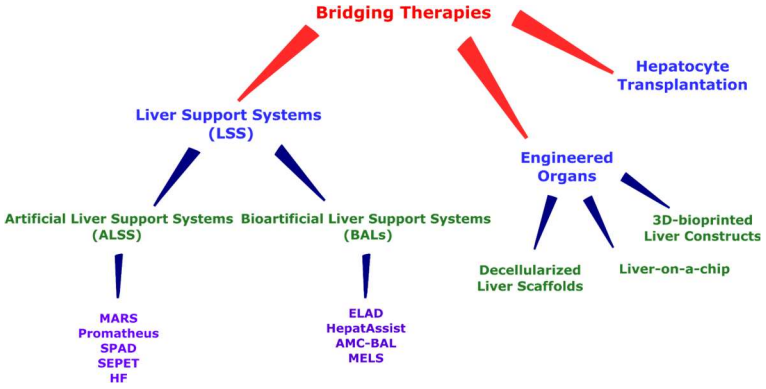


Figure 1.12. Bridging therapies in liver failure. The schematic illustrates the main categories of bridging therapies used in patients with acute or chronic liver failure as a bridge to transplantation or liver regeneration. The first category includes liver support systems (LSS), which can be divided into: artificial liver support systems (ALSS), such as molecular adsorbent recirculating system (MARS), Prometheus system, Single-pass albumin dialysis (SPAD), Selective Plasma Filtration Therapy (SEPET), hemofiltration (HF), as well as bioartificial support systems (BALs), including Extracorporeal Liver Assist Device (ELAD), HepatAssist, Academic Medical Center-bioartificial liver (AMC-BAL), and Modular Extracorporeal Liver Support (MELS). The second category comprises engineered liver organs, including decellularized liver scaffolds, liver-on-a-chip systems, and 3D-bioprinted liver models. The third category includes hepatocyte transplantation, which involves the administration of functional liver cells to restore metabolic activity.

1.6.1 Liver Support Systems (LSS)

1.6.1.1 Artificial Liver Support Systems

Artificial liver support systems (ALSS) are extracorporeal therapeutic devices designed to remove toxins from the blood through physicochemical mechanisms. They are intended to detoxify the blood and reduce liver damage. ALSS utilizes techniques such as hemodialysis, hemofiltration, adsorption, and albumin dialysis. Clinically, these systems are used in patients

with acute liver failure (ALF) or acute on chronic liver failure (ACLF), serving as a bridge to transplantation or regeneration [155]. A major limitation of ALSS is that they do not restore the full biological functions of the liver. Although they improve biochemical parameters and reduce clinical symptoms, they do not provide a definitive cure. Currently, the most widely used ALSS include the molecular adsorbent recirculating system (MARS), single-pass albumin dialysis (SPAD), fractionated plasma separation and adsorption system (Prometheus), selective plasma filtration therapy (SEPET), and hemofiltration (HF) [156], [157].

The Molecular Adsorbent Recirculating System (MARS), based on albumin dialysis (Figure 1.13), was developed by Stange's group in 1993 [158]. The system consists of three interconnected circuits. In the first circuit, the patient's blood flows through a dialysis membrane. In the second circuit, toxins diffuse into an albumin-containing solution. In the third circuit, the albumin is regenerated for recirculation. This configuration enables efficient removal of albumin-bound toxins, such as ammonia, bilirubin, bile acids, and inflammatory mediators. Clinical studies indicate that MARS improves hemodynamics stability and hepatic encephalopathy in patients with liver failure, although a significant reduction in overall mortality has not been achieved [156], [159].

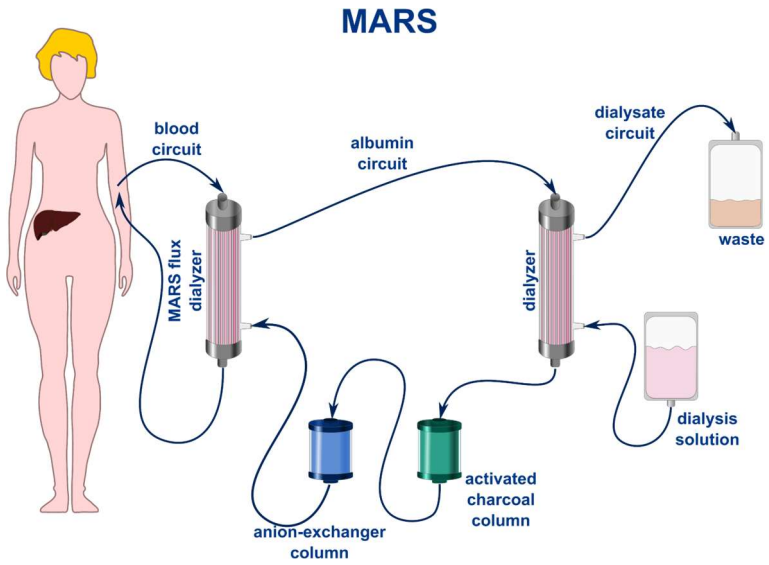


Figure 1.13. Molecular Adsorbent Recirculating System (MARS). The schematic illustrates three interconnected circuits. Blood from the patient passes through a MARS flux dialyzer, where toxins diffuse across the dialysis membrane into the albumin-containing dialysate (1 - patient blood circuit). Albumin binds toxins and removes them from patent's circulation (2 - albumin circuit). The albumin dialysate is recirculated and purified via activated charcoal columns and anion-exchange column. In the third circuit (dialysis circuit), waste products are removed from the dialysate. Detoxified blood is returned to the patient, while the albumin dialysate is continually recirculated and regenerated, enabling ongoing removal of toxins.

The Prometheus system, introduced in the late 1990s, separates the patient's plasma using a filter with a cut-off of approximately 250 kDa. The plasma then passes sequentially

through an anion-exchange column and a neutral adsorber before being returned to circulations and undergoing dialysis. This system effectively removes bilirubin and bile acids, demonstrating efficacy comparable to MARS. Nevertheless, clinical studies have not indicated a significant impact on patient survival [157].

In Selective Plasma Filtration Therapy (SEPET), blood is circulated through an extracorporeal system where plasma is separated from cellular components. The plasma is then filtered to remove small- and medium-sized molecules while preserving larger proteins and growth factors important for liver regeneration. The filtered plasma is recombined with the cellular fraction and returned to the patient. This method has been associated with improvements in liver failure function parameters and prolonged survival [160].

Single-pass albumin dialysis (SPAD) is a simplified form of albumin dialysis in which blood undergoes a single dialysis session with albumin-containing dialysate. Toxins, including bilirubin, bile acids, and protein-bound molecules, are transferred to the dialysate, which is then discarded. The procedure can be performed using standard dialysis equipment, making it widely accessible. However, SPAD only provides supportive therapy and does not replace full liver function [157].

Hemofiltration (HF) is an extracorporeal technique in which blood passes through a semipermeable membrane, and the filtered fluid is replaced with a substitution fluid. This method primarily eliminates small- and medium-sized molecules, such as ammonia, cytokines, and metabolites, but does not effectively eliminate albumin-bound toxins. Therefore, HF is often used in combination with other ALSS systems as a part of supportive therapy [161].

1.6.1.2 Bioartificial Liver Support Systems

Bioartificial liver support systems (BALs) are hybrid extracorporeal devices, containing biological material, particularly human hepatocytes, which provide not only detoxification but also essential metabolic liver functions, including protein synthesis [162], [163]. The optimal cell source for BAL systems is human hepatocytes; however, their limited availability and the difficulty of maintaining sufficient functional cell mass remain major constraints. Therefore, alternative cell sources are commonly used, including porcine hepatocytes, human hepatoma-derived cell lines, stem cell-derived hepatocyte-like cells, and reprogramming hepatocytes-like cells. Additional challenges associated with BALs include maintaining cell viability and functionality within the bioreactor, the risk of infections (especially zoonotic

transmission), and the high technological complexity of these devices. Similar to ALSS, BALs are designed to stabilize patients and serve as a bridge to liver regeneration or transplantation.

BAL liver support systems utilize various types of bioreactors, including hollow fiber bioreactors, floating/encapsulation-based bioreactors, multilayer membrane bioreactors, and scaffold-based bioreactors [163], [164]. These systems enable the development of different types of three-dimensional (3D) cell cultures. Their advantage over conventional two-dimensional (2D) cultures lies in their ability to better replicate liver physiology and provide a more relevant microenvironment. A major limitation of 2D cultures is their inability to reproduce liver tissue architecture [165]. As a result, cells cultured in monolayers lose important spatial interactions, leading to disruption in metabolic and signaling pathways.

In contrast, 3D systems used in BAL replicate key features of the *in vivo* environment, including cell-cell and cell-ECM interactions, which are essential for proper liver function [166], [167]. This leads to improved maintenance of metabolic activity and hepatocyte-specific gene expression. Furthermore, BAL systems incorporating bioreactors enable precise control of environmental parameters such as flow, oxygenation, and metabolite exchange. Proper liver function depends on interactions between hepatocytes and non-parenchymal cells; 3D models facilitate co-culture systems that enhance hepatocyte functionality [165], [167].

Overall, these features make BALs more physiologically relevant than conventional 2D cultures, increasing their potential in both clinical and research applications.

Several BAL systems have entered clinical trials, including Extracorporeal Liver Assist Device (ELAD), HepatAssist, Academic Medical Center-bioartificial liver (AMC-BAL), and Modular Extracorporeal Liver Support (MELS) [162], [163].

The Extracorporeal Liver Assist Device (ELAD) was developed in the early 1990s by Sussman et al. and was based on the human hepatoblastoma-derived C3A cell line [168]. Early clinical studies demonstrated good biocompatibility, hemodynamic stability, and improvements in selected metabolic parameters in patients with ALF [169]. A schematic representation of the ELAD system is shown in Figure 1.14. In this system, the patient's blood is circulated extracorporeally, and plasma is separated and directed through hollow fibers bioreactors at a flow rate of 150-300 mL/min. These bioreactors contain C3A cells seeded outside the semipermeable capillary membranes (70 kDa MWCO) with an initial cell mass of approximately 200 g per bioreactor. Within the bioreactors, the cells perform metabolic and synthetic functions, including detoxification and protein production. The treated plasma is subsequently filtered, recombined with blood components, and returned to the patient [170]. Despite promising early results, subsequent clinical trials did not demonstrate a significant

improvement in overall survival [169]. As a result, the system was further modified, including increasing the cell mass to approximately 440 g per bioreactor, introducing polysulfone membranes with a MWCO of 120 kDa, and increasing the flow rate to 500 mL/min. The ELAD system progressed to Phase II clinical trials and Phase III randomized clinical trials [171], [172]. Despite initial promise, these studies did not demonstrate a significant survival benefit, its development was ultimately discontinued in 2018.

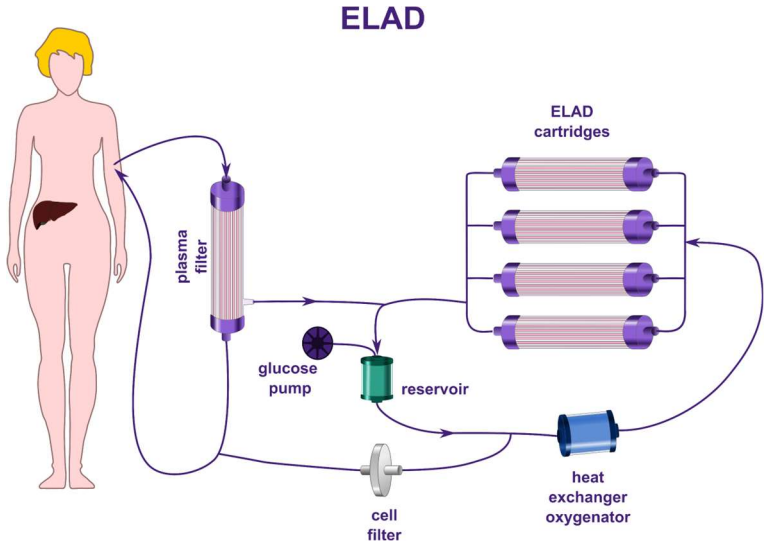


Figure 1.14. Schematic of an extracorporeal liver assist device (ELAD) used as a liver support system. The patient's blood flows through a plasma filter, where cellular elements are separated from plasma. The cellular components are returned to the body, while the plasma is directed to the next stage of the system. It then passes through ELAD cartridges containing hollow fiber bioreactors with human C3A liver cells, where metabolic processes, ammonia detoxification, and protein synthesis take place. To maintain cellular metabolic activity, the system is equipped with a glucose pump supplying substrates necessary for cell function. Additionally, a reservoir stabilizes plasma volume and flow within the system. Environmental conditions in the bioreactor are regulated by a heat exchanger and an oxygenator. After passing through the bioreactor, the plasma is filtered to prevent C3A cells from entering the patient's circulation, thereby increasing the safety of the therapy. Finally, the purified and metabolically modified plasma is recombined with the cellular components and returned to the patient.

HepatAssist is a system developed by Demetriou et al., which utilizes cryopreserved porcine hepatocytes cultured in hollow fibers bioreactors. Early Phase I clinical trials in patients with ALF demonstrated that the system was safe and well tolerated, providing temporary metabolic support without evidence of porcine endogenous retrovirus (PERV) transmission. In this system, the patient's blood is separated into cellular components and plasma. The plasma is then perfused through a bioreactor's capillaries containing approximately $5–7\times10^9$ porcine hepatocytes [173]. Within the bioreactor, detoxification and metabolic processes occur across a semipermeable membrane. The treated purified plasma is subsequently recombined with blood cells and returned to the patient [174], [175]. In a multicenter Phase II randomized controlled trial involving 171 patients with ALF, no significant improvement in 30-day survival

was observed [174]. Consequently, the development of HepatAssist was discontinued, and the system is considered a first-generation BAL. Nevertheless, it has contributed to the development of newer technologies, such as HepatiCan, which consists of a single-use BAL biocartridge and uses HepG2 cells encapsulated in alginate spheroids to improve reproducibility and clinical applicability [176].

The Modular Extracorporeal Liver Support (MELS) system was initially conceptualized by Gerlach et al. in 1994 and further developed in the early 2000s by Sauer and colleagues. It consists of three functional modules. CellModule, containing human or porcine hepatocytes responsible for metabolic activity, detoxification, and protein synthesis. DetoxModule, performing albumin dialysis to remove both albumin-bound and water-soluble toxins. DialysisModule, responsible for hemofiltration [177], [178], [179]. In the MELS system, the patient's blood is separated into plasma and cellular components. The plasma is circulated through a bioreactor containing approximately 400–600 g of hepatocytes and subsequently returned to the bloodstream [178]. Phase I clinical trials have shown that the system is safe, with no evidence of PERV transmission. However, these studies involved small patient cohorts and lacked randomization, limiting the strength of the conclusions [177].

The Academic Medical Center-Bioartificial Liver (AMC-BAL) AMC-BAL system was developed by Chamuleau's group [180] and operates on a principle similar to that of the MELS. It consists of three interconnected circuits. The blood circuit, where the patient’s blood is separated into plasma and cellular components. The bioreactor circuit - the core of the AMC-BAL. Plasma flows through a three-dimensional non-woven polyester matrix with approximately 10^{10} primary hepatocytes (usually porcine or human). The gas circuit is responsible for oxygen delivery and carbon dioxide removal [181]. Phase I clinical trials using porcine hepatocytes demonstrated that the system is safe and capable of supporting liver metabolic activity. However, its clinical application is limited by challenges related to oxygenation and mass transport, which require further improvement [182], [183]. To overcome limitations associated with xenogeneic cells, the system was later adapted to use the human HepaRG cell line derived from HCC. These cells can differentiate into hepatocytes-like cells and provide a more stable and scalable alternative. Experimental studies have demonstrated improvements in ammonia and bilirubin clearance, as well as increased albumin and urea production [184], [185], [186].

1.6.1.3 Cell-Based Therapy

Hepatocyte transplantation involves transplanting cells isolated from a portion of a donor's liver into a recipient. This method is less invasive than whole-organ transplantation, as the cells are administered through a catheter, most often into the portal vein, the splenic artery, or the splenic parenchyma. Being a radiological rather than a surgical procedure, it eliminates the need to open the patient's abdomen, reducing the risk of complications and shortening recovery time [187]. Similarly, to conventional organ transplantation, hepatocyte transplantation requires immunosuppressive therapy and monitoring of the liver [188]. This method is primarily used in patients with ALF to provide new hepatocytes that support liver function when it is uncertain whether the liver will regenerate. In contrast, liver transplantation represents a definitive and functionally irreversible treatment option. A major advantage of hepatocyte transplantation, in addition to its lower invasiveness, is that in many diseases, only a small proportion of functional hepatocytes, approximately 5–10%, is sufficient to achieve a clinical effect. Moreover, hepatocytes from livers unsuitable for whole organ transplantation can be used. The procedure can also be repeated, allowing supplementation of cell “doses” as needed [187]. This approach also allows assessment of a patient's response to therapy and can serve as a bridge before full organ transplantation [189]. Nevertheless, hepatocyte transplantation cannot replace liver transplantation due to its limited long-term efficacy. Transplanted cells often exhibit poor engraftment and limited persistence, with only a fraction integrating and functioning effectively. Moreover, this approach is ineffective in advanced cirrhosis and still necessitates immunosuppressive therapy [188].

Alternative cell-based therapies for liver support involve cell types other than hepatocytes. Mesenchymal stem cells (MSCs), derived from sources such as bone marrow, adipose tissue, and umbilical cord blood, exert their therapeutic effects primarily through a paracrine mechanism. They secrete growth factors, anti-inflammatory cytokines, and immunomodulatory molecules that support hepatocyte regeneration and reduce fibrosis. However, MSCs do not directly replace hepatocyte-specific metabolic functions [190], [191].

Liver progenitor cells (hepatoblast-like cells) represent another potentially therapeutic option. These immature cells can proliferate and differentiate into both hepatocytes and cholangiocytes. They may support liver regeneration, particularly when hepatocytes proliferation is impaired, and show promise in treating inherited metabolic disorders and acute liver failure. However, their clinical application remains experimental, as they require further maturation and present challenges in *in vitro* expansion and differentiation [135].

Induced pluripotent stem cells (iPSCs), which can differentiate into hepatocyte-like cells, are also being investigated as an alternative cell source. Nevertheless, their use is limited by an immature or semi-mature phenotype and potential tumorigenicity. Ongoing research aims to improve their functionality capacity and safety profile [154], [192].

Among available therapeutic approaches, liver transplantation remains the most effective treatment for end-stage liver disease, whereas cell-based therapies primarily play a supportive or bridging role by promoting regeneration, modulating inflammation, and reducing fibrosis without fully restoring metabolic function.

1.6.1.4 Other Methods

Liver decellularization is a method that involves the removal of cells from an organ while preserving the extracellular matrix (ECM) and the three-dimensional architecture of the organ [193], [194]. This approach allows for obtaining the biological scaffold that can be reseeded with cells and potentially used for the creation of functional organs or research models [193]. Such “reconstructed” organs better replicate the native cellular environment compared to two-dimensional cultures and can be used for studies of drug toxicity and metabolism [195]. In the case of human livers, organs that are not suitable for transplantation, such as damaged or hypoxic livers or organ fragments, are most commonly used. Animal livers, including those from rats, mice, and pigs, are also utilized [194].

3D printing (bioprinting) is promising continuously developing method used to generate mini-tissues and liver models. This approach utilizes patient-derived cells or stem cells, which are incorporated into bioinks composed of cells suspended in hydrogel matrices. These bioinks are then deposited layer-by-layer using specialized printers to build structures that mimic native tissue architecture. A critical aspect of this technique is the precise spatial organization of hepatocytes and the recreation of liver vasculature, which remains one of the major challenges in the field [196], [197].

1.6.2 Alternative Models of Hepatocytes

Due to the limited availability of human hepatocytes, as well as the high cost and technical challenges associated with their *in vitro*, alternative models such as iPSCs, human cancer cell lines are widely used in research. These models support a broad range of studies, including investigations of molecular mechanisms, carcinogenesis, hepatocyte-specific protein

activity, drug cytotoxicity, biomarkers identification, and the development of targeted therapies [149].

1.6.2.1 Induced Pluripotent Stem Cells (iPSCs)

iPSCs, are somatic cells that can be reprogrammed into a pluripotent state and subsequently differentiated into hepatocyte-like cells (HLCs). They provide a virtually unlimited source of patient-specific cells, enabling the development of personalized research models. The differentiation process partially recapitulates embryonic liver development, resulting in cells that express hepatocyte markers and exhibit basic metabolic functions [198]. HLCs derived from iPSCs are widely used in studies of drug metabolism, hepatotoxicity, and liver disease modeling, including those with a genetic basis [149]. However, a major limitation of this approach is the immature phenotype of HLCs, which resembles fetal hepatocytes. This immaturity is associated with reduced activity of key metabolic enzymes and limits the full replication of adult hepatocytes functions [149], [198]. To overcome these limitations, advanced culture systems, including three-dimensional (3D) cultures and organoids, are being developed These approaches improve cell functionality and better mimic the *in vivo* liver microenvironment [199].

1.6.2.2 Human Cancer Cell Lines

Due to the limited availability and culturing difficulties of hepatocytes, numerous cancer-derived and immortalized liver cell lines have been developed. These cell lines are easy to maintain, proliferate rapidly, and can be genetically modified, making them widely used and reproducible research model [200], [201], [202]. Commonly used liver-derived cell lines include HepG2, C3A, HepaRG, Huh7, and members of the SNU series. However, these models differ significantly in metabolic activity and gene regulation, making the appropriate selection of a cell line crucial depending on the research objective.

The HepG2 cell line, derived from hepatoblastoma (HB), retains certain hepatocyte-specific functions, such as plasma protein synthesis However, it exhibits limited cytochrome P450 (CYP450) enzyme activity, which restricts its usefulness in xenobiotic metabolism studies, although it is still used in anticancer research [200].

The C3A cell line, a subclone of HepG2, shows improved differentiation and stability compared to its parental line. Nevertheless, its drug biotransformation capacity remains limited [203].

In contrast, the HepaRG cell line, derived from hepatocellular carcinoma (HCC), can differentiate into hepatocyte-like cells and demonstrates high expression of key CYP450 enzymes, including CYP3A4 and CYP1A2. Additionally, these cells exhibit polarization ability and urea production, making them a valuable model for pharmacokinetic and hepatotoxicity studies [203].

The Huh7 cell line, also derived from HCC, is widely used in virological research, particularly in studies of HCV, as well as in drug metabolism research [200].

SNU cell lines (e.g., SNU398, SNU449, SNU475), derived from HCC, are characterized by significant genetic heterogeneity and chromosomal abnormalities, reflecting the complexity of liver cancer biology [204]. Many of these lines contain integrated HBV DNA, making them useful models for studying viral-host interactions and the HBV life cycle [205].

1.7 Human Hepatocyte-Derived Proliferating Cells as a Potentially New Source of Hepatic Cells

Liver diseases are among the leading cause of mortality worldwide. Despite significant therapeutic advances, liver transplantation (LT) remains the only effective treatment for end-stage liver disease. Globally, 5-20% of patients on transplant waiting lists die due to the insufficient availability of donor organs [206]. Therefore, there is an urgent to develop alternative therapeutic strategies capable of prolonging patient survival and improving quality of life until LT becomes available. Among bridging therapy approaches, BALs represent one of the most promising strategies, as they utilize metabolically active cells as their biological component. Although human hepatocytes are considered the optimal cell source for BALs, their limited availability and rapid *ex vivo* dedifferentiation necessitate the search for alternative cell sources capable of preserving essential metabolic functions.

During the course of this doctoral thesis, I aimed to optimize the liver cell isolation method developed at LTE IBBE PAS in order to improve both cells yield and viability. In addition, I proposed human Hepatocyte-Derived Proliferating Cells (hHDPCs) as a potential alternative cell source for applications such as BAL systems and cell-based therapies. Primary hepatocytes are particularly difficult to maintain *iv vitro* because, outside their natural microenvironment, they rapidly lose viability and metabolic activity while exhibiting limited

proliferating capacity. Importantly, prior research conducted at LTE IBBE PAS focused mainly on genetically modified liver cancer-derived cells, whereas I was the first researcher in the laboratory to work with primary human liver cells. The hHDPCs were isolated from resected human liver tissue using a mechanical and enzymatic digestion method. Here, I present a self-developed protocol for the isolation, identification, and culture of these cells, together with their comprehensive molecular and physiological characterization. During culture in commercially available hepatocyte medium supplemented with HGS, the cells underwent spontaneous dedifferentiation without the application of additional dedifferentiation-inducing factors. This approach aimed to generate liver-derived cells retaining selected hepatic functions while simultaneously acquiring proliferative capacity, thereby reflecting cellular processes of liver regeneration.

Importantly, hHDPCs retained several hepatocyte-specific functions, including albumin and urea production, while maintaining proliferative potential and an intermediate phenotype associated with liver regeneration. One of the objectives of this work was to identify the optimal transitional cellular state in which botch hepatocyte functionality and proliferative capacity are preserved.

Compared to commonly used hepatic models, hHDPCs offer several important advantages. Cancer-derived cell lines, such as HepG2, undergo metabolic reprogramming, that result in uncontrolled proliferation and reduced expression of hepatocyte-specific functions, thereby limiting their physiological relevance [207]. Similarly, although iPSCs represent a promising alternative, they frequently fail to achieve full functional maturity [149], [198]. In contrast, hHDPCs are directly derived from mature hepatocytes and therefore retain a more physiologically relevant phenotype, including partial preservation of hepatocytes-specific functions. Furthermore, iPSC culture is considerably more complex and expensive than hHDPCs culture due to the requirement for numerous specialized supplements and differentiation factors. Unlike hepatocytes, which rapidly lose functionality under standard culture conditions, hHDPCs maintain metabolic activity over extended periods, making them more suitable for long-term studies. At the same time, their proliferative capacity enables the generation of sufficient cell numbers, overcoming one of the major limitations associated with human hepatocytes.

The fact that hHDPCs are directly derived from individual patient further enhances their translational potential. Their proliferation capacity enables patient-specific drug testing, supports the development of personalized therapeutic strategies. Moreover, their autologous origin may reduce the risk of immune rejection in future cell-based therapies aimed at

supporting liver regeneration. These characteristics make hHDPCs particularly attractive not only for *in vitro* disease modeling but also for potential clinical applications.

Taken together, although hHDPCs still require further investigation and optimization, they represent a highly promising and potentially superior alterative to currently available hepatocyte models by combining physiological relevance, scalability, and translational applicability.

Thesis Statements:

1. It is possible to optimize the culture conditions of hepatocytes isolated from human liver tissue to obtain cells with acquired proliferative capacity while retaining essential hepatocyte functions.
2. The resulting stable cell line of proliferating cells derived from human hepatocytes (human Hepatocyte-Derived Proliferating Cells, hHDPCs) constitutes a novel source of functional biological material for use in a bioartificial liver.

Objectives of the Study:

To obtain a new biological material for a bioartificial liver, specifically: 1) derived from human liver isolates, with increased availability resulting from acquired proliferative capacity, and 2) stable under dynamic culture conditions in a hollow-fiber bioreactor.

Novel Contributions of the Study:

1. Development of a method for the dedifferentiation of hepatocytes, enabling them to acquire proliferative capacity while maintaining liver-specific functions, including the production of albumin and alpha-1 antitrypsin.
2. An average 50-fold increase in the number of hHDPCs is achieved over 12 passages.
3. The culture duration of hHDPCs under dynamic conditions was comparable to that of control hepatoblastoma cells and was approximately 12 days. Flow conditions had a more favorable effect on the metabolic functions of hHDPCs than on those of the cancer cell line.

2 Materials

2.1 Cells Used in the Experiments

Human hepatocytes were isolated from resected fragment of human livers obtained in cooperation with the Department of General, Transplant, and Liver Surgery at the University Clinical Center, Medical University of Warsaw, Poland. The Local Research Ethics Committee granted ethical approval for this study (reference number: KB/182/2008). The isolation procedure was performed using a modified method developed at the Laboratory of Tissue Engineering, IBBE PAS, and described by Zakrzewska et al. in 2017 [153]. In this study, cells isolated from resected fragments of human livers will be referred to as LCIs with H followed by the donor number, e.g., LCI(H53) or LCI(H72).

Human Hepatocyte-Derived Proliferating Cells (hHDPCs) are dedifferentiated cells derived from human hepatocytes isolated using the method mentioned above. The particular cells will be labelled as hHDPCs, followed by a plus sign (indicating the cell passage), the passage number, and the donor identifier from which they originate, e.g., hHDPCs+2(H37).

Table 2.1 presents the cancer cell lines and human tissue-derived isolated cells commercially available and used in this study.

Table 2.1. List of the cell lines used during course of experiments.

Type of cells	Characteristic	Donor	Company
HepG2 (HB-8065)	Human hepatoblastoma (HB) cell line*	Male, 15 y/o	American Type Culture Collection (ATCC), Manassas, VA, USA
C3A (CRL-10741)	HepG2/C3A, clonal derivative of HepG2**	Male, 15 y/o	
HOS (CRL-1543)	Human Osteosarcoma cell line	Female, 13 y/o	
HDFn (PCS-201-010)	Primary Dermal Fibroblast Normal; Human	-	
SH-SY5Y (CLR-2266)	Neuroblastoma cell line	Female, 4 y/o	
SNU449 (CRL-2234)	Hepatocellular Carcinoma (HCC)	Male 52 y/o	
SNU475 (CRL-2236)	Hepatocellular Carcinoma (HCC)	Male, 43 y/o	
hHs (HMCPTS; Lot no. Hu1994)	Primary Human Hepatocytes***	Female, 58 y/o	Thermo Fisher Scientific, Waltham, MA, USA
hHs (HMCPTS; Lot no. Hu8345)		Male, 47 y/o	
2 x hHs (HMCPTS; Lot no. Hu8449)		Female, 62 y/o	

hHs (HMCPTS; Lot no. Hu2098)		Male, 57 y/o	
HUVEC	Primary cells isolated from human umbilical cords	-	Laboratory of Diagnosis and Therapy Support of Metabolic Diseases, Nalecz Institute of Biocybernetics and Biomedical Engineering, Polish Academy of Sciences
C3A cells with overexpression of fluorescent protein EGFP (C3A_EGFP)	C3A cells genetically modified (with the use of lentiviral vector) to stably overexpress fluorescent marker [Samluk et al., 2013]	-	Laboratory of Tissue Engineering, Nalecz Institute of Biocybernetics and Biomedical Engineering, Polish Academy of Sciences

* HepG2 mistakenly identified as hepatocellular carcinoma (HCC) [208].

** During the series of experiments performed in this doctoral thesis, HepG2 and C3A cells were used interchangeably as hepatoblastoma-derived cell lines.

*** For the purposes of this work, commercial human hepatocytes from donor Hu1994 will be referred to as hH_1; those from Hu8345 as hH_2; those from Hu8449 as hH_3 or hH_5; and those from Hu2098 as hH_4.

2.2 Culture Media and Supplements

Table 2.2 and Table 2.3 present the basal culture media used for cell cultures and the ingredients used to supplement the culture media. In Table 2.4, the specific ingredients used to supplement the culture media are presented.

Table 2.2. Types of culture media used during experiments.

Reagent	Characteristic	Company
WEM	William's E Medium, GlutaMAX Supplement	Thermo Fisher Scientific, Waltham, MA, USA
AdDMEM/F12	Dulbecco's Modified Eagle Medium/Ham's F-12	
HepatoZYME-SFM	Hepatozyme-SFM is a serum-free medium	
DMEM	High glucose Dulbecco's Modified Eagle Medium	Sigma Aldrich, Poznan, Poland
M199	Medium 199	
MEM	Minimum Essential Medium Eagle	
Ham's F-12	Nutrient Mixture F-12 Ham	
HM	Hepatocyte Medium kit, cat. no. 5201	ScienCell, Carlsbad, CA, USA
EMEM	Eagle's Minimum Essential Medium	American Type Culture Collection (ATCC), Manassas, VA, USA
RPMI-1640	RPMI-1640 Medium	

Table 2.3. Basic culture media supplements.

Ingredients / supplements	Characteristic	Company
FBS	Heat-inactivated Fetal Bovine Serum	American Type Culture Collection (ATCC), Manassas, VA, USA
MEM NEAA	Nonessential amino acids solution	Biological Industries Inc., Beit-Haemek, Israel
P/S	Penicillin/Streptomycin Solution	
Sodium Bicarbonate	Maintain a stable, physiological pH of the culture medium when incubated in a 5% CO_2 atmosphere	Sigma Aldrich, Poznan, Poland
L-glutamine	L-glutamine	
ECGS	Endothelial Cell Growth Supplements	
HEPES	HEPES solution pH 7.0-7.6	
FBS	Fetal Bovine Serum from kit, cat. no. 5201	ScienCell, Carlsbad, CA, USA
HGS	Hepatocyte Growth Supplement from kit, cat. no. 5201	
P/S	Penicillin/Streptomycin Solution from kit, cat. no. 5201	
Heparin	Heparin	WZF Polfa S.A., Warsaw, Poland
glutaMAX	glutaMAX	Thermo Fisher Scientific, Waltham, MA, USA

Table 2.4. Additional culture media supplements.

Reagent	Characteristic	Company
Insulin	Insulin from bovine pancreas	BioReagent, Sigma Aldrich, Poznan, Poland
Hydrocortisone	Hydrocortisone	
NAC	*N*-Acetyl-L-cysteine	
Nic	Nicotinamide	
Cell Maintenance Supplement Pack	Hepatocyte Maintenance Supplement Pack contains Dexamethasone, cocktail solution of penicillin-streptomycin (P/S), and ITS+ (human recombinant insulin, human transferrin, selenium complex, BSA, and linoleic acid), GlutaMAX, and HEPES	Thermo Fisher Scientific, Waltham, MA, USA
N-2	N-2 Supplement (100×)	Thermo Fisher Scientific, Waltham, MA, USA
B-27	B-27 Supplement (50×)	
EGF	Human Epithelial Growth Factor Recombinant Protein	
HGF	Human Hepatocyte Growth Factor Recombinant Protein	
A83-01	A 83-01	STEMCELL, BIOKOM, Janki, Poland
For	Forskolin	

Y-27632	Y-27632 dihydrochloride	PeproTech, Cranbury, NJ, USA
FGF-10	Recombinant Human Fibroblasts Growth Factor-10	
BMP-7	Recombinant Human Bone Morphogenetic Protein 7	
RSpo1	Recombinant Human R-Spondin-1	
Nog	Recombinant Human Noggin	
Wnt-3a	Recombinant Human Wnt-3a Protein	RD System, Minneapolis, MN, USA
FGF-19	Recombinant Human Fibroblasts Growth Factor -19	
Gastrin	Gastrin I, Human	Sigma Aldrich, Poznan, Poland
FGF-4	Fibroblast Growth Factor-4 human	
DAPT	N-[N-(3,5-Difluorophenacetyl)-L-alanyl]-S-phenylglycine t-butyl ester	
Dex	Dexamethasone	

2.3 Other Ingredients Used During Experiments

The proteolytic enzymes used for cell isolation from tissue are presented in Table 2.5. The kits used in this study are presented in Table 2.6. The ingredients used to prepare buffers and solutions are listed in Table 2.7.

Table 2.5. List of used digestive enzymes.

Digestive enzyme	Concentration	Distributor
Collagenase I	0.1%	Thermo Fisher Scientific, Waltham, MA, USA
Collagenase II	0.1%	
Collagenase XI	0.05%	Sigma Aldrich, Poznan, Poland
Collagenase D	0.5mg/mL	
Liberase	0.08 U/mL; 0.28 U/mL; 0.8 U/mL	

Table 2.6. Commercial kits used during course of experiments.

Name	Application	Company
Pierce BCA Protein Assay Kit	Determination of protein concentration	Thermo Fisher Scientific, Waltham, Massachusetts, USA
Clarity Western ECL Substrate	Proteins detection	Bio-Rad, CA, USA
CytoPainter F-Actin Staining Kit	Apical vacuoles visualization	Abcam, Cambridge, United Kingdom
Glucose	Determination of the glucose concentration in the culture media	BioMaxima, Lublin, Poland

Total RNA Mini Plus	RNA isolation from cells	A&A Biotechnology, Gdansk, Poland
Bead-Beat Total RNA Mini	RNA isolation from tissue	
iScript Advanced cDNA Synthesis Kit	cDNA synthesis	Bio-Rad, CA, USA
SsoAdvanced SYBR Green Supermix	Preparation of the Real Time qPCR samples	Bio-Rad, CA, USA
QuantiChrom Urea Assay Kit	Determination of the urea concentration in the culture media	BioAssay Systems, Hayward, California, USA
Halt Protease Inhibitor Cocktail 100×; Halt Phosphate Inhibitor Cocktail 100×; EDTA 100×	Supplements for RIPA buffer, used for protein isolation	Thermo Fisher Scientific, Waltham, Massachusetts, USA

Table 2.7. Ingredients necessary for buffer or solution preparation.

Reagent	Company
Sodium chloride (NaCl)	Sigma Aldrich, Poznan, Poland
Hydrochloric acid (HCl)	POCH, Gliwice, Poland
Sodium Dodecyl Sulfate (SDS)	Sigma Aldrich, Poznan, Poland
Tween-20	Sigma Aldrich, Poznan, Poland
Bovine Serum Albumin (BSA)	Sigma Aldrich, Poznan, Poland
Formaldehyde (FA)	Sigma Aldrich, Poznan, Poland
Tris Base	Lab Empire, Rzeszow, Poland
Sulfuric acid (H_2SO_4)	POCH, Gliwice, Poland
Glycine	POCH, Gliwice, Poland
Beta-mercaptoethanol (ß-ME)	Sigma Aldrich, Poznan, Poland
30% solution of acrylamide/bis-acrylamide 37.5:1	Sigma Aldrich, Poznan, Poland
Ammonium Persulfate (APS)	Sigma Aldrich, Poznan, Poland
N,N,N',N'-tetramethylethane-1,2-diamine (TEMED)	Sigma Aldrich, Poznan, Poland
Sodium hydroxide (NaOH)	WARCHEM, Warsaw, Poland
Tri-Sodium Citrate ($Na_3C_6H_5O_7$)	CHEMPUR, Piekary Slaskie, Poland
TRI Reagent	Sigma Aldrich, Poznan, Poland
1-Bromo-3-Chloropropane	Sigma Aldrich, Poznan, Poland
Hanks' Balanced Salt Solution (HBSS)	Thermo Fisher Scientific, Waltham, Massachusetts, USA
70% solution of ethanol	Linegal Chemicals, Warsaw, Poland
95% solution of ethanol	POCH, Gliwice, Poland
Isopropanol	POCH, Gliwice, Poland
Methanol	CHEPUR, Piekary Slaskie, Poland
Ethylenediaminetetraacetic Acid (EDTA)	POCH, Gliwice, Poland
Acetone	WARCHEM, Warsaw, Poland
Trichloroacetic Acid (TCA)	Sigma Aldrich, Poznan, Poland
4′,6-diamidino-2-phenylindole (DAPI)	Sigma Aldrich, Poznan, Poland
Trypan blue	Sigma Aldrich, Poznan, Poland
Dimethyl Sulfoxide (DMSO)	ATCC, Manassas, Virginia, USA
Thiazolyl Blue Tetrazolium Bromide (MTT)	Sigma Aldrich, Poznan, Poland
StayRNA	A&A Biotechnology, Gdansk, Poland
Ammonium Chloride (NH_4Cl)	POCH, Gliwice, Poland

Sodium Bicarbonate ($NaHCO_3$)	POCH, Gliwice, Poland
Histofluid (a preservative glue)	Medlab Products, Raszyn, Poland

2.4 Antibodies and Primers Used in the Experiments

The antibodies used for flow cytometry (FC), immunostaining/immunofluorescence (IF), ELISA, and Western blot (WB) analyses are presented in Table 2.8. A list of primers used for Reverse Transcription Quantitative Polymerase Chain Reaction (RT-qPCR) is provided in Table 2.9. All primers were commercially obtained from Bio-Rad (Bio-Rad, CA, USA).

Table 2.8. List of antibodies used for FC, WB, IF, ELISA analysis.

Antibody	Marker	Concentration	Method	Company, cat. number
Primary antibodies				
Goat anti-human albumin, HRP conjugated	HRP	1:100 1: 10 000 1:100 1:50 000	FC WB IF ELISA	Bethyl, Warsaw, Poland, A80-129P
Goat anti-human albumin, HRP conjugated	HRP	1:500	ELISA	Bethyl, Warsaw, Poland, A80-129A
Goat anti-human albumin, FITC conjugated	FITC	1:100 1:10 000 1:100	FC WB IF	Bethyl, Warsaw, Poland, A80-129F
Rabbit anti-human albumin, unconjugated	-	1:100 1:1000 1:100	FC WB IF	Invitrogen, Thermo Fisher Scientific, Waltham, Massachusetts, USA, PA5-13476
Mouse anti-human arginase 1	-	1:50	WB	Santa Cruz, Dallas, Texas, USA, sc-365547
Mouse anti-human Hepatocyte Nuclear Factor 4 alpha, unconjugated	-	1:1000	WB	Invitrogen, Thermo Fisher Scientific, Waltham, Massachusetts, USA, MA1-199
Rabbit anti-human Hepatocyte Nuclear Factor 4 alpha, PE conjugated	PE	1:200 1:500	FC IF	Biorbyt, Cambridge, United Kingdom orb484959
Rabbit anti-human Hepatocyte Nuclear Factor 1 alpha, unconjugated	-	1:1000	WB	Invitrogen, Thermo Fisher Scientific, Waltham, Massachusetts, USA, PA5-79379
Rabbit anti-human Alpha-fetoprotein, unconjugated	-	1:240 1:1000 1:100	FC WB IF	Invitrogen, Thermo Fisher Scientific, Waltham, Massachusetts, USA, MA5-16321

Rabbit anti-human Alpha-1-Antitrypsin, unconjugated	-	1:100 1:100	FC IF	Bioss, Thermo Fisher Scientific, Waltham, Massachusetts, USA, BS-0096R
Rabbit anti-human Carbamoyl phosphate synthetase I, unconjugated	-	1:500	WB	Abcam, Cambridge, United Kingdom, EPR7493-3
Mouse anti-human Cytochrome P450 3A4, unconjugated		1:1000	WB	Invitrogen, Thermo Fisher Scientific, Waltham, Massachusetts, USA, MA5-17064
Rabbit anti-human Cytochrome P450 2E1, unconjugated	-	1:10 000	WB	Invitrogen, Thermo Fisher Scientific, Waltham, Massachusetts, USA, PA5-35351
Rabbit anti-human Cytochrome P450 3A4, FITC conjugated	FITC	1:100 1:100	FC IF	biorbyt, Cambridge, United Kingdom, orb13919
Rabbit anti-human glyceraldehyde-3-phosphate dehydrogenase, unconjugated	-	1:10 000	WB	Invitrogen, Thermo Fisher Scientific, Waltham, Massachusetts, USA, PA1-988
Mouse anti-human CD73, PE conjugated	PE	1:10 1:25	FC IF	Becton Dickinson, Warsaw, Poland, 550257
Mouse anti-human Integrin beta 1, PE conjugated	PE	1:200 1:200	FC IF	Abcam, Cambridge, United Kingdom, ab64629
Mouse anti-human CD44, APC conjugated	APC	1:100 1:100	FC IF	Abcam, Cambridge, United Kingdom, ab81424
Mouse anti-human CD45, APC conjugated	APC	1:10 1:25	FC IF	Becton Dickinson, Warsaw, Poland, 555485
Rabbit anti-human CD133, unconjugated	-	1:100 1:10000 1:100	FC WB IF	Abcam, Cambridge, United Kingdom, ab19898
Rabbit anti-human CD34, unconjugated	-	1:100 1:100	FC IF	Abcam, Cambridge, United Kingdom, ab81289
Rabbit anti-human Ki67, unconjugated	-	1:100 1:100	FC IF	Invitrogen, Thermo Fisher Scientific, Waltham, Massachusetts, USA, MA5-14520
Rabbit anti-human Vimentin, unconjugated	-	1:100 1:1000 1:100	FC WB IF	Invitrogen, Thermo Fisher Scientific, Waltham, Massachusetts, USA,

				MA5-16409
Goat IgG FITC isotype control	FITC	1:100 1:100	FC IF	Abcam, Cambridge, United Kingdom, ab37374
Rabbit IgG Phycoerythrin-Isotype Control	PE	1:200 1:200	FC IF	Abcam, Cambridge, United Kingdom, ab37407
Mouse APC Isotype Control	APC	1:100 1:100	FC IF	Becton Dickinson, Warsaw, Poland, 550854
Secondary antibodies				
Goat anti-mouse IgG Fc Cross-Adsorbed Secondary Antibody HRP	-	1:2000	WB	Invitrogen, Thermo Fisher Scientific, Waltham, Massachusetts, USA, 31439
goat anti-rabbit IgG H&L HRP	-	1:10 000	WB	Abcam, Cambridge, United Kingdom, ab97051
Alexa Fluor goat anti-rabbit IgG (H+L)	-	1:100 1:1000/1:2000	FC IF	Invitrogen, Thermo Fisher Scientific, Waltham, Massachusetts, USA, A11034
Goat anti-mouse IgG (H+L) Alex Fluor Plus 488		1:100 1:1000/1:2000	FC IF	Invitrogen, Thermo Fisher Scientific, Waltham, Massachusetts, USA, A32723

Table 2.9. List of primers used for RT-qPCR.

Gene Symbol	Gene Name	Unique Assay ID	Amplicon Length (bp)	Efficiency
AFP	alpha-fetoprotein	qHsaCID0017919	141	99
ACTB	β-actin	qHsaCED0036269	62	103
ALB	albumin	qHsaCID0017798	112	95
ARG1	Arginase 1, liver	qHsaCED0003959	67	100
CPS1	carbamoyl-phosphate synthase 1, mitochondrial	qHsaCID0037920	143	98
CYP2C8	cytochrome P450, family 2, subfamily C, polypeptide 8	qHsaCID0021321	119	96
CYP2E1	cytochrome P450, family 2, subfamily E, polypeptide 1	qHsaCED0044326	72	93
CYP3A4	cytochrome P450, family 3, subfamily A, polypeptide 4	qHsaCID0012316	98	101
GAPDH	glyceraldehyde-3-phosphate dehydrogenase	qHsaCED0038674	117	97
GLUL	glutamate-ammonia ligase	qHsaCED0001392	73	99

HNF1A	hepatocyte nuclear factor 1 homeobox A	qHsaCED0001918	61	99
HNF4A	hepatocyte nuclear factor 4, alpha	qHsaCID0015879	108	102
PXR	nuclear receptor subfamily 1, group I, member 2	qHsaCED0045230	96	97
RPS18	ribosomal protein S18	qHsaCED0037454	67	94
VIM	vimentin	qHsaCED0042034	104	95

2.5 Buffers and Reagents Used During Experiments

2.5.1 Buffers and Reagents for Western Blot Analysis

Lower (Resolving) Buffer (4×): To prepare a 4× lower buffer, 90.86 g of Tris base was dissolved in 300 mL of Milli-Q water. The pH was adjusted to 8.8 using HCl, and the final volume was brought to 500 mL with Milli-Q water. The buffer was stored at room temperature (RT).

Upper (Stacking) Buffer (4×): To prepare a 4× upper buffer, 30.3 g of Tris base was dissolved in 300 mL of Milli-Q water. The pH was adjusted to 6.8 using HCl, and the final volume was brought to 500 mL with Milli-Q water. The buffer was stored at RT.

Running Buffer: The 10× running buffer used for electrophoresis was prepared as described in Table 2.10.

Table 2.10. Composition of the running buffer.

Reagent	Amount	Final concentration
Tris base	15.14 g	250 mM
Glycine	72.07 g	1.92 M
SDS	50 mL (10%)	1 %
Milli-Q water	400 mL	-

The pH was adjusted to 8.3 using HCl, and the final volume was brought to 0.5 L with Milli-Q water. To prepare the 1× running buffer used in sodium dodecyl sulfate-polyacrylamide gel electrophoresis (SDS-PAGE), the stock solution was diluted 1:10 with Milli-Q water. The buffer was stored at 4°C.

Transfer Buffer: The 10× transfer buffer used for protein transfer onto membranes was prepared as described in Table 2.11.

Table 2.11. Composition of the transfer buffer.

Reagent	Amount	Final concentration
Tris base	15.14 g	250 mM
Glycine	72.07 g	1.92 M
Milli-Q water	400 mL	-

The pH was adjusted to 8.3 using HCl, and the final volume was brought to 0.5 L with Milli-Q water. To prepare the 1× transfer buffer, 100 mL of the stock buffer was mixed with 200 mL of ethanol, and the final volume was adjusted to 1 L with Milli-Q water. The buffer was stored at 4°C.

Tris-Buffered Saline with Tween-20 (TBST Buffer) (10×): The 10× TBST buffer, used for washing membranes after protein transfer, was prepared as described in Table 2.12.

Table 2.12. Composition of the TBST buffer.

Reagent	Amount	Final concentration
Tris base	12.2 g	0.5 M
NaCl	43.9 g	1.5 mM
Tween-20	5 mL	1 %
Milli-Q water	300 mL	-

The pH was adjusted to 7.4 using HCl, and the final volume was brought to 1 L with Milli-Q water. For preparing the 1× TBST buffer, the stock solution was diluted 1:10 with Milli-Q water. The buffer was stored at RT.

Membrane Stripping Buffers: Mild Stripping Buffer (pH 2.2) was prepared as described in Table 2.13.

Table 2.13. Composition of the mild stripping buffer.

Reagent	Amount
Glycine	1.5 g
SDS 10%	1 mL
Tween-20	1 mL
36% HCl	1 mL
Milli-Q water	Adjust to 100 mL

Strong Stripping Buffer was prepared as described in Table 2.14.

Table 2.14. Composition of the strong stripping buffer.

Reagent	Amount
Upper buffer (4×)	6.25 mL
Beta-mercaptoethanol (ß-ME)	342 µL
SDS 10%	4 mL
Milli-Q water	Adjust to 50 mL

(SDS) Solution (10%): To prepare the 10% SDS solution, 10 g of SDS powder was weighed and dissolved in 70 mL of Milli-Q water. The solution was heated to 50°C until the powder had completely dissolved. The final volume was adjusted to 100 mL with Milli-Q water. The solution was stored at RT.

Resolving Gel (12%): A 12% resolving gel was prepared by mixing the reagents listed in Table 2.15.

Table 2.15. Composition of the resolving gel.

Reagent	Amount
Acrylamide 30%	4 mL
Lower Buffer (4×)	2.4 mL
APS	100 µL
TEMED	20 µL
10% SDS	100 µL
Milli-Q water	3.38 mL

Stacking Gel (4%): A 4% stacking gel was prepared by mixing the reagents listed in Table 2.16.

Table 2.16. Composition of the stacking gel.

Reagent	Amount
Acrylamide 30%	600 µL
Upper Buffer (4×)	960 µL
APS	40 µL
TEMED	6 µL
10% SDS	40 µL
Milli-Q water	2.35L

Blocking Solution (5%): The blocking solution was prepared by dissolving 5 g of skim milk powder (SM, Gostyn, Poland) in 100 mL of 1× TBST buffer. The solution was stored at 4°C.

Enhanced Chemiluminescence (ECL) for Protein Imaging: The enhanced chemiluminescence substrate for Horseradish Peroxidase (HRP) (Bio-Rad, CA, USA) was prepared immediately before use by mixing Reagent A and Reagent B in a 1:1 ratio, and then applied to the membrane.

Sodium Azide Solution (10%): The 10% sodium azide (NaN_3) solution, used for secondary antibody deactivation, was prepared by weighing the required amount of NaN_3 powder and dissolving it in Milli-Q water.

Additional reagents and equipment used for Western blot (WB) analysis are listed in Table 2.17.

Table 2.17. Reagents and equipment for WB analysis.

Reagent	Characteristics	Company
PVDF membrane (pore size 0.2 µm)	Transfer membrane	Thermo Fisher Scientific, Waltham, Massachusetts, USA
Wide Range Color Protein Ladder	Range: 10-250 kDa	A&A Biotechnology, Gdansk, Poland
5×Sample Buffer (5×SB)	Stock solution 5× diluted into 1.5×	NZYtech, Lisboa, Portugal
Developer Dental Readymatic Kodak/Carestream	Ready to used solution	Marrodent, Warsaw, Poland
Fixative Dental Readymatic Kodak/Carestream	Ready to mused solution	
CL-X Posure Film	Clear-blue X-ray film especially for detection and documentation of protein	Thermo Fisher Scientific, Waltham, Massachusetts, USA

2.5.2 Buffer and Reagents for ELISA analysis

Wash Buffer: The wash buffer used for washing wells during the ELISA protocol was prepared according to Table 2.18 and stored at 4°C.

Table 2.18. The composition of the wash buffer.

Reagent	Amount
Tris Base	6.06 g
NaCl	8.2 g
6 M HCl	7 mL
Milli-Q water	Adjust to 1 L

Postcoat Buffer: The Postcoat buffer (blocking solution) was prepared by diluting commercially available Tris-buffered saline with Bovine Serum Albumin (BSA) (pH 8.0; Sigma Aldrich, Poznan, Poland) to a final volume of 1 L with Milli-Q water. The solution was stored at 4°C.

Conjugate Diluent Buffer: The Conjugate Diluent buffer was prepared by adding 0.5 mL of 10% Tween-20 to 100 mL of Postcoat Buffer. The solution was stored at 4°C.

Coating Buffer: The Coating buffer was prepared by dissolving one capsule of Carbonate–Bicarbonate Buffer (Sigma Aldrich, Poznan, Poland) in 100 mL of Milli-Q water. The solution was stored at 4°C.

Human Albumin Standard: The human albumin standard (22 mg/mL; Bethyl, Warsaw, Poland) was diluted to a final concentration of 400 ng/mL. The solution was stored at −20°C and thawed immediately before use.

TMB Substrate: The ready-to-use TMB (3,3′,5,5′-Tetramethylbenzidine) substrate for HRP (Biomibo, Warsaw, Poland) was stored at 4°C.

2.5.3 Solutions for Immunostaining

PBST: PBST solution was prepared by diluting 0.1% Tween-20 with PBS.

Blocking Solution (1% BSA): The blocking solution for immunohistochemistry was prepared by diluting a 5% BSA stock solution (BSA dissolved in PBS; Sigma Aldrich, Poznan, Poland) with PBST to obtain a 1% working solution.

Buffer for Protein Isolation: The radioimmunoprecipitation assay (RIPA) buffer (Thermo Fisher Scientific, Waltham, MA, USA) was freshly prepared and supplemented with Halt Protease Inhibitor Cocktail (100×), Halt Phosphatase Inhibitor Cocktail (100×), and EDTA (100×), each at a ratio of 1:100. The buffer was kept cold (4°C) until use.

2.5.4 Reagents for Liver Tissue Cell Isolation

Collagenase Solutions: All collagenase solutions were prepared under sterile conditions, filtered through 0.22 µm membranes, and stored at 4°C.

- **Collagenase I (0.1%)**: 500 mg of collagenase I powder was dissolved in 1 mL HBSS, then diluted with 9 mL HBSS to obtain a 5% solution. The stock was aliquoted and stored at −20°C. A 0.1% working solution was prepared by diluting 1 mL of the 5% stock with 49 mL HBSS.
- **Collagenase II (0.1%)**: A 1 g/mL stock solution was prepared by dissolving 1 g collagenase II powder in 1 mL HBSS, then diluted 1:10 to obtain a 10% solution, aliquoted,

and stored at −20 °C. The 0.1% working solution was prepared by diluting the 10% stock solution 1:100 in HBSS.

- **Collagenase D (0.5 mg/mL)**: A 20 mg/mL stock solution was prepared by dissolving 100 mg of collagenase D powder in 5 mL HBSS, aliquoted, and stored at −20°C. The 0.5 mg/mL working solution was prepared by diluting 1 mL of the stock with 39 mL HBSS.
- **Collagenase XI (0.05%)**: Prepared similarly to collagenase I, using a 5% stock solution diluted 1:100 with HBSS to obtain the 0.05% working solution.

Liberase Solution: The Liberase stock solution (13 U/mL) was diluted with sterile water to obtain working solutions at concentrations of 0.08 U/mL, 0.28 U/mL, and 0.8 U/mL. Aliquots were stored at −20°C and thawed immediately before use.

Percoll Solution: The Percoll solution (Sigma Aldrich, Poznan, Poland) with a final density of 1.04 g/mL was prepared using the following formula:

$$V_P = V_f \, x \, \frac{d - 0.1 \, x \, d_{out} - 0.9}{d_{NaCl} - 1}, \tag{1}$$

where V_P – Percoll volume [mL], V_f – Percoll final volume [mL], d – expected density [g/mL] (1.04 g/mL), d_{out} – output density [g/mL], and d_{NaCl} – density of 1.5 M NaCl [g/mL] = 1.058 g/mL.

Red Blood Cell Lysis Buffer: Either a commercially available 1× RBC Lysis Buffer (Thermo Fisher Scientific, Waltham, MA, USA) or a self-prepared buffer was used. The buffer composition was as follows: 1.55 M NH_4Cl, 100 mM $NaHCO_3$, and 1 mM EDTA. The working solution was prepared by diluting the 10× stock buffer 1:10 with Milli-Q water.

Collagen Solution for Coating Culture Surfaces: Human hepatocyte cultures were grown either on commercially available collagen type I-coated plates (rat tail) or on self-coated plates. The recommended collagen concentration was 5 µg/cm².

The collagen stock solution (50 µg/mL) was diluted with 20 mM acetic acid according to the following equations:

$$V_1 = \frac{\left(50 \, \frac{\mu g}{mL} of \; collagen\right) \cdot (Final \; Volume)}{(Initial \; concentration \; of \; collagen \left(\frac{\mu g}{mL}\right))}, \tag{2}$$

$$V_{acid} = \ Final\ Volume - V_1, \quad (3)$$

where V_1 – collagen solution volume, and V_{acid} – acid solution volume.

The required volume of collagen solution was added to the culture dishes at a concentration of 5 µg/cm², incubated for 1 h at RT, and then aspirated. The dishes were washed three times with PBS, air-dried under sterile conditions, and stored at 4°C.

Dried Genetically Modified Fibroblasts as a Culture Growth Surface

One approach to improving culture conditions involved the use of dried human fibroblasts (drHDFn), either genetically modified or unmodified. Stable genetic modifications were achieved by introducing additional copies of genes encoding Epidermal Growth Factor (EGF) or Hepatocyte Growth Factor (HGF) using lentiviral vectors. Cells modified according to the method described by Wencel et al. (2021) were used in the experiments [209]. Fibroblasts overexpressing either EGF or HGF were utilized, and the culture plates were prepared as follows: fibroblast cells were seeded into 24-well culture plates at the densities specified in Table 2.19.

Table 2.19. Seeding densities and types of fibroblast variants.

Cells density per well	Variants of dried fibroblasts
2×10^4	Nonmodified cells – drHDFn
2×10^4	Cells with overexpression of EGF – drHDFn_EGF
2×10^4	Cells with overexpression of HGF – drHDFn_HGF
$1\times10^4 + 1\times10^4$	Mix of cells with overexpression of EGF and HGF – drHDFn_EGF+HGF

The plates containing the cells were cultured for 24 hours at 37°C in a 5% CO_2 atmosphere. Subsequently, the culture medium was removed, and the plates were left to dry for 30 min under sterile conditions. The plates, sealed with Parafilm, were then stored at 4°C.

2.5.5 Other Reagents and Solutions Used in Experiments

Formaldehyde (4%): The 4% formaldehyde (FA) solution was prepared by diluting the 16% formaldehyde stock solution with Phosphate-buffered saline (PBS) to obtain a 4% solution. Aliquots were prepared, frozen, and stored at −20°C until use.

Sterile PBS: Sterile PBS was prepared by dissolving PBS tablets (Thermo Fisher Scientific, Waltham, MA, USA) in Milli-Q water (1 tablet per 100 mL). The solution was then filtered through a 0.22 µm membrane under sterile conditions in a laminar flow hood.

Trypsin-EDTA (0.25%): A total of 50 mL of 10× Trypsin stock solution (Biological Industries, Beit-Haemek, Israel) was diluted with 450 mL of PBS, and 685 µL of 0.5 M Ethylenediaminetetraacetic acid (EDTA) was added. The solution was filtered through a 0.22 µm membrane under sterile conditions, aliquoted, and stored at 4°C or −20°C.

Tween-20 (10%): A 10% Tween-20 solution was prepared by diluting the 100% stock solution 1:10 with PBS.

Triton X-100 (0.1%): A 10% Triton X-100 solution (Sigma Aldrich, Poznan, Poland) was prepared by diluting the 100% stock 1:10 with PBS. This 10% solution was then further diluted 1:100 to obtain a 0.1% working solution.

Fetal Bovine Serum in PBS (2%): A 2% Fetal Bovine Serum (FBS) solution was prepared by diluting 100% FBS with PBS.

2.5.6 Reagents Used for the Characterization of Polysulfone Capillary Membranes

Table 2.20 provides a list of reagents, substances, and solutions used for the characterization of polysulfone capillary membranes.

Table 2.20. Reagents and materials used for the characterization of polysulfone capillary membranes.

Name	Company
Polysulfone capillary membranes with pore size 0.2 µm	Vestergaard Frandsen, Lozanna, Switzerland
Bovine Serum Albumin (BSA) – 7.1 nm (67 kDa)	Fluka, Charlotte, North Carolina, USA
Green fluorescent polystyrene microspheres – 100 nm	EPRUI Biotech, Suzhou, China
Green fluorescent polystyrene microspheres – 200 nm	
Green fluorescent polystyrene microspheres – 500 nm	
Cytometer Setup and Tracking Beads – 2-3 µm	Becton Dickinson, Warsaw, Poland
Polyurethane resin FC 52/HPE 85; polyol; component A	JASSKOR, Warsaw, Poland
Polyurethane resin FC 52/HPE 40-85A-ISO; isocyanine; component B	
Silicone grease ROTISILON C	Carl Roth, Karlsruhe, Germany

2.5.7 Laboratory Equipment

The equipment required for the doctoral research is listed in Table 2.21. Laboratory materials and consumables used throughout the study are listed in Table 2.22.

Table 2.21. Laboratory equipment used in the study.

Name	Company
Biological safety cabinet class II NuAire LABGARD	NuAire, Plymouth, Massachusetts, USA
Incubator CO_2 for cell culture NuAire	
Flow cytometer BD FACSCanto II	Becton Dickinson, Warsaw, Poland
Inverted phase contrast microscope CKX41	Olympus, Warsaw, Poland
Fluorescence inverted microscope IX-71 equipped with the CS-S_MP-VF Multi Position module	
Confocal microscope Fluoview FV4000	
OLYMPUS Provi CM20 incubation monitoring system (demo version)	
Spectrophotometer with plate reader Synergy HT Bio-Tek	BIOKOM, Janki, Poland
Centrifuge 5415 R	Eppendorf, Warsaw, Poland
Automatic pipettes	
Automatic pipettor	
Mini centrifuge D1008	DLAB Scientific, Rowland St., California, USA
Thermomixer HCM100-Pro	
Spectrophotometer UV-Vis NanoDrop One	Thermo Fisher Scientific, Waltham, Massachusetts, USA
Spectrophotometer UV-Vis U-3010	Hitachi High-Technologies, Tokyo, Japan
Scanning electron microscope TM-1000	
Centrifuge MPW-352R	MPW, Warsaw, Poland
Autoclave Classic Prestige Medical	Bionovo, Legnica, Poland
Liquid nitrogen dewar Lab Systems LS3000	Worthington Industries, Columbus, Ohio, USA
Set for vertical electrophoresis and transfer Mini PROTEAN 3 Cell	Bio-Rad, Hercules, California, USA
CFX96 Connected Real-Time PCR Detection System	
iCycler Thermal Cycler	
Centrifuge LISA	AFI Group, Château-Gontier, France
Magnetic stirrer with heating IKA RTC basic	IKA, Warsaw, Poland
Shaker IKA Vortex 2	
Peristaltic pump Reglo-Digital ISM597A	Ismatec, Glattburg, Switzerland
Peristaltic pump L/S easy-load II 77202-60	Masterflex, Plock, Poland
Laboratory cradle KL-945	JW Electronic, Warsaw, Poland
Multichannel pipettes	Medlab, Raszyn, Polska
Laboratory scales WTB2000	Radwag, Warsaw, Poland

Goniometer DSA25	Krüss Optronic, Hamburg, Germany
Water Bath SWB	Stuart, Stone, United Kingdom
Sputter coater Emitech K550X	Quorum Technologies, Ashford, United Kingdom
Multifunctional instrument CX-705 (used for pH measurement)	Elmetron, Zabrze, Poland
Incubator KBC-65G	WAMED, Warsaw, Poland
Heater	Termiko, Cieszyn, Poland
Vacuum dryer SPT-200 BCM	Conbest, Krakow, Poland
Centrifuge (for pouring resin on modules)	Laboratory of Semi-Permeable Membranes and Bioreactors, Institute of Biocybernetics and Biomedical Engineering, Polish Academy of Sciences
Ultra-low temperature freezer MDF-DU502VX	PHC Corporation, Tokyo, Japan

Table 2.22. Materials and consumables used in the study.

Name	Company
Pipette tips (volume 10 µL, 200 µL, 1 mL)	Profilab, Warsaw, Poland
Pipette filter tips (volume 10 µL, 200 µL, 1 mL)	Googlab Scientific, Rokocin, Poland
Serological pipettes (volume 5 mL, 10 mL, 25 mL, 50 mL)	
Centrifuge tubes (volume 15 mL, 50 mL)	
Flasks for cell culture (surface 25 cm^2, 75 cm^2)	
6, 12, 24 and 96-well plates	Nest Scientific Biotechnology, Wuxi, Jiangsu, China
Cell culture dishes (size 60 mm)	
Injection syringes (volume 2 mL, 5 mL, 20 mL)	Becton Dickinson, Warsaw, Poland
Microcentrifuge tubes (volume 1.5 mL, 2 mL)	Bionovo, Legnica, Poland
Glass bottles	
Glass beakers	
Mr. Frosty Freezing Container	
Petri dishes (various diameter)	
Cryovials (volume 2 mL)	Biologix Plastics, Changzhou, Jiangsu, China
Cell scrapers	
PVDF membrane filters (pore size 0.22 µm)	Merck, Darmstadt, Germany
PVDF membrane mini filters (pore size 0.22 µm) Millex-GV	
Mesh at pore size 70 µm	
Scienceware polypropylene Buchner funnel	
Needles for luer lock syringes (various sizes)	
Microsep centrifugal filters, 0.5-5 mL sample volumes	Pall Corporation, Port Washington, New York, USA
Bürker counting chamber	Equimed, Warsaw, Poland

96-well maxi binding plates	Thermo Fisher Scientific, Waltham, Massachusetts, USA
6, 24-well coated plates, Collagen I, Rat Tail	
24-wells plates coated, Laminin	
Round-bottom tubes	Sarstedt, Nümbrecht, Germany
Pump tubing (interior diameter 1.85 mm)	Ismatec, Glattburg, Switzerland
Pump tubing (interior diameter 2.79 mm)	
Hemodialysis tubing A/V Set for Dialog	B.Braun Aeskulap Chifa, Nowy Tomysl, Poland
Scalpels Cutfix (number 22)	Linegal Chemicals, Warsaw, Poland

2.6 Computer Software

The following computer programs were used for data analysis, visualization, and documentation:

- ImageJ 1.53k, Wayne Rasband and contributors, National Institutes of Health, USA
- Statistica 10 software, Stat Soft. Inc., Tulsa, OK, USA.
- OriginPro, Version 2023. OriginLab Corporation, Northampton, MA, USA.
- OLYMPUS cellSens Dimension 3.2, OLYMPUS CORPORATION.
- Olympus OlyVIA 4.1, EVIDENT Technology Center Europe GmbH.
- BD FACSDiva Software, version 6.1.2, Becton, Dickinson and Company, New York, USA.
- BioRender, Fontana T., 2004, available at https://www.biorender.com/
- Inkscape 1.1, GNU General Public License, Version 3.
- Bio-Rad CFX Maestro 2.0, Version 5.0.021.0616, Bio-Rad, Hercules, California, USA.
- TM-1000 software, Hitachi TM-1000, Tokyo, Japan.
- UV Solutions 2.0, Hitachi High-tech Corporation, Tokyo, Japan.
- PyMOL, Version 3.1.6.1. Schrödinger, LLC.

3 Methods

3.1 Cell Culture Methods

3.1.1 Culture Media Composition and Preparation

3.1.1.1 Basic Culture Media

Almost all basal culture media used in this study were ready-to-use fluids, except for the DMEM, which was purchased as a powder. The DMEM powder was dissolved in 500 mL of distilled water, followed by the addition of 3.7 g of sodium bicarbonate. After brief stirring, the solution was adjusted to a final volume of 1 L with distilled water and filtered through a 0.2 μm filter. To obtain media specific for each cell line, the basal media were supplemented with various reagents. Tables 3.1–3.4 present the composition of the basic culture media adapted for the culture of specific cell types.

Table 3.1. Composition of media for the culture of C3A, HepG2, HOS, hHDPCs, hHs, and liver cells.

DMEM	
Concentration	**Reagent**
-	High glucose Dulbecco's Modified Eagle Medium
10%	FBS
1%	MEM NEAA
EMEM	
Concentration	**Reagent**
-	Eagle's Minimum Essential Medium
10%	FBS
1%	MEM NEAA
WEM	
Concentration	**Reagent**
-	William's E Medium, GlutaMAX Supplement
10%	FBS
1%	MEM NEAA
HM+HGS	
Concentration	**Reagent**
-	Hepatocyte Medium
10% or 5% or 2%	FBS
1%	HGS
1%	P/S
HZ	
Concentration	**Reagent**
	Hepatozyme-SFM, is a serum-free medium
200 mM	α-glutamine
1%	P/S

Table 3.2. Medium used for HUVEC culture.

M199	
Concentration	**Reagent**
-	Medium 199
15 IE/mL	Heparin
2 mL/100 mL	HEPES solution pH 7.0-7.6
10 µg/mL	Endothelial Cell Growth Supplements (ECGS)
100 U/mL /100 µg/mL	P/S solution
10%	FBS

Table 3.3. Medium used for SH-SY5Y culture.

MEM/F12	
Concentration/ratio	**Reagent**
1:1	Minimum Essential Medium Eagle/Nutrient Mixture F-12 Ham
15%	FBS
2 mM	glutaMAX
1%	MEM NEAA
100 U/mL /100 µg/mL	P/S solution

Table 3.4. Medium used for SNU475, SNU449 cultures.

RPMI-1640	
Concentration	**Reagent**
-	Medium RPMI-1640
10%	FBS

3.1.1.2 Culture Media Used for Inducing the Dedifferentiation of hHDPCs into Hepatocytes

To test the hHDPCs dedifferentiation into hepatocytes, culture media supplemented with various growth factors were used. Table 3.5 presents the composition of these media.

Table 3.5. Compositions of the culture media used for dedifferentiation of hHDPCs into hepatocytes.

HM	
Concentration	**Reagent**
	HM
2%	FBS
1%	P/S
HM+FGF-4+HGF	
Concentration	**Reagent**
	HM
2%	FBS
1%	P/S
10 ng/mL	FGF-4
10 ng/mL	HGF

HM+EGF+HGF	
Concentration	**Reagent**
	HM
2%	FBS
1%	P/S
10 ng/mL	EGF
10 ng/mL	HGF

3.1.1.3 Media for Obtaining Human Dedifferentiated Hepatocytes (hDHe) That Divide and Retain Hepatocyte Functions

The composition of the medium used for thawing and initial culture of human hepatocytes is presented in Table 3.6. The ingredients required for the preparation of the Expansion Medium (EM) are presented in Table 3.7. This medium was used in I stage of experiment to obtain dividing cells dedifferentiated from the human hepatocytes – human Dedifferentiated Hepatocytes (hDHe) – and was applied to cells cultured on plates coated with rat tail collagen type I. For cell cultures conducted on dried genetically modified fibroblasts (drHDFn_EGF+HGF), the culture medium listed in Table 3.8 was used.

After 5 days of culture, the composition of the expansion medium was changed. Table 3.9 contains the reagents required for the preparation of Expansion Medium_2 (EM_2). For cells cultured on drHDFn_EGF+HGF, the Expansion Medium_2* (EM_2*) was used, and its composition is listed in Table 3.10.

The Differentiation Medium (DM) was used in the II stage of experiment to obtain hepatocyte-like cells that divide yet retain hepatocyte functions. Table 3.11 contains the list of substances required for the preparation of this medium.

Table 3.6. The composition of the culture medium used for thawing and initial culture of human hepatocytes.

WG+I+H	
Concentration	**Reagent**
	William's E Medium, GlutaMAX™ Supplement
4 μg/mL	Insulin
50 μM	Hydrocortisone

Table 3.7. Composition of the Expansion Medium_1 (EM1) used for culturing cells on a collagen-coated surface.

Expansion Medium_1 (EM1)	
Concentration	**Reagent**
	AdDMEM/F12
1%	N-2 Supplement (100×)
1%	B-27 Supplement (50×),

1.25 mM	*N*-Acetyl-L-cysteine (NAc)
10 nM	Gastrin I, Human
10 mM	Nicotinamide (Nic)
5 μM	A 83-01
50 ng/mL	EGF
500 ng/mL	R-Spondin-1
100 ng/mL	FGF-10
25 ng/mL	HGF
25 ng/mL	Noggin
50 ng/mL	Wnt-3a
10 μM	Y-27632 dihydrochloride

Table 3.8. Composition of the Expansion Medium_1* (EM1*) used for culturing cells on the drHDFn_EGF+HGF growth surface.

Expansion Medium_1* (EM1*)	
Concentration	**Reagent**
	AdDMEM/F12
1%	N-2 Supplement (100×)
1%	B-27 Supplement (50×),
1.25 mM	*N*-Acetyl-L-cysteine (NAc)
10 nM	Gastrin I, Human
10 mM	Nicotinamide (Nic)
5 μM	A 83-01
500 ng/mL	R-Spondin-1
100 ng/mL	FGF-10
25 ng/mL	Noggin
50 ng/mL	Wnt-3a
10 μM	Y-27632 dihydrochloride

Table 3.9. Composition of the Expansion Medium_2 (EM2) used after 5 days of culturing cells on a collagen-coated surface.

Expansion Medium_2 (EM2)	
Concentration	**Reagent**
	AdDMEM/F12
1%	N-2 Supplement (100×)
1%	B-27 Supplement (50×),
1.25 mM	*N*-Acetyl-L-cysteine (NAc)
10 nM	Gastrin I, Human
10 mM	Nicotinamide (Nic)
5 μM	A 83-01
50 ng/mL	EGF
500 ng/mL	R-Spondin-1
100 ng/mL	FGF-10
25 ng/mL	HGF

Table 3.10. Composition of the Expansion Medium_2* (EM2*) used after 5 days of culturing cells on the drHDFn_EGF+HGF growth surface.

Expansion Medium_2* (EM2*)	
Concentration	**Reagent**
	AdDMEM/F12
1%	N-2 Supplement (100×)
1%	B-27 Supplement (50×),
1.25 mM	*N*-Acetyl-L-cysteine (NAc)
10 nM	Gastrin I, Human
10 mM	Nicotinamide (Nic)
5 µM	A 83-01
500 ng/mL	R-Spondin-1
100 ng/mL	FGF-10

Table 3.11. The composition of the Differentiation Medium (DM) used to generate hepatocyte-like cells.

Differentiation Medium (DM)	
Concentration	**Reagent**
	AdDMEM/F12
1%	N-2 Supplement (100×)
1%	B-27 Supplement (50×)
10 nM	Gastrin I, Human
500 µM	A 83-01
50 ng/mL	EGF
25 ng/mL	HGF
100 ng/ml	FGF-19
10µM	DAPT
25 ng/mL	BMP-7
30 µM	Dexamethasone

3.1.2 Cell Thawing

Cryovials containing 1 mL of cryopreserved cells were stored in liquid nitrogen. For thawing, the vials were removed from the dewar and placed in a water bath. Once partially thawed, 1 mL of warm medium was added to the cells, followed by transfer into a centrifuge tube containing 3 mL of culture medium. The suspension was centrifuged (5 min, 15°C, 163 RCF), the supernatant discarded, and the pellet resuspended in 1 mL of fresh medium. The cells were then seeded into culture vessels and incubated at 37°C with 5% CO_2.

3.1.3 Cell Passaging

In this doctoral study, ‘cell passage’ refers to splitting cells after they reach high confluency. The procedure began with removing the culture medium and washing the cells with PBS. Next, 0.25% trypsin–EDTA was added, and the culture was incubated at 37°C for

5 minutes (typically, depending on the cell type). Trypsin was neutralized with an equal volume of FBS-supplemented medium (1:1). The detached cells were dissociated into a single-cell suspension by pipetting up and down several times, transferred to a test tube, and centrifuged (5 min, 15°C, 163 RCF). The supernatant was discarded, and the pellet was resuspended in 900 µL of fresh culture medium. The resulting suspension was either frozen or seeded directly for further culture or cell counting.

3.1.4 Cell Counting Using the Bürker Chamber and Trypan Blue Exclusion

The trypan blue exclusion method was used to distinguish viable cells from dead ones, as only dead cells take up the dye due to compromised membrane integrity. Depending on the cell density, the suspension was either diluted in PBS or directly mixed 1:1 with 0.2% trypan blue. Then, 10 µL of the mixture was applied to a Bürker chamber, and cells were counted using an inverted phase-contrast microscope (CKX41; Olympus, Warsaw, Poland).

The final cell number was calculated using the following formula (4):

$$n_f = n_a \cdot d \cdot 10^4, \tag{4}$$

where n_f – final number of cells, n_a – average number of counted cells, and d – dilution factor.

3.1.5 Cell Freezing

To preserve biological material, the cell portions were frozen after each passage. The cell suspension in fresh culture medium was transferred into cryovials, and DMSO was added to a final concentration of 10% (0.1 mL DMSO per 1 mL cell suspension). The cryovials were placed in a freezing container at −80°C for 24 h, and then transferred to liquid nitrogen for long-term storage.

3.1.6 Cell Doubling Time

To calculate cell doubling time, cells were seeded in culture dishes and grown for several days. After trypsinization, cells were counted using the trypan blue exclusion method. Using the following formula (5) developed by Korzynska and Zychowicz (2008) [210], the cell doubling time was estimated:

$$T_2 = \frac{\Delta t}{log_2(\frac{\Delta N}{N_o+1})}, \tag{5}$$

where Δt- culture time, N_o – initial number of cells, and ΔN – increase in cell number.

3.2 Hepatocytes Isolation

3.2.1 Mechanical Dissociation and Enzymatic Digestion of the Liver Tissue

During the preparation of the doctoral thesis, resected fragments of liver tissue were obtained from 30 donors, and a total of 41 cell isolations were carried out using multiple liver fragments digested with selected collagenases. The hepatocyte isolation procedure was performed according to the method described by Zakrzewska et al. [153]. All procedures related to human hepatocyte isolation were performed under a laminar flow hood under sterile conditions. Throughout the process, a peristaltic pump was used to rinse the tissue with various solutions, maintaining a flow rate of 8–10 mL/min.

The liver tissue was first washed with cold PBS without Mg^{2+} and Ca^{2+} to remove blood cells until the solution became clear. Next, the PBS was replaced with a digestive enzyme solution (details of solution preparation are described in section 2.8.7, Reagents for Liver Cell Isolation), and the tissue was continuously rinsed. The volume of the collagenase solution depended on the tissue weight, i.e. 1 mL of enzyme was used per 1 g of tissue.

The tissue fragments were then cut into small pieces and incubated in a water bath at 37°C for 15 min with magnetic stirring. This step was repeated if necessary. The digested tissue was filtered using a Büchner funnel to remove larger fragments, , and then filtered through a 70 μm mesh. All these steps were performed on ice.

The tissue filtrate was centrifuged at 366 RCF for 7 min at 4°C. To lyse red blood cells, the pellet was resuspended in culture medium containing 1× RBC Lysis Buffer and shaken on a thermomixer at 37°C, 800 RPM for 5 min. The cell suspension was centrifuged as described above.

To separate cells from debris, the samples were centrifuged at 366 RCF for 20 min at 4°C using a Percoll solution with a density of 1.04 g/mL. The cells were then washed with culture medium and centrifuged again under the same conditions; this step was repeated once more.

Finally, the cells were counted using a Bürker chamber and the trypan blue exclusion method, then seeded into culture plates or prepared for flow cytometry analysis.

Table 3.12 provides an overview of liver samples collected from 30 patients, presenting information on their age, gender, diagnosed conditions, treatments received, formation of cell islands, and the collagenase type used for tissue digestion. Table 3.13 summarizes liver samples for which no cell isolation was performed; instead, direct analyses were conducted on the liver

tissue, including WB and RT-qPCR assays. Table 3.14 provides a summary of the liver samples available in the research team's collection. This biological material was obtained by other team members prior to the commencement of this doctoral study. For samples LCI(H33) and LCI(H38), experiments were conducted on liver tissue, whereas for the remaining samples, liver cell isolates were used. Table 3.15 presents information about donors of commercially available hepatocytes, including gender, age, cause of death, and other medical conditions. These data were obtained from the certificates of analysis accompanying each hepatocytes vial.

Table 3.12. A compilation of liver samples from patients, from which liver cells were isolated.

Experimental conditions									**Preliminary observation**
Sample number	**Sample name Liver cell isolate (LCI)**	**Gender**	**Age**	**Chemotherapy**	**Steatosis**	**Diabetes**	**Cancer/ metastases**	**Type of used collagenase**	**Cell islands formation**
1	H49	F	41	-	-	-	+	I	-
2	H50	M	68	+	-	-	+	II	-
3	H51	F	70	+	-	-	+	D	+
4	H52	F	58	-	-	-	+	II	+
5	H53	F	47	-	-	-	+	II	+
6	H54	F	45	-	+	-	+	II	-
7	H55	F	60	-	-	-	-	D	+
8	H56	M	32	-	-	-	-	II	+
9	H57	M	54	-	-	-	+	II	-
10	H58	M	68	-	-	-	+	II	+
11	H59	M	53	-	-	-	+	II	+
12	H60	M	50	+	-	-	+	II	-
13	H61	M	30	-	+	-	-	(II +D); II *	+
14	H62	M	78	-	-	-	+	D	-
15	H63	M	27	-	-	-	+	II + I	+
16	H64	F	70	+	-	-	+	II + XI	+
17	H65	F	60	-	-	-	-	II+XI+I	+
18	H66	M	60	-	-	-	+	(I+II+XI); (I+II) *	-
19	H67	M	67	-	-	-	+	(I+II); I *	+
20	H68	M	63	-	-	+	+	Liberase	-
21	H69	M	78	+	-	+	+	D	+

22	H70	F	67	+	-	-	+	XI; II; D; I *	+
23	H71	M	70	-	-	-	-	Liberase; (I+II+D) *	+
24	H72	F	65	-	-	-	+	Liberase; (I+II+XI) *	+
25	H73	F	38	+	-	-	+	I+II+D+XI	-
26	H74	F	49	-	-	-	-	II; Liberase *	+
27	H76	M	42	-	+	-	-	XI	+
28	H78	F	62	+	-	-	+	II; (II+D) *	+
29	H79	M	73	-	-	-	+	D+II	-
30	H84	F	52	-	+	-	-	XI; I *	-

* multiple liver tissue fragments subjected to digestion with selected collagenases

Table 3.13. A compilation of liver samples from patients, which were used for various experiments without prior cell isolation.

Sample number	Sample name Liver cell isolate (LCI)	Gender	Age	Chemotherapy	Steatosis	Diabetes	Cancer/ metastases
1	H75	F	28	+	-	-	+
2	H77	M	42	-	+	-	-
3	H81	M	77	-	-	-	+

Table 3.14. A compilation of liver samples from patients in the research team's collection. Cell isolation was performed before starting work on this doctoral thesis.

Sample number	Sample name Liver cell isolate (LCI)	Gender	Age	Chemotherapy	Steatosis	Diabetes	Cancer/ metastases	Type of used collagenase
1	H33	M	73	+	-	-	+	I
2	H35	M	65	-	+	-	-	I
3	H37	F	34	+	-	-	+	I
4	H38	M	61	-	+	-	-	II
5	H40	F	62	+	-	-	+	XI
6	H43	M	61	-	+	-	-	I

Table 3.15. Summary of information on donors of commercially available hepatocytes.

Sample number	Sample name	Gender	Age	Cause of death	Other
1	hH_1	F	58	N/A	Metastatic tumor
2	hH_2	M	47	Anoxia (CVA, Cerebrovascular Accident)	N/A
3; 5	hH_3; hH_5	F	62	Anoxia (Drug Intoxi-fication)	Hypothyroidism, Epilepsy, Chronic Obstructive Pulmonary Disease
4	hH_4	M	57	N/A	Metastatic tumor

3.2.2 Determination of Yield of Cell Isolation and Cell Viability

After liver cell isolation and cell counting, the yield of the isolation procedure (Y) was calculated using the following formula (6):

$$Y = \frac{LCN}{LTM}, \tag{6}$$

where Y – yield of liver cell isolation [$\times 10^6$ cells/g tissue], LCN – live cell number [$\times 10^6$ cells], LTM – liver tissue mass [g].

Cell viability was calculated using Equation (7):

$$V = \frac{LCN}{TCN}\ x\ 100\%, \tag{7}$$

where V – cell viability [%], TCN – total cell number [$\times 10^6$ cells].

3.2.3 Variants of Cultures of Isolated Cells

To improve and ensure optimal conditions for human hepatocyte culture, various culture media and growth substrates were employed. Cells isolated from liver tissues were seeded onto culture plates coated with different substances supporting cell adhesion, such as rat tail collagen type I, fibronectin, laminin, or dried genetically modified human fibroblasts overexpressing HGF. Additionally, several types of culture media were tested, including DMEM, William's E Medium (WEM), HepatoZYME-SFM (HZ), and Hepatocyte Medium supplemented with HGS (HM+HGS). All media were supplemented with various additives that enhance cell growth,

such as insulin, dexamethasone, HGF, EGF, amino acid solutions, or the commercially available Hepatocyte Growth Supplement (the detailed compositions of the media are presented in Table 3.1). The cells were seeded on the 24-well plates at a density of 0.5-1×10^6 cells per well.

3.3 Flow Cytometry

For flow cytometry (FC) analysis, cells were detached from the culture surface using 0.25% trypsin-EDTA and counted in a Bürker chamber using the trypan blue exclusion method. After each step in this protocol, cells were centrifuged for 5 min at 4°C at 700 RCF. Cell fixation was performed with 4% FA (100 µL per 1×10^6 cells for most cell types; for HDFn or hHDPCs, 100 µL per 2–5×10^5 cells) for 15 min at RT. Cells were then incubated with 0.1% Triton X-100 (the same volume as used for fixation) for 10 min at RT. Next, cells were incubated in 2% FBS diluted in PBS containing either a primary antibody or a fluorophore-conjugated antibody for 1 h at RT. If necessary, incubation with secondary antibodies was performed for 30 min at RT (the list of used antibodies is presented in Table 2.8). Finally, cell pellets were resuspended in 100 µL PBS, transferred into FACS tubes and analyzed using the FACS Canto II flow cytometer (BD, Warsaw, Poland). The obtained results are expressed as a percentage, this enables the estimation of protein expression on the population level. This method was described earlier in Zakrzewska et al. [153].

3.3.1 Flow Cytometric Determination of Cell Size and Granularity

The size and granularity of hHDPCs, C3A, HDFn, and hHs cells were evaluated using FC. All measurements were conducted under identical voltage settings: forward scatter [FSC; (corresponding to cell size)] at 300 V and side scatter [SSC; (corresponding to cell granularity)] at 400 V. The FSC parameter corresponds to cell size, whereas SSC reflects cell granularity. Each sample contained 1×10^6 cells.

3.4 Immunofluorescence

The presence of specific proteins in the cells was confirmed using immunostaining with specific antibodies. The medium was removed, and the wells were rinsed with PBS (after each step, the wells were washed three times with PBS). Cells were fixed with 4% FA for 15 min at RT, permeabilized with 0.1% Triton X-100 for 10 min at RT and blocked with 1% BSA for 30

min at RT. After overnight incubation with primary antibodies at 4°C, the wells were washed with PBS, followed by incubation with secondary antibodies for 30 min at RT. Finally, cell nuclei were stained with DAPI. Results were analyzed using a fluorescence inverted microscope (IX-71; Olympus, Warsaw, Poland).

3.5 Apical Vacuoles

For apical vacuole imaging, cells cultured on plates were first fixed with 4% FA for 15 min at RT and permeabilized with 0.1% Triton X-100 for 10 min at RT. The F-actin Staining Kit – Red Fluorescence (Cytopainter) was then applied according to the manufacturer's instructions using the phalloidin probe for 15 min at RT. Cell nuclei were counterstained with DAPI. After each step, wells were washed three times with PBS. Apical vacuoles were primarily visualized using an IX-71 inverted fluorescence microscope, and additionally, using the APX100 fluorescence microscope and the Fluoview FV4000 confocal microscope (both from Olympus, Warsaw, Poland).

For confocal imaging, cells were grown on coverslips, fixed, permeabilized as described above, mounted on glass slides and sealed with Histofluid, a preservative glue.

3.6 Enzyme-linked Immunosorbent Assay (ELISA)

To determine whether the tested cells were capable of secreting albumin, culture medium samples were collected during culture. The ELISA method was used to quantify the concentration of human albumin using a commercial kit, as described below.

First, the anti-human albumin antibody was diluted 1:500 in Coating Buffer. Maxi binding 96-well plates were coated with 100 µL of the antibody solution per well and incubated for 1 h at RT in the dark. After incubation, the solution was discarded, and the wells were washed twice with 100 µL of Wash Solution per well.

Next, 200 µL of Postcoat Solution (blocking solution) was added to each well, followed by incubation for 30 min at RT in the dark. Wells were washed twice with 200 µL of Wash Solution. Then, 100 µL of serially diluted albumin standards (400, 200, 100, 50, 25, 12.5, 6.25, 3.12 ng/mL), and diluted or undiluted samples were added and incubated for 1 h at RT in the dark.

After washing the wells twice with 100 µL of Wash Solution, HRP-conjugated anti-human antibody was diluted 1:50,000 in Conjugate Diluent, and 100 µL was added to each

well. The plate was incubated for 1 h at RT in the dark, followed by two washes with 100 µL of Wash Solution.

Then, 100 µL of TMB Substrate was added to each well and incubated for 15 min at 37°C with shaking on a thermomixer. The reaction was stopped by adding 100 µL of 0.2 M H_2SO_4 per well. Absorbance was measured at 450 nm using a Synergy HT Bio-Tek microplate reader (BIOKOM, Janki, Poland).

A standard curve was generated from the albumin standard dilutions to calculate the albumin concentration in the tested samples.

3.7 Thiazolyl Blue Tetrazolium Bromide (MTT) Assay

Cells were seeded into 96-well plates and cultured for several days without medium replacement. After removing the medium, MTT solution was added to each well at a final concentration of 0.25 mg/mL and incubated for 2 h at 37°C. Subsequently, 150 µL of isopropanol was added to each well and incubated for 15 min at 37°C. Absorbance was measured at 570 nm using the Synergy HT Bio-Tek plate reader.

3.8 Glucose Concentration Measurements

Glucose concentration in culture media was determined using a colorimetric glucose assay kit. In a 96-well plate, 2 µL of each sample or glucose standard (in triplicate) and 200 µL of color reagent were added per well. After mixing and incubation for 10 min at RT, absorbance was measured at 505 nm using the Synergy HT Bio-Tek microplate reader.

3.9 Western Blot Analysis

3.9.1 Protein Isolation from Cells

During the experimental cycles, protein isolation was performed either from cells seeded and cultured for several days or from directly thawed cells.

For isolation from cultured cells, the cells were first washed with PBS, collected by scraping, and suspended in RIPA buffer containing protease, phosphatase, and EDTA inhibitors. Samples were incubated at 4°C for 25 min with shaking at 350 RPM on a thermomixer, followed by centrifugation for 20 min at 4°C at 13,400 RCF. The supernatants were then transferred to new tubes, and protein concentration was determined using the BCA assay according to the manufacturer's protocol.

For isolation from thawed cells, samples of 1×10^6 cells were used. Thawed cells were mixed with culture medium and centrifuged at 366 RCF for 5 min at RT. The supernatants were discarded, and the pellets were washed with 1 mL PBS and centrifuged again under the same conditions. The resulting pellets were then resuspended in 0.5 mL of cold RIPA buffer containing protease, phosphatase, and EDTA inhibitors, and the procedure described above was followed.

3.9.2 Protein Isolation from Liver Tissue

Protein isolation from liver tissue was performed as follows: 20 mg of liver tissue was cut into small pieces, and 1 mL of RIPA buffer containing protease, phosphatase, and EDTA inhibitors was added. The tissue was gently minced with tweezers, and a small stir bar was added. Samples were incubated at 4°C for 2 h with shaking at 1000 RPM. After incubation, samples were centrifuged for 20 min at 4°C at 13,400 RCF, and the supernatants were collected for protein concentration analysis using the BCA assay.

3.9.3 Protein Concentration – BCA Assay

Protein concentrations were determined using the bicinchoninic acid (BCA) assay. Serial dilutions of the albumin standard (BSA) were prepared according to the manufacturer's instructions, from a stock solution of 2,000 µg/mL to a working concentration of 25 µg/mL. Working reagent (WR) was prepared by mixing reagents A and B at a 50:1 ratio. On a 96-well plate, 25 µL of each albumin dilution and sample (in triplicate) was pipetted, followed by the addition of 200 µL WR. The plate was shaken for 30 s and incubated at 37°C for 30 min. After cooling to RT, absorbance was measured at 562 nm using the Synergy HT Bio-Tek microplate reader. A standard curve prepared from BSA dilutions was used to calculate protein concentrations in the samples.

3.9.4 Protein Precipitation

Protein precipitation was performed using 10% trichloroacetic acid (TCA) at a 1:1 ratio. Samples were incubated on ice for 15 min, then centrifuged at 4°C at 15,700 RCF for 10 min. The supernatants were discarded, and pellets were washed twice with 0.5 mL of cold acetone, followed by centrifugation for 4 min at 4°C at 15,700 RCF. The pellets were then dried and

resuspended in 1.5× Sample Buffer (1.5× SB), followed by incubation at 55°C for 45 min with shaking at 1,300 RPM.

3.9.5 Electrophoresis

Protein separation was performed using SDS-PAGE with a 4% stacking gel and a 12% separation gel. Before loading, samples were heated to 95°C for 5 min. A total of 25 µg of protein was loaded per well. Wide Range Color Protein (10 – 250 kDa) was used as the protein ladder. Electrophoresis was performed in a running buffer, starting at 70 V and increasing to 150 V.

3.9.6 Membrane Transfer

Proteins separated on the gel were transferred onto a 0.2 µm polyvinylidene difluoride (PVDF) membrane. Before transfer, the membrane was activated in methanol for 2 min and rinsed in transfer buffer. The transfer sandwich was assembled in the following order: sponge, Whatman paper, membrane, gel, Whatman paper, sponge. The cassette was placed in the transfer apparatus, and the transfer was performed in transfer buffer at 210 mA for 2 h.

3.9.7 Antibody Labeling

After protein transfer, the membrane was washed with 1× TBST and blocked with 5% nonfat milk for 1 h at RT. Primary antibody incubation was performed either overnight at 4°C or for 1 h at RT, depending on the antibody. Secondary antibody incubation lasted 15 min, 30 min, 1 h, or 2 h at RT, depending on the antibody (the list of used antibodies is presented in Table 2.8).

3.9.8 Imaging

Proteins on membranes were visualized using an Enhanced Chemiluminescence (ECL) kit. The ECL solution was freshly prepared before use, applied to the membrane and incubated for 5 min at RT. Membranes were then placed in a developing cassette with X-ray film for an appropriate exposure time, depending on signal intensity. The films were subsequently developed, rinsed with water and fixed.

3.9.9 Membrane Stripping

For analyzing proteins with similar molecular weights, primary antibodies need to be stripped before re-incubation with the antibody:

- **Mild stripping:** Membranes were incubated twice with stripping buffer for 8 min at RT, washed three times with 1× TBST for 7 min, blocked for 30 min at RT and then re-probed with primary antibodies.
- **Strong stripping:** Membranes were incubated with strong stripping buffer at 50°C for 30 min, washed four times with 1× TBST for 5 min, blocked and processed as described above.
- **Secondary antibody deactivation:** When proteins had different sizes and primary antibodies were from different hosts, secondary antibodies were deactivated by incubating membranes in 10% NaN_3 for 20 min at RT, washed three times with 1× TBST for 5 min, blocked and then processed as above.

3.10 Gene Expression Analysis (RT-qPCR)

3.10.1 RNA Isolation from Cells

RNA isolation was performed for the following cell types: C3A, HepG2, SNU449, SNU475, hHs, and hHDPCs from donors (H37, H65, H72). Each vial contained 1×10^6 cells stored in stayRNA at −20°C. The cells were thawed on ice, washed with 1 mL of cold PBS and centrifuged (4°C, 5 min, 1,500 RCF).

For RNA extraction, the Total RNA Mini Plus kit was used. After centrifugation, the supernatant was discarded, and the pellet was resuspended in 400 µL of Fenozol, pipetted several times and vortexed for 5 s. Samples were then incubated for 5 min at 50°C in a thermomixer at 500 RPM. Next, 150 µL of ultrapure water was added, and the samples were vortexed for 15 s and incubated for 15 min at RT.

The mixture was centrifuged (15 min, 4°C, 13,400 RCF), and 400 µL of the supernatant was transferred to a new tube containing 400 µL of isopropanol. The sample was gently mixed by inverting the tube and then applied to a mini column, followed by centrifugation (1 min, 4°C, 13,400 RCF).

The mini column was transferred to a new tube, and 700 µL of washing solution A1 was added. The column was centrifuged (1 min, 4°C, 13,400 RCF). This washing step was repeated once. Next, 300 µL of solution A1 was added, and the column was centrifuged again (2 min, 4°C, 13,400 RCF).

Finally, the mini column was transferred to a fresh tube, 60 µL of ultrapure water was added, incubated for 2 min at RT and centrifuged (1 min, 4°C, 13,400 RCF). RNA concentration and purity were assessed using a NanoDrop One Spectrophotometer (Thermo Fisher Scientific, Waltham, Massachusetts, USA).

3.10.2 RNA Isolation from Liver Tissue

Following the manufacturer's protocol, RNA was isolated from tissue samples weighing 20–50 mg. Samples were placed in bead-beating tubes and supplemented with 800 µl of Fenozol. The total shaking time was 2 min, consisting of 20 s shaking intervals followed by 1 min of cooling on ice. Subsequently, the samples were incubated for 5 min at 50°C, after which 200 µl of chloroform was added and the tubes were mixed by gentle inversion.

The samples were then incubated for 3 min at RT and centrifuged for 10 min at 13,400 RCF. Approximately 450 µl of the supernatant was transferred to fresh tubes, combined with 250 µl of isopropanol, thoroughly mixed and loaded onto minicolumns. The columns were centrifuged for 1 min at 13,400 RCF.

Next, the minicolumns were placed in new collection tubes, and 700 µl of A1 washing solution was added, followed by centrifugation for 1 min at 13,400 RCF. This wash step was repeated twice. Subsequently, 200 µL of A1 washing solution was added to each minicolumn and centrifuged for 2 min at 13,400 RCF.

The minicolumns were transferred to fresh tubes, and 100 µl of ultrapure water was added. After a 3-minute incubation at RT, the samples were centrifuged for 1 min at 13,400 RCF. The resulting RNA preparations were stored at −20°C or −80°C until further use.

3.10.3 Reverse Transcription and cDNA Preparation

The conversion of isolated RNA into complementary DNA (cDNA) was performed using the Reverse Transcription Reagent iScript Advanced cDNA Synthesis Kit. For each sample, 1 µg of total RNA was used as a template for cDNA synthesis. The kit contains reagents such as dNTPs, oligo(dT) primers, random primers, reverse transcriptase, and an RNase inhibitor (the primers used in the study are listed in Table 2.9). According to the manufacturer's protocol, a reaction mixture containing commercial reagents and the RNA template was prepared, and cDNA synthesis was performed using the iCycler Thermal Cycler (Bio-Rad, Hercules, California, USA). The reaction program was as follows: incubation at 25°C for 5 min, reverse transcription at 46°C for 20 min, and enzyme inactivation at 95°C for 1 min. After

completion of the reaction, the samples were stored at 4°C and subsequently transferred to −20°C until further use.

3.10.4 Real-Time Detection of cDNA

According to the manufacturer's protocol, the RT-qPCR reaction mixture was prepared. The mixture consisted of SYBR Green Supermix, forward and reverse primers, nuclease-free water, and the cDNA template. After loading the samples onto a 96-well plate, the plate was sealed with a transparent film, vortexed for 30 s, and centrifuged at 4°C for 5 min at 4,500 RCF using an AFI LISA centrifuge (AFI Group, Château-Gontier, France). Subsequently, the plate was placed into the CFX96 Connected Real-Time PCR Detection System (Bio-Rad, Hercules, California, USA), and RT-qPCR analysis was performed. The thermal cycling program began with polymerase activation at 95°C for 2 min, followed by 40 cycles of denaturation at 95°C for 5 s and annealing at 60°C for 30 s.

3.11 hHDPCs Cultures Variants

3.11.1 Effect of Various Culture Media on hHDPCs Proliferation and Viability

Newly obtained human hepatocyte-derived proliferating cells (hHDPCs) were tested for proliferation in different culture media. For the experiment, cells at two passages (hHDPCs+3 and hHDPCs+8), derived from one donor (H65), were used. The following culture media were tested: DMEM, EMEM, William's E Medium (WEM), Hepatocyte Medium (HM), and Hepatocyte Medium supplemented with Hepatocyte Growth Supplements (HM+HGS). The detailed compositions of those media are provided in Table 3.1. After 6 days, cells were trypsinized and counted using the trypan blue exclusion method.

3.11.2 Long-Term Monitoring of Morphology and Proliferation of hHDPCs

The OLYMPUS Provi CM20 incubation monitoring system (demo version) was used to continuously observe cell growth directly in the incubator. This system enabled automated imaging of cultures at predefined positions, with images acquired every 4 hours from 5 observation fields per well (scale bar 200 µm). Additionally, the system automatically quantified the number of cells and culture confluency. For this experiment, the following cell types were used: LCIs derived from three donors (H40, H43, H74), C3A, HDFn, and

early-passage (+2) hHDPCs obtained from donor H74 [hHDPCs(H74)]. All cultures were conducted in 24-well plates coated with rat tail collagen type I. Two types of culture media were used: DMEM and HM+HGS. Cultures were maintained for 21 days. Medium exchange and sampling for further analyses were performed after 2, 6, 10, 13, 17, and 21 days of culture.

Complementary microscopic observations were also performed using an inverted fluorescence microscope Olympus IX71 (Olympus, Warsaw, Poland), equipped with the CS-S_MP-VF Multi Position module enabling image acquisition at the same positions within the culture vessels. Microphotographs were collected on days 3, 6, 8, 10, 13, 17, 20, and 21 of culture.

3.11.3 Mesenchymal Stem Cell Markers in hHDPCs

Human hepatocytes rapidly dedifferentiated into fibroblast-like cells after isolation. Because fibroblasts are cells of mesenchymal origin, it was verified to which cell type the hHDPCs are most closely related. For this purpose, protein markers specific and nonspecific for Mesenchymal Stem Cells (MSCs) were selected. CD29, CD73, and CD44 were used as positive MSC markers, whereas CD34, CD133, and CD45 were used as negative MSC markers (see Table 2.8). Flow cytometry was used to compare the production of MSC markers in different cell types. The following cell lines were used as a control: C3A, HDFn, Human Umbilical Vein Endothelial Cells (HUVEC), the neuroblastoma cell line SH-SY5Y, and hH_3. For each cell type, 2×10^5 cells per sample were seeded into T25 cm^2 culture flasks and cultured in media dedicated to the specified cell line. The compositions of the used media were presented in the Tables 3.1–3.3.

The experiment was conducted in three variants. In the first variant, the presence of MSC markers was analyzed in 11 consecutive passages of hHDPCs derived from a single donor (H37). In the second variant, MSC marker production was compared in hHDPCs obtained from three different donors (H37, H65, H72) at passages +2, +8, and +11. In the third variant, MSC marker expression was compared among six different cell types: hHDPCs, C3A, HDFn, hHs, HUVEC, and SH-SY5Y. In all cases, identical antibody concentrations were used independently of the cell type.

3.11.4 Re-differentiation of hHDPCs into Hepatocyte-like Cells Using Growth Factor-Supplemented Medium

In the course of this doctoral thesis, it was investigated whether hHDPCs can redifferentiate into hepatocyte-like cells in the presence of selected growth factors. For this purpose, hHDPCs derived from donor H72 were used at passages +2, +6, and +12. Cells were seeded at a density of 3×10^4 per well in 24-well plates.

Three variants of culture media were used, with their compositions presented in Table 3.5. The first medium variant was HM supplemented with FGF-4 and HGF (HM+F+H), the second contained HM supplemented with EGF and HGF (HM+E+H), and the third was the control medium consisting of HM without additional growth factors. The detailed compositions of media are presented in. The experiment was conducted for 21 days, with medium exchanges performed every 3–4 days, and samples were collected for subsequent analyses.

3.12 Characteristics of the Polysulfone Capillary Membranes

3.12.1 Scanning Electron Microscopy

Samples intended for scanning electron microscope (SEM) (Hitachi High-Technologies, Tokyo, Japan) were prepared according to standard procedures. Polysulfone capillary membranes were incubated in ethanol for 15 min, transferred to a dish containing liquid nitrogen, and fractured with a scalpel. Subsequently, the samples were dried at 80°C for 20 min. The SEM sample stage was prepared by attaching a graphite adhesive tape, and the membrane fragments were mounted in both vertical and horizontal orientations. A thin layer of gold was sputtered onto the samples using a sputter coater, and SEM imaging was then performed. The obtained SEM microphotographs were analyzed using the TM-1000 software.

3.12.2 Wettability Angle Measurements

Contact angle measurements were performed to determine the wettability of the membrane surface. The measurements were conducted using a DSA25 Krüss goniometer (Krüss Optronic, Hamburg, Germany). For the analysis, the fiber was fractured and the sample was placed on the measurement stage. A water droplet was dispensed using a microneedle. The software calculated the contact angle between the tangent to the droplet at the point of contact and the surface of the membrane. Contact angle measurements were used to determine membrane hydrophobicity. Hydrophilic surfaces are characterized by contact angles in the

range $0° < \theta < 90°$, whereas hydrophobic surfaces exhibit contact angles in the range $90° < \theta < 180°$. Measurements were taken at multiple locations on the fiber surface.

3.12.3 Ultrafiltration Measurements

Ultrafiltration measurements were performed to assess the permeability of the membrane capillaries. The procedure involved passing water through the module at a pressure of 100 hPa for 2 min. The permeate collected was then weighed, assuming that 1 g of water corresponds to 1 cm³. The ultrafiltration coefficient (UFC) of the membrane was calculated using Equation (8):

$$UFC = \frac{V}{A \cdot p \cdot T}, \tag{8}$$

where UFC is ultrafiltration coefficient [cm3/m2·hPa·min], V – volume of permeate [cm3], A – surface area [m2], p – pressure [hPa], and T – time [min].

3.12.4 Bovine Serum Albumin (BSA) Retention

Prior to the retention measurements, the bioreactors were rinsed with water for 15 min. A vacuum was applied to generate the retentate (solution retained by the membrane) and the permeate (solution passing through the membrane). A BSA solution at a concentration of 1 g/L was prepared, and the system was stabilized before use. The BSA solution was pumped through the system at a flow rate of 8 mL/min, with retentate and permeate collected simultaneously at the same flow rate. The absorbance of BSA was measured at 278 nm using a Hitachi U-3010 spectrophotometer (Hitachi High-Technologies, Tokyo, Japan), and a calibration curve was constructed to quantify the BSA concentration. Retention (R) was calculated using Equation (9):

$$R = \left(1 - \left(\frac{C_p}{C_o}\right)\right) \cdot 100\%, \tag{9}$$

where R – retention [%], C_p – BSA concentration in the permeate [g/L], C_o – BSA concentration in the retentate [g/L].

3.12.5 Membrane Cut-Off Determination

The membrane cut-off point was determined by performing retention experiments and analyzing the retentate using flow cytometry. Fluorescent polystyrene beads of different sizes were employed: 100, 200, and 500 nm beads with green fluorescence, and a mixture of 2 μm and 3 μm beads with red and green fluorescence. Initially, water was passed through the system, followed by bead suspensions. After 5 min of stabilization under vacuum, both retentate and permeate fractions were collected. The particle number in each fraction was quantified using a BD FACSCanto II flow cytometer.

3.12.6 Biocompatibility of the Polysulfone Membrane

Biocompatibility tests were performed using genetically modified C3A cells overexpressing enhanced green fluorescent protein (EGFP) (C3A_EGFP). Cells were cultured in standard DMEM supplemented with 10% FBS and 1% nonessential amino acids. Two experimental variants were performed:

1. **Conditioned Medium:** Membranes were incubated in culture medium, and the resulting conditioned medium was subsequently added to cell cultures.
2. **Direct Contact:** Cells were cultured directly with capillary membranes. Capillaries were cut into 1 cm fragments, sterilized, and incubated in PBS at RT for 24 h prior to use.

For the conditioned medium experiments, 100×1 cm membrane fragments were incubated with culture medium for 24 h at RT. Cells were seeded at a density of 0.2×10^5 cells per well in 1 mL of conditioned medium on 12-well plates.

For the direct contact experiments, 10×1 cm membrane fragments were incubated in PBS for 24 h at RT. Cells were seeded at the same density and volume as above, directly onto wells containing membrane fragments.

Both experiments were conducted for 3 days. Fluorescence microscopy was used to obtain microphotographs at 20× magnification (Olympus IX71, Warsaw, Poland).

3.13 Module Preparation

For testing cell cultures under dynamic conditions in this doctoral study, self-constructed hollow fiber bioreactors were used in cooperation with the Laboratory of Semi-Permeable Membranes and Bioreactors, IBBE PAS. First, bundles of capillary membranes were prepared, each consisting of 20 fibers, and tied with thread at both ends

(Figure 3.1A). The ends of the capillaries were melted at high temperature to prevent resin from entering the lumens (Figure 3.1B). The fiber bundle was placed inside an acrylic module housing. A mixture of two resin components, A and B, was prepared at a 3:1 ratio (Figure 3.1C). The components were thoroughly mixed and degassed in a vacuum dryer for several minutes to remove trapped air (Figure 3.1D).

Meanwhile, the mold for the module was prepared by lubricating its internal surfaces with grease. The capillary bundle was positioned inside the mold, which was then sealed. The mold containing the module was placed in a centrifuge and filled with resin (Figure 3.1E). Centrifugation was performed at 600 RPM for 2 h to ensure uniform resin distribution. After centrifugation, the module was removed from the mold and cured at 40°C for 24 h (Figure 3.1F, G). The following day, excess resin was trimmed from the module ends, and the integrity of the capillaries was examined under a magnifying glass to confirm that all lumens remained unobstructed (Figure 3.1H, I). The length of the capillaries within the module was then measured to calculate the total growth area. Finally, plastic caps were attached to both ends of the module, and the system was tested for tightness by passing compressed air through (Figure 3.1J).

The growth area (A) was estimated using the following Equation (10):

$$A = \pi \cdot d \cdot L \cdot n, \tag{10}$$

where A – capillaries surface in the module [mm^2], d – external diameter of the capillary [mm], L – length of the capillaries within the module (excluding the resin-covered sections) [mm], and n – number of the capillaries inside the module (here n = 20 for each bioreactor).

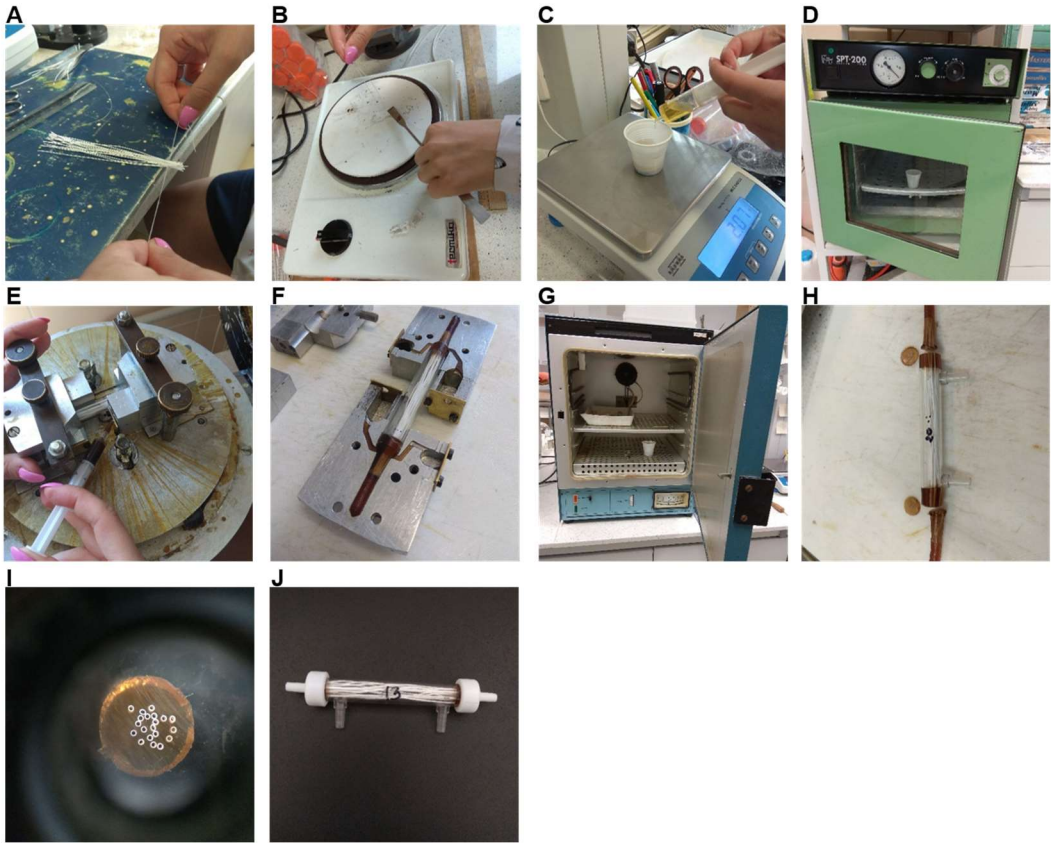


Figure 3.1. Steps in preparing a hollow fiber bioreactor. A) Capillary ends tied with a string. **B)** Capillary ends welded. **C)** Resin weighed. **D)** Degassing of the prepared resin mixture. **E)** Module filled with the resin mixture. **F)** Module after centrifugation. **G)** Module dried at 42°C for 24 h. **H)** Excess resin trimmed from module ends. **I)** Resin patch with capillaries, checked for capillary patency. **J)** Ready-to-use module.

3.13.1 Dynamic System – Preparation

To carry out cell culturing under dynamic conditions, an appropriate system was required. The system consisted of the following components: a peristaltic pump, tubing with connectors, a gas trap (oxygenator), the bioreactor, needles for collecting or draining fluid from the system, a needle with a filter for venting, and bottle containing fluid (PBS or culture medium) (Figure 3.2). After assembling and connecting all components, the apparatus was placed in an incubator (37°C, 5% CO_2), and the PBS was circulated through the system for 24 hours to stabilize it and check for leaks. The fluid flow rate was set at 10 mL/min. The next day, the PBS solution was replaced with culture medium in an open system. After connecting the culture medium, the system was ready to be seeded with cells.

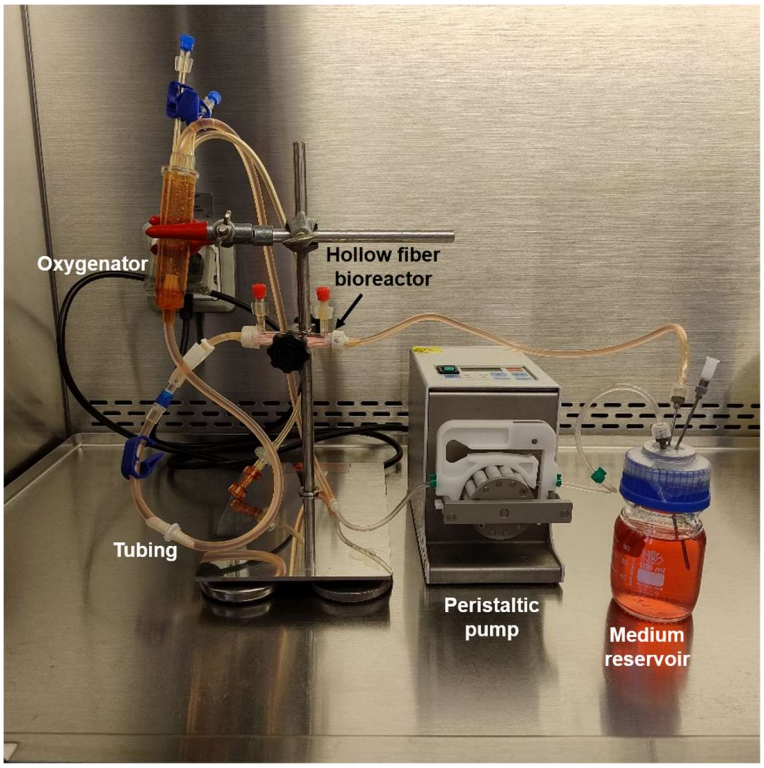


Figure 3.2. **System for dynamic culture.** The ready-to-use system contains of a hollow fiber bioreactor, a peristaltic pump, a medium reservoir, an oxygenator (bubble and gas trap), and the necessary tuning with connectors. The fluid flow rate was set at 10 mL/min.

3.13.2 Dynamic System – Cell Cultures

Both freshly thawed cells (hHs and LCIs) and cells previously cultured for several days (HepG2 and hHDPCs) were used in the experiments. Prior to seeding, all cells were counted using the trypan blue exclusion method.

In the dynamic culture system, cells were grown on the external surfaces of the capillaries. The appropriate number of cells was suspended in 3 mL of culture medium and introduced directly into the bioreactor through access ports in the module housing.

During the first hour after seeding, the module was rotated every 10 min to ensure uniform cell attachment across the entire capillary surface. Subsequently, the system was transferred to the incubator, and continuous fluid flow was initiated as described above. Approximately 120 mL of medium circulated through the closed-loop system throughout the culture period.

Dynamic cultures were maintained for 12 days. Samples of culture medium were collected on days 2, 5, 7, 9, and 12 for further analysis. As a control, parallel cell cultures were maintained under static conditions in T25 culture flasks (surface area 25 cm^2, comparable to the total surface area available inside the bioreactor). For cultures of commercially available hHs and LCIs, culture vessels were additionally coated with rat tail collagen type I.

3.13.3 Dynamic System – Sample Analysis

3.13.3.1 Albumin Production (ELISA)

Albumin production in the post-culture medium was determined for both dynamic and static cultures using ELISA. Samples from cancer cell line cultures (HepG2) and hHs, LCI(H43, H74, H37, H72), and hHDPCs were analyzed. For HepG2 and hHs cells, the culture media samples were diluted prior to measurements, whereas undiluted medium was used for hHDPCs and liver cell isolate samples. Media samples collected on days 2, 5, 7, 9, and 12 of culture were used for further evaluation.

3.13.3.2 Urea Production

Urea concentration in the culture medium was determined using the commercial QuantiChrom Urea Assay Kit, according to the manufacturer's instructions. Measurements were performed in a 96-well plate, with 50 µL of each sample added in duplicate to individual wells. To complete the reaction, 200 µL of the WR prepared by mixing Reagents A and B in a 1:1 ratio was added to each well. The plate was incubated for 50 min at RT, and absorbance was measured at 430 nm using a Synergy HT spectrophotometer.

4 Results

4.1 Isolation of Human Hepatocytes from Resected Liver Fragments and Liver Lysate Culture Variants

4.1.1 Quantitative Analysis of Liver Cell Isolation

Isolation of liver cells from resected human liver fragments was performed using the method developed at the LTE, BBE PAS [153]. A total of 41 cell isolations were carried out from 30 donors during the course of the doctoral study. Following isolation, the cells seeded onto culture plates were observed to form structures resembling islands, a characteristic colony of hepatocytes. Based on these observations, it was assumed that the cell islands, composed of polygonal-shaped cells, represented hepatocytes; however, this assumption required further confirmation through additional studies.

Table 3.12 summarizes the liver samples obtained from 30 patients from whom cells were isolated, including age, gender, diagnosed diseases, treatments applied, presence of cell island formation, and the type of collagenase used for tissue digestion. Among the 30 donors, 8 (27%) had undergone chemotherapy, 4 (13%) had steatosis, 2 (7%) - diabetes, 22 (73%) -cancer or metastases, and 5 (17%) were healthy donors.

After each liver tissue isolation, the following parameters were determined: isolation yield (Y) and cell viability (V). To calculate these parameters, the weight of the liver fragments used for isolation was also recorded. The detailed methods of calculation are described in section 3.2.2. Table 4.1 presents the mean values of these parameters for 30 liver donors: 14 isolations were performed for female donors and 16 for male donors. For female donors, the isolation yield was about 17% lower than for male donors, while the average donor age and liver tissue mass were similar between the two groups (no statistically significant differences were observed for isolation yield, liver tissue mass, or donor age). In contrast, cell viability differed significantly: viability in female donors was 96%, whereas in male donors it was 89% ($p < 0.05$).

Table 4.1. Average values of donor age, isolation yield, liver tissue mass, and cell viability were calculated for 30 hepatocyte donors.

	Donor age [years]	Liver tissue mass (*LTM*) [g]	Isolation yield (*Y*) [$\times 10^6$ live cells/g tissue]	Cell viability (*V*) [%]
Mean value±SD (n = 30)	57 ± 14	57.33 ± 61.49	1.68 ± 2.36	92 ± 8
Female (n = 14)	56 ± 11	54.99 ± 34.53	1.51 ± 1.50	96 ± 5
Male (n = 16)	57 ± 17	59.39 ± 79.16	1.82 ± 2.96	89 ± 9*

*$p<0.05$ for the comparison of cell viability (*V*) after isolation from female versus male donors. Statistical analysis was performed using one-way ANOVA followed by Duncan's *post-hoc* test. All results in the Table are presented with ±SD of the mean.

Table 4.2 presents a comparison of isolation yield (*Y*) and cell viability (*V*), along with donor age and organ weight (LTM), for donors classified by sex and chemotherapy. The table also provides data for the above-mentioned parameters divided according to the presence of cancer and the use or absence of chemotherapy. In addition, results obtained from healthy organ donors are included.

When comparing patients treated with chemotherapy with those who were not treated, isolation efficiency values were comparable in both groups. A similar pattern was observed for cell viability, with identical results of 92% in both groups. However, when sex was taken into account, among women who received chemotherapy, isolation efficiency was 1.1-fold lower than in women who were not treated, while cell viability was comparable and remained at a very high level (approximately 95%). In contrast, among men, the trend in isolation efficiency was reversed: patients who received chemotherapy had a 1.2-fold higher isolation efficiency than those who were not treated with chemotherapy. Cell viability in these two male groups was comparable and remained high (approximately 88%), although it was lower than that observed in women.

Isolation efficiency in patients diagnosed with cancer and treated with chemotherapy was 1.3-fold higher than in cancer patients who were not treated with chemotherapy. Cell viability after isolation was similar in both groups, reaching approximately 91%.

In healthy donors, when results were compared by sex, women had a 1.4-fold higher isolation efficiency than men. Cell viability was also higher in women by 6% (98%). The mean age of donors of both sexes was comparable. Notably**,** tissue fragments obtained from female

donors were, on average, three times larger than those obtained from male donors, which may affect the isolation parameters.

Table 4.2. Average values of donor age, liver tissue mass, isolation yield, and cell viability with respect to donor gender, cancer/metastases presence, chemotherapy treatment, or healthy donors.

	Donor age [years]	Liver tissue mass (LTM) [g]	Isolation yield (*Y*) [$\times 10^6$ live cells/g tissue]	Cell viability (*V*) [%]
Chemotherapy				
Mean value±SD				
Yes (n = 8)	63 ± 13	41.07 ± 23.83	1.70 ± 1.20	92 ± 10
No (n = 22)	54 ± 14	63.25 ± 69.96	1.67 ± 2.69	92 ± 8
Female				
Yes (n = 5)	61 ± 13	97.78 ± 7.48	1.43 ± 1.23	95 ± 7
No (n = 9)	53 ± 8	96.32 ± 3.96	1.56 ± 1.68	96 ± 4
Male				
Yes (n = 3)	65 ± 14	29.38 ± 11.03	2.14 ± 1.10	88 ± 15
No (n = 13)	55 ± 17	66.31 ± 86.81	1.74 ± 3.28	89 ± 8
Cancer with chemotherapy (n = 8)	63 ± 13	41.07 ± 23.38	1.70 ± 1.20	92 ± 10
Cancer without chemotherapy (n = 14)	57 ± 14	48.38 ± 56.90	2.18 ± 3.26	91 ± 8
Healthy donors				
Mean value±SD (n = 5)	54 ± 14	70.98 ± 43.48	1.04 ± 0.62	96 ± 5
Female (n = 3)	56 ± 6	97.33 ± 30.04	1.17 ± 0.79	98 ± 0
Male (n = 2)	51 ± 27	31.45 ± 23.41	0.84 ± 0.40	92 ± 8

Table 4.3 presents the isolation parameters (donor age, liver tissue mass, isolation yield, cell viability), including the donor's sex, the cell's ability to form islands, and the influence of chemotherapy on cell islands formation. For specimens obtained from female donors, cell isolation yield was 20% lower when the cells formed islands in culture than when they did not form islands. In this group, the liver tissue mass was nearly twice as high, and the donor age was 22 years higher compared with donors whose cells did not form islands. However, the cell

viability was similar in both groups. For male donors, the isolation yield for island-forming cells was approximately 43% lower than for non-island-forming specimens. Moreover, the male donors in the island-forming group were 12 years younger, and their average liver tissue mass was nearly 60% higher than in the non-island-forming group. The cell viability was similar in both groups.

Regarding the influence of chemotherapy on the ability of cells to form islands (Table 4.3), the highest isolation yield (2.48×10^6 live cells/g tissue) and highest cell viability (98%) were obtained in the group with chemotherapy present (marked Yes) and no island formation (marked No) - Yes/No subgroup. The average liver tissue mass in this group was approximately 43 g, and the average donor age was 52 years. In the donor group without chemotherapy and without island formation (No/No subgroup), the isolation yield was 13% lower than in the Yes/No subgroup. Cell viability was 87%, the average donor age was 61 years, and the liver tissue mass was nearly 30 g. In the subgroup without chemotherapy but with the island-forming cell (No/Yes subgroup), the isolation yield was 58% lower than in the Yes/No subgroup. Cell viability was 93%, and cells were isolated from tissue fragments weighing approximately 84 g, with an average donor age of 52 years. Finally, in the subgroup with chemotherapy and island-forming cells (Yes/Yes), the lowest isolation yield was observed (50% lower than for the Yes/No subgroup). The cell viability was 89%, tissue mass averaged 40 g, and this group included the oldest donors (69 years on average).

Table 4.3. Average values of donor age, liver tissue mass, isolation yield, and cell viability, including the ability to form cell islands by donor gender and the impact of chemotherapy on island formation.

Groups and subgroups	Donor age [years]	Liver tissue mass (LTM) [g]	Isolation yield (*Y*) [$\times10^6$ live cells/g tissue]	Cell viability (*V*) [%]
Ability to form cell islands				
Female				
Yes (n = 10)	61 ± 8	63.40 ± 34.92	1.41 ± 1.69	96 ± 5
No (n = 4)	44 ± 6	33.98 ± 26.12	1.76 ± 1.02	95 ± 6
Male				
Yes (n = 9)	52 ± 20	82.00 ± 100.8	1.37 ± 2.62	88 ± 9
No (n = 7)	64 ± 10	30.30 ± 19.4	2.40 ± 3.48	89 ± 10

Influence of chemotherapy treatments on forming cell islands				
Chem*/Isl**				
Yes/Yes (n = 5)	69 ± 6	39.68 ± 23.31	1.23 ± 0.99	89 ± 12
Yes/No (n = 3)	52 ± 15	43.38 ± 26.34	2.48 ± 1.26	98 ± 3
No/Yes (n = 14)	52 ± 15	83.81 ± 80.44	1.45 ± 2.43	93 ± 6
No/No (n = 8)	61 ± 12	29.39 ± 18.84	2.15 ± 3.48	87 ± 9

*Chem – Chemotherapy

**Isl – Islands

Among the liver cell isolations performed, 19 (63%) were successful, while 11 (37%) did not result in colony formation. Figure 4.1 presents the number of liver cell isolations, along with information about the donors' gender and whether the isolated cells did or did not form cell islands after isolation. Sixteen isolations were performed from male donors, and in half of these cases, the isolated cells formed islands, while in the second half, they did not. For female donors, the distribution differed: among the 14 isolations performed, cell islands were obtained in 10 cases (71%).

Considering all cell isolations, Table 4.4 presents the proportions of isolations from female and male donors and indicates whether the isolated cells formed islands. The highest percentage (33%) was recorded for island-forming cells from female donors, whereas the absence of island formation among female donors accounted for 13%. Among male donors, both island-forming and non-island-forming cells accounted for 27% each.

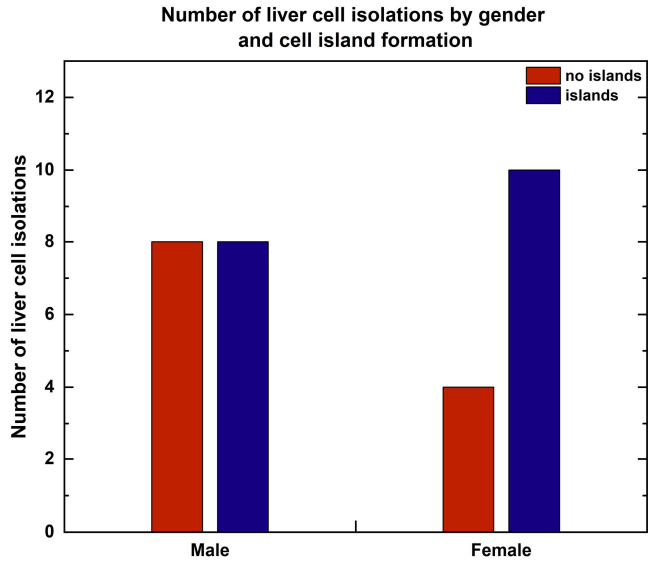


Figure 4.1. Distribution of liver cell isolations by sex and cell island formation. The total number of liver donors was 30. Sixteen isolations were carried out for male donors and fourteen for female donors.

Table 4.4. Percentage and total number of isolations showing or not showing hepatocyte island formation, by patient sex and age group.

	Islands (subgroup Yes)		No islands (subgroup No)		
	Female (F)	**Male (M)**	**Female (F)**	**Male (M)**	**Total**
Sum	10	8	4	8	30
%	**33**	**27**	**13**	**27**	**100**
F+M islands [%]	**60**				
F+M no islands [%]			**40**		

Another approach to presenting the statistics of cell isolations involved dividing the isolations by donor age group and determining whether the cells formed cell islands (Figure 4.2). The highest number of liver cell isolations – 13, was performed in middle-aged donors (46–65 years). The results showed that cell islands were formed in samples obtained from 8 of these isolations, representing 62% of this group. For young donors (18–45 years), 7 cell isolations were performed, and in 4 (57%), the cells formed islands. In the oldest donor group (66–99 years), 10 liver cell isolations were performed, and cells from 6 isolations formed islands (60%).

Table 4.5 presents the percentage distribution of hepatocyte island formation according to donor sex and age group. The results indicate that, in the youngest age group, 43% of cells isolated from female donors did not form islands, whereas 57% of those from male donors did. In the middle-aged group, 54% of cell isolations from female donors resulted in island formation, while only 8% did not. For male donors, the trend was reversed: 8% of isolations resulted in island formation, whereas 31% did not. In the oldest donor age group, 30% of cells isolated from female donors formed islands, and no cases were recorded in which the cells failed to form islands. Among male donors in this group, 30% of isolations resulted in island formation, whereas 40% did not.

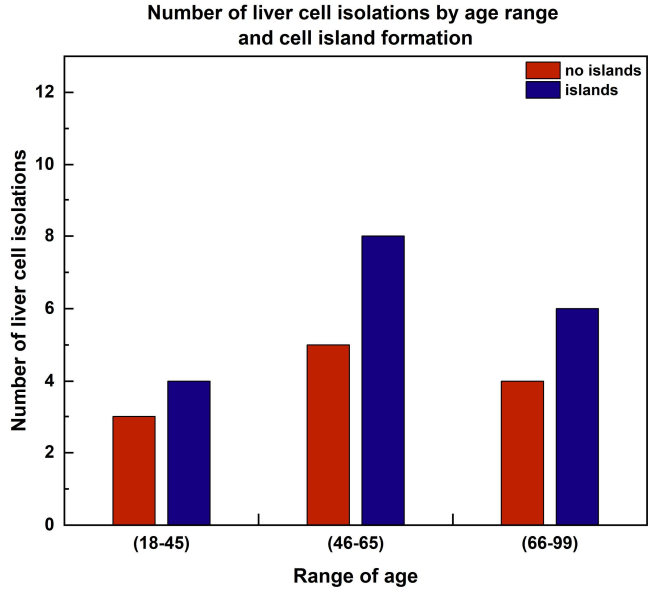


Figure 4.2. Distribution of liver cell isolations by donor age group and cell island formation. The results were divided into three age ranges: young donors (18–45 years), middle-aged donors (46–65 years), and older donors (66–99 years). The total number of liver donors was 30, including 7 cell isolations from young donors, 13 from middle-aged donors, and 10 from older donors.

Table 4.5. Percentage and total number of isolations showing or not showing hepatocyte island formation, by patient sex and age group, calculated for each age group.

	Islands present (subgroup Yes)		Islands absent (subgroup No)		
Age range	**Female (F)**	**Male (M)**	**Female (F)**	**Male (M)**	**Total**
18-45	0	4	3	0	7
%	**0**	**57**	**43**	**0**	**100**
46-65	7	1	1	4	13
%	**54**	**8**	**8**	**31**	**100**
66-99	3	3	0	4	10
%	**30**	**30**	**0**	**40**	**100**

Another way to present the distribution of liver cell isolations was by comparing the number of isolations performed using different types of digestive enzymes (collagenases) and assessing whether the isolated cells formed cell islands (Figure 4.3 and Table 4.6). The total number of donors was 30; however, some tissue samples were partially divided, and different types of collagenases were used for the isolations, resulting in a total of 41 cell isolations. The highest number of liver cell isolations (13) was performed using collagenase type II; cell islands were observed in 9 isolations (69%), whereas in 4 isolations (31%), the cells did not form islands. In the case of collagenase type D use, a high number of island-forming cells was observed in cell cultures, with islands present in 4 out of 5 isolations (80%). Favorable results were obtained in isolations performed with the commercial collagenase mixture (types I and II), known as Liberase, where islands formed in two out of four isolations (50%); similar to

cultures obtained using collagenase type I. When collagenase type XI was used, island formation occurred in two out of three isolations (67%). For the collagenase mixtures (I+II), (II+D), and (I+II+XI), islands were observed in 2 out of 3 isolations (67%). For the use of mixtures (II+XI), (I+II+D), one isolation was performed for each, and in both cases, the cells formed islands. Finally, for the use of mixture (I+II+D+XI), only one isolation was performed, and island formation was not observed (Figure 4.3).

Cell isolations that resulted in the formation of cell clusters constituted 22% of all 41 isolations performed using collagenase type II, while those in which no clusters were formed accounted for 10%. In the case of isolations conducted with collagenase type D, 10% led to the formation of cell colonies, whereas 2% did not, across all 41 isolations performed. For the remaining collagenases or collagenase mixtures used, isolations that resulted in either the formation or absence of cell clusters represented less than 5% for each variant in relation to the total number of isolations.

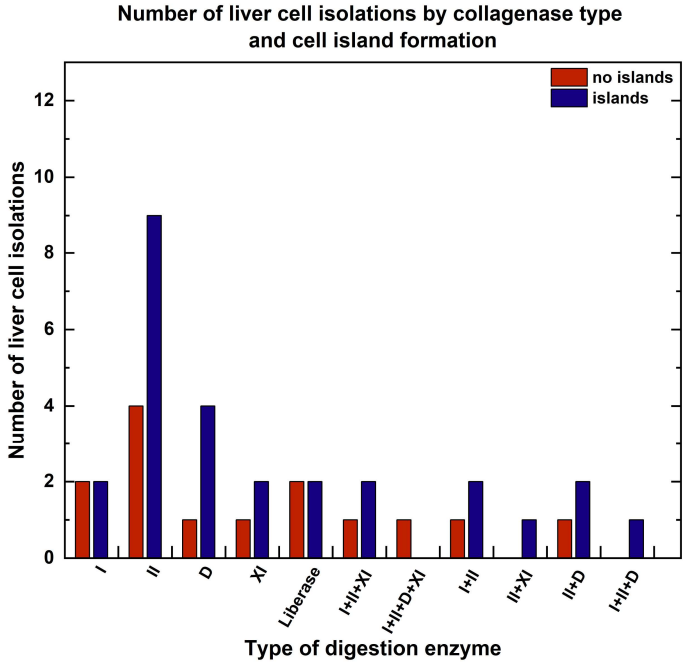


Figure 4.3. Distribution of liver cell isolations by type or mixture of digestive enzymes and cell island formation. In total, 41 liver cell isolations were performed using various collagenases: type I (4 isolations), type II (13 isolations), type D (5 isolations), and type XI (3 isolations). The commercial Liberase preparation was used for 4 isolations. For the enzyme mixtures, the numbers of isolations were as follows: (I+II+XI) – 2; (I+II+D+XI) – 1; (I+II) – 3; (II+XI) – 1; (II+D) – 3; (I+II+D) – 1.

Table 4.6. Percentage and total number of isolations with or without hepatocyte island formation, by type or mixture of digestive enzyme.

	Islands		Number of isolations	Percentage of isolations for digestion enzyme		Percentage of all isolations	
Enzyme type	Present	Absent		Present [%]	Absent [%]	Present [%]	Absent [%]
I	2	2	4	50	50	5	5
II	9	4	13	69	31	22	10
D	4	1	5	80	20	10	2
XI	2	1	3	67	33	5	2
Liberase	2	2	4	50	50	5	5
I+II+XI	2	1	3	67	33	5	2
I+II+D+XI	0	1	1	0	100	0	2
I+II	2	1	3	67	33	5	2
II+XI	1	0	1	100	0	2	0
II+D	2	1	3	67	33	5	2
I+II+D	1	0	1	100	0	2	0
Sum	**27**	**14**	**41**			**66**	**34**

4.1.2 Cell Islands and Culture Conditions

During culture of liver-isolated cells, microphotographs were taken to document morphological changes in the cells, caused by dedifferentiation, division, or cell death. Cell morphology varied depending on the culture medium and growth surface used. Observation of isolated cell cultures revealed that the number of cell islands ranged from 1 to 12 per well. Moreover, differences in island size were observed, with some islands being smaller and others larger. In some cases, the cell islands were observed after 24 h from isolation, while in others, after a few days of culture.

From the liver sample designated LCI(H53), cells were isolated using collagenase type I and cultured with DMEM or WEM. The results showed that cells forming islands in DMEM were more flattened, resulting in larger island structures than those cultured in WEM. Moreover, the size of cell islands was observed to change during culture. Micrographs taken one day after isolation were captured at 10× magnification, while those from subsequent days were taken at 6.4× (Figure 4.4). Cell islands also differed in the number of cells per island in DMEM, an island consisted of approximately 133 cells (Figure 4.4A), whereas in WEM, an island comprised about 63 cells (Figure 4.4B).

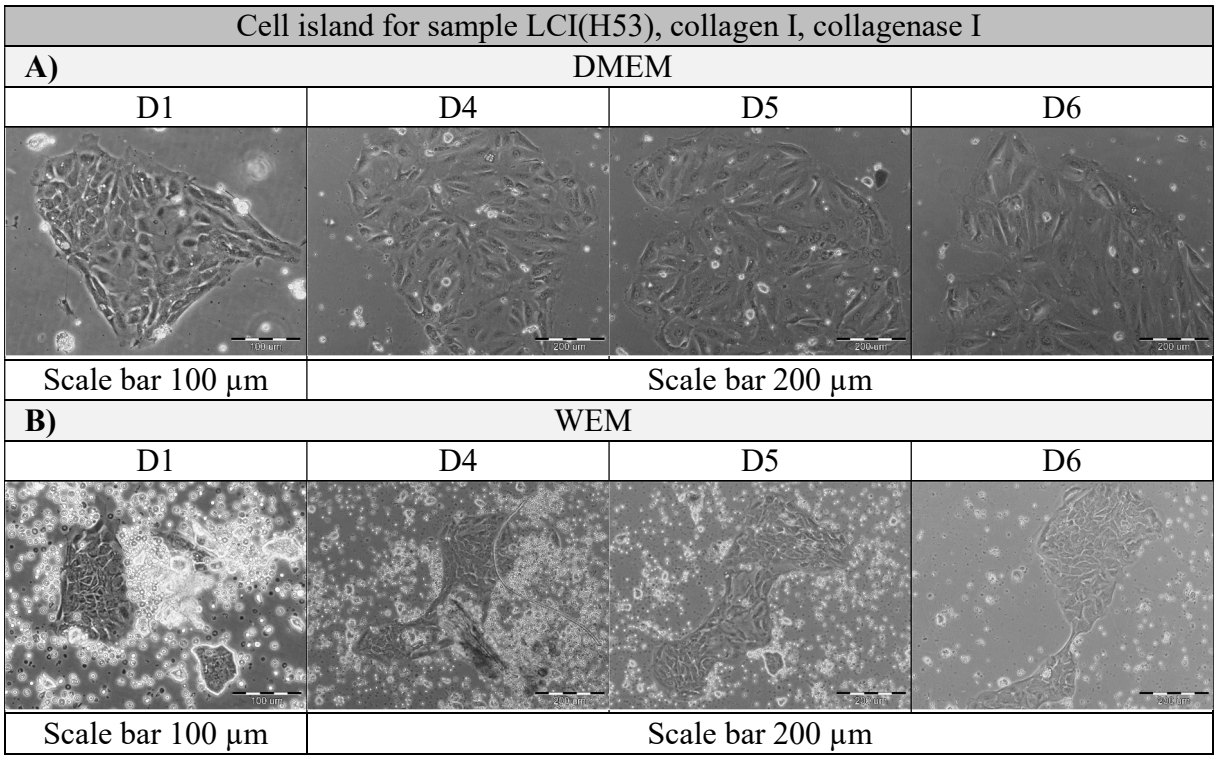


Figure 4.4. Representative images showing morphological changes in cell islands obtained from liver tissue specimen H53 [LCI(H53)]. Cells were isolated using collagenase type I. Observations were performed for six days. Cells were seeded at a density of 0.5×10^6 cells per well on 24-well plates coated with rat tail collagen type I. Cultures were conducted in DMEM or William's E medium (WEM). Microphotographs were taken using an Olympus IX71 fluorescence microscope at 10× or 6.4× magnification. **A)** Cells cultured in DMEM; scale bar: 100 µm (day 1) and 200 µm (subsequent days). **B)** Cells cultured in William's E medium; scale bar: 100 µm (day 1) and 200 µm (subsequent days).

Cells isolated from another liver donor, LCI(H72), using a mixture of collagenases (I+II+XI), were cultured on plates coated with collagen type I in two different media: HepatoZYME-SFM (HZ) and Hepatocyte Medium supplemented with HGS (HM+HGS). Distinct cellular behaviors were observed depending on the medium. In HZ medium, no cell islands were visible one day after isolation, but they appeared on the second day. After five days of culture, the cells began detaching from the surface, and further observations were discontinued (Figure 4.5A). In contrast, cells cultured in HM+HGS medium retained visible islands after 5 days, and by the seventh day, an increased number of cells exhibiting hepatocyte- and fibroblast-like morphology was observed. By the tenth day of culture, cell division was evident, and the cell morphology predominantly shifted from polygonal, hepatocyte-like, toward spindle-shaped, fibroblast-like cells (Figure 4.5B).

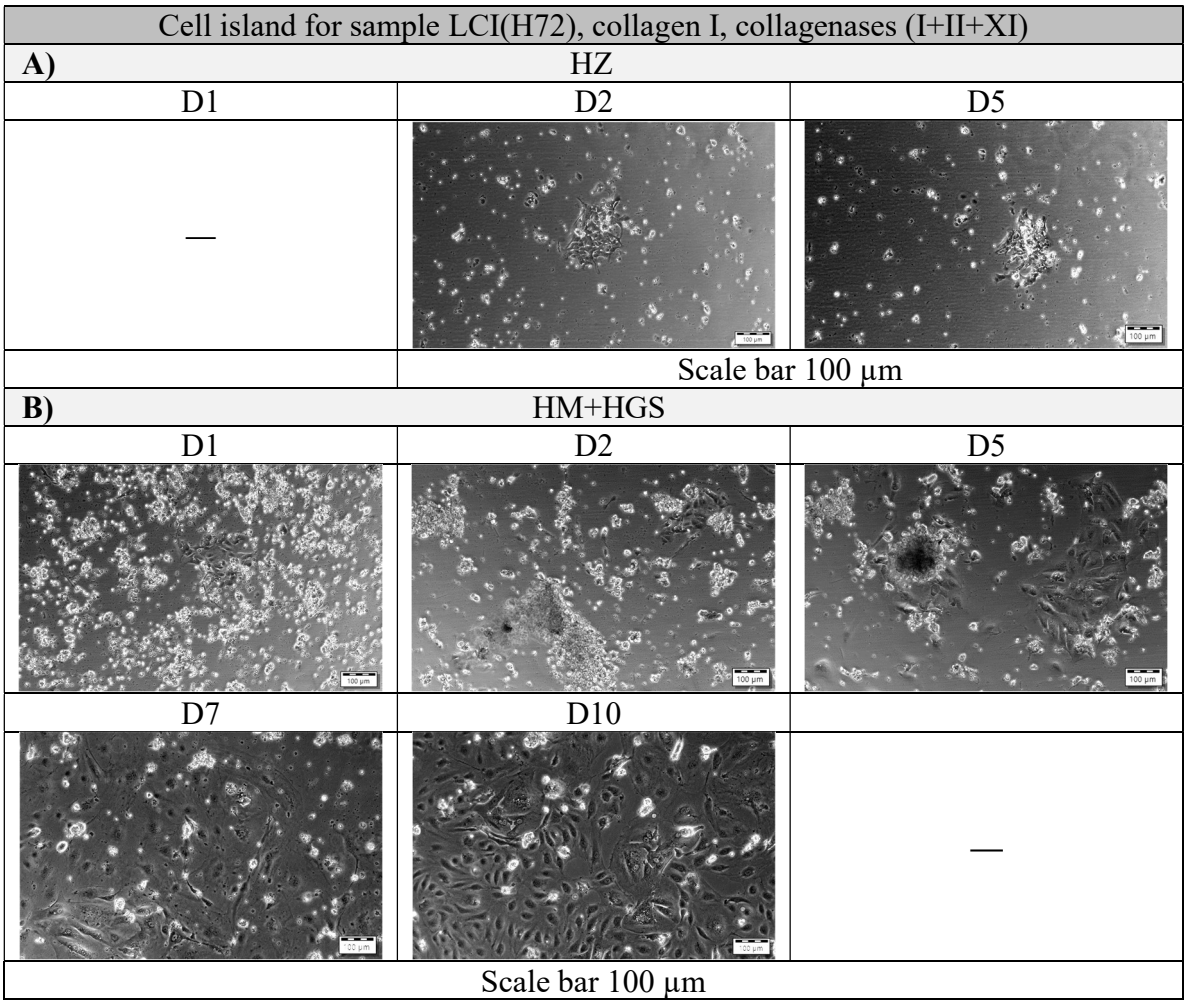


Figure 4.5. Representative images showing changes in the morphology of cell islands from liver sample H72 [LCI(H72)]. Observations were carried out for up to 10 days. Cells were seeded at a density of 0.5×10^6 cells per well on 24-well plates coated with rat tail collagen type I and cultured in either HZ or HM+HGS medium. Microphotographs were taken using an Olympus IX71 fluorescence microscope at 10× magnification. **A)** Cells isolated with collagenases (I+II+XI) and cultured in HZ medium (images taken after 2 and 5 days; scale bar: 100 µm). **B)** Cells isolated with the same enzyme mixture and cultured in HM+HGS medium (images taken after 1, 2, 5, 7, and 10 days; scale bar: 100 µm).

Another example of cell islands formation refers to another liver donor, LCI(H74). During isolation, the commercially available Liberase enzyme was used for tissue digestion. Notably, the first islands were observed only after 6 days of culture. The culture was subsequently monitored for 13 days, during which phenotypic changes toward fibroblast-like cells and active cell division were observed (Figure 4.6).

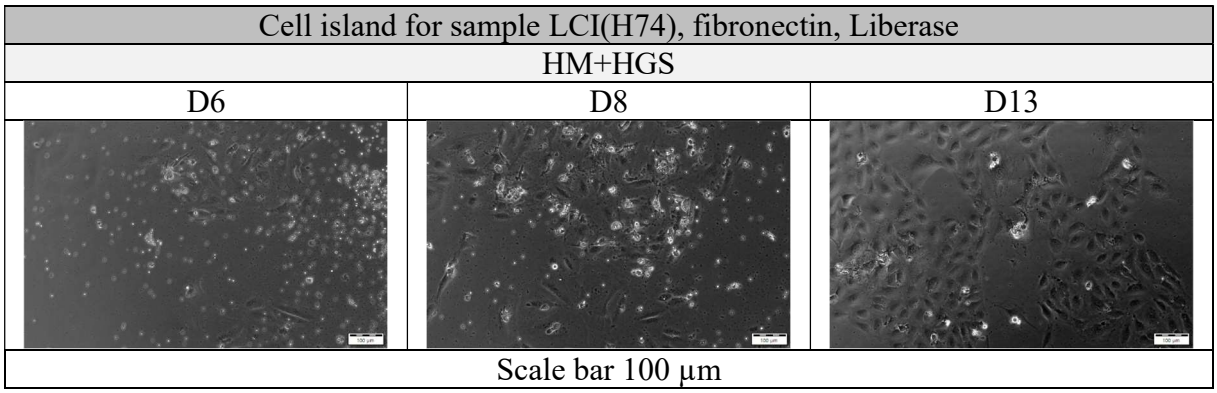


Figure 4.6. R**epresentative images showing morphological changes in cell islands isolated from liver tissue specimen H74 [LCI(H74)].** Observations were performed for 13 days. Cells were isolated using Liberase, seeded at a density of 1×10^6 cells per well on 24-well plates coated with fibronectin, and cultured in HM+HGS medium. Microphotographs were taken using an Olympus IX71 fluorescence microscope at 10× magnification. Scale bar: 100 μm.

4.1.3 Summary of the isolation conditions

Data on the conditions for hepatocyte isolation from liver tissue and their ability to form islands are presented in graphs illustrating the conditions most favorable for hepatocyte culture (Figure 4.7). The effects of different growth culture surfaces (collagen, fibronectin, drHDFn) and culture media (DMEM+FBS, DMEM-FBS [DMEM without FBS], HM+HGS, WEM+FBS, WEM-FBS) on island formation were analyzed.

The highest island formation was observed in cultures grown on collagen with HM+HGS medium, followed by cultures grown on both DMEM variants. The lowest island formation was observed in collagen-based cultures supplemented with both of the WEM medium variants. In cultures grown on drHDFn, the rate of island formation was similar across all tested media, including DMEM+FBS, WEM+FBS, and WEM-FBS. However, the island formation rate under these conditions was approximately 2-fold lower than that observed in collagen-based cultures. Cultures grown on fibronectin were evaluated using three media types (DMEM+FBS, DMEM-FBS, and HM+HGS). In this case, the highest island formation rate, approximately twice as high, was observed in cultures supplemented with DMEM+FBS compared to HM+HGS, whereas no island formation was detected in cultures maintained in DMEM without FBS (Figure 4.7A).

A comparison of island formation rates and isolation efficiency across different media types is presented in Figure 4.7B. The highest isolation efficiency of liver cells was observed in cultures supplemented with WEM+FBS; however, the island formation rate for this condition was not the highest. The highest island formation rate was obtained in cultures with WEM-FBS, although the isolation efficiency under these conditions was 1.3-fold lower. Both

DMEM+FBS and DMEM-FBS exhibited comparable isolation efficiencies and island formation coefficients. In contrast, the lowest isolation efficiency and islands formation coefficient were observed for cultures maintained in HM+HGS medium.

Comparison of island formation rates with cell viability demonstrated that cell viability exceeded 90% for all tested media, ranging from 90% to 96%. The lowest cell viability (90%) and the lowest island formation rate were observed in cultures grown in HM+HGS medium. Conversely, the highest cell viability (96%), together with an intermediate island formation rate, was obtained in cultures supplemented with DMEM-FBS (Figure 4.7C).

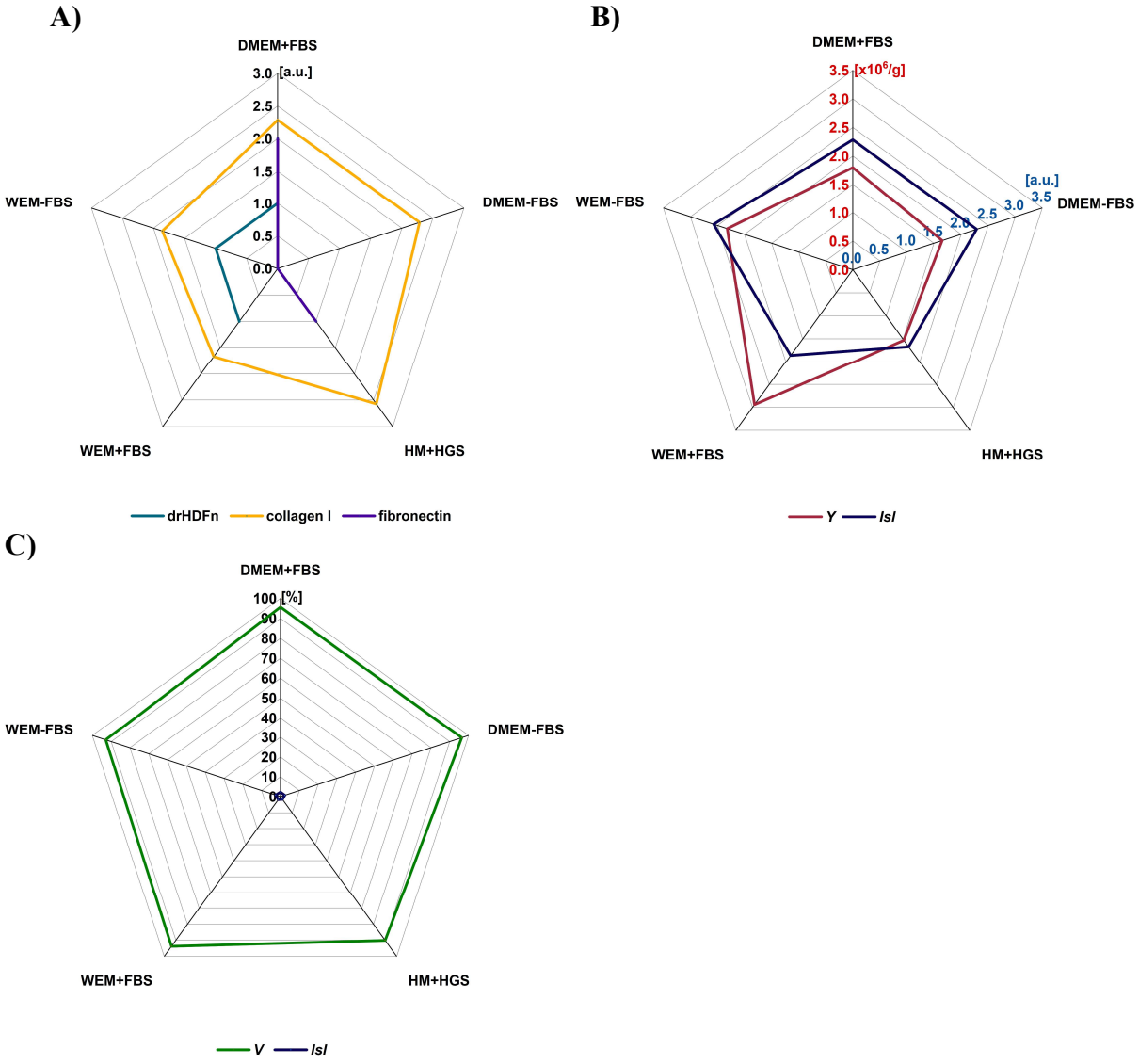


Figure 4.7. Summary of optimal conditions for hepatocyte culture. Isolated liver cells were cultured in various media, including DMEM supplemented or not with FBS (DMEM+FBS, DMEM-FBS), WEM supplemented or not with FBS (WEM+FBS, WEM-FBS), and HM+HGS. **A)** Comparison of cells cultured under different culture conditions, including culture media and growth surfaces (collagen type I, fibronectin, and drHDFn [dried human fibroblasts]), with respect to cell island formation. **B)** Comparison of cell island (*Isl*) formation rates across different media types and isolation efficiency (*Y*). **C)** Comparison of cell island (*Isl*) formation rates in cultures grown in different media with cell viability (*V*).

4.1.4 Detection of Albumin Production by Cell Islands – Immunocytostaining

To confirm the presence of hepatocytes in the liver isolates and their ability to form cell islands, immunocytostaining with an antibody detecting human albumin was performed. Albumin is localized in the cytoplasm of hepatocytes. Twenty-four and forty-eight hours after cell isolation from two different liver donors (H58 and H67, respectively), albumin detection was carried out (Figure 4.8A and B). Commercially available human hepatocytes (hH_2) were used as a positive control and analyzed after two days of culture (Figure 4.8C). Green fluorescence in the cytoplasm confirmed albumin production by both isolated liver cells and control hepatocytes.

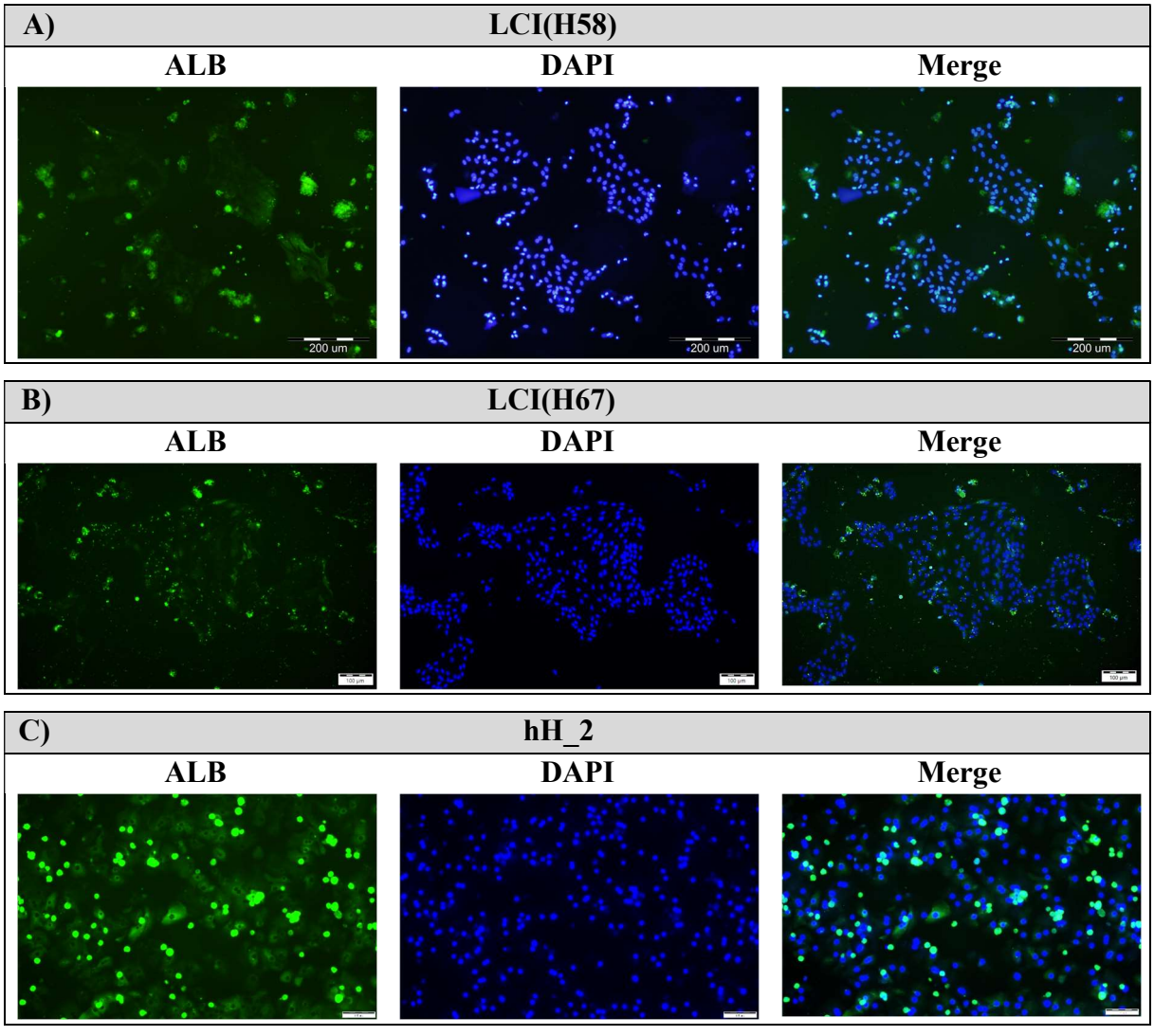


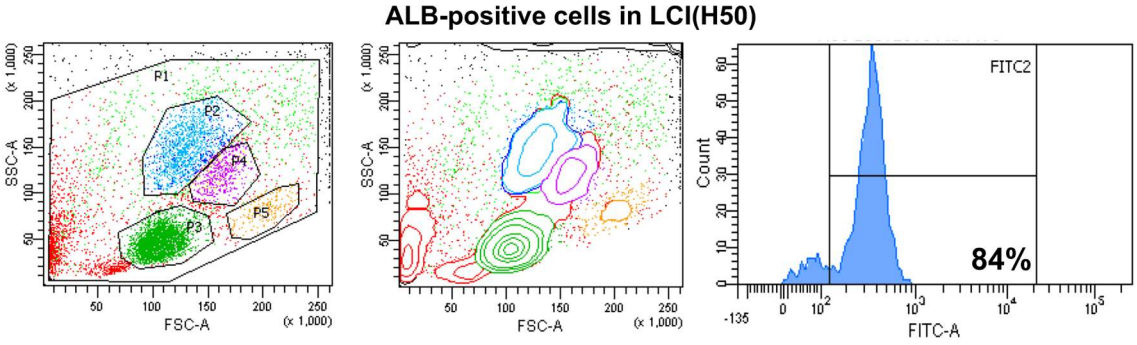
Figure 4.8. Images of immunocytostained cells producing albumin. Cells were seeded at densities of 0.5×10^6 (LCIs) and 0.15×10^6 (hH_2) per well on 24-well plates coated with rat tail collagen type I. Cells were labeled with FITC-conjugated anti-human albumin antibody (green), and nuclei were stained with DAPI (blue). **A)** Immunocytostaining of LCI(H53), performed 24 h after isolation. **B)** Immunocytostaining of LCI(H67), performed 48 h after isolation. **C)** Immunocytostaining of hH_2, performed after 48 h of culture. Microphotographs were taken using an Olympus IX71 fluorescence microscope at 10× magnification. Scale bar: 100 µm.

4.1.5 Flow Cytometric Detection of Human Hepatocytes in Isolates

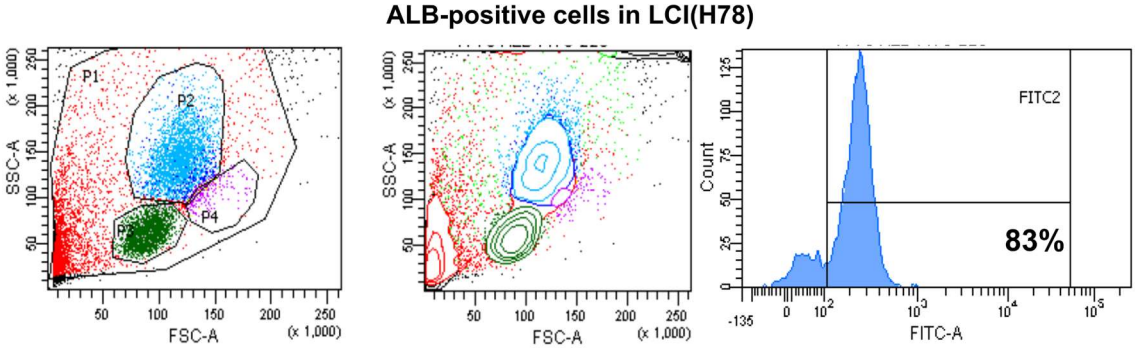
After isolating cells from liver tissue, they were subjected to flow cytometric analysis, which revealed differences in the distribution of cell populations among samples derived from different patients. This finding confirms the presence of various liver cell types in the isolates following tissue digestion. Figure 4.9 presents representative distributions of cell populations for samples LCI(H50 and H78) and hHs. In this study, the analysis focused on identifying the hepatocyte population; other cell types were not characterized.

The results presented in Figure 4.9 demonstrate that, depending on the tissue origin, different populations of isolated cells were obtained. Hepatocytes were detected within population 2 (P2) in sample LCI(H50). Among five distinct populations, albumin protein expression was observed exclusively in P2, as shown in the dot, contour, and histogram plots (Figure 4.9A). The proportion of albumin-positive cells in this population was 84%. For sample LCI(H78), three distinct cell populations were detected, with albumin-positive cells again localized to P2 (Figure 4.9B), comprising 83% of that population. Additionally, the population profiles and albumin-positive cell percentages were compared with hHs. As shown in Figure 4.9C, a single homogeneous population was observed, containing 89% albumin-positive cells.

A)



B)



C)

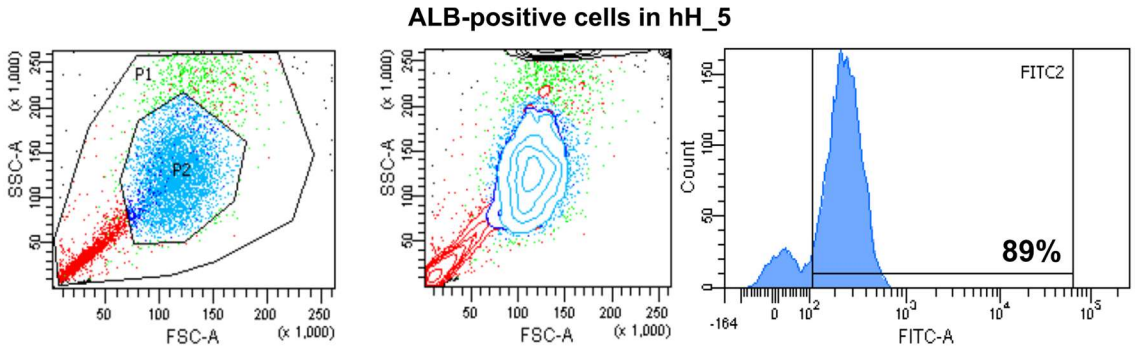


Figure 4.9. Cytometric identification of human hepatocytes was performed in the liver isolates. Albumin detection was performed on the tested samples containing 1×10^6 cells per tube, which included two isolates from different donors LCI(H50 and H78) and commercial human hepatocytes from donor hH_5. Each panel presents a dot plot (left), a contour plot (center), and a histogram (right), illustrating the fluorescence intensity of albumin-positive cells. Population regions (P1–P5) are indicated on the dot plots. The P1 gate includes all detected cells, whereas P2–P5 represent specific subpopulations. **A)** Flow cytometric analysis of LCI(H50). **B)** Flow cytometric analysis of LCI(H78). **C)** Flow cytometric analysis of hH_5. A single measurement was performed for each sample (n = 1); therefore, neither standard deviation (SD) nor statistical analysis was conducted.

Further flow cytometric analyses were performed to detect hepatocyte-specific proteins in the fresh isolated cells (except thawed hH_1, and LCI(H65 and H72). In addition to albumin (ALB), the following proteins were examined: alpha-1-antitrypsin (A1AT), cytochrome P450 3A4 (CYP3A4), and hepatocyte nuclear factor 4α (HNF4α). Commercial human hepatocytes from a 58-year-old female donor served as a positive control. Seventeen samples were analyzed in total (n = 17), of which sixteen originated from liver isolates. Six samples were derived from male donors and eleven from female donors. The patient ages ranged from 27 to 78 years.

Albumin-positive cells were detected in all samples, ranging from 32% (H74) to 97% (H52). Among the sixteen liver cell isolates, five [LCI(H53, H63, H69, H72, and H74)] contained fewer than 50% albumin-positive cells. In the hH_1 control, 70% of cells were albumin-positive, whereas most other isolates [LCI((H49, H50, H51, H52, H55, H60, H61, H65, H71, and H78)] contained more than 70% albumin-positive cells (Figure 4.10).

More than 70% of albumin-positive cells were detected in 4 out of 6 men (67%) and 6 out of 11 women (55%) (Figure 4.10).

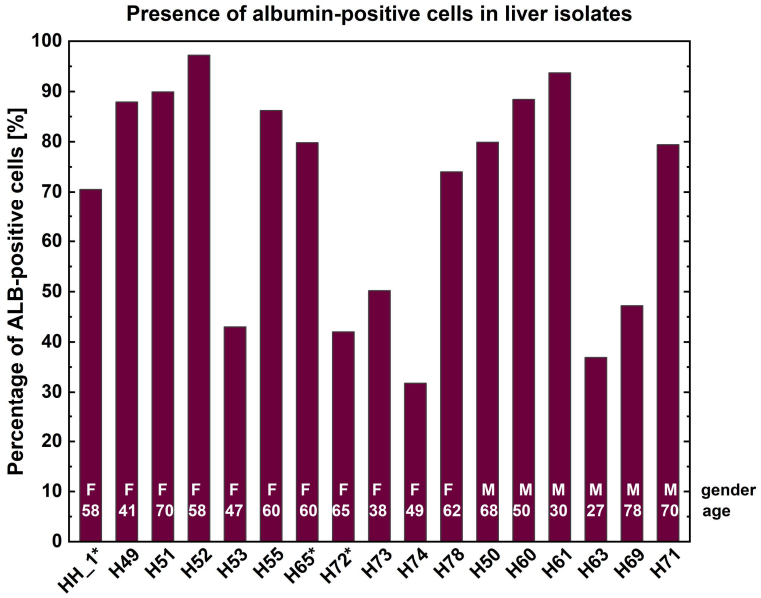


Figure 4.10. Percentage of albumin-positive cells isolated from resected human liver fragments. Flow cytometric analysis was performed on cells isolated from sixteen liver donors, LCI(H49–H78). *Analysis performed from thawed cells without cell culture: commercial human hepatocytes (hH_1) and LCI(H65 and H72). hH_1 was used as a control. Donor age and gender are indicated on the graph: female (F), male (M). Each analysis included 1×10^6 cells. Single measurements were performed; therefore, standard deviation (SD) and statistical analyses were not conducted.

Alpha-1-antitrypsin (A1AT) protein expression was also evaluated in the same seventeen samples. In the hH_1 control, 5% of cells were A1AT-positive. No positive cells were detected in samples H65 and H72. Among the remaining isolates, the percentage of A1AT-positive cells ranged from 12% to 99%. Six samples LCI(H53, H61, H63, H69, H71, and H73) contained fewer than 50% A1AT-positive cells, while eight LCI(H49, H50, H51, H52, H55, H60, H74, and H78) exhibited values above 50% (Figure 4.11).

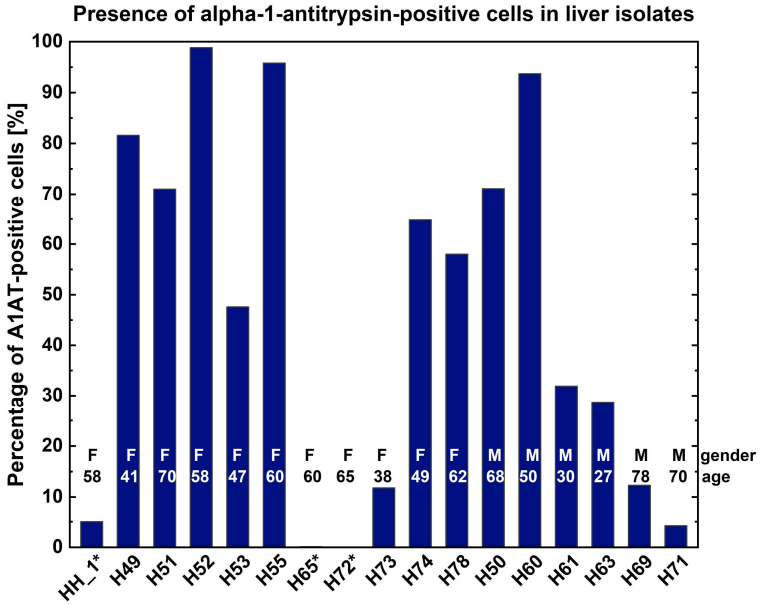


Figure 4.11. Percentage of alpha-1 antitrypsin (A1AT)-positive cells isolated from resected human liver fragments. Flow cytometric analysis was performed for sixteen LCIs and the hH_1 control (n = 17). *Analysis

performed from thawed cells without cell culture: commercial human hepatocytes (hH_1) and LCI(H65 and H72). Each analysis included 1×10^6 cells. Donor age and gender (F – female, M – male) are indicated in the graph. Single measurements were performed; therefore, standard deviation (SD) and statistical analyses were not conducted.

The presence of cytochrome P450 3A4 (CYP3A4) was subsequently examined in selected isolates LCI(H69, H71, H72, H73, H74, and H78) due to limited biological material. hH_1 served as a control. The isolates were derived from four female and two male donors aged 38–78 years. In hH_1, 21% of cells were CYP3A4-positive; a comparable value (24%) was observed for sample LCI(H69). Less than 5% positive cells were detected in samples LCI(H71, H72, and H78), whereas notably higher levels were found in LCI(H73) (88%) and LCI(H74) (64%) (Figure 4.12). Moreover, the percentage of CYP3A4-positive cells was higher in younger patients (38 and 49 years old; samples LCI(H73 and H74), respectively) than in older patients.

Analysis of HNF4α protein expression was performed in 7 samples from different donors (5 females and 2 males, aged 38–78 years). In hH_1, 48% of cells were HNF4α-positive, representing the highest value observed. In liver isolates, the proportion of HNF4α-positive cells ranged from 2% to 41% (Figure 4.12).

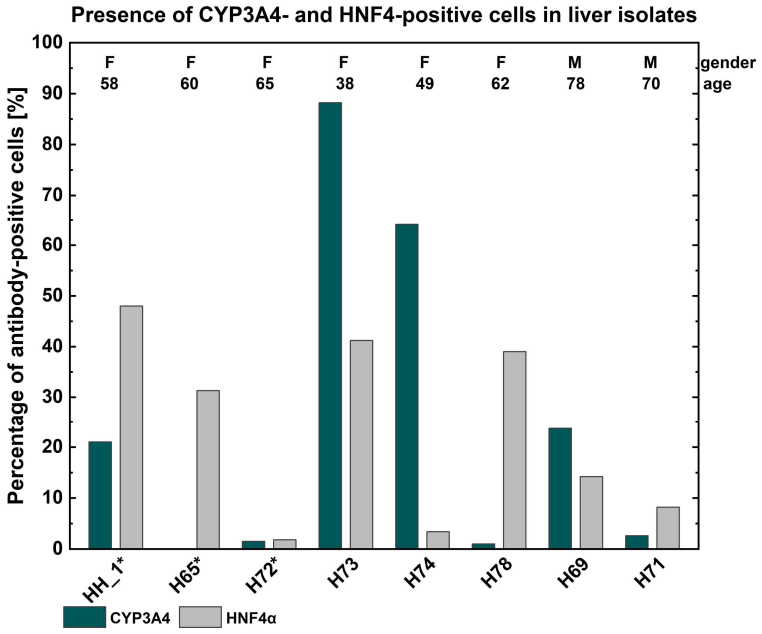


Figure 4.12. Percentage of CYP3A4- and HNF4α-positive cells isolated from resected human liver fragments. Flow cytometric analysis was performed for LCIs from the following donors: H65 (except CYP3A4), H69, H71, H72, H73, H74, and H78. hH_1 served as the control. *Analysis performed from thawed cells without cell culture: commercial human hepatocytes (hH_1) and LCI(H65 and H72). hH_1 was used as a control. Donor age and gender (F – female, M – male) are indicated on the graph. Each sample contained 1×10^6 cells. Results for CYP3A4 are shown in green, and for HNF4α in grey. Single measurements were performed; therefore, standard deviation (SD) and statistical analyses were not conducted.

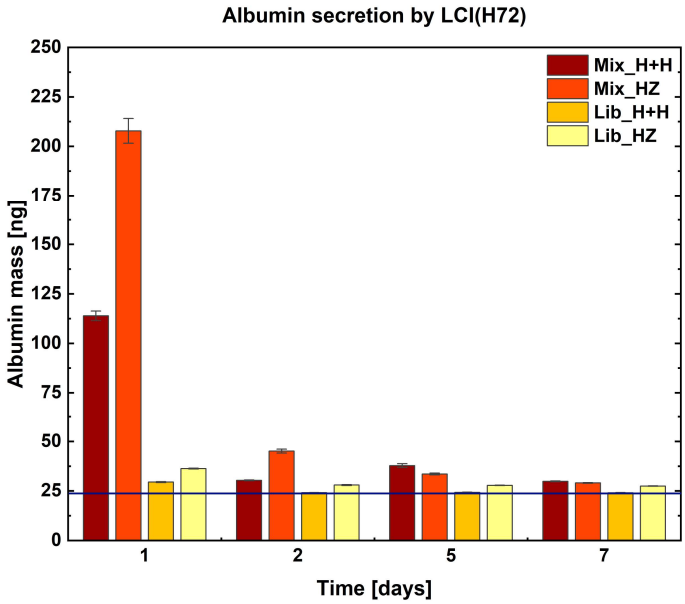
4.1.6 Albumin Secretion – ELISA

To verify whether the cells isolated from human livers secreted albumin, culture medium samples were collected during cultivation and analyzed using an enzyme-linked immunosorbent assay (ELISA). The results demonstrated that albumin-producing cells were present among the isolates, confirming the presence of hepatocytes. Moreover, the findings indicated rapid dedifferentiation of hepatocytes under *ex vivo* conditions.

For cells isolated using a collagenase enzyme mixture (Mix) and cultured in HepatoZYME-SFM medium (HZ), albumin secretion reached a high level (208 ng) after one day. However, within two days, albumin production decreased nearly 5-fold and continued to decline over subsequent days, stabilizing at a low constant level (Figure 4.13).

Cells isolated using the same collagenase mixture but cultured in Hepatocyte Medium supplemented with HGS (H+H) produced approximately half the albumin level (114 ng) after one day compared with the HZ culture. In this case, albumin production also decreased rapidly over time. For cells isolated with Liberase (Lib) and cultured in either medium, albumin secretion remained low (approximately 30 ng) even after one day and decreased only slightly thereafter (Figure 4.13).

A)



A1)

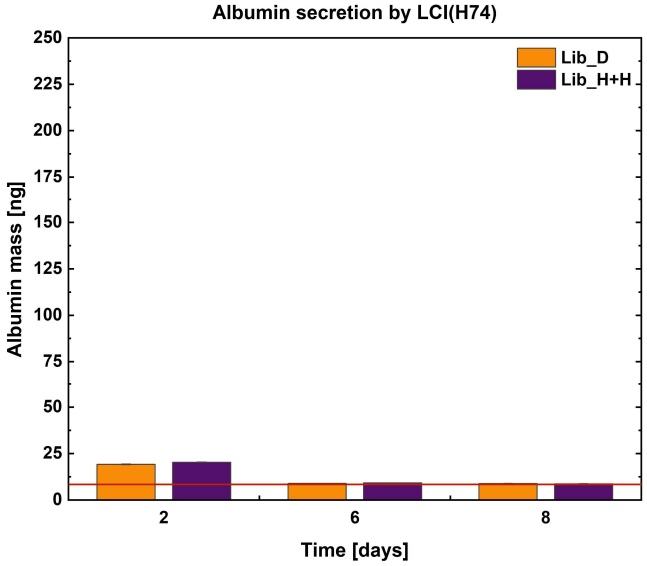
		Mix_ H+H	Mix_ H+H	Mix_ H+H	Mix_ H+H	Mix_ HZ	Mix_ HZ	Mix_ HZ	Mix_ HZ	Lib_ H+H	Lib_ H+H	Lib_ H+H	Lib_ H+H	Lib_ HZ	Lib_ HZ	Lib_ HZ	Lib_ HZ
		1	2	5	7	1	2	5	7	1	2	5	7	1	2	5	7
Mix_ H+H	1		0.000 029	0.000 063	0.000 023	0.00 0117	0.00 0117	0.00 0033	0.00 0017	0.000 019	0.000 011	0.000 011	0.000 011	0.00 0056	0.00 0017	0.00 0018	0.00 0011
Mix_ H+H	2	0.000 029		0.004 445	0.826 910	0.00 0023	0.00 0033	0.17 6228	0.62 0669	0.734 637	0.025 289	0.027 679	0.026 117	0.01 8653	0.37 8412	0.35 5255	0.29 7041
Mix_ H+H	5	0.000 063	0.004 445		0.002 858	0.00 0056	0.00 3018	0.09 2838	0.00 1419	0.002 178	0.000 013	0.000 020	0.000 013	0.52 8207	0.00 0410	0.00 0365	0.00 0250

Mix_ H+H	**7**	0.000 023	0.826 910	0.002 858		0.00 0019	0.00 0029	0.13 8903	0.75 7012	0.885 807	0.038 594	0.041 827	0.039 923	0.01 3088	0.48 0539	0.45 4498	0.38 6014
Mix_ HZ	**1**	0.000 117	0.000 023	0.000 056	0.000 019		0.00 0063	0.00 0029	0.00 0017	0.000 017	0.000 011	0.000 011	0.000 010	0.00 0033	0.00 0018	0.00 0011	0.00 0011
Mix_ HZ	**2**	0.000 117	0.000 033	0.003 018	0.000 029	0.00 0063		0.00 0071	0.00 0019	0.000 023	0.000 011	0.000 011	0.000 011	0.00 0677	0.00 0017	0.00 0017	0.00 0018
Mix_ HZ	**5**	0.000 033	0.176 228	0.092 838	0.138 903	0.00 0029	0.00 0071		0.09 1268	0.118 946	0.000 745	0.000 834	0.000 786	0.24 5861	0.03 9792	0.03 6815	0.02 8041
Mix_ HZ	**7**	0.000 017	0.620 669	0.001 419	0.757 012	0.00 0017	0.00 0019	0.09 1268		0.851 565	0.067 493	0.071 373	0.070 526	0.00 7289	0.65 1468	0.62 6542	0.54 4773
Lib_ H+H	**1**	0.000 019	0.734 637	0.002 178	0.885 807	0.00 0017	0.00 0023	0.11 8946	0.85 1565		0.049 278	0.052 828	0.051 226	0.01 0502	0.54 9742	0.52 4062	0.44 9917
Lib_ H+H	**2**	0.000 011	0.025 289	0.000 013	0.038 594	0.00 0011	0.00 0011	0.00 0745	0.06 7493	0.049 278		0.948 968	0.995 875	0.00 0034	0.14 4700	0.15 2033	0.17 9783
Lib_ H+H	**5**	0.000 011	0.027 679	0.000 020	0.041 827	0.00 0011	0.00 0011	0.00 0834	0.07 1373	0.052 828	0.948 968		0.948 920	0.00 0036	0.15 1034	0.15 4571	0.17 4400
Lib_ H+H	**7**	0.000 011	0.026 117	0.000 013	0.039 923	0.00 0010	0.00 0011	0.00 0786	0.07 0526	0.051 226	0.995 875	0.948 920		0.00 0029	0.15 0506	0.16 0616	0.19 3816
Lib_ HZ	**1**	0.000 056	0.018 653	0.528 207	0.013 088	0.00 0033	0.00 0677	0.24 5861	0.00 7289	0.010 502	0.000 034	0.000 036	0.000 029		0.00 2374	0.00 2149	0.00 1508
Lib_ HZ	**2**	0.000 017	0.378 412	0.000 410	0.480 539	0.00 0018	0.00 0017	0.03 9792	0.65 1468	0.549 742	0.144 700	0.151 034	0.150 506	0.00 2374		0.94 5890	0.83 6935
Lib_ HZ	**5**	0.000 018	0.355 255	0.000 365	0.454 498	0.00 0011	0.00 0017	0.03 6815	0.62 6542	0.524 062	0.152 033	0.154 571	0.160 616	0.00 2149	0.94 5890		0.87 8994
Lib_ HZ	**7**	0.000 011	0.297 041	0.000 250	0.386 014	0.00 0011	0.00 0018	0.02 8041	0.54 4773	0.449 917	0.179 783	0.174 400	0.193 816	0.00 1508	0.83 6935	0.87 8994	

Figure 4.13. Albumin secretion measured in cells isolated from liver sample LCI(H72). A) Cells were seeded at a density of 0.5×10^6 cells per well on 24-well plates coated with rat tail collagen type I and cultured in either HZ or HM+HGS medium. Culture media were collected after 1, 2, and 5 days of culture for sandwich ELISA analysis over a total culture period of seven days. Mix, mixture of collagenases I, II, and XI (2:1:1 ratio); Lib, Liberase; HZ, HepatoZYME-SFM medium; H+H, Hepatocyte Medium supplemented with HGS. The baseline is shown in blue. **A1)** Statistical significance (p) for Figure 4.13A. Statistical significance was assessed by multivariate analysis of variance (MANOVA) with Duncan's *post-hoc* test. Results are presented as mean ± SD (n = 4). Significance levels: *p<0.05, **p<0.01, ***p<0.001.

An analogous ELISA performed on cells isolated from liver LCI(H74) also confirmed the presence of hepatocytes. Cells were isolated using Liberase and cultured in either DMEM (D) or Hepatocyte Medium supplemented with HGS (H+H). Albumin production increased after two days of culture (20 ng), followed by a 2-fold decrease to 9 ng on the sixth and subsequent days (Figure 4.14).

A)



A1)

		D	D	D	H+H	H+H	H+H
		2	6	8	2	6	8
D	2		0.000149	0.000099	0.000380	0.000992	0.000066
D	6	0.000149		0.296698	0.000082	0.004824	0.028083
D	8	0.000099	0.296698		0.000060	0.001853	0.114878
H+H	2	0.000380	0.000082	0.000060		0.000115	0.000050
H+H	6	0.000992	0.004824	0.001853	0.000115		0.000497
H+H	8	0.000066	0.028083	0.114878	0.000050	0.000497	

Figure 4.14. Measurement of albumin secretion in cells isolated from liver sample LCI(H74). A) Cells were isolated using Liberase, seeded at a density of 1×10^6 cells per well on 24-well plates coated with fibronectin, and cultured in HM+HGS medium. Culture media were collected after 2 and 6 days of culture for sandwich ELISA analysis. The total culture period lasted eight days. Lib – Liberase; D – DMEM medium; H+H – Hepatocyte Medium supplemented with HGS. The baseline is shown in red. **A1)** Statistical significance (p) for Figure 4.14A. Statistical significance was assessed using MANOVA with Duncan's *post-hoc* test. Results are presented as mean ± SD (n = 2). Significance levels: *p<0.05, **p<0.01, ***p<0.001.

4.1.7 Genes Expression in Liver Tissue Isolates – RT-qPCR

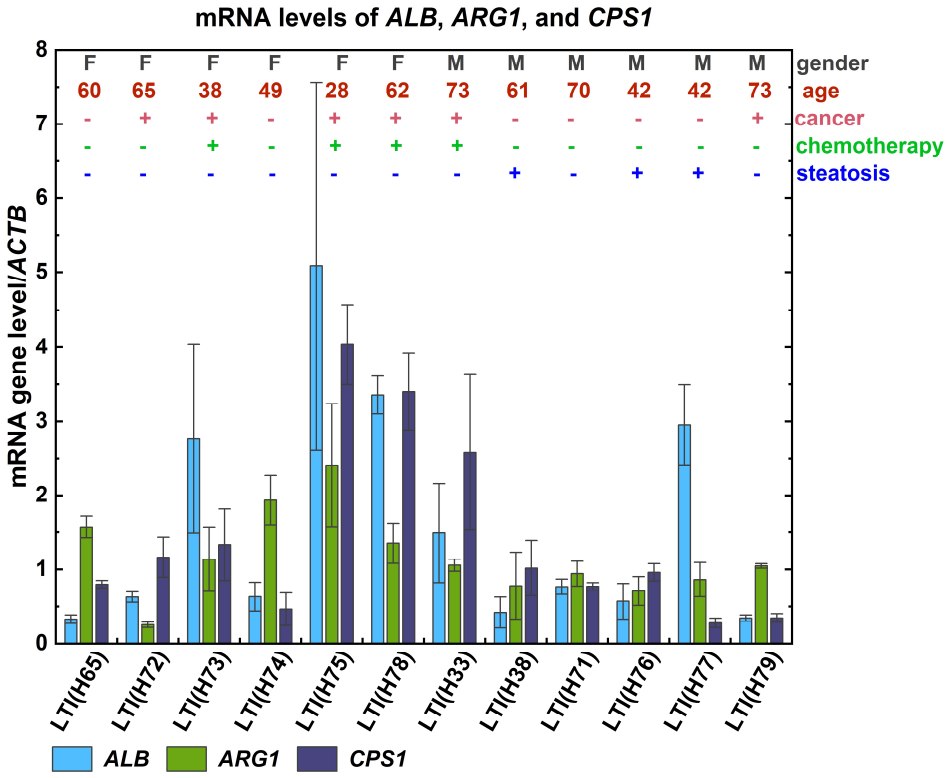
The expression of the following genes at the mRNA level were examined: albumin (*ALB*), arginase 1 (*ARG1*), carbamoyl-phosphate synthase 1 (*CPS1*), hepatocyte nuclear factor 4α (*HNF4α*), hepatocyte nuclear factor 1α (*HNF1α*), cytochrome P450 3A4 (*CYP3A4*), cytochrome P450 2C8 (*CYP2C8*), cytochrome P450 2E1 (*CYP2E1*), alpha-fetoprotein (*AFP*), and vimentin (*VIM*). β-actin (*ACTB*) was used as the housekeeping control gene. RNA was isolated from liver tissue, and the samples were referred to as liver tissue isolate (LTI).

The analysis was performed for 12 samples from different donors, designated as LTI(H33, H38, H65, H71–H79). Samples were obtained from six female (F) and six male (M) donors aged 28–73 years. The study also considered whether the donors had undergone chemotherapy and whether they had liver fibrosis.

Analysis of *ALB* expression showed that donors who received chemotherapy generally exhibited higher mRNA levels than those who did not. Samples with elevated *ALB* expression included LTI(H33, H73, H75, H77, and H78). The highest expression value (5.1) was observed in LTI(H75). Expression levels in LTI(H73) and LTI(H77) were approximately 2-fold lower, 1.5-fold lower in LTI(H78), and 3.4-fold lower in LTI(H33). In LTI(H71), the expression was nearly 7-fold lower than in LTI(H75), whereas in LTI(H72, H74, and H76) it was 8-fold lower. Sample LTI(H38) exhibited a 12-fold decrease relative to LTI(H75), and LTI(H65 and H79) showed transcript levels 15-fold lower. Notably, LTI(H77) was an exception: this donor had not undergone chemotherapy but showed elevated *ALB* expression, likely due to severe fatty liver disease. Expression levels for LTI(H77) and LTI(H38) differed significantly, although both donors had liver steatosis without cancer (Figure 4.15).

ARG1 transcript expression was higher in samples LTI(H65, H74, H75, and H78), and markedly lower in LTI(H72). The highest expression level (2.4) was observed in LTI(H75); expression in LTI(H65) was 1.5-fold lower, in LTI(H74) 1.2-fold lower, and in LTI(H78) 2.3-fold lower. In LTI(H72), mRNA expression was approximately 10-fold lower than in LTI(H75). Expression levels were 2-fold lower in samples LTI(H33, H73, and H79); 2.7-fold lower in LTI(H71) and LTI(H77); and 3.2-fold lower in LTI(H38) and LTI(H76) (Figure 4.15).

Expression of *CPS1* was higher in samples LTI(H33, H75, and H78), and lower in LTI(H74, H77, and H79). Sample LTI(H75) had the highest mRNA expression value (4), while LTI(H33) and LTI(H78) exhibited levels 1.6- and 1.2-fold lower, respectively. In LTI(H74), transcript expression was nearly 9-fold lower, and in LTI(H77) and LTI(H79), it was fourteen- and 12-fold lower, respectively. Samples LTI(H38, H65, H71, H72, H73, and H76) showed similar expression levels. However, compared with LTI(H75), gene expression was 3.2-fold lower in LTI(H72) and LTI(H73); 4-fold lower in LTI(H38) and LTI(H76); and 5-fold lower in LTI(H65) and LTI(H71) (Figure 4.15).



A)

ALB	LTI(H71)	LTI(H72)	LTI(H73)	LTI(H74)	LTI(H33)	LTI(H38)	LTI(H65)	LTI(H75)	LTI(H76)	LTI(H77)	LTI(H78)	LTI(H79)
LTI(H71)		1.000000	0.076978	1.000000	0.985608	0.999983	0.999827	0.000127	1.000000	0.035968	0.006215	0.999876
LTI(H72)	1.000000		0.044467	1.000000	0.948930	1.000000	0.999996	0.000127	1.000000	0.019959	0.003288	0.999998
LTI(H73)	0.076978	0.044467		0.045203	0.621187	0.018637	0.012499	0.019977	0.035106	1.000000	0.997126	0.013345
LTI(H74)	1.000000	1.000000	0.045203		0.950504	1.000000	0.999996	0.000127	1.000000	0.020311	0.003349	0.999997

LTI(H33)	0.985608	0.948930	0.621187	0.950504		0.819897	0.735147	0.000160	0.922686	0.416117	0.123453	0.749840
LTI(H38)	0.999983	1.000000	0.018637	1.000000	0.819897		1.000000	0.000127	1.000000	0.007996	0.001274	1.000000
LTI(H65)	0.999827	0.999996	0.012499	0.999996	0.735147	1.000000		0.000127	1.000000	0.005296	0.000853	1.000000
LTI(H75)	0.000127	0.000127	0.019977	0.000127	0.000160	0.000127	0.000127		0.000127	0.044504	0.194794	0.000127
LTI(H76)	1.000000	1.000000	0.035106	1.000000	0.922686	1.000000	1.000000	0.000127		0.015533	0.002501	1.000000
LTI(H77)	0.035968	0.019959	1.000000	0.020311	0.416117	0.007996	0.005296	0.044504	0.015533		0.999924	0.005663
LTI(H78)	0.006215	0.003288	0.997126	0.003349	0.123453	0.001274	0.000853	0.194794	0.002501	0.999924		0.000908
LC(H79)	0.999876	0.999998	0.013345	0.999997	0.749840	1.000000	1.000000	0.000127	1.000000	0.005663	0.000908	

B)

ARG1	LTI(H71)	LTI(H72)	LTI(H73)	LTI(H74)	LTI(H33)	LTI(H38)	LTI(H65)	LTI(H75)	LTI(H76)	LTI(H77)	LTI(H78)	LTI(H79)
LTI(H71)		0.207933	0.999539	0.010863	0.999998	0.999920	0.317675	0.000153	0.997660	1.000000	0.862275	0.999999
LTI(H72)	0.207933		0.034455	0.000128	0.077795	0.584063	0.000320	0.000127	0.768037	0.369216	0.003311	0.084746
LTI(H73)	0.999539	0.034455		0.081831	1.000000	0.936975	0.811904	0.000502	0.822537	0.990519	0.998967	1.000000
LTI(H74)	0.010863	0.000128	0.081831		0.036413	0.001713	0.934146	0.724175	0.000791	0.004420	0.431472	0.033151
LTI(H33)	0.999998	0.077795	1.000000	0.036413		0.990439	0.605427	0.000253	0.949088	0.999582	0.983650	1.000000
LTI(H38)	0.999920	0.584063	0.936975	0.001713	0.990439		0.083747	0.000129	1.000000	1.000000	0.456698	0.992705
LTI(H65)	0.317675	0.000320	0.811904	0.934146	0.605427	0.083747		0.057218	0.042003	0.173277	0.998584	0.580604
LTI(H75)	0.000153	0.000127	0.000502	0.724175	0.000253	0.000129	0.057218		0.000128	0.000135	0.005397	0.000238
LTI(H76)	0.997660	0.768037	0.822537	0.000791	0.949088	1.000000	0.042003	0.000128		0.999956	0.290344	0.957427
LTI(H77)	1.000000	0.369216	0.990519	0.004420	0.999582	1.000000	0.173277	0.000135	0.999956		0.678538	0.999735
LTI(H78)	0.862275	0.003311	0.998967	0.431472	0.983650	0.456698	0.998584	0.005397	0.290344	0.678538		0.979446
LC(H79)	0.999999	0.084746	1.000000	0.033151	1.000000	0.992705	0.580604	0.000238	0.957427	0.999735	0.979446	

C)

CPS1	LTI(H71)	LTI(H72)	LTI(H73)	LTI(H74)	LTI(H33)	LTI(H38)	LTI(H65)	LTI(H75)	LTI(H76)	LTI(H77)	LTI(H78)	LTI(H79)
LTI(H71)		0.973540	0.769072	0.996226	0.000155	0.999489	1.000000	0.000127	0.999958	0.884716	0.000127	0.953005
LTI(H72)	0.973540		0.999985	0.481609	0.001976	0.999997	0.985135	0.000127	0.999920	0.170946	0.000127	0.259221
LTI(H73)	0.769072	0.999985		0.188040	0.009425	0.994933	0.821480	0.000127	0.981581	0.048423	0.000128	0.081223
LTI(H74)	0.996226	0.481609	0.188040		0.000128	0.789164	0.991949	0.000127	0.878990	0.999966	0.000127	1.000000
LTI(H33)	0.000155	0.001976	0.009425	0.000128		0.000546	0.000166	0.001438	0.000357	0.000127	0.256285	0.000127
LTI(H38)	0.999489	0.999997	0.994933	0.789164	0.000546		0.999846	0.000127	1.000000	0.401094	0.000127	0.540399
LTI(H65)	1.000000	0.985135	0.821480	0.991949	0.000166	0.999846		0.000127	0.999992	0.842133	0.000127	0.927812
LTI(H75)	0.000127	0.000127	0.000127	0.000127	0.001438	0.000127	0.000127		0.000127	0.000127	0.624674	0.000127
LTI(H76)	0.999958	0.999920	0.981581	0.878990	0.000357	1.000000	0.999992	0.000127		0.517825	0.000127	0.662208
LTI(H77)	0.884716	0.170946	0.048423	0.999966	0.000127	0.401094	0.842133	0.000127	0.517825		0.000127	1.000000
LTI(H78)	0.000127	0.000127	0.000128	0.000127	0.256285	0.000127	0.000127	0.624674	0.000127	0.000127		0.000127
LC(H79)	0.953005	0.259221	0.081223	1.000000	0.000127	0.540399	0.927812	0.000127	0.662208	1.000000	0.000127	

Figure 4.15. Expression mRNA levels of *ALB*, *ARG1*, and *CPS1* genes in LTIs. Tissue fragments were obtained from twelve donors LTI(H33, H38, H65, H71, H72, H73, H74, H75, H76, H77, H78, and H79). RNA was isolated

from 50 mg of tissue using the Bead-Beat Total RNA Mini kit, and samples were analyzed using the RT-qPCR method. The housekeeping gene β-actin (*ACTB*) served as the internal control. Gene expression levels were calculated using the comparative Ct (ΔΔCt) method, with the average RQ across all samples for a given gene serving as the calibrator. Final expression levels were determined as the ratio of the RQ of each target gene to the RQ of *ACTB*. The graph includes information on donor gender, age, cancer or liver fibrosis status, and chemotherapy treatment. Bars representing *ALB* expression are shown in blue, *ARG1* in green, and *CPS1* in purple. **A)** Statistical significance (p) for *ALB* expression in Figure 4.15. **B)** Statistical significance (p) for *ARG1* expression in Figure 4.15. **C)** Statistical significance (p) for *CPS1* expression in Figure 4.15. Statistical analysis was performed using one-way ANOVA followed by Duncan's *post-hoc* test. Results are shown as mean ± SD of four replicates (n = 4). Significance levels: **p*<0.05, ***p*<0.01, ****p*<0.001.

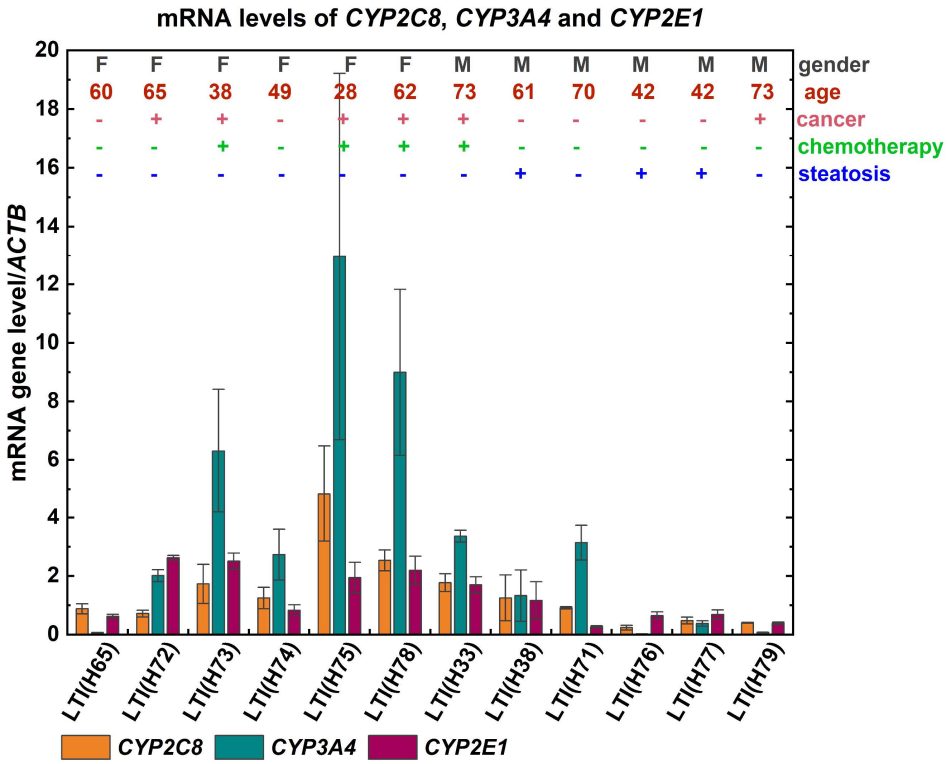
The next genes examined were three members of the cytochrome P450 family: *CYP3A4*, *CYP2C8*, and *CYP2E1*.

Analysis of *CYP3A4* mRNA expression revealed markedly elevated levels in samples LTI(H73, H75, and H78). The highest expression was detected in LTI(H75) (value of 13). Expression in LTI(H78) and LTI(H73) was 1.4-fold and 2-fold lower, respectively. Elevated transcript expression was also observed in samples LTI(H33, H71, H72, and H74); however, compared with LTI(H75), expression was 4-fold lower in LTI(H33) and LTI(H71), 6-fold lower in LTI(H72), and nearly 5-fold lower in LTI(H74). In sample LTI(H38), the expression was nearly 10-fold lower than in LTI(H75). Among the remaining samples, LTI(H77) showed low *CYP3A4* mRNA expression (0.4), representing a 34-fold decrease relative to LTI(H75). The lowest levels were detected in samples LTI(H65, H76, and H79), with 230-fold, 662-fold, and 185-fold lower expression than in LTI(H75), respectively. Elevated *CYP3A4* expression was observed in donors who had undergone chemotherapy LTI(H73, H75, H78, H33). However, increased transcript expression was also observed in samples from donors without cancer and without chemotherapy treatment, LTI(H77, H74). A similar expression level was observed in sample LTI(H72), obtained from a donor with cancer who had not received chemotherapy (Figure 4.16).

For the second cytochrome P450 gene, *CYP2C8*, higher mRNA expression was detected in the LTI (H75 and H78) samples. Sample LTI(H75) reached a value of 4.8, while LTI(H78) exhibited nearly a 2-fold decrease. Expression in LTI(H33 and H73) was approximately 3-fold lower than in LTI(H75), and in LTI(H38) and LTI(H74), 4-fold lower. In the LTI(H65 and H71) samples, *CYP2C8* transcript levels were 5-fold lower relative to LTI(H75). Samples LTI(H72, H77, and H79) showed 7-, 10-, and 12-fold lower expression, respectively. The lowest transcript level was observed in LTI(H76), which exhibited a 20-fold decrease relative to LTI(H75). Similar to *CYP3A4*, increased *CYP2C8* expression correlated with samples from donors with cancer treated with chemotherapy (Figure 4.16).

The final gene analyzed from the cytochrome P450 family was *CYP2E1*, which overall showed the lowest mRNA expression levels among the three genes. The highest *CYP2E1* expression was observed in samples LTI(H72) and LTI(H73), unlike *CYP3A4* and *CYP2C8*, in which LTI(H75) showed the highest expression. For sample LTI(H72), expression reached 2.6, which was 1.04-fold higher than in LTI(H73). Expression in LTI(H78), LTI(H75), and LTI(H33) was 1.2-, 1.3-, and 1.5-fold lower, respectively, compared with LTI(H72). In LTI(H38), *CYP2E1* transcript levels were 2-fold lower, and in LTI(H74), 3-fold lower than in LTI(H72). In samples LTI(H65, H76, and H77), expression was approximately 4-fold lower, while in LTI(H71) and LTI(H79), levels were 9-fold and nearly 7-fold lower, respectively.

As with the other cytochrome genes, increased *CYP2E1* expression was observed in samples from donors with cancer who had undergone chemotherapy LTI(H73, H75, H78, H33). The exception was sample LTI(H72), which showed the highest expression despite originating from a donor with cancer who had not received chemotherapy. Interestingly, sample LTI(H79), also derived from a donor with cancer who did not undergo chemotherapy, showed one of the lowest *CYP2E1* mRNA expression levels (Figure 4.16).



A)

CYP2C8	LTI(H71)	LTI(H72)	LTI(H73)	LTI(H74)	LTI(H33)	LTI(H38)	LTI(H65)	LTI(H75)	LTI(H76)	LTI(H77)	LTI(H78)	LTI(H79)
LTI(H71)		0.999998	0.717040	0.999538	0.650399	0.999476	1.000000	0.000127	0.891195	0.995356	0.018507	0.983686
LTI(H72)	0.999998		0.416299	0.977391	0.354813	0.975920	1.000000	0.000127	0.989666	0.999983	0.005284	0.999761
LTI(H73)	0.717040	0.416299		0.989667	1.000000	0.990429	0.671051	0.000127	0.040717	0.150181	0.734470	0.103065

LTI(H74)	0.999538	0.977391	0.989667		0.979747	1.000000	0.998973	0.000127	0.416292	0.780243	0.127423	0.673275
LTI(H33)	0.650399	0.354813	1.000000	0.979747		0.981037	0.602522	0.000127	0.031346	0.120419	0.794885	0.081484
LTI(H38)	0.999476	0.975920	0.990429	1.000000	0.981037		0.998852	0.000127	0.409646	0.774054	0.130415	0.666227
LTI(H65)	1.000000	1.000000	0.671051	0.998973	0.602522	0.998852		0.000127	0.917292	0.997528	0.015276	0.989916
LTI(H75)	0.000127	0.000127	0.000127	0.000127	0.000127	0.000127	0.000127		0.000127	0.000127	0.000278	0.000127
LTI(H76)	0.891195	0.989666	0.040717	0.416292	0.031346	0.409646	0.917292	0.000127		0.999983	0.000281	1.000000
LTI(H77)	0.995356	0.999983	0.150181	0.780243	0.120419	0.774054	0.997528	0.000127	0.999983		0.001091	1.000000
LTI(H78)	0.018507	0.005284	0.734470	0.127423	0.794885	0.130415	0.015276	0.000278	0.000281	0.001091		0.000691
LC(H79)	0.983686	0.999761	0.103065	0.673275	0.081484	0.666227	0.989916	0.000127	1.000000	1.000000	0.000691	

B)

CYP3A4	**LTI(H71)**	**LTI(H72)**	**LTI(H73)**	**LTI(H74)**	**LTI(H33)**	**LTI(H38)**	**LTI(H65)**	**LTI(H75)**	**LTI(H76)**	**LTI(H77)**	**LTI(H78)**	**LTI(H79)**
LTI(H71)		0.999762	0.616486	1.000000	1.000000	0.984628	0.651363	0.000131	0.635318	0.782510	0.017207	0.657267
LTI(H72)	0.999762		0.196104	0.999997	0.998749	0.999998	0.972520	0.000127	0.968610	0.993109	0.002216	0.973871
LTI(H73)	0.616486	0.196104		0.439298	0.711184	0.073944	0.008571	0.004072	0.008019	0.015225	0.807730	0.008784
LTI(H74)	1.000000	0.999997	0.439298		0.999999	0.998171	0.813790	0.000128	0.800781	0.907729	0.008307	0.818496
LTI(H33)	1.000000	0.998749	0.711184	0.999999		0.964329	0.554389	0.000134	0.538168	0.694451	0.025202	0.560400
LTI(H38)	0.984628	0.999998	0.073944	0.998171	0.964329		0.999249	0.000127	0.999025	0.999954	0.000661	0.999320
LTI(H65)	0.651363	0.972520	0.008571	0.813790	0.554389	0.999249		0.000127	1.000000	1.000000	0.000159	1.000000
LTI(H75)	0.000131	0.000127	0.004072	0.000128	0.000134	0.000127	0.000127		0.000127	0.000127	0.291509	0.000127
LTI(H76)	0.635318	0.968610	0.008019	0.800781	0.538168	0.999025	1.000000	0.000127		1.000000	0.000156	1.000000
LTI(H77)	0.782510	0.993109	0.015225	0.907729	0.694451	0.999954	1.000000	0.000127	1.000000		0.000193	1.000000
LTI(H78)	0.017207	0.002216	0.807730	0.008307	0.025202	0.000661	0.000159	0.291509	0.000156	0.000193		0.000160
LC(H79)	0.657267	0.973871	0.008784	0.818496	0.560400	0.999320	1.000000	0.000127	1.000000	1.000000	0.000160	

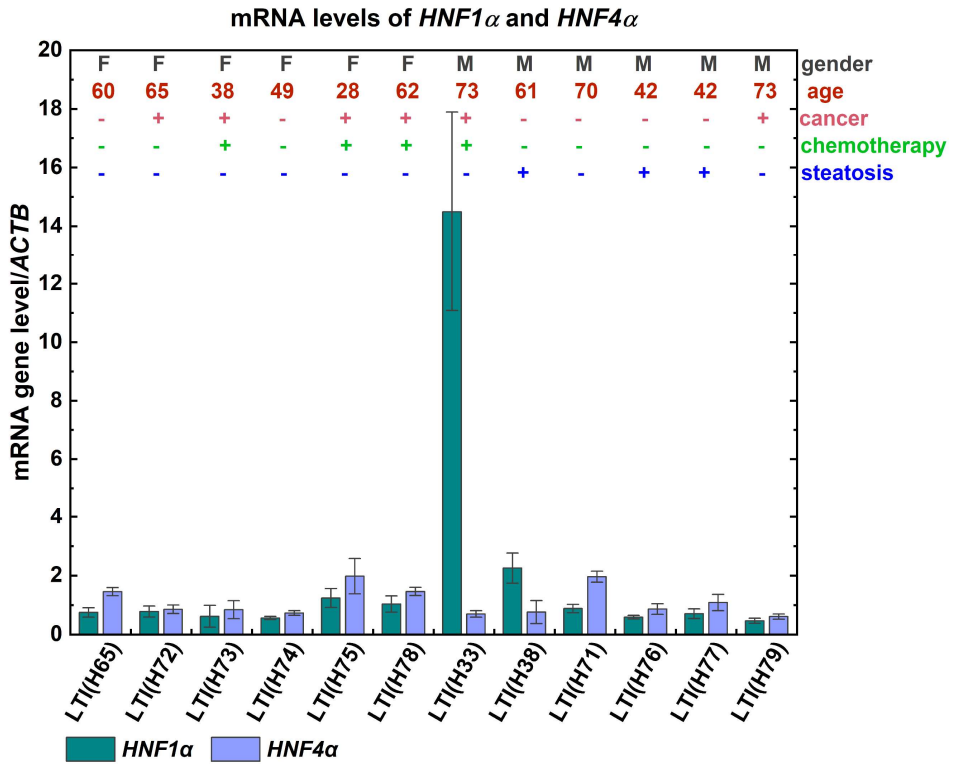
C)

CYP2E1	**LTI(H71)**	**LTI(H72)**	**LTI(H73)**	**LTI(H74)**	**LTI(H33)**	**LTI(H38)**	**LTI(H65)**	**LTI(H75)**	**LTI(H76)**	**LTI(H77)**	**LTI(H78)**	**LTI(H79)**
LTI(H71)		0.000127	0.000127	0.345050	0.000132	0.010841	0.894243	0.000127	0.850884	0.756832	0.000127	0.999984
LTI(H72)	0.000127		0.999989	0.000127	0.007585	0.000130	0.000127	0.125676	0.000127	0.000127	0.722572	0.000127
LTI(H73)	0.000127	0.999989		0.000127	0.032114	0.000150	0.000127	0.351647	0.000127	0.000127	0.956438	0.000127
LTI(H74)	0.345050	0.000127	0.000127		0.016215	0.918598	0.998169	0.000752	0.999366	0.999936	0.000141	0.705927
LTI(H33)	0.000132	0.007585	0.032114	0.016215		0.434096	0.001260	0.990712	0.001659	0.002707	0.512622	0.000166
LTI(H38)	0.010841	0.000130	0.000150	0.918598	0.434096		0.384417	0.045360	0.446701	0.561999	0.002202	0.047052
LTI(H65)	0.894243	0.000127	0.000127	0.998169	0.001260	0.384417		0.000155	1.000000	1.000000	0.000127	0.995556
LTI(H75)	0.000127	0.125676	0.351647	0.000752	0.990712	0.045360	0.000155		0.000167	0.000201	0.990570	0.000127
LTI(H76)	0.850884	0.000127	0.000127	0.999366	0.001659	0.446701	1.000000	0.000167		1.000000	0.000127	0.990365
LTI(H77)	0.756832	0.000127	0.000127	0.999936	0.002707	0.561999	1.000000	0.000201	1.000000		0.000128	0.971004
LTI(H78)	0.000127	0.722572	0.956438	0.000141	0.512622	0.002202	0.000127	0.990570	0.000127	0.000128		0.000127
LC(H79)	0.999984	0.000127	0.000127	0.705927	0.000166	0.047052	0.995556	0.000127	0.990365	0.971004	0.000127	

Figure 4.16. Expression of *CYP3A4*, *CYP2C8*, and *CYP2E1* genes at the transcript level in LTIs. Tissue fragments were obtained from resected fragments of human liver from 12 donors, designated as LTI(H33, H38, H65, H71, H72, H73, H74, H75, H76, H77, H78, and H79). Gene expression analysis was performed using the RT-qPCR method. The housekeeping gene β-actin (*ACTB*) serves as the internal control. Gene expression levels were calculated using the comparative Ct (ΔΔCt) method, and values were determined as the ratio of the RQ of each target gene to the RQ of *ACTB*. The graph presents donors' gender, age, cancer or liver steatosis status, and chemotherapy treatment. Bars representing *CYP2C8* expression are shown in orange, *CYP3A4* in green, and *CYP2E1* in pink. **A)** Statistical significance (p) for *CYP2C8* gene expression in Figure 4.16. **B)** Statistical significance (*p*) for *CYP3A4* gene expression in Figure 4.16. **C)** Statistical significance (*p*) for *CYP2E1* gene expression in Figure 4.16. Statistical analysis was performed using one-way ANOVA followed by Duncan's *post-hoc* test. Results are presented as mean ± SD of four replicates (n = 4). Significance levels: **p*<0.05, ***p*<0.01, ****p*<0.001.

The expression levels of two genes from the transcription factor family, *HNF4α* and *HNF1α*, were examined. For *HNF4α*, the highest transcript expression values were obtained in samples LTI(H75) and LTI(H71), with mean differences of 1.98 and 1.96, respectively. Elevated mRNA levels were also detected in samples LTI(H78) and LTI(H65), which were 1.4-fold lower than those in LTI(H75). The remaining samples exhibited similar *HNF4α* expression levels in the LTI(H72, H73, H76, and H77), which were approximately 2-fold lower, whereas in LTI(H33, H38, H74, and H79), it was 3-fold lower than in LTI(H75). Notably, the highest expression levels for this gene were found in samples derived from a donor with cancer after chemotherapy and from a donor without cancer (Figure 4.17).

For the second transcription factor gene, *HNF1α*, mRNA expression was markedly elevated in sample LTI(H33), reaching a 14.5-fold increase. The second-highest transcript levels were observed in sample LTI(H38), which were approximately 6-fold lower than in LTI(H33). Slightly elevated expression compared with the remaining samples was observed for LTI(H75) and LTI(H78), with expression being 12- and 14-fold lower than in LTI(H33), respectively. The lowest *HNF1α* mRNA expression level was observed in sample LTI(H79), indicating a 31-fold decrease relative to LTI(H33). The other samples, LTI(H65, H71, H72, H73, H74, H76, and H77), displayed a comparable expression pattern, averaging approximately 20-fold lower than LTI(H33). Similar to *HNF4α*, the highest *HNF1α* expression levels were observed in samples derived from a chemotherapy-treated cancer patient and from a patient without cancer but with fatty liver disease (Figure 4.17).



A)

HNF1α	LTI(H71)	LTI(H72)	LTI(H73)	LTI(H74)	LTI(H33)	LTI(H38)	LTI(H65)	LTI(H75)	LTI(H76)	LTI(H77)	LTI(H78)	LTI(H79)
LTI(H71)		1.000000	1.000000	0.999999	0.000127	0.740491	1.000000	0.999996	1.000000	1.000000	1.000000	0.999981
LTI(H72)	1.000000		1.000000	1.000000	0.000127	0.651170	1.000000	0.999950	1.000000	1.000000	1.000000	0.999999
LTI(H73)	1.000000	1.000000		1.000000	0.000127	0.501987	1.000000	0.999088	1.000000	1.000000	0.999980	1.000000
LTI(H74)	0.999999	1.000000	1.000000		0.000127	0.452982	1.000000	0.998029	1.000000	1.000000	0.999933	1.000000
LTI(H33)	0.000127	0.000127	0.000127	0.000127		0.000127	0.000127	0.000127	0.000127	0.000127	0.000127	0.000127
LTI(H38)	0.740491	0.651170	0.501987	0.452982	0.000127		0.623592	0.951677	0.477018	0.585399	0.854194	0.371725
LTI(H65)	1.000000	1.000000	1.000000	1.000000	0.000127	0.623592		0.999905	1.000000	1.000000	1.000000	1.000000
LTI(H75)	0.999996	0.999950	0.999088	0.998029	0.000127	0.951677	0.999905		0.998630	0.999792	1.000000	0.993800
LTI(H76)	1.000000	1.000000	1.000000	1.000000	0.000127	0.477018	1.000000	0.998630		1.000000	0.999963	1.000000
LTI(H77)	1.000000	1.000000	1.000000	1.000000	0.000127	0.585399	1.000000	0.999792	1.000000		0.999998	1.000000
LTI(H78)	1.000000	1.000000	0.999980	0.999933	0.000127	0.854194	1.000000	1.000000	0.999963	0.999998		0.999599
LC(H79)	0.999981	0.999999	1.000000	1.000000	0.000127	0.371725	1.000000	0.993800	1.000000	1.000000	0.999599	

B)

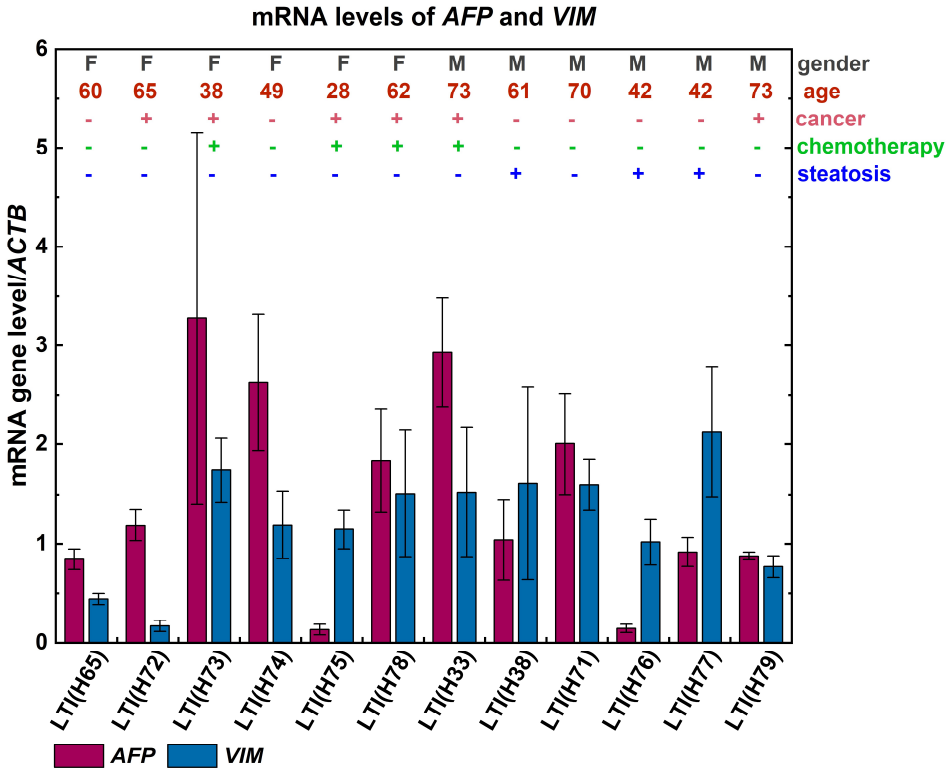
HNF4α	LTI(H71)	LTI(H72)	LTI(H73)	LTI(H74)	LTI(H33)	LTI(H38)	LTI(H65)	LTI(H75)	LTI(H76)	LTI(H77)	LTI(H78)	LTI(H79)
LTI(H71)		0.000164	0.000156	0.000130	0.000129	0.000134	0.261269	1.000000	0.000171	0.002004	0.273890	0.000127
LTI(H72)	0.000164		1.000000	0.999922	0.999335	0.999997	0.093664	0.000154	1.000000	0.982667	0.088268	0.970997
LTI(H73)	0.000156	1.000000		0.999974	0.999701	0.999999	0.080209	0.000148	1.000000	0.974047	0.075490	0.980403
LTI(H74)	0.000130	0.999922	0.999974		1.000000	1.000000	0.018294	0.000129	0.999842	0.751781	0.017071	0.999943
LTI(H33)	0.000129	0.999335	0.999701	1.000000		1.000000	0.011689	0.000128	0.998861	0.646123	0.010889	0.999997
LTI(H38)	0.000134	0.999997	0.999999	1.000000	1.000000		0.029847	0.000132	0.999993	0.852528	0.027910	0.999331
LTI(H65)	0.261269	0.093664	0.080209	0.018294	0.011689	0.029847		0.261269	0.093664	0.080209	0.018294	0.011689
LTI(H75)	1.000000	0.000154	0.000148	0.000129	0.000128	0.000132	0.261269		0.000171	0.002004	0.273890	0.000127
LTI(H76)	0.000171	1.000000	1.000000	0.999842	0.998861	0.999993	0.093664	0.000171		0.982667	0.088268	0.970997
LTI(H77)	0.002004	0.982667	0.974047	0.751781	0.646123	0.852528	0.080209	0.002004	0.982667		0.075490	0.980403
LTI(H78)	0.273890	0.088268	0.075490	0.017071	0.010889	0.027910	0.018294	0.273890	0.088268	0.075490		0.980403
LC(H79)	0.000127	0.970997	0.980403	0.999943	0.999997	0.999331	0.011689	0.000127	0.970997	0.980403	0.980403	

LTI(H65)	0.261269	0.093664	0.080209	0.018294	0.011689	0.029847		0.220972	0.104834	0.696214	1.000000	0.003168
LTI(H75)	1.000000	0.000154	0.000148	0.000129	0.000128	0.000132	0.220972		0.000159	0.001559	0.232135	0.000127
LTI(H76)	0.000171	1.000000	1.000000	0.999842	0.998861	0.999993	0.104834	0.000159		0.987477	0.098887	0.962146
LTI(H77)	0.002004	0.982667	0.974047	0.751781	0.646123	0.852528	0.696214	0.001559	0.987477		0.679434	0.344366
LTI(H78)	0.273890	0.088268	0.075490	0.017071	0.010889	0.027910	1.000000	0.232135	0.098887	0.679434		0.002937
LC(H79)	0.000127	0.970997	0.980403	0.999943	0.999997	0.999331	0.003168	0.000127	0.962146	0.344366	0.002937	

Figure 4.17. Expression of *HNF4α* and *HNF1α* genes at the mRNA level in LTIs. Gene analysis was performed using RT-qPCR. On liver tissue fragments obtained from 12 patients**,** designated LTI(H33, H38, H65, H71, H72, H73, H74, H75, H76, H77, H78, and H79). β-actin (*ACTB*) served as the internal control (housekeeping gene). Gene expression levels were calculated using the comparative Ct (ΔΔCt) method, with values expressed as the ratio of the RQ of each target gene to the RQ of the *ACTB* control. The graph also indicates patient gender, age, presence of cancer or liver steatosis, and chemotherapy treatment. Bars representing *HNF1α* expression are shown in green, and those for *HNF4α* in purple. A) Statistical significance (*p*) for *HNF1α* gene expression in Figure 4.17. B) Statistical significance (*p*) for *HNF4α* gene expression in Figure 4.17. Statistical analysis was performed using one-way analysis of variance (ANOVA) followed by Duncan's *post-hoc* test. Results are presented as mean ± SD (n=4). Significance levels: **p*<0.05, ***p*<0.01, ****p*<0.001.

The next gene analyzed was *AFP*. Higher transcript levels were observed in LTI(H73, H74, H71, H78, and H33) samples. The highest expression was detected in sample LTI(H73), with a relative value of 3.3. In sample LTI(H33), the expression was 1.1-fold lower, while in LTI(H74) it was 1.2-fold lower than in LTI(H73). Samples LTI(H71) and LTI(H78) showed transcript levels lower than in LTI(H73) by 1.6-fold and 1.8-fold, respectively. In samples LTI(H38) and LTI(H72), *AFP* expression was approximately 3-fold lower, whereas in LTI(H65, H77, and H79) it was about 4-fold lower. The lowest expression was observed in samples LTI(H75 and H76), where *AFP* levels were approximately 24-fold lower than in LTI(H73). For the *AFP* gene, elevated expression occurred in both oncological and non-oncological patients (Figure 4.18).

Expression of the *VIM* gene was also assessed. Higher *VIM* expression was observed in samples LTI(H77, H78, H73, H71, H38, and H33), whereas the lowest mRNA level was in LTI(H72). Expression levels were similar among the remaining samples, LTI(H65, H74, H75, H76, and H79). Relative to sample LTI(H77) – the sample with the highest *VIM* expression (2.1) – expression was approximately 1.3-fold lower in LTI(H33, H38, H71, H73, and H78); about 2-fold lower in LTI(H74, H75, and H76); 3-fold lower in LTI(H79); and 5-fold lower in LTI(H65). In sample LTI(H72), *VIM* expression was approximately 13-fold lower than in LTI(H77) (Figure 4.18).



A)

AFP	LTI(H71)	LTI(H72)	LTI(H73)	LTI(H74)	LTI(H33)	LTI(H38)	LTI(H65)	LTI(H75)	LTI(H76)	LTI(H77)	LTI(H78)	LTI(H79)
LTI(H71)		0.818174	0.237209	0.966765	0.684577	0.619410	0.352821	0.011001	0.011783	0.447329	1.000000	0.395227
LTI(H72)	0.818174		0.003123	0.115768	0.023800	1.000000	0.999756	0.492661	0.509312	0.999976	0.954010	0.999910
LTI(H73)	0.237209	0.003123		0.951496	0.999750	0.001256	0.000425	0.000128	0.000128	0.000637	0.112993	0.000503
LTI(H74)	0.966765	0.115768	0.951496		0.999928	0.054572	0.018898	0.000325	0.000342	0.028424	0.850017	0.022861
LTI(H33)	0.684577	0.023800	0.999750	0.999928		0.009974	0.003140	0.000148	0.000150	0.004864	0.444499	0.003853
LTI(H38)	0.619410	1.000000	0.001256	0.054572	0.009974		0.999999	0.707562	0.723418	1.000000	0.837803	1.000000
LTI(H65)	0.352821	0.999756	0.000425	0.018898	0.003140	0.999999		0.915817	0.924035	1.000000	0.584078	1.000000
LTI(H75)	0.011001	0.492661	0.000128	0.000325	0.000148	0.707562	0.915817		1.000000	0.852941	0.028883	0.889270
LTI(H76)	0.011783	0.509312	0.000128	0.000342	0.000150	0.723418	0.924035	1.000000		0.864515	0.030820	0.899078
LTI(H77)	0.447329	0.999976	0.000637	0.028424	0.004864	1.000000	1.000000	0.852941	0.864515		0.687454	1.000000
LTI(H78)	1.000000	0.954010	0.112993	0.850017	0.444499	0.837803	0.584078	0.028883	0.030820	0.687454		0.632482
LC(H79)	0.395227	0.999910	0.000503	0.022861	0.003853	1.000000	1.000000	0.889270	0.899078	1.000000	0.632482	

B)

VIM	LTI(H71)	LTI(H72)	LTI(H73)	LTI(H74)	LTI(H33)	LTI(H38)	LTI(H65)	LTI(H75)	LTI(H76)	LTI(H77)	LTI(H78)	LTI(H79)
LTI(H71)		0.005660	0.999999	0.983459	1.000000	1.000000	0.049331	0.962837	0.832274	0.890011	1.000000	0.367461
LTI(H72)	0.005660		0.001699	0.120345	0.010293	0.005070	0.999388	0.162414	0.329097	0.000162	0.011450	0.796478
LTI(H73)	0.999999	0.001699		0.875542	0.999938	1.000000	0.016459	0.807148	0.569424	0.986833	0.999889	0.169056
LTI(H74)	0.983459	0.120345	0.875542		0.996732	0.978872	0.511423	1.000000	0.999993	0.205082	0.997712	0.975928
LTI(H33)	1.000000	0.010293	0.999938	0.996732		1.000000	0.082750	0.990011	0.921764	0.784988	1.000000	0.503203
LTI(H38)	1.000000	0.005070	1.000000	0.978872	1.000000		0.044711	0.954641	0.811741	0.905106	1.000000	0.344733

LTI(H65)	0.049331	0.999388	0.016459	0.511423	0.082750	0.044711		0.606093	0.835407	0.000673	0.090512	0.997071
LTI(H75)	0.962837	0.162414	0.807148	1.000000	0.990011	0.954641	0.606093		1.000000	0.154339	0.992479	0.990298
LTI(H76)	0.832274	0.329097	0.569424	0.999993	0.921764	0.811741	0.835407	1.000000		0.066277	0.933634	0.999750
LTI(H77)	0.890011	0.000162	0.986833	0.205082	0.784988	0.905106	0.000673	0.154339	0.066277		0.762446	0.009730
LTI(H78)	1.000000	0.011450	0.999889	0.997712	1.000000	1.000000	0.090512	0.992479	0.933634	0.762446		0.529125
LC(H79)	0.367461	0.796478	0.169056	0.975928	0.503203	0.344733	0.997071	0.990298	0.999750	0.009730	0.529125	

Figure 4.18. *AFP* and *VIM* gene expression at the mRNA level in LTIs. Expression levels were analyzed in resected human liver fragments using RT-qPCR. Tissue fragments were collected from 12 patients designated LTI(H33, H38, H65, H71, H72, H73, H74, H75, H76, H77, H78, and H79). RNA was isolated from 50 mg of liver tissue using the Bead-Beat Total RNA Mini Kit. Each sample was analyzed in four replicates. The housekeeping gene β-actin (*ACTB*) served as an internal control. Gene expression levels were calculated using the comparative Ct (ΔΔCt) method, with the average RQ value for all samples for a given gene serving as the calibrator. Expression levels were determined as the ratio of the RQ of each target gene to that of the *ACTB* control. The graph also indicates patient gender, age, cancer or liver steatosis status, and chemotherapy treatment. Bars representing *AFP* expression are shown in pink, and those for *VIM* in blue. **A)** Statistical significance (*p*) for *AFP* expression in Figure 4.18. **B)** Statistical significance (*p*) for *VIM* expression in Figure 4.18. Statistical analysis was performed using one-way ANOVA followed by Duncan's post-hoc test. Results are presented as mean ±SD (n = 4). Significance levels: **p*<0.05, ***p*<0.01, ****p*<0.001.

4.2 Human Hepatocyte-Derived Proliferating Cells (hHDPCs) as a New Model of Human Hepatocytes

4.2.1 hHDPCs Characteristics

The newly obtained cells, derived from dedifferentiated human hepatocytes isolated from resected human liver fragments, were designated as human Hepatocyte-Derived Proliferating Cells (hHDPCs). These cells were analyzed to assess their metabolic and morphological similarities to human hepatocytes (hH_2; hHs), HDFn, and C3A.

Table 4.7 presents the range of FSC (corresponding to cell size) and SSC (corresponding to cell granularity) values for the studied cell populations, as well as the values measured at the population centers. The results indicate that, in terms of cell size, hHDPCs are comparable to hHs and C3A, whereas HDFn cells are the largest. In contrast, when granularity is considered, hHDPCs are similar to hHs, with values approximately half of those observed for C3A and HDFn (Figure 4.19).

Table 4.7. Comparison of size and granularity between hHDPCs, C3A, HDFn, and hHs.

	Range		Population center	
Cell type	**FSC 'size'**	**SSC 'granularity'**	**FSC**	**SSC**
C3A	80-200	65-240	135	130
HDFn	100-225	70-250	150	130
hHDPCs	70-210	35-230	120	80
hH_2	75-200	20-170	130	75

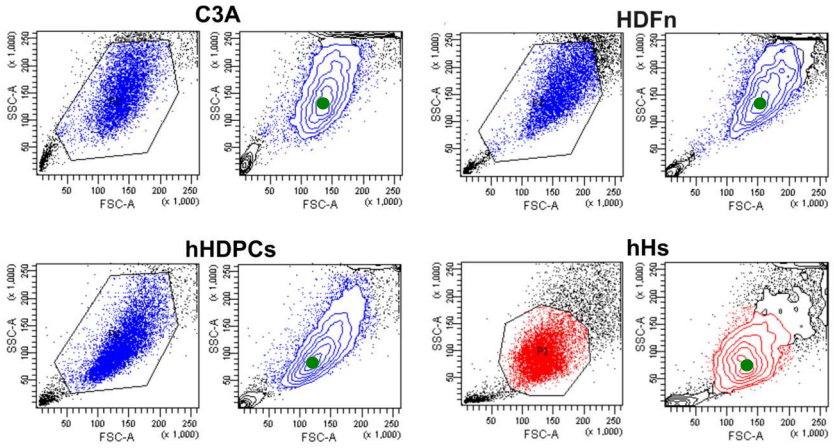


Figure 4.19. Cytometric comparison of the distribution of hHDPCs, C3A, HDFn, and hH_2 cell populations. Flow cytometric analysis was performed on hHDPCs, C3A, HDFn, and hH_2. Cells were cultured for 2 days, trypsinized, and counted using the Trypan Blue exclusion method. Subsequently, 1×10^6 cells from each sample were collected, fixed with 4% formaldehyde, and analyzed. Measurement parameters were FSC at 300 V, and SSC at 400 V. Left-hand graphs (dot-plots) represent the population distribution of individual cells, whereas right-hand graphs (contour plots) depict the contour-line population distribution. FSC and SSC values were obtained from the contour-plots, with the centers of the studied populations marked by green dots. A single measurement was performed for each cell type (n = 1).

4.2.1.1 Comparison of Apical Vacuole Formation Different Cell Types

To perform apical vacuole (AV) imaging, fixed C3A cells were incubated with an F-actin Staining Kit containing a red fluorescent phalloidin-conjugated probe. This probe binds specifically to actin filaments, enabling visualization of actin-based structures such as apical vacuoles. Apical vacuoles, precursors of liver *bile canaliculi*, form between two or more apical cell membranes and appear as ring-shaped structures. As shown in Figure 4.20 A, B, C3A cells are capable of forming AVs, and these structures are observed at junctions involving three or more apical cell membranes.

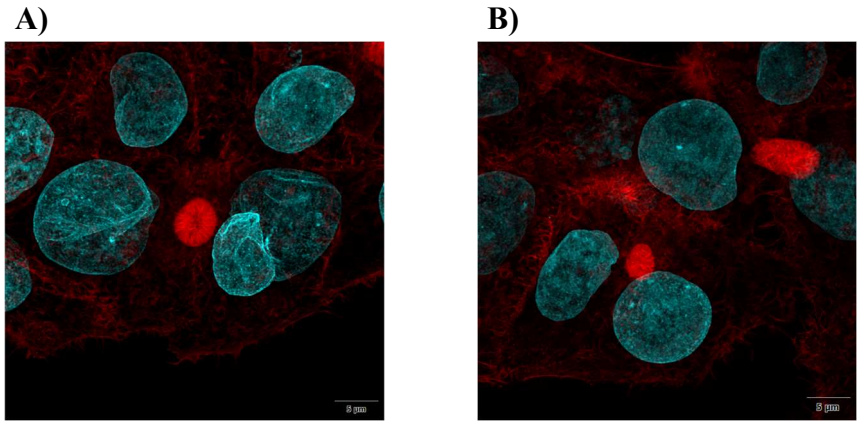


Figure 4.20. Apical vacuoles (AV) are present between C3A cells. Cells were seeded at a density of 4×10^5 cells onto microscope cover glasses (3.6 cm^2) and cultured for 2 days in DMEM medium. Cells were stained with the F-actin Staining Kit – Red Fluorescence – Cytopainter, labeling actin filaments in red, while nuclei were stained with DAPI (blue). Apical vacuoles are visualized as bright red, ring-shaped structures at cell junctions. Images were obtained using a confocal laser-scanning microscope (Fluoview FV4000), at 60× magnification with oil immersion (scale bar = 5 µm) (Olympus, Warsaw, Poland).

Commercially available human hepatocytes were examined for their ability to form apical vacuoles under standard, flat, static culture conditions. Thawed hepatocytes (hH_2) were cultured for two days, fixed, and stained with the red fluorescent probe for actin, while nuclei were stained with DAPI. As shown in Figure 4.21, merged images revealed no characteristic ring-shaped structures in hepatocytes. Instead, phalloidin staining highlighted F-actin filaments throughout the entire cell cytoplasm. These results indicate that, under the tested culture conditions, human hepatocytes do not form apical vacuoles as the ring-shaped structures formed by the cells are not present and, consequently, may indicate a loss of cell polarity.

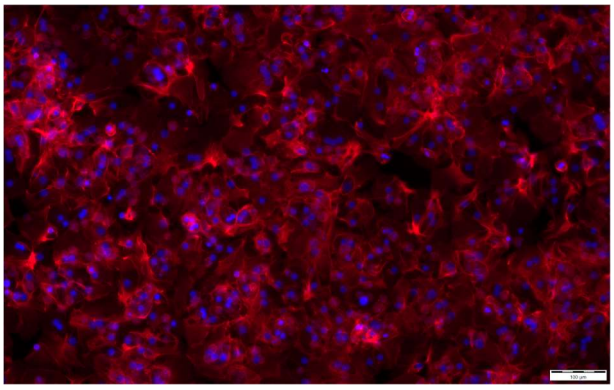


Figure 4.21. Apical vacuoles in human hepatocytes. Cells were seeded at a density of 5×10^5 cells per well in a 24-well plate and cultured for 2 days. Phalloidin staining (red) for actin filaments visualization, merged with nuclei stained using DAPI (blue). Images were acquired using a fluorescence inverted microscope (Olympus IX-71), at 10× magnification (scale bar = 100 µm).

To compare AV formation among different cell types, C3A cells, HDFn, and hHDPCs were analyzed. C3A cells served as the positive control due to their known ability to form AVs.

HDFn cells served as the negative control, while hHDPCs, derived from dedifferentiated human hepatocytes, were tested for AV formation capacity.

Results confirmed that C3A cells form AVs, visualized as red ring-shaped structures at cell–cell junctions (Figure 4.22A, green arrows). In contrast, no apical vacuoles were observed in HDFn cells; only phalloidin-stained F-actin filaments were visible (Figure 4.22B). Similarly, hHDPCs failed to form AVs. Although small red dots were occasionally observed at the cell periphery, they did not localize between cells, suggesting that hHDPCs lack the ability to form apical vacuoles and exhibit no cell membrane polarization (Figure 4.22C).

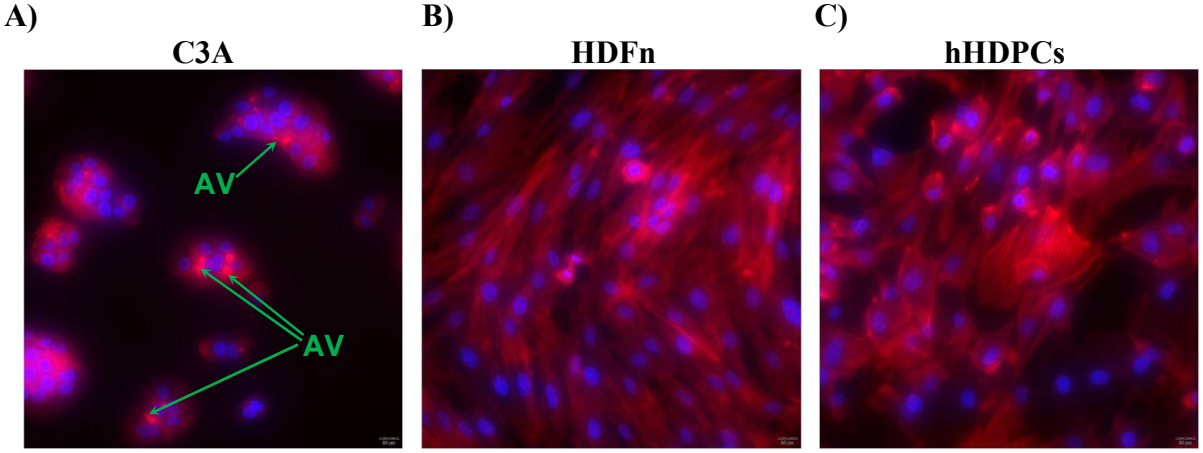


Figure 4.22. Comparison of apical vacuole formation in C3A, HDFn, and hHDPCs. F-actin staining (red) was performed for three cell types: C3A, HDFn, and hHDPCs. Nuclei were counterstained with DAPI (blue). **A)** C3A cells, positive control, forming AVs (green arrows). **B)** HDFn cells, negative control, with no AV formation. **C)** hHDPCs, tested for AV formation. Cells were seeded at a density of 5×10^4 cells and cultured for 2 days in media specific for each cell type. Images were taken using an Olympus APX100 fluorescence microscope (Olympus, Warsaw, Poland) at 40× magnification (scale bar = 20 µm).

4.2.1.2 hHDPCs are Positive for Hepatocyte-Specific Proteins – Immunofluorescence

Immunofluorescence analysis was performed to detect the expression of specific proteins, including ALB, A1AT, CYP3A4, HNF4α, AFP, VIM, and Ki67, in hHDPCs from various passages and donors, as well as in control cell types: hH_2, C3A, and HDFn.

Immunolabeling with anti-human albumin antibodies was performed for the following hHDPCs cell types: hHDPCs+0(H37), hHDPCs+4(H76), and hHDPCs+8(H63). The results demonstrated that hHDPCs from the analyzed passages and donors produced albumin, visualized as green fluorescence. hH_2 and C3A cells served as positive controls, as these cell types are known to express albumin, whereas HDFn cells, which do not produce albumin, were used as negative controls (Figure 4.23A).

The next analyzed liver protein was A1AT, whose green fluorescence signal was detected in all examined hHDPCs samples (hHDPCs+0(H37), hHDPCs+4(H65),

hHDPCs+8(H63)) as well as in all control cell types, including hH_2, C3A, and surprisingly, HDFn (Figure 4.23B).

Analysis of CYP3A4 protein expression in the tested cells revealed that the hHDPCs are capable of producing this typical hepatocyte P450 cytochrome isoenzyme at low levels (samples: hHDPCs+0(H37), hHDPCs+4(H65), and hHDPCs+12(H72)). Interestingly, no protein signal was detected in hH_2 cells, which served as a positive control. In contrast, the C3A cells exhibited protein expression at similarly low levels to the hHDPCs. As expected, no fluorescence signal was observed in the HDFn cells, which served as a negative control (Figure 4.23C).

For the analysis of the hepatocyte transcription factor HNF4α, C3A, HDFn, hHs, hHDPCs+0(H37), hHDPCs+4(H76), and hHDPCs+12(H72) cells were examined. A red fluorescence signal or green fluorescence in the case of the hHDPCs+4(H76) was detected in all analyzed cell types. However, fluorescence was predominantly localized in the cell nuclei, as expected, only in the hH_2 cells, with minimal signal detected in the entire cell. In contrast, in the remaining cell types, the observed signal originated exclusively from the cytoplasm (Figure 4.23D).

The AFP protein, as a marker of immature hepatocytes and cancer cells, was detected at high levels only in C3A cells. No protein signal was observed in either HDFn or hH_2 cells, whereas in the various hHDPCs samples (hHDPCs+0(H37), hHDPCs+4(H65), hHDPCs+8(H63)), the fluorescence signal intensity was low yet evident (Figure 4.23E).

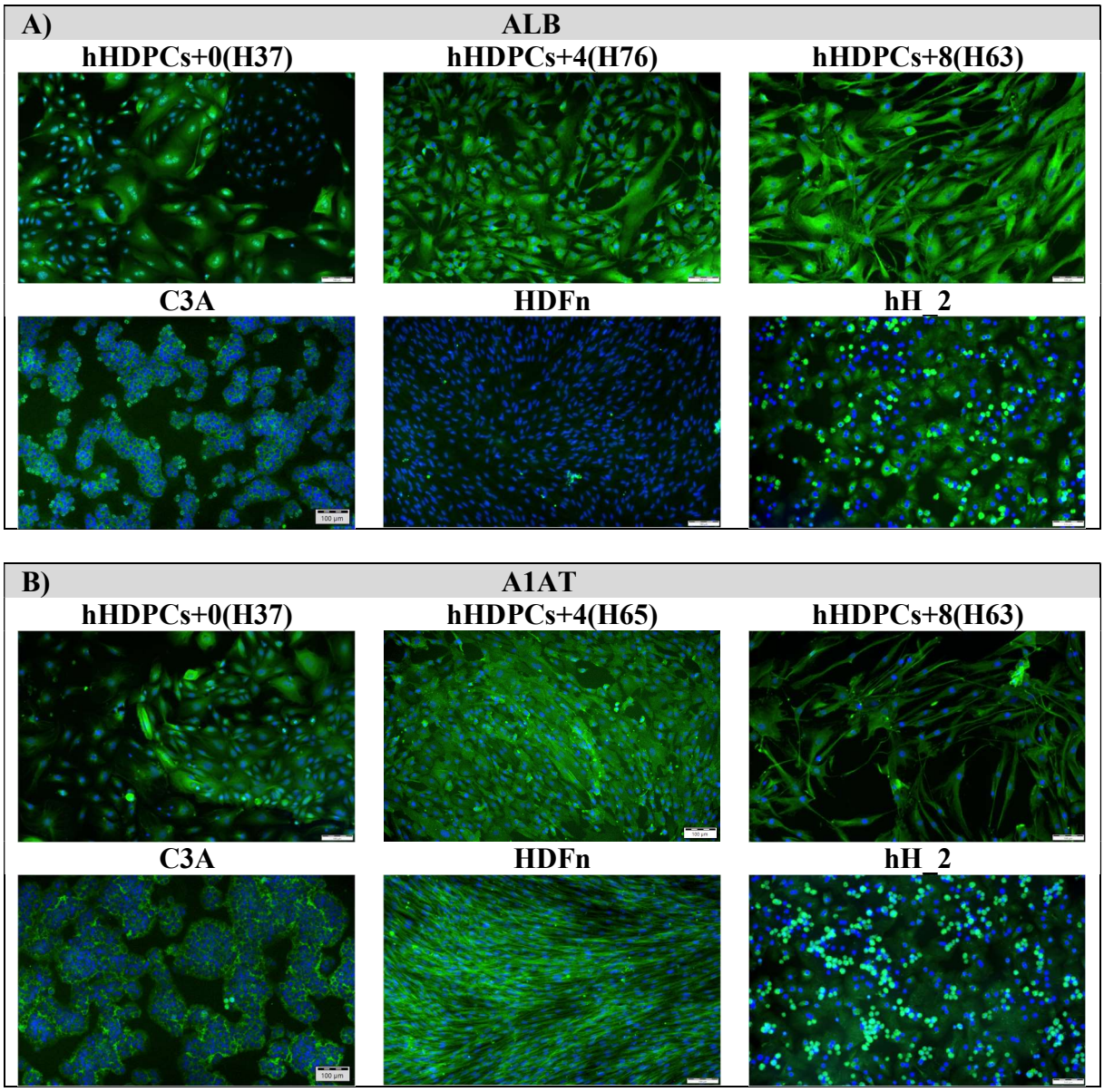
Another analyzed protein was Ki67, a marker indicative of cellular proliferation. The protein signal (green fluorescence) was detected in nearly all tested cell types (C3A, HDFn, hHDPCs+0(H37), hHDPCs+8(H63), hHDPCs+12(H72)), with the exception of hH_2. In the case of hHs, the green fluorescence observed in the images originated from unattached cells (Figure 4.23F).

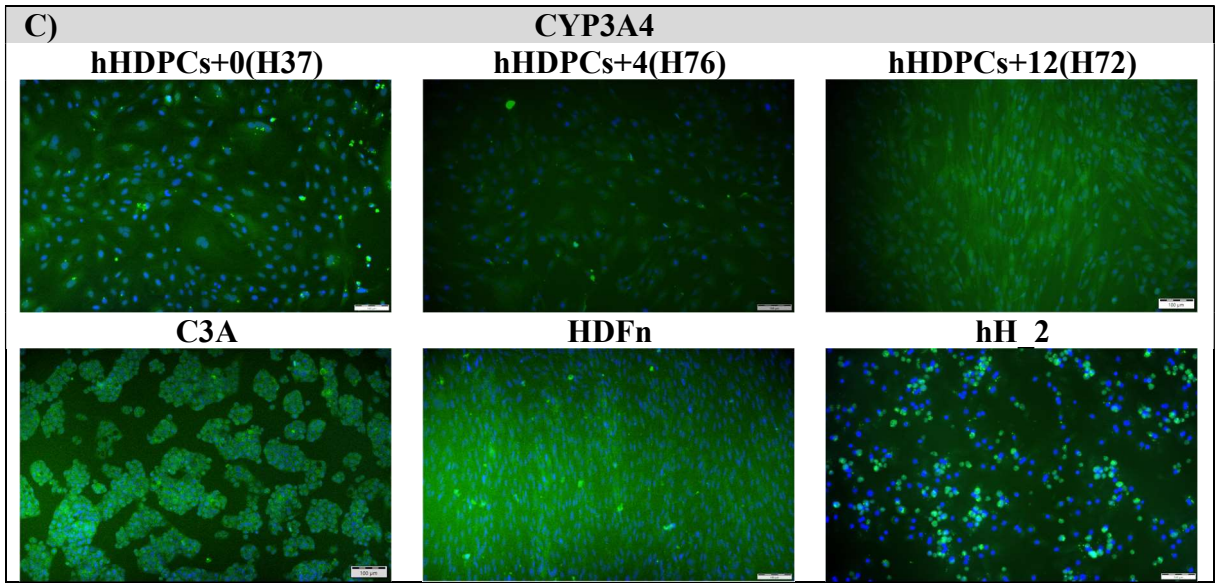
During the experiment the presence of CK18 in cells was also analyzed, which is a marker expressed by hepatocytes. The results indicated that this protein is present at low levels in hHDPCs+1(H63), hDPCs+6(H76) and ihHDPCs+10(H37). Importantly, the images show that CK18 protein expression increases with passage number, regardless of the sample donor. Low level of CK18 expression was observed in hH_2, whereas no expression was detected in the C3A cell. HDFn cells were not analyzed (Figure 4.23G).

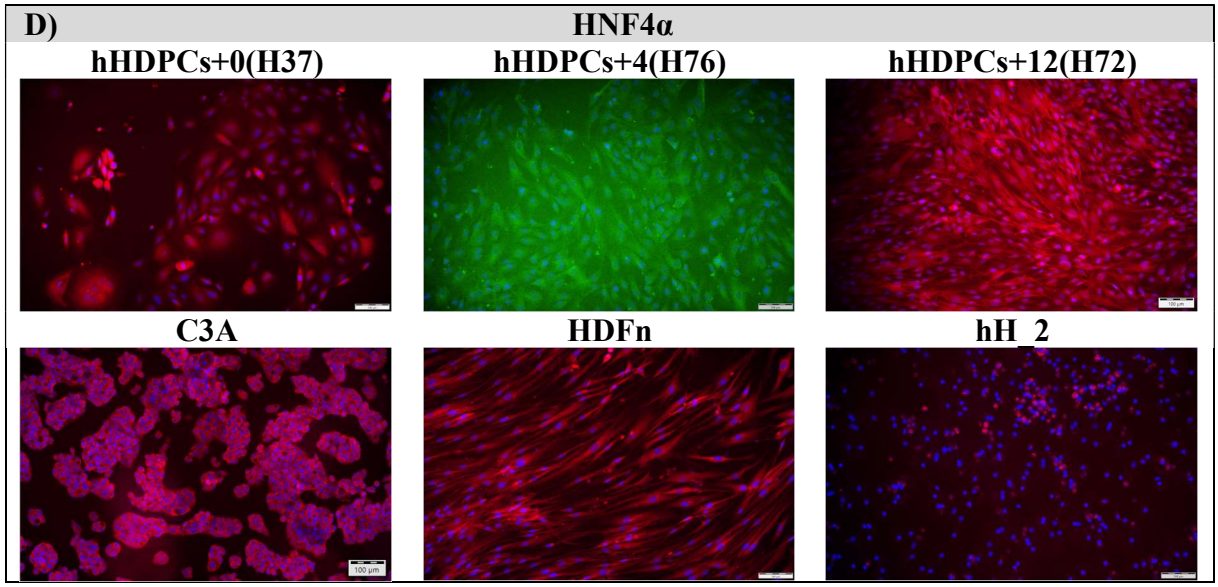
Another analyzed protein was CK19, a marker of both cancer cells and immature hepatocytes. CK19 was detected at low levels in some cells at the initial passage hHDPCs+0(H37), while other cells were negative. CK19 expression was not observed in

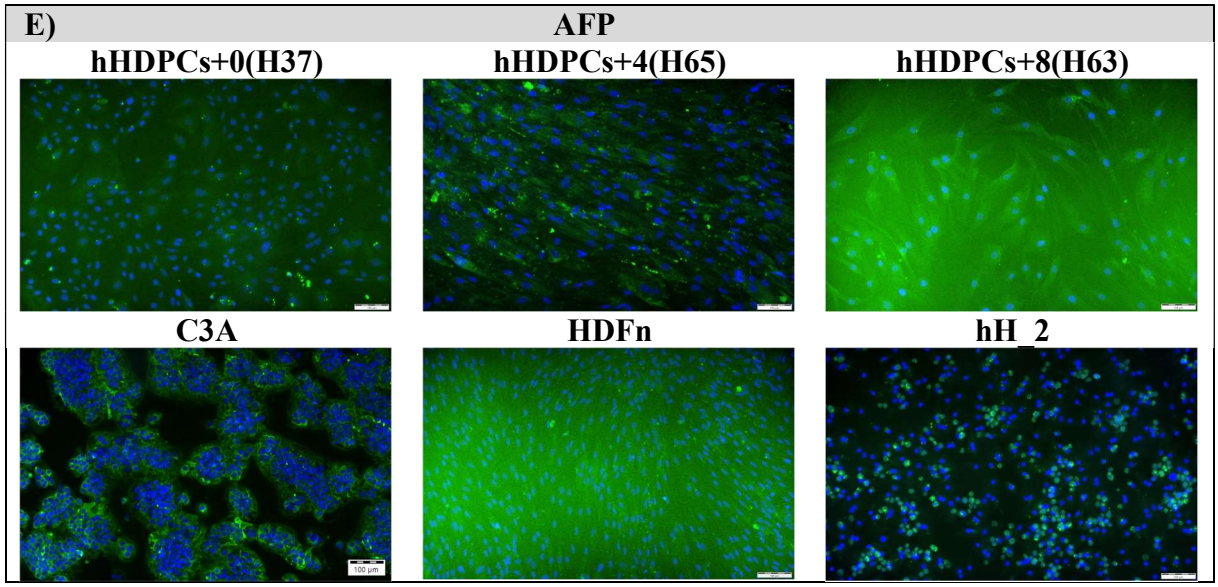
hHDPCs+4(H65) and hHDPCs+12(H72). Among the control cell types (C3A, HDFn, hH_2), only for C3A protein expression was observed, although at a low level (Figure 4.23H).

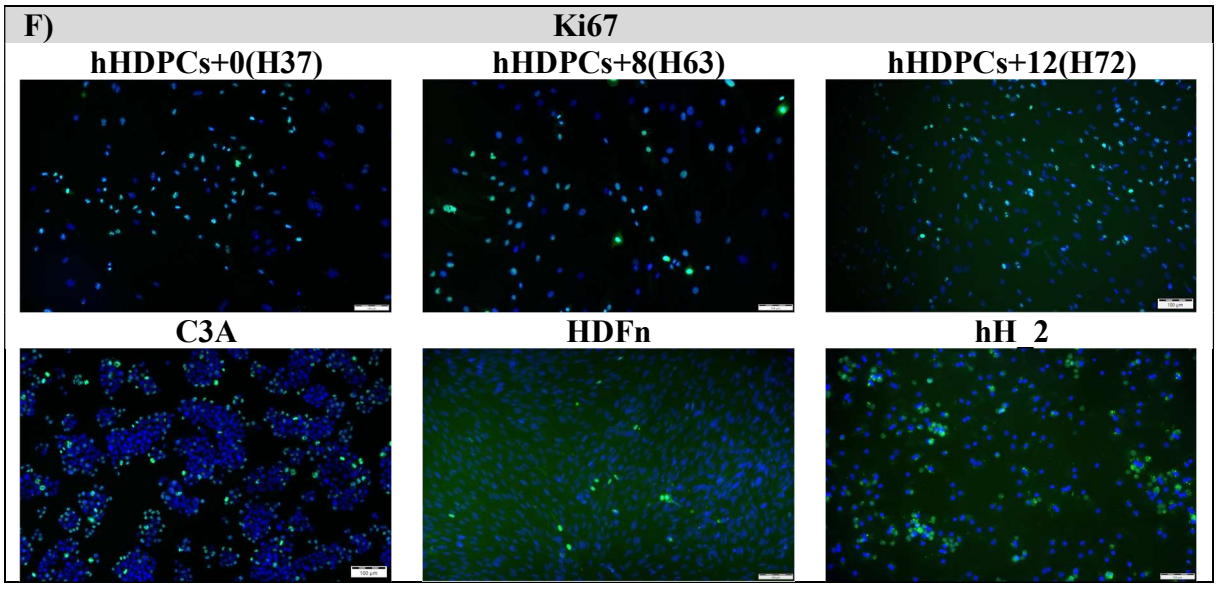
The final protein examined for its presence in the cells was vimentin, a marker specific for fibroblasts. A strong green fluorescence signal was detected in HDFn, as well as in hHDPCs+0(H37) and hHDPCs+4(H65). In contrast, the signal observed in hHDPCs+5(H65) was weaker than that in the other cell types. Furthermore, no Vim signal was detected in hH_2 and C3A (Figure 4.23I).

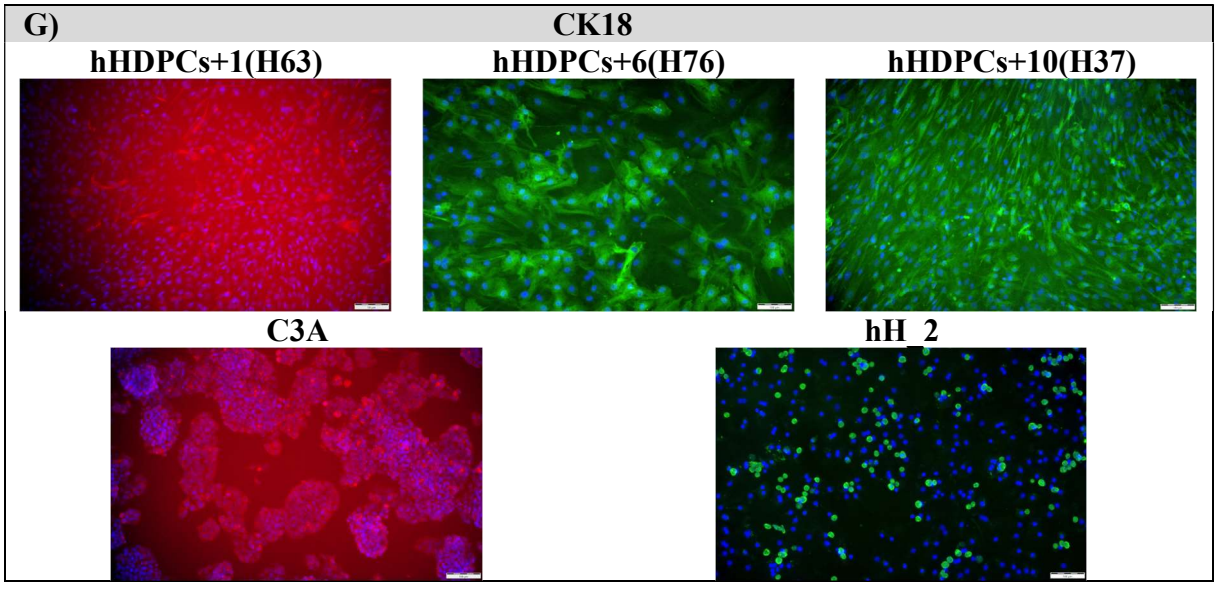


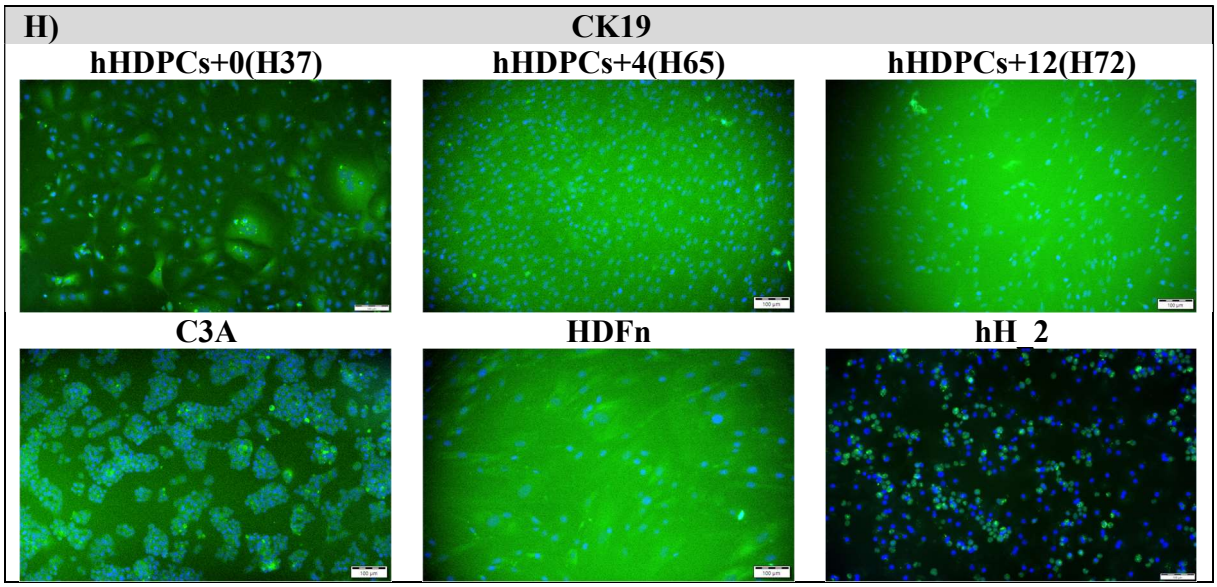

C)
CYP3A4
hHDPCs+0(H37)
hHDPCs+4(H76)
hHDPCs+12(H72)
C3A
HDFn
hH_2


D)
HNF4α
hHDPCs+0(H37)
hHDPCs+4(H76)
hHDPCs+12(H72)
C3A
HDFn
hH_2


E)
AFP
hHDPCs+0(H37)
hHDPCs+4(H65)
hHDPCs+8(H63)
C3A
HDFn
hH_2


F)
Ki67
hHDPCs+0(H37)
hHDPCs+8(H63)
hHDPCs+12(H72)
C3A
HDFn
hH_2


G)
CK18
hHDPCs+1(H63)
hHDPCs+6(H76)
hHDPCs+10(H37)
C3A
hH_2


H)
CK19
hHDPCs+0(H37)
hHDPCs+4(H65)
hHDPCs+12(H72)
C3A
HDFn
hH_2

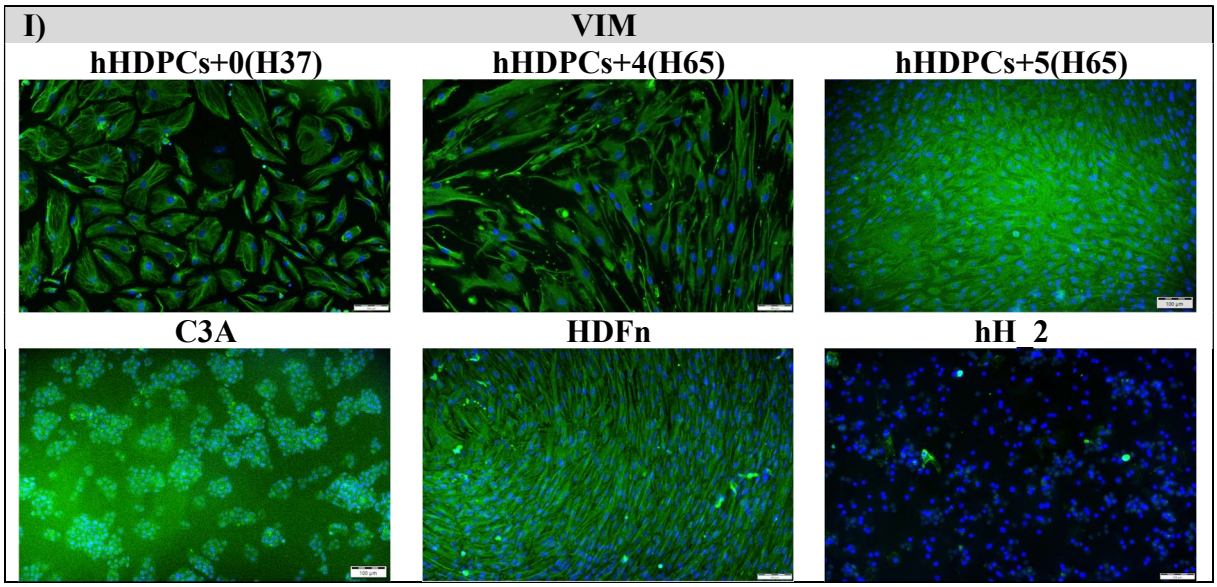


Figure 4.23. Expression of hepatic markers in different cell types. Tested cells were seeded in 24-well plates and cultured in media specific to each cell type. hH_2, C3A, and HDFn cells served as controls. C3A and HDFn cells were cultured in DMEM, whereas all hHDPCs and hH_2 cells were maintained in Hepatocyte Medium supplemented with HGS. Cells were seeded at densities appropriate for each cell type. Prior to immunocytochemical analysis, cells were cultured for 2–5 days and subsequently fixed. Cell nuclei were counterstained with DAPI (blue). **A)** Albumin (ALB) expression was detected in the following hHDPCs: hHDPCs+0(H37), hHDPCs+4(H76), and hHDPCs+8(H63). Albumin-producing cells exhibited green fluorescence. **B)** Alpha-1 antitrypsin (A1AT) expression was observed in hHDPCs+0(H37), hHDPCs+4(H65), and hHDPCs+8(H63), indicated by green fluorescence. **C)** Cytochrome P450 3A4 (CYP3A4) expression was detected in hHDPCs derived from different donors (H37, H76, H72) and representing distinct passages (+0, +4, +12). Green fluorescence corresponded to CYP3A4 expression. **D)** Hepatocyte nuclear factor 4 alpha (HNF4α) expression was analyzed in hHDPCs+0(H37), hHDPCs+4(H76), and hHDPCs+12(H72) cells. HNF4α was visualized as red fluorescence or green fluorescence in the case of hHDPCs+4(H76). **E)** Alpha-fetoprotein (AFP) expression was examined in hHDPCs+0(H37), hHDPCs+4(H65), and hHDPCs+8(H63) cells and was indicated by green fluorescence. **F)** The proliferation marker Ki67 was assessed in hHDPCs+0(H37), hHDPCs+8(H63), and hHDPCs+12(H72) cells, appearing as a green fluorescent signal. **G)** CK18 expression was analyzed in hHDPCs+1(H63), hHDPCs+6(H76), hHDPCs+10(H37), C3A, and hH_2. In case of hHDPCs+1(H63) and C3A protein expression was indicated by red color, and for other samples by green. **H)** CK19 expression was examined for the hHDPCs+0(H37), hHDPCs+4(H65), hHDPCs+12(H72), C3A, HDFn, hH_2. CK19-producing cells exhibited green fluorescence. **I)** Vimentin (VIM) expression was analyzed in hHDPCs+0(H37), hHDPCs+4(H65), and hHDPCs+5(H65) cells and visualized by green fluorescence. Merged micrographs were acquired using an Olympus IX-71 inverted fluorescence microscope at 10× magnification (scale bar: 100 µm), with the same exposure settings.

4.2.1.3 hHDPCs are Positive for Hepatocyte-Specific Proteins – FC

A comprehensive series of experiments was undertaken to characterize hHDPCs, with flow cytometric analyses performed to quantify the expression levels of hepatocyte-specific proteins across multiple cell isolates and passages. The data presented in Figure 4.24A-C illustrate representative findings obtained from LCI derived from two donors (H65 and H72)

and their corresponding passages (various lines of hHDPCs). HepG2 and human hepatocytes (hH_1) were included as reference controls.

For donor H65, results are provided for the liver cell isolates and passages +1 and +4; whereas for donor H72, data encompass passages +1, +4, +7, and +11. The proteins analyzed included albumin (ALB), Hepatocyte Nuclear Factor 4α (HNF4α), and Cytochrome P450 3A4 (CYP3A4). Due to the limited availability of material, CYP3A4 expression was not assessed in the LCI(H65) nor in the hHDPCs+1(H72).

Figure 4.24A summarizes the percentages of ALB-positive cells. All samples exhibited albumin expression; however, the proportions varied across passages. For H65-derived material, 80% of cells in the LCI were ALB-positive; this proportion decreased to 40% at passage +1 but subsequently increased to 83% at passage +4. In the case of H72-derived samples, 51% of cells in the liver lysate expressed albumin; the percentage declined to 27% at passage +1, rose to 54% at passage +4, dropped to 18% at passage +7, and increased again to 48% at passage +11 (Figure 4.24A). Among the control groups, 62% of HepG2 cells and 71% of hHs were ALB-positive.

Expression analysis of HNF4α in the hHDPCs revealed more pronounced variability than that observed for albumin (Figure 4.24B). For H65-derived samples, 31% of cells in the liver lysate were HNF4α-positive; this proportion increased to 67% at passage +1, followed by a marked decline to 8% at passage +4. In H72-derived material, 14% of cells in the LCI expressed HNF4α; this increased to 42% at passage +1, decreased to 9% at passage +4, dropped sharply to 1% at passage +7, and rose again to 20% at passage +11. In the reference controls, HNF4α expression was detected in 40% of the HepG2 cells and 48% of the hHs.

Due to the limited number of samples, CYP3A4 expression analysis was not performed for the H65 liver lysate or the hHDPCs+1(H72). In hHDPCs derived from the H65, 93% of cells at passage +1 were CYP3A4-positive, whereas this percentage decreased sharply to 7% at passage +4. For H72-derived samples, 14% of LCI expressed CYP3A4; this percentage decreased to 3% at passage +4, became undetectable at passage +7, and then increased dramatically to 98% at passage +11 (Figure 4.24C). Among the reference groups, 1% of HepG2 cells and 21% of hHs expressed CYP3A4.

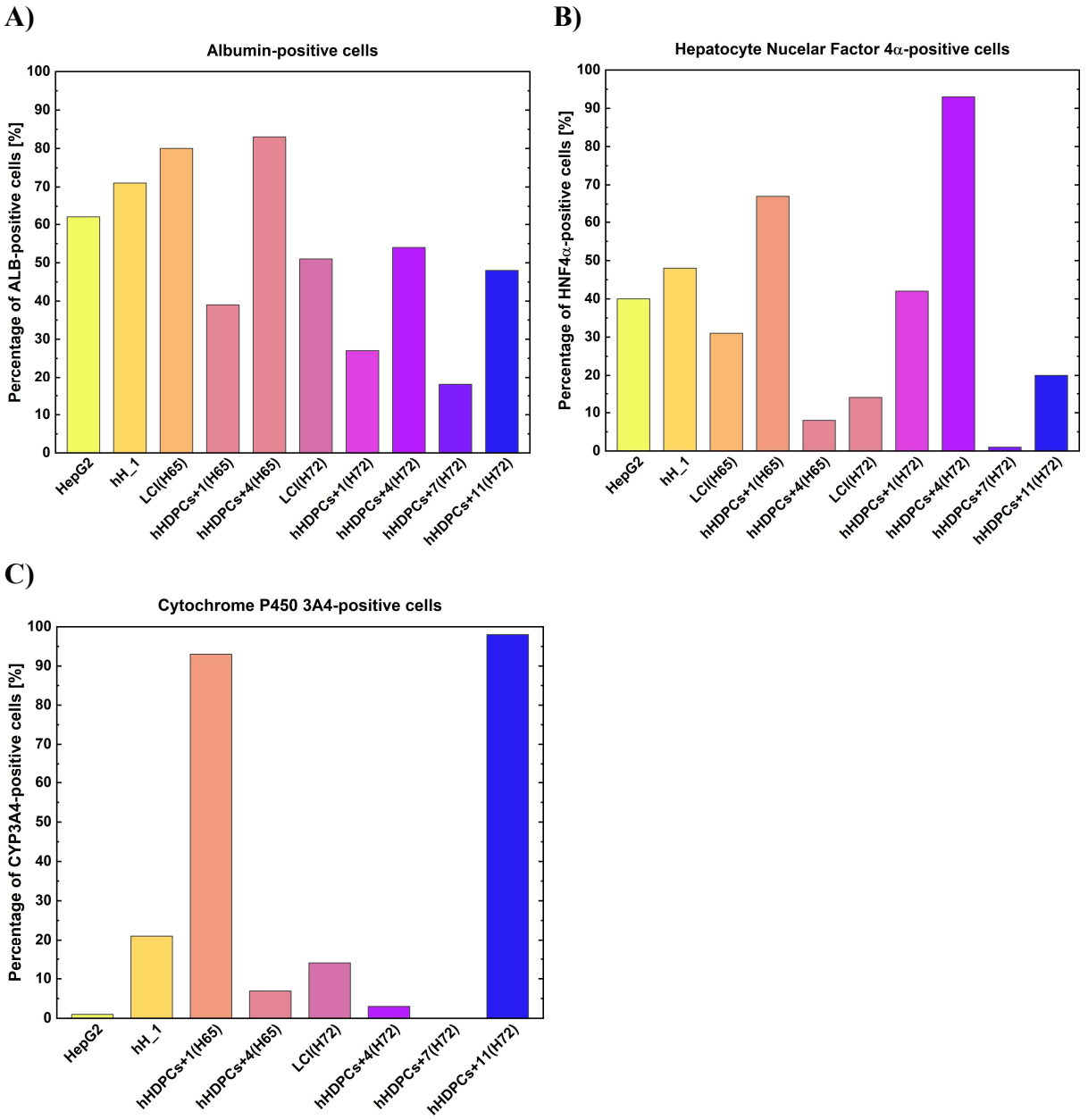


Figure 4.24. Comparison of the Percentage of Antibody-Positive Cells in Liver Isolates and in Liver-Derived Cell Lines at Different Passages. Flow cytometric analysis was performed for LCIs from two donors (H65 and H72) and for hHDPCs derived from these isolates at various passages (hHDPCs+1(H65), hHDPCs+4(H65), hHDPCs+1(H72), hHDPCs+4(H72), hHDPCs+7(H72), hHDPCs+11(H72)). HepG2 cells and human hepatocytes (hH_1) were included as controls. Three hepatocyte-specific proteins were analyzed: albumin (ALB), Hepatocyte Nuclear Factor 4α (HNF4α), and Cytochrome P450 3A4 (CYP3A4). A total of 2×10^5 cells were used for the analysis of each sample. **A)** Graph representing the percentage of ALB-positive cells for the following samples: LCI(H65), hHDPCs+1(H65), hHDPCs+4(H65), LCI(H72), hHDPCs+1(H72), hHDPCs+4(H72), hHDPCs+7(H72), hHDPCs+11(H72). **B)** Graph showing the percentage of HNF4α-positive cells for the same sample set: LCU(H65), hHDPCs+1(H65), hHDPCs+4(H65), LCI(H72), hHDPCs+1(H72), hHDPCs+4(H72), hHDPCs+7(H72), hHDPCs+11(H72). **C)** Graph illustrating the percentage of CYP3A4-positive cells for the following samples: hHDPCs+1(H65), hHDPCs+4(H65), LCI(H72), hHDPCs+4(H72), hHDPCs+7(H72), hHDPCs+11(H72). Each sample was analyzed in a single replicate; therefore, neither standard deviations nor statistical analyses were calculated.

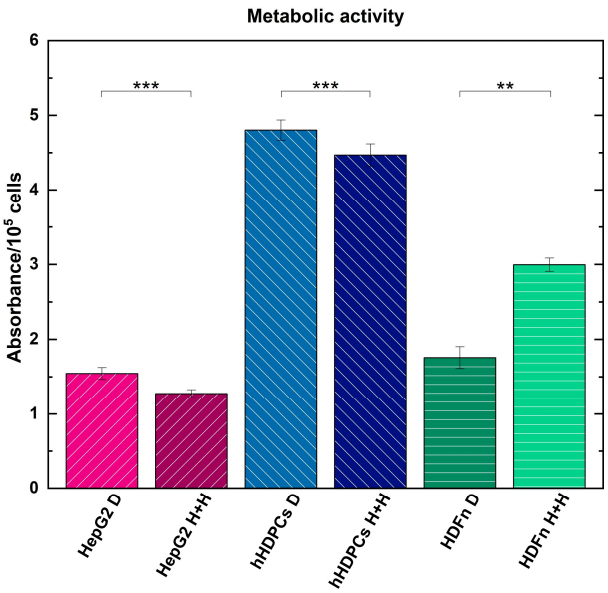
4.2.2 Comparison of hHDPCs, HepG2, and HDFn Cultures

4.2.2.1 MTT Assay

The thiazolyl blue tetrazolium bromide (MTT) assay was used to assess the mitochondrial activity of the tested cells. The metabolic activity of the hHDPCs was determined for cells at passage +3, obtained from donor H65. The hHDPCs were compared with the HepG2 and the HDFn. In addition, mitochondrial activity was evaluated in cells cultured in two types of media: DMEM (D) and HM supplemented with HGS (H+H).

The results indicated that, among all tested cell types, the hHDPCs exhibited the highest metabolic activity in both conditions. The hHDPCs showed about a 1.1-fold higher activity in DMEM than in H+H ($p<0.01$). The HDFn cells displayed about a 1.6-fold lower activity in DMEM than in H+H ($p<0.01$). HepG2 cells showed a 1.2-fold lower activity in H+H than in DMEM ($p<0.01$) (Figure 4.25A). Comparison of metabolic activity between different cell types cultured in the same medium showed that the hHDPCs cultured in DMEM exhibited 2.7-fold and 3.2-fold higher mitochondrial activity than the HDFn and HepG2, respectively ($p<0.001$ for both). Similarly, the hHDPCs cultured in H+H exhibited the highest metabolic activity, approximately 1.5-fold higher than the HDFn ($p<0.01$), and about 3.5-fold higher than the HepG2 ($p<0.001$) (Figure 4.25A). Moreover, a similar pattern was observed for the hHDPCs and the HepG2 cells, which exhibited the highest metabolic activity when cultured in DMEM, approximately 1.2-fold higher than when cultured in H+H. In contrast, the HDFn cells cultured in H+H exhibited approximately 1.7-fold higher metabolic activity compared with those cultured in DMEM (Figure 4.25A).

A)



A1)

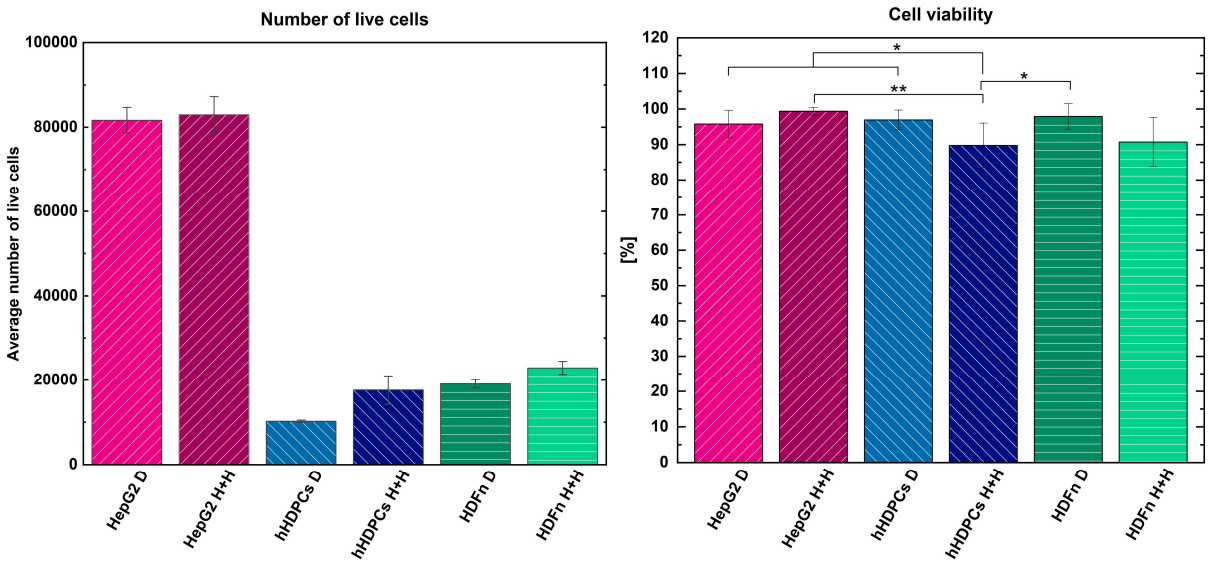
		HepG2	HepG2	hHDPCs	hHDPCs	HDFn	HDFn
		D	H+H	D	H+H	D	H+H
HepG2	**D**		0.000206	0.000031	0.000053	0.001546	0.000063
HepG2	**H+H**	0.000206		0.000026	0.000031	0.000063	0.000053
hHDPCs	**D**	0.000031	0.000026		0.000124	0.000053	0.000063
hHDPCs	**H+H**	0.000053	0.000031	0.000124		0.000063	0.000121
HDFn	**D**	0.001546	0.000063	0.000053	0.000063		0.000121
HDFn	**H+H**	0.000063	0.000053	0.000063	0.000121	0.000121	

Figure 4.25. Comparison of metabolic activity among HepG2, HDFn, and hHDPCs determined by the MTT assay. Cells were seeded in 96-well plates at densities of 3×10^4 cells per well for HepG2 and 1×10^4 cells per well for HDFn and hHDPCs. Cultures were maintained in DMEM (D) or HM supplemented with HGS (H+H) for 4 days without medium change. Seven biological replicates were analyzed. **A)** Absorbance values normalized to cell number. **A1)** Statistical significance (p values) for Figure 4.25A, calculated using multivariate analysis of variance (MANOVA) followed by Duncan's *post-hoc* test. Results are presented as mean ± SD (n=7). Statistical significance was defined as: *p<0.05, **p<0.01, ***p<0.001.

The average cell counts at the end of the experiment indicated that the HepG2 cells exhibited the fastest proliferation, with nearly a 3-fold increase in cell number in both media; however, this difference was not statistically significant. The hHDPCs showed the slowest proliferation, with a 1.02-fold increase in DMEM and an almost 2-fold increase in H+H, neither of which reached statistical significance. The HDFn cells displayed intermediate proliferation, with approximately a 2-fold increase in DMEM and a 2.3-fold increase in H+H over 4 days (with no statistically significant difference) (Figure 4.26A).

Among the tested cell types, the lowest and comparable cell viability (approximately 90%) was observed for the hHDPCs and the HDFn cultured in H+H (not statistically significant), whereas HepG2 exhibited a viability of approximately 99% ($p<0.001$ compared with hHDPCs). For all cell types cultured in DMEM, cell viability was similar, at approximately 97%, with no statistically significant differences among the tested cell types (Figure 4.26B).

A) **B)**



A1)

Statistical significance for number of live cells		HepG2	HepG2	hHDPCs	hHDPCs	HDFn	HDFn
		D	H+H	D	H+H	D	H+H
HepG2	D		0.199804	0.000060	0.000082	0.000113	0.000235
HepG2	H+H	0.199804		0.000050	0.000060	0.000082	0.000113
hHDPCs	D	0.000060	0.000050		0.373964	0.010093	0.003992
hHDPCs	H+H	0.000082	0.000060	0.373964		0.028168	0.010093
HDFn	D	0.000113	0.000082	0.010093	0.028168		0.373964
HDFn	H+H	0.000235	0.000113	0.003992	0.010093	0.373964	

B1)

Statistical significance for cell viability		HepG2	HepG2	hHDPCs	hHDPCs	HDFn	HDFn
		D	H+H	D	H+H	D	H+H
HepG2	D		0.384394	0.760283	0.029499	0.590486	0.200115
HepG2	H+H	0.384394		0.541509	0.007291	0.702250	0.054592
hHDPCs	D	0.760283	0.541509		0.019312	0.792256	0.137829
hHDPCs	H+H	0.029499	0.007291	0.019312		0.013269	0.243532
HDFn	D	0.590486	0.702250	0.792256	0.013269		0.097074
HDFn	H+H	0.200115	0.054592	0.137829	0.243532	0.097074	

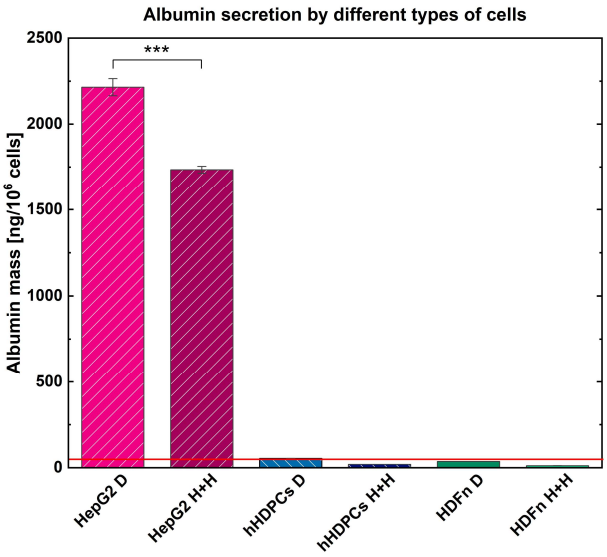
Figure 4.26. Average number of live cells and cell viability in HepG2, HDFn, and hHDPCs cultures. Cells were seeded in 96-well plates at densities of 3×10^4 cells per well for HepG2 and 1×10^4 cells per well for HDFn and hHDPCs, and cultured for 4 days without medium replacement in DMEM (D) or HM supplemented with HGS (H+H). Cells were trypsinized and counted using the trypan blue exclusion method. Two biological replicates were analyzed. **A)** Average number of live cells for the different cell types cultured with D and H+H media. **A1)** Statistical significance (p values) for Figure 4.26A. **B)** Cell viability for the different cell types cultured in D and H+H media. **B1)** Statistical significance (p values) for Figure 4.26B. Statistical significance was determined using MANOVA followed by Duncan's *post-hoc* test. Results are presented as mean ± SD (n=2). Statistical significance was defined as: *p<0.05, **p<0.01, ***p<0.001.

4.2.2.2 Albumin Secretion

To evaluate albumin secretion, hHDPCs, HepG2, and HDFn cells were cultured in two types of media: DMEM (D) and HM supplemented with HGS (H+H). Albumin secretion levels in the post-culture medium were quantified using an enzyme-linked immunosorbent assay (ELISA), absorption measurements were normalized to the number of harvested cells (Supplementary Figure S8.1).

The results showed that only the HepG2 cells secreted detectable levels of albumin in both media. Moreover, HepG2 cells cultured with DMEM secreted 1.3-fold more albumin than those cultured in H+H ($p<0.01$). In contrast, hHDPCs and HDFn cells exhibited albumin levels comparable to the blank baseline, as indicated by the red line in Figure 4.27A.

A)



A1)

Statistical significance for albumin secretion		HepG2	HepG2	hHDPCs	hHDPCs	HDFn	HDFn
		D	H+H	D	H+H	D	H+H
HepG2	**D**		0.000172	0.000095	0.000038	0.000066	0.000032
HepG2	**H+H**	0.000172		0.000172	0.000066	0.000095	0.000038
hHDPCs	**D**	0.000095	0.000172		0.240465	0.523201	0.170483
hHDPCs	**H+H**	0.000038	0.000066	0.240465		0.534485	0.788855
HDFn	**D**	0.000066	0.000095	0.523201	0.534485		0.401933
HDFn	**H+H**	0.000032	0.000038	0.170483	0.788855	0.401933	

Figure 4.27. Albumin secretion by hHDPCs, HepG2, and HDFn cells. Cells were seeded in 24-well plates at densities of 7×10^4 cells per well for HepG2 and 2.5×10^4 cells per well for hHDPCs and HDFn, with three replicates per cell type. Cultures were maintained in DMEM (D) or HM supplemented with HGS (H+H) for 4 days. The red line indicates the baseline. **A)** Albumin secretion level in the post-cultured media. **A1)** Statistical significance (p values) for Figure 4.27A, calculated using MANOVA followed by Duncan's *post-hoc* test. Results are presented as mean ± SD (n=3). Significance levels: *p<0.05, **p<0.01, ***p<0.001.

4.2.2.3 Glucose Consumption

Glucose consumption was measured over 4 days in hHDPCs, HepG2, and HDFn cells cultured in DMEM (D) or HM supplemented with HGS (H+H). It should be noted that DMEM contains a high glucose concentration (4.5 g/L), whereas HM contains a physiological glucose concentration (1 g/L). Two variants of glucose consumption calculations were performed, which revealed differences between the behavior of single cells and that of entire cell populations. The first approach involved calculating glucose consumption per single cell, while the second assessed the percentage of glucose consumed by cell cultures. All glucose consumption measurements were normalized to the number of harvested cells (Supplementary Figure S8.1).

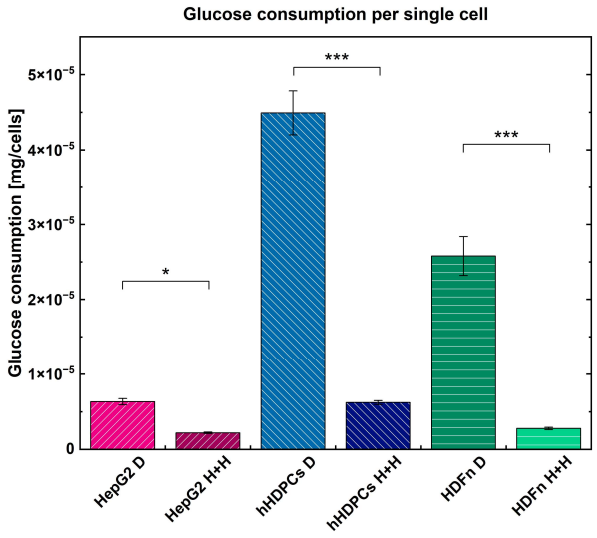
Considering glucose consumption per single cell (Figure 4.28A), among all tested variants, the highest amount of glucose (4.5×10^{-5} mg) was consumed by hHDPCs cultured in DMEM, which was 7.5-fold higher than in hHDPCs cultured in H+H ($p<0.001$). A single HDFn cell cultured in DMEM also consumed a relatively high amount of glucose (2.6×10^{-6} mg), which was 9-fold higher than in H+H ($p<0.001$). In HepG2 cultures, the differences between DMEM and H+H were less pronounced than in hHDPCs or HDFn. However, a single HepG2 cell cultured in DMEM still consumed more glucose (6.3×10^{-6} mg), approximately 2.2-fold more than in H+H ($p<0.05$).

Comparison of glucose consumption per single cell between cell types cultured in the same medium (Figure 4.28A) showed that a single hHDPC cell cultured in DMEM consumed 1.7-fold more glucose than HDFn ($p<0.01$), and 7-fold more than HepG2 ($p<0.001$). In the case of HDFn cell cultures in DMEM, a single cell consumed 4-fold more glucose than a single HepG2 cell ($p<0.01$). Differences in glucose consumption per single cell cultured in H+H were less pronounced than in DMEM. The highest glucose consumption was observed in hHDPCs, which consumed approximately 2-fold more glucose than HDFn ($p<0.05$) and 3-fold more than HepG2 ($p<0.05$).

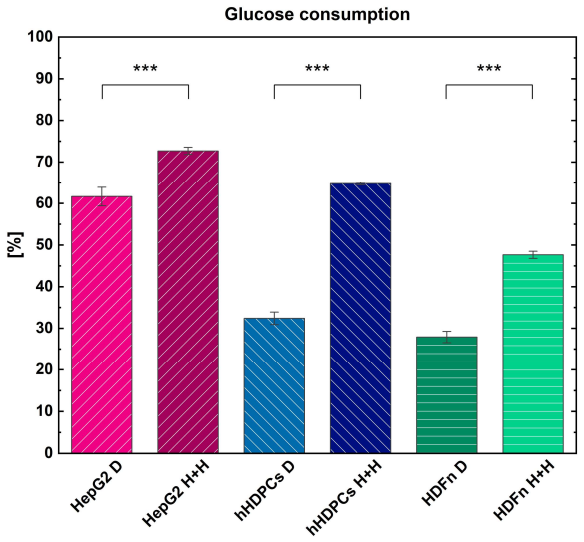
When comparing the percentage of glucose consumption by cell cultures grown in different media (Figure 4.28B), HepG2 exhibited the highest proportion of glucose consumption among all tested cell types under both conditions. The highest percentage was observed for HepG2 cultured in H+H (73%), which was 1.2-fold higher than in DMEM (62%) ($p<0.001$). hHDPCs cultured in H+H consumed 65% of the available glucose, which was approximately 2-fold higher than in DMEM (32%) ($p<0.001$). HDFn cells cultured in H+H consumed 48% of the available glucose, which was 1.7-fold higher than in DMEM (28%)

(p<0.001) (Figure 4.28B). Comparison of glucose consumption across cell types cultured in DMEM showed that HepG2 consumed 1.9-fold more glucose than hHDPCs (p<0.001) and 2.2-fold more than HDFn (p<0.001). In H+H mdium, HepG2 consumed 1.1-fold more glucose than hHDPCs (p<0.01) and 1.5-fold more than HDFn (p<0.001). hHDPCs cultured in DMEM consumed 1.1-fold more glucose than HDFn (p<0.05), and in H+H, 1.3-fold more (p<0.001).

A)



B)



A1)

Glucose consumpt. by single cell		HepG2	HepG2	hHDPCs	hHDPCs	HDFn	HDFn
		D	H+H	D	H+H	D	H+H
HepG2	D		0.012400	0.000095	0.934809	0.000172	0.023712
HepG2	H+H	0.012400		0.000032	0.012482	0.000038	0.666507
hHDPCs	D	0.000095	0.000032		0.000066	0.000172	0.000038
hHDPCs	H+H	0.934809	0.012482	0.000066		0.000095	0.022448
HDFn	D	0.000172	0.000038	0.000172	0.000095		0.000066
HDFn	H+H	0.023712	0.666507	0.000038	0.022448	0.000066	

B1)

Glucose consumption [%]		HepG2	HepG2	hHDPCs	hHDPCs	HDFn	HDFn
		D	H+H	D	H+H	D	H+H
HepG2	D		0.000095	0.000095	0.014272	0.000066	0.000172
HepG2	H+H	0.000095		0.000038	0.000177	0.000032	0.000066
hHDPCs	D	0.000095	0.000038		0.000066	0.001577	0.000172
hHDPCs	H+H	0.014272	0.000177	0.000066		0.000038	0.000095
HDFn	D	0.000066	0.000032	0.001577	0.000038		0.000095
HDFn	H+H	0.000172	0.000066	0.000172	0.000095	0.000095	

Figure 4.28. Glucose consumption by hHDPCs, HepG2, and HDFn cells. Cells were seeded at densities of 7×10^4 (HepG2) and 2.5×10^4 (hHDPCs and HDFn) cells per well in 24-well plates and cultured for 4 days in DMEM (D) or HM supplemented with HGS (H+H), with three replicates per medium type. Glucose measurements were normalized to the number of harvested cells. **A)** Glucose consumption per single cell. **A1)** Statistical significance (p values) for Figure 4.28A. **B)** Percentage of glucose consumption by different cell types cultured with D or H+H. **B1)** Statistical significance (p values) for Figure 4.28B. Statistical significance was determined using MANOVA followed by Duncan's *post-hoc* test. Results are presented as mean ± SD (n=3). Significance levels: *p<0.05, **p<0.01, ***p<0.001.

4.2.3 Effect of Various Culture Media on hHDPCs Proliferation and Viability

The proliferation rate of hHDPCs was evaluated in different culture media: DMEM, EMEM, WEM, HM, and HM+HGS. The experiment was performed using hHDPCs at passages +3 and +8 derived from a single donor (H65). A schematic representation of the culture plate layout is shown in Figure 4.29.

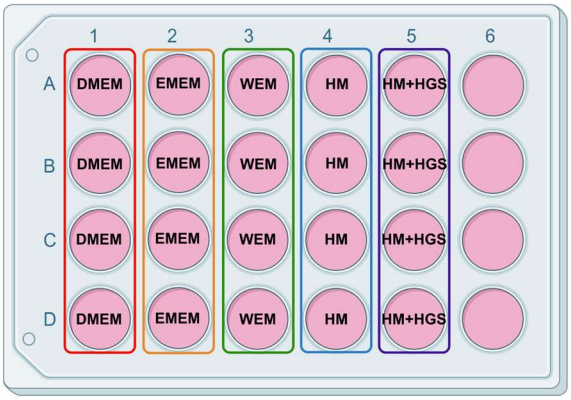


Figure 4.29. **Scheme of experiment for hHDPCs culture in different media.** Cells were cultured with the following media: high glucose Dulbecco's Modified Eagle Medium (DMEM), Eagle's Minimum Essential Medium (EMEM), William's E Medium (WEM), Hepatocyte Medium (HM), and Hepatocyte Medium supplemented with hepatocyte growth supplement (HM+HGS). Cells were seeded at a density of 2×10^4 cells per well and cultured for 6 days. All experimental conditions were performed in four replicates.

4.2.3.1 Cell Number and Cell Doubling Time by hHDPCs Cultured in Various Media

The highest cell numbers were obtained in cultures maintained in HM and HM+HGS for both analyzed cell passages. Cells at the lower passage (hHDPCs+3) exhibited markedly higher proliferation over the 6-day culture period compared with cells at the higher passage (hHDPCs+8). Specifically, hHDPCs+3 cells cultured in DMEM showed an approximately 5.5-fold increase in cell number relative to hHDPCs+8 ($p<0.0001$). Similarly, proliferation of hHDPCs+3 cells in EMEM was nearly 4-fold higher ($p<0.0001$), while cells cultured in WEM showed a 3-fold increase ($p<0.0001$) compared with hHDPCs+8. In HM and HM+HGS, lower passage cells reached 2-fold ($p<0.0001$) and 2.5-fold ($p<0.0001$) higher cell counts, respectively, than their higher-passage counterparts (Figure 4.30A).

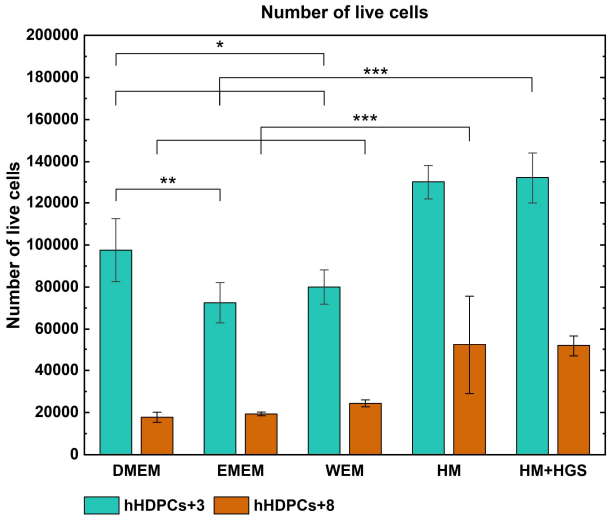
Analysis of cell doubling time revealed that hHDPCs+3 cells cultured in HM or HM+HGS required approximately 2.5 days to double their number (not statistically significant). Cells cultured in EMEM required 4 days, in DMEM 3 days ($p<0.05$), and in WEM 3.5 days (not statistically significant compared with DMEM or EMEM) (Figure 4.30B).

For hHDPCs+8, only cultures in HM and HM+HGS doubled their cell number over a 6-day period, requiring approximately 5.5 days for both media (not statistically significant). Cells

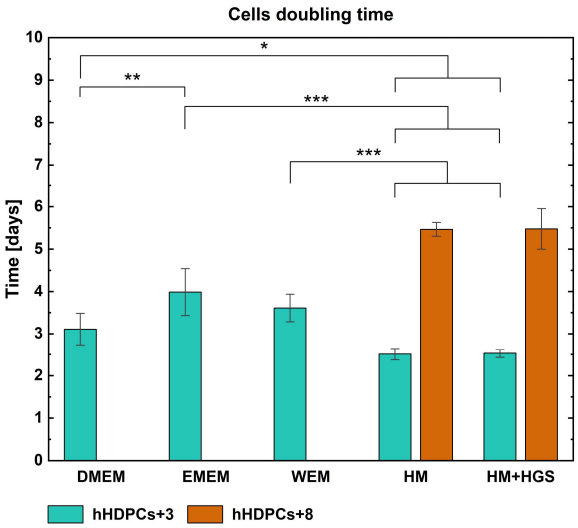
cultured in the other media required a longer period of time to double in number. Moreover, the addition of HGS to the medium did not significantly influence doubling time during the 6-day culture period, regardless of passage (Figure 4.30B).

High cell viability was maintained in both cell passages (+3 and +8), ranging from 92% to 99%. The exception was hHDPCs+8 culture in DMEM, which exhibited 88% viability. Statistical significance was observed only for hHDPCs+8 cultures: cell viability in DMEM (88%) was significantly lower than in HM+HGS (99%; $p<0.001$), which represented the highest value observed in the experiment (Figure 4.30C).

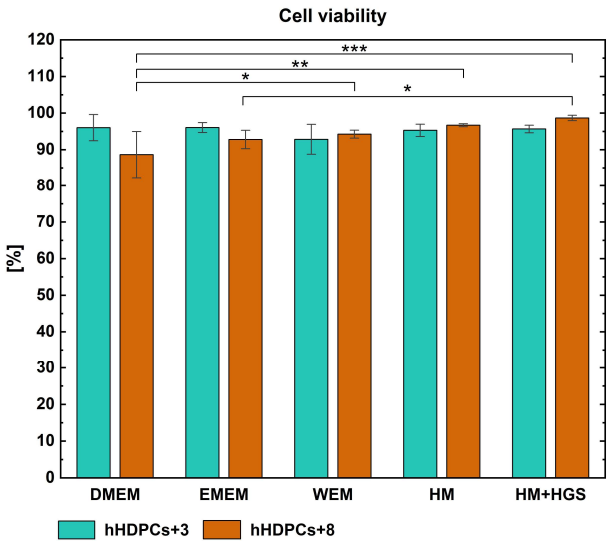
A)



B)



C)



A1)

Statistical significance for number of live cells		hHDPCs+3	hHDPCs+3	hHDPCs+3	hHDPCs+3	hHDPCs+3	hHDPCs+8	hHDPCs+8	hHDPCs+8	hHDPCs+8	hHDPCs+8
		DMEM	EMEM	WEM	HM	HM+HGS	DMEM	EMEM	WEM	HM	HM+HGS
hHDPCs+3	DMEM		0.004110	0.031088	0.000342	0.000204	0.000020	0.000023	0.000027	0.000056	0.000037

hHDPCs+3	**EMEM**	0.004110		0.339808	0.000053	0.000034	0.000027	0.000034	0.000054	0.014015	0.015701
hHDPCs+3	**WEM**	0.031088	0.339808		0.000061	0.000053	0.000023	0.000027	0.000034	0.001692	0.001772
hHDPCs+3	**HM**	0.000342	0.000053	0.000061		0.797725	0.000019	0.000020	0.000023	0.000034	0.000027
hHDPCs+3	**HM+HGS**	0.000204	0.000034	0.000053	0.797725		0.000018	0.000019	0.000020	0.000027	0.000023
hHDPCs+8	**DMEM**	0.000020	0.000027	0.000023	0.000019	0.000018		0.617696	0.286479	0.000129	0.000144
hHDPCs+8	**EMEM**	0.000023	0.000034	0.000027	0.000020	0.000019	0.617696		0.522783	0.000370	0.000359
hHDPCs+8	**WEM**	0.000027	0.000054	0.000034	0.000023	0.000020	0.286479	0.522783		0.001530	0.001402
hHDPCs+8	**HM**	0.000056	0.014015	0.001692	0.000034	0.000027	0.000129	0.000370	0.001530		0.948931
hHDPCs+8	**HM+HGS**	0.000037	0.015701	0.001772	0.000027	0.000023	0.000144	0.000359	0.001402	0.948931	

B1)

Statistical significance for hHDPCs+3	DMEM	EMEM	WEM	HM	HM+HGS
DMEM		0.003341	0.055958	0.029404	0.031523
EMEM	0.003341		0.140250	0.000099	0.000073
WEM	0.055958	0.140250		0.000660	0.000682
HM	0.029404	0.000099	0.000660		0.942305
HM+HGS	0.031523	0.000073	0.000682	0.942305	

B2)

Statistical significance for hHDPCs+8	HM	HM+HGS
HM		0.970285
HM+HGS	0.970285	

C1)

Statistical significance for viability hHDPCs+3	DMEM	EMEM	WEM	HM	HM+HGS
DMEM		0.988365	0.138579	0.716578	0.850613
EMEM	0.988365		0.142009	0.714085	0.847811
WEM	0.138579	0.142009		0.212479	0.174189
HM	0.716578	0.714085	0.212479		0.844819
HM+HGS	0.850613	0.847811	0.174189	0.844819	

C2)

Statistical significance for viability hHDPCs+8	DMEM	EMEM	WEM	HM+HGS	HM
DMEM		0.078047	0.027578	0.003717	0.000749
EMEM	0.078047		0.518348	0.112472	0.024990
WEM	0.027578	0.518348		0.284231	0.074039
HM	0.003717	0.112472	0.284231		0.379893
HM+HGS	0.000749	0.024990	0.074039	0.379893	

Figure 4.30. Comparison of cell number, doubling time, and viability across different passages and culture media. hHDPCs at passages +3 and +8, derived from a single donor (H65), were seeded in 24-well plates at a density of 2.5×10^4 cells per well and cultured for 6 days. Each culture condition was performed in four replicates. The following media were tested: DMEM, EMEM, WEM, HM, and HM+HGS. Cell numbers were determined using the trypan blue exclusion method. **A)** Average cell number for hHDPCs+3 and hHDPCs+8 cultured in different media. **A1)** Statistical significance (p values) for differences between passages across media (Figure 4.30A). Statistical analyses were performed using MANOVA followed by Duncan's *post-hoc* test. **B)** Doubling time for hHDPCs+3 and hHDPCs+8 in different media. **B1)** Statistical significance (p values) for hHDPCs+3 (Figure 4.30B). **B2)** Statistical significance (p values) for hHDPCs+8 (Figure 4.30B). Estimations were performed

only for cells cultured in HM and HM+HGS. **C)** Cell viability of hHDPCs+3 and hHDPCs+8 cultured in different media. **C1)** Statistical significance (p values) for hHDPCs+3 (Figure 4.30C). **C2)** Statistical significance (p values) for hHDPCs+8 (Figure 4.30C). Differences between hHDPCs+3 and hHDPCs+8 across the tested media were analyzed using ANOVA followed by Duncan's *post-hoc* test. Results are presented as mean values ± SD (n = 4). For all samples in the experiment, statistical significance thresholds were set as follows: *p < 0.05, **p < 0.01, ***p < 0.001.

4.2.3.2 Glucose Consumption by hHDPCs Cultured in Various Media

Glucose consumption was analyzed in hHDPCs at passages +3 and +8 over a 6-day culture period. Cells at the lower passage (+3) generally consumed more glucose than hHDPCs at passage +8. Specifically, hHDPCs+3 consumed 2.5-fold more glucose in DMEM than hHDPCs+8 ($p<0.001$). In EMEM, hHDPCs+3 utilized 1.03-fold more glucose than hHDPCs+8; however, this difference was not statistically significant. In WEM, cells at passage +3 consumed nearly twice as much glucose as those at passage +8 ($p<0.001$). In HM, glucose consumption by hHDPCs+3 was 1.5-fold higher than in hHDPCs+8 ($p<0.001$), whereas in HM+HGS, the difference was minimal (1.05-fold, not statistically significant) (Figure 4.31A).

When considering the percentage of glucose consumed by the cultures, hHDPCs+3 utilized almost all available glucose in EMEM (98%), WEM (93%), HM (95%), and HM+HGS (94%), with the exception of DMEM, where only 73% of glucose was consumed. In contrast, hHDPCs+8 cells consumed the least glucose in DMEM (30%), followed by WEM (50%), HM (63%), and HM+HGS (89%). The highest consumption by hHDPCs+8 was observed in EMEM (95%). A comparison of hHDPCs+8 cultured in HM and HM+HGS showed that HGS supplementation increased glucose utilization (Figure 4.31A).

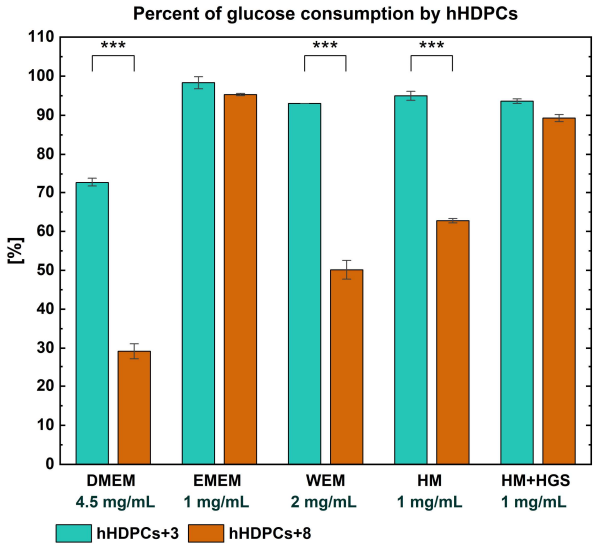
Analysis of glucose consumption at the cellular level showed an opposite trend: hHDPCs+8 consumed more glucose per harvested cell (sum of live and dead cells) than hHDPCs+3 in almost all media. In most cases, glucose uptake per cell was nearly 2-fold higher in hHDPCs+8, except in EMEM, where it was approximately 3-fold higher. A similar pattern was observed across media (Figure 4.31B).

For hHDPCs+3, the highest glucose uptake per 10^6 harvested cells was observed in DMEM (11.9 mg/10^6 cells). Uptake in WEM was approximately 1.4-fold lower (not statistically significant), in EMEM 2-fold lower ($p<0.05$), and in HM and HM+HGS more than 4-fold lower (both $p<0.01$).

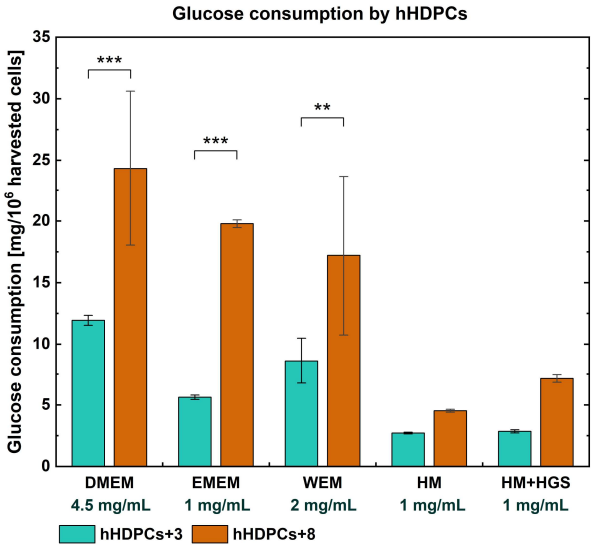
For hHDPCs+8, the highest glucose uptake per 10^6 harvested cells was also observed in DMEM (24 mg/10^6 cells). In EMEM, cells consumed approximately 1.2-fold less glucose than in DMEM (not statistically significant), and in WEM, 1.4-fold less ($p<0.01$). At passage +8,

differences between HM and HM+HGS were observed, as cells cultured in the presence of HGS utilized approximately 1.6-fold more glucose than those cultured in HM alone. Compared with DMEM, glucose consumption in HM+HGS and HM was approximately 3.4-fold and 5-fold lower, respectively ($p<0.001$ for both media) (Figure 4.31B).

A)



B)



A1)

Statistical significance for glucose consum. [%]		hHDPCs+3	hHDPCs+3	hHDPCs+3	hHDPCs+3	hHDPCs+3	hHDPCs+8	hHDPCs+8	hHDPCs+8	hHDPCs+8	hHDPCs+8
		DMEM	EMEM	WEM	HM	HM+HGS	DMEM	EMEM	WEM	HM	HM+HGS
hHDPCs+3	DMEM		0.000026	0.000068	0.000029	0.000035	0.000187	0.000029	0.000187	0.000100	0.000044
hHDPCs+3	EMEM	0.000026		0.008401	0.318492	0.166489	0.000025	0.341052	0.000029	0.000029	0.010753
hHDPCs+3	WEM	0.000068	0.008401		0.041823	0.084944	0.000044	0.038068	0.000100	0.000188	0.845611
hHDPCs+3	HM	0.000029	0.318492	0.041823		0.628066	0.000029	0.922454	0.000035	0.000044	0.052431
hHDPCs+3	HM+HGS	0.000035	0.166489	0.084944	0.628066		0.000029	0.579710	0.000044	0.000068	0.102197
hHDPCs+8	DMEM	0.000187	0.000025	0.000044	0.000029	0.000029		0.000026	0.000100	0.000068	0.000035
hHDPCs+8	EMEM	0.000029	0.341052	0.038068	0.922454	0.579710	0.000026		0.000029	0.000035	0.049045
hHDPCs+8	WEM	0.000187	0.000029	0.000100	0.000035	0.000044	0.000100	0.000029		0.000187	0.000068
hHDPCs+8	HM	0.000100	0.000029	0.000188	0.000044	0.000068	0.000068	0.000035	0.000187		0.000102
hHDPCs+8	HM+HGS	0.000044	0.010753	0.845611	0.052431	0.102197	0.000035	0.049045	0.000068	0.000102	

B1)

Statistical significance for glucose consum. per cell		hHDPCs+3	hHDPCs+3	hHDPCs+3	hHDPCs+3	hHDPCs+3	hHDPCs+8	hHDPCs+8	hHDPCs+8	hHDPCs+8	hHDPCs+8
		DMEM	EMEM	WEM	HM	HM+HGS	DMEM	EMEM	WEM	HM	HM+HGS
hHDPCs+3	DMEM		0.023130	0.181053	0.002354	0.002437	0.000130	0.004967	0.038844	0.009991	0.070381
hHDPCs+3	EMEM	0.023130		0.246403	0.276492	0.284659	0.000027	0.000047	0.000228	0.650200	0.530279
hHDPCs+3	WEM	0.181053	0.246403		0.038012	0.039651	0.000036	0.000302	0.002494	0.128718	0.540207

hHDPCs+3	**HM**	0.002354	0.276492	0.038012		0.954245	0.000020	0.000023	0.000039	0.481344	0.108889
hHDPCs+3	**HM+HGS**	0.002437	0.284659	0.039651	0.954245		0.000022	0.000024	0.000043	0.490770	0.112833
hHDPCs+8	**DMEM**	0.000130	0.000027	0.000036	0.000020	0.000022		0.071097	0.009697	0.000023	0.000030
hHDPCs+8	**EMEM**	0.004967	0.000047	0.000302	0.000023	0.000024	0.071097		0.294449	0.000033	0.000104
hHDPCs+8	**WEM**	0.038844	0.000228	0.002494	0.000039	0.000043	0.009697	0.294449		0.000105	0.000767
hHDPCs+8	**HM**	0.009991	0.650200	0.128718	0.481344	0.490770	0.000023	0.000033	0.000105		0.311150
hHDPCs+8	**HM+HGS**	0.070381	0.530279	0.540207	0.108889	0.112833	0.000030	0.000104	0.000767	0.311150	

Figure 4.31. Glucose consumption by hHDPCs cultured in different media. hHDPCs derived from a single donor (H65) at passages +3 and +8 were cultured for 6 days in 24-well plates at a density of 2.5×10^4 cells per well. Four replicates were performed for each condition. The media tested were: DMEM (4.5 mg/mL glucose), EMEM (1 mg/mL), WEM (2 mg/mL), HM (1 mg/mL), and HM+HGS (1 mg/mL). Glucose consumption was measured using a commercial colorimetric assay based on absorbance readings. **A)** Percentage of glucose consumed by the cell cultures after 6 days of incubation. **A1)** Statistical significance (p values) for differences in the percentage of glucose consumption between hHDPCs+3 and hHDPCs+8 across the tested media (Figure 4.31A). **B)** Glucose consumption expressed as mg per 10^6 harvested cells (sum of live and dead cells) for hHDPCs+3 and hHDPCs+8 across the tested media. B1) Statistical significance (p values) for differences in glucose consumption (mg per 10^6 harvested cells) for Figure 4.31B. Statistical analysis was performed using MANOVA followed by Duncan's *post-hoc* test. Data are presented as mean ± SD, n = 4, with significance levels set at *p<0.05, **p<0.01, ***p<0.001.

4.2.3.3 Albumin Secretion by hHDPCs Cultured in Various Media

Albumin secretion by hHDPCs at passage +3 and +8 was measured in post-culture media from DMEM, EMEM, WEM, HM, and HM+HGS cultures. Albumin levels were quantified using a sandwich ELISA. No detectable albumin was observed in any of the culture media samples (data not shown).

4.2.4 Effect of Hepatocyte Growth Supplement (HGS) on hHDPCs Proliferation

The effect of Hepatocyte Growth Supplement (HGS) on hHDPCs proliferation was studied using cells at three different passages (+5, +8, +12). Cells were cultured in DMEM (D) or hepatocyte medium (H), in the absence or presence of HGS (D+H, H+H). All samples were derived from a single donor (H65). The detailed composition of the media is provided in Table 3.1. The experimental design is illustrated in Figure 4.32.

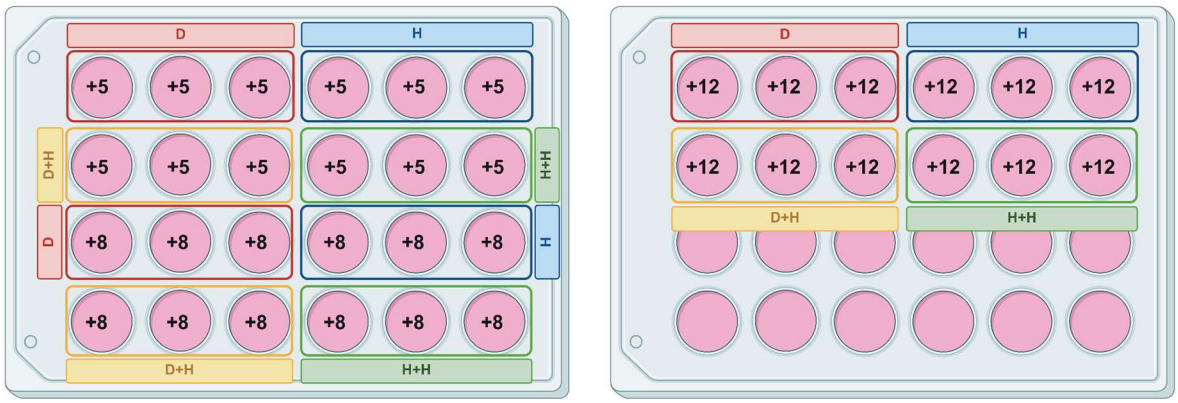


Figure 4.32. Experimental design: effect of HGS on hHDPCs proliferation. hHDPCs from donor H65 were analyzed at three passages: +5, +8, and +12. To determine the influence of HGS on cell proliferation, cells were cultured in DMEM (D) or Hepatocyte Medium (H), either without supplementation or with HGS (D+H, H+H). Cells were seeded at a density of 2.5×10^4 per well in 24-well plates and cultured for 4 days.

The highest cell numbers were obtained for the middle passage (+8). At the lowest passage (+5), cell counts were 1.7-fold lower in DMEM and 1.4-fold lower in the other media compared with passage +8. Cultures maintained in HM and HM+HGS showed significantly higher cell numbers than those cultured in DMEM for both lower passages. At the highest passage (+12), cell numbers remained low across all media (Figure 4.33A).

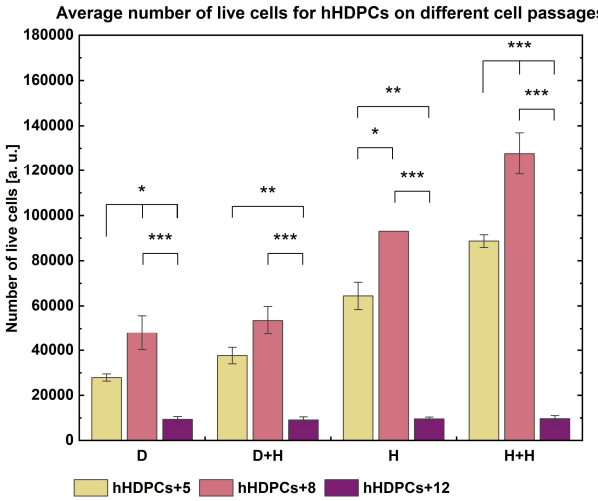
The results indicate that HGS enhanced cell proliferation in a passage- and medium-dependent manner. Cells at passage +8 proliferated faster, whereas passage +5 cells divided more slowly (approximately 1.5-fold lower than passage +8), and passage +12 cells exhibited reduced proliferation, with average cell numbers around 9×10^4 in all media.

Cell proliferation increased in HM supplemented with HGS; cell counts were approximately 1.4-fold higher than in HM alone at both passages +5 and +8. In DMEM, the effect of HGS was weaker, proliferation increased about 1.3-fold at passage +5 and 1.1-fold at passage +8 (Figure 4.33A).

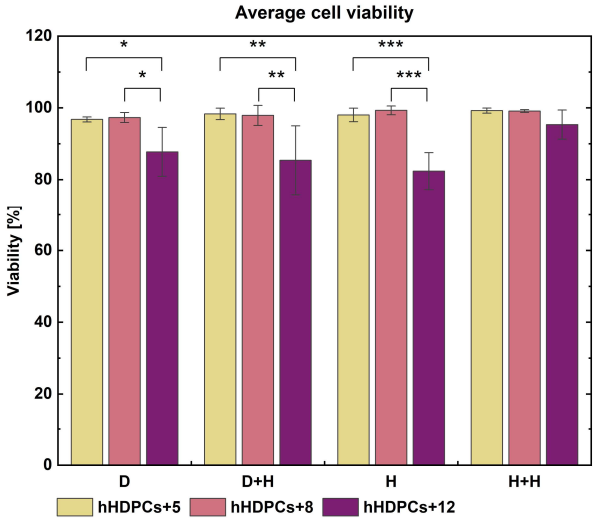
Cell viability analysis demonstrated that hHDPCs at lower and middle passages cultured in all media types maintained high viability levels (97–99%). At passage +12, the highest viability was observed in HM+HGS (95%), whereas other conditions showed reduced viability (82–85%) (Figure 4.33B).

Microscopic observations confirmed these findings. After 4 days of culture, the highest cell numbers were obtained at the middle passage (+8) across all tested media. The highest proliferation rate was observed in HM+HGS and HM, whereas the lowest cell numbers were observed at passage +12, regardless of the medium used (Supplementary Figure S8.2).

A)



B)



A1)

		D	D	D	D+H	D+H	D+H	H	H	H	H+H	H+H	H+H
		+5	+8	+12	+5	+8	+12	+5	+8	+12	+5	+8	+12
D	+5		0,046097	0,026829	0,206827	0,003774	0,028964	0,000154	0,000028	0,022364	0,000024	0,000021	0,030469
D	+8	0,046097		0,000231	0,371483	0,236934	0,000237	0,017599	0,000085	0,000227	0,000041	0,000020	0,000247
D	+12	0,026829	0,000231		0,001663	0,000037	0,972050	0,000024	0,000021	0,979051	0,000020	0,000019	0,954925
D+H	+5	0,206827	0,371483	0,001663		0,054520	0,001783	0,002618	0,000036	0,001445	0,000028	0,000024	0,001881
D+H	+8	0,003774	0,236934	0,000037	0,054520		0,000034	0,159231	0,000620	0,000042	0,000213	0,000032	0,000031
D+H	+12	0,028964	0,000237	0,972050	0,001783	0,000034		0,000021	0,000020	0,954925	0,000019	0,000019	0,979051
H	+5	0,000154	0,017599	0,000024	0,002618	0,159231	0,000021		0,014053	0,000028	0,004868	0,000054	0,000020
H	+8	0,000028	0,000085	0,000021	0,000036	0,000620	0,000020	0,014053		0,000024	0,568935	0,000071	0,000019
H	+12	0,022364	0,000227	0,979051	0,001445	0,000042	0,954925	0,000028	0,000024		0,000021	0,000020	0,938473
H+H	+5	0,000024	0,000041	0,000020	0,000028	0,000213	0,000019	0,004868	0,568935	0,000021		0,000173	0,000019
H+H	+8	0,000021	0,000028	0,000019	0,000024	0,000032	0,000019	0,000054	0,000071	0,000020	0,000173		0,000013
H+H	+12	0,030469	0,000247	0,954925	0,001881	0,000031	0,979051	0,000020	0,000019	0,938473	0,000019	0,000013	

B1)

		D	D	D	D+H	D+H	D+H	H	H	H	H+H	H+H	H+H
		+5	+8	+12	+5	+8	+12	+5	+8	+12	+5	+8	+12
D	+5		0,877565	0,015902	0,683141	0,752897	0,003811	0,736992	0,517043	0,000523	0,527637	0,542953	0,668897
D	+8	0,877565		0,013350	0,782047	0,856499	0,003068	0,839446	0,604548	0,000408	0,615559	0,631488	0,584493
D	+12	0,015902	0,013350		0,009198	0,010120	0,487672	0,010342	0,005754	0,140690	0,005755	0,005838	0,031937
D+H	+5	0,683141	0,782047	0,009198		0,907674	0,002001	0,929049	0,792096	0,000259	0,801630	0,814778	0,437102
D+H	+8	0,752897	0,856499	0,010120	0,907674		0,002241	0,972363	0,717048	0,000297	0,728214	0,744959	0,488754
D+H	+12	0,003811	0,003068	0,487672	0,002001	0,002241		0,002275	0,001218	0,375469	0,001215	0,001233	0,008609
H	+5	0,736992	0,839446	0,010342	0,929049	0,972363	0,002275		0,735982	0,000296	0,746159	0,761151	0,478325
H	+8	0,517043	0,604548	0,005754	0,792096	0,717048	0,001218	0,735982		0,000156	0,981644	0,958875	0,313844

H	**+12**	0,000523	0,000408	0,140690	0,000259	0,000297	0,375469	0,000296	0,000156		0,000160	0,000161	0,001253
H+H	**+5**	0,527637	0,615559	0,005755	0,801630	0,728214	0,001215	0,746159	0,981644	0,000160		0,973770	0,321140
H+H	**+8**	0,542953	0,631488	0,005838	0,814778	0,744959	0,001233	0,761151	0,958875	0,000161	0,973770		0,331837
H+H	**+12**	0,668897	0,584493	0,031937	0,437102	0,488754	0,008609	0,478325	0,313844	0,001253	0,321140	0,331837	

Figure 4.33. Average number of live cells and cell viability of hHDPCs at passages +5, +8, and +12 cultured in DMEM (D) or HM (H), with or without HGS supplementation (D+H, H+H). A) Cells were seeded in 24-well plates at a density of 2.5×10^4 per well and cultured for 4 days. After culture, cells were trypsinized and counted using the trypan blue exclusion method. Each condition was tested in triplicate. **A1)** Statistical significance (p values) for the data shown in Figure 4.33A. **B)** Cell viability of hHDPCs at different passages cultured with D, D+H, H, and H+H. **B1)** Statistical significance (p values) for the data presented in Figure 4.33B. Statistical analysis was performed using MANOVA followed by Duncan's *post-hoc* test. Results are presented as mean ± SD (n=3), with significance levels set at *p<0.05, **p<0.01, ***p<0.001.

4.2.5 Protein Expression Fluctuations During hHDPCs Passaging

4.2.5.1 Albumin Expression – FC

Human hepatocyte-derived proliferating cells (hHDPCs) are differentiated cells derived from isolated hepatocytes; therefore, it was important to examine whether they retain the ability to produce albumin and at which cell passages this function is preserved. FC was used to quantify the percentage of albumin-positive cells. The hHDPCs derived from four donors (H37, H60, H63, and H76) were analyzed. Cells from each donor were cultured for up to ten passages in HM+HGS, with each passage lasting between 3 and 8 days. Positive controls included the C3A, hH_1, and LCI(H65). The HOS and HDFn cell lines were used as negative controls.

The results (Figure 4.34) demonstrated the presence of albumin-positive cells at all analyzed passages for all hHDPCs donors. The lowest percentage of albumin-expressing cells (14%) was observed in hHDPCs derived from donor H76 at passage +8, while the remaining samples at this passage exhibited values ranging from 25% to 30%. The highest percentage (90%) was detected in hHDPCs from donor H37 at passage +10. For the other donors at the same passage, albumin-positive cells ranged from 20% to 40%.

Notably, fluctuations in albumin expression varied between donors. The hHDPCs from donor H60 displayed approximately 50% albumin-positive cells at the earliest passages, followed by variable but consistently lower levels at later passages, which never exceeded 50%. In contrast, hHDPCs derived from donor H37 showed much higher levels, with 82% at passage +1, 86% at +5, 81% at +7, and 90% at +10. In later passages, the percentage of albumin-positive cells decreased, ranging from 50% to 19%.

The hHDPCs from donor H63 behaved similarly to those from donor H37 at early passages (+1 to +6), showing 80% at +1, 57% at +3, 67% at +4, and 70% at +6; however, at later passages, the values ranged between 47% and 29%, resembling the pattern observed for donor H60. Samples from donor H76 followed a trend similar to that observed for donor H60, with levels above 50% only at passages +2 (57%), +5 (56%), and +6 (74%), while the remaining passages ranged from 50% to 14% (Figure 4.34). No albumin-positive cells were detected in the negative controls, HOS and HDFn. Among the positive controls, C3A showed 86%, hHs 70%, and LCI samples 88% of albumin-positive cells (Figure 4.34, inserted graph).

The presence of albumin in hHDPCs, which were dedifferentiated from hepatocytes, was also assessed using immunofluorescence. The analysis was conducted across twelve consecutive cell passages. The results, presented in Supplementary Figure S8.3, confirmed the presence of albumin in dedifferentiating hepatocytes at every passage. Moreover, variations in albumin signal intensity were observed across passages, consistent with the flow cytometry-based findings. Additionally, sequential images also revealed morphological changes in the cells, showing a transition from the cuboidal shape typical of hepatocytes to the spindle-shaped morphology characteristic of fibroblasts.

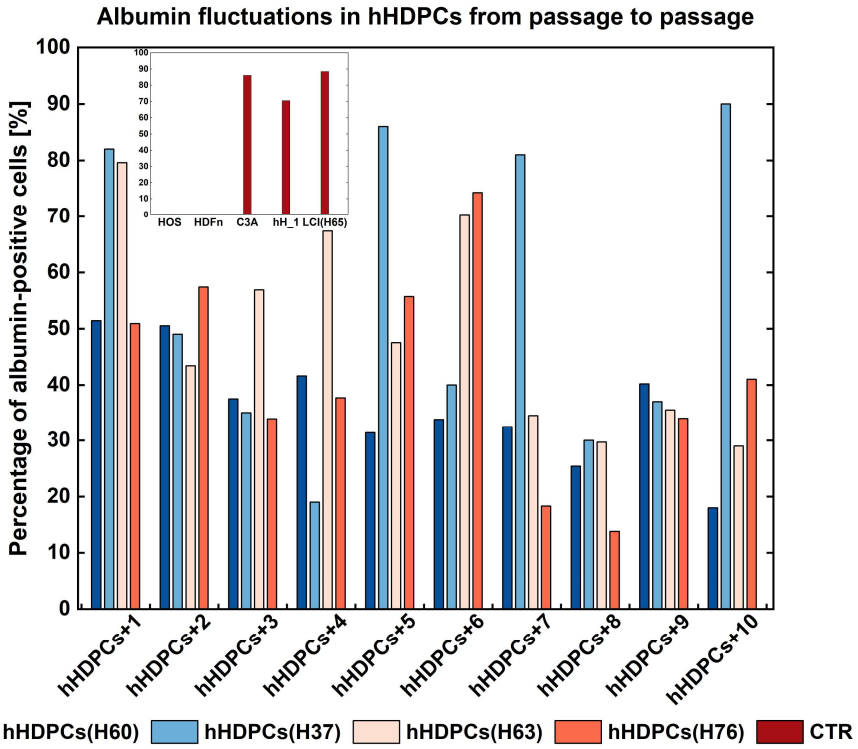


Figure 4.34. Albumin expression across ten passages of hHDPCs. The analysis was performed on hHDPCs derived from four liver donors (H60, H37, H63, H76). Control cell lines included HOS, HDFn, and C3A, as well as hH_1 and LCI(H65). Albumin expression was assessed by flow cytometry. Cells were seeded at a density of 0.4×10^6 cells per 25 cm² culture flask in HM+HGS medium. Each passage was cultured for 3–8 days, after which cells were detached using trypsin and counted with the trypan blue exclusion method. For cytometric analysis, 0.2×10^6 cells per sample were analyzed in a single replicate; therefore, no statistical analysis was performed.

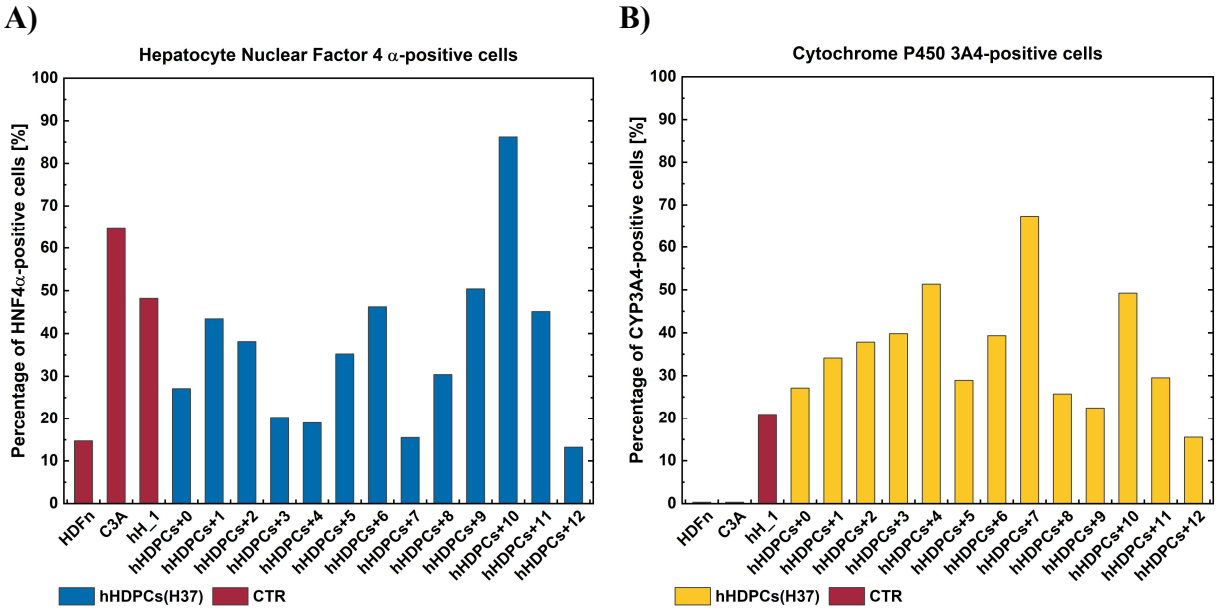
4.2.5.2 Passage to Passage Changes in Expression of Other Protein – FC

Using hHDPCs derived from the H37 liver, protein expression changes were analyzed across 12 cell passages. The following proteins were examined: HNF4α, CYP3A4, and vimentin (VIM, a fibroblast-specific protein).

For HNF4α, the highest percentage of HNF4α-positive cells was observed at passage +0 (86%), which was the only passage exceeding 50%. This value was notably higher than in the controls, where C3A showed 65%, hH_1 48%, and HDFn approximately 15%. The lowest level of HNF4α expression was detected at passage +12 (13%), similar to the value measured in HDFn cells (Figure 4.35A).

For CYP3A4, the highest percentage of expressing cells (67%) was observed at passage +7, whereas the lowest (15.5%) occurred at passage +12. Passages +7 and +4 (51%) were the only ones with levels above 50%. Among the control cells, no CYP3A4-positive cells were detected in C3A or HDFn, while hHs displayed 20% expression (Figure 4.35B).

Regarding vimentin, fluctuations in expression were also observed across passages. However, compared with the other analyzed proteins, the overall expression levels were consistently lower. None of the hHDPC passages exceeded 50%; the highest level was detected at passage +0 (36%; protein detection was performed after 10 days of culture), and the lowest at passage +4 (4.4%). Among the controls, Vim was absent in C3A and hHs but present in HDFn cells at 27% (Figure 4.35C).



C)

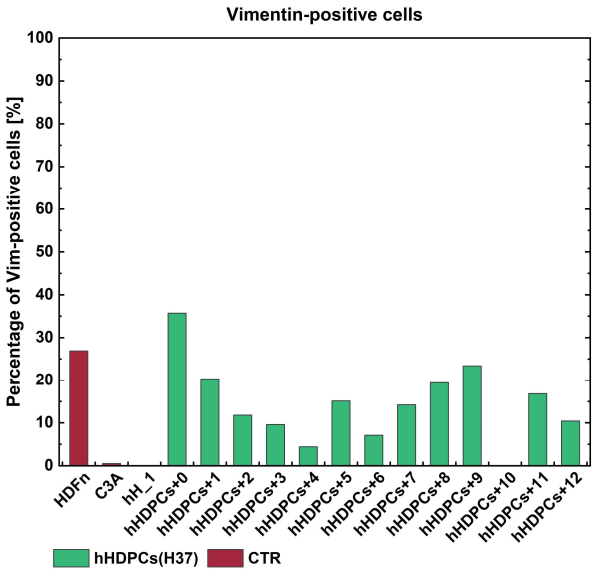


Figure 4.35. Protein expression changes during long-term culture of hHDPCs. The study analyzed hepatocyte nuclear factor 4α (HNF4α), cytochrome P450 3A4 (CYP3A4), and vimentin (Vim) across 12 consecutive passages of hHDPCs derived from donor H37. Flow cytometry measurements for each sample were performed using 0.2×10^6 cells. Samples were incubated with antibodies according to the established protocol. **A)** Percentage of HNF4α-positive cells across hHDPCs passages and control cells (HDFn, C3A, hH_1). A total of 12 passages were analyzed. **B)** Percentage of CYP3A4-positive cells across hHDPCs passages and control cells (HDFn, C3A, hHs). **C)** Percentage of Vim-positive cells across hHDPCs passages and control cells (HDFn, C3A, hH_1). A total of 12 passages were analyzed, with +0 representing unpassaged, but divided cells. Imunocytostainng for cells at passage +0 was performed after 10 days of culture. For hHDPCs+10, the analysis was not performed due to insufficient cell numbers. Each sample was analyzed in a single replicate; therefore, no statistical analysis was conducted.

4.2.5.3 Protein Expression in hHDPCs – Western Blot

Relative changes in protein expression levels in hHDPCs were analyzed using the semi-quantitative Western blot technique. The following proteins were examined: ALB, AFP, two transcription factors: HNF4α and HNF1α, two proteins from the cytochrome P450 family: CYP3A4 and CYP2E1, as well as two proteins involved in the urea cycle: carbamoyl phosphate synthetase I (CPS1) and arginase 1 (ARG1). Additionally, the pentaspan transmembrane glycoprotein (CD133) and the fibroblast-specific protein vimentin (VIM) were analyzed.

The study was conducted using hHDPCs derived from different donors (H37, H40, H43, H65, H72) and various cell passages. As controls, HDFn, C3A, hH_2, LCI(H40), LCI(H35), and a liver tissue isolate from donor H81 [LTI(H81)] were used. The housekeeping gene Glyceraldehyde 3-phosphate dehydrogenase (GAPDH) served as a loading control for protein normalization.

The results demonstrated that all hHDPCs samples obtained from different donors expressed albumin. Representative results shown in Figure 4.36 showed characteristic albumin bands with a molecular weight of 67 kDa. Protein expression levels in these cells varied with

both the cell type and the passage number. For the hHDPCs derived from donor H43, albumin expression levels at passages +1 and +7 were 0.32 and 0.21, respectively, indicating similar expression at these passages. Passage +3, however, was particularly notable, as albumin expression increased nearly 3-fold compared with passage +1, reaching 0.92. In hHDPCs from donor H40, albumin expression decreased with increasing passage number. Between passages +1 and +3, expression levels were similar (2.3 and 2.1, respectively). At passage +7, however, expression decreased markedly by about 26-fold, reaching 0.09. Analysis of hHDPCs from donor H37 revealed similar albumin expression levels at passages +0 and +6 (0.43 and 0.38, respectively). At passage +3, albumin expression decreased 11-fold, reaching 0.04 (Figure 4.37A). In HDFn, no albumin expression was detected, in contrast to other cell types. Among the reference isolates, the highest albumin expression was observed in LCI(H40) (11.0), whereas the lowest was detected in LCI(H35) (0.2). LTI(H81) and hHs exhibited similar expression levels of 1.7 and 1.75, respectively, while C3A showed an expression level of 0.7 (Figure 4.37A).

Representative Western blot results for HNF4α, shown in Figure 4.36, demonstrated its expression in all tested cell types. In hHs, three distinct bands at 52 kDa, 46 kDa, and 42 kDa were detected. In C3A, two bands at 52 kDa and 42 kDa were observed. In some hHDPCs samples at various passages [hHDPCs+6, +10, +13(H72), hHDPCs+3(H37)] as well as in HDFn, two bands at 42 kDa and 40 kDa were present. In contrast, samples hHDPCs+2(H72), hHDPCs+0(H37), hHDPCs+6(H37), as well as the LTI and LCI controls, exhibited a single 42 kDa band (Figure 4.36). HNF4α expression in hHDPCs derived from donor H65 decreased progressively with increasing passage number: at passage +3, expression was 0.42, at passage +7, it dropped to 0.35, and at passage +11, it reached 0.2 (Figure 4.37B). In hHDPCs from donor H72, fluctuations in HNF4α expression were observed across passages. The highest expression was detected at passage +2 (2.33), whereas passages +3, +7, and +11 showed similar levels (approximately 0.38). Intermediate expression levels (~0.99) were observed at passages +6, +10, and +13. In hHDPCs derived from donor H43, HNF4α expression slightly increased with passage number: 0.6 at +1, 0.7 at +3, and 0.74 at +7. In contrast, cells from donor H40 exhibited a 3-fold decrease in expression between passages +1 (1.7) and +7 (0.6). For hHDPCs from donor H37, expression increased 2-fold from passage +0 (0.98) to passage +3 (2.03), but decreased 4-fold at passage +7 (0.5) (Figure 4.37B). In control cells, HNF4α expression was undetectable in LCI(H40) only. LCI(H35) exhibited expression at 0.3, whereas LTI and HDFn showed similar levels (0.45). The hHs and C3A demonstrated higher expression levels of 1.07 and 1.3, respectively.

Representative results for HNF1α, presented in Figure 4.36, showed two bands (72 kDa and 90 kDa) for hHs and C3A. In contrast, all other samples (LTI, HDFn, LCI, hHDPCs from H65 and H72 at passages +3, +7, +11) displayed a single band at 72 kDa. Overall, HNF1α expression was low in hHDPCs. No expression was detected in hHDPCs from donors H43 and H40. For samples derived from donor H65, expression levels at passages +3, +7, and +11 were 0.08, 0.04, and 0.06, respectively (Figure 4.37C). In hHDPCs from donor H72, the highest expression was detected at passage +2 (0.6), whereas the lowest occurred at passage +3 (0.01). At passages +6 and +7, expression levels were 0.3 and 0.08, respectively, while passages +10 to +13 exhibited a similar level of approximately 0.14. In samples derived from donor H37, HNF1α expression at passages +0 and +6 was comparable (0.11 and 0.12), whereas passage +3 showed a slightly elevated level of 0.19 (Figure 4.37C). HNF1α was not detected in LCI cells, while LTI and HDFn exhibited similar expression levels (approximately 1.0). The hHs and C3A demonstrated expression levels of 1.83 and 2.1, respectively.

The CYP3A4 protein appeared as a single band at 50 kDa in hHs, C3A, and LCI(H40) cells (Figure 4.36). No expression was detected in any hHDPCs, nor in LCI(H35) or HDFn controls. LCI(H40), LTI(H81), and C3A exhibited similar expression levels (0.4), while hHs showed the highest level (2.97) (Figure 4.37D). The second cytochrome P450 family member, CYP2E1, appeared as a single band at 52 kDa in hHs and LTI samples (Figure 4.36), with expression levels of 1.06 and 1.52, respectively (Figure 4.37D). A 150 kDa band corresponding to CPS1, a key urea cycle protein, was observed only in hHs and LTI(H81) samples (Figure 4.36). Expression levels in hHs and LTI were 3.5 and 0.6, respectively, with hHs exhibiting 6-fold higher expression level (Figure 4.37E).

AFP was detected exclusively in C3A as two bands (70 kDa and 50 kDa) (Figure 4.36), with a total expression level of 2.5 (Figure 4.37G). Arginase 1 (ARG1) appeared as a single 35 kDa band in hHs, LTI, and LCI samples (Figure 4.36). Expression levels in hHs and LTI were similar (0.67), whereas LCI showed lower expression (0.4) (Figure 4.37F). CD133 appeared as a 130 kDa band in hHs and C3A (Figure 4.36). Expression in hHs was 1.8, which was approximately 9-fold higher than in C3A (Figure 4.37F).

Finally, vimentin (VIM), a fibroblast-specific protein, was analyzed. No signal was detected in hHs, LTI, LCI(H35), or C3A. In other samples, multiple bands between 40 - 70 kDa were observed, with the strongest band at 67 kDa (Figure 4.36). LCI(H40) exhibited only a single band at 40 kDa.

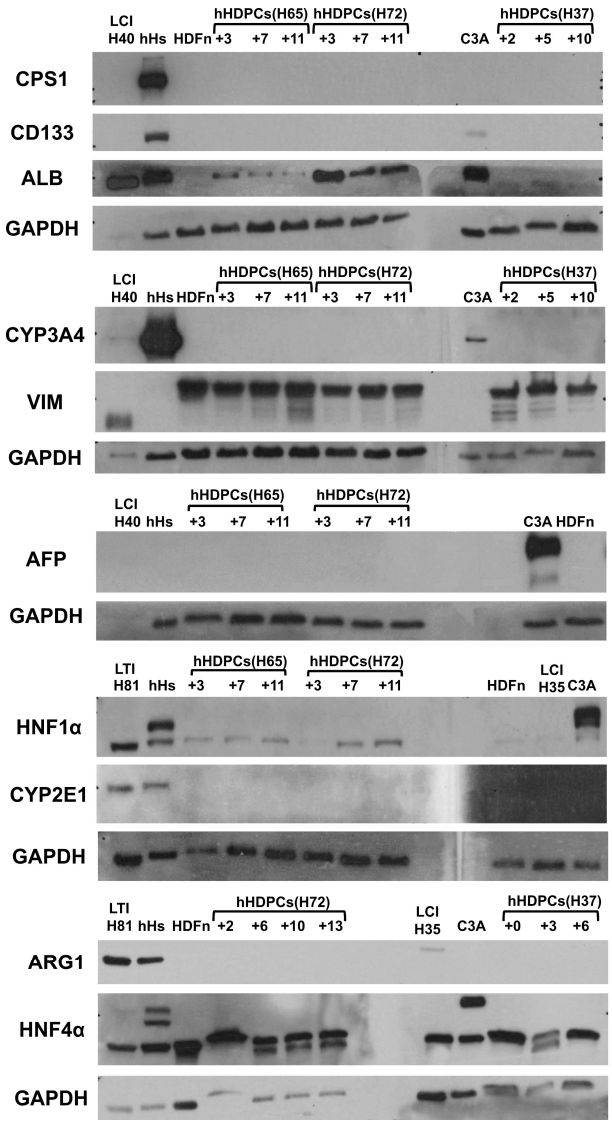
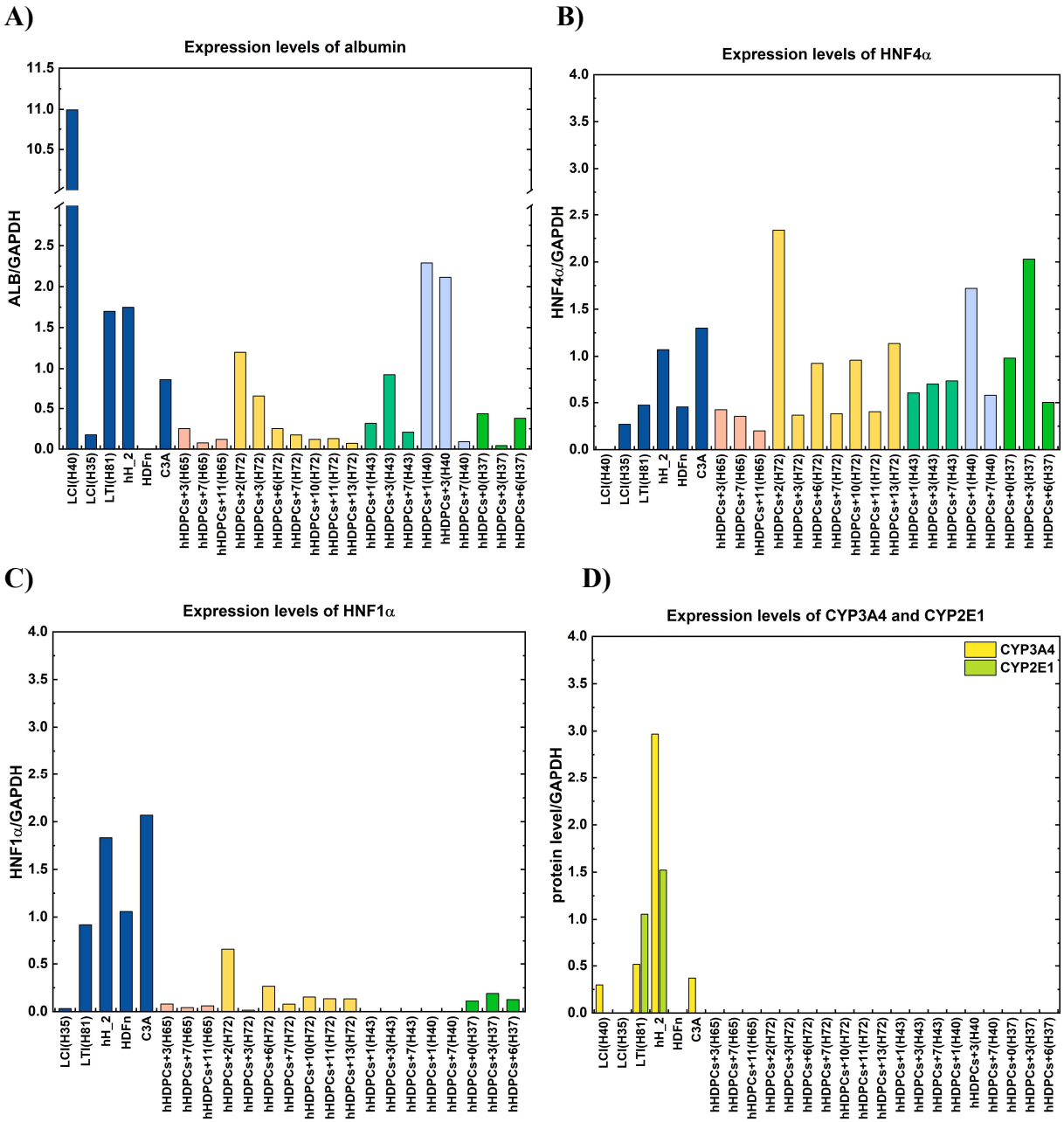


Figure 4.36. Western blot analysis of hHDPCs. Protein expression levels were examined in the following cell types: hHDPCs (at different cell passages) from five donors (H37, H40, H43, H65, H72) and, as controls, hH_2, C3A, HDFn, and LCI from two donors (H35 and H40), and a LTI from donor H81. The figure presents representative results obtained during the analysis of protein expression. The results for hHDPCs were obtained at the following passages: +0, +2, +3, +5, +6, +10 for donor H37; +3, +7, +11 for donor H65; and +2, +3, +6, +7, +10, +11, +13 for donor H72. Each sample was loaded onto the gel at a total protein amount of 25 µg. During the experiment, the levels of the following proteins were examined, with their predicted molecular sizes indicated: albumin (ALB) – 67 kDa, arginase 1 (ARG1) – 35 kDa, alpha-1-fetoprotein (AFP) – 70 kDa, Hepatocyte Nuclear Factor 4α (HNF4α) – 53 kDa, Hepatocyte Nuclear Factor 1α (HNF1α) – 67 kDa, cytochrome P450 3A4 (CYP3A4) – 55 kDa, cytochrome P450 2E1 (CYP2E1) – 56 kDa, carbamoyl phosphate synthetase I (CPS1) – 150 kDa, pentaspan transmembrane glycoprotein (CD133) – 130 kDa, and vimentin (VIM) – 56 kDa. Protein normalization was achieved using the housekeeping gene Glyceraldehyde 3-phosphate dehydrogenase (GAPDH; 36 kDa) as a loading control.


A)
Expression levels of albumin
ALB/GAPDH
B)
Expression levels of HNF4α
HNF4α/GAPDH
C)
Expression levels of HNF1α
HNF1α/GAPDH
D)
Expression levels of CYP3A4 and CYP2E1
CYP3A4
CYP2E1
protein level/GAPDH
LCI(H40)
LCI(H35)
LTI(H81)
hH_2
HDFn
C3A
hHDPCs+3(H65)
hHDPCs+7(H65)
hHDPCs+11(H65)
hHDPCs+2(H72)
hHDPCs+3(H72)
hHDPCs+6(H72)
hHDPCs+7(H72)
hHDPCs+10(H72)
hHDPCs+11(H72)
hHDPCs+13(H72)
hHDPCs+1(H43)
hHDPCs+3(H43)
hHDPCs+7(H43)
hHDPCs+1(H40)
hHDPCs+7(H40)
hHDPCs+0(H37)
hHDPCs+3(H37)
hHDPCs+6(H37)

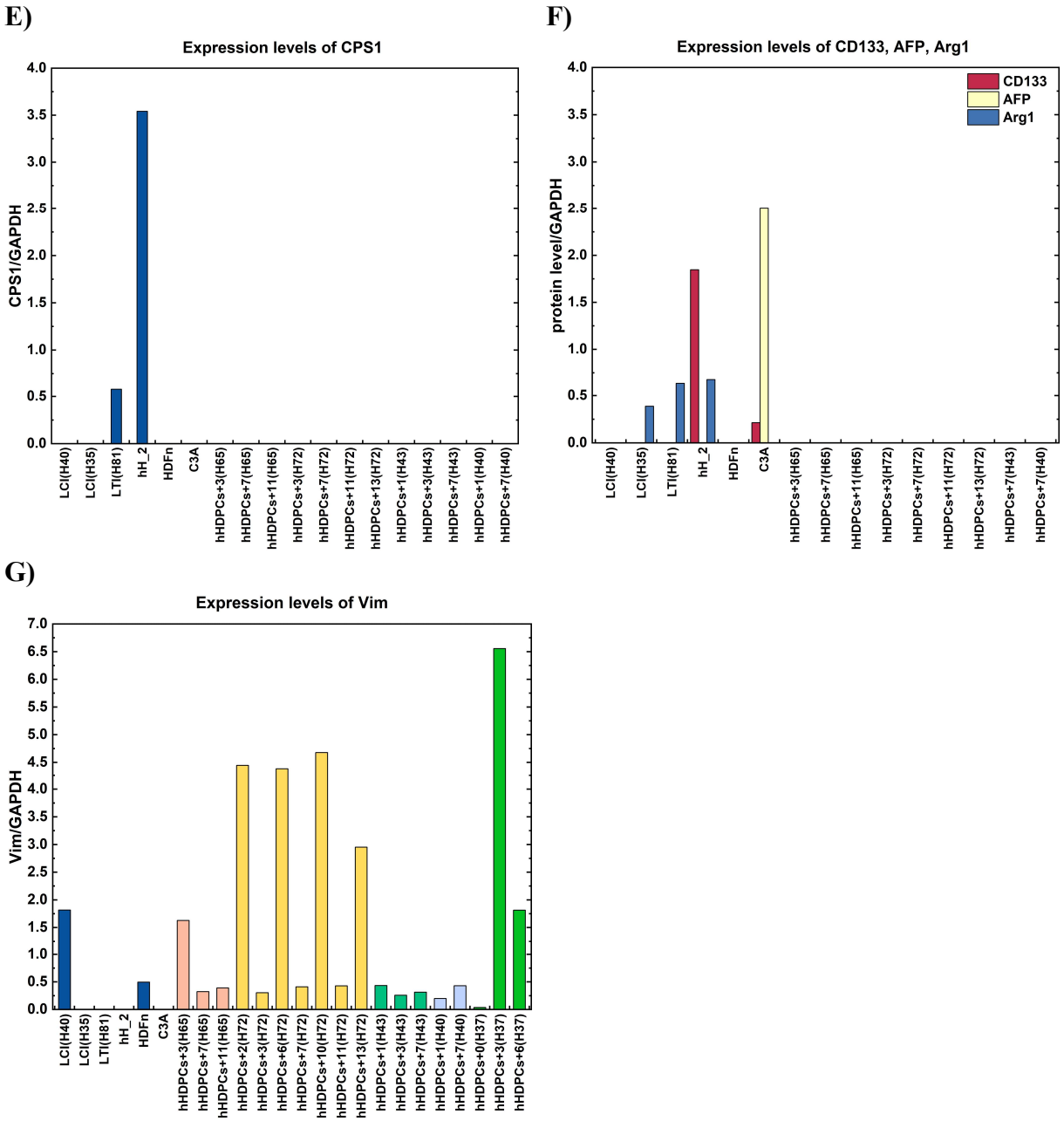


Figure 4.37. Protein expression levels. Protein expression levels were analyzed in the following cell types: hHDPCs (at different cell passages) from five donors (H37, H40, H43, H65, H72) and, as controls, hH_2, C3A, HDFn, LCI(H35), LCI(H40), and LTI(H81). Protein expression levels were calculated based on the ratio of the immunofluorescence signal density of the target protein to that of the reference protein GAPDH. **A)** Graph showing albumin (ALB) expression in the following cell types: LCI (H35 and H40), LTI(H81), C3A, hHs, HDFn, and hHDPCs at the indicated passages: for donor H65: +3, +7, +11; for donor H72: +2, +3, +6, +7, +10, +11, +13; for donor H43: +1, +3, +7; for donor H40: +1, +3, +7; for donor H37: +0, +2, +3, +5, +6, +10. **B)** Graph showing Hepatocyte Nuclear Factor 4α (HNF4α) expression for LCI (H35 and H40), LTI(H81), hHs, HDFn, C3A, and hHDPCs at the following passages: for donor H65: +3, +7, +11; for donor H72: +2, +3, +6, +7, +10, +11, +13; for donor H43: +1, +3, +7; for donor H40: +1, +7; H37 +0, +3, +6. **C)** Graph showing Hepatocyte Nuclear Factor 1α (HNF1α) expression for LCI(H35), LTI(H81), hHs, HDFn, C3A, and hHDPCs at the following passages: for donor H65: +3, +7, +11; for donor H72: +2, +3, +6, +7, +10, +11, +13; for donor H43: +1, +3, +7; for donor H40: +1, +7; for donor H37: +0, +3, +6. **D)** Graph showing the expression of two cytochrome P450 proteins: CYP3A4 (highlighted in yellow) and CYP2E1 (highlighted in green), for LCI (H35 and H40), LTI(H81), hHs, HDFn, C3A, and hHDPCs at the following passages: for donor H65: +3, +7, +11; for donor H72: +2, +3, +6, +7, +10, +11, +13; for donor H43: +1, +3, +7; for donor H40: +1, +3, +7; for donor H37: +0, +3, +6. **E)** Graph showing carbamoyl

phosphate synthetase I (CPS1) expression for LCI (H35 and H40), LTI(H81), hHs, HDFn, C3A, and hHDPCs at the following passages: for donor H65: +3, +7, +11; for donor H72: +3, +7, +11, +13; for donor H43: +1, +3, +7; for donor H40: +1, +7. **F)** Graph showing the expression of pentaspan transmembrane glycoprotein (CD133, highlighted in dark pink), alpha-1-fetoprotein (AFP, highlighted in light yellow), and arginase 1 (ARG1, highlighted in dark blue) for LCI (H35 and H40), LTI(H81), hHs, HDFn, C3A, and hHDPCs at the following passages: for donor H65: +3, +7, +11; for donor H72: +3, +7, +11, +13; for donor H43: +7; H40 +7. **G)** Graph showing vimentin (VIM) expression for LCI (H35 and H40), LTI(H81), hHs, HDFn, C3A, and hHDPCs at the following passages: for donor H65: +3, +7, +11; for donor H72: +2, +3, +6, +7, +10, +11, +13; for donor H43: +1, +7; for donor H40: +1, +7; for donor H37: +0, +3, +6. Due to high variability in immunofluorescent signal density across each sample replicates, standard deviations were not calculated. Therefore, only the average signal intensity is presented to allow indirect estimation of changes in protein levels.

4.2.5.4 Long-Term Culture of hHDPCs

Long-term cultures consisting of consecutive cell passages were performed for hHDPCs dedifferentiated from liver cells isolated from four donors, LCI(H37, H60, H63, H76). Cells that had dedifferentiated and divided but had not yet undergone the first passage were designated as hHDPCs+0.

For hHDPCs(H37), the first passage was performed after 10 days of culture; for hHDPCs(H60), after 12 days; for hHDPCs(H63), after 16 days; and for hHDPCs(H76), after 21 days from the start of culture. The results indicate that dedifferentiated cells from different donors exhibit variability in both the rate of dedifferentiation and the rate of cell division between passages. Consequently, differences in cell growth were observed during the long-term cultures.

In the case of the hHDPCs(H37), 12 passages were performed over 74 days, resulting in a total cell number exceeding 24×10^6 (Figure 4.38A). This indicates that cell growth between passage +0 and passage +12 increased 5-fold. For hHDPCs(H60), the culture lasted 93 days, during which 13 passages were completed, and the total cell number reached 12.5×10^6 cells (Figure 4.38B), corresponding to a 14.5-fold increase between passage +0 and passage +13. For hHDPCs(H63), 10 passages were carried out over 106 days, resulting in a total of more than 14×10^6 cells (Figure 4.38C) and an 11-fold increase in cell number. In the case of hHDPCs(H76), 10 passages were performed over 112 days, yielding over 12×10^6 cells (Figure 4.38D) and the highest overall growth among all samples – nearly an 84-fold increase between passage +0 and passage +10.

The total culture duration varied among hHDPCs from different donors; therefore, increases in cell number were compared at passage +10 for each cell type. At passage +10, hHDPCs(H37) yielded nearly 22×10^6 cells, hHDPCs(H60) yielded nearly 10×10^6 cells, hHDPCs(H63) yielded over 14×10^6 cells, and hHDPCs(H76) yielded approximately 12×10^6

cells. It is worth noting that after cell isolation, the number of hepatocytes in the cell lysate is unknown, whereas the total cell number is known. The initial number of hepatocytes that dedifferentiated into hHDPCs varied across donors. The results demonstrate substantial differences in cell growth capacity among the hHDPCs derived from different donors, with hHDPCs(H37) showing nearly twice the cell production compared with the other three cell types.

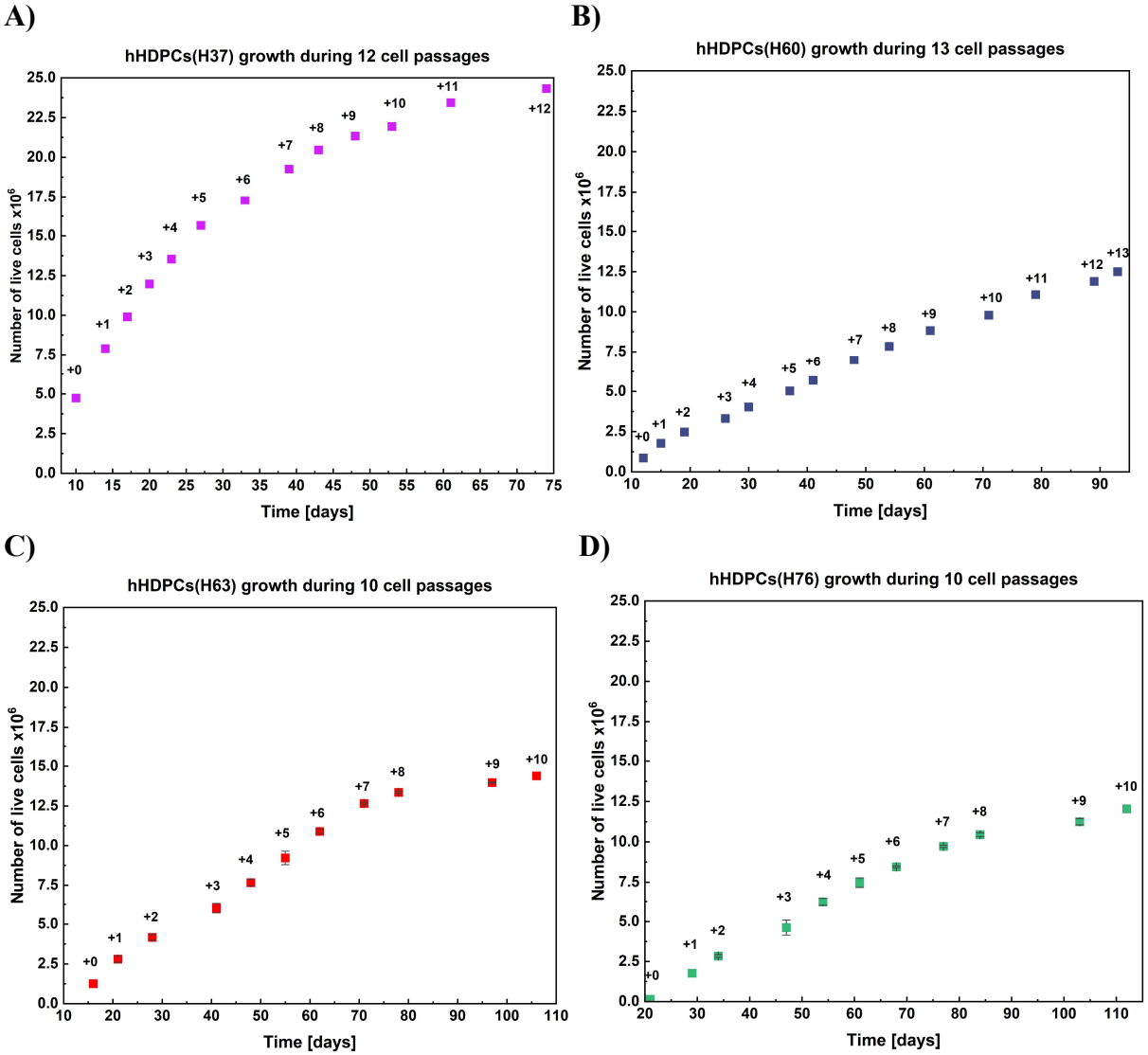


Figure 4.38. Comparison of cell growth during long-term cultures. The experiment was conducted on hHDPCs cells derived from four donors (H37, H60, H63, and H76). Liver isolates were thawed and seeded onto culture plates. After several days, once the cells dedifferentiated and began to proliferate, they were designated as hHDPCs. Following cell expansion, consecutive passages were performed and marked with a "+" sign followed by the passage number (+0, +1, etc.). Passage +0 represents dedifferentiated and divided hHDPCs that had not yet been passaged. After each passage, the cells were trypsinized and counted using the trypan blue exclusion method. The graphs present the total number of cells obtained after each passage. Cell number versus culture day plots include data points for specific passages, which are indicated by their passage numbers. **A)** Graph of cell number versus culture day for hHDPCs derived from donor H37, from passage +0 to +12. Each passage was analyzed in a single replicate; therefore, neither SD nor statistical analysis was performed. **B)** Graph of cell number versus culture day for hHDPCs derived from donor H60, from passage +0 to +13. Each measurement was performed in

a single replicate; thus, no SD or statistical analysis was conducted. **C)** Graph of cell number versus culture day for hHDPCs derived from donor H63, from passage +0 to +10. Measurements for each passage were performed in duplicate; the results are presented as mean values ± SD (n = 2), with no statistical analysis performed. **D)** Graph of cell number versus culture day for hHDPCs derived from donor H76, from passage +0 to +10. Measurements for each passage were performed in duplicate; the results are presented as mean values ± SD (n = 2), with no statistical analysis performed.

4.2.6 Long-Term Monitoring of Morphology and Proliferation of hHDPCs

Since new cells – hHDPCs that dedifferentiate from hepatocytes – were obtained, morphological changes and cell divisions during culture were monitored using the OLYMPUS Provi CM20 system (details described in section 3.11.2). Figure 4.39 shows the experimental design.

For this experiment, the following cell types were used: LCIs derived from three donors (H40, H43, H74), C3A, HDFn, and hHDPCs(H74). Two types of culture media were used: DMEM and HM+HGS.

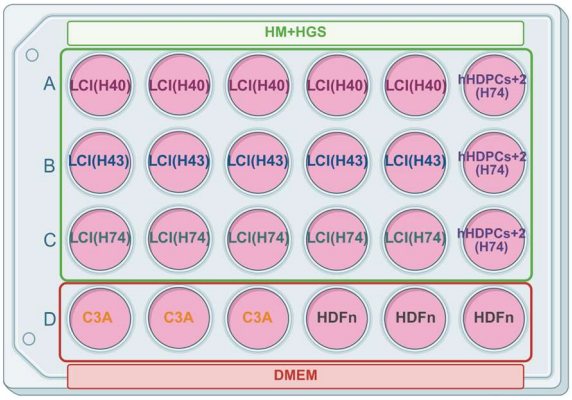


Figure 4.39. Experimental design. The following cell types were analyzed: three LCI(H40, H43, H74), C3A, HDFn, and hHDPCs+2(H74). C3A and HDFn were cultured in DMEM, whereas LCIs and hHDPCs were maintained in HM+HGS medium. Cells were seeded in 24-well plates coated with rat tail collagen type I at the following densities: 1.5×10^6 [LCI(H40, H43, H74)], 1×10^4 [hHDPCs+2(H74), HDFn], and 3×10^4 (C3A). Cultures were maintained for 21 days with scheduled medium changes.

4.2.6.1 Cell Proliferation and Cell Confluency

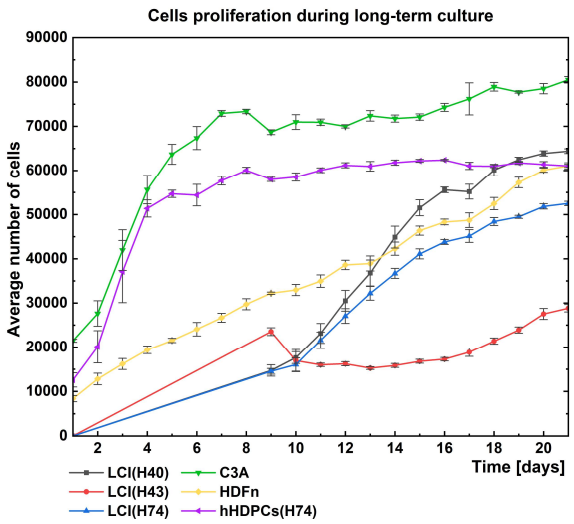
To assess proliferation dynamics, the OLYMPUS Provi CM20 system was also used to determine the number of cells during the entire 21-day culture period Figure 4.40).

The results showed that the C3A cell line proliferated rapidly during the first 8 days of culture, reaching approximately 7.4×10^4 cells per well. Subsequently, the cell number continued to increase, and by the end of the experiment, an average of 8×10^4 cells per well was obtained. hHDPCs(H74) exhibited strong proliferative potential, with cell numbers increasing steadily and reaching approximately 6×10^4 cells per well by day 8. After this time point, a slight decline

in cell numbers was observed, which stabilized at approximately 6.1×10^4 cells per well until day 21. In the case of HDFn, a gradual increase in cell number was observed. After 21 days of culture, the number of cells reached approximately 6.1×10^4 per well, a value similar to that observed for hHDPCs(H74). In liver cell isolates, cell growth was slower and more variable. Due to issues related to waste accumulation in the culture wells, cell numbers were analyzed starting from day 9 of culture, when all suspended elements had been completely removed during the medium exchange. In LCI(H40) cultures, the number of cells increased progressively, reaching 4.5×10^4 cells per well on day 14, which was higher than the number observed for HDFn on the same day (4.2×10^4). After 21 days of culture, the cell number reached 6.4×10^4. LCI(H74) exhibited a similar growth pattern, with cell numbers increasing from approximately 1.4×10^4 on day 9 to 5.2×10^4 by day 21. In the case of LCI(H43), the initial cell number was relatively high (2.3×10^4); however, the proliferation rate was limited, and by day 21, cultures contained only about 2.9×10^4 cells per well (Figure 4.40A).

The obtained results demonstrated that C3A reached 60% confluency after 5 days of culture, and this level remained stable until day 21. hHDPCs(H74) reached nearly 83% confluency after 8 days; however, this value subsequently declined slightly to approximately 77%, remaining stable thereafter. In HDFn cultures, confluency reached 74% after 11 days and remained stable for the remainder of the experiment. In contrast, LCIs displayed delayed increases in confluency, primarily due to significant cell debris during the early stages of culture. For LCI(H40), confluency increased gradually from 31% on day 8 to 67% on day 17. In the case of LCI(H74), confluency increased from 26% on day 8 to 67% on day 19. The LCI(H43) isolate demonstrated the highest initial confluency (34%), which increased to approximately 48% after 20 days of culture (Figure 4.40B).

A)



B)

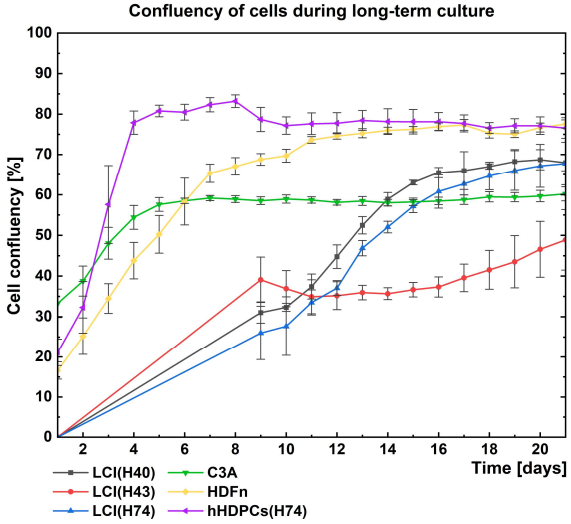


Figure 4.40. Changes in cell number and confluency dynamics in long-term cultures. The proliferation of three LCIs (H40, H43, H74), hHDPCs(H74), C3A, and HDFn was monitored using the OLYMPUS Provi CM20 system for 21 days. Cells were seeded at the following densities: 3×10^4 (C3A), 1×10^4 [HDFn, hHDPCs(H74)], and 1.5×10^6 [LCI(H40, H43, H74]. Cell counts were automatically determined every 4 hours. Media were exchanged after 2, 6, 10, 13, 17, and 21 days of culture. **A)** Average number of cells during long-term culture. **B)** Dynamics of confluency in long-term cultures. Results are shown as mean ± SD; n = 3 for C3A, HDFn, hHDPCs(H74), and n = 5 for each LCI.

4.2.6.2 Microscopic Observations

During the 21-day cell culture period, in addition to counting cells and calculating the percentage of confluence using the OLYMPUS Provi CM20 system software, morphological alterations and cell divisions were also monitored in the analyzed samples. Figure 4.41 presents representative images obtained with this system. Furthermore, it can be observed that cells that initially formed hepatocyte islands immediately after isolation began to divide after several days of culture. In the LCI(H40) sample, cell division was first noted on day 5 of culture. However, in the LCI(H74) sample, after 2 days of culture, a single cell can be observed dividing and forming an island of cells (Supplementary Figure S8.4A). Representative images of the control cell lines C3A, HDFn, and hHDPCs+2(H74) are additionally presented in Supplementary Figure S8.4B, C, D.

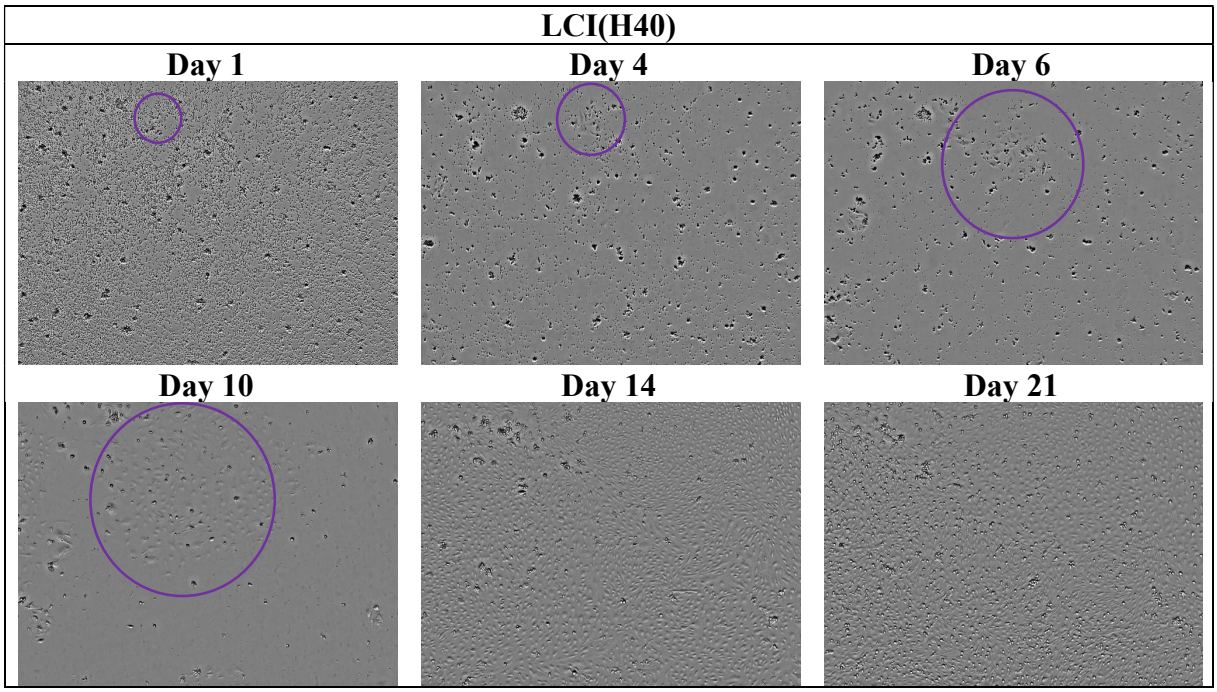
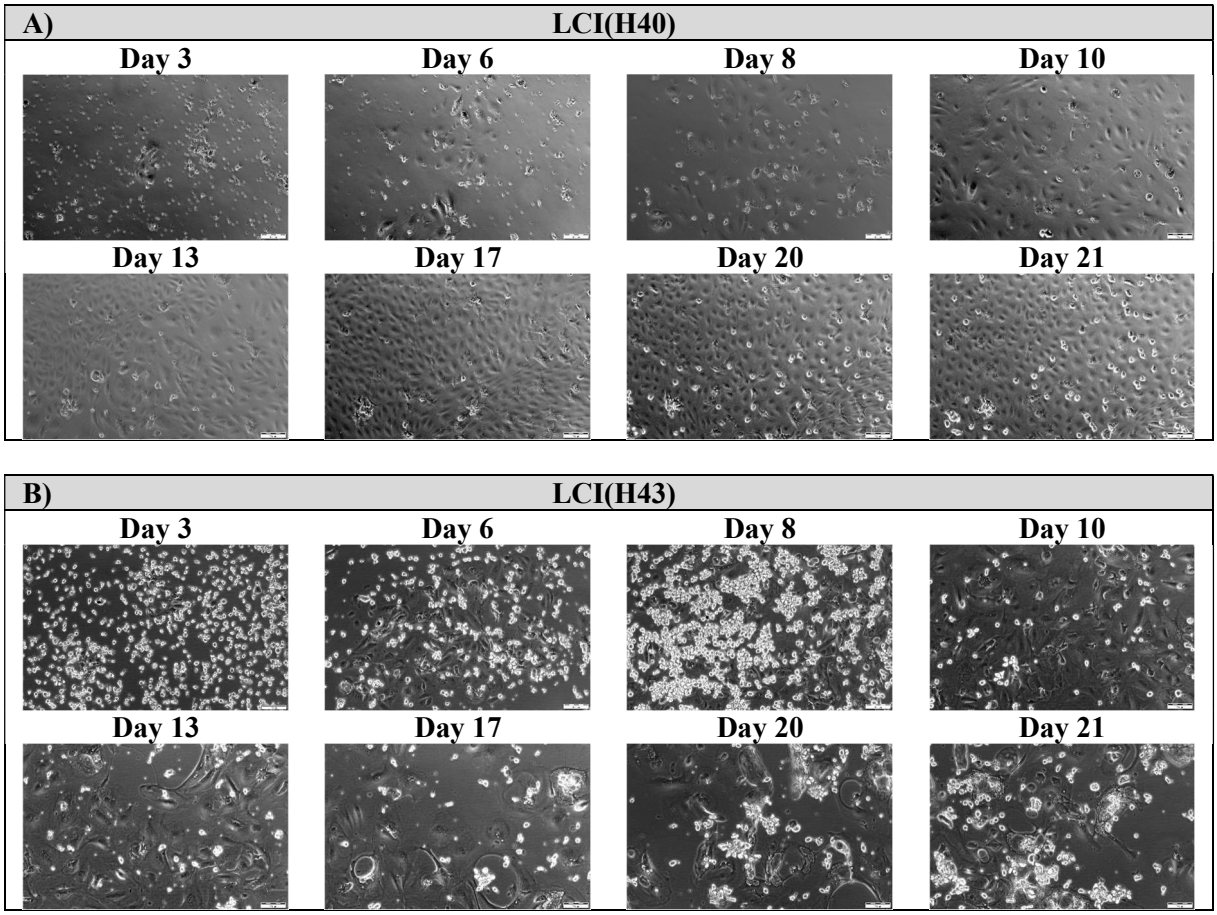


Figure 4.41. Observation of morphological changes and proliferation of liver cell isolates. Micrographs illustrate morphological transformations of the LCI(H40) during the 21-day culture period. Images were captured using the OLYMPUS Provi CM20 system at 4× magnification. Photographs were taken every 4 hours; however, only selected representative images are presented in the figure. The purple circle indicates a hepatocyte island that began proliferating after several days in culture.

The continuous monitoring system was equipped with a 4× magnification lens. Therefore, additional micrographs were obtained using an inverted fluorescence microscope at 10× magnification, which allows image acquisition at identical positions within the wells of the culture plate (Figure 4.42). The results obtained with this microscope also confirmed the ability of cells forming islands to proliferate as early as day 5 of culture. Moreover, it was observed that cells within individual LCIs exhibit different behavior. For instance, in Figure 4.42A, a cell island from LCI(H40) sample can be seen initiating division, and by day 17 of culture, full confluency is observed in the area viewed under the microscope. In contrast, in sample LCI(H43) (within the same monitored area of the well), the cells in the initial island divided; however, by day 13, fewer cells remained, and these cells were larger compared to those in sample LCI(H40). Furthermore, by day 17, cells began to degrade and detach from the culture surface (Figure 4.42B). Similarly, cells from LCI(H74) exhibited behavior comparable to that observed for LCI(H43). Cells within the island divided after 6 days of culture. By day 13, dividing cells were observed outside the initially monitored area, while the cells from the originally observed island had detached from the culture surface (Figure 4.42C).



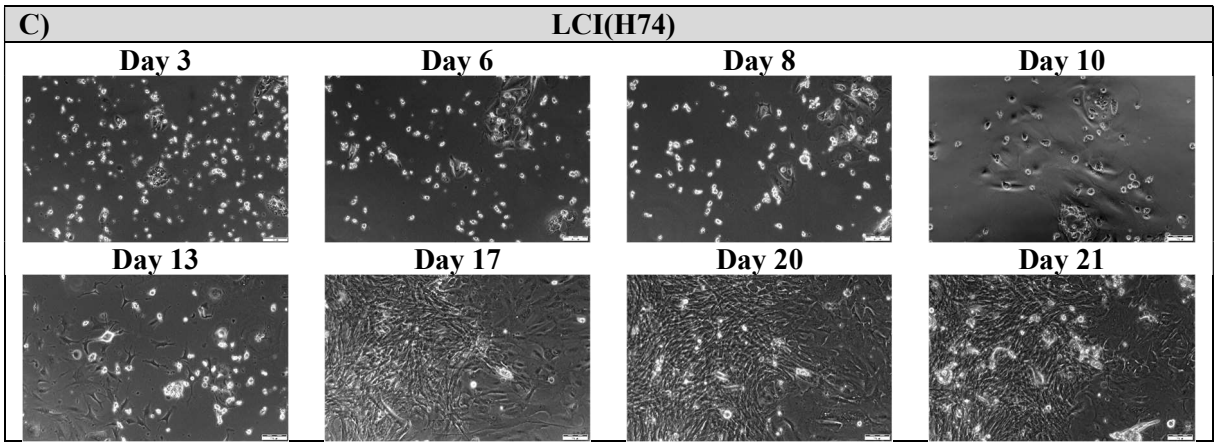


Figure 4.42. Morphological changes and proliferation of liver cell isolates. Cells were seeded in 24-well plates coated with rat tail collagen type I, at a density of 1.5×10^6 cells per well. LCIs were obtained from three donors: H40, H43, and H74. Cultures were maintained for 21 days, with medium changes every 2–3 days. **A)** Cell changes during 21 days of culture for sample LCI(H40). **B)** Cell changes observed for sample LCI(H43). **C)** Cell changes obtained for sample LCI(H74). Images were acquired using an inverted fluorescence microscope Olympus XI71 (Olympus, Warsaw, Poland), at 10× magnification (scale bar 100 μm), equipped with the CS-S_MP-VF Multi Position module, which enabled image acquisition at the same positions within the culture vessels.

4.2.6.3 Albumin Secretion (ELISA)

During the experiment, the secretion of albumin in the culture medium was also assessed using quantitative ELISA assay. Based on the data obtained from the cell culture monitoring system, the ELISA results were recalculated to determine daily albumin secretion by the cells. The findings indicate that among the investigated cell types, only C3A cells secreted albumin at a high level. Moreover, the amount of albumin secreted by C3A increased with culture duration: after 2 days, the secretion was 110 ng, while after 17 days it reached 8696 ng. However, after 21 days of culture, the mass of the secreted albumin in the culture medium decreased slightly to 8867 ng (Figure 4.43). For the other examined cell types, only low albumin production was detected, as shown in Figure 4.43. The results indicate that on day 2, albumin secretion levels were 5.8 ng for LCI(H43), 5.2 ng for LCI(H40), and 4.7 ng for LCI(H74), while both hHDPCs(H74) and HDFn exhibited identical values of 4 ng. After 6 days of culture, the albumin mass for all cell types reached 4 ng, and by day 21, the levels remained unchanged. It should be emphasized that, except for C3A, the results obtained for all cell types were at the detection limit of the ELISA method (values approached blank levels).

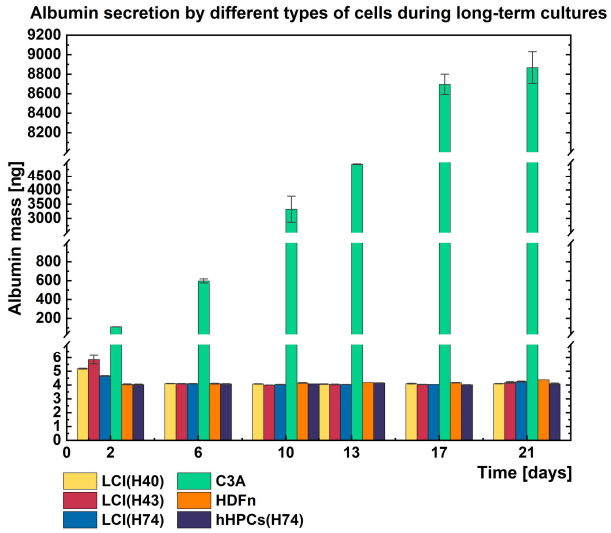
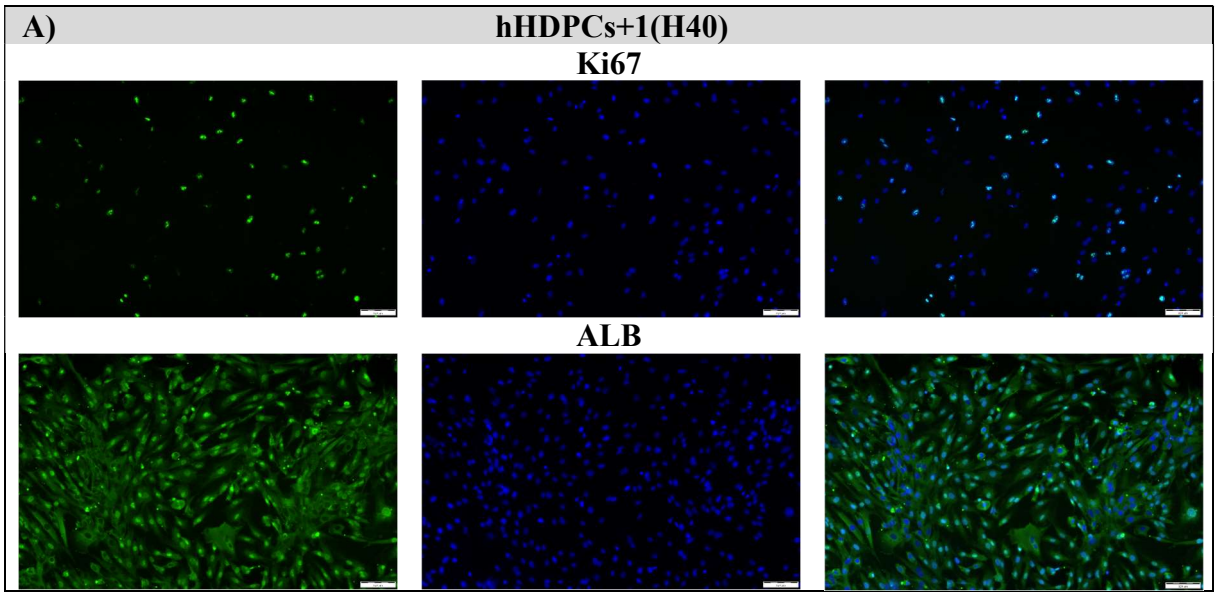


Figure 4.43. Albumin secretion by cells during long-term culture. Cells were cultured for 21 days, with the medium replaced every 2–3 days, in 24-well plates coated with rat tail collagen type I. Seeding densities were as follows: 3×10^4 for C3A, 1×10^4 for HDFn and hHDPCs(H74), and 1.5×10^6 for LCI (H40, H43, and H74). The albumin mass in the post-culture medium was determined by ELISA. Data are presented as mean ± SD; n = 2 for each cell type.

4.2.6.4 Immunocytostaining of hHDPCs After Long-Term Culture

At the conclusion of the experiment, cells derived from LCIs were detached, counted, and seeded into culture wells for immunostaining with antibodies against ALB and Ki67. Cells were plated at a density of 6×10^4 cells per well in 24-well plates and cultured for 24 h. Subsequently, the cells were prepared for immunostaining according to the protocol described in section 3.4 Immunofluorescence. After passaging, LCIs were designated as hHDPCs at the first passage. The results demonstrate that these cells retain proliferative capacity, as confirmed by expression of Ki67, and maintain their ability to produce albumin, as observed intracellularly (Figure 4.44).



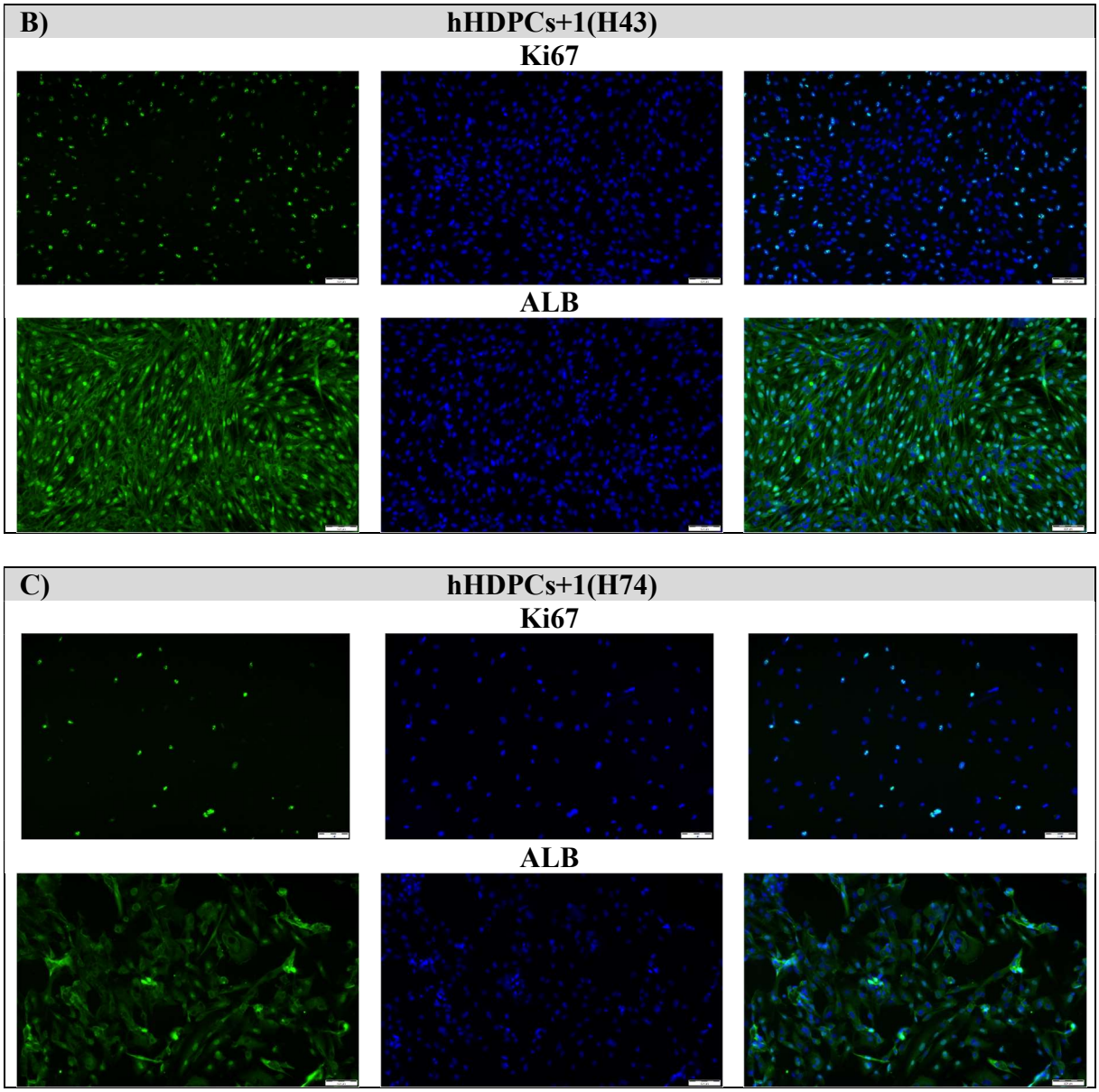


Figure 4.44. Detection of albumin and proliferation marker in cells after long-term culture. Cells [hHDPCs+1(H40), hHDPCs+1(H43), hHDPCs+1(H74)] were seeded at a density of 6×10^4 cells per well in 24-well plates and cultured for 24 h. Immunocytostaining was then performed for albumin (ALB) and Ki67 (a proliferation marker). In the images, ALB is shown in green within the cell cytoplasm (lower left panels), Ki67 appears as green punctate signals within the cell nuclei (upper left panels), and nuclei are counterstained with DAPI in blue (middle panels). The right panels present merged images. Micrographs were taken using an Olympus XI71 inverted fluorescence microscope (Olympus, Warsaw, Poland) at 10× magnification (scale bar: 100 µm).

4.2.7 Mesenchymal Stem Cell Markers in hHDPCs

Detection of positive (CD29, CD73, CD44) and negative (CD34, CD133, CD45) MSC markers were performed in the following cell types: hHDPCs, C3A, HDFn, HUVEC, SH-SY5Y, and hH_3, using flow cytometry analysis.

4.2.7.1 MSC Markers Across Passages

In the first experimental variant, the percentage of cells positive for individual MSC markers was analyzed for passages +0 to +11 in hHDPCs derived from donor H37. Due to insufficient cell material, passage +10 was not included. The results demonstrated that hHDPCs underwent gradual changes in the expression of analyzed proteins during subsequent passages. It was observed that all positive MSC markers (CD44, CD29, CD73), as well as two negative markers (CD133 and CD34) were present in hHDPCs, whereas CD45 was not detected in any passage (Figure 4.45).

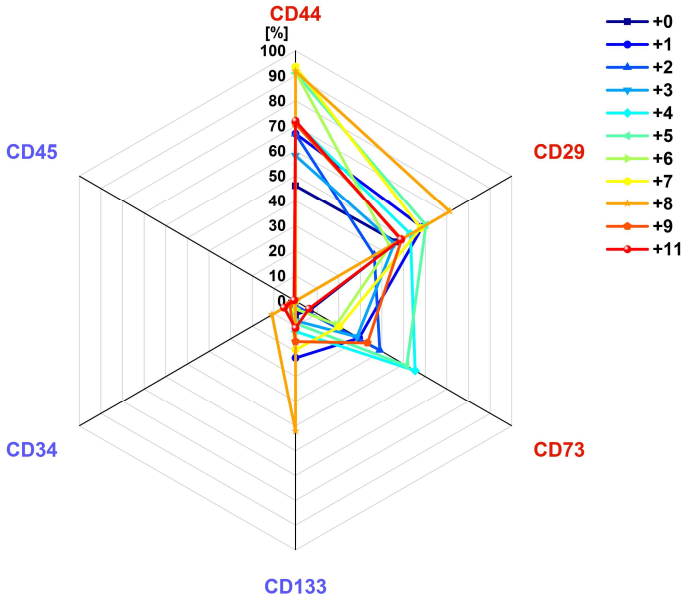


Figure 4.45. Expression levels of positive and negative MSC markers in consecutive passages of hHDPCs. hHDPCs derived from donor H37 were cultured in T25 cm^2 flasks in HM+HGS medium. Cells were regularly passaged, and flow cytometry analysis was performed. Positive MSC markers (CD44, CD29, CD73) are indicated in red, whereas negative MSC markers (CD34, CD133, CD45) are indicated in blue. The analysis was performed on 2×10^5 cells per sample. Measurements were conducted in single replicates; therefore, neither standard deviation (SD) nor statistical analysis was performed.

4.2.7.2 Comparison of MSC Markers in Different hHDPCs

In the second experimental variant, hHDPCs from donors H37, H65, and H72 were analyzed at passages +2, +8, and +11. The results indicated donor-dependent variability in protein expression at identical passages. For example, at passage +2, positive MSC markers were consistently detected, while negative markers were present at low levels, with less than 5% of CD133-positive cells (Figure 4.46A). In contrast, at passage +8, the proportion of CD133-positive cells ranged between 4% and 29% (Figure 4.46B). At passage +11, similarly

to passage +2, negative markers were detected only at low levels, ranging from 3% to 11% (Figure 4.46C).

A comparison of positive marker expression across passages revealed that CD44 was consistently detected at high levels: 67–82% at passage +2, 71–96% at passage +8, and 72–96% at passage +11. For CD29, positivity was observed in 36–80% of cells at passage +2, 31–54% at passage +8, and 43–76% at passage +11. CD73 expression was lower and more variable, ranging from 21 to 40% at passage +2, 14–98% at passage +8, and 6–37% at passage +11.

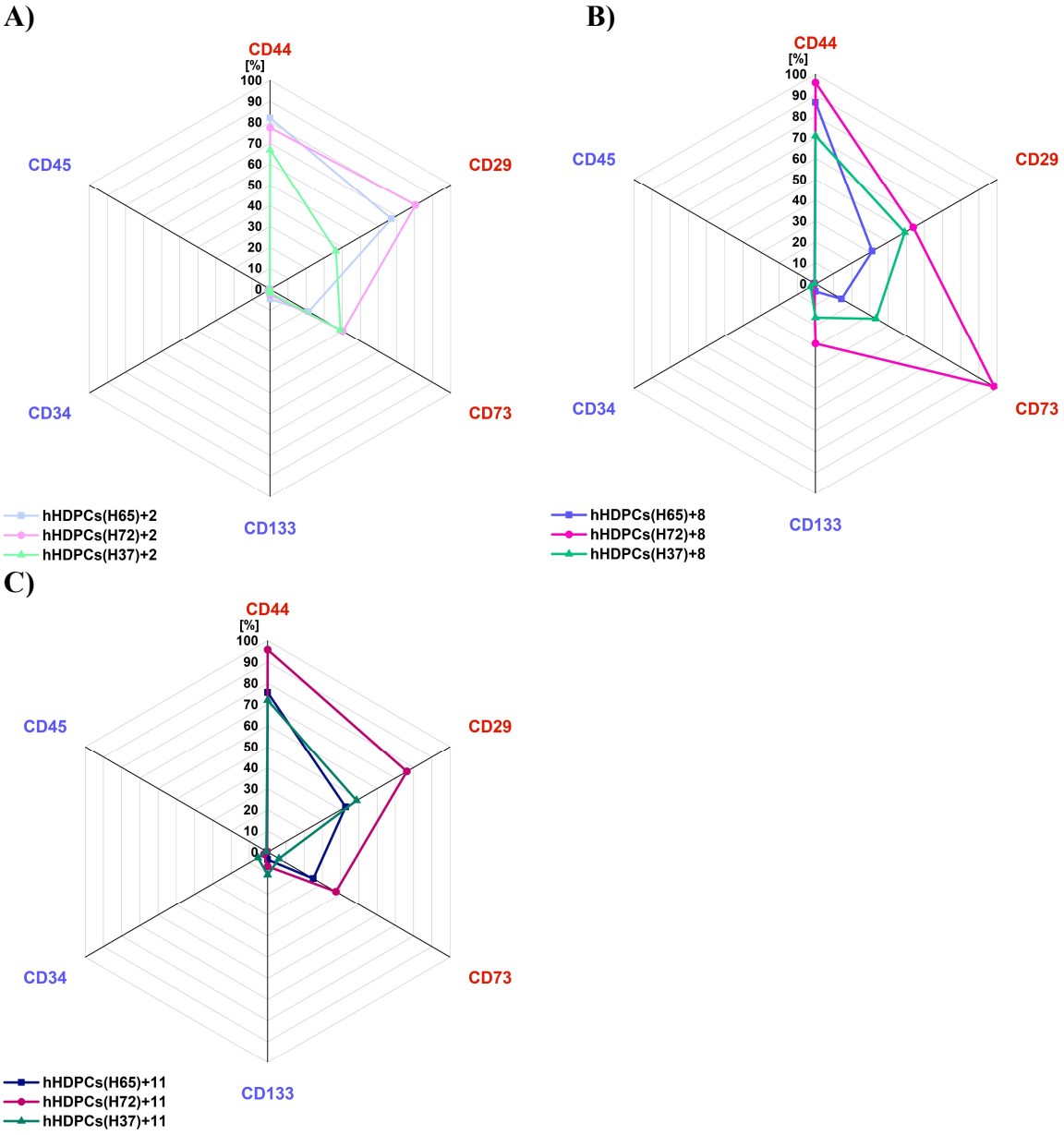


Figure 4.46. Detection of MSC markers in hHDPCs derived from three donors (H37, H65, H72) and analyzed at passages +2, +8, and +11. Cells were thawed and seeded at a density of 2×10^5 in T25 cm^2 flasks containing HM+HGS. The cells were cultured for 6 days, after which cytometric analysis was performed. Positive MSC markers (CD44, CD29, CD73) are indicated in red, whereas negative markers (CD34, CD133, CD45) are indicated in blue. **A)** Detection of positive and negative MSC markers in hHDPCs(H65, H72, and H37) at passage

+2. **B)** Detection of positive and negative MSC markers in hHDPCs(H65, H72, and H37) at passage +8. **C)** Detection of positive and negative MSC markers in hHDPCs(H65, H72, and H37) at passage +11. Each sample was analyzed in a single replicate; therefore, neither SD nor statistical analysis was performed.

4.2.7.3 MSC Markers in Different Types of Cells

In the third experimental variant, MSC marker expression was compared among hHDPCs(H37), HDFn, hH_3, C3A, SH-SY5Y, and HUVEC (Figure 4.47). In hHDPCs, 75% of cells were positive for CD44, 52% for CD29, 23% for CD73, 17% for CD133, and 4% for CD34, while CD45 was not detected. In C3A cells, neither negative MSC markers nor CD44 were detected, and only low expression of CD29 (10%) and CD73 (13%) was observed. In hHs, CD44 and CD45 were not detected; however, CD29 (35%), CD73 (21%), CD133 (14%), and CD34 (10%) were observed.

In HDFn, a high percentage of positive markers was observed. CD44 reached the highest level among all tested cell types (96%), whereas CD29 and CD73 were detected at 58% and 52%, respectively. Among the negative MSC markers, 8% of cells were positive for both CD133 and CD34, while CD45 was not detected. In SH-SY5Y cells, none of the tested markers were expressed. In HUVEC, with the exception of CD45, both positive and negative markers were detected. The expression values were as follows: CD44 – 23%, CD29 – 48%, CD73 – 16%, CD34 – 7%, CD133 – 33%.

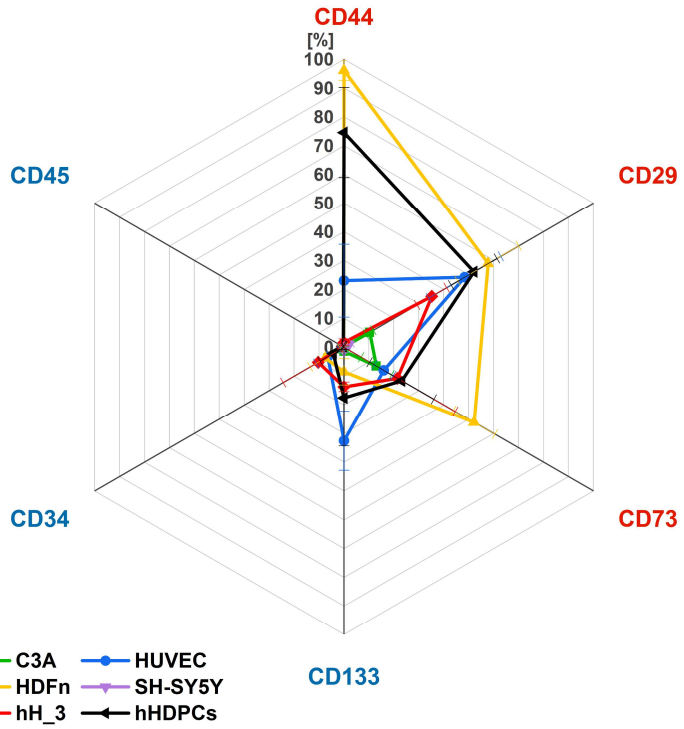


Figure 4.47. Expression of positive and negative MSC markers in different cell types (hHDPCs, HDFn, hH_3, C3A, SH-SY5Y, HUVEC). For each cell type, 2×10^5 cells per sample were seeded into T25 cm^2 culture flasks and cultured in media, dedicated to the specific cell line. Flow cytometry analysis was performed on 2×10^5

cells per sample. Positive markers (CD44, CD29, CD73) are shown in red; negative markers (CD34, CD133, CD45) are shown in blue. For C3A, HDFn, HUVEC, and SH-SY5Y, the experiments were performed in three replicates (n = 3), whereas for hHs, two replicates were performed (n = 2). For hHDPCs, average values obtained from 11 cell passages are presented (n = 11). Results are shown as mean value of the percentage of marker-positive cells.

4.2.8 Re-differentiation of hHDPCs into Hepatocyte-like Cells Using Growth Factor-Supplemented Medium

The investigation whether hHDPCs are capable of re-differentiating into hepatocyte-like cells in the presence of selected growth factors was performed using hHDPCs derived from donor H72 at passages +2, +6, and +12. Three variants of culture media were applied during the experiment: HM supplemented with FGF-4 and HGF (HM+F+H), HM supplemented with EGF and HGF (HM+E+H), and HM without additional growth factors (control). The experimental design is illustrated in Figure 4.48.

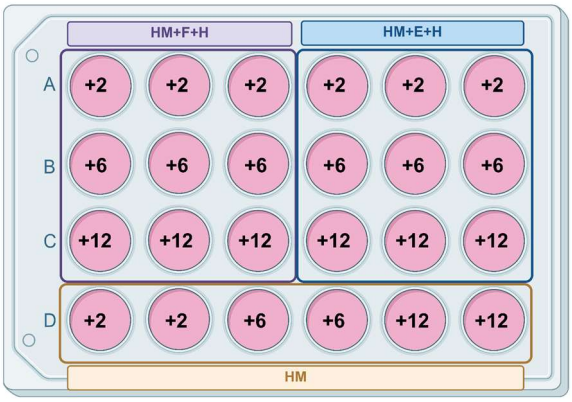
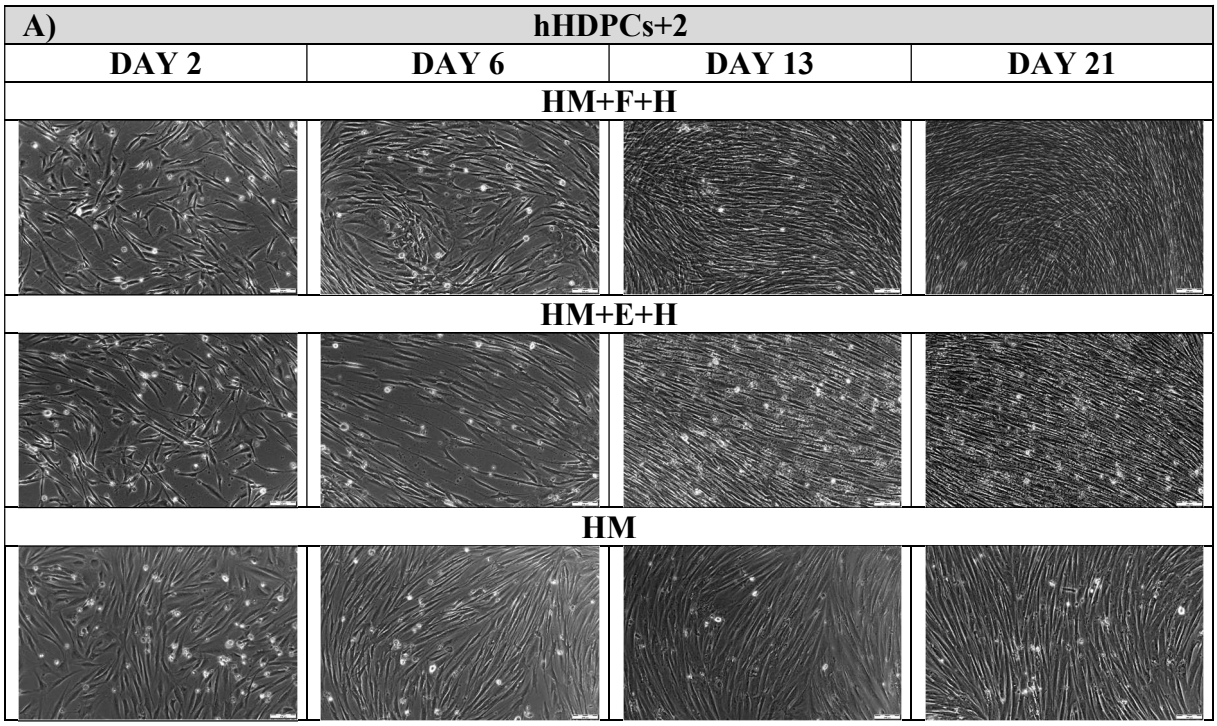


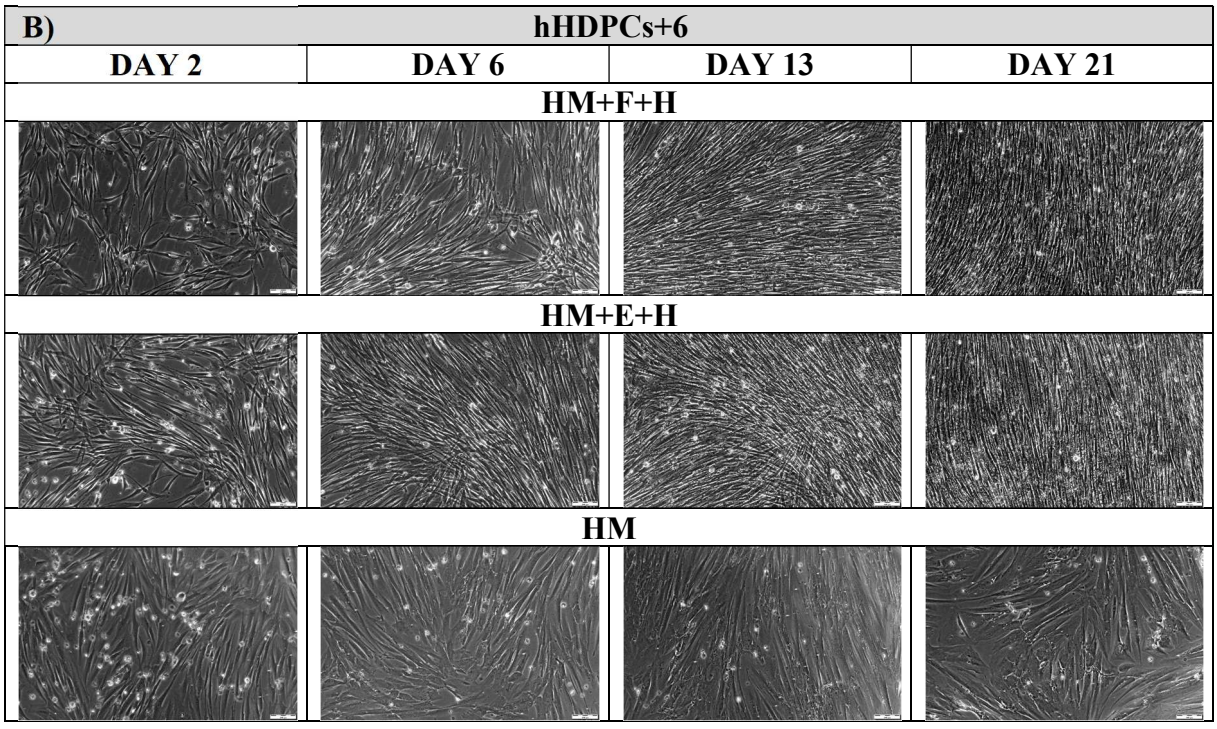
Figure 4.48. Experimental plan for the re-differentiation of hHDPCs into hepatocyte-like cells. hHDPCs at passages +2, +6, and +12, derived from donor H72, were analyzed. Cells were seeded at a density of 3×10^4 per well in 24-well plates and cultured for 21 days with regular medium exchange. Three variants of culture media were used: control (HM supplemented with FBS and antibiotics), HM+F+H (HM supplemented with FBS, antibiotics, FGF-4, and HGF), and HM+E+H (HM supplemented with FBS, antibiotics, EGF, and HGF). Variants HM+F+H and HM+E+H were performed in triplicate, while control cultures were prepared in duplicate.

4.2.8.1 Microscopy Observation of hHDPCs Cultured in Different Conditions

Microscopic observation of hHDPC cultures at passages +2, +6, and +12 in different media (HM, HM+F+H, HM+E+H) revealed that the presence of growth factors promoted cell proliferation. This effect was most pronounced in lower passages (+2 and +6), where after 21 days of culture the cells exhibited an elongated, spindle-shaped morphology and demonstrated extensive proliferation, which was not observed in the control HM cultures without growth factors (Figure 4.49A, B). In cultures derives from higher passages (+12), a slight increase in cell number was observed in the presence of growth factors, while cells grown

in basic HM medium showed poor adhesion to the substrate after 2 days, in contrast to those in HM+F+H and HM+E+H conditions (Figure 4.49C). Importantly, no morphological changes from spindle-shaped fibroblast-like cells to polygonal hepatocyte-like cells were observed during the culture period (Figure 4.49).





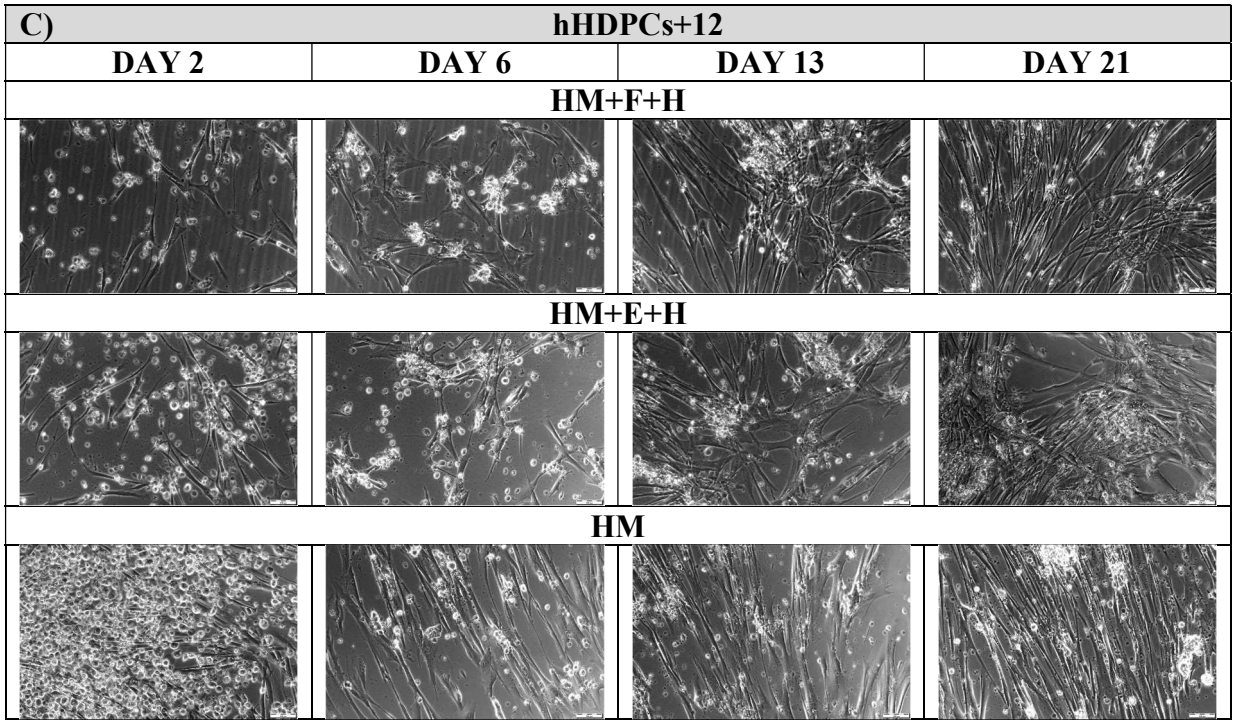
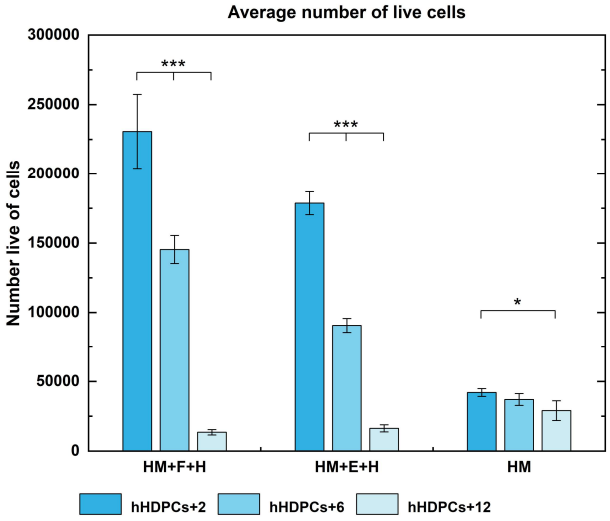


Figure 4.49. Morphological changes of hHDPCs at different passages cultured in media with or without growth factor supplementation. Cells were cultured for 21 days, and microphotographs were taken after 2, 6, 13, and 21 days. Culture variants included HM (control; Hepatocyte Medium supplemented with FBS and antibiotics), HM+F+H (supplemented with FBS, antibiotics, FGF-4, and HGF), and HM+E+H (supplemented with FBS, antibiotics, EGF, and HGF). **A)** Passage +2. **B)** Passage +6. **C)** Passage +12. Microphotographs were taken using an inverted fluorescent microscope Olympus IX71 (Olympus, Warsaw, Poland) at 10× magnification (scale bar = 100 μm).

4.2.8.2 Cell Number

After 21 days of culture, cells were trypsinized and counted as described in sections 3.1.3 Cell Passaging and 3.1.4 Cell Counting Using Bürker Chamber and Trypan Blue Exclusion**.** The results demonstrated that supplementation with growth factors (FGF-4, HGF, EGF) stimulated the proliferation of hHDPCs. The highest numbers of viable cells were obtained for hHDPCs+2 cultured in supplemented media, with the most pronounced increase observed in the HM+F+H condition ($p<0.001$). In comparison, hHDPCs cultured in HM+E+H yielded fewer cells: approximately 1.6-fold lower for passage +2 and approximately 2-fold lower for passage +6 relative to the HM+F+H condition ($p<0.001$). At passage +12, cells exhibited a very low proliferation rate during the 21-day culture period. Furthermore, at this passage, cell numbers in cultures supplemented with growth factors were reduced by approximately half compared with the control HM medium (Figure 4.50A).

A)



A1)

		hHDPCs +2	hHDPCs +2	hHDPCs +2	hHDPCs +6	hHDPCs +6	hHDPCs +6	hHDPCs+ 12	hHDPCs+ 12	hHDPCs+ 12
		F+H	**E+H**	**HM**	**F+H**	**E+H**	**HM**	**F+H**	**E+H**	**HM**
hHDPCs+ 2	**F+ H**		0.000210	0.000045	0.000092	0.000070	0.000037	0.000028	0.000031	0.000033
hHDPCs+ 2	**E+ H**	0.000210		0.000070	0.000637	0.000092	0.000045	0.000031	0.000033	0.000037
hHDPCs+ 2	**HM**	0.000045	0.000070		0.000092	0.000210	0.295552	0.000212	0.000354	0.021813
hHDPCs+ 6	**F+ H**	0.000092	0.000637	0.000092		0.000210	0.000070	0.000033	0.000037	0.000045
hHDPCs+ 6	**E+ H**	0.000070	0.000092	0.000210	0.000210		0.000092	0.000037	0.000045	0.000070
hHDPCs+ 6	**HM**	0.000037	0.000045	0.295552	0.000070	0.000092		0.000662	0.001115	0.109370
hHDPCs+ 12	**F+ H**	0.000028	0.000031	0.000212	0.000033	0.000037	0.000662		0.606953	0.006342
hHDPCs+ 12	**E+ H**	0.000031	0.000033	0.000354	0.000037	0.000045	0.001115	0.606953		0.011806
hHDPCs+ 12	**HM**	0.000033	0.000037	0.021813	0.000045	0.000070	0.109370	0.006342	0.011806	

Figure 4.50. Number of viable cells in hHDPCs cultures during re-differentiation experiments. hHDPCs at passages +2, +6, and +12 were cultured in 24-well plates at a density of 3 x 10^4 per well for 21 days. Control cultures were maintained in HM medium supplemented with FBS and antibiotics. whereas experimental cultures were performed in HM+F+H (HM supplemented with FBS, antibiotics, FGF-4, and HGF), and HM+E+H (HM supplemented with FBS, antibiotics, EGF, and HGF). Experimental variants with HM+F+H and HM+E+H were performed in triplicate, while controls were prepared in duplicate. **A1)** Statistical significance (p) was performed for Figure 4.50; analysis was conducted using MANOVA followed by Duncan's *post-hoc* test. Data are presented as mean ± SD (n = 2–3). Statistical significance was assumed at *p < 0.05, **p < 0.01, ***p < 0.001.

4.2.8.3 Albumin Production – ELISA

Albumin production in post-culture media was determined using quantitative ELISA assays for samples collected after 3, 6, 9, 13, 16, and 21 days of culture. However, the albumin secretion levels in the post-culture media for all experimental variants were below the assay's limit of detection (data not shown).

4.3 Human Dedifferentiated Hepatocytes (hDHes) Dividing and Retaining Hepatocyte Functions

To establish a long-term culture of dividing and functionally active human hepatocytes, cells were cultured on various growth surfaces using specialized culture media. The experiment was conducted in two stages. During the first stage, cells were maintained in an expansion medium (EM), whereas in the second stage, a differentiation medium (DM) was applied. The media were prepared according to the protocols described by Huch et al. (2015) and Garnier et al. (2018) [211], [212]. The experimental design is illustrated in Figure 4.51. The first stage was focused on inducing hepatocyte proliferation, while the second stage aimed to promote the differentiation of the proliferating cells while preserving hepatocyte-specific functions.

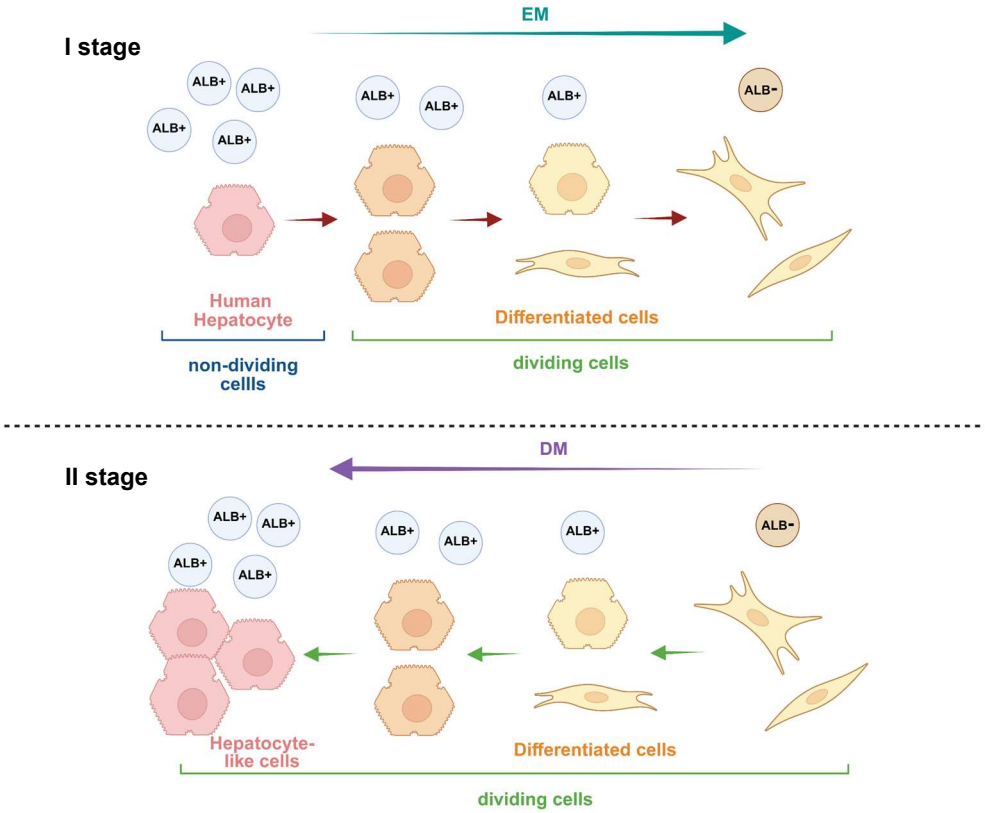


Figure 4.51. Schematic representation of the experiment design, stages I and II. Abbreviations: Alb^{+} - albumin production; Alb^{-} - gradual loss of albumin production; EM - expansion medium; DM - differentiation medium.

4.3.1 Stage I – Proliferating Hepatocyte-Like Cells

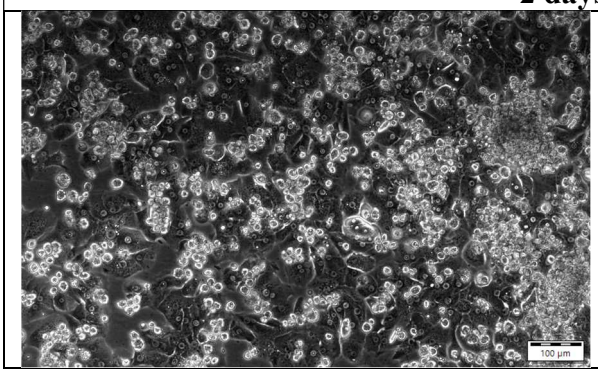
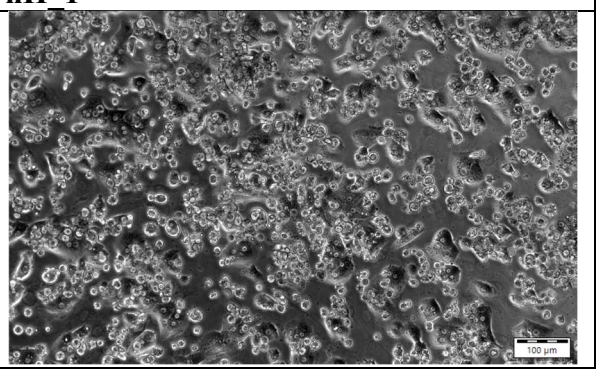
The first stage began with the thawing of cryopreserved human hepatocytes (hH_1). The cells were seeded into 24-well plates coated either with rat tail collagen type I or with dried fibroblasts overexpressing EGF and HGF (drHDFn_EGF+HGF). The cultures were carried out for 2 days in WG+I+H medium (Table 3.6) at a density of 3×10^{5} cells per well. Subsequently,

the medium was replaced with EM1 or EM1* (Table 3.7 and Table 3.8). EM1* was used exclusively for cells cultured on the drHDFn_EGF+HGF substrate and did not contain exogenous HGF or EGF. After 5 days, the medium was replaced with EM2 or EM2* (Table 3.9 and Table 3.10). Cells were cultured for a total of 48 days, after which the culture was terminated due to cell detachment and presumed cell death. However, it cannot be excluded that cells detached together with fibroblasts and remained viable, as this possibility was not experimentally verified. Throughout the culture period, cell morphology was monitored by microscopy and representative images are presented in Figure 4.52.

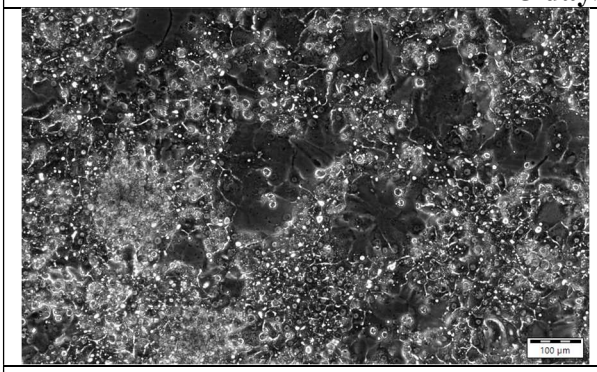
During culture, when hepatocytes (hH_1) that had started to divide were designated as human dedifferentiated hepatocytes (hDHes). The passage number was indicated by a plus sign ("+") followed by a number (e. g., +1). Cells that had not yet been passaged were defined as hDHes+0. After 9 days of culture, the cells were trypsinized, reseeded into new wells, and subjected to the first passage (hDHes+1)**.**

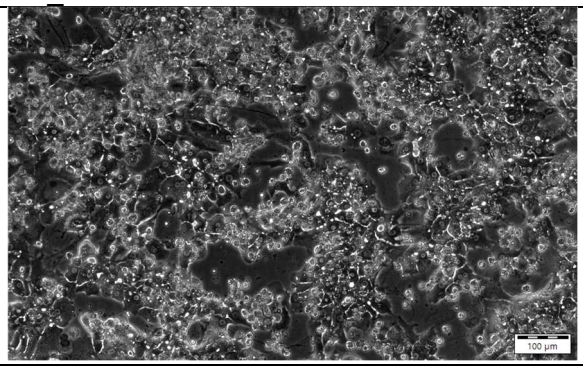
Cultures grown on the dried fibroblast substrate were maintained for 21 days, during which one passage was performed. Cells cultured on this substrate exhibited slower attachment and reduced spreading compared to those cultured on collagen, as clearly visible in images acquired after 9 days of culture (Figure 4.52).

In contrast, hepatocytes cultured on collagen-coated surfaces were maintained for 48 days, during which five passages were performed. Microscopic analysis revealed that between passages +1 and +4, hDHes displayed active proliferation and underwent a morphological transition from polygonal, hepatocyte-like shape to spindle-shaped, fibroblast-like cells. Following the fifth passage, cell proliferation slowed down, eventually leading to cell death.

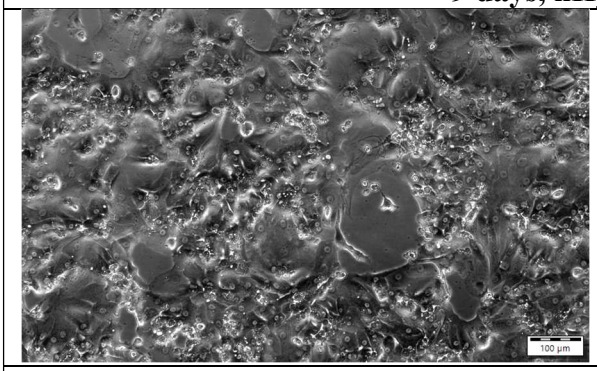
Cells cultured on the growth surface	
Collagen	**drHDFn_EGF+HGF**
2 days, hH_1	
	

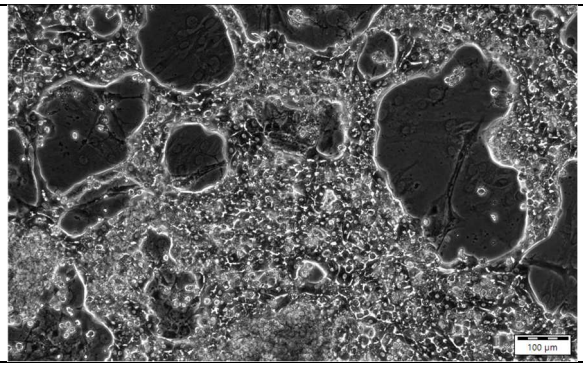
5 days, hH_1



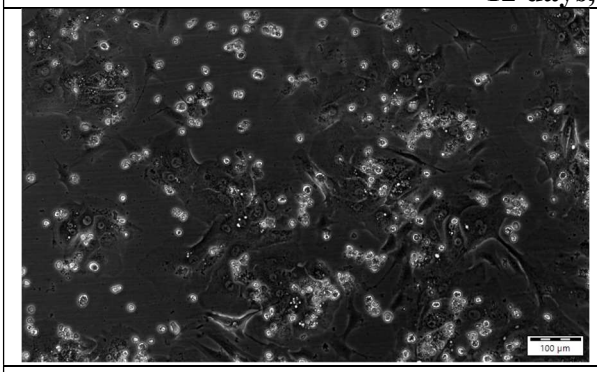


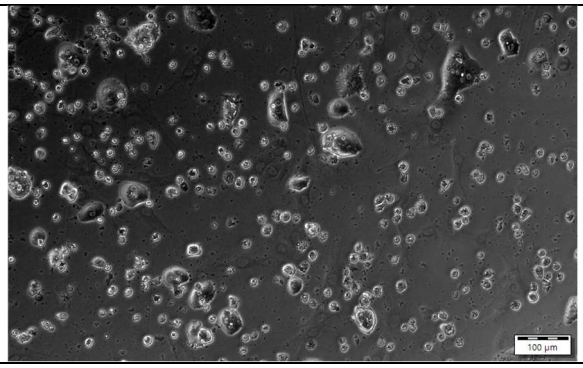
9 days, hH_1/hDHes+0



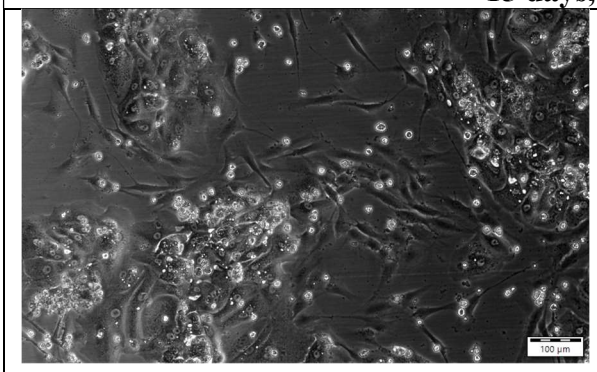


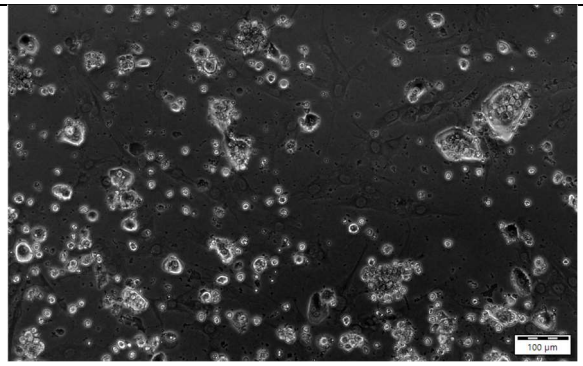
12 days, hDHes+1

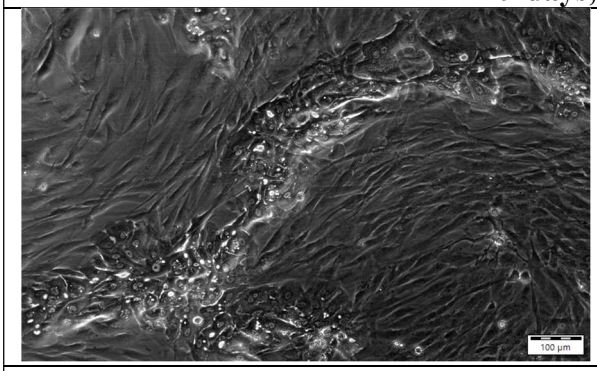
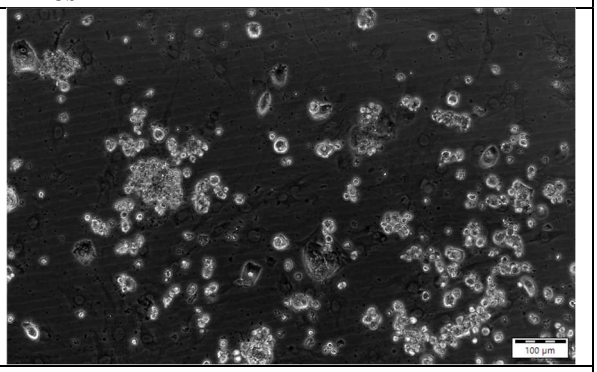
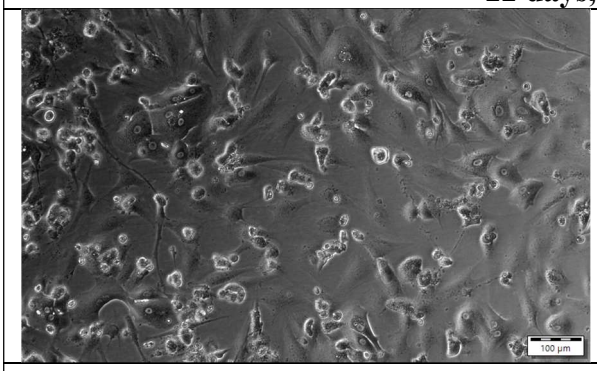
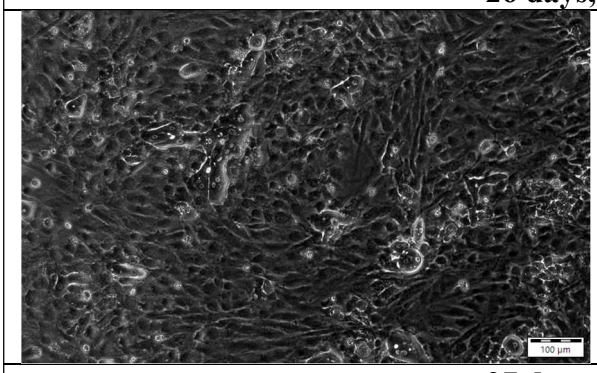
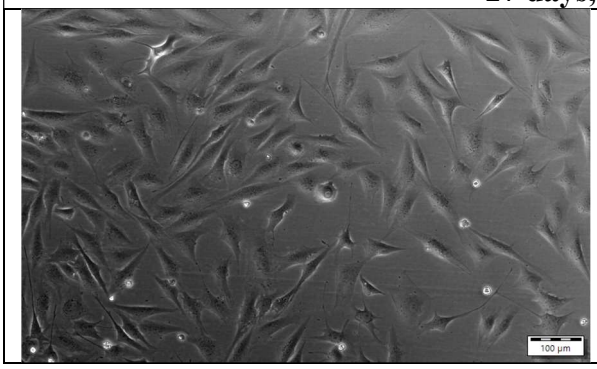


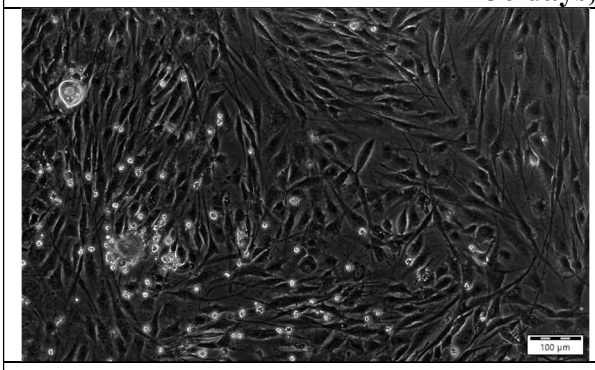
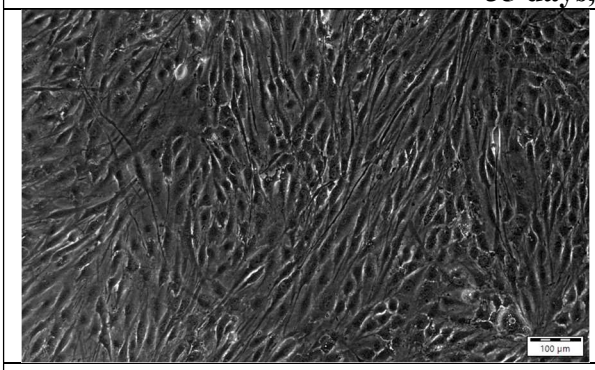
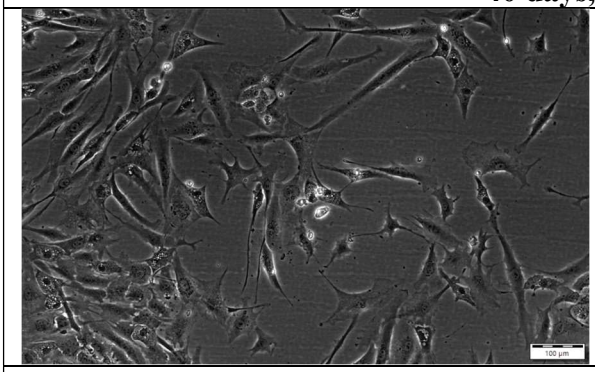
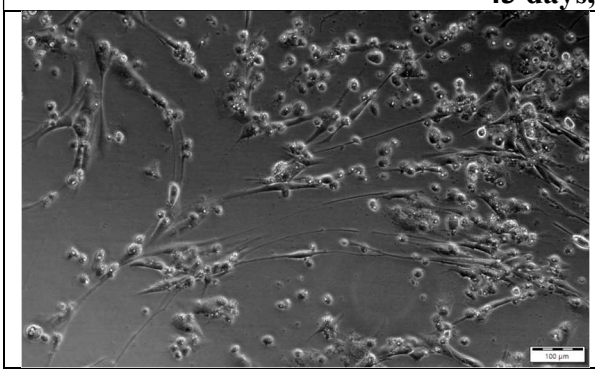


15 days, hDHes+1





19 days, hDHes+1	
	
22 days, hDHes+2	
	—
26 days, hDHes+2	
	—
27 days, hDHes+3	
	—

30 days, hDHes+3	
	—
35 days, hDHes+4	
	—
40 days, hDHes+5	
	—
43 days, hDHes+5	
	—

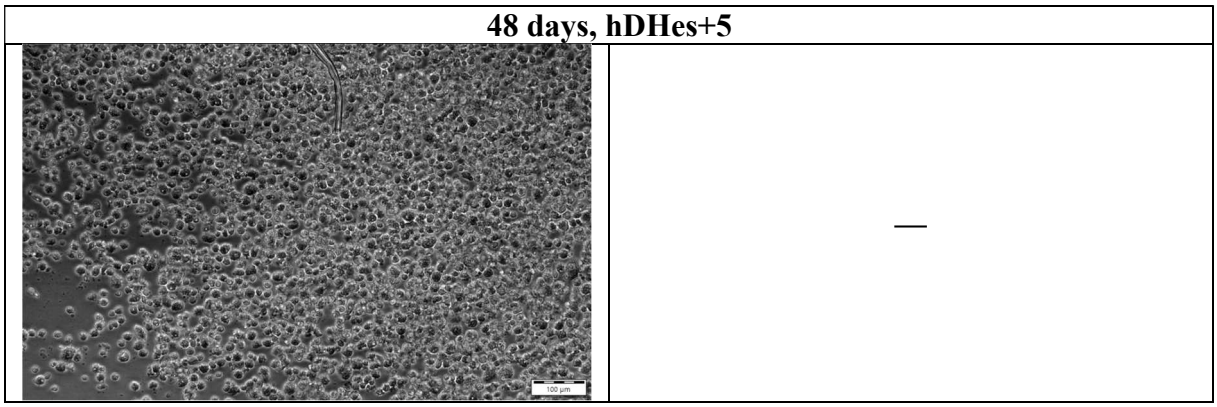


Figure 4.52. Morphological changes of cells cultured in expansion medium (EM). Human hepatocytes (hH_1) were seeded at a density of 3×10^5 cells per well on plates coated either with rat tail collagen type I or with dried fibroblasts overexpressing EGF and HGF (drHDFn_EGF+HGF). Four wells were prepared for each condition. Abbreviations: hHs – human hepatocytes; hDHes – human dedifferentiated hepatocytes; "+" followed by a number indicates the passage number. Cells cultured on collagen were maintained for 48 days with five passages, whereas cells cultured on drHDFn_EGF+HGF were maintained for 21 days with one passage. Images were taken using an Olympus IX-71 fluorescence microscope at 10× magnification (scale bar = 100 µm).

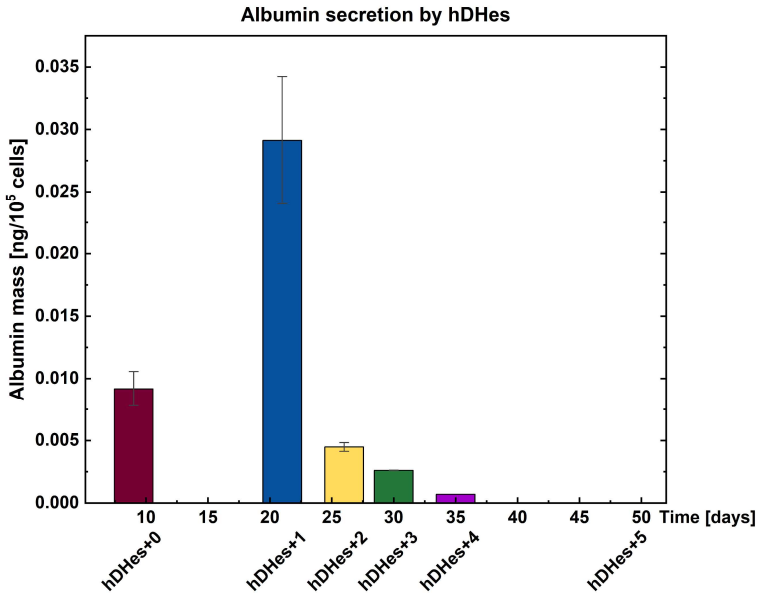
During serial passaging of hDHes, the total cell number was quantified. In cultures maintained on collagen-coated surfaces, total cell number increased from 1.2×10^6 to 3.34×10^6 over five passages. In contrast, cultures grown on drHDFn_EGF+HGF were initiated with 1.2×10^6 cells; however, after 9 days, only 6.2×10^5 cells were counted (Table 4.8).

Table 4.8. Comparison of cell number across individual passages under different culture conditions.

	Number of harvested cells	
Cell passage	**Collagen plate**	**drHDFn_EGF+HGF**
hH_1/hDHes+0	1.2×10^6	6.2×10^5
hDHes+1	2.1×10^5	0
hDHes+2	7.7×10^5	-
hDHes+3	4.4×10^5	-
hDHes+4	7.8×10^5	-
hDHes+5	0	-
Final cell number	**3.34×10^6**	**6.2×10^5**

Albumin production in the culture medium was determined using a quantitative sandwich ELISA assay. In cells cultured on collagen, albumin production in hDHes+1 increased 1.6-fold compared with hH_1/hDHes+0 ($p<0.001$). In contrast, albumin production in hDHes+2 decreased nearly 2-fold relative to hDHes+1 ($p<0.01$). In subsequent passages, albumin production decreased drastically and remained at a similarly low level, with no statistically significant differences observed among passages +3, +4, and +5 (Figure 4.53). Cells cultured on dried fibroblasts also produced albumin; however, the levels were lower, and the differences did not reach statistical significance (Supplementary Figure S8.5). A comparison of

cell cultures grown on collagen with those grown on drHDFn_EGF+HGF demonstrated that hDHes+0 cultured on dried fibroblasts produced approximately 2-fold less albumin than those cultured on collagen ($p<0.01$), while hDHes+1 cultured on drHDFn_EGF+HGF produced approximately 4-fold less albumin than cells cultured on collagen ($p<0.01$) (Supplementary Figure S8.6).



A)

	hH_1/hDHes+0	hDHes+1	hDHes+2	hDHes+3	hDHes+4	hDHes+5
hH_1/hDHes+0		0.000367	0.074161	0.000129	0.000098	0.000080
hDHes+1	0.000367		0.000149	0.000082	0.000060	0.000050
hDHes+2	0.074161	0.000149		0.000307	0.000189	0.000161
hDHes+3	0.000129	0.000082	0.000307		0.840987	0.838631
hDHes+4	0.000098	0.000060	0.000189	0.840987		0.992487
hDHes+5	0.000080	0.000050	0.000161	0.838631	0.992487	

Figure 4.53. Albumin production by hHs and hDHes cultured in expansion medium (EM) on collagen-coated surfaces. Human hepatocytes (hH_1) were seeded at a density of 3×10^5 cells per well onto rat tail collagen type I. Dedifferentiation occurred within 9 days (hDHes+0), after which the first passage (hDHes+1) was performed. Subsequent passages were carried out on days 21, 26, 30, 35, and 40, corresponding to hDHes+2 through hDHes+5. The total culture duration was 48 days. Albumin production was quantified using a sandwich ELISA assay (n = 3). **A)** Statistical analysis of the data shown in Figure 4.53. One-way ANOVA followed by Duncan's *post-hoc* test was applied. Data are presented as mean ± SD; *p < 0.05, **p < 0.01, ***p < 0.001.

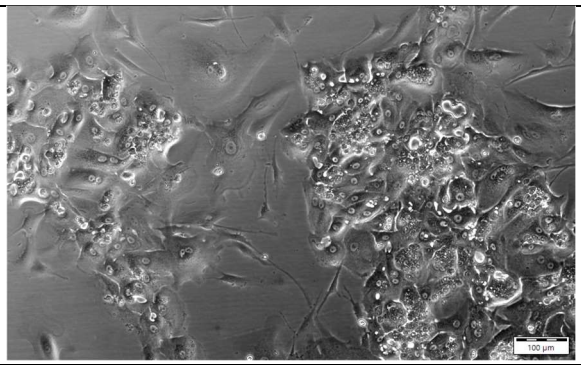
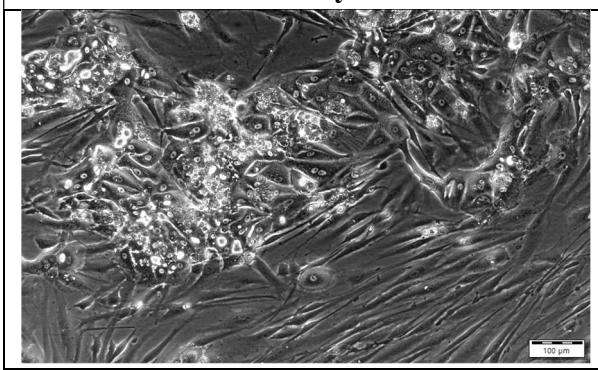
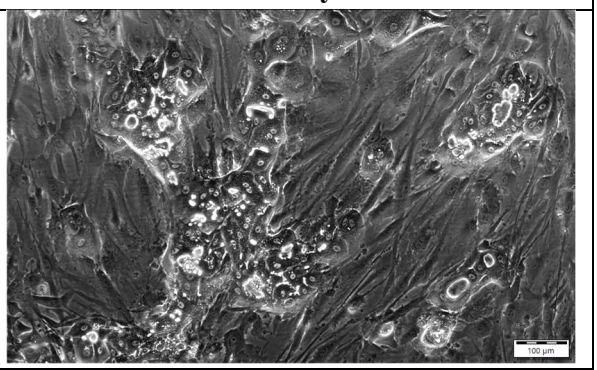
Due to the unsuccessful maintenance of hepatocytes on the dried fibroblast substrate, all subsequent experiments were conducted only on collagen-coated plates. These results demonstrated that hepatocytes cultured in EM on collagen underwent dedifferentiation and proliferation, confirming the successful completion of the first experimental stage.

4.3.2 Stage II – Proliferating Hepatocyte-Like Cells with Restored Hepatocyte Functions

Results from Stage I were used to determine the most suitable passage for initiating Stage II. The second stage began with thawing hDHes at passage 4, which were cultured in EM for 7 days, then passaged (hDHes+5) and transferred to DM (Table 3.11). After 8 days in DM, cell death was observed, and the culture was terminated on day 15.

In an alternative approach, hDHes+2 cells were thawed and cultured in EM supplemented with BMP-7 (a protein belonging to the TGF-β family of growth factors that regulates cell proliferation) for 7 days, followed by passaging. Cell death occurred after 6 days, and repeating the experiment under identical conditions resulted in the same outcome.

In the third approach, hDHes+0 cells were cultured in EM+BMP-7 for 8 days, after which the medium was switched to DM. Cells were passaged on day 16 (hDHes+1), followed by subsequent passages on days 20 (hDHes+2) and 30 (hDHes+3). Cell death occurred by day 33, leading to termination of the experiment. Throughout the entire culture period, no morphological reversion from spindle-shaped to polygonal hepatocyte-like cells was observed (Figure 4.54).

<table>
<tr><th colspan="2">hDHes+0</th></tr>
<tr><th colspan="2">EM</th></tr>
<tr><th colspan="2">8 day</th></tr>
<tr><td colspan="2"></td></tr>
<tr><th colspan="2">DM</th></tr>
<tr><th>12 day</th><th>16 day</th></tr>
<tr><td></td><td></td></tr>
</table>

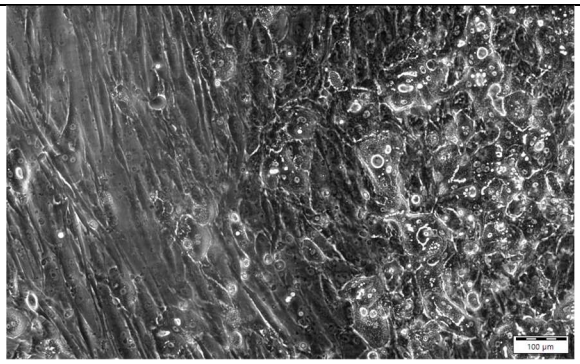
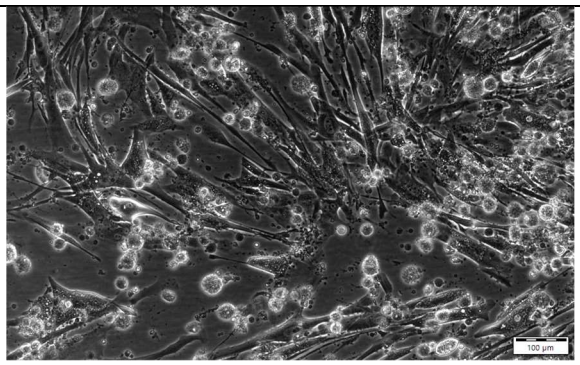
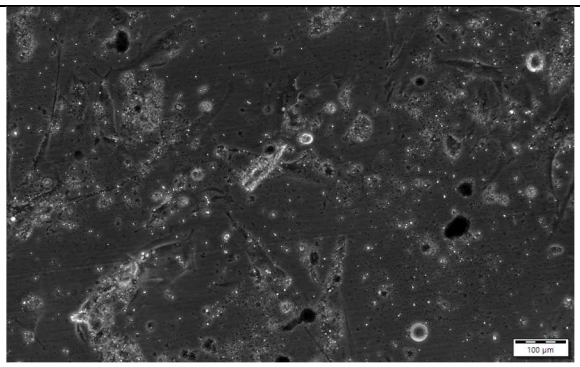
hDHes+1. DM
20 day

hDHes+2. DM
29 day

hDHes+3. DM
33 day


Figure 4.54. Morphology of hDHes cultured during Stage II on collagen-coated surfaces. hDHes were seeded at a density of 1×10^5 cells per well onto rat tail collagen type I. Cells were initially cultured in expansion medium (EM), after which the medium was replaced with differentiation medium (DM) on day 8. The culture was maintained for 33 days, during which three passages were performed (hDHes+1, hDHes+2, and hDHes+3). Images were acquired using an Olympus IX-71 fluorescence microscope at 10× magnification (scale bar = 100 μm).

During the 33-day culture period, cells were trypsinized for subsequent passage and counted. The average number of viable cells per well is presented in Figure 4.55. A slight increase in cell number was observed between the initial seeding and the first passage, followed by an approximately 1.5-fold decrease by the second passage, ultimately leading to complete cell death by the third passage.

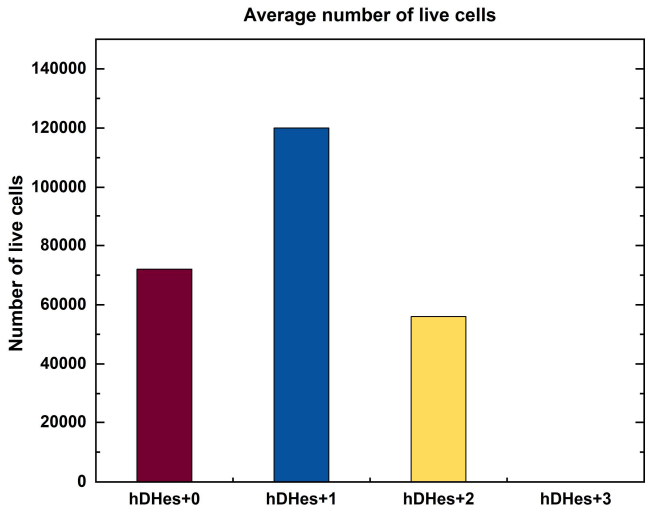
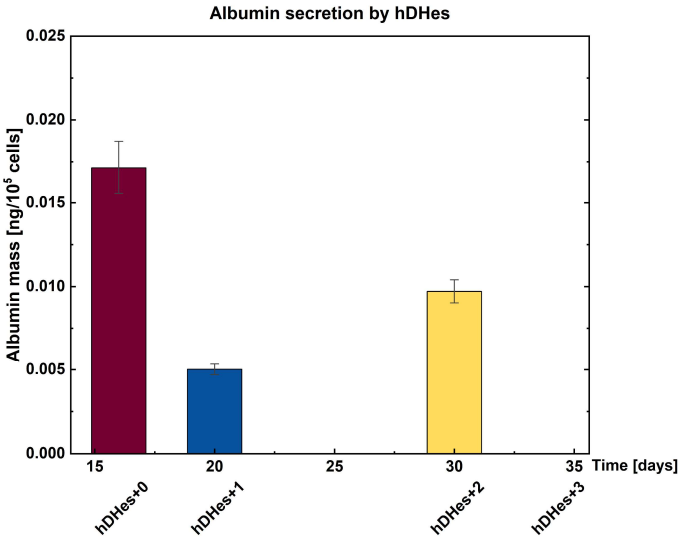


Figure 4.55. Cell growth during the differentiation culture of hDHes at different passages. All cultures were performed in 24-well plates. At the beginning of the experiment, hDHes at passage +0 were cultured in EM. After several days, the medium was replaced with DM, and all subsequent passages were carried out in DM. Cells were seeded at a density of 1×10^5 cells per well. After several days of culture, cells were passaged into two wells at 3.6×10^4 cells per well (hDHes+1). The next passage (hDHes+2) was seeded into three wells at 2.5×10^4 cells per well, and for the final passage (hDHes+3), cells were seeded into two wells at 2.8×10^4 cells per well. After each passage, cells were trypsinized, pooled, and counted using the trypan blue exclusion method. As these results were obtained from a single experiment, standard deviation and statistical analyses were not performed.

ELISA analysis showed that during culture in EM, albumin production by hDHes+0 increased. However, following the switch to DM, albumin secretion decreased. Albumin production decreased approximately 2-fold from hDHes+0 to hDHes+1 ($p < 0.001$), followed by a slight, non-significant decrease between hDHes+1 and hDHes+2. A further 1.5-fold reduction was observed in hDHes+3 ($p < 0.01$) (Figure 4.56).

A)



A1)

	hDHes+0	hDHes+1	hDHes+2	hDHes+3
hDHes+0		0.000223	0.000100	0.000077
hDHes+1	0.000223		0.294623	0.001519
hDHes+2	0.000100	0.294623		0.005323
hDHes+3	0.000077	0.001519	0.005323	

Figure 4.56. Albumin production by hDHes cultured in differentiation medium (DM) on collagen-coated surfaces. A) hDHes were seeded at a density of 1×10^5 cells per well. The first passage (hDHes+1) was performed on day 16, followed by hDHes+2 on day 20, and hDHes+3 on day 30. Albumin production were measured using ELISA in triplicate (n = 3). **A1)** Statistical analysis of the data shown in Figure 4.56 was performed using one-way ANOVA followed by Duncan's *post-hoc* test. Samples collected during EM culture were excluded from the analysis. Data are presented as mean ± SD. n = 3. Significance levels: *p < 0.05, **p < 0.01, ***p < 0.001.

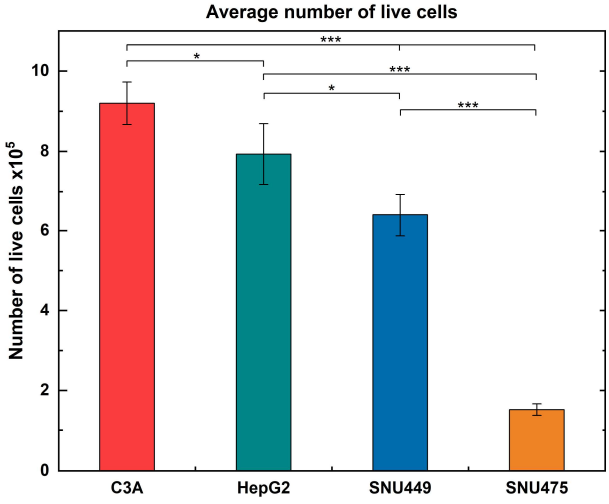
4.4 Comparative Analysis of Tumor Models of Hepatocytes

4.4.1 Proliferation, Cell Doubling Time, and Morphology of Selected Liver Cancer Cell Lines

In this part of the experiments, differences between selected liver cancer cell lines were analyzed. Hepatoblastoma (HB) cells, including C3A and HepG2, and hepatocellular carcinoma (HCC) cells, represented by SNU449 and SNU475, were examined. The compositions of the culture media used are presented in Tables 3.1–3.4.

Cells were cultured for 4 days without a medium replacement, after which they were detached from the culture surface and counted. Higher cell numbers were observed for HB cell lines, with the highest value for C3A, followed by HepG2 ($p<0.05$). In contrast, both HCC cell lines exhibited lower cell numbers. Moreover, SNU475 showed the lowest proliferation rate, with a cell number six times lower than that of C3A ($p<0.001$) (Figure 4.57).

A)



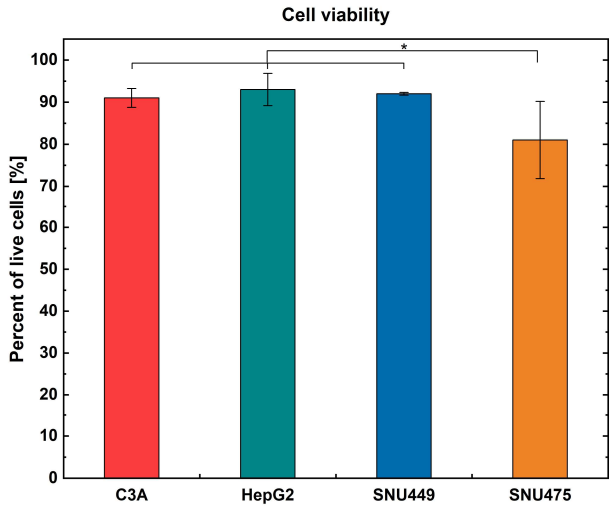
A1)

Statistical significance	C3A	HepG2	SNU449	SNU475
C3A		0.026651	0.000496	0.000077
HepG2	0.026651		0.011251	0.000100
SNU449	0.000496	0.011251		0.000224
SNU475	0.000077	0.000100	0.000224	

Figure 4.57. Differences in cell numbers obtained during the 4-day culture of liver cancer cell lines. A) Cells were seeded at a density of 1.5×10^5 per well in 12-well plates and cultured for 4 days without changing the medium. C3A cells were cultured in DMEM, HepG2 in EMEM, and both SNU cell lines in RPMI-1640. On the final day, cells were detached from the growth surface by trypsinization and counted using the trypan blue exclusion method. Each variant was prepared in three replicates. **A1)** Statistical significance (p) for Figure 4.57A. Data were analyzed using one-way ANOVA followed by Duncan's *post-hoc* test. Results are presented as mean ± SD (n = 3). Statistical significance: *p<0.05, **p<0.01, ***p<0.001.

At the same time, the experiment allowed for the determination of the viability of the studied liver cancer cell lines. The results showed that both HB cell lines and SNU449 exhibited cell viabilities above 90% (with no statistically significant differences between them). In contrast, SNU475 showed a viability of approximately 80% (p<0.05) (Figure 4.58).

A)



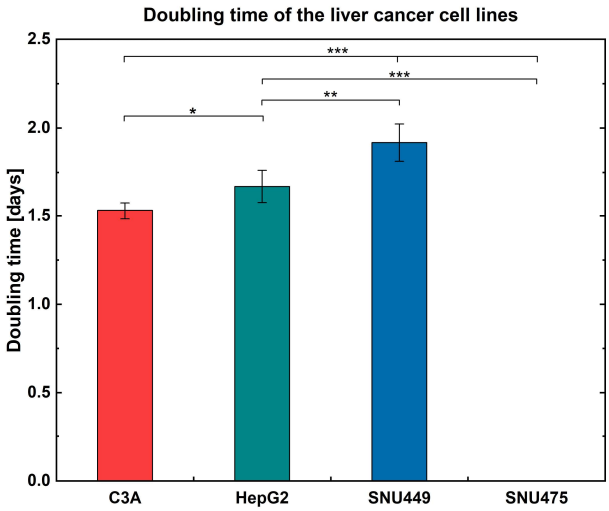
A1)

Statistical significance	C3A	HepG2	SNU449	SNU475
C3A		0.684512	0.783439	0.045781
HepG2	0.684512		0.880946	0.030177
SNU449	0.783439	0.880946		0.034629
SNU475	0.045781	0.030177	0.034629	

Figure 4.58. Comparison of cell viability among liver cancer cell lines. A) Cells were seeded at a density of 1.5×10^5 per well in 12-well plates and cultured for 4 days without changing the medium. Dedicated culture media were used for each cell line: C3A – DMEM, HepG2 – EMEM, SNU449 and SNU475 – RPMI-1640. The experiment was performed in triplicate. Cell viability was calculated as the ratio of live cells to the total number of cells (live + dead). **A1)** Statistical significance (p) for Figure 4.58A. Results were analyzed using one-way analysis of variance (ANOVA) followed by Duncan's *post-hoc* test. Data are presented as mean ± SD (n = 3). Levels of significance: *p<0.05, **p<0.01, ***p<0.001.

The cell doubling time was also determined (Figure 4.59). The results indicated that HB cells divided faster than HCC cells. C3A cells showed the shortest doubling time, requiring approximately 1.5 days to double their number ($p<0.05$), whereas HepG2 cells required 1.7 days. SNU449 cells doubled their number after 2 days of culture ($p<0.001$), while SNU475 cells did not divide during the 4-day experiment ($p<0.001$).

A)



A1)

Statistical significance	C3A	HepG2	SNU449	SNU475
C3A		0.047209	0.000339	0.000223
HepG2	0.047209		0.003482	0.000100
SNU449	0.000339	0.003482		0.000077
SNU475	0.000223	0.000100	0.000077	

Figure 4.59. Doubling time of liver cancer cell lines. A) Cells were cultured for 4 days without changing the medium in 12-well plates at a density of 1.5×10^5 per well. Dedicated media were used for each cell line: DMEM for C3A, EMEM for HepG2, and RPMI-1640 for SNU449 and SNU475. Each condition was performed in triplicate. The doubling time was calculated according to Equation (5) (for details, see section 3.1.6). **A1)** Statistical significance (p) for Figure 4.59A. Results were analyzed using one-way analysis of variance (ANOVA) followed by Duncan's *post-hoc* test. Data are presented as mean ± SD (n = 3). Levels of significance: *$p<0.05$, **$p<0.01$, ***$p<0.001$.

A comparison of the phenotypes of liver cancer cell lines showed that hepatoblastoma cells (C3A and HepG2) grew on top of each other, forming cell aggregates, whereas hepatocellular carcinoma cells (SNU449 and SNU475) grew as a monolayer covering the culture surface. Additionally, HCC cells were more flattened than HB cells and therefore occupy a larger surface area (Figure 4.60).

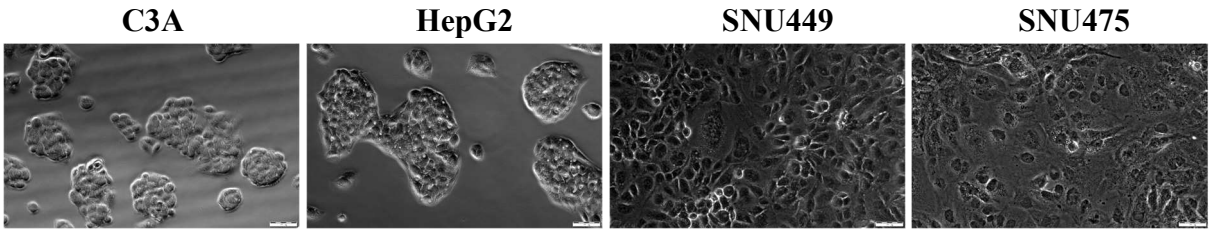
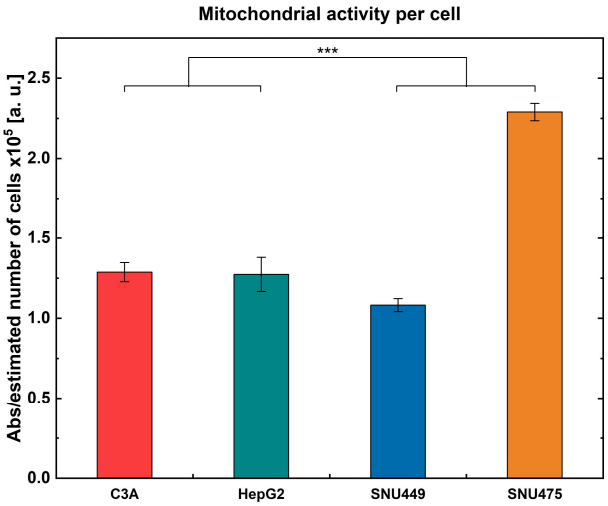


Figure 4.60. Phenotypic differences between liver cancer cell lines. The images show liver cancer cell lines derived from hepatoblastoma (HB; C3A and HepG2) and hepatocellular carcinoma (HCC; SNU449 and SNU475). Cells were seeded at a density of 8×10^4 per well in 24-well plates and cultured for 3 days. Microphotographs were taken using an Olympus IX71 fluorescence microscope under visible light at 20× magnification (scale bar: 50 µm).

4.4.2 Metabolic Activity of Liver Cancer Cell Lines (MTT)

Mitochondrial activity of liver cancer cell lines (C3A, HepG2, SNU449, and SNU475) was assessed using the MTT assay. The highest metabolic activity was observed in SNU475 cells ($p<0.001$). For C3A and HepG2, the values were approximately 1.7-fold lower (with no statistically significant difference between them), whereas for SNU449, the activity was about two-fold lower (Figure 4.61).

A)



A1)

Statistical significance	C3A	HepG2	SNU449	SNU475
C3A		0.735949	0.000141	0.000151
HepG2	0.735949		0.000261	0.000072
SNU449	0.000141	0.000261		0.000058
SNU475	0.000151	0.000072	0.000058	

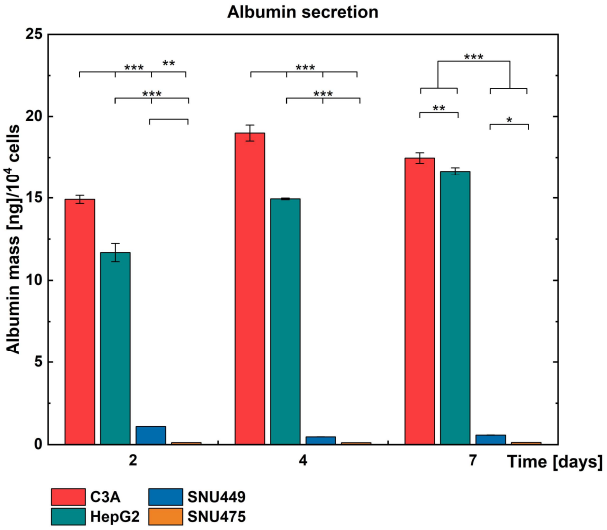
Figure 4.61. Metabolic activity of liver cancer cell lines per cell. A) Mitochondrial activity was determined using the MTT assay, and absorbance measurements were normalized to the estimated cell number. Cultures were carried out for 4 days without changing the medium. Cells were seeded in 96-well plates at a density of 3×10^4 cells per well. The experiment was performed in six replicates for each cell line. **A1)** Statistical significance (p) for Figure 4.61A. Results were analyzed using one-way analysis of variance (ANOVA) followed by Duncan's *post-hoc* test. Data are presented as mean ± SD (n = 6). Levels of significance: *p<0.05, **p<0.01, ***p<0.001.

4.4.3 Albumin Production by Liver Cancer Cell Lines (ELISA)

The results showed that both HB cell lines secreted albumin, with C3A producing it at a higher level than HepG2, particularly during the first 4 days of culture – approximately 1.3-fold higher ($p<0.001$). After 7 days, albumin production in the culture medium were similar for both cell lines, although still slightly higher for C3A, by approximately 1.07-fold ($p<0.01$).

Moreover, albumin secretion by C3A changed over the 7-day culture period: it increased up to day 4 and then began to decrease. In contrast, HepG2 showed a continuous increase in albumin secretion levels throughout the culture (Figure 4.62). For the HCC cell lines, the pattern was different. No albumin was detected in the culture medium of SNU475, while SNU449 showed a very low level of albumin secretion, approximately 14-fold lower than C3A. Additionally, after 2 days of culture, the albumin production in SNU449 decreased about 2-fold (Figure 4.62).

A)



A1)

Statistical significance	C3A	HepG2	SNU449	SNU475
C3A		0.000223	0.000100	0.000077
HepG2	0.000223		0.000223	0.000100
SNU449	0.000100	0.000223		0.004468
SNU475	0.000077	0.000100	0.004468	

A2)

Statistical significance	C3A	HepG2	SNU449	SNU475
C3A		0.000223	0.000100	0.000077
HepG2	0.000223		0.000223	0.000100
SNU449	0.000100	0.000223		0.114008
SNU475	0.000077	0.000100	0.114008	

A3)

Statistical significance	C3A	HepG2	SNU449	SNU475
C3A		0.001062	0.000100	0.000077
HepG2	0.001062		0.000223	0.000100
SNU449	0.000100	0.000223		0.023710
SNU475	0.000077	0.000100	0.023710	

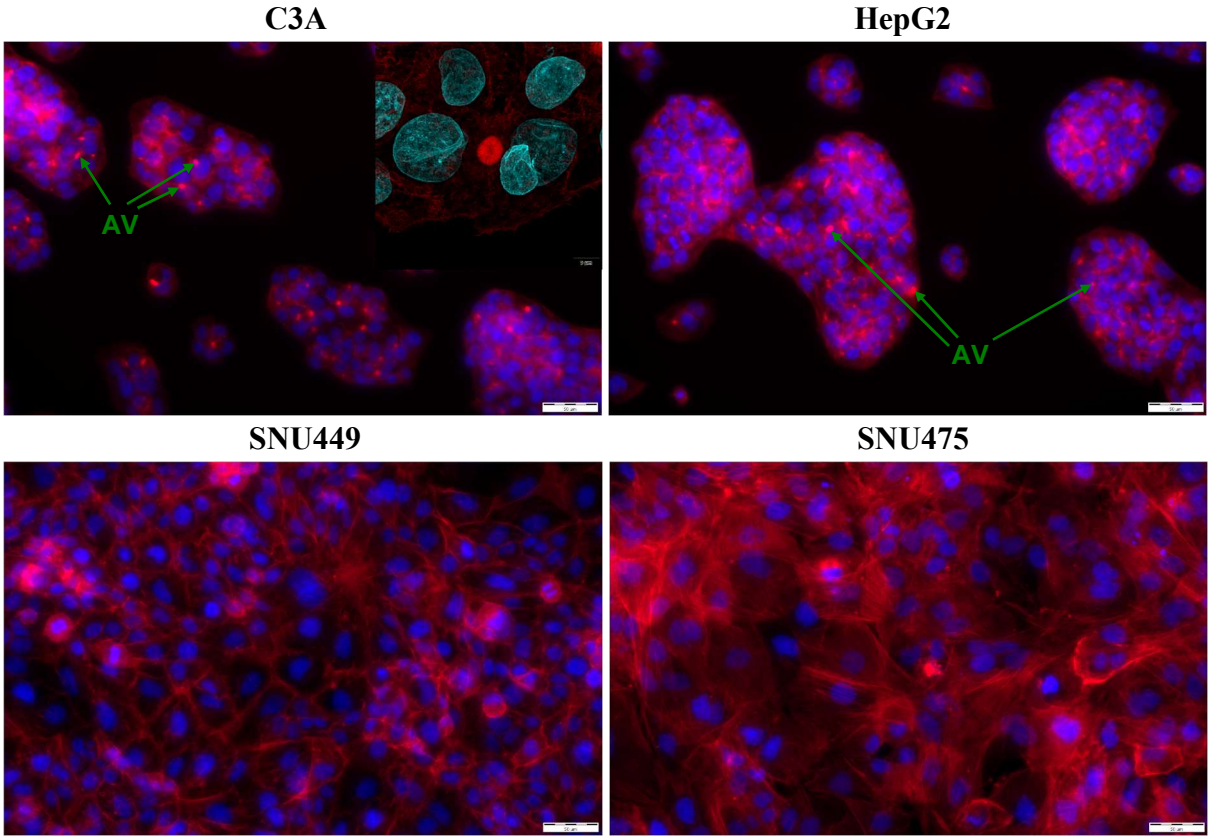
Figure 4.62. Albumin secretion by liver cancer cell lines. A) Cells were seeded in T25 culture flasks at a density of 1×10^6 cells per flask and cultured for 7 days. Medium samples were collected after 2, 4, and 7 days. Albumin production in the collected media was determined using the sandwich enzyme-linked immunosorbent assay (ELISA). **A1)** Statistical significance (p) for day 2 of culture in panel A). **A2)** Statistical significance (p) for day 4 of culture in panel A). **A3)** Statistical significance (p) for day 7 of culture in panel A). Results were analyzed using one-way analysis of variance (ANOVA) followed by Duncan's *post-hoc* test. Data are presented as mean ± SD (n = 3). Levels of significance: *p<0.05, **p<0.01, ***p<0.001.

4.4.4 Apical Vacuoles Formation

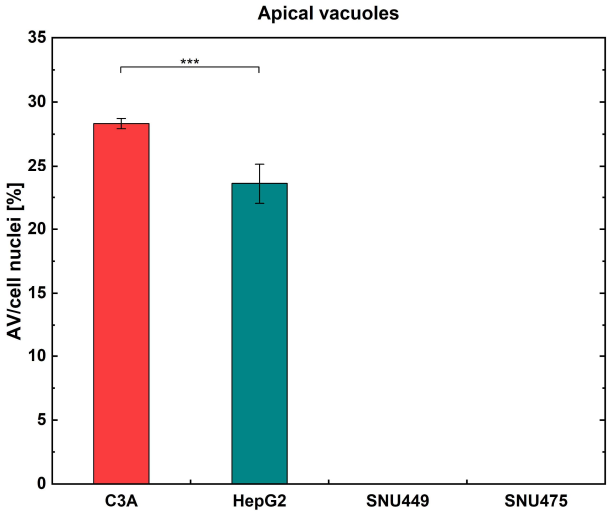
Apical vacuoles (AVs) are functional and structural precursors of *bile canaliculi* and indicate cell polarity, which is essential for specific cellular functions. They are formed at the junctions of three or more apical membranes of adjacent cells.

The ability of the studied cells to form AVs was assessed by labeling F-actin with red-fluorescent phalloidin. In microscopic images, these structures appeared as red dots or rings. The obtained results showed that C3A and HepG2 cells formed AVs (green arrows in Figure 4.63A), whereas both SNU cell lines did not (Figure 4.63A). Furthermore, C3A cells formed significantly more AVs than HepG2 cells (p<0.001) (Figure 4.63B).

A)



B)



B1)

Statistical significance	C3A	HepG2
C3A		0.000188
HepG2	0.000188	

Figure 4.63. Formation of Apical Vacuoles (AVs) by liver cancer cell lines. Cells were seeded at a density of 8×10^4 per well in 24-well plates and cultured for 3 days. Cells were stained with F-actin (red), and cell nuclei were counterstained with DAPI (blue). **A)** The merged microphotographs taken with a fluorescence microscope (Olympus IX71) at 20× magnification (scale bar 50 µm), and the inset microphotograph was acquired using a confocal laser scanning microscope (FLUOVIEW FV4000) at 60× magnification (scale bar 5µm). AVs, appearing as bright red dots or ring-like structures, are indicated in the images with green arrows, and are present in C3A and HepG2. **B)** The number of apical vacuoles in the cells was estimated as a ratio of AVs to cell nuclei. Counting was performed in 5 fields of view at 20× magnification for each cell type. **B1)** Statistical significance (p) for Figure 4.63B. Results were analyzed using the one-way analysis of variance (ANOVA) and Duncan's *post-hoc* test. Results are presented as mean value ± SD, n=5. Level of significance: *p<0.05, **p<0.01, ***p<0.001.

4.4.5 Protein Production and Gene Expression in Selected Liver Cancer Cell Lines

Western blot (WB) and RT-qPCR analysis were performed to examine the levels of hepatocyte-specific protein production and gene expression, respectively, in liver tumor cell lines. In addition to C3A, HepG2, SNU449, and SNU475 cells, samples from human hepatocyte (hH_2) and liver cell lysate from donor H40 [LCI(H40] were also analyzed. For LCI sample, only WB analysis was performed.

The presence of the following proteins and genes was examined: albumin (ALB), arginase 1 (ARG1), carbamoyl phosphate synthetase I (CPS1), two transcription factors: hepatocyte nuclear factor 1α (HNF1α) and 4α (HNF4α), and three cytochrome P450 family members: CYP3A4, CYP2C8, and CYP2E1. Additionally, only protein expression of alpha-fetoprotein (AFP) and only gene expression of *GLUL* and *PXR* were analyzed. The housekeeping gene *RPS18* was used as an internal control for RT-qPCR, while glyceraldehyde 3-phosphate dehydrogenase (GAPDH) was used as a loading control for WB.

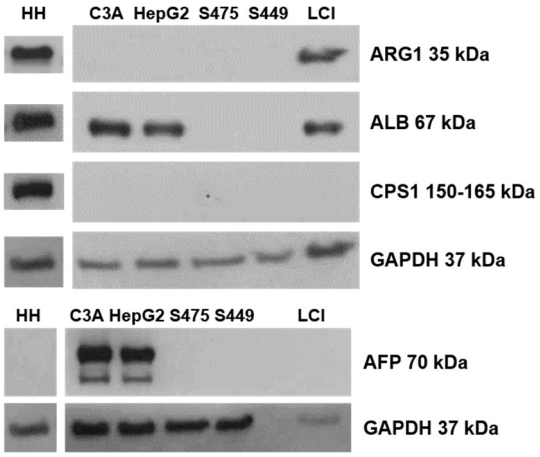
The results indicated significant differences in protein expression between HB-derived and HCC-derived cells. For albumin, the most abundant plasma protein produced in the liver, a specific signal at 67 kDa was observed in C3A and HepG2 cells, as well as in the hHs and LCI controls (Figure 4.64A). C3A cells exhibited a 1.1-fold higher ALB expression than HepG2 cells, although, this difference was not statistically significant. No ALB signal was detected in the analyzed HCC cell lines (Figure 4.64B). RT-qPCR analysis showed that hHs, C3A, and HepG2 cells, unlike both SNU cell lines, synthesized mRNA for the albumin gene. The highest expression level was observed in hHs cells, which was more than twice that observed in the cancer cell lines. HepG2 cells exhibited a 1.2-fold higher *ALB* expression than C3A cells; however, this difference was not statistically significant (Figure 4.64B).

AFP, a marker of immature hepatocytes or tumor cells, was detected exclusively in HB-derived cells as two bands at 70 kDa and 50 kDa. C3A cells exhibited 1.25-fold higher AFP protein expression compared to HepG2 cells; however, this difference was not statistically significant. No AFP protein expression was observed in HCC-derived cell lines, despite their cancerous origin (Figure 4.64A, C). *AFP* gene expression was not analyzed.

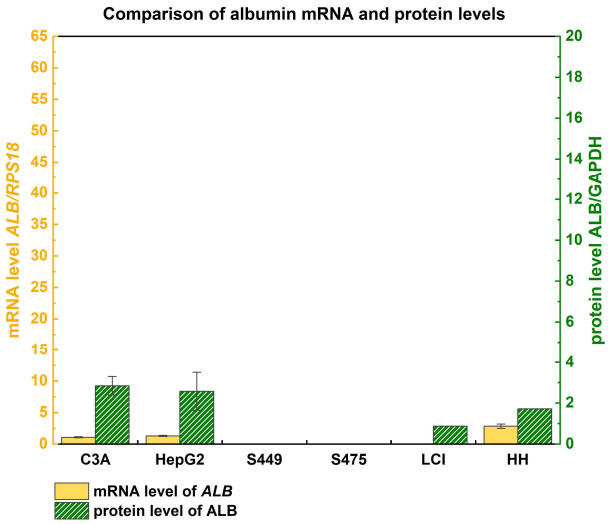
Arginase 1 and CPS1, key enzymes involved in the urea cycle, showed distinct expression patterns. For ARG1, a 35 kDa band was present in hHs and LCI samples, with LCI showing nearly twice the signal intensity observed in hHs (Figure 4.64A, D). None of the liver cancer cell lines produced ARG1 protein. At a gene level, *ARG1* expression was detected in all examined cell types, with the highest expression observed in hHs cells, which was 67-fold higher than in HepG2 cells. Among the tumor cell lines, HepG2 exhibited the highest *ARG1* expression, approximately 6-fold higher than C3A and SNU475 ($p<0.001$) and about 15-fold higher than SNU449 ($p<0.001$) (Figure 4.64D).

CPS1 protein expression was observed only in hHs, with a band at 150-160 kDa (Figure 4.64A, E). *CPS1* gene expression was also highest in hHs cells, approximately 19-fold higher than in SNU449 cells. Among the cancer cell lines, SNU449 showed the highest *CPS1* expression. C3A and HepG2 exhibited similar expression levels, approximately 2-fold lower than SNU449 ($p<0.01$). *CPS1* expression was not detected in SNU475 cells (Figure 4.64E).

A)



B)



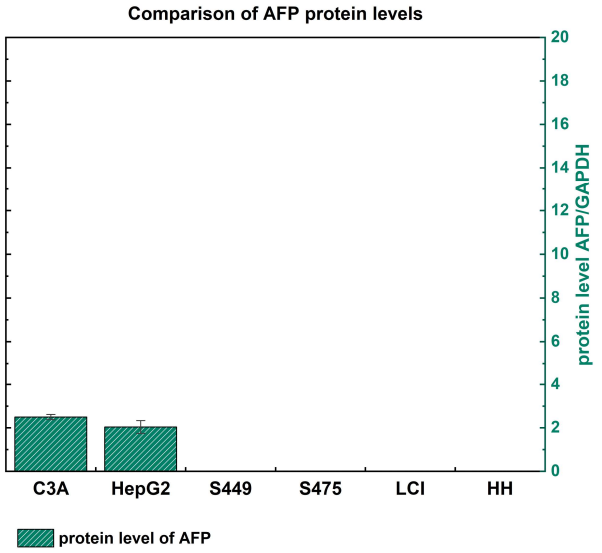
B1)

Statistical significance ALB protein	C3A	HepG2
C3A		0.675638
HepG2	0.675638	

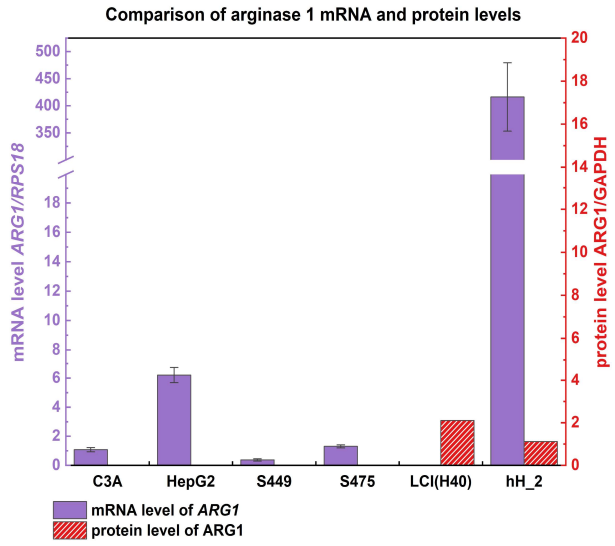
B2)

Statistical significance *ALB* gene	C3A	HepG2
C3A		0.199625
HepG2	0.199625	

C)



D)



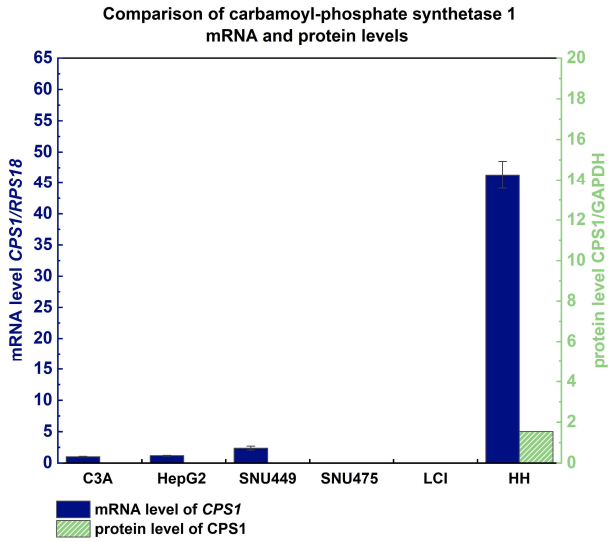
C1)

Statistical significance AFP protein	C3A	HepG2
C3A		0.066106
HepG2	0.066106	

D1)

Statistical significance *ARG1* gene	C3A	HepG2	SNU449	SNU475
C3A		0.000101	0.139817	0.601837
HepG2	0.000101		0.000077	0.000223
SNU449	0.139817	0.000077		0.069560
SNU475	0.601837	0.000223	0.069560	

E)



E1)

Statistical significance *CPS1* gene	C3A	HepG2	SNU449	SNU475
C3A		0.584071	0.001950	0.007617
HepG2	0.584071		0.003337	0.004198
SNU449	0.001950	0.003337		0.000117
SNU475	0.007617	0.004198	0.000117	

Figure 4.64. Comparison of protein and gene expression in liver cancer cell lines. The expression of hepatocyte-specific proteins and genes was analyzed in liver cancer cell lines and control cells using Western blot (WB) and RT-qPCR. Protein and gene expression levels were compared among the following cell types: C3A, HepG2, SNU449 (S449), SNU475 (S475), and human hepatocytes (hH_2). For WB analysis, a liver cell isolate [LCI(H40)] was also included. The analyzed proteins included albumin (ALB, 67 kDa), arginase 1 (ARG1, 35 kDa), carbamoyl phosphate synthetase I (CPS1, 150-160 kDa), alpha-fetoprotein (AFP, 70 kDa), and glyceraldehyde 3-phosphate dehydrogenase (GAPDH, 37 kDa), which served as a loading control. Each sample (25 µg of total protein) was loaded onto a polyacrylamide gel. Signal detection was performed on X-ray films using an ECL kit. Band intensities were quantified using ImageJ software, and protein expression levels were calculated as the ratio of the target protein to GAPDH.

For gene expression analysis, total RNA was isolated from 1×10^6 cells per sample. The following genes were analyzed: *ALB*, *ARG1*, and *CPS1*. The housekeeping gene *RPS18* was used as an internal control. Relative gene expression levels were calculated using the comparative Ct (ΔΔCt) method, with C3A cells serving as the calibrator. Expression levels were determined based on the ratio of the relative quantification (RQ) values for each gene to the RQ value of *RPS18*. **A)** Representative WB images of the analyzed proteins. **B)** Quantification of ALB protein and *ALB* gene expression levels. **B1)** Statistical significance (p values) for ALB protein expression (corresponding to Figure 4.64B). **B2)** Statistical significance (p values) for *ALB* gene expression (corresponding to Figure 4.64B). **C)** Quantification of AFP protein expression levels. **C1)** Statistical significance (p values) for AFP protein expression (corresponding to Figure 4.64C). **D)** Quantification of ARG1 protein and *ARG1* gene expression levels. **D1)** Statistical significance (p values) for *ARG1* gene expression (corresponding to Figure 4.64D). **E)** Quantification of CPS1 protein and gene *CPS1* gene expression levels. **E1)** Statistical significance (p values) for *CPS1* gene expression (corresponding to Figure 4.64E). Statistical analysis was performed using the one-way analysis of variance (ANOVA) followed by Duncan's *post-hoc* test. Results are presented as mean ± SD (n=3 for HCC cell lines; n = 1 for hHs and LCI). Statistical significance was defined as: *p<0.05, **p<0.01, ***p<0.001. For hHs and LCI samples, only single experiment was analyzed; therefore, no statistical analysis was performed.

Analysis of HNF4α protein expression showed that this protein was produced by hHs, LCI, C3A, and HepG2 cells. In C3A, HepG2, and hHs cells, expression levels were comparable, however, HepG2 exhibited slightly higher HNF4a expression than C3A cells (1.1-fold difference, not statistically significant). The highest expression was observed in LCI; however, unlike the other samples, the signal appeared at 45 kDa rather than at 52 kDa. The HNF4α signal in LCI was 4.6-fold higher than in hHs cells and 3.4-fold higher than in HepG2 cells. No HNF4α protein expression was detected in SNU cell lines (Figure 4.65A, B).

For the second transcription factor, HNF1α, protein signals were observed in all samples, although with notable differences. In hHs, C3A, and HepG2 cells, three bands were detected at 80 kDa, 67 kDa, and 61 kDa. The highest signal was obtained in hHs cells, with expression levels 1.4-fold higher than in HepG2 cells. Among HB-derived cells, HepG2 showed 1.2-fold higher HNF1α expression than C3A, although this difference was not statistically significant. In both HCC cell lines, HNF1α appeared as two bands at 67 kDa and 61 kDa, with similar expression levels in SNU449 and SNU475, which were approximately 9-fold lower than in HepG2 cells ($p<0.001$). The lowest HNF1α protein expression was observed in LCI, where only a weak band at 67 kDa was detected, representing a 51-fold reduction compared to the hHs cells and a 36-fold reduction compared to the HepG2 (Figure 4.65A, C).

At the mRNA level, *HNF4α* transcripts were not detected in SNU449 or SNU475 cells. In turn, C3A and HepG2 cells exhibited low *HNF4α* expression, approximately 29-fold lower than in hHs cells (Figure 4.65B). For *HNF1α*, no gene expression was detected in SNU475 cells, whereas SNU449 expressed the gene at a low level, approximately 3-fold lower than in C3A and HepG2 cells ($p<0.01$). Expression levels in C3A and HepG2 were comparable and approximately 64-fold lower than those observed in hHs cells (Figure 4.65C).

The next group of analyzed proteins comprised three members of the cytochrome P450 family. CYP3A4 was detected at 50 kDa in all samples except for both SNU cell lines. The highest expression was observed in hHs cells and was approximately 2-fold higher than in LCI and C3A cells. Among HB-derived cell lines, C3A showed approximately 3.5-fold higher CYP3A4 expression than HepG2 cells ($p<0.01$). CYP2E1 protein was also detected at 56 kDa, exclusively in hHs cells. CYP2C8 protein was also detected only in hHs cells and appeared as two bands at 50 kDa and 40 kDa (Figure 4.65A, D, E, F).

Consistent with the protein expression analysis, gene expression of cytochrome P450 family members *CYP3A4*, *CYP2E1*, and *CYP2C8* was also examined. *CYP3A4* showed extremely high expression in hHs cells; approximately 22,620-fold higher than in HepG2 cells.

Among the cancer cell lines, HepG2 exhibited the highest expression, approximately 3-fold higher than C3A cells ($p<0.05$). No *CYP3A4* gene expression was detected in either SNU cell line (Figure 4.65D).

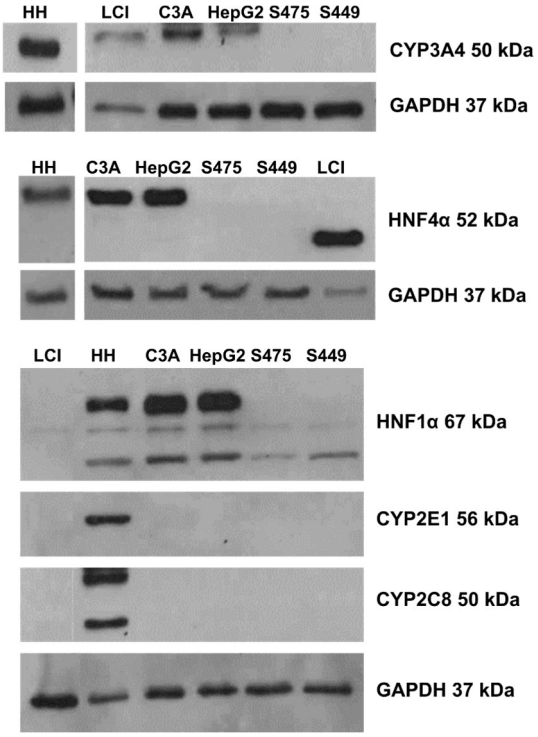
Analysis of *CYP2E1* gene expression revealed the highest level in hHs cells, similar to *CYP3A4*. *CYP2E1* transcripts were also detected in both SNU cell lines. Among the cancer cells, SNU449 showed the highest expression, although it was approximately 812-fold lower than in hHs cells. Comparison between SNU449 and SNU475 showed that SNU475 expressed nearly 4-fold lower levels of *CYP2E1* ($p<0.001$). C3A and HepG2 cells exhibited comparable *CYP2E1* expression levels, approximately 10-fold lower than those observed in SNU449 cells ($p<0.001$) (Figure 4.65E).

The third cytochrome P450 gene analyzed was *CYP2C8*, which was expressed in all examined cell types. hHs cells showed the highest *CYP2C8* expression, approximately 452-fold higher than SNU449 cells. Among the tumor cell lines, SNU449 exhibited the highest *CYP2C8* expression, approximately 1.6-fold higher than in SNU475 ($p<0.05$) and 2-fold higher than in C3A ($p<0.001$). The lowest *CYP2C8* expression was observed in HepG2 cells, nearly 5-fold lower than in SNU449 ($p<0.001$) (Figure 4.65F).

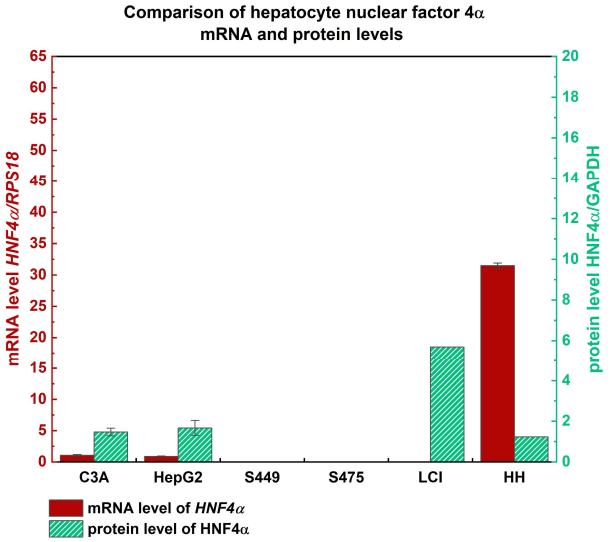
Another gene analyzed was *GLUL*, which was expressed in C3A, HepG2, and SNU449 cells. Notably, this gene was not expressed in hHs cells. *GLUL* expression was also not detected in SNU475. Expression levels in C3A and HepG2 cells were similar (differences not statistically significant) and where almost five-fold higher than those observed in SNU449 cells ($p<0.001$) (Figure 4.65G).

The next analyzed gene was *PXR*, which was expressed in hHs, C3A, and HepG2 cells. Expression levels in C3A and HepG2 cells were very similar but significantly lower ($p<0.001$), approximately 55-fold, than in hHs cells. No *PXR* expression was detected in SNU449 and SNU475 cells (Figure 4.65H).

A)



B)



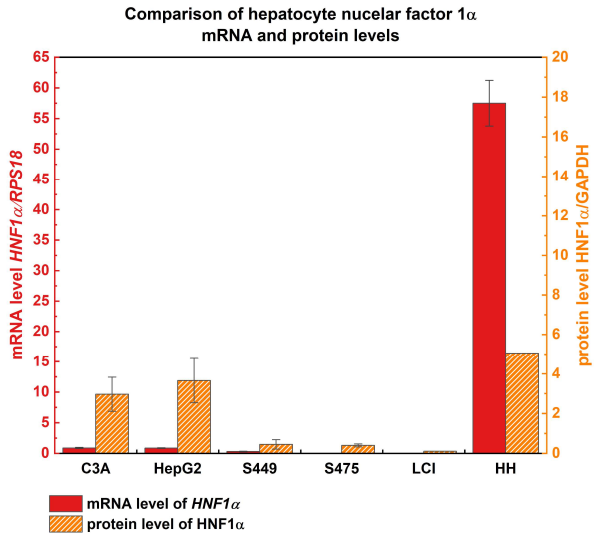
B1)

Statistical significance HNF4α protein	C3A	HepG2
C3A		0.440797
HepG2	0.440797	

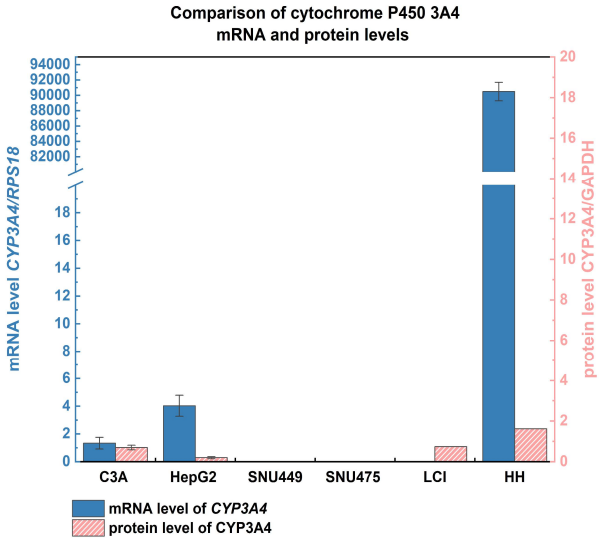
B2)

Statistical significance *HNF4α* gene	C3A	HepG2	SNU449	SNU475
C3A		0.051290	0.000077	0.000100
HepG2	0.051290		0.000102	0.000223
SNU449	0.000077	0.000102		1.000000
SNU475	0.000100	0.000223	1.000000	

C)



D)



C1)

Statistical significance HNF1α protein	C3A	HepG2	SNU449	SNU475
C3A		0.276860	0.002865	0.003070
HepG2	0.276860		0.000856	0.000870
SNU449	0.002865	0.000856		0.930814
SNU475	0.003070	0.000870	0.930814	

C2)

Statistical significance *HNF1α* gene	C3A	HepG2	SNU449	SNU475
C3A		0.884549	0.004132	0.000399
HepG2	0.884549		0.004176	0.000429
SNU449	0.004132	0.004176		0.061132
SNU475	0.000399	0.000429	0.061132	

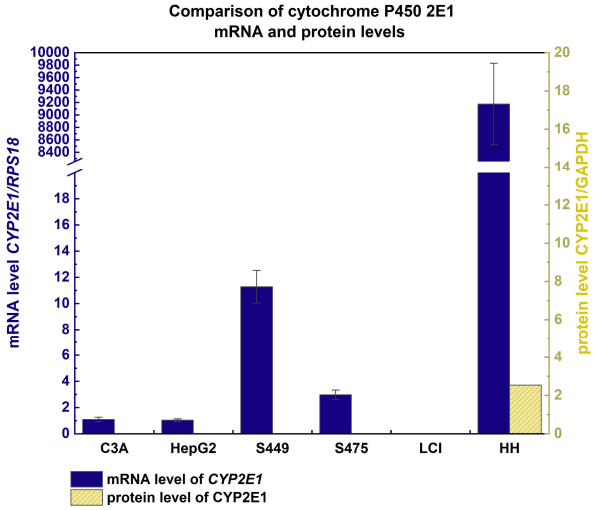
D1)

Statistical significance CYP3A4 protein	C3A	HepG2
C3A		0.002351
HepG2	0.002351	

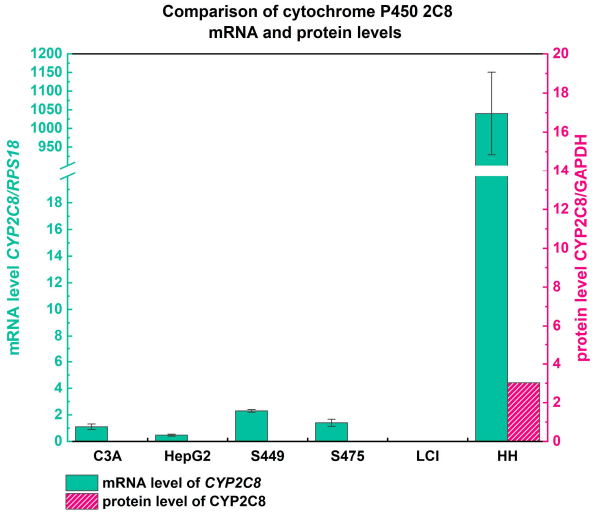
D2)

Statistical significance *CYP3A4* gene	C3A	HepG2	SNU449	SNU475
C3A		0.017549	0.177922	0.194142
HepG2	0.017549		0.002697	0.003062
SNU449	0.177922	0.002697		1.000000
SNU475	0.194142	0.003062	1.000000	

E)



F)



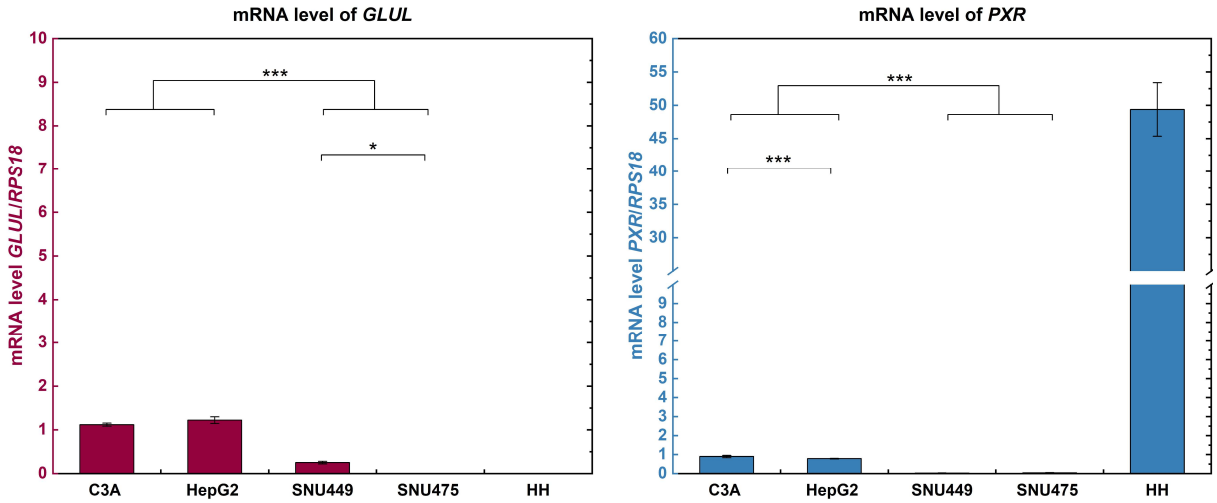
E1)

Statistical significance *CYP2E1* gene	C3A	HepG2	SNU449	SNU475
C3A		0.952729	0.000107	0.109515
HepG2	0.952729		0.000084	0.111869
SNU449	0.000107	0.000084		0.000250
SNU475	0.109515	0.111869	0.000250	

F1)

Statistical significance *CYP2C8* gene	C3A	HepG2	SNU449	SNU475
C3A		0.086536	0.007893	0.385565
HepG2	0.086536		0.000794	0.024814
SNU449	0.007893	0.000794		0.025394
SNU475	0.385565	0.024814	0.025394	

G) **H)**



G1)

Statistical significance *GLUL* gene	C3A	HepG2	SNU449	SNU475
C3A		0.239054	0.000224	0.000100
HepG2	0.239054		0.000101	0.000077
SNU449	0.000224	0.000101		0.015503
SNU475	0.000100	0.000077	0.015503	

H1)

Statistical significance *PXR* gene	C3A	HepG2	SNU449	SNU475
C3A		0.000444	0.000077	0.000100
HepG2	0.000444		0.000100	0.000223
SNU449	0.000077	0.000100		0.494800
SNU475	0.000100	0.000223	0.494800	

Figure 4.65. Selected protein production and gene expression in liver cancer cell lines. WB and RT-qPCR analysis were used to assess the expression levels of hepatocyte nuclear factor 4α (HNF4α), hepatocyte nuclear factor 1α (HNF1α), cytochrome P450 3A4 (CYP3A4), cytochrome P450 2E1 (CYP2E1), and cytochrome P450 2C8 (CYP2C8) in liver cancer cell lines and control cells. In addition, gene expression level of *GLUL* and *PXR* were analyzed. Protein and gene expression were examined in the following cell types: C3A, HepG2, SNU449 (S449), SNU475 (S475), human hepatocytes (hH_2). For WB analysis, a LCI(H40) was also included. The expected molecular weights were as follows: HNF4α – 52 kDa, HNF1α – 67 kDa, CYP3A4 – 50 kDa, CYP2E1 – 56 kDa, CYP2C8 – 50 kDa. For each sample, 25 µg of total protein was loaded onto the gel and incubated with the corresponding antibodies. Signals were detected using an ECL kit and X-ray films. GAPDH (37 kDa) was used as a WB loading control. Band intensities were quantified using ImageJ software, and protein expression levels were calculated as a ratio of the target protein to the reference protein. For gene expression analysis, the housekeeping gene *RPS18* was used as an internal control. Relative gene expression levels were calculated using the comparative Ct (ΔΔCt) method, with C3A cells serving as the calibrator. Expression levels are presented as a ratio of the relative quantification (RQ) values for each target gene to the RQ value of *RPS18*. **A)** Representative WB images of the analyzed proteins. **B)** Quantification of HNF4α protein and *HNF4α* gene expression levels. **B1)** Statistical significance (p values) for HNF4α protein expression (corresponding to Figure 4.65B). **B2)** Statistical significance (p values) for *HNF4α* gene expression (corresponding to Figure 4.65B). **C)** Quantification of HNF1α protein and *HNF1α* gene expression levels. **C1)** Statistical significance (p values) for HNF1α protein expression (corresponding to Figure 4.65C). **C2)** Statistical significance (p values) for *HNF1α* gene expression (corresponding to Figure 4.65C). **D)** Quantification of CYP3A4 protein and *CYP3A4* gene expression levels. **D1)** Statistical significance (p values) for CYP3A4 protein expression (corresponding to Figure 4.65D). **D2)** Statistical significance (p values) for *CYP3A4* gene expression (corresponding to Figure 4.65D). **E)** Quantification of CYP2E1 protein and *CYP2E1* gene expression levels. **E1)** Statistical significance (p values) for *CYP2E1* gene expression (corresponding to Figure 4.65E). **F)** Quantification of CYP2C8 protein and *CYP2C8* gene expression levels. **F1)** Statistical significance (p values) for *CYP2C8* gene

expression (corresponding to Figure 4.65F). **G)** Quantification of *GLUL* gene expression levels. **G1)** Statistical significance (p values) for *GLUL* gene expression (corresponding to Figure 4.65G). **H)** Quantification of *PXR* gene expression levels. **H1)** Statistical significance (p values) for *PXR* gene expression (corresponding to Figure 4.65H). Statistical analysis was performed using the one-way analysis of variance (ANOVA) followed by Duncan's *post-hoc* test. Data are presented as mean ± SD (n=3 for HCC cell lines; n = 1 for hHs and LCI). Statistical significance was defined as: *p<0.05, **p<0.01, ***p<0.001. For hHs and LCI samples, only one biological replicate was available, therefore, statistical analysis was performed only among the cancer cell lines.

4.5 Dynamic Cell Cultures in Capillary Bioreactors

4.5.1 Preparation of the Hollow Fiber Bioreactor System

4.5.1.1 Dimensions and Cross-Sectional Structure of Capillary Membranes

Scanning electron microscopy (SEM) analysis of the polysulfone capillary membranes revealed a porous structure on both the inner and outer surfaces. The inner surface exhibited larger pore sizes compared to the outer surface (Figure 4.66A, B). Cross-sectional SEM images show changes in the membrane pore size from the inner to the outer region (Figure 4.67A, B). The average pore size on the external membrane surface was 0.26 ± 0.09 µm. SEM analysis also enabled measurements of the capillary diameters. The average outer diameter was 588 ± 24 µm, whereas the inner diameter measured 400 ± 36 µm (Figure 4.67C).

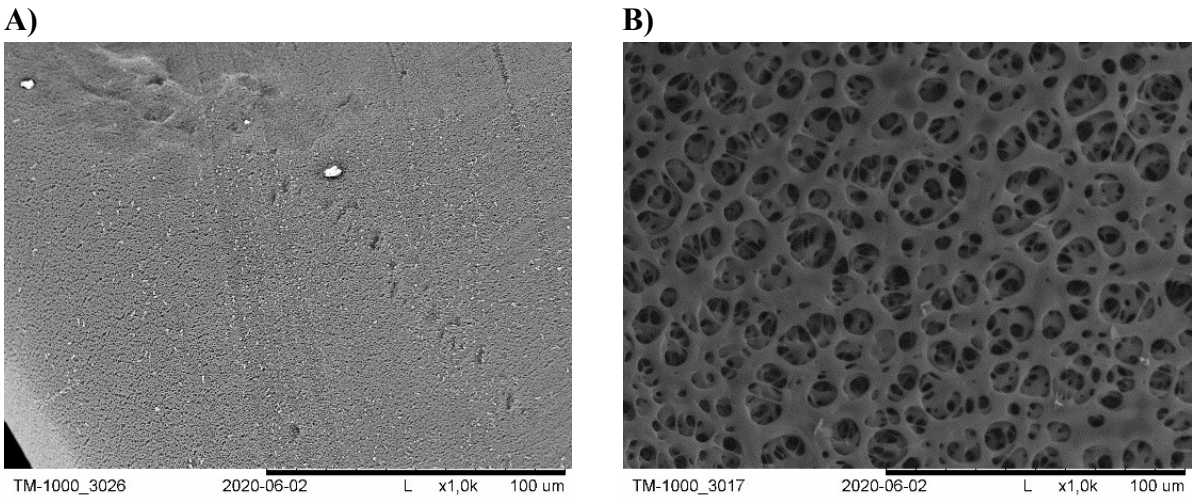


Figure 4.66. Structure of the inner and outer surfaces of a capillary membrane. A) Outer surface of the membrane. **B)** Inner surface of the membrane. Images were obtained using a scanning electron microscope (Hitachi TM-1000) at 1000× magnification (scale bar: 100 µm).

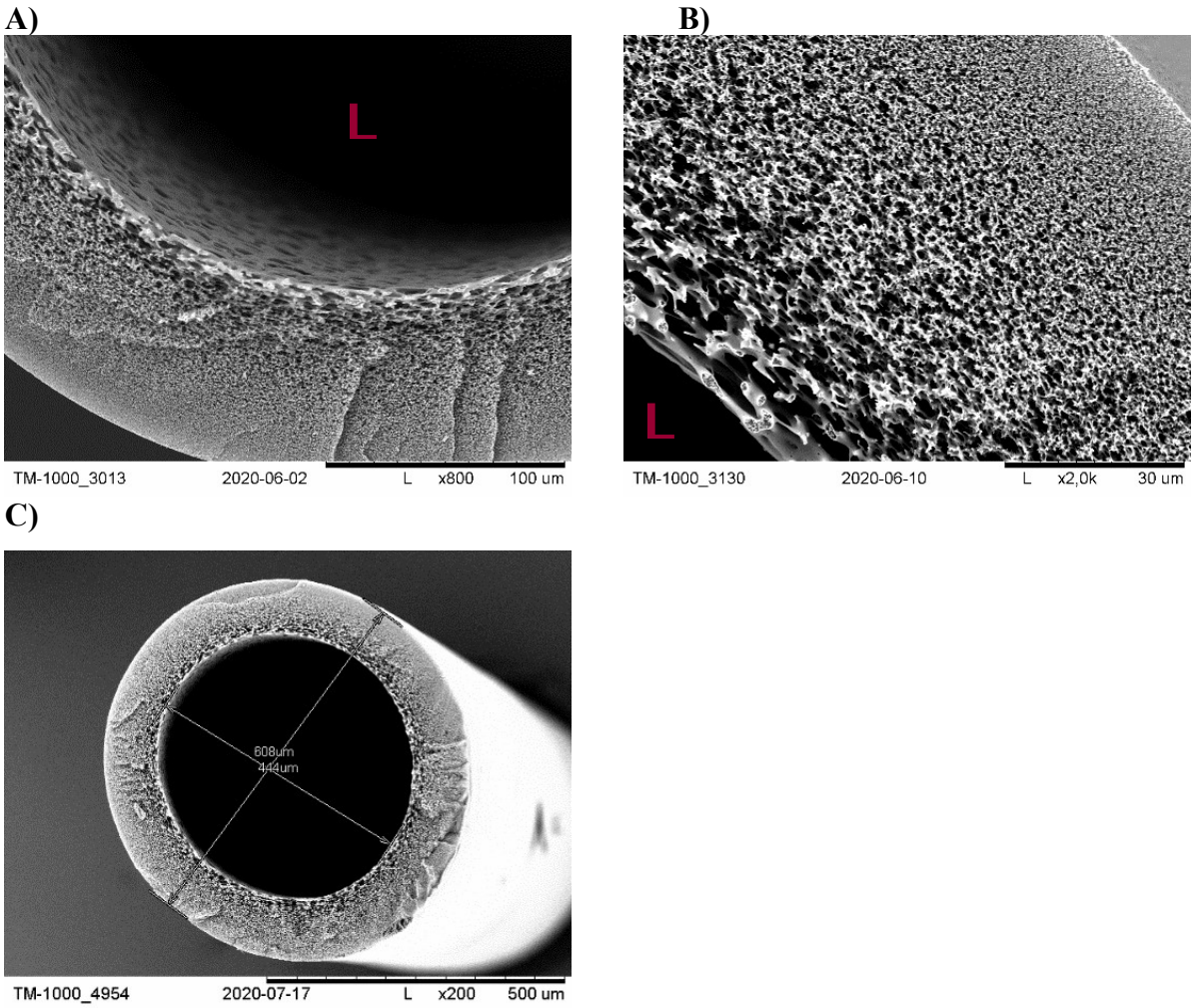


Figure 4.67. Cross-section of the capillary membrane. Micrographs were taken using a scanning electron microscope (Hitachi TM-1000). **A)** Cross-section at 1000× magnification (scale bar: 100 µm). **B)** Cross-section at 2000× magnification (scale bar: 30 µm). The capillary lumen was marked as red "L". **C)** Measures of the capillary diameters at 200× magnification (scale bar: 500 µm).

4.5.1.2 Wettability Analysis

The wettability of the capillary membrane surface was evaluated using the sessile drop method with a DSA25 Krüss goniometer. The contact angle was defined as the angle between the tangent to the droplet at the contact point and the membrane surface, as described in section 3.12.2. The rate at which the droplet spreads on the tested surface, reflected by changes in the contact angle, determines the material's surface properties, specifically hydrophobicity or hydrophilicity. This parameter is of particular importance for cell culture applications, as cells preferentially adhere to hydrophilic surfaces. Figure 4.68 presents a water droplet placed on the surface of a crushed capillary membrane. In the present study, the wettability measurements of the polysulfone capillary membrane yielded a contact angle of 61.02 ± 5.78°, confirming its

hydrophilic nature of the membrane surface. Measurements were performed at multiple points on the membrane surface, and the reported value represents the mean of these replicates.

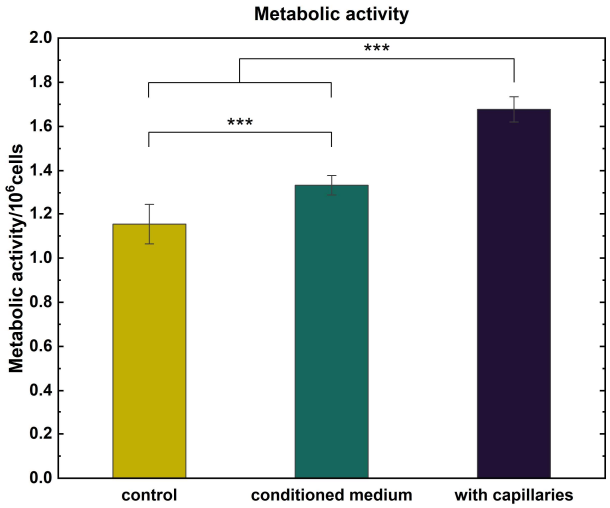


Figure 4.68. Contact angle measurement of a water droplet on the surface of a polysulfone capillary membrane. The surface wettability was evaluated using the sessile drop method with a DSA25 Krüss goniometer. The image shows a representative droplet on the crushed membrane surface used for contact angle determination.

4.5.1.3 Investigation of Membrane Cytotoxicity

The cytotoxicity of polysulfone capillary membranes was evaluated using the MTT assay, which measures the metabolic activity of cells (C3A_EGFP) cultured either in the presence of membranes or in membrane-conditioned medium. The results demonstrated that cells cultured with capillaries exhibited the highest metabolic activity ($p<0.001$), followed by cells cultured in conditioned medium ($p<0.001$), in comparison with the control culture (Figure 4.69).

A)



A1)

statistical significance	control	conditioned medium	with capillaries
control		0.000429	0.000089
conditioned medium	0.000429		0.000167
with capillaries	0.000089	0.000167	

Figure 4.69. Metabolic activity of C3A_EGFP cells cultured in membrane-conditioned medium or in the presence of polysulfone capillary membranes. A) Cells were cultured for 3 days either with conditioned medium (medium collected after 24 h incubation with capillaries) or directly with capillary membranes (10 capillaries, each 1 cm in length). Control cultures were maintained under standard conditions. Experiments were conducted in 12-well plates at a seeding density of 0.2×10^5 cells per well. MTT assay results, representing six biological replicates (n = 6), were normalized to cell number. **A1)** Statistical significance for Figure 4.69. Statistical analyses were performed using ANOVA followed by Duncan's *post-hoc* test. Data are presented as mean ± SD. Levels of significance are indicated as follows: *p<0.05, **p<0.01, ***p<0.001.

After 3 days of culture, the effect of the membrane on cell viability was also evaluated. The results showed that cell viability was high across all culture variants, ranging from 98% to 99% of viable cells (Figure 4.70).

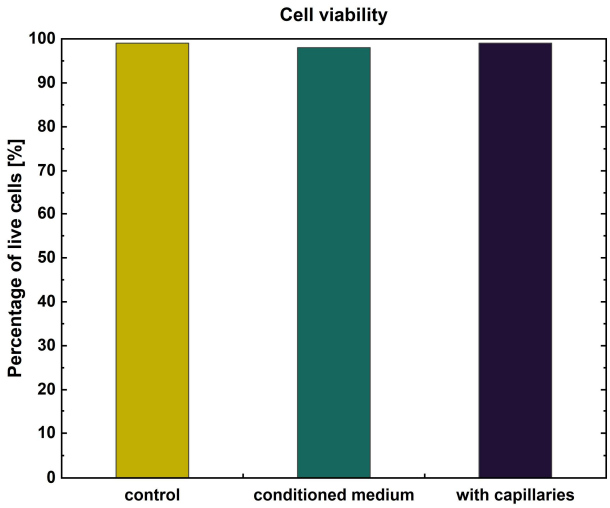


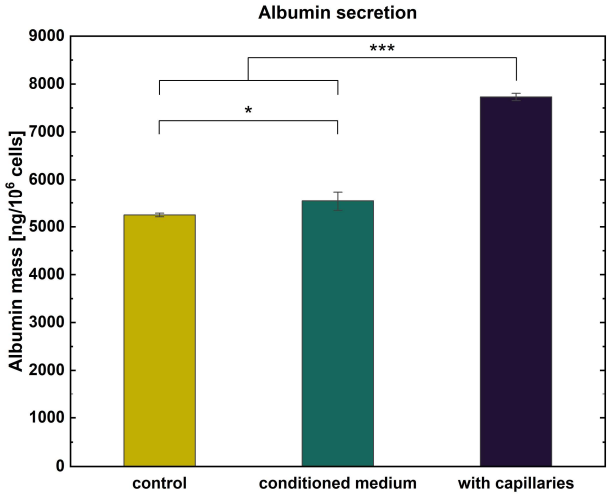
Figure 4.70. Cell viability of cells cultured in membrane-conditioned medium or in the presence of polysulfone capillary membranes. Cells were seeded at a density of 0.2×10^5 cells per well in a 24-well plate and cultured for 3 days. The experiment was performed under three conditions. In the control conditions, cells were cultured in standard DMEM. In the second condition, cells were cultured in conditioned medium (medium collected after 24 h of incubation with capillaries). In the third condition, cells were cultured directly with capillary membranes (10 capillaries, each 1 cm in length). Cells were then trypsinized and counted using the trypan blue exclusion method. The study was performed as a single biological replicate.

4.5.1.4 Albumin Secretion - ELISA

An ELISA assay was employed to determine albumin production in the culture medium produced by C3A_EGFP cells under different conditions. Albumin, as the most abundant protein synthesized by hepatocytes, serves as a key indicator of cell functionality in culture. After normalization for cell number, ELISA results revealed that C3A_EGFP cells cultured with capillary membranes produced the highest levels of albumin compared with the control

(p<0.001). Cells cultured in conditioned medium produced albumin at levels similar to the control (p<0.05) (Figure 4.71).

A)



A1)

statistical significance	control	conditioned medium	with capillaries
control		0.028060	0.000113
conditioned medium	0.028060		0.000235
with capillaries	0.000113	0.000235	

Figure 4.71. Albumin secretion by C3A_EGFP cells cultured in membrane-conditioned medium or in the presence of polysulfone capillary membranes. A) Cells were cultured for 3 days in 12-well plates at a seeding density of 0.2×10^5 cells per well, in standard DMEM, conditioned medium, or with capillary membranes. The study included three biological replicates (n = 3). **A1)** Statistical significance for Figure 4.71. Statistical analyses were performed using ANOVA followed by Duncan's *post-hoc* test. Data are presented as mean ± SD. Levels of significance are indicated as follows: *p<0.05, **p<0.01, ***p<0.001.

4.5.1.5 Ultrafiltration Measurements

After characterizing the membrane, the hollow fiber bioreactors were prepared for dynamic cultures. Ultrafiltration measurements were carried out for three selected self-constructed bioreactors. Since membrane ultrafiltration values vary over time, the measurements were repeated for the tested bioreactors after one week. For further details, see section 3.12.3.

In the first set of ultrafiltration measurements (U1), the results obtained for three independent bioreactors ranged from 185 to 192 $cm^3/m^2\cdot hPa\cdot min$ (Table 4.9). For each bioreactor, repeated measurements conducted after one week of operation showed a decrease in membrane ultrafiltration. The subsequent ultrafiltration values (U2) ranged from 116 to 137 $cm^3/m^2\cdot hPa\cdot min$ (Table 4.9), indicating that the ultrafiltration coefficient decreased by 37% for the first bioreactor, by 32% for the second, and by 29% for the third module, with an average decrease of UFC equal 33%.

Table 4.9. Ultrafiltration values (U1, U2) obtained during measurements performed for three independent hollow fiber bioreactors.

	Ultrafiltration 1 (U1, 1 day) [$cm^3/m^2 \cdot hPa \cdot min$]	Ultrafiltration 2 (U2, 7 days) [$cm^3/m^2 \cdot hPa \cdot min$]
Module 1	185	116
Module 2	186	126
Module 3	192	137

4.5.1.6 Retention Measurements

Determining the membrane cut-off point was of crucial importance. For this purpose, membrane retention measurements were conducted. Bovine serum albumin (BSA) and fluorescent polystyrene beads of various sizes were employed to assess membrane retention. Measurements involving BSA were performed using a spectrophotometer, whereas measurements with polystyrene beads were carried out using a flow cytometer. Detailed information on the measurement procedure is provided in sections: 3.12.4.

The obtained results (Table 4.10) demonstrated that small particles with sizes below 0.2 µm, such as BSA and 100 nm beads, freely passed through the membrane, resulting in 0% retention. In contrast, larger particles – 200 nm beads, which became embedded within the membrane and were unable to pass through, exhibited a retention of 97%. Particles exceeding 200 nm in size, specifically 500 nm, 2 µm, and 3 µm beads, were completely retained by the membrane, corresponding to 100% retention. Figure 4.72 presents a dot plot illustrating the size differences of the tested beads (Cytometer Setup and Tracking Beads). Population 1 (P1) represents the distributions of 2 µm beads (red dots), while populations 2 (P2) corresponds to the distributions of 3 µm beads (green dots).

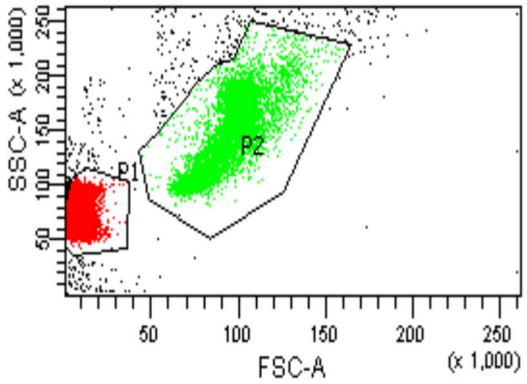


Figure 4.72. Populations of fluorescent beads of different sizes (FSC). Population 1 (P1) represents 2 µm beads (red), whereas population 2 (P2) represents 3 µm beads (green).

Table 4.10. Membrane retention values determined for different types of particles.

Type of molecule	Retention [%]
Bovine serum albumin 67 kDa; 8 nm	0
Green Fluorescent Beads – 100 nm	0
Green Fluorescent Beads – 200 nm	97
Green Fluorescent Beads – 500 nm	100
Cytometer Setup and Tracking Beads (2 μm and 3 μm)	100

4.5.2 Dynamic Cultures

4.5.2.1 Comparison of Albumin Secretion by Cells under Dynamic and Static Conditions

A comparison between dynamic and static culture conditions was performed for four cell types: HepG2, hHs (hH_3; hH_4; hH_5), LCIs (H69 and H72), and four samples of hHDPCs at +2 cell passage [hHDPC(H43), hHDPC(H74), hHDPC(H37), hHDPC(H72)]. For dynamic cultures, cells were seeded into a hollow fiber bioreactor (on the outer membrane surface), whereas for static conditions, cells were seeded into T25 culture flasks (25 cm^2). Detailed procedures are described in the section 3.13. To ensure comparability, the same number of cells was used for both dynamic and static conditions, although the seeding density differed among cell types.

Albumin secretion levels in the culture media were determined using the ELISA method after culturing the various cell types. Figure 4.73 shows the dynamic to static ratio (Dyn/Stat) obtained for cultures of different cell types. The lowest dynamic to static culture ratio was observed for the cancer cell line HepG2. The ratio for hHs was intermediate and fell between the values obtained for two LCI samples: it was higher than that for LCI(H69) but lower than that for LCI(H72). The highest Dyn/Stat ratio was observed for all hHDPCs samples. These results indicated also that hHDPCs behaved more similarly to hHs than to HepG2 cells. Therefore, they can be successfully used in dynamic cultures, where such conditions promote the albumin secretion (Figure 4.73).

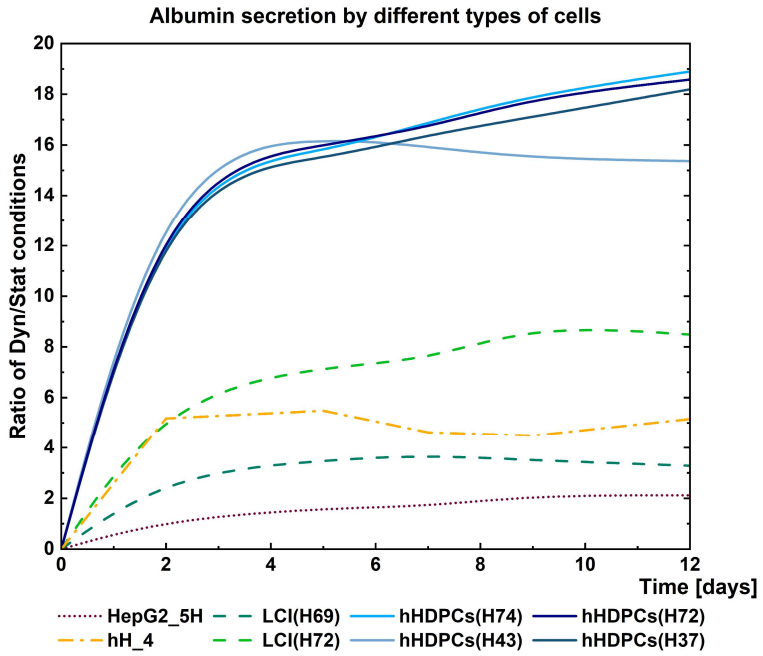


Figure 4.73. Albumin secretion by different cell types under dynamic and static conditions. The dynamic to static ratio (Dyn/Stat) of albumin secretion is shown for the following cell types: HepG2_5H, hH_4, LCIs (H69, H72), and hHDPCs (H43, H74, H37, H72). All cells were cultured in Hepatocyte Medium supplemented with HGS, 2% FBS, and 1% P/S. To ensure comparability, the same number of cells was seeded into the bioreactor and T25 flasks for each cell type; however, seeding densities varied: HepG2 at 5×10^6, hH_4 at $3{,}72\times10^6$, LCIs (H69, H72) at 5×10^6 and 20×10^6 respectively, and hHDPCs (H43, H37, H72) at 2.5×10^6, and hHDPC(H74) at 2.3×10^6 cells. Under the static conditions, hHs and LCIs were cultured on a rat tail collagen type I coated surface. All cultures were maintained for 12 days without medium exchange. For dynamic cultures, the flow rate was 10 mL/min. Media samples were collected every 2–3 days, and albumin production was determined using ELISA. The experiment was performed in three technical replicates (n = 3).

The results obtained under dynamic and static conditions were also compared for a single cell type. A total of five HepG2 cultures were analyzed: two cultured in DMEM medium (D) and three in hepatocyte medium supplemented with HGS (HM+HGS; H).

The comparison of the dynamic to static ratio showed that both HepG2 samples cultured in DMEM (HepG2_1D, HepG2_2D) exhibited higher values than those cultured in HM+HGS, which suggest that cells cultured in DMEM improve the albumin production under dynamic conditions. Among the three samples cultured in HM+HGS, two (HepG2_4H and HepG2_5H) showed similar Dyn/Stat ratios, whereas HepG2_3H differed markedly from the other samples (Figure 4.74).

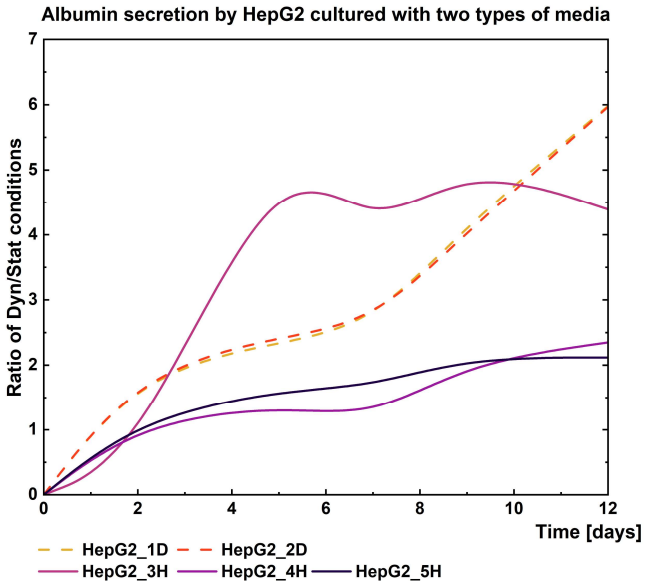


Figure 4.74. Albumin secretion by HepG2 cell lines under dynamic and static conditions. Cells were seeded at 5×10^6 per culture vessel and maintained for 12 days without medium exchange. DMEM (D) and HM+HGS (H) media were used. Two DMEM cultures (HepG2_1D, HepG2_2D) and three HM+HGS cultures (HepG2_3H, HepG2_4H, HepG2_5H) were analyzed. Albumin secretion levels in post-culture media were determined using ELISA. Experiments were performed in three technical replicates (n = 3). Statistical analysis was not conducted, as each culture was treated as an independent experiment.

Figure 4.75 presents the dynamic to static ratio of albumin secretion by human hepatocytes (hHs). The experiment was performed using three hepatocyte samples obtained from different donors (hH_3, hH_4, hH_5). Results showed diverse cell behavior. For two samples (hH_4 and hH_5), dynamic conditions enhanced albumin secretion, particularly in hH_4. In contrast, for sample hH_3, similar levels of albumin secretion were obtained under both dynamic and static conditions.

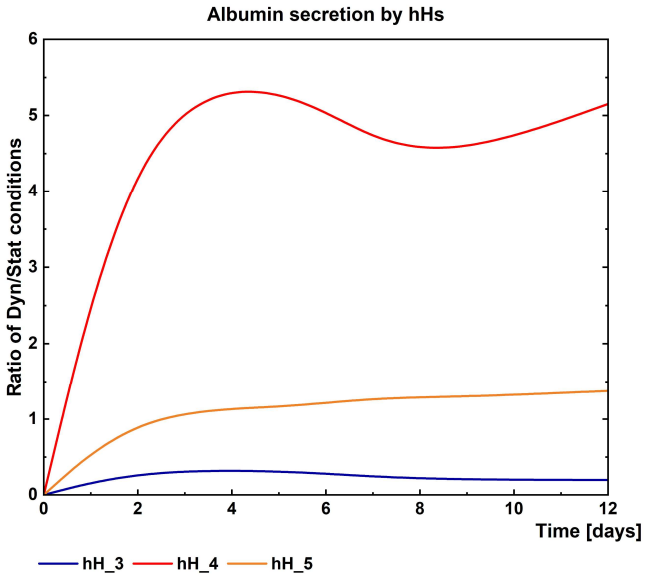


Figure 4.75. Albumin secretion during dynamic and static culture of human hepatocytes (hHs). The experiments were conducted over 12 days using hepatocyte medium supplemented with HGS, without medium

replacement. Cells were thawed and directly seeded into a bioreactor and T25 flasks coated with rat tail collagen type I. For both dynamic (Dyn) and static (Stat) conditions, equal numbers of cells were used: hH_3 – 5×10^6, hH_4 – 3.72×10^6, and hH_5 – 2.8×10^6. Albumin production in post-culture media were determined using ELISA. Experiments were performed in three replicates, each treated as an independent experiment; therefore, no statistical analysis was conducted.

4.5.2.2 Comparison of Urea Production in Cells under Dynamic and Static Conditions

The ability of different cell types to produce urea was also investigated under dynamic and static culture conditions. The study was performed using the same post-culture medium samples that were used for the ELISA assay, including HepG2, hHs, LCIs, and hHDPCs.

The results revealed that, similarly to albumin secretion, dynamic conditions promoted higher urea synthesis compared with static conditions. Moreover, urea production was detected in all analyzed cell types (Figure 4.76).

Analysis of the dynamic to static ratio showed that all hHDPC samples exhibited an upward trend in urea production under dynamic conditions throughout the 12-day culture period, among all tested cell types. Interestingly, the Dyn/Stat ratio for HepG2 and hHs was intermediate between the results for two LCI samples. LCI(H72) exhibited a higher Dyn/Stat ratio than LCI(H69).

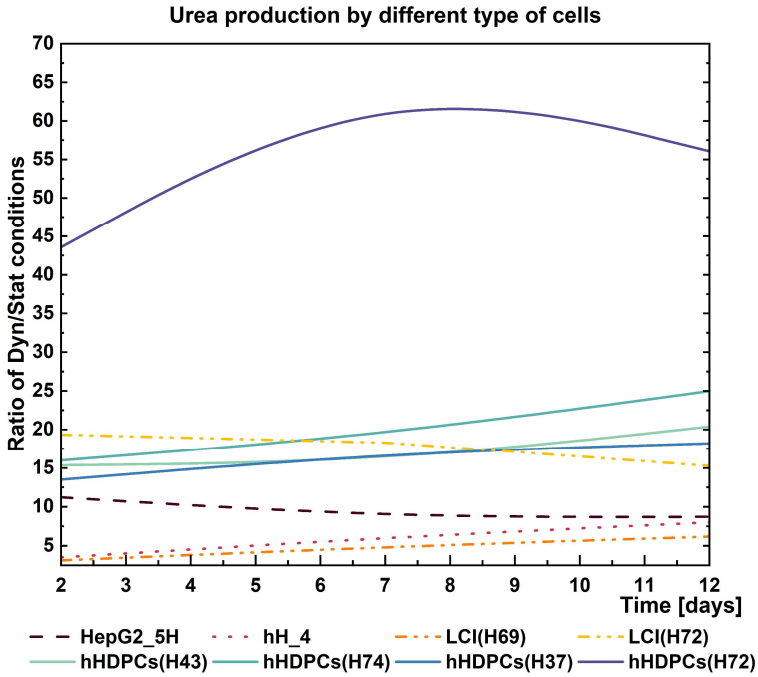


Figure 4.76. Urea production by different cell types under dynamic (Dyn) and static (Stat) culture conditions. The experiment included the following cell types: HepG2, hHs, LCIs (H69 and H72), and four hHDPCs specimens: hHDPC(H43), hHDPC(H74), hHDPC(H37), and hHDPC(H72). All cells were cultured in hepatocyte medium supplemented with HGS, 2% FBS, and 1% P/S solution. For each cell type, equal numbers of cells were seeded into the bioreactor and T25 flasks; however, seeding densities differed: 5×10^6 for HepG2, $3{,}72\times10^6$ for hH_4, 5×10^6 and 20×10^6 for the LCI (H69, H72 respectively), 2.5×10^6 for hHDPC(H43), hHDPC(H74), and hHDPC(H37), and 2.3×10^6 for hHDPC(H72). Cultures were maintained for 12 days without

medium exchange, and dynamic cultures were maintained at a flow rate of 10 mL/min. Urea concentrations were determined using the QuantiChrom Urea Assay Kit. Each cell type was tested in a single experimental run. Values are presented as mean ± SD, with SD calculated from technical replicates (n = 3). No statistical analysis was performed.

A comparative analysis of urea production was conducted for the liver cancer cell line HepG2, cultured in two media: DMEM (D) and Hepatocyte Medium supplemented with HGS (HM+HGS; H). Analysis of dynamic to static ratio of urea production showed that culture in DMEM enhanced the urea production, in contrast to cultures with HM+HGS medium (Figure 4.77).

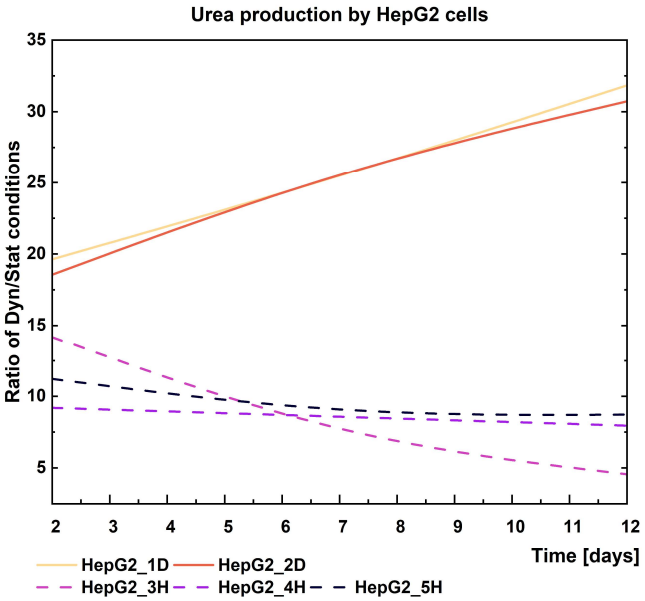


Figure 4.77. Urea production by HepG2 cell lines under dynamic (Dyn) and static (Stat) culture conditions. The dynamic to static ratio was determined using HepG2 cells in five independent experimental runs. Two experiments were performed in DMEM (D) [HepG2_1D, HepG2_2D] and three in hepatocyte medium supplemented with HGS (H) [HepG2_3H, HepG2_4H, HepG2_5H]. Prior to the experiments, cells were cultured for several days and then seeded at a density of 5×10^6 cells into a hollow-fiber bioreactor and T25 flasks. Cultures were maintained for 12 days without medium replacement. Urea concentrations were measured on day 2, 7, and 12 using the QuantiChrom Urea Assay Kit. Results are presented as mean ± SD, with SD calculated from three technical replicates. Each experiment was treated as an independent repetition; therefore, no statistical analysis was performed.

Urea production by hHs was assessed in three independent replicates, using cells obtained from three donors: hH_3, hH_4, hH_5. Urea production was detected in all hHs specimens. The highest dynamic to static ratio was observed for hH_5, an intermediate ratio for hH_4, and the lowest for hH_3 (Figure 4.78).

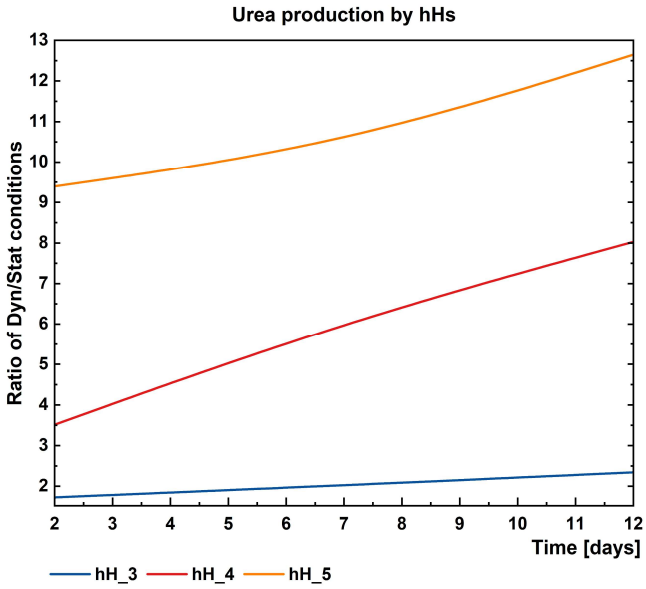


Figure 4.78. Urea production by human hepatocytes under dynamic (Dyn) and static (Stat) culture conditions. The experiment was conducted in three independent replicates (hH_3, hH_4, hH_5), using cells obtained from three different donors. Equal numbers of cells were seeded into both dynamic and static cultures: 5×10^6 for hH_3, 3.72×10^6 for hH_4, and 2.8×10^6 for hH_5. Following thawing, cells were directly seeded into a hollow fiber bioreactor and T25 flasks. Cultures were maintained for 12 days in hepatocyte medium supplemented with HGS, without medium replacement. Urea concentrations were measured using the QuantiChrom Urea Assay Kit. The results are presented as mean ± SD, with SD calculated from technical replicates (n = 3). Statistical analysis was not performed, as each replicate was considered an independent experiment.

5 Discussion

In this doctoral thesis, I aimed to modify the liver cell isolation method developed at LTE IBBE PAS in order to achieve high cell yield and viability. Additionally, I sought to obtain hepatocyte-derived cells that retained their essential functions and could serve as a novel cell source for potential applications in bioartificial liver systems.

The cell line derived from by differentiating isolated human hepatocytes was designed as human Hepatocyte-Derived Proliferating Cells (hHDPCs). These cells retained selected hepatocyte characteristics while simultaneously exhibiting proliferative capacity, making them a promising novel cell source. In the following sections, I discuss the methods used for liver cell isolation and culture and present the characteristics of the newly established hHDPCs.

5.1 Optimization of Liver Tissue Isolation Protocol and Cell Cultures

During the course of this doctoral thesis, I performed 41 cell isolations from tissue samples obtained from 30 donors. The isolation procedure was based on the method developed at the LTE BBE PAS, previously described by Zakrzewska et al. (2017). The original protocol involves mechanical dissociation combined with enzymatic digestion and was designed for the rapid and efficient preparation of biological material from small liver fragments flow cytometric analysis. According to the authors, this method is relatively simple and less damaging to cells compared with more complex isolation procedures [153].

I modified the original isolation protocol to improve both the efficiency of cell isolation and the quality of the resulting biological material for *in vitro* applications. These modifications included the use of different combinations of collagenases during tissue digestion, applied either individually or in various volume ratios. In addition, I cultured the isolated cells under different experimental conditions using several culture media, including DMEM and hepatocyte-dedicated media such as Williams' E medium (WEM) and Hepatocyte Medium (HM). The media were supplemented with compounds supporting hepatocyte culture, including insulin, dexamethasone, and a commercial hepatocyte growth supplement (HGS), although the exact composition of this supplement was not disclosed by the manufacturer. I also evaluated cell growth and morphology in media supplemented with or without FBS. Furthermore, I tested different ECM coatings, including type I collagen derived from rat tail, laminin, and fibronectin. Additional experiments were performed using culture systems involving genetically modified human fibroblasts overexpressing HGF and EGF.

The data presented in Table 3.12 indicate that more than 70% of the donor tissues were obtained from patients diagnosed with primary liver cancer or liver metastases, rendering this organ unsuitable for transplantation. Approximately 20% of the donors presented other medical conditions that also excluded the possibility of LT. Only 17% of the analyzed tissue samples originated from healthy donors. Although the number of analyzed samples was relatively limited (n = 30), these observations may reflect the ongoing clinical problem associated with insufficient donor organ availability. Therefore, the development of effective methods for human hepatocyte isolation and optimization of hepatocyte culture conditions remains an important research objective.

To evaluate the effectiveness of the modified isolation procedure, I compared the obtained values of isolation yield (*Y*) and cell viability (*V*) with data from the literature. A comparison of the isolation methods and the obtained parameters is presented in Table 5.1. The results obtained using the modified protocol based on mechanical dissociation and enzymatic digestion were comparable to, or within the range of, values reported in previous studies. The mean donor age across the compared studies was similar; however, the average weight of liver tissue used for isolation varied considerably. It should also be emphasized that liver samples used in this study originated from different anatomical regions of the liver, which may have additionally influenced isolation efficiency. Guy et al. (2025) demonstrated that perfused liver fragments with preserved vasculature yielded the highest hepatocyte isolation efficiency, whereas non-perfused fragments produced lower cell yield [213]. Similarly, Lee et al. (2014) reported that factors such as hepatic steatosis, cold ischemia time, perfused liver weight, and previous chemotherapy significantly reduced the both hepatocyte yield and viability [214]. Taken together, these observations indicate that efficient isolation of viable human hepatocytes remains technically challenging and continues to require further methodological optimization.

Although the modified protocol used in this study resulted in one of the lowest isolation yields reported in Table 5.1, the isolated cells maintained very high viability, indicating they remained in good condition after isolation. These findings suggest that the isolation method developed at LTE IBBE PAS [153], together with the modifications introduced in this doctoral thesis, may be particularly suitable for processing small liver tissue fragments (up to 100 g), rather than larger tissue samples or whole organs. However, this approach inherently limits the total number of isolated cells, as previously noted by Zakrzewska et al. (2017) [153].

Importantly, the rapid isolation of highly viable cells enabled me to observe cellular behavior during culture and facilitated the performance of various biological assays. In the

future, such approaches may contribute to the development of personalized therapeutic strategies tailored to individual patients. Compared with the classical two-step collagenase perfusion technique, the modified protocol described in this study may also offer practical advantages, including shorter processing time, lower technical complexity, reduced cellular stress, and improved viability of the obtained cell preparations.

Table 5.1. Comparison of donor characteristics, isolation yield, cell viability, and isolation methods between the present study and published literature.

	Donor age [years]	***Y* [cell number $\times 10^6$/g tissue]**	**LTM [g]**	***V* [%]**	**Method of cells isolation**
This study (n = 30)	57±14	1.68±2.36	57.33±61.49	92±8	Mechanical dissociation and enzymatic digestion of tissue, with modifications
Zakrzewska et al. [153] (n = 41)	55±14	3.90±2.77	-	97±2	Mechanical dissociation and enzymatic digestion of tissue
Alexandrova et al. [215] (n = 58)	54±16	2.6±3.8	1836±407	64±26	Modified three-step collagenase perfusion
Lee et al. [214] (n = 1032, for V); (n = 1028, for Y)	-	13.04±0.4	-	77±0.3	Two-step collagenase perfusion technique, with modifications
Gramignoli et al. [216] (n = 42)	53±17	8.2±5.7	66±38	77±9	Two-step collagenase perfusion technique, with modifications
Serralta et al. [217] (n = 14)	58±13	7.9±4.5	~3	91±7	Microperfusion of tissue with collagenase
Pfeiffer et al. [218] (n = 12)	-	14.8±6.6	-	77±4	Two-step EDTA/collagenase perfusion technique

My observation on a higher yield of isolated cells from male donors was consistent with the findings reported by Zakrzewska et al. (2017) [153]. At the same time, I observed lower cell viability in male donor samples than in samples from female donors. In contrast to my observations, Zakrzewska et al. did not report gender-related differences in hepatocyte viability but pointed at increased ALB content in male hepatocytes when compared to the female counterparts. It should be emphasized, however, that the differences observed in isolation yield in my study were not statistically significant, whereas the differences in cell viability reached statistical significance (Table 4.1).

The observed differences in isolation yield and hepatocyte viability between male and female donors may be associated with the biological effects of sex hormones on liver tissue

organization, hepatocyte metabolism, and cellular stress response. Sex hormones, particularly estrogens, are known to influence extracellular matrix (ECM) remodeling, inflammatory signaling, and mitochondrial function, all of which may affect the efficiency of hepatocyte isolation procedures. Previous studies have demonstrated that 17β-estradiol exerts hepatoprotective effects by supporting mitochondrial biogenesis and reducing oxidative stress in hepatocytes, as described by Galmés-Pascual et al. (2017) [219]. Estrogens have also been shown to modulate inflammatory responses by reducing the production of pro-inflammatory cytokines [220] [221]. Furthermore, estrogens may influence liver tissue architecture through the regulation of ECM remodeling and hepatic stellate cell activation, potentially resulting in a more compact tissue organization [222], as also discussed in [223] and [224].

Such structural differences may reduce the accessibility of digestive enzymes during tissue dissociation and could partially explain the lower isolation yield observed in samples obtained from female donors. On the other hand, lower estrogen-mediated hepatoprotection in male donors may increase cellular susceptibility to isolation-induced stress, which could contribute to the lower hepatocyte viability observed in my study.

Taken together, these observations suggest that donor sex may represent an important factor influencing hepatocyte isolation outcomes. Therefore, optimization of isolation protocols with consideration of donor gender may improve both isolation yield and post-isolation cell viability.

Following liver cell isolation, a subset of cells formed so-called cell islands, which became the main focus of this study. Interestingly, the phenomenon of hepatocyte islands or colonies has been extensively investigated both *in vivo* and *ex vivo*. In this thesis, the term cell islands refer to adherent multicellular hepatocyte structures formed *in vitro*, regardless of whether they originated from clonal proliferation or spontaneous aggregation.

Current *in vivo* studies support a model in which liver parenchyma regeneration occurs through diffuse clonal expansion, defined as the local proliferation of cells derived from a single hepatocyte without the requirement for a dedicated stem cell niche. Wang et al. (2015) demonstrated that diploid Axin2+ hepatocytes located in the perivenous zone are capable of proliferation and clonal expansion, gradually occupying larger regions of the liver lobule [225]. Subsequently, Wei et al. (2021) and He et al. (2021) demonstrated that zone 2 hepatocytes also contribute significantly to liver homeostasis and regeneration. Their findings suggest that the contribution of individual hepatic zones to clonal expansion is dynamic and depends on physiological conditions and tissue injury [226], [227].

In this context, clonal islands observed *in vivo* reflect the expansion of single hepatocytes during both tissue homeostasis and regeneration. In contrast, similar observations in *ex vivo* conditions are considerably more difficult to interpret. Following isolation, hepatocytes may form structures called colonies or islands, which can arise either through clonal proliferation or spontaneous cellular aggregation. Several studies have demonstrated that hepatocytes retain the ability to form colonies and partially proliferate *in vitro*. Cho et al. (2008) described a technique enabling hepatocyte expansion in culture, indicating the possibility of proliferative growth outside of the organism [228]. Yamasaki et al. (2006) demonstrated that single hepatocytes are capable of generating proliferative colonies *in vitro*, which subsequently undergo proliferation and differentiation [229].

At the same time, determining whether an observed island is truly clonal remains challenging because hepatocytes retain strong adhesive properties after isolation and tend to spontaneously aggregate. This phenomenon has been demonstrated in numerous studies, including organoid-based models. Brophy et al. (2009) showed that hepatocytes rapidly form aggregates under optimal culture conditions while maintaining differentiated hepatic gene expression and function [230]. Similarly, Yuasa et al. (1993) demonstrated that hepatocyte aggregation significantly affects cell survival and maintenance of metabolic activity. The authors suggested that aggregate formation is a natural characteristic of hepatocytes cultured *in vitro* and does not necessarily result from the proliferation of a single cell [231].

Consequently, the observed islands may arise not only from the proliferation of a single hepatocyte but also through the fusion or aggregation of multiple hepatocytes of different origins. Therefore, in this doctoral thesis, these structures are referred to as hepatocyte islands or cell islands. The issue of cellular clonality and its verification using time-lapse microscopy will be discussed in subsequent sections of this thesis.

I considered the isolation procedure successful when islands of adherent cells were observed in culture (Figure 4.1). In the liver cell isolation, 60% of cases were considered successful, as the cells formed islands (Figure 4.1 and Table 4.4). This finding was interpreted as evidence of successful modification of the mechanical dissociation and enzymatic digestion protocol. Isolations performed using biological material obtained from male donors were successful in 50% of cases, whereas material obtained from female donors resulted in successful island formation in 71% of cases. These observations are consistent with the previously discussed hypothesis that female hepatocytes are more viable, potentially associated with the protective effects of female sex hormones.

Using donor age as a criterion for island formation (Figure 4.2 and Table 4.5), most isolations were performed using biological material obtained from middle-aged donors (46–65 years). Islands were obtained in 54% of female donor samples and 8% of male donor samples, yielding a total success rate of 62% within this age group. In the oldest donor group, despite fewer performed isolations, 60% of procedures resulted in successful island formation. In the youngest age group, 57% of isolations were successful; however, only 7 isolations were performed.

No studies directly evaluating the relationship between donor age and the ability to form hepatocyte islands were identified in the available literature. Therefore, the obtained results were indirectly compared with studies investigating the influence of donor age on hepatocyte isolation yield and cell viability. Mitry et al. demonstrated a significant negative correlation between donor age and hepatocyte viability [232]. However, several other studies, including those by Solanas et al. (2022) and Meng et al. (2016), did not confirm a significant influence of donor age or reported only a weak association between donor age and hepatocyte viability or isolation yield [233], [234]. The authors of these studies indicated that factors other than donor age may significantly influence hepatocyte viability. These include liver fibrosis, cold ischemia time, the anatomical site of tissue collection, and the overall clinical condition of the donor. Liver fibrosis is particularly important because it significantly reduces hepatocyte viability and tends to progress with age, as demonstrated by Bonora-Centelles et al. (2010) [235].

During hepatocyte isolation, selecting an appropriate digestive enzyme is a critical factor affecting both isolation yield and post-isolation cell viability. Enzyme activity, protease content, digestion time, and digestion intensity all influence the quality of the obtained cell population. Excessively aggressive digestion may improve tissue dissociation efficiency but simultaneously induce substantial cellular damage, thereby reducing cell viability and functional integrity. Conversely, insufficient digestion may limit the release of cells from the extracellular matrix, resulting in poor isolation efficiency and limited applicability for downstream culture and analysis.

Manufacturer guidelines provide detailed specifications for the application of individual collagenase types depending on the tissue characteristics and extracellular matrix density. Collagenase types I and II are commonly used for the digestion of soft and moderately dense tissues. Collagenase type I is frequently applied for tissues such as liver, lung, and adipose tissue, whereas collagenase type II is more suitable for tissues characterized by higher extracellular matrix density, including cartilage, bone, heart tissue, and selected liver samples.

In contrast, collagenase type XI exhibits higher enzyme activity and is intended for the digestion of connective tissues requiring degradation of a highly fibrotic extracellular matrix, including scarred or cancerous tissues, due to its relatively high proteolytic activity compared with other collagenase variants discussed in this study. Collagenase D and Liberase enzyme mixtures are commonly used in isolation protocols that require high cell quality and viability, including protocols for hepatocyte and pancreatic islet isolation. These enzyme preparations enable more controlled tissue dissociation while reducing damage to cellular structures [236], [237], [238].

In the isolation protocol used in this doctoral thesis, treatment with collagenase II was the most effective method for promoting island formation (Figure 4.3 and Table 4.6). It should be noted that most tissues from which cells were isolated using collagenase II originated from patients with liver cancer or liver metastases, which may have influenced tissue architecture and increased extracellular matrix density. Therefore, collagenase II, which is suitable for tissues with higher matrix density, may have been more effective under these experimental conditions.

Importantly, collagenase D, despite being less aggressive toward cells during the isolation process, also yielded favorable results, with a predominance of samples forming islands compared with samples that did not form islands. However, these observations should be interpreted cautiously because the number of samples analyzed for each collagenase variant or enzyme mixture was not equivalent. Consequently, no definitive conclusions can be drawn regarding the superiority of a specific collagenase type for hepatocyte isolation. Furthermore, numerous additional factors must be considered during optimization of the isolation procedure.

In addition to different isolation conditions, I tested various cell culture conditions after isolation from liver tissue in order to determine the optimal conditions for hepatocyte culture. The example cell islands shown in Figure 4.4–Figure 4.6 were obtained during culture on various types of ECM coatings (collagen, laminin, fibronectin, and dried genetically modified fibroblasts overexpressing EGF and HGF). Various culture media, DMEM with and without FBS, and media dedicated to hepatocyte culture, such as HM+HGS or WEM with or without FBS, were used. Based on these images, I observed different effects of culture conditions on hepatocyte behavior.

I observed that cells do not form islands under all conditions, or that only a small number of islands are formed under certain culture conditions. For example, culturing in HZ medium revealed that a few cell islands detached after a short time (Figure 4.5A). The opposite effect was observed for cells cultured in HM+HGS, where cells in islands started to divide

(Figure 4.5B). It is worth emphasizing that in the cases described here, I used the same digesting enzyme and the same culture medium for the isolation of the same sample. This further demonstrates the significant impact of the culture medium on cell behavior and the importance of selecting appropriate conditions for the desired culture outcome. It also indicates that not every cell on an island proliferates.

Simultaneously with obtaining cell islands after isolation, I identified and confirmed whether the cells forming islands were hepatocytes. To this end, I performed a series of basic identification tests, such as immunofluorescence (IF) and flow cytometry (FC) to detect intracellular albumin, as well as ELISA tests to detect albumin secreted by the cells into the post-culture medium. After labeling the cells with an antibody against human albumin, I observed that the cells forming the islands were positive for immunostaining.

Already in the 1970s, the group of Feldmann, among others, demonstrated the identification of hepatocytes by immunohistochemistry, where they detected albumin in hepatocytes [239]. Thus, the IF test results confirmed that the cells forming the islands were indeed hepatocytes (Figure 4.8).

Initially, FC analysis, confirms the presence of hepatocytes in the liver isolates. I performed the studies on 16 patient samples, using commercial human hepatocytes from a female donor as a control. Depending on the sample, I observed several cell populations, however, hepatocytes were identified only in population 2 (P2) (Figure 4.9), which was also consistent with the results presented by Zakrzewska et al. (2017), where different cell populations were also observed in different patient samples, and hepatocytes were also antibody-identified in P2 [153].

Furthermore, in 10 of 16 samples, I observed a percentage of albumin-positive cells at or above the level of control hepatocytes (70%) (Figure 4.10). Consequently, the method I used enables the acquisition of high-quality hepatocytes for various studies, including flow cytometric analysis and cell culture.

Interestingly, I observed that the albumin level in liver isolated cells (LCIs) was 12% higher in men than in women (but statistical analysis was not performed), which also confirms the results obtained by Zakrzewska et al. (2017) [153]. The authors of the publication suggest that the donor's gender influences the functionality of isolated hepatocytes and that material from male donors may be more suitable for therapeutic applications.

Moreover, I did not observe any dependence on patient age, as the percentage of albumin-positive cells isolated from both groups of patients, over 65 and younger individuals, could be either above or below 70%.

In addition to albumin, I examined the presence of other hepatocyte-specific proteins, which complement the dataset used to identify them. In the case of A1AT analysis (Figure 4.11), I observed that more than 50% of A1AT-positive cells were obtained from LCIs of female donors in 6 out of 10 samples (excluding control hepatocytes, these samples also came from a female donor). Interestingly, middle-aged men had the highest A1AT levels, while young donors had average protein levels, and donors over 70 had very low A1AT levels. I did not find literature data directly addressing the relationship between donor gender or age and A1AT expression in isolated hepatocytes using flow cytometry. However, it should be noted that the described result is only observational due to the small study group.

Another protein that confirmed hepatocyte identity in LCI was CYP3A4, which I detected in samples from donors of both sexes (Figure 4.12). Due to the lack of induction and cytochrome activity tests, this result cannot be interpreted in terms of protein activity or enzymatic function; it only confirms the presence of this protein in the liver isolate sample. In the case of FC analysis, I did not find any literature examining CYP3A4 presence in hepatocytes isolated from donors; most studies focus primarily on enzymatic activity rather than expression level.

In the LCI samples, HNF4α protein level was also analyzed and was detected in all tested samples, although the percentage of HNF4α-positive cells varied widely among donors (Figure 4.12). These results suggest that the isolated cells exhibit a mature hepatocyte phenotype. However, no correlation was observed between HNF4α expression and donor gender, age, or disease entity. However, the analysis was performed on a small study group, including only two male donors and, together with the controls, six female donors, which limited the ability to detect meaningful trends. I did not find literature demonstrating an influence of gender or age on HNF4α expression levels.

5.2 Albumin Secretion by Hepatocytes

One of the fundamental functions of hepatocytes is their ability to secrete albumin, which can also serve as a marker of the functional quality of these cells. Measurement of albumin levels in the culture medium from samples LCI(H72) and LCI(H74) (Figure 4.13 and Figure 4.14) revealed the presence of this protein in the post-cultured medium, confirming that hepatocytes were present among the isolated cells and that they were functional. However, the albumin level rapidly decreased during culture, indicating the initiation of cell dedifferentiation, which might be associated with the loss of hepatocyte-specific functions *ex vivo*. Furthermore,

it can be observed that both the isolation method and the culture conditions strongly influenced cell behavior. In the case of the LCI(H72) sample, the low albumin level in the medium (Figure 4.13) may indicate less favorable isolation and/or cell culture conditions, which may directly result in fewer cells capable of producing albumin or poorer cell conditions. In this case, using Liberase for tissue digestion and culturing cells in HM+HGS or HZ medium did not yield the expected results. In contrast, when a mixture of collagenases [I, II, and XI, in a 2:1:1 ratio] was used to digest the liver tissue, the albumin level in the medium was significantly higher than in cells after Liberase digestion, where the same culture medium was used.

I used Liberase to digest the tissue from the LCI(H74) sample and cultured the cells in DMEM and HM+HGS media. Unfortunately, after 6 days of culture, the albumin level was already comparable to the blank level for both media (Figure 4.14). When comparing albumin secretion by cells from the LCI(H74) (Figure 4.14) and LCI(H72) samples (Figure 4.13), I observed that after 2 days of culture, LCI(H74) cells exhibited lower albumin secretion than LCI(H72) cells under HM+HGS conditions. It should be emphasized, however, that this comparison concerns samples digested with Liberase but cultured on different substrates: type I collagen for (LCI(H72)) and fibronectin for (LCI(H74)). Both collagen and fibronectin are important components of the ECM, whose influence on maintaining hepatocyte phenotype and function is well documented. Through integrin-dependent signaling, the ECM regulates the expression of hepatocyte-specific genes, including the albumin gene. These results suggest that differences in albumin secretion levels may result from different effects of both the culture medium and ECM components on cell function. Similar observations were presented in the work of Watanabe et al., who showed that the albumin concentration in the post-culture medium, determined by ELISA, was lower in cells cultured on laminin compared to collagen, even though the *ALB* gene expression level remained at a similar level [240]. The obtained result also demonstrates how strongly cell isolation and culture conditions affect the preservation of hepatocyte function and how rapidly cell dedifferentiation may occur *ex vivo*.

5.3 Gene Expression in Liver Tissue Isolates

I also investigated the expression levels of genes specific to hepatocytes. RNA was isolated directly from liver tissue samples, and the expression of the following genes was analyzed: *ALB*, *ARG1*, *CPS1*, *CYP3A4*, *CYP2C8*, *CYP2E1*, *HNF4α*, *HNF1α*, and *AFP*. I also analyzed the expression of the *VIM* gene, which is not specific to hepatocytes. The obtained results were evaluated for potential correlations with donor sex, age, cancer status, prior

chemotherapy, and hepatic steatosis. I analyzed 12 samples obtained from 6 female and 6 male donors. Among these patients, cancer was diagnosed in 6 individuals (4 females and 2 males), 4 patients had undergone chemotherapy treatment (3 females and 1 male), and hepatic steatosis was detected in 3 patients, all of whom were male.

Analysis of hepatocyte-specific gene expression in cells isolated from liver tissue obtained from different donors revealed considerable variability among the analyzed samples. The expression profiles of *ALB*, *ARG1*, and *CPS1* indicated differences in the functional status and metabolic activity of hepatocytes between the investigated isolates (Figure 4.15). Among all analyzed samples, the LTI(H75) sample exhibited the highest expression of all three genes, which may indicate the best-preserved hepatocytic phenotype and high metabolic activity of the cells. Elevated expression of these genes was also observed in the LTI(H33) and LTI(H78), suggesting that the isolated cells retained well-preserved functional hepatocyte characteristics. In contrast, isolates LTI(H72), LTI(H74), LTI(H76), and LTI(H79) were characterized by reduced transcript levels, which may indicate impaired hepatocyte function, a lower degree of cellular differentiation, or the influence of pathological factors associated with donor condition. Moreover, I did not observe any correlation between gene expression levels and donor age or sex. However, I observed that donors who had undergone chemotherapy tended to exhibit higher *ALB* expression, although this relationship was not unequivocal. This was particularly evident in sample LTI(H77), which originated from a donor who had not received chemotherapy treatment but exhibited elevated *ALB* expression despite severe hepatic steatosis. This finding suggests that hepatic metabolic alterations may influence the expression of hepatocyte-specific genes. At the same time, significant differences between the LTI(H77) and LTI(H38) samples, despite the presence of steatosis in both cases, indicate substantial biological heterogeneity among donors (Figure 4.15).

The differences in *ALB*, *CPS1*, and *ARG1* expression levels observed in this study may result from both individual biological variability among donors and coexisting pathological conditions, such as hepatic steatosis, previous anticancer treatment, or other pathological states that were not analyzed in this study. Similar relationships have previously been described in studies investigating the quality and functionality of isolated human hepatocytes. Numerous studies have demonstrated that the expression of *ALB* and *CPS1* correlates with the maintenance of a mature hepatocyte phenotype and metabolic function. In contrast, reduced levels of these markers have been observed under conditions of liver injury, cellular stress, hepatocyte dedifferentiation, or during culture [241], [242].

The obtained results are consistent with literature reports indicating substantial interindividual variability in the expression of hepatocyte-specific genes in human hepatocyte cultures. It has been demonstrated that the expression of genes associated with hepatocyte metabolic function may differ significantly among donors due to genetic factors, environmental influences, and the clinical condition of the donor. Rogue et al. (2011) demonstrated substantial variability in transcript levels of genes associated with amino acid metabolism, lipid metabolism, and hepatocyte functions among populations of human hepatocytes. The authors observed variability in albumin expression levels among six donors; however, these differences were not drastic. The study did not analyze the samples with respect to donor sex, age, or disease status [243]. Similarly, Peng et al. (2025) observed considerable heterogeneity in the expression of hepatocyte markers, including albumin, among different batches of human hepatocytes. However, the authors did not evaluate these results according to donor sex or age [244].

The analysis of expression of genes belonging to the cytochrome P450 family revealed substantial variability among the investigated liver tissue isolates (Figure 4.16). The expression of *CYP3A4*, *CYP2C8*, and *CYP2E1* reflects the metabolic activity of hepatocytes as well as their capacity to metabolize drugs and other xenobiotic compounds.

I observed the highest expression levels of *CYP3A4* and *CYP2C8* in sample LTI(H75), suggesting high detoxification activity and well-preserved metabolic function of hepatocytes in this isolate. Elevated transcript levels of these genes were also detected in samples LTI(H73) and LTI(H78), whereas the lowest expression levels were observed in isolates LTI(H65), LTI(H76), and LTI(H79). Particularly pronounced differences were observed for *CYP3A4*, whose expression in some samples was several hundred-fold lower compared with LTI(H75) (female donor, 28 years), indicating substantial functional heterogeneity among donors.

These findings are consistent with the literature, which indicates sex-dependent regulation of *CYP3A4* expression. Wolbold et al. (2003) reported higher *CYP3A4* mRNA transcript levels in women than in men, indicating sex-dependent regulation of *CYP3A4* expression at the transcriptional level [245]. Similarly, Schirmer et al. (2007) demonstrated that CYP3A4 protein expression and enzymatic activity are influenced by both genetic polymorphisms and sex, and that interactions occur between these factors. The authors reported sex-dependent effects of selected *CYP3A4* polymorphisms, with certain genetic variants being associated with higher *CYP3A4* expression and activity, particularly in women [246]. Using microarray-based transcriptomic analysis, Zhang et al. (2011) demonstrated that a substantial proportion of liver genes exhibit sexual dimorphism. The authors also confirmed higher *CYP3A4* expression in women [247]. In contrast, I did not observe any correlation between

CYP3A4 expression levels and donor age consistent with previous reports. Chen et al. (2015) reported no significant association between age and hepatic *CYP3A4* mRNA expression in adult liver samples, although developmental stage-dependent differences were observed during early postnatal life [248].

When analyzing the relationship between *CYP3A4* expression and the presence of cancer, including liver metastases, as well as previous chemotherapy treatment, I observed elevated *CYP3A4* expression in most patients presenting one or both of these factors. However, available literature indicates that it cannot be unequivocally concluded that oncological patients or chemotherapy-treated individuals exhibit increased *CYP3A4* expression, since this depends on numerous biological and therapeutic factors. Srikanth et al. (2004) demonstrated that *CYP3A4* gene expression, protein level, and enzymatic activity depend on the type and dose of the administered anticancer drug [249].

In the investigated group, hepatic steatosis was identified in 3 patients, all of whom were male. In two of these patients, *CYP3A4* mRNA levels were low or undetectable (Figure 4.16). Studies performed using human biopsy material and *in vitro* models demonstrated that hepatic steatosis, particularly NAFLD and nonalcoholic steatohepatitis (NASH), generally leads to reduced *CYP3A4* expression, although this effect may vary depending on disease stage and other metabolic factors. It should be emphasized, however, that the analyzed literature studies did not evaluate *CYP3A4* mRNA expression in NAFLD or NASH patients with consideration of sex differences [250], [251].

For the *CYP2C8* gene, I did not observe any clear effect of sex, age, or hepatic steatosis on gene expression levels (Figure 4.16). However, I observed that *CYP2C8* mRNA levels were elevated in some patients diagnosed with cancer and previously treated with chemotherapy compared with the remaining analyzed individuals. Available literature data indicate only a minor influence of sex on *CYP2C8* expression. Naraharisetti et al. (2010) demonstrated comparable *CYP2C8* mRNA and protein expression levels in male and female human liver tissue, suggesting a minimal role of sex in the regulation of *CYP2C8*. Furthermore, variability in *CYP2C8* activity was primarily associated with genetic polymorphisms rather than sex [252].

Within the investigated group, I did not observe any association between *CYP2E1* expression levels and donor sex or age. Data regarding the influence of sex on *CYP2E1* expression in humans remains limited. Most studies have focused on enzyme activity and have reported higher activity of CYP2E1 in males than in females, as reviewed by Aljohmani et al. (2025) [253]. However, Liu et al. (2021) observed a tendency toward higher *CYP2E1* mRNA expression in children than in adults in an analysis of approximately 100 human liver samples.

The authors also reported higher *CYP3A4* and *CYP2E1* mRNA expression in women compared with men; however, these differences did not reach statistical significance [254].

In this study, elevated expression of CYP genes was more frequently observed in samples derived from donors with cancer who had undergone chemotherapy treatment, which may indicate induction of drug-metabolizing enzymes in response to prior exposure to chemotherapeutic compounds. However, this relationship was not unequivocal, as some samples obtained from donors without chemotherapy also exhibited increased expression of selected CYP genes. These findings suggest that, in addition to anticancer treatment, individual donor characteristics, liver metabolic status, coexisting pathological alterations, and the type of administered therapy may substantially influence cytochrome P450 expression levels.

Overall, the obtained results indicate considerable heterogeneity in the metabolic activity of isolated hepatocytes and confirm high interindividual variability in cytochrome P450 gene expression among donors of human liver tissue. Particularly high heterogeneity was observed for *CYP3A4*, whose expression may vary among individuals due to genetic factors, environmental influences, and previous drug exposure. Similar observations were reported by Rodríguez-Antona et al., who demonstrated substantial interindividual differences in CYP enzyme activity in human liver tissue [255].

The analysis of liver-related transcription factors *HNF4α* and *HNF1α* revealed a heterogeneous expression profile among the analyzed liver tissue isolates (Figure 4.17). These genes play a key role in maintaining the mature hepatocyte phenotype and in regulating the expression of genes involved in metabolism and detoxification functions of liver cells. I observed the highest level of *HNF4α* expression in samples LTI(H75) and LTI(H71), suggesting well-preserved hepatocyte identity in these isolates. Elevated expression was also detected in LTI(H78) and LTI(H65), whereas the remaining isolates showed a relatively similar, moderately reduced transcript level. Compared with other analyzed genes, differences in *HNF4α* expression were relatively small, suggesting more stable regulation of this transcription factor among donors. The highest *HNF1α* mRNA expression was detected in sample LTI(H33), whereas most other isolates exhibited several-fold lower transcript levels. Particularly low expression was observed in sample LTI(H79). Such differences may indicate individual biological heterogeneity among donors and varying degrees of preservation of hepatocyte regulatory functions. Elevated expression of HNF4α and HNF1α was observed both in samples obtained from donors who had undergone chemotherapy and in patients without cancer but with coexisting hepatic steatosis. This suggests that transcription factor expression may be

influenced not only by prior anticancer treatment but also by liver metabolic status and individual donor biological characteristics.

Available studies indicate that sex influences the expression profiles of hepatocyte genes and liver metabolism, particularly those involved in detoxification and drug metabolism pathways. *HNF4α* is considered a key regulator of these transcriptional networks and is involved in sex-dependent regulation of hepatic gene expression, including genes from the cytochrome P450 family[256], [257]. However, direct associations between *HNF4α* expression levels and donor sex remain poorly characterized.

Similarly, for HNF1α, I did not observe a correlation between gene expression levels and patient sex or age. As in the case of *HNF4α*, the literature does not indicate a direct relationship between *HNF1α* expression and these factors, but rather suggests an indirect role of this gene in the regulation of multiple signaling pathways. Transcriptomic studies of human liver performed by Rahman RU et al. (2026) indicate that hepatocyte gene expression profiles are influenced by donor characteristics such as sex and age, which modulate metabolic and cellular function-related pathways [257]. Furthermore, reduced *HNF1α* expression has been associated with loss of hepatocyte differentiated state, activation of EMT-like processes, and tumor progression. In a study by Pelletier et al. (2011), inhibition of *HNF1α* in liver cancer cell lines led to cellular dedifferentiation and increased expression of mesenchymal markers, suggesting an important role of this factor in maintaining hepatocyte homeostasis [258]. In addition, *HNF1α* has been implicated in the response of cancer cells to anticancer therapy. Fujino et al. (2021) reported increased *HNF1α* expression in chemotherapy-resistant cancer cells, suggesting a role of this factor in regulating adaptive mechanisms related to cellular stress and drug metabolism [259].

Overall, the results indicate that *HNF4α* and *HNF1α* expression may reflect the degree of preservation of the mature hepatocyte phenotype and the metabolic potential of isolated human liver tissue samples.

The analysis of *AFP* and *VIM* mRNA expression revealed a heterogeneous expression profile among the analyzed liver tissue isolates, which may reflect differences in hepatocyte maturity, regenerative activation, and phenotypic alterations (Figure 4.18). The highest *AFP* expression levels were observed in samples LTI(H73), LTI(H74), LTI(H71), LTI(H78), and LTI(H33), whereas the lowest transcript levels were detected in samples LTI(H75) and LTI(H76). Particularly noteworthy was sample LTI(H75), which simultaneously exhibited high expression of genes characteristic of mature hepatocytes, including *ALB*, *ARG1*, *CPS1*, and *CYP3A4*, along with very low *AFP* mRNA expression level. This may indicate a well-preserved

mature hepatocyte phenotype. In contrast, the elevated *AFP* expression observed in samples LTI(H73), LTI(H33), and LTI(H78) may suggest partial activation of regenerative processes, cellular stress, or a less mature cellular phenotype. High *AFP* expression was observed in both oncological and non-oncological donors, indicating that AFP mRNA expression was not exclusively associated with cancer.

A similar trend was observed for the *VIM* mRNA expression levels. The highest *VIM* expression levels were detected in samples LTI(H77), LTI(H78), LTI(H73), LTI(H71), LTI(H38), and LTI(H33), whereas the lowest expression was observed in sample LTI(H72). Elevated *VIM* mRNA expression may indicate activation of processes associated with cellular stress, tissue remodeling, or partial loss of the mature hepatocyte phenotype. I did not observe any correlation between *AFP* or *VIM* expression levels and any of the analyzed factors, including sex, age, cancer, chemotherapy treatment, or steatosis.

Available data on the influence of sex, age, or liver steatosis on *AFP* gene expression are limited and mostly indirect, as the majority of studies have focused on *AFP* mRNA expression in the context of hepatocellular carcinoma (HCC) and hepatocyte dedifferentiation processes. Previous studies demonstrated that *AFP* mRNA expression is markedly elevated in HCC tissue compared with healthy liver tissue. Moreover, *AFP* expression has been associated with tumor cells exhibiting a more progenitor-like phenotype, suggesting a relationship between *AFP* expression, hepatocyte dedifferentiation, and activation of developmental programs, as reported by He et al. (1999) and Chen et al. (2020) [260], [261].

Similarly, available data regarding the relationship between *VIM* mRNA expression and factors such as sex, age, cancer, liver steatosis, or chemotherapy exposure remain limited and inconsistent. Most studies analyze *VIM* expression in the context of global transcriptomic alterations associated with EMT and cancer cell dedifferentiation rather than demographic characteristics of donors.

In summary, the obtained results suggest that the expression profiles of the analyzed genes are influenced by both individual biological characteristics of the donors and pathological liver conditions, as well as previous anticancer treatment. The observed variability among isolates is consistent with literature reports describing the high heterogeneity of human hepatocytes and highlights the significant impact of donor variability on the functional properties of isolated liver cells.

5.4 Human Hepatocyte-Derived Proliferating Cells (hHDPCs) as a New Model of Human Hepatocytes

5.4.1 hHDPCs Characteristics

The isolation method which I used enabled me to obtain a heterogeneous population of liver-derived cells. Some isolated cells formed cell islands, and their subset exhibited proliferative activity. In terms of novelty of my work, in opposite to results published by other authors where they used dedicated growth and other mitogenic factors to obtain dedifferentiated cells, I elaborated a new method of proliferating hepatocytes derivation based on their natural inclination to form cell islands and to initiate *ex vivo* processes resembling those present in the regenerating liver. Suggesting, it was necessary to establish whether the isolated hepatocytes had acquired proliferative capacity or whether other cell types present in the culture, including fibroblasts, were responsible for the observed cell divisions. The newly identified cells were termed human Hepatocyte-Derived Proliferating Cells (hHDPCs). In the following sections, I characterize these cells and evaluate whether they retain hepatocyte-specific functions and, if so, for how long these properties are maintained. I also investigate whether these cells can undergo controlled dedifferentiation processes.

One of the earliest phenotypic changes observed during hepatocyte dedifferentiation *in vitro* is the transition from a hexagonal epithelial morphology to a spindle-shaped, fibroblast-like phenotype. Measurements of cell size and granularity demonstrated that the hHDPCs population was more heterogeneous than the C3A and HDFn populations, in contrast to hHs (Figure 4.19 and Table 4.7). Within the hHDPCs population, based on cytometric scatter parameters, I observed both hepatocyte-like and fibroblast-like cells, suggesting that these cells represent an intermediate phenotypic state.

Cell membrane polarization was evaluated based on the cell's capability to form apical vacuoles (AVs), which are functional and structural precursors of *bile canaliculi*. Proper formation of these structures is essential for hepatocyte function as it ensures intracellular transport related to detoxification processes [209]. Current studies demonstrated that hHDPCs do not form AVs, unlike C3A cells, in which AVs are visible as dot-like or ring-like F-actin structures (Figure 4.20 and Figure 4.22A). In contrast, hHs are highly polarized *in vivo*; however, following isolation and during dedifferentiation *in vitro*, they lose this polarized organization and, similarly to hHDPCs, do not form AVs (Figure 4.21 and Figure 4.22). The absence of AV formation may result from the use of conventional two-dimensional (2D) culture systems, which do not support multipolar hepatocyte polarization. Indeed, previous reports

have demonstrated the formation of these structures in three-dimensional (3D) culture models. Deharde et al. confirmed that hepatocytes cultured in a sandwich configuration, in which cells are embedded between layers of extracellular matrix components such as collagen and/or Matrigel, retain the ability to form Avs [262]. Furthermore, Wrzesinski et al. and Gaskell et al. demonstrated that C3A cells are capable of forming aggregates that resemble early 3D tissue organization, enabling them to retain selected hepatocyte-specific functions. In addition, Wencel et al. reported the presence of ring-shaped actin structures corresponding to AVs formations between C3A cells [263], [264], [265].

The results of my study are consistent with literature data indicating that hepatocytes cultured under 2D conditions progressively lose their polarity. Therefore, the characterization of the hHDPCs should be extended to include sandwich culture models for both hHDPCs and hHs. Such culture conditions may promote AV formation. On the other hand, the absence of AVs structure in hHDPCs cultured in 2D conditions may suggest that, although these cells originate from hepatocytes, dedifferentiation alters their ability to fully maintain hepatocyte-specific structural organization.

Another aspect of the hHDPCs characterization was the evaluation of hepatocyte-specific protein expression in the hHDPCs derived from different donors and maintained at various passages. The analysis included proteins characteristic of mature hepatocytes, including: ALB, A1AT, CYP3A4, HNF4α, and CK18, as well as immature hepatocyte markers such as AFP and CK19. In addition, I assessed the proliferation marker Ki67 and the mesenchymal marker VIM.

The results demonstrated that the hHDPCs derived from different donors and cultured at various passages expressed ALB, A1AT, CYP3A4, HNF4α, and CK18. However, the expression levels of these proteins did not change linearly across passages but, instead, displayed a fluctuating pattern (Figure 4.23A, B, C, D, G), which is discussed in greater detail in the following sections of this thesis. In contrast, AFP expression remained very low in the hHDPCs samples (Figure 4.23E), whereas CK19 expression gradually decreased with increasing passage number (Figure 4.23H).

Analysis of the proliferation marker Ki67 revealed that, despite numerous proliferating cells observed microscopically, a substantial proportion of cells did not express this protein (Figure 4.23F). Miller et al. (2018) demonstrated that Ki67 reflects only a transient state of cells progressing through the G1, S, G2, and M phases of the cell cycle and rapidly disappears once cells enter the quiescent G0 phase [266]. These findings may indicate asynchronous proliferation within the hHDPCs population, with cells at different phases of the cell cycle.

Alternatively, they may reflect population heterogeneity, characterized by the presence of both intensely proliferating cell fractions and fractions with a more quiescent or differentiated phenotype.

VIM expression was evaluated to assess the differentiation status and phenotypic plasticity of the hHDPCs, as mature hepatocytes do not normally express this protein, whereas it is characteristic of mesenchymal cells. Meyer et al. (2013) demonstrated that stimulation with transforming growth factor-β1 (TGF-β1) induces vimentin expression in hepatocytes within four days of culture [267]. Similarly, Kaimori et al. (2007) detected weak and diffuse VIM expression in hepatocytes after only 24 h of culture. Following TGF-β1 stimulation, these authors observed strong VIM expression after 48 h, accompanied by the acquisition of a more spindle-shaped morphology [268]. The reported changes in VIM expression, including its induction and heterogeneous distribution pattern, may be interpreted not only as a feature of hepatocyte dedifferentiation but also as evidence of a transient state of cellular plasticity referred to as partial epithelial-to-mesenchymal transition (partial EMT). During partial EMT, cells simultaneously exhibit epithelial and mesenchymal characteristics without undergoing complete phenotypic conversion. Such an intermediate state has previously been described in hepatocytes exposed to culture-related stress and TGF-β1 stimulation, where epithelial and mesenchymal markers coexist despite partial preservation of hepatocyte identity [267], [268]. Importantly, Meyer et al. also emphasized that not every dedifferentiation process in hepatocytes should be classified as EMT [267]. Based on these observations, the increased presence of VIM in the hHDPCs compared with hepatocytes may indicate partial dedifferentiation and suggest partial EMT, during which the cells gradually acquire mesenchymal characteristics (Figure 4.23I).

Taken together, obtained results indicate that hHDPCs represent a hepatocyte-derived cell population, as evidenced by the expression of hepatocyte-specific proteins. However, these cells also exhibit incomplete phenotypic stabilization and substantial plasticity that changes with increasing passage number. It should also be noted that the transcription factor HNF4α, which is expected to display nuclear localization, was detected in the cytoplasm of hHDPCs. In addition, both HNF4α and HNF1α exhibited distinct banding patterns in WB analysis (Figure 4.36) These findings may suggest a partial reorganization of the hepatocyte transcriptional network during the generation of hHDPCs. Although the hHDPCs may initially resemble hepatic progenitor cells, the overall results suggest that they more likely represent dedifferentiated hepatocytes displaying a transient progenitor-like phenotype. The absence of stable expression of progenitor-associated markers, such as AFP and CK19, precludes

classifying these cells as classical hepatic progenitor cells. Instead, the observed phenotype appears to reflect a transitional dedifferentiation state resembling processes occurring during liver regeneration. Similar phenomena, in which mature hepatocytes acquire progenitor-like proliferative capacity, have previously been described in the literature. However, these processes are typically accompanied by increased expression of progenitor markers such as AFP and CK19, as demonstrated by Fu et al. (2019) [269].

5.4.2 Comparison of hHDPCs, HepG2, and HDFn Cultures

The MTT assay was used to evaluate changes in cellular metabolic activity under different culture conditions. Because the study involved media differing in glucose concentration and the presence of the hepatocyte growth supplement (HGS), this method allowed assessment of the cells' metabolic state rather than solely their viability. This is particularly important in studies involving liver cells, whose function is closely associated with energy metabolism.

The obtained results demonstrated differences in metabolic activity among the analyzed cell types. The HepG2 cells exhibited higher metabolic activity in high-glucose medium (Figure 4.25), suggesting a preference for glycolytic metabolism. This phenomenon is characteristic of cancer cells and is commonly referred to as the Warburg effect [270].

Among all analyzed cell types, hHDPCs exhibited the highest metabolic activity (Figure 4.25). This finding further supports their hepatocytic origin and incomplete dedifferentiation and remains consistent with their regenerative status. Under physiological *in vivo* conditions, hepatocytes display high metabolic activity and retain the ability to switch between different metabolic pathways, including gluconeogenesis and oxidative substrate metabolism. Importantly, experimental studies have demonstrated substantial differences between the metabolism of hepatocytes and cancer-derived cell lines. Bissell et al. (1978) showed that hepatocytes consume less glucose and rely more heavily on oxidative metabolism than tumor-derived liver cell lines, which exhibit enhanced glycolytic activity [271]. Interestingly, despite the higher cell count in HM+HGS medium, hHDPCs exhibited reduced metabolic activity under these conditions. This observation may suggest a shift toward a more balanced metabolic state that more closely resembles physiological *in vivo* conditions. High-glucose media, such as DMEM, may induce non-physiological metabolic stimulation, leading to increased ATP production and enhanced glycolytic activity, as demonstrated by Shiroyama et al. (2001) [272]. Furthermore, prolonged exposure to abnormal glucose concentrations has

been shown to alter hepatocyte metabolic pathways, insulin sensitivity, and detoxification capacity (Davidson et al., 2016) [273]. In contrast, culture conditions characterized by lower glucose availability, such as HM supplemented with HGS, may not indicate impaired cellular function. Instead, they may reflect a metabolic state more representative of physiological liver conditions, in which hepatocytes are not continuously exposed to excess glucose. This interpretation is further supported by studies demonstrating that culture conditions, including medium composition, significantly influence hepatocyte bioenergetics and metabolic phenotype, as reported by Dabos et al. (2004) [274].

In the case of the HDFn cells, the observed trend was the opposite of that in hHDPCs, with metabolic activity increased in HM+HGS medium (Figure 4.25). This may indicate greater adaptive capacity of fibroblasts to changing environmental conditions.

At the same time, the high and relatively stable viability observed across all experimental conditions indicates that the differences detected in the MTT assay primarily reflect alterations in metabolic activity rather than differences in cell survival.

Glucose consumption by cells is commonly used as an indicator of cellular metabolic activity, reflecting the utilization of energy-producing pathways, particularly glycolysis, as well as cellular adaptation to environmental conditions. The obtained results demonstrated the influence of both cell type and culture medium composition on glucose metabolism. In all analyzed cell types, glucose consumption per cell was higher under DMEM culture conditions than in HM+HGS (Figure 4.28A). This observation suggests an increased dependence on glycolytic metabolism in DMEM. In contrast, culture in HM+HGS was associated with lower glucose consumption and a metabolic shift toward more energy-efficient mitochondrial processes linked to oxidative phosphorylation. Under physiological conditions, oxidative phosphorylation represents the dominant ATP-producing pathway in cells with a stable metabolic phenotype.

This observation is consistent with reports demonstrating that glucose deprivation or reduced glucose availability induces increased mitochondrial activity and a shift toward oxidative metabolism in the HepG2 cells, as shown by Weber et al. (2002) [275]. Furthermore, Schicht et al. (2022) demonstrated that culture medium composition significantly alters the metabolic profile of hepatoma cell lines, leading to changes in gene expression and metabolic functions [276].

Glucose is a critical component of culture media, serving as both an energy source and a substrate for multiple cellular processes. However, both excessively high and excessively low glucose concentrations may substantially influence cellular metabolism and phenotype. Na et

al. (2014) demonstrated that hepatocytes cultured under high-glucose conditions proliferate more slowly and exhibit altered morphology compared with cells maintained under lower glucose concentrations [277]. Similarly, Davidson et al. (2016) showed that prolonged exposure to hyperglycemic conditions induces metabolic and phenotypic alterations in hepatocytes, including lipid accumulation, impaired insulin sensitivity, and disrupted glucose regulation compared with normoglycemic conditions [273].

The literature further indicates that excess glucose may act not only as an energy substrate but also as a cellular stress factor, potentially contributing to metabolic dysfunction and oxidative stress. The phenomenon of glucotoxicity has been described in hepatocytes as well as in other cell types [278], [279]. Among the analyzed cell types, hHDPCs exhibited the highest metabolic activity in DMEM, which may represent an adaptive response to *in vitro* conditions that differ substantially from the physiological cellular environment. In contrast, the reduction in glucose consumption observed in HM+HGS across all analyzed cell types suggests a shift in metabolic phenotype toward more efficient utilization of energy substrates, potentially involving greater reliance on oxidative phosphorylation. Cassim et al. (2018) demonstrated that hepatocyte isolation and *in vitro* culture induce substantial metabolic alterations, including disturbances in redox balance and mitochondrial function, indicating metabolic stress and reprogramming of cellular energy pathways [280].

Analysis of glucose consumption by the entire culture revealed a different pattern at the population level. In the hHDPCs culture, the overall percentage of glucose consumption was higher in HM+HGS than in DMEM, despite lower glucose consumption when normalized per cell (Figure 4.28B). This phenomenon may be explained by the higher number of cells observed under HM+HGS conditions (Supplementary Figure S8.1), suggesting that this environment supports hHDPCs survival or functional stabilization while simultaneously reducing individual cellular metabolic demand. This may indicate more efficient utilization of energy substrates under conditions more closely resembling the physiological hepatic environment. A similar relationship was observed in the HDFn cells, which exhibited higher glucose consumption per cell in DMEM and reduced consumption in HM+HGS, accompanied by increased total glucose utilization at the culture level. The increased number of fibroblasts in HM+HGS suggests that these conditions promote cell survival or proliferation, whereas the lower glucose consumption per cell may reflect a shift in metabolic strategy. Fibroblasts are known to possess high metabolic plasticity and the ability to dynamically regulate the balance between glycolysis and mitochondrial metabolism depending on environmental conditions, thereby enabling adaptation

to fluctuations in nutrient availability, as demonstrated by Gohil et al. (2010) and Protasoni et al. (2023) [281], [282].

HepG2 cells exhibited a distinct metabolic profile, characterized by higher overall glucose consumption in HM+HGS compared with DMEM, despite reduced glucose consumption when normalized per cell. Moreover, despite lower cell numbers, HepG2 cells maintained relatively high glucose utilization, suggesting sustained glycolytic activity independent of proliferation rate. This observation is consistent with the Warburg effect, in which elevated glucose metabolism is maintained regardless of proliferation dynamics.

Taken together, the obtained results suggest the presence of two distinct models of metabolic regulation. hHDPCs and HDFn cells exhibited environmentally dependent metabolic adaptation and the ability to undergo metabolic reprogramming in response to culture conditions. In contrast, HepG2 cells maintained high glucose utilization regardless of culture conditions, reflecting sustained tumor cell reprogramming.

Albumin secretion in hepatocytes occurs through the constitutive secretory pathway and may serve as an indicator of the cellular differentiation stages. Classical studies demonstrated that, following synthesis in the endoplasmic reticulum (ER), albumin is transported through the Golgi apparatus and continuously secreted without intracellular storage. For example, Yokota and Fahimi (1981), using immunocytochemical methods, demonstrated the presence of albumin throughout the entire secretory pathway, confirming that its intracellular transport is continuous and highly organized [283]. In turn, Fries et al. (1984) showed that the transport of secretory proteins from the ER to the Golgi apparatus occurs with different kinetics, suggesting the existence of selective and regulated transport mechanisms rather than passive protein flow [284]

One of the earliest points at which disturbances in albumin secretion may occur is the ER. In healthy hepatocytes, albumin rapidly achieves its proper conformation and exits the ER efficiently. However, studies conducted in the early 1990s demonstrated that disturbances in protein folding may lead to intracellular retention of secretory proteins. Lodish and Kong (1993) showed that retention of secretory proteins within the ER may result from transient impairment of disulfide bond formation. They demonstrated that treatment with dithiothreitol (DTT) reversibly retained proteins requiring disulfide bonds within the ER, despite the overall secretory pathway remaining functionally intact [285].

Another critical stage is transport between the ER and the Golgi apparatus. Fries et al. (1984) demonstrated that albumin normally passes through this stage relatively rapidly; however, the process remains tightly regulated and susceptible to disruption [284]. In cells undergoing dedifferentiation accompanied by loss of hepatocyte-specific features, disturbances

in ER export sites and reduced efficiency of Coat Protein Complex II (COPII)-dependent transport have been observed. As a consequence, secretory proteins may be retained within the ER before reaching the Golgi apparatus. This results in decreased extracellular albumin secretion and may simultaneously lead to intracellular albumin accumulation. Previous studies demonstrated that efficient ER export requires both COPII vesicle formation and the presence of specialized ER exit sites. Disruption of these structures causes retention of secretory cargo within the ER and impairs further transport to the Golgi apparatus [286], [287], [288].

The next regulatory level involves the Golgi apparatus and the *trans*-Golgi network (TGN). Webb et al. (2005) demonstrated that this stage strongly depends on intracellular signaling pathways, as inhibition of tyrosine phosphorylation resulted in albumin accumulation within the TGN region and impaired secretion. Dedifferentiated hepatocytes frequently exhibit Golgi fragmentation and disturbed cellular polarity, which may further contribute to inefficient protein sorting and export [289].

The final stage regulating albumin secretion involves vesicular transport and exocytosis. Ikonen et al. (1995) demonstrated that secretory proteins are transported in specialized vesicles distinct from those carrying membrane proteins. In dedifferentiated cells, disturbances in cytoskeletal organization, Rab protein function, SNARE-dependent transport, and overall vesicular trafficking have frequently been reported [290], [291], [292]. Such alterations may result in intracellular albumin accumulation despite preserved protein synthesis [289], [284]. Although current results demonstrated that the hHDPCs produce albumin, I was unable to detect albumin secretion into either of the analyzed conditioned culture media (Figure 4.27). Considering the mechanisms described above, this finding may indicate phenotypic alterations during the dedifferentiation, including partial disruption or dysregulation of the albumin secretory pathway.

In contrast, HepG2 cells exhibited a markedly different phenotype. High albumin production was detected in both analyzed media, indicating that the secretory pathway remained functionally active in these cells. Interestingly, albumin secretion was higher in high-glucose DMEM than in hepatocyte-dedicated medium, with differences in glucose availability between the culture conditions. Elevated glucose concentrations may stimulate the HepG2 metabolism and enhance albumin production, whereas hepatocyte-specific medium may promote a more stable and physiologically relevant metabolic state associated with lower albumin secretion.

According to the available literature, the most probable sites of impairment include the ER (protein folding defects and ER stress), COPII-dependent ER-to-Golgi transport, and ER exit sites, and for later stages of Golgi sorting and exocytosis. The obtained results are

consistent with literature reports describing loss of the hepatocyte phenotype accompanied by progressive disorganization of the secretory pathway and intracellular accumulation of proteins despite preserved translation.

Importantly, none of the mechanisms described above was directly investigated in the present study. Nevertheless, analysis of these processes could provide valuable insight into the biology of hHDPCs and help identify which stage of the secretory pathway is impaired. Such studies may also reveal whether albumin secretion can be restored, increasing the usefulness of hHDPCs as an experimental model and their potential for clinical applications.

5.4.3 Optimization of hHDPCs culture conditions

Already in the 1980s, it was shown that the type of culture medium and its supplementation affect hepatocyte condition. Enat et al. (1984) developed several culture media that influenced hepatocyte survival, including serum-supplemented medium (SSM), serum-free hormonally defined medium (DM), and medium supplemented with both serum and hormones (SSM/DM) [293]. Currently, commercial media for hepatocyte culture are also available, such as Hepatocyte Culture Medium (HCM), HepatoZYME-SFM, and William's E Medium (WEM). In 2020, Toba et al. compared five commercial media: Hepatocyte Culture Medium (HCM), HepatoZYME-SFM, Cellartis Power Primary HEP Medium, DMEM/F12, and William's E Medium. The aim of the study was to determine which medium is the most suitable for culturing hepatocytes and human iPS cell-derived hepatocyte-like cells (human iPS-HLCs). However, the authors showed that hepatocytes are highly demanding cells under *in vitro* conditions and that the optimal culture medium has still not been clearly identified [294].

In this study, I evaluated the effect of different culture media (DMEM, EMEM, WEM, HM, and HM+HGS) on the behavior of developed in our lab hHDPCs (Figure 4.30). The media differed in composition, especially in glucose concentration, which was analyzed during the experiment. The results showed that both passage number and culture medium composition significantly affect the proliferation rate and metabolism of the hHDPCs. Clear differences were observed between low-passage (+3) and high-passage (+8) cells. These differences suggested gradual changes in cellular phenotype during passaging. High-passage cells showed lower proliferative capacity and altered glucose metabolism. Low-passage cells were characterized by high proliferation, shorter doubling time, and high viability in all tested media.

The decrease in the hHDPCs proliferation rate with increasing passage number suggested progressive cellular ageing. Hayflick and Moorhead (1961) demonstrated that human

diploid cells have a limited capacity for *in vitro* division. They observed a gradual decrease in proliferation during subsequent passages, followed by complete growth arrest. This study formed the basis for the concept of replicative senescence [295]. Similar observations were reported by Wagner et al. (2008), who studied mesenchymal stem cells during subsequent passages. The authors showed that cell ageing is a gradual and organized process. With increasing passage number, the cells showed lower proliferative activity, morphological changes, and reduced differentiation potential. Metabolic and functional alterations were also observed, indicating progressive senescence of the cell population [296]. Schäuble et al. (2012) studied primary human fibroblasts during long-term culture. They observed gradual cell cycle arrest and increased heterogeneity within the cell population. The number of senescent cells increased with subsequent passages. The authors suggested that cellular senescence develops progressively in different subpopulations rather than occurring simultaneously in all cells [297]. Based on the aforementioned literature data, I concluded that subsequent passages of the hHDPCs were associated with a gradual loss of proliferative activity and metabolic changes characteristic of cellular ageing. However, cell ageing was not the only factor affecting cell behavior. Changes related to ongoing cell transformation also had to be considered.

Expanding on the previously discussed aspect of the influence of glucose availability on the hHDPCs performance. Hayashi et al. (2024) demonstrated that hyperglycemia can cause hepatocyte damage due to mitochondrial metabolic overload. Excess glucose increased the production of reactive oxygen species (ROS), induced endoplasmic reticulum stress, activated apoptotic pathways, and finally caused cell damage. The authors also showed that cellular dysfunction appeared before the loss of viability, suggesting that metabolic overload is an early mechanism of glucose toxicity [278]. The results of this study showed that high glucose concentration in DMEM did not improve the hHDPCs proliferation in either low- or high-passage cells. In high-passage cells, hyperglycemic conditions reduced cell number and viability. In contrast, media dedicated to hepatocyte culture and containing lower glucose concentrations (HM and HM+HGS) promoted the highest proliferation of low-passage cells. This may suggest that the hHDPCs maintain a more physiological metabolic profile under moderate glucose conditions.

Analysis of glucose utilization also showed clear differences between passages. High-passage cells consumed more glucose per cell while showing lower proliferation efficiency. This may indicate a shift toward less efficient energy pathways, including increased glycolysis. Similar metabolic changes were described by Liu et al. (2016), who observed increased glycolysis and reduced oxidative phosphorylation in stressed or dedifferentiated

hepatocytes [298]. The obtained results suggested adaptive stress-related metabolic reprogramming rather than neoplastic transformation of the hHDPCs. Moreover, high-passage cells showed greater variability across media conditions, which may indicate reduced adaptive capacity during long-term culture. In contrast, low-passage cells showed more stable proliferative and metabolic responses.

In summary, the obtained results showed that the hHDPCs had the highest functional stability and proliferation efficiency at low passages and under moderate glucose conditions. Increasing passage number led to higher sensitivity to environmental conditions and reduced proliferative activity. These observations are consistent with cellular ageing and metabolic adaptation described in the literature. Furthermore, the results suggested that the hHDPCs, similarly to hepatocytes, are sensitive to hyperglycemic conditions and that excess glucose may lead to metabolic overload and impaired cellular function. Better results observed in media with lower glucose concentration may indicate that these cells maintain a more physiological metabolic profile under moderate energy substrate availability. Based on the conducted experiments, HM+HGS was selected as the main medium for the hHDPCs culture. This medium was also previously selected for isolated hepatocyte culture (Figure 4.7).

5.4.4 Effect of Hepatocyte Growth Supplement (HGS) on hHDPCs Proliferation

Given the previous results, I decided to investigate whether the improved the hHDPCs culture conditions were associated with HGS supplementation. I also wanted to determine whether HGS could improve the performance of other media, such as DMEM. This aspect was also important from a financial perspective because DMEM is cheaper and more widely available than HM.

In this study, I analyzed the effect of HGS on the proliferation and viability of the hHDPCs at passages +5, +8, and +12 in four culture conditions: DMEM, DMEM+HGS, HM, and HM+HGS (Figure 4.33). The obtained results showed that HGS supplementation significantly affected the proliferation rate and viability of the hHDPCs, especially in cells at lower passages. The strongest effect was observed in HM supplemented with HGS (HM+HGS). This suggests that the components present in HGS support hepatocyte function and proliferative activity.

Although the exact composition of HGS is not disclosed by the manufacturer, the supplement is known to contain growth factors, hormones, and nutrients required for hepatocyte culture. Therefore, the observed effects may result from the activation of signaling pathways

related to cell proliferation, metabolism, and survival. Similar observations were reported by Enat et al. (1984), who demonstrated that hepatocytes cultured in hormonally defined medium showed increased proliferation rate and better maintenance of cellular function compared to standard culture conditions [293]. These findings indicate that appropriate supplementation of the culture medium is important for maintaining hepatocyte activity *in vitro*. In the present study, the strongest effect of HGS supplementation was observed in low-passage cells. However, with increasing passage number, the effect gradually decreased, especially under DMEM conditions. This may indicate that cells progressively lose their ability to respond to proliferative signals over the long term in culture. Similar observations were described by Wagner et al. (2008), who showed that cells gradually lose proliferative potential and responsiveness to environmental stimuli during subsequent passages [296]. Therefore, the limited effectiveness of HGS at later passages may result from progressive cellular senescence and phenotypic changes developing during long-term culture. At the same time, HM supplemented with HGS maintained relatively high cell viability even at later passages. This may suggest a partial protective effect of the supplement. Similar observations were reported by Xiang et al. (2019), who demonstrated that long-term maintenance of hepatocyte survival and function *in vitro* requires properly selected environmental conditions and supplementation supporting cellular homeostasis [299]. The authors also emphasized that even small changes in culture conditions may significantly affect hepatocyte phenotype stability and cell survival.

The obtained results should also be considered in the context of differences in culture medium composition, especially glucose concentration. Analysis of HGS supplementation under different culture conditions revealed significant differences in the hHDPCs response. In DMEM and DMEM+HGS conditions, only small differences in cell number and viability were observed. This suggests that under high-glucose conditions, the effect of HGS supplementation on cell proliferation and survival is limited. A different effect was observed in HM medium. In this case, HGS supplementation significantly increased cell number at passages +5 and +8. This suggests that physiological glucose concentration and the factors present in HGS worked together to support the hHDPCs proliferation and stabilization. However, at passage +12, this effect became weaker, and similar cell numbers were observed regardless of HGS supplementation. This suggests that, at later passages, the main limiting factor is the loss of proliferative capacity associated with cellular senescence rather than culture conditions alone.

Overall, the results indicate that the effectiveness of HGS supplementation strongly depends on both culture medium composition and cell passage number. The strongest response was observed under physiological glucose conditions, whereas the effect was weaker under

hyperglycemic conditions. This may indicate reduced metabolic adaptation and impaired responsiveness to growth signals under less favorable conditions. Furthermore, the gradual decline in supplementation effectiveness at later passages suggests that progressive cellular senescence and phenotypic destabilization become dominant limiting factors during long-term culture. These results confirm that appropriate medium composition and supplementation are crucial for maintaining cells with hepatocyte-like characteristics *in vitro*.

5.4.5 Protein Expression Fluctuations During hHDPCs Passaging

Due to previous observations showing variable levels of hepatocyte-specific proteins during subsequent passages of the hHDPCs, I analyzed the expression of ALB, HNF4α, CYP3A4, and VIM during 10–12 consecutive passages (Figure 4.34 and Figure 4.35). Because hepatocytes rapidly dedifferentiate *in vitro* and lose their specialized functions, I expected a gradual decrease in ALB, HNF4α, and CYP3A4 expression with increasing passage number. At the same time, I expected an increase in VIM expression.

Instead, the obtained results showed fluctuating changes in the expression of the analyzed proteins. These observations suggest that the hHDPCs do not undergo simple unidirectional dedifferentiation. Instead, the cells may exist in an intermediate state between hepatocyte and mesenchymal phenotypes. The cells retained some hepatocyte characteristics while also exhibiting features of mesenchymal cells, such as increased proliferation, spindle-shaped morphology, cytoskeletal changes, and VIM expression. Processes related to EMT play an important role during liver regeneration. EMT-related changes in hepatocytes can increase cellular plasticity and support adaptation to injury and regenerative conditions. In the hHDPCs, the observed changes may indicate a partial EMT-like state. EMT is not considered a simple binary process. Cells can exist in different intermediate states depending on environmental conditions and intracellular signaling. In the classical view, three types of EMT are described: type 1, type 2, and type 3. These correspond to developmental, regenerative, and cancer-related processes, respectively. EMT type 2 is closely linked to tissue repair and inflammation. It is also characterized by partial reversibility of the cellular phenotype [138]. More recent models suggest that EMT is not a simple binary process. Instead, there is a continuous spectrum of intermediate states. These include hybrid epithelial/mesenchymal (E/M) states, in which cells coexpress epithelial and mesenchymal markers while partially retaining the identity of their original cell type [300], [301]. In this view, EMT does not always lead to full transdifferentiation. Instead, it can produce stable or temporary intermediate states.

These states may support cellular plasticity, survival, and proliferation under changing environmental conditions. Different experimental models have described such EMT-related states in hepatocytes. Miura et al. (2024) showed that hepatocytes can enter a hybrid E/M state associated with increased plasticity and partial loss of mature hepatocyte features. In this model, cells can also gain the ability to transdifferentiate, including toward intestinal epithelial-like cells. This indicates strong changes in cell identity [302]. In contrast, Xie et al. (2024) described a reversible proliferative state in hepatocytes. In this system, EMT-related changes are limited and mainly support proliferation and cytoskeletal remodeling. Importantly, cells can return to a functional hepatocyte state, which is consistent with a regenerative type of EMT (type 2 EMT) [303]. Ying et al. (2024) showed another mechanism of liver regeneration. In their model, regeneration is mainly supported by extracellular vesicle signaling. This process does not require strong activation of EMT and allows hepatocytes to maintain their identity with minimal phenotypic change [304]. In contrast to the models described by Miura et al. [302], where EMT is associated with the loss of mature hepatocyte features, and the model described by Xie et al. [303], where EMT is transient and reversible, the hHDPCs show a stable partial EMT-like state with regenerative features. This state does not lead to full dedifferentiation or redifferentiation but maintains the cells in a stable intermediate phenotype. This is supported, among other things, by the presence of intracellular albumin during subsequent cell passages. This model also differs from the observations of Ying et al. [304], where liver regeneration occurs mainly through extracellular signaling without clear EMT activation.

An interesting feature of the hHDPCs, described earlier in this Section, is the presence of intracellular albumin expression, despite its secretion into the culture medium. This suggests that the cells retain a partially active hepatocyte program, but have lost aspects of functional maturity related to cell polarity and active secretory transport. This phenomenon may be linked to partial activation of EMT-related processes. EMT is associated with changes in cytoskeletal organization, cell architecture, and intracellular transport mechanisms.

Mature hepatocytes are characterized by a cytoskeletal organization mainly based on microtubules and actin filaments, with very low expression of VIM. During dedifferentiation and EMT, VIM expression is induced. It becomes strongly upregulated and is a typical intermediate filament of cells with a more mesenchymal phenotype and a reorganized cell architecture. Vimentin, as an intermediate filament, plays an active role in intracellular transport. It interacts with both microtubules and actin filaments. In this way, it influences cytoskeletal organization and the movement of intracellular structures. Although these processes were mainly described in non-hepatocyte models, they are considered to be widely

involved in cytoskeletal remodeling during EMT and dedifferentiation [305], [306]. Studies summarized by Leggett et al. (2021) also showed that VIM network remodeling is associated with changes in cell morphology, loss of polarity, and increased migratory capacity, which are typical features of EMT. In dedifferentiating cells, changes in cytoskeletal connections occur together with changes in intracellular transport organization [307]. Xing et al. (2025) also demonstrated that the vimentin network can directly participate in intracellular transport in hepatocytes, including regulation of vesicle transport and movement of cellular components [308].

Based on these observations and the results obtained for the hHDPCs, reduced albumin secretion may be linked to cytoskeletal remodeling and changes in intracellular transport associated with EMT and dedifferentiation processes. In addition, the presence of VIM and spindle-shaped morphology suggests that the cells remain in an intermediate state between hepatocyte and mesenchymal phenotypes. This state is typical of regenerative processes, in which increased proliferation and cellular plasticity occur alongside reduced hepatocyte maturation. Furthermore, considering the observed behavior of the hHDPCs, including relatively low Ki67 expression, which suggests that not all cells in the G1 phase are actively progressing through the cell cycle, as well as the fluctuating expression of liver-specific proteins, two phenomena should be considered: cellular asynchrony and partial synchronization. Asynchrony means that cells are in different phases of the cell cycle. In a healthy liver, most hepatocytes are in the G0 or early G1 phase, meaning they normally do not divide synchronously. However, during partial hepatectomy, hepatocytes can temporarily enter the cell cycle in a coordinated manner. This is shown by a synchronized increase in DNA synthesis about 24–36 hours after liver resection (Grisham, 1962; Li et al., 2014) [309], [310]. Similar results were observed in mice, where markers of S and M phase confirmed synchronized progression of many hepatocytes after injury (Miyaoka et al., 2012) [311]. Despite this coordinated response, hepatocytes do not become fully synchronized. Proliferation occurs in several overlapping waves, which creates temporal heterogeneity in the population (Zou et al., 2012) [312]. This shows that even under strong regenerative stimulation, cell cycle entry is not fully simultaneous but involves different subpopulations at different times [312], [311].

Cell differentiation involves changes in gene expression, metabolism, and cell structure, and is not directly linked to the cell cycle. However, the differentiation state and cell cycle are partially connected processes. In the liver, mature hepatocytes are mostly differentiated, asynchronous, and rarely proliferating. During regeneration, there is a temporary activation of

the cell cycle and partial synchronization of proliferation. After regeneration, the system returns to an asynchronous state typical for homeostasis. Based on the literature and the results obtained for the hHDPCs, I concluded that both asynchrony and partial synchronization processes are present in these cells.

5.4.6 Long-Term Culture of hHDPCs

Due to the proliferative capacity of the hHDPCs, the next step in the study was to evaluate how long these cells could be maintained in culture and how many passages could be performed. During long-term culture, I observed a clear increase in cell number. However, the results differed between samples. This depended on the donor, the quality of cell isolation, and the initial number of hepatocytes in the liver cell isolate. During 2–3 months of culture, 10–13 passages were performed, and a 5- to 84-fold increase in cell number was observed, depending on the sample (Figure 4.38). It should be emphasized that these calculations included only cells that had already divided and were ready for passaging. Therefore, the actual increase in cell number was likely much higher. This was related to the unknown initial number of isolated hepatocytes and the inability to determine how many cells underwent dedifferentiation into the hHDPCs.

Different models describing the proliferative potential of liver-derived cells and iPSCs have been reported in the literature. In contrast to the hHDPCs, which showed a limited number of divisions, iPSCs can be maintained in culture for very long periods. Cruvinel et al. (2020) showed that iPSCs could be passaged more than 50 times while maintaining pluripotency and the ability to differentiate into all three germ layers [313]. Levy et al. (2015) described a method for long-term *ex vivo* proliferation of human hepatocytes. Because mature hepatocytes normally have limited proliferative capacity, the authors developed a system that temporarily induced them to enter a proliferative state. Afterwards, the cells were redifferentiated into functional hepatocytes using OSM stimulation and controlled HPV E6/E7 expression. Using this method, the cells achieved up to 40 population doublings and regained hepatocyte functions after proliferation [314]. McClelland et al. (2008) established culture conditions supporting short-term *ex vivo* self-renewal of human hepatic stem cells (hHpSCs). The cells were initially maintained under proliferative, non-differentiating conditions and subsequently differentiated into hepatocyte-like and biliary cells after changes in culture conditions. The differentiation process was associated with reduced proliferation and increased expression of mature liver markers. The authors reported that the cells maintained proliferative capacity, colony-forming

ability, and progenitor phenotype for more than 1 month of culture, although the number of passages was not specified. The doubling time was approximately 24 hours, and the colonies increased in cell number around 16-fold within 7–10 days. After reaching confluence, proliferation slowed down. The total culture period lasted around 2 months [315]. Compared with the models described above, the hHDPCs showed several differences. The hHDPCs were cultured under unchanged conditions in HM+HGS medium throughout the experiments. In the method presented in this study, dedifferentiation of the hHDPCs occurred spontaneously and was not induced by additional factors. The hHDPCs were generated by selective expansion of proliferating cells originating from hepatocyte islands. The hHDPCs proliferated throughout the culture period, although the proliferation rate gradually decreased at higher passages. In contrast to the observations reported by McClelland et al. (2008), I did not observe reduced proliferation after reaching confluence.

Notably, the other experiments showed that the hHDPCs retained some hepatocyte-related functions without acquiring a progenitor phenotype. This was supported by the lack of AFP expression and the rapid loss of CK19 expression, which became undetectable even at early passages. These results may also reflect the regenerative status of the hHDPCs.

Using the OLYMPUS Provi CM20 system for continuous culture monitoring, it was determined whether the observed cell islands had a clonal or aggregative character, as discussed earlier in this work. Several methods can be used to confirm clonality, including single-cell seeding, time-lapse microscopy, and lineage tracing.

Long-term cultures were performed without passaging using thawed the LCI samples obtained from three donors, and phenotypic changes in the cells were monitored for 21 days, until they reached the hHDPCs+0 stage, defined as proliferating cells that had not yet been passaged. The system captured images of the same areas of the culture well every 4 hours. This allowed us to observe that some cells within the islands proliferated (Figure 4.41), while others died. Moreover, cell divisions originating from an individual cell that were not originally associated with a cell island were also observed (Supplementary Figure S8.4A).

These observations are consistent with those of Yang et al. (2010), who showed that single hepatic progenitor cells can form proliferating colonies *ex vivo*. The authors tracked the development of colonies derived from a single parental cell and confirmed the clonal expansion potential of these cells [316]. My observations are also consistent with the earlier findings of Yuasa et al. (1993). The authors reported that after isolation, hepatocytes form cell islands that support cell survival and maintenance of metabolic functions. However, these islands do not

necessarily show clonal proliferation [231]. Taken together, these observations indicate that the studied cells may display both clonal and aggregative behavior.

In addition to image acquisition, the software automatically counted cells and calculated confluency. However, these measurements were limited to five selected fields within each culture well. Before the analysis, the system also had to be trained to recognize cells. For the LCI samples, measurements began after 8 days of culture because the thawed isolates initially contained substantial cellular debris. Only after 8 days had the debris decreased enough for reliable cell counting. The results showed that during the transition from the LCIs to hHDPCs+0, the cells gradually acquired proliferative features. At the end of the experiment, two samples, LCI(H40) and LCI(H74), reached cell numbers and confluency levels similar to the hHDPCs+2 and the HDFn controls. In contrast, the LCI(H43) behaved differently, showing lower proliferative potential and lower confluency. This suggests that donor origin also influences cell behavior. It should also be noted that the actual number of the C3A cells was much higher than the software indicated. After 21 days of culture, C3A cells reached 100% confluency. However, the software was optimized for counting single cells rather than aggregates, which are commonly formed by the C3A cells. Therefore, the C3A results should be treated as approximate. In this experiment, I considered microscopic observations to be more reliable and informative (Supplementary Figure S8.4B).

After 21 days of culture, the cells were passaged, and intracellular albumin was confirmed in all samples (Figure 4.43). However, albumin was not secreted into the culture medium in any sample (Figure 4.44). These results indicate that the cells retained some hepatocyte-related functions despite the phenotypic changes observed during culture

5.4.7 Mesenchymal Stem Cell Markers in hHDPCs

Previous studies have shown that hepatocytes can exhibit high phenotypic plasticity *in vitro*. During culture, they may partially lose liver-specific functions and acquire some mesenchymal features. In addition, hepatocyte isolation may also include resident liver mesenchymal cells, such as hepatic stellate cells and interstitial fibroblasts. Therefore, I performed a controlled analysis to determine whether the hHDPCs had fully dedifferentiated into mesenchymal cells or whether the proliferating cells were of mesenchymal origin.

To investigate this, the expression of mesenchymal stem cell (MSC) markers was analyzed, including positive (CD73, CD29, CD44) and negative MSC markers (CD34, CD45, CD133). The obtained results showed that the hHDPCs did not correspond to a classical

mesenchymal cell population. Instead, they exhibited a dynamic and heterogeneous marker expression profile during subsequent passages.

Flow cytometry analysis performed over 11 consecutive passages revealed fluctuating expression of MSC markers (Figure 4.45). These changes were consistent with the previously observed variability in ALB, HNF4α, CYP3A4, and VIM expression. This supports earlier observations suggesting that the hHDPCs exist in an intermediate phenotypic state, remaining between a hepatocyte-like and a more mesenchymal phenotype. The results also support the presence of a transient partial EMT-like program.

I also observed differences between donors, despite the same passage number. This may indicate that individual biological variability and the initial condition for the cells influence the dedifferentiation process. At passage +2, the MSC marker profile was more similar to the hepatocyte phenotype. In contrast, at passage +8, expression of positive MSC markers and some negative markers increased, suggesting higher population heterogeneity and a shift of some cells toward a more mesenchymal phenotype. At passage +12, I observed a partial decrease in MSC marker expression (Figure 4.46), this may indicate a reduction in the mesenchymal-like subpopulation and a partial shift toward a more epithelial phenotype.

Comparison of hHDPCs with other cell lines (HUVECs, hHFs, HDFn, and SH-SY5Y) showed that hHDPCs occupied an intermediate position between hHs and HDFn. At the same time, hHDPCs did not resemble the C3A, HUVEC, or SH-SY5Y cell lines (Figure 4.47). This further supports the hybrid phenotypic nature of hHDPCs.

MSC marker analysis in different types of hepatocyte-like cells has been performed by several research groups. Luo et al. (2018) described a population of adult rat hepatocyte-derived mesenchymal-like stem cells (arHMSCs). These cells exhibited fibroblast-like morphology and expressed mesenchymal markers, such as CD29, CD44, CD90, VIM, and α-SMA. FC analysis at passage +3 showed very high expression of CD29 and CD90, while CD44 and CD73 expression was lower. Expression of CD34 and CD45 was absent or very low. Based on these findings, the authors described the arHMSCs as a stable mesenchymal-like population derived from hepatocytes [317]. In contrast to the model described by Luo et al., hHDPCs showed much greater phenotypic heterogeneity. MSC marker expression was highly variable between passages and donors. This pattern does not correspond to the stable the arHMSC phenotype, especially for CD29, which showed almost complete positivity in classical MSC-like populations. In addition, the hHDPCs contained CD133-positive cells, whereas the arHMSCs did not. This may indicate activation of a dedifferentiation program associated with epithelial plasticity and partial EMT. Another important difference is that the hHDPCs maintained

expression of hepatocyte markers, such as albumin, HNF4α, and CYP3A4, even in the presence of mesenchymal markers. In the Luo model, hepatocyte marker expression was largely lost in the mesenchymal state and reappeared only after redifferentiation into hepatocyte-like cells. The results suggest that hHDPCs do not represent a stable hepatocyte-derived mesenchymal stem cell population similar to the arHMSCs. Instead, they appear to represent a dynamic and transitional phenotypic state in which hepatocyte and mesenchymal features coexist. Furthermore, the fluctuating expression of CD29, CD44, and CD73 across passages suggests that these markers depend on the current cell state rather than stable mesenchymal identity.

Covas et al. (2008) described mesenchymal stem cells isolated from fetal liver that showed stable, similar expression of MSC markers, including CD29, CD44, CD73, CD90, and CD105, and lacked CD34 and CD45 expression. This phenotype corresponds to the classical MSC profile and represents a clearly defined mesenchymal population *in vitro* [318]. In contrast, the hHDPCs exhibited a heterogeneous, unstable MSC marker profile, which does not correspond to the classical MSC phenotype described by Covas et al.

The results on MSC marker analysis, together with previous observations, support the hypothesis that the hHDPCs neither constitute a stable mesenchymal population nor a fully mature hepatocyte phenotype. Instead, they appear to exist in a transitional state associated with cellular plasticity. The obtained data also suggest that the hHDPCs do not originate from mesenchymal cells. Rather, the observed marker profile indicates persistent partial EMT activation and a dynamic balance between epithelial and mesenchymal features. This state may resemble regenerative processes observed in the liver *in vivo*, in which hepatocytes undergo concurrent temporary dedifferentiation and redifferentiation.

5.4.8 Attempts to Re-differentiation of hHDPCs Into Hepatocyte-Like Cells Using Growth Factors

For many years, researchers have been trying to obtain new sources of hepatocyte- For many years, researchers have been seeking new sources of hepatocyte-like cells for research and therapy, mainly because of the limited availability of liver donors. One approach is based on controlled culture conditions that allow cells to dedifferentiate and later redifferentiate into hepatocyte-like cells. Therefore, I also attempted to redifferentiate hHDPCs toward a hepatocyte-like phenotype.

Three different hHDPCs passages were used to determine whether the passage stage affected the cells' susceptibility to differentiation. This experiment was based on the study by Herrera et al. (2006), in which the authors used medium supplemented with FGF-4 and HGF

for differentiation of liver-derived stem cells [319]. In my study, additionally was used a variant supplemented with EGF+HGF. Both supplemented variants were cultured in HM medium without HGS supplementation. FGF-4, EGF, and HGF are commonly used during hepatocyte differentiation because they mimic signaling pathways involved in liver development and regeneration.

The obtained results showed that supplementation with FGF-4+HGF or EGF+HGF significantly stimulated hHDPCs proliferation, especially at lower passages. However, the cells did not regain the polygonal morphology typical of mature hepatocytes. Instead, they became more elongated and fibroblast-like. In addition, albumin secretion into the culture medium was not detected. Cells cultured in FGF-4+HGF conditions showed a stronger proliferative response than cells cultured with EGF+HGF. This suggests that the applied growth factors mainly promoted cell expansion rather than hepatocyte redifferentiation. An interesting observation was the lack of a proliferative response at the highest analyzed passage (+12). In these cells, both FGF-4+HGF and EGF+HGF conditions resulted in lower cell numbers than those cultured in basal HM medium. This may indicate progressive proliferative exhaustion during long-term culture and partial loss of the ability to respond properly to mitogenic stimulation.

Under conditions of prolonged stimulation of HGF-, EGF-, and FGF-4-related pathways may destabilize the proliferative-regenerative phenotype of the hHDPCs or increase cellular stress instead of promoting further expansion. It is also possible that late passages selected a subpopulation of cells better adapted to basal culture conditions than to strong mitogenic stimulation. The observed proliferative effect is consistent with the biological role of the applied growth factors. HGF is one of the main hepatocyte mitogens activated during liver regeneration and stimulates proliferation, migration, and cell survival [82]. EGF also promotes proliferation of hepatocytes and progenitor cells while supporting maintenance of a proliferative and plastic phenotype [88]. FGF-4 plays an important role during liver development and early hepatocyte differentiation, but it is also associated with progenitor-like and developmental characteristics [320]. Taken together, these observations suggest that the applied growth factor combinations mainly supported maintenance of a regenerative and proliferative intermediate state rather than full hepatocyte redifferentiation.

In contrast to my model, Herrera et al. studied liver stem cell-derived progenitor cells (HLSCs). These cells exhibited progenitor features, high proliferative potential, partial commitment to the hepatocyte lineage, and the ability to differentiate into mature hepatocyte-like cells. The differences between my results and those obtained by Herrera et al. may suggest that the hHDPCs originated from mature hepatocytes that had already undergone

partial dedifferentiation before growth factor stimulation. In this situation, the applied growth factors may have acted mainly as regenerative and proliferative stimuli, similar to liver regeneration *in vivo*. As a result, the cells showed increased proliferation and acquired a more fibroblast-like phenotype instead of regaining mature hepatocyte characteristics.

An important factor influencing the results in this study was that the hHDPCs were cultured without HGS supplementation. Under standard conditions, HGS supports the maintenance of hepatocyte phenotype, cell survival, and basic metabolic activity. The absence of this supplement may have weakened signals stabilizing hepatocyte identity and increased the cells' susceptibility to a more plastic state. As a consequence, the cells may have become more dependent on alternative signaling pathways, such as HGF-, EGF-, and FGF-4-dependent activation of proliferation and survival. This could have favored the maintenance of a transitional phenotype with partial EMT-like features. In this context, the lack of full hepatocyte redifferentiation may result both from the absence of stabilizing factors (HGS) and from the dominance of proliferation-promoting signals over maturation-related processes.

It is possible that effective redifferentiation of hHDPCs would require culture conditions specifically optimized for this cell type. Selection of the appropriate cell passage may also be important for achieving more efficient hepatocyte-like differentiation.

5.4.9 Human Dedifferentiated Hepatocytes (hDHes) Dividing and Retaining Hepatocyte Functions

In another attempt to expand human hepatocytes in culture, a transient proliferative state was inducted in cells isolated from human liver parenchyma. Commercially available human hepatocytes were cultured in Expansion Medium (EM), which promoted cell proliferation while reducing hepatocyte-specific functions. The proliferating cells were subsequently transferred to Differentiation Medium (DM), where they retained proliferative activity and regained hepatocyte characteristics. These cells were termed human Dedifferentiated Hepatocytes (hDHes).

The experimental design was based on the studies of Garnier et al. (2018) and Huch et al. (2015) [212], [211], while the composition of the EM and DM media was adopted from the latter one. In both studies, liver cells were cultured and expanded in three-dimensional Matrigel-based organoid systems. Matrigel is a complex extracellular matrix derived from murine sarcoma that is rich in laminin, collagen IV, and growth factors, including FGF and EGF. It supports the maintenance of the progenitor cell niche and the spatial organization characteristic of organoids. However, the use of Matrigel has several important limitations,

including batch-to-batch variability, the presence of undefined biologically active components, and its animal and tumorous origin. These factors may influence the behaviour of human cells and limit the translational potential of such culture systems (Benton et al., 2014; Aisenbrey and Murphy, 2020) [321], [322].

Therefore, this study aimed to develop a simplified culture model free of animal-derived components. For this purpose, a collagen substrate and genetically modified dried fibroblasts overproducing EGF and HGF (drHDFn_EGF+HGF) were used along with EM. Dried fibroblasts form a biologically active layer containing extracellular matrix proteins and provide cell–ECM interactions that more closely resemble physiological conditions than standard plastic culture surfaces. Wencel et al. (2017) demonstrated that dried fibroblasts improved the C3A cell adhesion, supported albumin secretion, and stabilized hepatocyte function during short-term culture [265]. Unlike the organoid cultures described by Huch et al. and Garnier et al., the cells in the present study were maintained in a conventional two-dimensional culture system. As mentioned earlier, Numerous studies have shown that 2D culture conditions lead to a rapid loss of hepatocyte functions, impaired cell polarization, and hepatocyte dedifferentiation. In contrast, 3D culture systems preserve metabolic activity and hepatocyte phenotype more effectively (Godoy et al., 2013; Bell et al., 2016) [149], [151].

In the first stage of the experiment, it was demonstrated that culturing human hepatocytes in EM on a type I collagen substrate enabled transient cell proliferation. The cells underwent five passages, and their number increased nearly threefold (Table 4.8). At the same time, increased proliferation was accompanied by a gradual loss of hepatocyte function, as evidenced by reduced albumin production (Figure 4.53). In addition, the cells changed their morphology from the typical polygonal shape characteristic of hepatocytes to an elongated spindle-like fibroblastic morphology (Figure 4.52). As in the case of the hHDPCs, these observations may indicate the initiation of hepatocyte dedifferentiation and EMT-like transitions, processes that are associated with the loss of mature hepatocyte markers and increased proliferative activity (Kaimori et al., 2007; Meyer et al., 2013) [267], [268]. The results of this study are partially consistent with those of Garnier et al., who demonstrated that hepatocytes can dedifferentiate into a progenitor-like state under 3D organoid culture conditions. However, in contrast to their model, cell proliferation in the present study was temporary and ended with cell death after several passages. This finding may indicate the important role of the 3D microenvironment in maintaining the long-term proliferative potential of dedifferentiated hepatocytes.

Notably, interesting results were also observed in cultures grown on dried fibroblasts overproducing EGF and HGF. Despite previous reports by Wencel et al. (2017), who did not observe adhesion problems in short-term cultures using dried fibroblasts, in the present study, an increase in the hDHes number led to detachment of the cell layer along with the fibroblast substrate. This prevented long-term culture and limited the system to a single passage [265]. The observed detachment can be explained in terms of cell adhesion mechanics and traction force generation. Adherent cells maintain internal cytoskeletal tension resulting from actin–myosin activity regulated by the RhoA/ROCK pathway. This tension is transmitted to the substrate through integrins (Schierbaum et al., 2019; Bhadriraju et al., 2007) [323], [324]. In this system, cells act as active generators of mechanical forces that may exceed the mechanical strength of the dried fibroblast layer, leading to local adhesion loss or progressive detachment of the cell feeder layer (Guillot & Lecuit, 2013) [325]. Disruption of hepatocyte–extracellular matrix interactions affects both cell morphology and function (Bissell et al., 1987) [326], while changes in adhesion can modulate RhoA activity (Dohda et al., 2004) [327], a key regulator of cytoskeletal organization and cellular tension (Hall, 1998; Bhadriraju et al., 2007) [324], [328]. Therefore, layer detachment can be interpreted as a mismatch between active cellular forces and a mechanically unstable substrate. Although dried fibroblasts provide a biologically active extracellular matrix, they do not fully recreate a stable hepatocyte niche, particularly under long-term proliferative conditions. Unlike organized 3D systems or stable ECM scaffolds, the drHDFn layer may undergo mechanical destabilization during rapid hDHes expansion.

Additionally, comparative analysis of albumin secretion over 21 days showed lower albumin levels and a progressive decline with increasing hDHes proliferation in cultures grown in EM on drHDFn_EGF+HGF compared with collagen-based cultures. This suggests that dried fibroblast substrates may support short-term maintenance of hepatocyte function, but are mechanically and biologically insufficient for long-term preservation of the hepatocyte phenotype. These results highlight the important role of the extracellular matrix microenvironment in regulating hepatocyte function. In collagen-based cultures, the observed effects may result from more physiological cell–ECM interactions, whereas EGF and HGF signaling in the expansion medium may promote a shift toward a proliferative phenotype at the expense of metabolic function. According to the literature, excessive or uncontrolled activation of growth factor signaling pathways may destabilize the hepatocyte phenotype and promote dedifferentiation [329], [330].

It should also be noted that the actual concentrations of EGF and HGF present in dried fibroblasts were not controlled. In the drHDFn_EGF+HGF condition, the expansion medium

was not supplemented with exogenous EGF and HGF, unlike in collagen-based cultures. Hepatocytes are highly sensitive to mitogenic signals and can rapidly adapt to excess mitogenic signals, which, *in vitro,* may result in loss of phenotype and accelerated dedifferentiation. Consequently, excessive or unstable signaling may have contributed to the observed decline in cellular function. The literature indicates that EGF has a dual role: it stimulates hepatocyte proliferation (Kimura et al.; Liu et al., 2013) [331], [332] but also may promote dedifferentiation, loss of hepatocyte phenotype, and activation of EMT-related pathways (Pagan et al. 1997) [330]. These results highlight the importance of precise selection of microenvironmental conditions and control of growth factor signaling during hepatocyte culture.

In the second stage of the experiment, conducted exclusively on the collagen substrate, an attempt was made to maintain proliferation while restoring hepatocyte function using differentiation medium (DM). Despite three passages, stable redifferentiation was not achieved, and the cells eventually died. This failure may be attributed to several factors, including loss of culture continuity after the expansion phase (cells were frozen and then thawed for differentiation phase), mismatch between DM composition and the highly dedifferentiated state of the cells, and the use of a two-dimensional culture system, which, unlike spheroid and organoid models, does not provide an appropriate spatial microenvironment for redifferentiation (Huch et al., 2015; Garnier et al., 2018). In 3D systems described in the literature, both culture architecture and medium composition are carefully optimized to maintain a balance between proliferation and differentiation, which may be crucial for successful redifferentiation. Interestingly, the highest increase in the hDHes number was observed at passage +1, suggesting a transient state of high cellular plasticity.

It is possible that prolonged culture without further passaging could have supported partial redifferentiation and reacquisition of hepatocyte features, similar to observations in organoid systems described by Garnier et al. and Huch et al.

The experiment demonstrated that cell expansion can be initiated and sustained without the need for organoid formation. These findings suggest that organoid formation is not a prerequisite for the expansion phase, thereby simplifying the culture workflow and potentially reducing the time and resources required for cell propagation.

5.4.10 Comparative Analysis of Tumor Models of Hepatocytes

In this work, four liver cancer-derived cell lines commonly used as hepatocyte models in research and for drug testing were compared. The analyzed lines originated from two types of liver cancer: HepG2 and C3A derived from hepatoblastoma (HB) [200], [208], and SNU449 and SNU475 representing hepatocellular carcinoma (HCC) [333], [334]. Morphological, phenotypic, and metabolic changes were analyzed during culture, together with differences in protein and mRNA expression between the cell lines. The results revealed relevant phenotypic differences between the HB- and the HCC-derived lines, which can influence their selection for specific research and medical applications.

The C3A cells exhibited the highest proliferation rate among all analyzed lines, whereas the SNU475 cells showed the slowest growth *ex vivo* (Figure 4.57). Morphological analysis confirmed further differences. C3A and HepG2 cells formed relatively small cell islands with less flattened morphology. In contrast, both SNU cell lines formed a more homogeneous monolayer composed of larger, highly flattened cells (Figure 4.60). The presence of apical vacuoles, especially in the C3A cells, was also observed. These structures were absent in both SNU449 and SNU475 cells (Figure 4.63). The absence of AVs in SNU449 and SNU475 suggests a loss of mature hepatocyte characteristics, especially those connected to cell membrane polarization. These results may indicate that HCC-derived cell lines exhibit a more mesenchymal phenotype, whereas HB-derived cell lines exhibit rather epithelial features. This is consistent with the literature data, where, for example, Nguyen et al. (2022) describe SNU475 cells as highly invasive and characterized by dynamic cytoskeletal reorganization, consistent with a morphology involving increased cell spreading and, consequently, a more mesenchymal characteristic [334].

In contrast, Oz et al. (2021) demonstrated that the HepG2 cells exhibit an epithelial phenotype, form compact organoids, maintain strong intercellular connections, and exhibit limited migration and invasion capacity. This phenotype indicates lower tumor aggressiveness and greater similarity to normal liver tissue. The SNU449 cells, on the other hand, exhibit a mesenchymal phenotype, with cells forming loose, irregular structures, easily separating from each other, and demonstrating high migration and invasion capacity. The presence of these features indicates activation of the EMT process and greater tumor aggressiveness. The SNU475 line exhibits intermediate features between epithelial and mesenchymal phenotypes, forming partially ordered structures and demonstrating moderate migration capacity. This suggests partial EMT and high plasticity of these cancer cells [333].

Additional confirmation of the more differentiated phenotype of C3A and HepG2 cells provided analysis of albumin secretion, which revealed the highest secretory activity in the C3A cells, slightly lower in the HepG2, very low in the SNU449, and practically undetectable in the SNU475. This also confirms the results obtained from mRNA and WB analysis and indicates that C3A and HepG2 demonstrate significantly better preservation of liver function than SNU lines. These observations correspond to the division of HCC lines into epithelial and mesenchymal phenotypes described in the literature. Fuchs et al. (2008) demonstrated that SNU449 and SNU475 cells with mesenchymal features exhibit greater resistance to EGFR inhibitors compared to cells with a more epithelial phenotype. In contrast, the HepG2 cell line, characterized by epithelial features, is more sensitive to the applied treatment [335]. However, it should be noted that this line is currently considered a model of hepatoblastoma rather than classic HCC [208]. Nwosu et al. (2018) demonstrated that liver cancer cell lines are not biologically equivalent and differ in their metabolic profiles of human tumors. Lines with an epithelial phenotype, such as HepG2, Huh7, and Hep3B, exhibit a more hepatocyte-like metabolic gene expression profile and better resemble well-differentiated liver tumors. In contrast, lines with a mesenchymal phenotype, such as SNU449, show reduced expression of hepatocyte-associated metabolic genes and present a more immature, dedifferentiated profile, consistent with more aggressive and metastatic forms of liver cancer. The authors emphasize that EMT is associated not only with changes in cell migration and invasiveness but also with significant metabolic reprogramming. Consequently, the choice of cell line is crucial for the interpretation of liver cancer research results and should reflect the specific biological type of the tumor [336].

An interesting observation was the highest metabolic activity per cell in the SNU475 line, despite virtually no proliferation. This indicates that high metabolic activity does not necessarily correlate with active proliferation or preserved hepatocyte function.

Differences between the cell lines were also observed in HNF4α expression. The highest protein levels were detected in the HepG2 cells, slightly lower in the C3A, while expression was very low and comparable in both SNU lines. HNF4α plays a key role in maintaining the hepatocyte transcriptional program, regulating genes involved in metabolism, cell polarity, and secretory functions. Reduced HNF4α expression in SNU449 and SNU475 correlates with the absence of albumin expression, loss of apical vacuole structures, and undetectable CYP3A4 levels. The higher HNF4α expression in the HepG2 compared with the C3A may suggest a stronger maintenance of hepatocyte-related transcriptional regulation, despite the C3A showing more developed secretory activity.

Significant differences in CYP3A4 expression were also observed. The highest protein level among the analyzed lines was detected in the C3A cells, followed by HepG2. However, expression remained low compared with the hHs. The protein was undetectable in both SNU lines. CYP3A4 is one of the main drug-metabolizing enzymes in hepatocytes; therefore, higher expression in C3A suggests relatively better preservation of detoxification-related functions compared with HepG2. This is in line with previous reports indicating that C3A, as a HepG2 subclone, was selected for a more hepatocyte-like phenotype and higher functional activity [203]. The absence of CYP3A4 in the SNU lines further confirms the loss of classical hepatocyte functions in these cells.

Another observation was the lack of detectable CYP2E1 and CYP2C8 protein expression in all analyzed lines, despite the presence of mRNA, particularly for *CYP2E1* and *CYP2C8* in SNU449. This suggests that these genes may be subject to post-transcriptional or translational regulation. It is also possible that protein levels were below the detection threshold of the method used. The discrepancy between mRNA and protein levels may be biologically relevant, as it indicates that transcript abundance does not always directly reflect functional protein expression. In the case of SNU449, the combination of high *CYP2E1* and *CYP2C8* mRNA levels with the absence of detectable protein may indicate partial preservation of transcriptional activity related to hepatocyte metabolism, together with impaired translation or protein stability.

Interesting results were obtained for urea cycle-related genes *ARG1* and *CPS1*. mRNA analysis showed the highest *ARG1* expression in HepG2 cells, low levels in C3A and SNU475, and very low levels in SNU449. *CPS1* expression was highest in SNU449, low in C3A and HepG2, and undetectable in SNU475. In hepatocytes, both proteins are typically highly expressed, whereas in the analyzed cancer cell lines, despite detectable transcripts, ARG1 and CPS1 proteins were not observed in any line.

ARG1 and CPS1 are key enzymes of the urea cycle and are considered markers of mature hepatocytes. However, in both HB and HCC-derived lines, their expression is frequently dysregulated at multiple regulatory levels, which is also supported by literature data (Missiaen et al., 2022) [337]. More detailed results concerning *CPS1* and *ARG1* expression and their analysis are discussed in the subsequent sections.

When comparing mRNA expression with protein levels, the particularly notable finding was the high *CPS1* and *CYP2E1* mRNA expression in SNU449, combined with the absence of detectable hepatocyte-specific proteins such as albumin, CYP3A4, ARG1, or CPS1. These results suggest that SNU449 may retain parts of a transcriptional program related to

mitochondrial and nitrogen metabolism, but without full translation into a functional hepatocyte phenotype. This may reflect metabolic reprogramming characteristic of aggressive HCC, where selected pathways remain transcriptionally active but are not efficiently translated into functional proteins. The lack of detectable CPS1 and ARG1 protein in all analyzed lines further indicates that even more hepatocyte-like models, such as C3A and HepG2, do not fully reproduce mature hepatocyte metabolism *in vitro*. This highlights the limitations of classical hepatoblastoma and HCC-derived models in studying liver metabolic functions and suggests caution when interpreting results based solely on mRNA expression.

Taken together, these results indicate that C3A and HepG2 retain a more mature and functional hepatocyte-like phenotype, whereas SNU449 and especially SNU475 exhibit a more dedifferentiated, mesenchymal phenotype of HCC. This has important implications for model selection: C3A and HepG2 appear more suitable for studies of hepatocyte function, metabolism, and hepatotoxicity, while SNU449 and SNU475 may better represent aggressive, poorly differentiated hepatocellular carcinoma and processes associated with EMT, migration, and therapy resistance [202].

5.4.11 Dynamic Culture System

Bioartificial liver (BAL) support systems represent a promising therapeutic approach for the alternative treatment of liver failure, but their development is still limited by the availability and functionality of suitable cell sources. In this work, I constructed a simplified BAL model using a hollow-fiber bioreactor incorporating hHDPCs as an alternative cell source. This enabled the evaluation of these cells under dynamic conditions that better reflect the hepatocyte *in vivo* environment.

In such systems, membranes play a key role not only as a physical scaffold for cells but also as selective barriers regulating the transport of oxygen, CO_2, nutrients, and metabolites. Previous studies have shown that membrane properties, particularly pore size and distribution, significantly affect mass transfer efficiency and cell behavior, including proliferation and metabolic activity [338], [339], [340]. The physicochemical properties of the membrane surface are also important determinants of cell–substrate interactions. Surface modifications, especially changes in hydrophilicity, can influence cell adhesion and organization [341]. For example, Wei et al. demonstrated that mouse fibroblasts exhibited greater adhesion on materials with higher wettability [342]. These findings suggest that both the membrane's structural characteristics and its surface properties may affect the functionality of the cell source used in

the BAL model. This highlights the importance of carefully selecting bioreactor components when designing liver support systems.

For the purpose of the current bioreactor model by characterizing polysulfone hollow-fiber membranes obtained from Vestergaard-Frandsen. SEM analysis confirmed the porous structure of the membrane surfaces, while cross-sectional imaging revealed heterogeneous pore sizes. This enabled the exchange of substances between cells cultured on the outer membrane surface and the culture medium flowing inside the capillaries. The measurements also confirmed that the pore size was consistent with the manufacturer's declared value of 0.2 μm and that the membrane exhibited hydrophilic properties. Ultrafiltration measurements performed one week apart showed a decrease in membrane performance after storage in distilled water. This may have resulted from biofilm formation or the adsorption of environmental contaminants. Since distilled water is not sterile, microbial contamination of the membrane surface could occur. Previous studies on polysulfone ultrafiltration membranes have shown that reductions in filtration flux are primarily associated with adsorption and biological fouling, whereas structural changes of the material, such as swelling in water, have only a minor effect [343], [344], [345]. The retention results indicated a distinct separation threshold in the range of approximately 150–200 nm, consistent with the nominal membrane pore size of 0.2 μm. Particles with a diameter of 100 nm were not retained, whereas retention of 200 nm particles increased to 97%, indicating a sharp transition between permeating and retained fractions. Larger particles (500 nm and 2–3 μm) were completely retained. These results indicate that the membrane enables efficient mass exchange while preventing cell penetration into the capillary lumen.

Moreover, the membrane intended for cell culture must be non-toxic to cells. Therefore, the C3A_EGFP cells were cultured under three experimental conditions: standard monolayer culture, culture in conditioned medium, and culture on capillary membranes. The results showed that culture on capillaries increased cellular metabolic activity compared with the control conditions, while maintaining very high cell viability. Furthermore, culture on capillary membranes enhanced cellular function, as indicated by increased albumin secretion. Taken together, these findings indicate that the membrane is suitable for cell culture. Its properties suggest it may support cell growth and function by enabling efficient mass exchange, promoting improved cell adhesion, and lacking cytotoxic effects.

After characterizing the membrane, I prepared hollow-fiber bioreactors and conducted cell cultures under dynamic conditions. Post-culture medium samples were collected to determine albumin and urea concentrations. All cell types were cultured in the same

hepatocyte-dedicated medium (HM+HGS) supplemented with 2% FBS and exposed to identical flow conditions. In our previous BAL model, the C3A cells and their genetically modified derivatives were cultured under dynamic conditions [346]. We have shown that these conditions led to increased albumin production compared with monolayer culture conducted under static conditions. In the current model, different cell types were evaluated under static and dynamic culture conditions.

The obtained values for the albumin secretion ratio under dynamic and static conditions (Figure 4.73) indicate clear differences in cellular responses to mechanical stimuli generated by culture medium flow. The lowest value of this parameter was observed for the HepG2 cell line, suggesting limited sensitivity of these cells to dynamic culture conditions and a reduced ability to adapt their secretory function to enhanced mass transfer and the low but measurable shear stress present in the system. Shear stress is a mechanical force acting parallel to the cell surface and is generated by fluid flow over cells. Under physiological conditions, it occurs naturally within hepatic blood vessels and serves as an important regulator of hepatocyte function. Literature data have shown that shear stress influences hepatocyte metabolism and promotes the maintenance of its liver-specific functions [347], [348]. Consequently, dynamic culture conditions may support the preservation or restoration of a more physiological cellular phenotype, resulting in increased secretion of liver-specific proteins, including albumin.

In studies of Pallakan et al. (2013), hollow-fiber bioreactors have shown that HepG2 cells respond to dynamic culture conditions by increasing metabolic activity, including glucose consumption and ammonia detoxification. However, the effects on secretory functions such as albumin and urea production appear to be more variable and strongly dependent on flow parameters and bioreactor design [349]. Jakubowska et al. demonstrated that increasing flow rates in cultures of C3A cells enhanced both albumin and urea secretion [346].

The comparison of the HepG2 cultures grown in two media (DMEM and HM+HGS) suggests that DMEM supports higher metabolic activity, potentially leading to increased protein synthesis, including albumin production. In contrast, HM+HGS appears to limit the metabolic activity of HepG2 cells, resulting in lower albumin secretion (Figure 4.74). Under dynamic conditions, this difference became even more pronounced, as reflected by higher Dyn/Stat ratios in cells cultured in DMEM. This effect may result from the combined influence of elevated metabolic activity and improved mass transport under perfusion conditions. Therefore, the higher albumin production observed in DMEM may not necessarily reflect a more physiological hepatocyte phenotype but could instead be associated with the increased metabolic activity characteristic of cancer-derived cell lines.

In the case of the hH_4 cells, intermediate Dyn/Stat values were observed. This may indicate a partial preservation of the physiological response to flow stimulation and suggest that the applied culture conditions did not fully support the functional response of these cells. In contrast, the LCI samples exhibited a heterogeneous response [LCI(H69) < hHs < LCI(H72)], which may reflect differences in the initial hepatocyte content of the isolates and variations in cell maturity and functionality within this group (Figure 4.73). Tilles et al. demonstrated using a microchannel flat-plate bioreactor that hepatocyte functions, including albumin and urea synthesis, are strongly influenced by flow conditions and shear stress. Moderate perfusion enhanced these functions, whereas excessive shear stress reduced them [347]. Similarly, Abu-Absi et al. showed that hepatocytes cultured in hollow-fiber perfusion systems maintained stable albumin and urea production over extended culture periods while preserving liver-specific functions [350]. Experiments conducted using hepatocytes from different donors demonstrated significant variability in cellular responses to the dynamic culture conditions (Figure 4.75). In samples hH_4 and hH_5, albumin secretion increased under flow conditions, with this effect being particularly pronounced in the hH_4. In contrast, no significant differences between dynamic and static conditions were observed for sample hH_3. These findings indicate substantial interindividual variability among hepatocytes, which may result from differences in cellular functional status, maturity, expression of hepatocyte-specific genes, or sensitivity to mechanical stimuli. The lack of response observed in the hH_3 may be associated with limited mechanosensitivity of the cells and a high basal albumin production rate under static conditions. These results emphasize the importance of donor selection and cell source characterization in dynamic culture studies and suggest that the effects associated with enhanced mass exchange may depend strongly on donor-specific characteristics as well as the cells' condition.

Notably, the highest Dyn/Stat values were observed for the hHDPCs, suggesting a pronounced response of these cells to dynamic culture conditions and an increased capacity for albumin secretion under medium flow conditions. Interestingly, the near-undetectable levels of albumin observed in static hHDPCs cultures indicate a loss or substantial weakening of the hepatocyte-like phenotype under conventional 2D culture conditions, as discussed previously in this work. Under dynamic conditions, where medium flow promotes rapid mass exchange, increased albumin secretion was observed. Nevertheless, it should be emphasized that albumin levels remained comparable to the blank control during the initial culture period and exceeded background levels only at later time points. Therefore, the observed effect was not immediate

but developed progressively during culture under flow conditions. These findings may indicate a partial restoration of hepatocyte-specific functions in all hHDPCs samples tested.

Dynamic conditions promoted not only increased albumin secretion but also enhanced urea synthesis, confirming their positive effect on hepatocyte metabolic function. Urea production was observed in all analyzed cell types; however, the magnitude of the response to flow conditions varied. Again, the highest Dyn/Stat values, together with an increasing trend over time, were observed in the hHDPCs, indicating their ability to adapt to dynamic conditions and progressively enhance their metabolic activity. HepG2 and hHs cells exhibited an intermediate response, whereas differences were observed between LCI samples, with LCI(H72) showing higher activity than LCI(H69). These findings suggest that enhanced mass exchange under dynamic conditions not only stimulates hepatocyte function but may also support the long-term stabilization and development of metabolic activity. However, this effect appears to depend strongly on cell type and cellular condition.

Despite the observed production of urea by the HepG2 cells, WB analysis did not reveal the presence of key urea cycle enzymes, including CPS1 and ARG1, which were readily detectable in hHs. This apparent discrepancy suggests that the detected urea may result from residual urea cycle activity, although the corresponding proteins could not be detected by WB because their levels were below the assay's detection limit, or from alternative pathways of nitrogen metabolism. Impairment of the urea cycle does not necessarily indicate a complete loss of function, as even low levels of enzymatic activity may result in measurable urea production. Additionally, alternative metabolic pathways may contribute to partial ammonia detoxification. These observations are consistent with the literature, reports indicating impaired ammonia detoxification in the HepG2 cells compared with primary hepatocytes due to reduced expression of urea cycle enzymes, particularly OTC and ARG1. Mavri-Damelin et al. (2007) demonstrated that genetic restoration of the missing enzymes partially recovered urea cycle activity in the HepG2 cells. However, the efficiency of the restored pathway remained lower than that observed in primary hepatocytes, reflecting the neoplastic origin and altered metabolism of these cells [351]]. Similarly, Jakubowska et al. (2024) showed that the C3A cells possess an inefficient urea cycle and limited ammonia detoxification capacity. Restoration of OTC and ARG1 expression significantly improved urea cycle function, and this effect was further enhanced under dynamic culture conditions in a hollow-fiber BAL model [346]. In the HepG2 cells, ammonia detoxification relies less on the urea cycle than in primary hepatocytes. Choi et al. (2000) demonstrated that the HepG2 cells preferentially detoxify ammonia through

glutamine synthesis rather than through the urea cycle. Consequently, ammonia is incorporated into glutamine, which can subsequently be utilized in cellular biosynthetic processes [352].

A similar discrepancy between enzyme detection and urea production was also observed in the hHDPCs. Although CPS1 and ARG1 proteins were not detected by WB analysis, an increase in urea production was observed under dynamic culture conditions. In addition to the hypothesis that the hHDPCs retain low levels of urea cycle activity, suggesting residual but functional nitrogen metabolism, alternative mechanisms should also be considered. Several processes described in the literature may contribute to apparent urea production independently of a fully functional urea cycle. One possible explanation is extracellular arginase activity resulting from the release of ARG1 into the culture medium. Peters et al. (2008) demonstrated that primary hepatocytes and liver slices can release active arginase into the culture supernatant, leading to the extracellular conversion of arginine into urea independently of intracellular ureagenesis. The authors emphasized that the presence of urea in the medium does not necessarily reflect active urea cycle function within hepatocytes [353]. Another potential mechanism involves arginase 2 (ARG2), a mitochondrial enzyme that catalyzes the conversion of arginine into ornithine and urea independently of the canonical hepatic urea cycle. Zhang et al. (2024) demonstrated that ARG2 contributes to mitochondrial arginine metabolism and can influence nitrogen handling and oxidative metabolism even when the activity of other urea cycle enzymes is limited [354]. This mechanism may partially explain the increase in urea concentration observed in the hHDPCs cultures. Although the manufacturer of the HM medium does not disclose its complete formulation, the medium, according to the report, contains amino acids essential for cell survival, including arginine, which may serve as a substrate for ARG2-mediated urea production. Therefore, the increased urea concentration observed during the hHDPCs culture may result from one or more of the mechanisms discussed above, including residual ureagenesis, extracellular arginase activity, or ARG2-dependent arginine metabolism. Consequently, the exact source of urea produced by the hHDPCs remains unclear and requires further investigation. The most reliable method for assessing true urea cycle activity is the use of stable nitrogen isotopes, such as $^{15}NH4+$, which allow direct tracking of ammonium incorporation into urea. This approach was used, among others, by Lee et al. (2000), who evaluated urea cycle function by measuring the formation of ^{15}N-labeled urea, a direct marker of ureagenesis [355]. However, this aspect was not investigated in the present study.

The obtained results demonstrate that the hHDPCs exhibit substantial donor-dependent functional heterogeneity in both albumin secretion and urea production. While most samples showed a relatively coordinated increase in both functional parameters over time, sample

hHDPCs(H72) displayed a distinct phenotype characterized by reduced albumin secretion and markedly elevated urea production. These findings suggest that the transitional cellular state is associated with an altered balance between synthetic and metabolic functions, reflecting partial decoupling of hepatocyte-specific activities. Overall, urea production appears to be more sensitive to donor-specific and temporal variability than albumin secretion, highlighting the functional plasticity of hepatocyte-derived cells under in vitro conditions.

The beneficial effects of dynamic culture conditions are likely due to complex changes in the cellular microenvironment. Medium flow improves mass transport, enhances oxygen and nutrient availability, facilitates metabolite removal, and stabilizes local concentration gradients. In addition, dynamic culture modulates cell–matrix interactions and activates mechanotransduction pathways. Therefore, the observed enhancement of hepatocyte function under dynamic conditions should be interpreted as the combined effect of multiple physicochemical factors acting simultaneously.

Taken together, these findings suggest that flow conditions provide an important functional stimulus for cells exhibiting a more physiological hepatocyte-like phenotype. Among the analyzed cell populations, hHDPCs showed the strongest functional response to enhanced.

6 Conclusions

A modified original liver cell isolation protocol developed at Laboratory of Tissue Engineering IBBE PAS, based on mechanical tissue fragmentation and enzymatic digestion, enabled the efficient recovery of a broad spectrum of liver cell populations, including hepatocytes. Compared with the gold-standard two-step collagenase perfusion method, the developed approach is faster, less expensive, and technically less demanding. However, its application is limited to relatively small liver tissue fragments that do not require vascular perfusion. Efficient cell isolation resulted in the generation of high-quality biological material characterized by high viability, enabling the establishment of adherent cell cultures. A tendency toward higher isolation efficiency was observed in samples from male donors, whereas lower cell viability was observed in samples derived from female donors. These observations may indicate a potential influence of donor sex on hepatocyte isolation outcomes. Based on the results obtained under the different culture conditions, HM supplemented with HGS was selected as the most suitable medium for subsequent cell culture experiments. An important stage of the study involved the isolation of cells forming characteristic cell islands. Notably, cell islands were most frequently observed in cultures established from isolations preformed using collagenase II or D. The use of various analytical techniques confirmed that hepatocytes were present within the isolated liver cell population and that these very ones formed cellular islands. The isolated hepatocytes secreted albumin into the culture medium, further indicating their good viability following isolation. In addition to albumin, the presence of other hepatocyte-specific proteins, such as A1AT, HNF4α, and CYP3A4, was also demonstrated. Interestingly, protein and mRNA expression levels varied between donors, indicating that both differences among donors and the coexistence of different pathological conditions may influence the condition of the cells after isolation. Following isolation and *ex vivo*, hepatocytes underwent rapid dedifferentiation, accompanied by the loss of specialized hepatic functions and the acquisition of proliferative capacity, what became the basis for the establishment of a new hepatocyte-derived cell line. The characterization of these cells therefore became a central objective of the present study.

The newly obtained cell population was designated as human Hepatocyte-Derived Proliferating Cells (hHDPCs). The inability of the hHDPCs to form apical vacuoles indicates a loss of cell polarity, a feature that has also been reported in commercially available hepatocytes (hHs). In contrast, tumor C3A cells showed a well-defined polarized organization characteristic of epithelial cell lines. One of the most important features of the hHDPCs phenotype is the

maintenance of selected hepatocyte-associated markers despite extensive passaging. Notably, hHDPCs retain proliferative capacity for approximately 12 consecutive passages while preserving the expression of ALB and CK18 and maintaining detectable levels of HNF4A and HNF1A proteins. The sustained production of ALB and CK18 is particularly significant because primary hepatocytes cultured under conventional two-dimensional conditions typically lose these markers rapidly and undergo progressive dedifferentiation or degeneration. The absence of CK19 expression, together with only trace levels of AFP, suggests that the hHDPCs do not undergo complete conversion toward either a progenitor-like or cholangiocyte-like phenotype. Furthermore, the continued activity of HNF4A and HNF1A indicates partial preservation of the hepatocyte-specific regulatory network. However, the characteristics of the detected proteins suggest functional alterations. HNF4A was predominantly localized in the cytoplasm rather than in the nucleus, which may indicate impaired transcriptional activity. In addition, differences observed in the Western blot profile of HNF1A between hHDPCs and primary human hepatocytes may reflect the loss of post-translational modifications characteristic of the mature state of hepatocyte. A relatively low level of the cell proliferation marker Ki67 was observed in the hHDPCs, which generally exhibit a high proliferative capacity. This finding may indicate heterogeneity within the hHDPCs population, which simultaneously exhibits both cell cycle synchronization and asynchrony. It may also suggest a transitional state of the hHDPCs characteristic of liver regeneration process. Another factor observed in the hHDPCs confirming their regenerative status was the presence of VIM, whose expression level was increased compared with the hHs, where it is not expressed. Furthermore, the presence of VIM in differentiating hHDPCs may indicate the initiation of cytoskeletal reorganization and partial EMT, together contributing to a transitional state characteristic of the regenerating liver. The obtained results demonstrated significant differences in metabolic activity between the studied cell types (HepG2, hHDPCs, HDFn) and culture conditions (DMEM, HM+HGS), while maintaining high viability across all experimental groups. This indicates that the observed changes primarily reflected alterations in cellular metabolism rather than differences in cell survival. The hHDPCs exhibited the highest metabolic activity, whereas the HepG2 cells showed a preference for high-glucose conditions, consistent with their cancerous phenotype and enhanced glycolytic metabolism. At the same time, the reduced metabolic activity of the hHDPCs under HM+HGS conditions, despite increased cell number, and the reduced glucose consumption per cell, suggest a shift toward more physiological and energy-efficient oxidative metabolic pathways. Compared to other cell models, the hHDPCs exhibit an intermediate phenotype: they are more metabolically sensitive than the HDFn, which

are characterized by high plasticity but do not exhibit the constitutively high glycolytic activity typical of the HepG2 cells. This suggests that the hHDPCs best reflect a more physiological yet sensitive metabolic profile dependent on the culture environment. A key observation during the hHDPCs characterization was that, unlike the HepG2 cells, albumin was not detected in the post-culture medium of the hHDPCs, despite its intracellular presence being confirmed by several tests. This suggests phenotypic changes occurring in the hHDPCs during dedifferentiation in culture, which may indicate an impaired albumin secretion pathway and, consequently, a partial loss of hepatocytic functions.

The developed hHDPCs' performance demonstrated that both culture medium composition and cell passage number significantly influence their proliferation rate and metabolism. Cells at early passages were characterized by higher proliferative activity, greater functional stability, and better adaptation to culture conditions compared with cells at higher passages. With increasing passage number, a decrease in proliferative capacity and metabolic alterations indicative of progressive cellular senescence were observed. High glucose concentrations did not improve the hHDPCs growth and, in late-passage cells, led to reduced cell number and viability. Moreover, excess glucose may exert metabolic stress and disrupt metabolic homeostasis. The most favorable culture conditions were provided by HM+HGS medium, which supported the maintenance of a more physiological metabolic profile and high proliferative efficiency. These results indicate that the hHDPCs exhibit hepatocyte-like characteristics, including sensitivity to hyperglycemic conditions, and that their functional potential is highest in early culture passages. Based on studies of isolated hepatocytes isolated from human liver fragments, HM+HGS medium was selected as the optimal culture condition, as it provided the most suitable environment for cell maintenance. This medium was also selected for the hHDPCs, further supporting the hypothesis of their hepatocyte-derived origin. Supplementation of the culture medium with HGS enhances the proliferation and survival of hHDPCs; however, its effectiveness depends on both medium composition and cell passage number. The strongest effect was observed in HM+HGS medium, particularly in low-passage cells, indicating a synergistic effect between growth factors present in HGS and physiological glucose conditions. As passage number increased, the effect of HGS gradually decreased, suggesting a progressive loss of cellular responsiveness to proliferative signals due to senescence. Overall, the results confirmed that maintaining hepatocyte-like properties of the hHDPCs requires both appropriate supplementation and optimal metabolic culture conditions.

Despite a clear shift away from the mature hepatocyte phenotype, the hHDPCs retained several characteristics indicative of partial hepatocyte identity. During long-term culture, the

hHDPCs exhibited a high proliferative capacity, with an average of approximately 50-fold increase in cell number over 12 passages. The cells displayed both clonal growth, evidenced by the division of progeny from a single parental cell, and the ability to form cell islands. Furthermore, some cells within these islands retained proliferative activity, whereas others remained non-proliferative. Despite a gradual decline in proliferative activity in subsequent passages, both cell types retained certain hepatocyte characteristics, including albumin expression, while lacking markers of progenitor cells. These results suggest that hHDPCs constitute a distinct cell population with the capacity for long-term proliferation and partial preservation of hepatocyte functions, and that their properties depend on both culture duration and individual donor characteristics. The acquisition of proliferative capacity by hepatocytes is a characteristic feature of liver regeneration and further supports the notion that the newly established hHDPCs represent a transitional cellular state.

Another characteristic feature of hHDPCs is the dynamic variability of marker expression across successive passages. Fluctuations were observed in the expression of hepatocyte-specific markers, as well as in non-hepatocyte-associated markers, including VIM, CD44, CD29, CD73, and, in some cases, CD133 and CD34. These changes did not follow a linear pattern. Neither a progressive loss of hepatocyte-associated markers nor a sustained increase in mesenchymal or progenitor-associated markers was observed. Instead, the expression profiles suggest the existence of dynamic adaptive cellular states. Such variability may reflect a combination of cellular plasticity, partial EMT process, adaptive cytoskeletal remodeling, transient regenerative programs, and an unstable balance between hepatocyte-like and proliferation-associated phenotypes. Importantly, vimentin expression together with persistent CK18 expression and the absence of CK19 support the notion that hHDPCs undergo only partial EMT rather than complete fibroblastic conversion. This observation further supports the interpretation that hHDPCs occupy an intermediate phenotypic state characterized by substantial cellular plasticity.

Despite retaining the ability to synthesize albumin, hHDPCs did not efficiently secrete this protein into the culture medium, failed to form apical vacuoles, and exhibited predominantly cytoplasmic rather than nuclear localization of HNF4A. Together, these observations suggest a loss of hepatocyte polarization, impaired secretory activity, and partial disruption of the hepatocyte-specific transcriptional program. Furthermore, hHDPCs lacked detectable CPS1 and ARG1 expression and exhibited only very low levels of CYP3A4, suggesting impairment of selected metabolic and detoxification pathways characteristic of mature hepatocytes.

Attempts to redifferente toward a mature hepatocyte phenotype resulted in enhanced proliferation and a shift toward a more spindle-shaped morphology. This occurred despite supplementation with growth factors such as FGF-4, HGF, and EGF, which are commonly used to support hepatocyte maintenance and differentiation. These observations may suggest that, under stimulation conditions, hHDPCs derived from hepatocytes acquire a more fibroblast-like morphology. One possible explanation for this response is the absence of HGS supplementation in the HM medium. Since HGS contributes to the stabilization of hepatocyte culture conditions and phenotype, its removal may have facilitated further dedifferentiation and promoted progression toward a more adaptive proliferative state. Overall, the results indicate that hHDPCs do not redifferente toward hepatocyte-like cells under growth factor stimulation conditions.

Presented here is an alternative simplified model for the expansion and redifferentiation of commercially available human hepatocytes (hDHes) that was developed without the use of Matrigel or three-dimensional organoid culture systems. Two growth surfaces were evaluated: type I collagen and dried fibroblasts overexpressing EGF and HGF (drHDFn_EGF+HGF). Under EM medium and on collagen-coated surfaces, hepatocytes proliferated for five passages, achieving nearly a threefold increase in cell number. However, this process was accompanied by a gradual decline in albumin secretion and a morphological shift from a typical hepatocyte-like phenotype to a spindle-shaped morphology. This suggests dedifferentiation and a loss of functions characteristic of mature hepatocytes, which is also consistent with observations in hHDPCs. Attempts to redifferentiate the cells using DM medium did not result in a stable restoration of the hepatocyte phenotype or sustained proliferation. The results indicate that the expansion phase of hepatocytes may be initiated and maintained in 2D cultures without the need for organoid formation. In cultures grown on dried fibroblasts, impaired cell adhesion and the cell layer detachment were observed during periods of increased proliferation, limiting long-term culture stability. In addition, albumin secretion levels were lower than those observed in collagen-based cultures, suggesting insufficient support for the maintenance of hepatocyte-specific functions. Overall, these findings indicate that both the composition and the mechanical stability of the extracellular microenvironment are critical determinants of hepatocyte proliferation, differentiation, and functional maintenance. The results demonstrated that human hepatocytes can undergo transient proliferation in two-dimensional culture systems; however, this is accompanied by a progressive loss of the mature hepatocyte phenotype. The use of differentiation medium did not enable efficient or stable redifferentiation of the cells, highlighting the importance of appropriate spatial architecture and the cellular

microenvironment present in 3D organoid systems. Among the tested growth surfaces, type I collagen proved more suitable for maintaining hepatocyte functions than dried fibroblasts overproducing EGF and HGF. Although dried fibroblasts represent a potential alternative to Matrigel and reduce reliance on animal-derived matrices, their limited mechanical stability restricts their applicability for long-term culture. Despite these limitations, the developed system constitutes a simplified platform that may serve as a useful basis for further studies on hepatocyte proliferation, dedifferentiation, and phenotype stabilization.

A comparative analysis was performed on four liver-derived cancer cell lines, including HepG2 and C3A (hepatoblastoma-derived) and SNU449 and SNU475 (hepatocellular carcinoma, HCC). The results revealed clear phenotypic differences between hepatoblastoma-derived and HCC-derived cell lines. HepG2 and C3A cells exhibited a more differentiated, hepatocyte-like phenotype characterized by higher proliferative activity, the presence of apical structures, albumin secretion, and expression of HNF4α and CYP3A4. In contrast, SNU449 and SNU475 displayed a more mesenchymal, poorly differentiated phenotype associated with features consistent with epithelial–mesenchymal transition (EMT), loss of hepatocyte function, and a lack of expression of most hepatocyte-specific proteins analyzed. Accordingly, HepG2 and C3A cell lines may represent more suitable models for studies of hepatocyte function, hepatic metabolism, and hepatotoxicity. In contrast, SNU449 and SNU475 appear more appropriate for investigations of aggressive HCC phenotypes, including tumor progression, invasiveness, and treatment resistance. These findings emphasize the importance of selecting an appropriate in vitro model depending on the specific research question.

A simplified bioartificial liver (BAL) model was developed using a bioreactor with polysulfone capillaries and hHDPCs as an alternative cell source. One element of the bioreactor design was the characterization of polysulfone membrane capillaries and the assessment of their cytotoxicity. The obtained results showed that the membrane's pore size, pore size gradient, hydrophilic nature, and 97% retention of 0.2 μm particles are properties that favor cell culture. These characteristics facilitate efficient mass transfer through the membrane and enhance cell adhesion to its surface. Dynamic culture conditions in the BAL bioreactor enhanced cells' metabolic and secretory functions, likely through improved mass exchange and stimulation of mechano-transduction pathways. Among the cell populations analyzed (HepG2, hHs, and LCIs), the hHDPCs exhibited the greatest increase in albumin secretion and urea production, suggesting high sensitivity to flow conditions and potential functional similarities to primary hepatocytes. Moreover, the results suggest that dynamic culture conditions may promote the acquisition of a more hepatocyte-like phenotype by the hHDPCs. Under flow conditions,

albumin production in the culture medium increased over the course of cultivation, whereas in static cultures it remained at the limit of detection throughout the experiment. Furthermore, the hHDPCs derived from different donors exhibited distinct responses to the applied culture conditions, both in terms of albumin secretion and urea production. In particular, one donor-derived cell population showed a markedly different response, further supporting the donor-dependent nature of the hHDPCs behavior. These findings indicate that the hHDPCs may represent a promising cell source for bioartificial liver applications; however, the mechanisms underlying the observed increase in urea production require further investigation.

The main advantage of the hHDPCs over classical models such as the HepG2 cells or iPSC-derived hepatocyte-like cells may lie in their ability to retain a dynamic adaptive response, partial hepatocyte identity, and long-term proliferative capacity under dynamic culture conditions. Although the hHDPCs undergo dedifferentiation toward a fibroblast-like phenotype, they do not appear to undergo complete EMT. Moreover, the observed fluctuations in both positive and negative MSC-associated markers suggest that the hHDPCs do not represent a stable mesenchymal population, but rather occupy a transitional, plastic cellular state.

The major advantages of the hHDPCs model include its long-term proliferative capacity and the ability to maintain selected hepatocyte-associated characteristics during extended culture. The hHDPCs adapt efficiently to dynamic culture conditions, tolerate exposure to flow , and exhibit an active metabolic response under different experimental settings. Importantly, the cells retain expression of ALB, HNF4A, HNF1A, and CK18 despite partial loss of mature hepatocyte functions. The pronounced biological plasticity of the hHDPCs makes this model particularly useful for investigating transient hepatocyte states, cellular regeneration, loss and recovery of hepatocyte function, metabolic remodeling, cytoskeletal reorganization, and epithelial–mesenchymal plasticity during dedifferentiation. At the same time, several limitations should be acknowledged. These include incomplete metabolic maturation, impaired albumin secretion, loss of hepatocyte polarization, and phenotypic variability, as fluctuations in marker expression may complicate experimental standardization and reproducibility. The obtained data suggest that hHDPCs represent a population of hepatocyte-derived cells that can adapt to long-term in vitro culture conditions. These cells appear to adopt a regenerative-adaptive state characterized by considerable metabolic and phenotypic plasticity. Their phenotype does not fully correspond to either mature hepatocytes, classical hepatic progenitor cells, or fibroblast-like cells. Instead, the hHDPCs appear to represent a transitional cellular

state characteristic of liver regeneration, which retains selected hepatocyte-associated features while simultaneously exhibiting adaptive responses to long-term culture.

A significant advantage of the hHDPCs is their ability to divide, thereby increasing cell availability. In contrast, hepatocytes exhibit limited ex *vivo* proliferation and rapidly lose their essential functions. The obtained results suggest that the simultaneous proliferative activity of the hHDPCs, while maintaining part of essential hepatocyte function, makes them a promising source of cells that can replace hepatocytes in such applications as BALs.

Based on their biological characteristics, the hHDPCs may constitute a valuable model for studies of cellular adaptation to *in vitro* culture, the effects of perfusion and mechanical stimulation on cell behavior, and mechanisms involved in stabilization of the hepatocyte phenotype. Furthermore, they may be useful for investigating liver regeneration, tissue remodeling, loss and recovery of hepatocyte function, epithelial–mesenchymal plasticity, and alterations in nitrogen and glucose metabolism.

Because the hHDPCs can be derived from individual donors and the obtained results demonstrated donor-dependent differences in cellular responses, they may provide a valuable platform for the development of patient-specific *in vitro* models, for example hepatotoxicity test of new drugs. Such systems could support future studies aimed at investigating inter-individual variability in cellular behavior, disease mechanisms, and therapeutic susceptibility, thereby contributing to the advancement of personalized medicine approaches.

Final Thoughts

A modification of the liver cell isolation method developed at LTE IBBE PAS enabled the production of high-quality biological material suitable for, among other applications, adherent cell cultures. However, the obtained biological material exhibited considerable variability during culture, which depended on donor-specific characteristics, isolation conditions, and culture conditions. Nevertheless, the isolated cells demonstrated proliferative potential while partially retaining hepatocyte-specific functions. These findings confirm the first hypothesis of this study, demonstrating that it is possible to establish culture conditions for isolated hepatocytes that enable cell proliferation while preserving key hepatocyte functions.

The cells selected based on their proliferative capacity, designed as human Hepatocyte-Derived Proliferating Cells (hHDPCs), represent a unique, long-term proliferating population of hepatocyte-like cells that retains partial hepatocyte identity while simultaneously undergoing extensive adaptive plasticity and metabolic remodeling. This phenotype corresponds neither to mature hepatocytes nor to classical progenitor cells; rather, it resembles regenerative hepatocytes adapting to *in vitro* culture conditions and a dynamic perfusion environment. It should be emphasized that hHDPCs are dedifferentiated cells of hepatocyte origin that have lost some of their characteristic hepatocyte features. Therefore, further studies are required to better characterize these cells and to identify strategies for stabilizing their phenotype, which could improve the reproducibility of experimental outcomes. Despite these limitations, the hHDPCs appear to represent a promising source of hepatocyte replacement cells.

The hHDPCs demonstrated improved metabolic performance under flow conditions, thereby supporting the second hypothesis of this doctoral thesis. Owing to their ability to proliferate, survive long-term, and partially preserve hepatocyte-specific functions, these cells may constitute a novel source of functional biological material for bioartificial liver systems. Furthermore, they provide a valuable model for studying liver regeneration and hepatocyte adaptation to both two-dimensional and three-dimensional culture environments.

7 References

[1] L. M. Biga *et al*, *Anatomy & Physiology* , 1st ed. Corvallis, OR : OpenStax/Oregon State University , 2019.

[2] A. D. J. P. Claude Couinaud, *Surgical anatomy of the liver revisited*. Paris: Paris, 1989.

[3] K. H. Liau, L. H. Blumgart, and R. P. DeMatteo, 'Segment-oriented approach to liver resection', *Surgical Clinics of North America*, vol. 84, no. 2, pp. 543–561, 2004, doi: 10.1016/j.suc.2003.12.003.

[4] A. Özkan *et al.*, 'The influence of chronic liver diseases on hepatic vasculature: A liver-on-a-chip review', *Micromachines (Basel).*, vol. 11, no. 5, 2020, doi: 10.3390/MI11050487.

[5] D. Chambers, C. Huang, and G. Matthews, 'Liver Function', in *Basic Physiology for Anaesthetists*, Cambridge University Press, 2019, ch. 66, pp. 299–306. doi: 10.1017/9781108565011.069.

[6] E. L. LeCluyse, R. P. Witek, M. E. Andersen, and M. J. Powers, 'Organotypic liver culture models: Meeting current challenges in toxicity testing', *Crit. Rev. Toxicol.*, vol. 42, no. 6, pp. 501–548, Jul. 2012, doi: 10.3109/10408444.2012.682115.

[7] T. Xiao, Z. Jin, J. Deng, and W. Meng, 'Liver regeneration: cytokine regulation targeting hepatocytes and beyond', *Life Medicine*, vol. 5, no. 1, pp. 1–46, Jan. 2026, doi: 10.1093/lifemedi/lnag004.

[8] R. Panday, C. P. Monckton, and S. R. Khetani, 'The Role of Liver Zonation in Physiology, Regeneration, and Disease', *Semin. Liver Dis.*, vol. 42, no. 01, pp. 001–016, Feb. 2022, doi: 10.1055/s-0041-1742279.

[9] A. Soto-Gutierrez, A. Gough, L. A. Vernetti, D. Taylor, and S. P. Monga, 'Pre-clinical and clinical investigations of metabolic zonation in liver diseases: The potential of microphysiology systems', *Exp. Biol. Med.*, vol. 242, no. 16, pp. 1605–1616, Oct. 2017, doi: 10.1177/1535370217707731.

[10] R. Manco and S. Itzkovitz, 'Liver zonation', *J. Hepatol.*, vol. 74, no. 2, pp. 466–468, 2021, doi: 10.1016/j.jhep.2020.09.003.

[11] Z. Kmieć, *Cooperation of Liver Cells in Health and Disease*, vol. 161. in Advances in Anatomy Embryology and Cell Biology, vol. 161. Berlin, Heidelberg: Springer Berlin Heidelberg, 2001. doi: 10.1007/978-3-642-56553-3.

[12] W. Seo, 'Hepatic non-parenchymal cells: Master regulators of alcoholic liver disease?', *World J. Gastroenterol.*, vol. 22, no. 4, p. 1348, 2016, doi: 10.3748/wjg.v22.i4.1348.

[13] D. L. Knook and E. Ch. Sleyster, 'Isolated parenchymal, Kupffer and endothelial rat liver cells characterized by their lysosomal enzyme content', *Biochem. Biophys. Res. Commun.*, vol. 96, no. 1, pp. 250–257, 1980, doi: 10.1016/0006-291X(80)91207-3.

[14] L. Qin and J. M. Crawford, 'Anatomy and Cellular Functions of the Liver', in *Zakim and Boyer's Hepatology*, Elsevier, 2018, pp. 2-19.e4. doi: 10.1016/B978-0-323-37591-7.00001-X.

[15] A. Zeigerer, A. Wuttke, G. Marsico, S. Seifert, Y. Kalaidzidis, and M. Zerial, 'Functional properties of hepatocytes in vitro are correlated with cell polarity maintenance', *Exp. Cell Res.*, vol. 350, no. 1, pp. 242–252, 2017, doi: 10.1016/j.yexcr.2016.11.027.

[16] S. WL. Barmore W, Azad F, *Physiology, Urea Cycle. [Updated 2023 May 8]*. StatPearls [Internet], Treasure Island (FL). doi: https://www.ncbi.nlm.nih.gov/books/NBK513323/.

[17] A. Panwar, P. Das, and L. P. Tan, '3D Hepatic Organoid-Based Advancements in LIVER Tissue Engineering', *Bioengineering*, vol. 8, no. 11, p. 185, 2021, doi: 10.3390/bioengineering8110185.

[18] C. Kupffer, 'Ueber Sternzellen der Leber', *Archiv für Mikroskopische Anatomie*, vol. 12, no. 1, pp. 353–358, 1876, doi: 10.1007/BF02933897.

[19] A. Sródka, R. W. Gryglewski, and W. Szczepariski, 'Browicz or Kupffer cells?', *Pol. J. Pathol.*, vol. 57, no. 4, pp. 183–5, 2006, [Online]. Available: http://www.ncbi.nlm.nih.gov/pubmed/17285760

[20] L. J. Dixon, M. Barnes, H. Tang, M. T. Pritchard, and L. E. Nagy, 'Kupffer Cells in the Liver', in *Comprehensive Physiology*, vol. 3, no. 2, Wiley, 2013, pp. 785–797. doi: 10.1002/cphy.c120026.

[21] L. Bouwens, P. De Bleser, K. Vanderkerken, B. Geerts, and E. Wisse, 'Liver Cell Heterogeneity: Functions of Non-Parenchymal Cells', *Enzyme*, pp. 155–168, 2017, doi: 10.1159/000468782.

[22] M. Werner *et al.*, 'All-In-One: Advanced preparation of Human Parenchymal and Non-Parenchymal Liver Cells', *PLoS One*, vol. 10, no. 9, p. e0138655, 2015, doi: 10.1371/journal.pone.0138655.

[23] E. Wisse, 'An electron microscopic study of the fenestrated endothelial lining of rat liver sinusoids', *J. Ultrastruct. Res.*, vol. 31, no. 1–2, pp. 125–150, 1970, doi: 10.1016/S0022-5320(70)90150-4.

[24] K. Vekemans and F. Braet, 'Structural and functional aspects of the liver and liver sinusoidal cells in relation to colon carcinoma metastasis', *World J. Gastroenterol.*, vol. 11, no. 33, p. 5095, 2005, doi: 10.3748/wjg.v11.i33.5095.

[25] R. Malik, C. Selden, and H. Hodgson, 'The role of non-parenchymal cells in liver growth', *Semin. Cell Dev. Biol.*, vol. 13, no. 6, pp. 425–431, 2002, doi: 10.1016/S1084952102001301.

[26] T. Tsuchida and S. L. Friedman, 'Mechanisms of hepatic stellate cell activation', *Nat. Rev. Gastroenterol. Hepatol.*, vol. 14, no. 7, pp. 397–411, 2017, doi: 10.1038/nrgastro.2017.38.

[27] Y. Wang and C. Zhang, 'The Roles of Liver-Resident Lymphocytes in Liver Diseases', *Front. Immunol.*, vol. 10, p. 1582, 2019, doi: 10.3389/fimmu.2019.01582.

[28] J. M. Banales, R. C. Huebert, T. Karlsen, M. Strazzabosco, N. F. LaRusso, and G. J. Gores, 'Cholangiocyte pathobiology', *Nat. Rev. Gastroenterol. Hepatol.*, vol. 16, no. 5, pp. 269–281, 2019, doi: 10.1038/s41575-019-0125-y.

[29] M. Gordillo, T. Evans, and V. Gouon-Evans, 'Orchestrating liver development', *Development*, vol. 142, no. 12, pp. 2094–2108, Jun. 2015, doi: 10.1242/dev.114215.

[30] K. Meyer *et al.*, ' Bile canaliculi remodeling activates YAP via the actin cytoskeleton during liver regeneration ', *Mol. Syst. Biol.*, vol. 16, no. 2, Feb. 2020, doi: 10.15252/msb.20198985.

[31] J. Gburek, B. Konopska, and K. Gołąb, 'Renal Handling of Albumin—From Early Findings to Current Concepts', *Int. J. Mol. Sci.*, vol. 22, no. 11, p. 5809, May 2021, doi: 10.3390/ijms22115809.

[32] G. J. Quinlan, G. S. Martin, and T. W. Evans, 'Albumin', *Hepatology*, vol. 41, no. 6, pp. 1211–1219, Jun. 2005, doi: 10.1002/hep.20720.

[33] T. J. Peters, *All About Albumin*. Elsevier, 1995. doi: 10.1016/B978-0-12-552110-9.X5000-4.

[34] J. R. Carvalho and M. V. Machado, 'New Insights About Albumin and Liver Disease', *Ann. Hepatol.*, vol. 17, no. 4, pp. 547–560, Jul. 2018, doi: 10.5604/01.3001.0012.0916.

[35] M. Bernardi, 'Effective albumin – A novel paradigm in the management of decompensated liver cirrhosis', *J. Transl. Int. Med.*, vol. 11, no. 1, pp. 11–14, May 2023, doi: 10.2478/jtim-2022-0070.

[36] N. Wu *et al.*, 'Albumin, an interesting and functionally diverse protein, varies from "native" to "effective" (Review).', *Mol. Med. Rep.*, vol. 29, no. 2, Feb. 2024, doi: 10.3892/mmr.2023.13147.

[37] V. Mishra and R. J. Heath, 'Structural and Biochemical Features of Human Serum Albumin Essential for Eukaryotic Cell Culture', *Int. J. Mol. Sci.*, vol. 22, no. 16, p. 8411, Aug. 2021, doi: 10.3390/ijms22168411.

[38] C. Leggio, L. Galantini, and N. V. Pavel, 'About the albumin structure in solution: cigar Expanded form versus heart Normal shape', *Physical Chemistry Chemical Physics*, vol. 10, no. 45, p. 6741, 2008, doi: 10.1039/b808938h.

[39] S. Sugio, A. Kashima, S. Mochizuki, M. Noda, and K. Kobayashi, 'Crystal structure of human serum albumin at 2.5 Å resolution', *Protein Engineering, Design and Selection*, vol. 12, no. 6, pp. 439–446, Jun. 1999, doi: 10.1093/protein/12.6.439.

[40] D. Levitt and M. Levitt, 'Human serum albumin homeostasis: a new look at the roles of synthesis, catabolism, renal and gastrointestinal excretion, and the clinical value of serum albumin measurements', *Int. J. Gen. Med.*, vol. 9, pp. 229–255, Jul. 2016, doi: 10.2147/IJGM.S102819.

[41] M. A. Ashraf *et al.*, 'Albumin: A Review of Market Trends, Purification Methods, and Biomedical Innovations', *Curr. Issues Mol. Biol.*, vol. 47, no. 5, p. 303, Apr. 2025, doi: 10.3390/cimb47050303.

[42] S. O. Brennan and K. Nakayama, 'Furin has the proalbumin substrate specificity and serpin inhibitory properties of an in situ hepatic convertase', *FEBS Lett.*, vol. 338, no. 2, pp. 147–151, Jan. 1994, doi: 10.1016/0014-5793(94)80353-6.

[43] Y. Misumi, K. Oda, T. Fujiwara, N. Takami, K. Tashiro, and Y. Ikehara, 'Functional expression of furin demonstrating its intracellular localization and endoprotease activity for processing of proalbumin and complement pro-C3.', *J. Biol. Chem.*, vol. 266, no. 25, pp. 16954–9, Sep. 1991, [Online]. Available: http://www.ncbi.nlm.nih.gov/pubmed/1885622

[44] A. Baral, 'Albumin: Bountiful Arrow in the Quiver of Liver and Its Significance in Physiology', *Livers*, vol. 5, no. 2, p. 27, Jun. 2025, doi: 10.3390/livers5020027.

[45] H. K. Dewangan, 'Albumin as Natural Versatile Drug Carrier for Various Diseases Treatment', in *Sustainable Agriculture Reviews 43.*, Springer, Cham, 2020, ch. 8, pp. 239–268. doi: 10.1007/978-3-030-41838-0_8.

[46] S. S. Samban *et al.*, 'An Insight Into the Role of Alpha-Fetoprotein (AFP) in the Development and Progression of Hepatocellular Carcinoma', *Mol. Biotechnol.*, vol. 66, no. 10, pp. 2697–2709, Oct. 2024, doi: 10.1007/s12033-023-00890-0.

[47] K. Liu *et al.*, 'Structural characteristics of alpha-fetoprotein, including N-glycosylation, metal ion and fatty acid binding sites', *Commun. Biol.*, vol. 7, no. 1, p. 505, Apr. 2024, doi: 10.1038/s42003-024-06219-0.

[48] P. Chaudhari, L. Tian, A. Deshmukh, and Y.-Y. Jang, 'Expression kinetics of hepatic progenitor markers in cellular models of human liver development recapitulating hepatocyte and biliary cell

fate commitment', *Exp. Biol. Med.*, vol. 241, no. 15, pp. 1653–1662, Sep. 2016, doi: 10.1177/1535370216657901.

[49] Y. Lu, B. Lin, and M. Li, 'The role of alpha-fetoprotein in the tumor microenvironment of hepatocellular carcinoma', *Front. Oncol.*, vol. 14, Apr. 2024, doi: 10.3389/fonc.2024.1363695.

[50] T. B. Tomasi, 'Structure and Function of Alpha-Fetoprotein', *Annu. Rev. Med.*, vol. 28, no. 1, pp. 453–465, Feb. 1977, doi: 10.1146/annurev.me.28.020177.002321.

[51] M. Zhu, B. Lin, P. Zhou, and M. Li, 'Molecular Analysis of AFP and HSA Interactions with PTEN Protein.', *Biomed Res. Int.*, vol. 2015, p. 256916, 2015, doi: 10.1155/2015/256916.

[52] T. Morinaga, M. Sakai, T. G. Wegmann, and T. Tamaoki, 'Primary structures of human alpha-fetoprotein and its mRNA.', *Proceedings of the National Academy of Sciences*, vol. 80, no. 15, pp. 4604–4608, Aug. 1983, doi: 10.1073/pnas.80.15.4604.

[53] A. A. Terentiev and N. T. Moldogazieva, 'Structural and functional mapping of α-fetoprotein', *Biochemistry (Moscow)*, vol. 71, no. 2, pp. 120–132, Feb. 2006, doi: 10.1134/S0006297906020027.

[54] K. H. Kim, S. Y. Lee, D. G. Kim, S.-Y. Lee, J. Y. Kim, and J. S. Yoo, 'Absolute Quantification of *N* -Glycosylation of Alpha-Fetoprotein Using Parallel Reaction Monitoring with Stable Isotope-Labeled *N* -Glycopeptide as an Internal Standard', *Anal. Chem.*, vol. 92, no. 18, pp. 12588–12595, Sep. 2020, doi: 10.1021/acs.analchem.0c02563.

[55] M. Fromme, F. Klebingat, P. Ellis, and P. Strnad, 'Alpha-1 antitrypsin deficiency-associated liver disease: From understudied disorder to the poster child of genetic medicine', *Hepatol. Commun.*, vol. 9, no. 5, May 2025, doi: 10.1097/HC9.0000000000000699.

[56] E. C. Lewis, 'Expanding the Clinical Indications for α1-Antitrypsin Therapy', *Molecular Medicine*, vol. 18, no. 6, pp. 957–970, Jun. 2012, doi: 10.2119/molmed.2011.00196.

[57] A. LARSSON, M. PALM, L. HANSSON, S. BASU, and O. AXELSSON, 'Reference values for α_1 -acid glycoprotein, α_1 -antitrypsin, albumin, haptoglobin, C-reactive protein, IgA, IgG and IgM during pregnancy', *Acta Obstet. Gynecol. Scand.*, vol. 87, no. 10, pp. 1084–1088, Oct. 2008, doi: 10.1080/00016340802428146.

[58] L. Paczek, W. Michalska, and I. Bartlomiejczyk, 'Trypsin, elastase, plasmin and MMP-9 activity in the serum during the human ageing process', *Age Ageing*, vol. 37, no. 3, pp. 318–323, Mar. 2008, doi: 10.1093/ageing/afn039.

[59] S. M. Janciauskiene, R. Bals, R. Koczulla, C. Vogelmeier, T. Köhnlein, and T. Welte, 'The discovery of α1-antitrypsin and its role in health and disease', *Respir. Med.*, vol. 105, no. 8, pp. 1129–1139, Aug. 2011, doi: 10.1016/j.rmed.2011.02.002.

[60] E. M. Marijanovic *et al.*, 'Reactive centre loop dynamics and serpin specificity', *Sci. Rep.*, vol. 9, no. 1, p. 3870, Mar. 2019, doi: 10.1038/s41598-019-40432-w.

[61] J. Yang, X. Bai, G. Liu, and X. Li, 'A transcriptional regulatory network of HNF4α and HNF1α involved in human diseases and drug metabolism', *Drug Metab. Rev.*, vol. 54, no. 4, pp. 361–385, Oct. 2022, doi: 10.1080/03602532.2022.2103146.

[62] L. Amicone, C. Cicchini, and A. Marchetti, 'HNF4α as a Master Regulator of Epigenetic Dynamics in Epithelial Cells', *Genes (Basel).*, vol. 17, no. 1, p. 41, Dec. 2025, doi: 10.3390/genes17010041.

[63] H. Hamdy *et al.*, 'Hepatocyte nuclear factor 4-Alpha: a key regulator in liver carcinogenesis', *Cellular Oncology*, vol. 48, no. 4, pp. 885–897, Aug. 2025, doi: 10.1007/s13402-025-01064-7.

[64] ‘HNF4a’. [Online]. Available: https://www.uniprot.org/uniprotkb/P41235/entry#sequences

[65] D. E. Frigo, M. Bondesson, and C. Williams, ‘Nuclear receptors: from molecular mechanisms to therapeutics’, *Essays Biochem.*, vol. 65, no. 6, pp. 847–856, Nov. 2021, doi: 10.1042/EBC20210020.

[66] H. Qian *et al.*, ‘An HNF1α-regulated feedback circuit modulates hepatic fibrogenesis via the crosstalk between hepatocytes and hepatic stellate cells’, *Cell Res.*, vol. 25, no. 8, pp. 930–945, Aug. 2015, doi: 10.1038/cr.2015.84.

[67] H. H. Lau, N. H. J. Ng, L. S. W. Loo, J. B. Jasmen, and A. K. K. Teo, ‘The molecular functions of hepatocyte nuclear factors – In and beyond the liver’, *J. Hepatol.*, vol. 68, no. 5, pp. 1033–1048, May 2018, doi: 10.1016/j.jhep.2017.11.026.

[68] N. Narayana, Q. Hua, and M. A. Weiss, ‘The dimerization domain of HNF-1α: structure and plasticity of an intertwined four-helix bundle with application to diabetes mellitus 1 1Edited by M. F. Summers’, *J. Mol. Biol.*, vol. 310, no. 3, pp. 635–658, Jul. 2001, doi: 10.1006/jmbi.2001.4780.

[69] ‘HNF1a’. [Online]. Available: https://www.uniprot.org/uniprotkb/P20823/entry#sequences

[70] Y. Zhang *et al.*, ‘CYP3A4 and CYP3A5: the crucial roles in clinical drug metabolism and the significant implications of genetic polymorphisms’, *PeerJ*, vol. 12, no. 12, p. e18636, Dec. 2024, doi: 10.7717/peerj.18636.

[71] P. Acharya, M. Liao, J. C. Engel, and M. A. Correia, ‘Liver Cytochrome P450 3A Endoplasmic Reticulum-associated Degradation’, *Journal of Biological Chemistry*, vol. 286, no. 5, pp. 3815–3828, Feb. 2011, doi: 10.1074/jbc.M110.186981.

[72] ‘CYP3A4’. [Online]. Available: https://www.uniprot.org/uniprotkb/P08684/entry#structure

[73] J. Yang *et al.*, ‘Cytochrome P450 Turnover: Regulation of Synthesis and Degradation, Methods for Determining Rates, and Implications for the Prediction of Drug Interactions’, *Curr. Drug Metab.*, vol. 9, no. 5, pp. 384–393, Jun. 2008, doi: 10.2174/138920008784746382.

[74] J. Massart, K. Begriche, and B. Fromenty, ‘Cytochrome P450 2E1 should not be neglected for acetaminophen-induced liver injury in metabolic diseases with altered insulin levels or glucose homeostasis’, *Clin. Res. Hepatol. Gastroenterol.*, vol. 45, no. 1, 2021, doi: 10.1016/j.clinre.2020.05.018.

[75] R. Harjumäki, C. S. Pridgeon, and M. Ingelman-Sundberg, ‘CYP2E1 in Alcoholic and Non-Alcoholic Liver Injury. Roles of ROS, Reactive Intermediates and Lipid Overload’, *Int. J. Mol. Sci.*, vol. 22, no. 15, p. 8221, Jul. 2021, doi: 10.3390/ijms22158221.

[76] P. R. Porubsky, K. M. Meneely, and E. E. Scott, ‘Structures of human cytochrome P-450 2E1: Insights into the binding of inhibitors and both small molecular weight and fatty acid substrates’, *Journal of Biological Chemistry*, vol. 283, no. 48, pp. 33698–33707, 2008, doi: 10.1074/jbc.M805999200.

[77] ‘CYP2E1’. [Online]. Available: https://www.uniprot.org/uniprotkb/P05181/entry#sequences

[78] X.-S. Lai, L.-P. Yang, X.-T. Li, J.-P. Liu, Z.-W. Zhou, and S.-F. Zhou, ‘Human CYP2C8: Structure, Substrate Specificity, Inhibitor Selectivity, Inducers and Polymorphisms’, *Curr. Drug Metab.*, vol. 10, no. 9, pp. 1009–1047, Nov. 2009, doi: 10.2174/138920009790711832.

[79] G. A. Schoch, J. K. Yano, M. R. Wester, K. J. Griffin, C. D. Stout, and E. F. Johnson, ‘Structure of Human Microsomal Cytochrome P450 2C8’, *Journal of Biological Chemistry*, vol. 279, no. 10, pp. 9497–9503, Mar. 2004, doi: 10.1074/jbc.M312516200.

[80] C. Yan *et al.*, 'Elucidating the Substrate Specificity of Cytochrome P450 Enzymes: Insights into N- and S-Containing Small-Molecule Metabolism', *Engineering*, vol. 54, pp. 229–250, Nov. 2025, doi: 10.1016/j.eng.2025.07.029.

[81] 'CYP2C8'. [Online]. Available: https://www.uniprot.org/uniprotkb/P10632/entry#sequences

[82] A. B. Fajardo-Puerta, M. Mato Prado, A. E. Frampton, and L. R. Jiao, 'Gene of the month: *HGF*', *J. Clin. Pathol.*, vol. 69, no. 7, pp. 575–579, Jul. 2016, doi: 10.1136/jclinpath-2015-203575.

[83] M. Kimura, H. Moteki, and M. Ogihara, 'Role of Hepatocyte Growth Regulators in Liver Regeneration', *Cells*, vol. 12, no. 2, p. 208, Jan. 2023, doi: 10.3390/cells12020208.

[84] T. Nakamura and S. Mizuno, 'The discovery of Hepatocyte Growth Factor (HGF) and its significance for cell biology, life sciences and clinical medicine', *Proceedings of the Japan Academy, Series B*, vol. 86, no. 6, pp. 588–610, 2010, doi: 10.2183/pjab.86.588.

[85] O. Mungunsukh, E. McCart, and R. Day, 'Hepatocyte Growth Factor Isoforms in Tissue Repair, Cancer, and Fibrotic Remodeling', *Biomedicines*, vol. 2, no. 4, pp. 301–326, Nov. 2014, doi: 10.3390/biomedicines2040301.

[86] Y. Zhao, W. Ye, Y. D. Wang, and W. D. Chen, 'HGF/c-Met: A Key Promoter in Liver Regeneration', *Front. Pharmacol.*, vol. 13, no. March, pp. 1–10, 2022, doi: 10.3389/fphar.2022.808855.

[87] C. Hadjittofi, M. Feretis, J. Martin, S. Harper, and E. Huguet, 'Liver regeneration biology: Implications for liver tumour therapies', *World J. Clin. Oncol.*, vol. 12, no. 12, pp. 1101–1156, Dec. 2021, doi: 10.5306/wjco.v12.i12.1101.

[88] C. Tito, S. Masciarelli, G. Colotti, and F. Fazi, 'EGF receptor in organ development, tissue homeostasis and regeneration', *J. Biomed. Sci.*, vol. 32, no. 1, p. 24, Feb. 2025, doi: 10.1186/s12929-025-01119-9.

[89] M. Kawanaka *et al.*, 'Correlation between serum cytokeratin-18 and the progression or regression of non-alcoholic fatty liver disease', *Ann. Hepatol.*, vol. 14, no. 6, pp. 837–844, Nov. 2015, doi: 10.5604/16652681.1171767.

[90] P. Strnad, C. Stumptner, K. Zatloukal, and H. Denk, 'Intermediate filament cytoskeleton of the liver in health and disease', *Histochem. Cell Biol.*, vol. 129, no. 6, p. 735, Jun. 2008, doi: 10.1007/s00418-008-0431-x.

[91] J.-Y. Zhuo, D. Lu, W.-Y. Tan, S.-S. Zheng, Y.-Q. Shen, and X. Xu, 'CK19-positive Hepatocellular Carcinoma is a Characteristic Subtype', *J. Cancer*, vol. 11, no. 17, pp. 5069–5077, 2020, doi: 10.7150/jca.44697.

[92] J. Zhuo *et al.*, 'The distinct responsiveness of cytokeratin 19-positive hepatocellular carcinoma to regorafenib', *Cell Death Dis.*, vol. 12, no. 12, p. 1084, Nov. 2021, doi: 10.1038/s41419-021-04320-4.

[93] R. Masuzaki, K. C. Ray, J. Roland, R. Zent, Y. A. Lee, and S. J. Karp, 'Integrin β1 Establishes Liver Microstructure and Modulates Transforming Growth Factor β during Liver Development and Regeneration', *Am. J. Pathol.*, vol. 191, no. 2, pp. 309–319, Feb. 2021, doi: 10.1016/j.ajpath.2020.10.011.

[94] D. Cohen, F. Lázaro-Diéguez, and A. Müsch, 'Bile canaliculi formation in primary hepatocytes requires α1β1 integrin-dependent adherens junction re-organization', *J. Cell Sci.*, vol. 138, no. 23, Dec. 2025, doi: 10.1242/jcs.264412.

[95] M. Barczyk, S. Carracedo, and D. Gullberg, ‘Integrins’, *Cell Tissue Res.*, vol. 339, no. 1, pp. 269–280, Jan. 2010, doi: 10.1007/s00441-009-0834-6.

[96] K. Ikeda, K. Horie, S. Inoue, and B. Blumberg, ‘Physiological Functions and Pathological Roles of PXR’, *J. Endocr. Soc.*, vol. 9, no. 9, pp. 1–10, Jul. 2025, doi: 10.1210/jendso/bvaf119.

[97] B. Frieg, B. Görg, H. Gohlke, and D. Häussinger, ‘Glutamine synthetase as a central element in hepatic glutamine and ammonia metabolism: novel aspects’, *Biol. Chem.*, vol. 402, no. 9, pp. 1063–1072, Aug. 2021, doi: 10.1515/hsz-2021-0166.

[98] Y. Zhou, T. Eid, B. Hassel, and N. C. Danbolt, ‘Novel aspects of glutamine synthetase in ammonia homeostasis’, *Neurochem. Int.*, vol. 140, no. July, p. 104809, Nov. 2020, doi: 10.1016/j.neuint.2020.104809.

[99] L. Zhang, Y. Zou, Y. Lu, Z. Li, and F. Gao, ‘Unraveling the therapeutic potential of carbamoyl phosphate synthetase 1 (CPS1) in human diseases’, *Bioorg. Chem.*, vol. 130, no. September 2022, p. 106253, Jan. 2023, doi: 10.1016/j.bioorg.2022.106253.

[100] S. K. Heuser, J. Li, S. Pudewell, A. LoBue, Z. Li, and M. M. Cortese-Krott, ‘Biochemistry, pharmacology, and in vivo function of arginases’, *Pharmacol. Rev.*, vol. 77, no. 1, p. 100015, Jan. 2025, doi: 10.1124/pharmrev.124.001271.

[101] ‘Arg1’. [Online]. Available: https://www.uniprot.org/uniprotkb/P05089/entry#sequences

[102] J. Ivaska, H.-M. Pallari, J. Nevo, and J. E. Eriksson, ‘Novel functions of vimentin in cell adhesion, migration, and signaling’, *Exp. Cell Res.*, vol. 313, no. 10, pp. 2050–2062, Jun. 2007, doi: 10.1016/j.yexcr.2007.03.040.

[103] M. G. Mendez, S. Kojima, and R. D. Goldman, ‘Vimentin induces changes in cell shape, motility, and adhesion during the epithelial to mesenchymal transition’, *The FASEB Journal*, vol. 24, no. 6, pp. 1838–1851, Jun. 2010, doi: 10.1096/fj.09-151639.

[104] P.-W. Wang, T.-H. Wu, T.-Y. Lin, M.-H. Chen, C.-T. Yeh, and T.-L. Pan, ‘Characterization of the Roles of Vimentin in Regulating the Proliferation and Migration of HSCs during Hepatic Fibrogenesis’, *Cells*, vol. 8, no. 10, p. 1184, Oct. 2019, doi: 10.3390/cells8101184.

[105] R. G. Wells, ‘the Epithelial-to-Mesenchymal Transition in Liver Fibrosis: Here Today, Gone Tomorrow?’, *Hepatology*, vol. 51, no. 3, pp. 737–740, Mar. 2010, doi: 10.1002/hep.23529.

[106] M. Dominici *et al.*, ‘Minimal criteria for defining multipotent mesenchymal stromal cells. The International Society for Cellular Therapy position statement’, *Cytotherapy*, vol. 8, no. 4, pp. 315–317, 2006, doi: 10.1080/14653240600855905.

[107] K. P. Alcedo, J. L. Bowser, and N. T. Snider, ‘The elegant complexity of mammalian ecto-5′-nucleotidase (CD73)’, *Trends Cell Biol.*, vol. 31, no. 10, pp. 829–842, Oct. 2021, doi: 10.1016/j.tcb.2021.05.008.

[108] A. Pedrycz-Wieczorska *et al.*, ‘CD44 as a Central Integrator of Inflammation and Fibrosis: From Molecular Signaling to Environmental Modulation’, *Int. J. Mol. Sci.*, vol. 26, no. 18, p. 8870, Sep. 2025, doi: 10.3390/ijms26188870.

[109] A. Santoro, M. Grimaldi, C. Marino, E. Napolitano, M. Buonocore, and A. M. D’Ursi, ‘Cell Surface Markers of Mesenchymal Stem Cells: Current Knowledge and Advances in Characterization Technologies’, ., vol. 16, no. 1, p. 10, Dec. 2025, doi: 10.3390/life16010010.

[110] A. Wright, M. L. Arthaud-Day, and M. L. Weiss, ‘Therapeutic Use of Mesenchymal Stromal Cells: The Need for Inclusive Characterization Guidelines to Accommodate All Tissue Sources

and Species', *Front. Cell Dev. Biol.*, vol. 9, no. February, pp. 1–18, Feb. 2021, doi: 10.3389/fcell.2021.632717.

[111] J. S. NIELSEN and K. M. MCNAGNY, 'CD34 is a Key Regulator of Hematopoietic Stem Cell Trafficking to Bone Marrow and Mast Cell Progenitor Trafficking in the Periphery', *Microcirculation*, vol. 16, no. 6, pp. 487–496, Aug. 2009, doi: 10.1080/10739680902941737.

[112] P. Pleskač, C. A. Fargeas, R. Veselska, D. Corbeil, and J. Skoda, 'Emerging roles of prominin-1 (CD133) in the dynamics of plasma membrane architecture and cell signaling pathways in health and disease', *Cell. Mol. Biol. Lett.*, vol. 29, no. 1, p. 41, Mar. 2024, doi: 10.1186/s11658-024-00554-0.

[113] A. Rheinländer, B. Schraven, and U. Bommhardt, 'CD45 in human physiology and clinical medicine', *Immunol. Lett.*, vol. 196, no. January, pp. 22–32, Apr. 2018, doi: 10.1016/j.imlet.2018.01.009.

[114] H. Devarbhavi, S. K. Asrani, J. P. Arab, Y. A. Nartey, E. Pose, and P. S. Kamath, 'Global burden of liver disease: 2023 update', *J. Hepatol.*, vol. 79, no. 2, pp. 516–537, Aug. 2023, doi: 10.1016/j.jhep.2023.03.017.

[115] T. Jing Xing, 'Clinical Classification of Liver Failure: Consensus, Contradictions and New Recommendations', *J. Clin. Gastroenterol. Hepatol.*, vol. 01, no. 02, pp. 1–5, 2017, doi: 10.21767/2575-7733.1000016.

[116] C. Gan *et al.*, 'Liver diseases: epidemiology, causes, trends and predictions', *Signal Transduct. Target. Ther.*, vol. 10, no. 1, p. 33, Feb. 2025, doi: 10.1038/s41392-024-02072-z.

[117] F. Idalsoaga, A. V. Kulkarni, O. Y. Mousa, M. Arrese, and J. P. Arab, 'Non-alcoholic Fatty Liver Disease and Alcohol-Related Liver Disease: Two Intertwined Entities', *Front. Med. (Lausanne).*, vol. 7, no. August, pp. 1–17, Aug. 2020, doi: 10.3389/fmed.2020.00448.

[118] H. Wazir *et al.*, 'Diagnosis and Treatment of Liver Disease: Current Trends and Future Directions', *Cureus*, vol. 15, no. 12, Dec. 2023, doi: 10.7759/cureus.49920.

[119] K. Baviskar, A. Kshirsagar, H. Raut, and M. R. N. Shaikh, 'Overview: Global burden of liver disease', *International Journal of Pharmaceutical Chemistry and Analysis*, vol. 11, no. 1, pp. 1–10, Mar. 2024, doi: 10.18231/j.ijpca.2024.001.

[120] F. Martin *et al.*, 'Organ Donation and Transplantation Worldwide: The Global Observatory on Donation and Transplantation 2024 Report', *Transplantation*, vol. 110, no. 3, pp. e655–e669, Mar. 2026, doi: 10.1097/TP.0000000000005657.

[121] T. E. Starzl, A. J. Demetris, and D. Van Thiel, 'Liver Transplantation', *New England Journal of Medicine*, vol. 321, no. 15, pp. 1014–1022, Oct. 1989, doi: 10.1056/NEJM198910123211505.

[122] Y. Zhai, H. Petrowsky, J. C. Hong, R. W. Busuttil, and J. W. Kupiec-Weglinski, 'Ischaemia–reperfusion injury in liver transplantation—from bench to bedside', *Nat. Rev. Gastroenterol. Hepatol.*, vol. 10, no. 2, pp. 79–89, Feb. 2013, doi: 10.1038/nrgastro.2012.225.

[123] A. A. Pillai and J. Levitsky, 'Overview of immunosuppression in liver transplantation', *World J. Gastroenterol.*, vol. 15, no. 34, p. 4225, 2009, doi: 10.3748/wjg.15.4225.

[124] T. Ivanics, P. Abreu, E. De Martin, and G. Sapisochin, 'Changing Trends in Liver Transplantation: Challenges and Solutions', *Transplantation*, vol. 105, no. 4, pp. 743–756, Apr. 2021, doi: 10.1097/TP.0000000000003454.

[125] S. Feng and J. C. Lai, 'Expanded Criteria Donors', *Clin. Liver Dis.*, vol. 18, no. 3, pp. 633–649, Aug. 2014, doi: 10.1016/j.cld.2014.05.005.

[126] P. Burra *et al.*, 'EASL Clinical Practice Guidelines: Liver transplantation', *J. Hepatol.*, vol. 64, no. 2, pp. 433–485, Feb. 2016, doi: 10.1016/j.jhep.2015.10.006.

[127] I. Vodkin and A. Kuo, 'Extended Criteria Donors in Liver Transplantation', *Clin. Liver Dis.*, vol. 21, no. 2, pp. 289–301, May 2017, doi: 10.1016/j.cld.2016.12.004.

[128] S. A. Muller *et al.*, 'Partial liver transplantation-living donor liver transplantation and split liver transplantation', *Nephrology Dialysis Transplantation*, vol. 22, no. Supplement 8, pp. viii13–viii22, Sep. 2007, doi: 10.1093/ndt/gfm653.

[129] A. Humar *et al.*, 'Liver regeneration after adult living donor and deceased donor split-liver transplants', *Liver Transplantation*, vol. 10, no. 3, pp. 374–378, Mar. 2004, doi: 10.1002/lt.20096.

[130] R. X. Sousa Da Silva, A. Weber, P. Dutkowski, and P. Clavien, 'Machine perfusion in liver transplantation', *Hepatology*, vol. 76, no. 5, pp. 1531–1549, Nov. 2022, doi: 10.1002/hep.32546.

[131] N. Wang *et al.*, 'Liver regeneration: unraveling the molecular mechanisms and clinical application', *J. Transl. Med.*, vol. 23, no. 1, p. 1409, Dec. 2025, doi: 10.1186/s12967-025-07412-3.

[132] L. D. DeLeve, 'Liver sinusoidal endothelial cells and liver regeneration', *Journal of Clinical Investigation*, vol. 123, no. 5, pp. 1861–1866, May 2013, doi: 10.1172/JCI66025.

[133] C. Yin, K. J. Evason, K. Asahina, and D. Y. R. Stainier, 'Hepatic stellate cells in liver development, regeneration, and cancer', *Journal of Clinical Investigation*, vol. 123, no. 5, pp. 1902–1910, May 2013, doi: 10.1172/JCI66369.

[134] Y. Zhao, S. Zhao, S. Liu, W. Ye, and W. Chen, 'Kupffer cells, the limelight in the liver regeneration', *Int. Immunopharmacol.*, vol. 146, no. September 2024, p. 113808, Jan. 2025, doi: 10.1016/j.intimp.2024.113808.

[135] J. Han, A. Sung, H. Jeong, and Y. Jung, 'Liver Progenitor Cells: Cellular Origins, Plasticity, and Signaling Pathways in Liver Regeneration', *Biology (Basel).*, vol. 14, no. 10, p. 1361, Oct. 2025, doi: 10.3390/biology14101361.

[136] A. Elchaninov, P. Vishnyakova, V. Glinkina, T. Fatkhudinov, and G. Sukhikh, 'Liver Regeneration as a Model for Studying Cellular Plasticity in Mammals: The Roles of Hepatocytes and Cholangiocytes', *Cells*, vol. 14, no. 15, p. 1129, Jul. 2025, doi: 10.3390/cells14151129.

[137] N. Tanimizu, N. Ichinohe, M. Yamamoto, H. Akiyama, Y. Nishikawa, and T. Mitaka, 'Progressive induction of hepatocyte progenitor cells in chronically injured liver', *Sci. Rep.*, vol. 7, no. 1, p. 39990, Jan. 2017, doi: 10.1038/srep39990.

[138] R. Kalluri and R. A. Weinberg, 'The basics of epithelial-mesenchymal transition', *Journal of Clinical Investigation*, vol. 119, no. 6, pp. 1420–1428, Jun. 2009, doi: 10.1172/JCI39104.

[139] G. Giannelli, P. Koudelkova, F. Dituri, and W. Mikulits, 'Role of epithelial to mesenchymal transition in hepatocellular carcinoma', *J. Hepatol.*, vol. 65, no. 4, pp. 798–808, Oct. 2016, doi: 10.1016/j.jhep.2016.05.007.

[140] N. G. Anderson, 'The Mass Isolation of Whole Cells from Rat Liver', *Science (1979).*, vol. 117, no. 3049, pp. 627–628, Jun. 1953, doi: 10.1126/science.117.3049.627.

[141] I. Mandl, J. D. MacLennan, E. L. Howes, R. H. DeBellis, and A. Sohler, 'ISOLATION AND CHARACTERIZATION OF PROTEINASE AND COLLAGENASE FROM CL. HISTOLYTICUM 12', *Journal of Clinical Investigation*, vol. 32, no. 12, pp. 1323–1329, Dec. 1953, doi: 10.1172/JCI102861.

[142] E. Y. Lasfargues, ‘Cultivation and behavior in vitro of the normal mammary epithelium of the adult mouse’, *Anat. Rec.*, vol. 127, no. 1, pp. 117–129, Jan. 1957, doi: 10.1002/ar.1091270111.

[143] R. B. Howard, A. K. Christensen, F. A. Gibbs, and L. A. Pesch, ‘THE ENZYMATIC PREPARATION OF ISOLATED INTACT PARENCHYMAL CELLS FROM RAT LIVER’, *J. Cell Biol.*, vol. 35, no. 3, pp. 675–684, Dec. 1967, doi: 10.1083/jcb.35.3.675.

[144] M. N. Berry and D. S. Friend, ‘HIGH-YIELD PREPARATION OF ISOLATED RAT LIVER PARENCHYMAL CELLS’, *J. Cell Biol.*, vol. 43, no. 3, pp. 506–520, Dec. 1969, doi: 10.1083/jcb.43.3.506.

[145] M. N. Berry, A. R. Grivell, M. B. Grivell, and J. W. Phillips, ‘Isolated hepatocytes - past, present and future’, *Cell Biol. Toxicol.*, vol. 13, no. 4–5, pp. 223–233, Jul. 1997, doi: 10.1023/A:1007402505482.

[146] P. O. Seglen, ‘Preparation of Isolated Rat Liver Cells’, *Methods Cell Biol.*, vol. 13, no. C, pp. 29–83, 1976, doi: 10.1016/S0091-679X(08)61797-5.

[147] P. O. Seglen, ‘Preparation of rat liver cells’, *Exp. Cell Res.*, vol. 74, no. 2, pp. 450–454, Oct. 1972, doi: 10.1016/0014-4827(72)90400-4.

[148] R. H. Bhogal *et al.*, ‘Isolation of primary human hepatocytes from normal and diseased liver tissue: A one hundred liver experience’, *PLoS One*, vol. 6, no. 3, pp. 1–8, 2011, doi: 10.1371/journal.pone.0018222.

[149] P. Godoy *et al.*, ‘Recent advances in 2D and 3D in vitro systems using primary hepatocytes, alternative hepatocyte sources and non-parenchymal liver cells and their use in investigating mechanisms of hepatotoxicity, cell signaling and ADME’, *Arch. Toxicol.*, vol. 87, no. 8, pp. 1315–1530, Aug. 2013, doi: 10.1007/s00204-013-1078-5.

[150] M. Gomez-Lechon, M. Donato, J. Castell, and R. Jover, ‘Human Hepatocytes in Primary Culture: The Choice to Investigate Drug Metabolism in Man’, *Curr. Drug Metab.*, vol. 5, no. 5, pp. 443–462, Oct. 2004, doi: 10.2174/1389200043335414.

[151] C. C. Bell *et al.*, ‘Characterization of primary human hepatocyte spheroids as a model system for drug-induced liver injury, liver function and disease’, *Sci. Rep.*, vol. 6, no. 1, p. 25187, May 2016, doi: 10.1038/srep25187.

[152] C. Poggel *et al.*, ‘Isolation of Hepatocytes from Liver Tissue by a Novel, Semi-Automated Perfusion Technology’, *Biomedicines*, vol. 10, no. 9, p. 2198, Sep. 2022, doi: 10.3390/biomedicines10092198.

[153] K. E. Zakrzewska, A. Samluk, A. Wencel, K. Dudek, D. G. Pijanowska, and K. D. Pluta, ‘Liver tissue fragments obtained from males are the most promising source of human hepatocytes for cell-based therapies – Flow cytometric analysis of albumin expression’, *PLoS One*, vol. 12, no. 8, p. e0182846, Aug. 2017, doi: 10.1371/journal.pone.0182846.

[154] K. D. Pluta, M. Ciezkowska, M. Wisniewska, A. Wencel, and D. G. Pijanowska, ‘Cell-based clinical and experimental methods for assisting the function of impaired livers – Present and future of liver support systems’, *Biocybern. Biomed. Eng.*, vol. 41, no. 4, pp. 1322–1346, Oct. 2021, doi: 10.1016/j.bbe.2021.06.005.

[155] R. Tandon and S. Froghi, ‘Artificial liver support systems’, *J. Gastroenterol. Hepatol.*, vol. 36, no. 5, pp. 1164–1179, May 2021, doi: 10.1111/jgh.15255.

[156] E. Gadour *et al.*, ‘Safety and efficacy of Single-Pass Albumin Dialysis (SPAD), Prometheus, and Molecular Adsorbent Recycling System (MARS) liver haemodialysis vs. Standard Medical

Therapy (SMT): meta-analysis and systematic review', *Gastroenterology Review*, vol. 19, no. 2, pp. 101–111, 2024, doi: 10.5114/pg.2024.139297.

[157] C. J. Karvellas, N. Gibney, D. Kutsogiannis, J. Wendon, and V. G. Bain, 'Bench-to-bedside review: Current evidence for extracorporeal albumin dialysis systems in liver failure', *Crit. Care*, vol. 11, no. 3, p. 215, 2007, doi: 10.1186/cc5922.

[158] J. Stange, W. Ramlow, S. Mitzner, R. Schmidt, and H. Klinkmann, 'Dialysis against a Recycled Albumin Solution Enables the Removal of Albumin-Bound Toxins', *Artif. Organs*, vol. 17, no. 9, pp. 809–813, Sep. 1993, doi: 10.1111/j.1525-1594.1993.tb00635.x.

[159] Stange *et al.*, 'Molecular Adsorbent Recycling System (MARS): Clinical Results of a New Membrane-Based Blood Purification System for Bioartificial Liver Support', *Artif. Organs*, vol. 23, no. 4, pp. 319–330, Apr. 1999, doi: 10.1046/j.1525-1594.1999.06122.x.

[160] J. Rozga, Y. Umehara, A. Trofimenko, T. Sadahiro, and A. A. Demetriou, 'A Novel Plasma Filtration Therapy for Hepatic Failure: Preclinical Studies', *Therapeutic Apheresis and Dialysis*, vol. 10, no. 2, pp. 138–144, Apr. 2006, doi: 10.1111/j.1744-9987.2006.00355.x.

[161] P. Papamichalis *et al.*, 'Liver replacement therapy with extracorporeal blood purification techniques current knowledge and future directions', *World J. Clin. Cases*, vol. 11, no. 17, pp. 3932–3948, Jun. 2023, doi: 10.12998/wjcc.v11.i17.3932.

[162] Y.-T. He, Y.-N. Qi, B.-Q. Zhang, J.-B. Li, and J. Bao, 'Bioartificial liver support systems for acute liver failure: A systematic review and meta-analysis of the clinical and preclinical literature', *World J. Gastroenterol.*, vol. 25, no. 27, pp. 3634–3648, Jul. 2019, doi: 10.3748/wjg.v25.i27.3634.

[163] Q. Jiang, Y. Su, X. Cao, H. Zhang, J. Zhang, and L. Li, 'Bioartificial liver: Where lies the path ahead—A review', *Hepatol. Commun.*, vol. 9, no. 9, Sep. 2025, doi: 10.1097/HC9.0000000000000788.

[164] R. Sakiyama, B. J. Blau, and T. Miki, 'Clinical translation of bioartificial liver support systems with human pluripotent stem cell-derived hepatic cells', *World J. Gastroenterol.*, vol. 23, no. 11, p. 1974, 2017, doi: 10.3748/wjg.v23.i11.1974.

[165] M. A. Tutty, D. Movia, and A. Prina-Mello, 'Three-dimensional (3D) liver cell models - a tool for bridging the gap between animal studies and clinical trials when screening liver accumulation and toxicity of nanobiomaterials', *Drug Deliv. Transl. Res.*, vol. 12, no. 9, pp. 2048–2074, Sep. 2022, doi: 10.1007/s13346-022-01147-0.

[166] J. Park and D. Lee, 'Bioartificial liver systems: current status and future perspective', *J. Biosci. Bioeng.*, vol. 99, no. 4, pp. 311–319, Apr. 2005, doi: 10.1263/jbb.99.311.

[167] Y. Wang *et al.*, 'Current development of bioreactors for extracorporeal bioartificial liver (Review)', *Biointerphases*, vol. 5, no. 3, pp. FA116–FA131, Sep. 2010, doi: 10.1116/1.3521520.

[168] N. L. Sussman, G. T. Gislason, C. A. Conlin, and J. H. Kelly, 'The Hepatix Extracorporeal Liver Assist Device: Initial Clinical Experience', *Artif. Organs*, vol. 18, no. 5, pp. 390–396, May 1994, doi: 10.1111/j.1525-1594.1994.tb02221.x.

[169] A. Ellis, 'Pilot-controlled trial of the extracorporeal liver assist device in acute liver failure', *Hepatology*, vol. 24, no. 6, pp. 1446–1451, Dec. 1996, doi: 10.1053/jhep.1996.v24.pm0008938179.

[170] G. T. Gislason, D. D. Lobdell, J. H. Kelly, and N. L. Sussman, 'A Treatment System for Implementing an Extracorporeal Liver Assist Device', *Artif. Organs*, vol. 18, no. 5, pp. 385–389, May 1994, doi: 10.1111/j.1525-1594.1994.tb02220.x.

[171] Teperman L., ‘The ELAD Study Group. Bilirubin Improvement correlates with 90- day survival with use of the ELAD systemin a randomized, controlled study of subjects with acute alcoholic hepatitis or acute decompensation of cirrhosis [abstract]’, *Am J Transplant*, vol. 13(Suppl 5, 2013.

[172] J. Thompson *et al.*, ‘Extracorporeal cellular therapy (ELAD) in severe alcoholic hepatitis: A multinational, prospective, controlled, randomized trial’, *Liver Transplantation*, vol. 24, no. 3, pp. 380–393, Mar. 2018, doi: 10.1002/lt.24986.

[173] M. P. van de Kerkhove, R. Hoekstra, R. A. F. M. Chamuleau, and T. M. van Gulik, ‘Clinical Application of Bioartificial Liver Support Systems’, *Ann. Surg.*, vol. 240, no. 2, pp. 216–230, Aug. 2004, doi: 10.1097/01.sla.0000132986.75257.19.

[174] A. A. Demetriou *et al.*, ‘Prospective, Randomized, Multicenter, Controlled Trial of a Bioartificial Liver in Treating Acute Liver Failure’, *Ann. Surg.*, vol. 239, no. 5, pp. 660–670, May 2004, doi: 10.1097/01.sla.0000124298.74199.e5.

[175] C. Mullon and Z. Pitkin, ‘The HepatAssist® Bioartificial Liver Support System: clinical study and pig hepatocyte process’, *Expert Opin. Investig. Drugs*, vol. 8, no. 3, pp. 229–235, Mar. 1999, doi: 10.1517/13543784.8.3.229.

[176] E. Erro *et al.*, ‘Evaluation of a single-use bioartificial liver (BAL) biocartridge consisting of cryopreservable alginate encapsulated liver cell spheroids as a component of HepatiCan™, a novel bioartificial liver device’, *Front. Bioeng. Biotechnol.*, vol. 13, no. August, pp. 1–17, Aug. 2025, doi: 10.3389/fbioe.2025.1572254.

[177] I. M. Sauer *et al.*, ‘Clinical extracorporeal hybrid liver support – phase I study with primary porcine liver cells’, *Xenotransplantation*, vol. 10, no. 5, pp. 460–469, Sep. 2003, doi: 10.1034/j.1399-3089.2003.00062.x.

[178] I. M. Sauer and J. C. Gerlach, ‘Modular Extracorporeal Liver Support’, *Artif. Organs*, vol. 26, no. 8, pp. 703–706, Aug. 2002, doi: 10.1046/j.1525-1594.2002.06931_1.x.

[179] J. C. Gerlach, J. Encke, O. Hole, C. Müller, C. J. Ryan, and P. Neuhaus, ‘BIOREACTOR FOR A LARGER SCALE HEPATOCYTE IN VITRO PERFUSION’, *Transplantation*, vol. 58, no. 9, pp. 984–988, Nov. 1994, doi: 10.1097/00007890-199411150-00002.

[180] M. F. Moedas *et al.*, ‘Advances in methods for characterization of hepatic urea cycle enzymatic activity in HepaRG cells using UPLC-MS/MS’, *Anal. Biochem.*, vol. 535, pp. 47–55, Oct. 2017, doi: 10.1016/j.ab.2017.07.025.

[181] L. M. Flendrig *et al.*, ‘In vitro evaluation of a novel bioreactor based on an integral oxygenator and a spirally wound nonwoven polyester matrix for hepatocyte culture as small aggregates’, *J. Hepatol.*, vol. 26, no. 6, pp. 1379–1392, Jul. 1997, doi: 10.1016/S0168-8278(97)80475-8.

[182] M.-P. Van De Kerkhove *et al.*, ‘Phase I Clinical Trial with the AMC-Bioartificial Liver’, *Int. J. Artif. Organs*, vol. 25, no. 10, pp. 950–959, Oct. 2002, doi: 10.1177/039139880202501009.

[183] M. P. van de Kerkhove, P. P. C. Poyck, T. Deurholt, R. Hoekstra, R. A. F. M. Chamuleau, and T. M. van Gulik, ‘Liver Support Therapy: An Overview of the AMC-Bioartificial Liver Research’, *Dig. Surg.*, vol. 22, no. 4, pp. 254–264, 2005, doi: 10.1159/000088055.

[184] G. A. A. Nibourg *et al.*, ‘Liver Progenitor Cell Line HepaRG Differentiated in a Bioartificial Liver Effectively Supplies Liver Support to Rats with Acute Liver Failure’, *PLoS One*, vol. 7, no. 6, p. e38778, Jun. 2012, doi: 10.1371/journal.pone.0038778.

[185] C. Gu, P. Li, W. Liu, Y. Zhou, and W. Tan, 'The role of insulin in transdifferentiated hepatocyte proliferation and function in serum-free medium', *J. Cell. Mol. Med.*, vol. 23, no. 6, pp. 4165–4178, Jun. 2019, doi: 10.1111/jcmm.14303.

[186] G. A. Nibourg, R. A. Chamuleau, T. M. van Gulik, and R. Hoekstra, 'Proliferative human cell sources applied as biocomponent in bioartificial livers: a review', *Expert Opin. Biol. Ther.*, vol. 12, no. 7, pp. 905–921, Jul. 2012, doi: 10.1517/14712598.2012.685714.

[187] J. Nulty, H. Anand, and A. Dhawan, 'Human Hepatocyte Transplantation: Three Decades of Clinical Experience and Future Perspective', *Stem Cells Transl. Med.*, vol. 13, no. 3, pp. 204–218, Mar. 2024, doi: 10.1093/stcltm/szad084.

[188] Z. Sun *et al.*, 'Hepatocyte transplantation: The progress and the challenges', *Hepatol. Commun.*, vol. 7, no. 10, Oct. 2023, doi: 10.1097/HC9.0000000000000266.

[189] R. D. Heath, F. Ertem, B. S. Romana, J. A. Ibdah, and V. Tahan, 'Hepatocyte transplantation: Consider infusion before incision', *World J. Transplant.*, vol. 7, no. 6, pp. 317–323, Dec. 2017, doi: 10.5500/wjt.v7.i6.317.

[190] P. Liu *et al.*, 'Immunomodulatory role of mesenchymal stem cell therapy in liver fibrosis', *Front. Immunol.*, vol. 13, no. January, pp. 1–10, Jan. 2023, doi: 10.3389/fimmu.2022.1096402.

[191] W.-C. Huang, Y.-C. Li, P.-X. Chen, K. S.-K. Ma, and L.-T. Wang, 'Mesenchymal stem cell therapy as a game-changer in liver diseases: review of current clinical trials', *Stem Cell Res. Ther.*, vol. 16, no. 1, p. 3, Jan. 2025, doi: 10.1186/s13287-024-04127-y.

[192] C. A. Lee, S. Sinha, E. Fitzpatrick, and A. Dhawan, 'Hepatocyte transplantation and advancements in alternative cell sources for liver-based regenerative medicine', *J. Mol. Med.*, vol. 96, no. 6, pp. 469–481, 2018, doi: 10.1007/s00109-018-1638-5.

[193] Q. Dai, W. Jiang, F. Huang, F. Song, J. Zhang, and H. Zhao, 'Recent Advances in Liver Engineering With Decellularized Scaffold', *Front. Bioeng. Biotechnol.*, vol. 10, no. February, Feb. 2022, doi: 10.3389/fbioe.2022.831477.

[194] K. H. Hussein *et al.*, 'Liver tissue engineering using decellularized scaffolds: Current progress, challenges, and opportunities', *Bioact. Mater.*, vol. 40, no. May, pp. 280–305, Oct. 2024, doi: 10.1016/j.bioactmat.2024.06.001.

[195] T. Mir *et al.*, 'Whole Liver Derived Acellular Extracellular Matrix for Bioengineering of Liver Constructs: An Updated Review', *Bioengineering*, vol. 10, no. 10, p. 1126, Sep. 2023, doi: 10.3390/bioengineering10101126.

[196] W. Shi, Z. Zhang, and X. Wang, 'The Prospect of Hepatic Decellularized Extracellular Matrix as a Bioink for Liver 3D Bioprinting', *Biomolecules*, vol. 14, no. 8, p. 1019, Aug. 2024, doi: 10.3390/biom14081019.

[197] W. Li *et al.*, 'Application of 3D Bioprinting in Liver Diseases', *Micromachines (Basel).*, vol. 14, no. 8, p. 1648, Aug. 2023, doi: 10.3390/mi14081648.

[198] Q. Luo *et al.*, 'Pluripotent Stem Cell-Derived Hepatocyte-like Cells: Induction Methods and Applications', *Int. J. Mol. Sci.*, vol. 24, no. 14, 2023, doi: 10.3390/ijms241411592.

[199] R. Ju *et al.*, 'Hepatocyte-like cells and liver organoids: the application of iPSCs and their derivants for treating liver diseases', *Mater. Adv.*, vol. 5, no. 21, pp. 8419–8431, 2024, doi: 10.1039/D4MA00373J.

[200] V. A. Arzumanian, O. I. Kiseleva, and E. V. Poverennaya, ‘The Curious Case of the HepG2 Cell Line: 40 Years of Expertise’, *Int. J. Mol. Sci.*, vol. 22, no. 23, p. 13135, Dec. 2021, doi: 10.3390/ijms222313135.

[201] K. Zeilinger, N. Freyer, G. Damm, D. Seehofer, and F. Knöspel, ‘Cell sources for *in vitro* human liver cell culture models’, *Exp. Biol. Med.*, vol. 241, no. 15, pp. 1684–1698, Sep. 2016, doi: 10.1177/1535370216657448.

[202] M. J. Wisniewska *et al.*, ‘Variable expression of hepatic genes in different liver tumor cell lines: conclusions for drug testing’, *Front. Cell Dev. Biol.*, vol. 13, 2025, doi: 10.3389/fcell.2025.1646602.

[203] L. J. Nelson *et al.*, ‘Human Hepatic HepaRG Cells Maintain an Organotypic Phenotype with High Intrinsic CYP450 Activity/Metabolism and Significantly Outperform Standard HepG2/C3A Cells for Pharmaceutical and Therapeutic Applications.’, *Basic Clin. Pharmacol. Toxicol.*, vol. 120, no. 1, pp. 30–37, Jan. 2017, doi: 10.1111/bcpt.12631.

[204] H.-J. Hwang, G.-J. Kim, G.-B. Lee, J.-T. Oh, Y.-H. Chun, and S.-H. Park, ‘A comprehensive karyotypic analysis on Korean hepatocellular carcinoma cell lines by cross-species color banding and comparative genomic hybridization’, *Cancer Genet. Cytogenet.*, vol. 141, no. 2, pp. 128–137, Mar. 2003, doi: 10.1016/S0165-4608(02)00671-4.

[205] I. Zaiets, O. Chazova, S. Gunewardena, and S. O. Gudima, ‘HCC-derived SNU cell lines as model systems to study HBV life cycle’, *J. Virol.*, vol. 99, no. 10, pp. 1–36, Oct. 2025, doi: 10.1128/jvi.01144-25.

[206] C. Thomas *et al.*, ‘Demand, Waitlisting and Transplantation Around the World: The Axiomatic View of Scarcity in Liver Transplantation’, *Clin. Transplant.*, vol. 40, no. 3, 2026, doi: 10.1111/ctr.70508.

[207] S. Park and M. N. Hall, ‘Metabolic reprogramming in hepatocellular carcinoma: mechanisms and therapeutic implications’, *Exp. Mol. Med.*, vol. 57, no. 3, pp. 515–523, Mar. 2025, doi: 10.1038/s12276-025-01415-2.

[208] D. López-Terrada, S. W. Cheung, M. J. Finegold, and B. B. Knowles, ‘Hep G2 is a hepatoblastoma-derived cell line’, *Hum. Pathol.*, vol. 40, no. 10, pp. 1512–1515, Oct. 2009, doi: 10.1016/j.humpath.2009.07.003.

[209] A. Wencel, M. Ciezkowska, M. Wisniewska, K. E. Zakrzewska, D. G. Pijanowska, and K. D. Pluta, ‘Effects of genetically modified human skin fibroblasts, stably overexpressing hepatocyte growth factor, on hepatic functions of cocultured C3A cells’, *Biotechnol. Bioeng.*, vol. 118, no. 1, pp. 72–81, Jan. 2021, doi: 10.1002/bit.27551.

[210] A. Korzyńska and M. Zychowicz, ‘A method of estimation of the cell doubling time on basis of the cell culture monitoring data’, *Biocybern. Biomed. Eng.*, vol. 28, no. 4, pp. 75–82, 2008.

[211] M. Huch *et al.*, ‘Long-Term Culture of Genome-Stable Bipotent Stem Cells from Adult Human Liver’, *Cell*, vol. 160, no. 1–2, pp. 299–312, Jan. 2015, doi: 10.1016/j.cell.2014.11.050.

[212] D. Garnier *et al.*, ‘Expansion of human primary hepatocytes in vitro through their amplification as liver progenitors in a 3D organoid system’, *Sci. Rep.*, vol. 8, no. 1, p. 8222, May 2018, doi: 10.1038/s41598-018-26584-1.

[213] T. Guy *et al.*, ‘High-yield isolation of primary human hepatocytes from small liver samples’, *In vitro models*, pp. 245–259, 2025, doi: 10.1007/s44164-025-00097-4.

[214] S. M. L. Lee *et al.*, 'An Algorithm that Predicts the Viability and the Yield of Human Hepatocytes Isolated from Remnant Liver Pieces Obtained from Liver Resections', *PLoS One*, vol. 9, no. 10, p. e107567, Oct. 2014, doi: 10.1371/journal.pone.0107567.

[215] K. Alexandrova *et al.*, 'Large-Scale Isolation of Human Hepatocytes for Therapeutic Application', *Cell Transplant.*, vol. 14, no. 10, pp. 845–853, Nov. 2005, doi: 10.3727/000000005783982530.

[216] R. Gramignoli *et al.*, 'Development and Application of Purified Tissue Dissociation Enzyme Mixtures for Human Hepatocyte Isolation', *Cell Transplant.*, vol. 21, no. 6, pp. 1245–1260, Jun. 2012, doi: 10.3727/096368911X600939.

[217] A. Serralta, M. T. Donato, F. Orbis, J. V. Castell, J. Mir, and M. J. Gómez-Lechón, 'Functionality of cultured human hepatocytes from elective samples, cadaveric grafts and hepatectomies', *Toxicology in Vitro*, vol. 17, no. 5–6, pp. 769–774, Oct. 2003, doi: 10.1016/S0887-2333(03)00122-X.

[218] E. Pfeiffer *et al.*, 'Featured Article: Isolation, characterization, and cultivation of human hepatocytes and non-parenchymal liver cells', *Exp. Biol. Med.*, vol. 240, no. 5, pp. 645–656, May 2015, doi: 10.1177/1535370214558025.

[219] B. M. Galmés-Pascual *et al.*, '17β-estradiol improves hepatic mitochondrial biogenesis and function through PGC1B', *Journal of Endocrinology*, vol. 232, no. 2, pp. 297–308, Feb. 2017, doi: 10.1530/JOE-16-0350.

[220] S. Ali Mondal *et al.*, '17α-estradiol, a lifespan-extending compound, attenuates liver fibrosis by modulating collagen turnover rates in male mice', *American Journal of Physiology-Endocrinology and Metabolism*, vol. 324, no. 2, pp. E120–E134, Feb. 2023, doi: 10.1152/ajpendo.00256.2022.

[221] Y. Kamada *et al.*, 'Estrogen deficiency worsens steatohepatitis in mice fed high-fat and high-cholesterol diet', *American Journal of Physiology-Gastrointestinal and Liver Physiology*, vol. 301, no. 6, pp. G1031–G1043, Dec. 2011, doi: 10.1152/ajpgi.00211.2011.

[222] I. Shimizu, 'Female hepatology: Favorable role of estrogen in chronic liver disease with hepatitis B virus infection', *World J. Gastroenterol.*, vol. 13, no. 32, p. 4295, Aug. 2007, doi: 10.3748/wjg.v13.i32.4295.

[223] L. Xu *et al.*, 'The Hepatoprotective and Hepatotoxic Roles of Sex and Sex-Related Hormones', *Front. Immunol.*, vol. 13, Jul. 2022, doi: 10.3389/fimmu.2022.939631.

[224] M. Shen and H. Shi, 'Sex Hormones and Their Receptors Regulate Liver Energy Homeostasis', *Int. J. Endocrinol.*, vol. 2015, pp. 1–12, 2015, doi: 10.1155/2015/294278.

[225] B. Wang, L. Zhao, M. Fish, C. Y. Logan, and R. Nusse, 'Self-renewing diploid Axin2+ cells fuel homeostatic renewal of the liver', *Nature*, vol. 524, no. 7564, pp. 180–185, Aug. 2015, doi: 10.1038/nature14863.

[226] Y. Wei *et al.*, 'Liver homeostasis is maintained by midlobular zone 2 hepatocytes', *Science (1979).*, vol. 371, no. 6532, Feb. 2021, doi: 10.1126/science.abb1625.

[227] L. He *et al.*, 'Proliferation tracing reveals regional hepatocyte generation in liver homeostasis and repair', *Science (1979).*, vol. 371, no. 6532, Feb. 2021, doi: 10.1126/science.abc4346.

[228] C. H. Cho, F. Berthiaume, A. W. Tilles, and M. L. Yarmush, 'A new technique for primary hepatocyte expansion in vitro', *Biotechnol. Bioeng.*, vol. 101, no. 2, pp. 345–356, Oct. 2008, doi: 10.1002/bit.21911.

[229] C. Yamasaki *et al.*, 'Growth and differentiation of colony-forming human hepatocytes in vitro', *J. Hepatol.*, vol. 44, no. 4, pp. 749–757, Apr. 2006, doi: 10.1016/j.jhep.2005.10.028.

[230] C. M. Brophy *et al.*, 'Rat hepatocyte spheroids formed by rocked technique maintain differentiated hepatocyte gene expression and function #', *Hepatology*, vol. 49, no. 2, pp. 578–586, Feb. 2009, doi: 10.1002/hep.22674.

[231] C. Yuasa, Y. Tomita, M. Shono, K. Ishimura, and A. Ichihara, 'Importance of cell aggregation for expression of liver functions and regeneration demonstrated with primary cultured hepatocytes', *J. Cell. Physiol.*, vol. 156, no. 3, pp. 522–530, Sep. 1993, doi: 10.1002/jcp.1041560311.

[232] R. R. Mitry *et al.*, 'Human Hepatocyte Isolation and Relationship of Cell Viability to Early Graft Function', *Cell Transplant.*, vol. 12, no. 1, pp. 69–74, Jan. 2003, doi: 10.3727/000000003783985197.

[233] E. Solanas *et al.*, 'How Donor and Surgical Factors Affect the Viability and Functionality of Human Hepatocytes Isolated From Liver Resections', *Front. Med. (Lausanne).*, vol. 9, no. May, pp. 1–9, May 2022, doi: 10.3389/fmed.2022.875147.

[234] F. Y. Meng *et al.*, 'Hepatocyte isolation from resected benign tissues: Results of a 5-year experience', *World J. Gastroenterol.*, vol. 22, no. 36, pp. 8178–8186, 2016, doi: 10.3748/wjg.v22.i36.8178.

[235] A. Bonora-Centelles *et al.*, 'Functional Characterization of Hepatocytes for Cell Transplantation: Customized Cell Preparation for Each Receptor', *Cell Transplant.*, vol. 19, no. 1, pp. 21–28, Jan. 2010, doi: 10.3727/096368909X474267.

[236] 'Collagenase_man'. Accessed: Apr. 29, 2026. [Online]. Available: https://documents.thermofisher.com/TFS-Assets/LSG/manuals/Collagenase_man.pdf

[237] 'Collagenases from Clostridium histolyticum'. Accessed: Apr. 29, 2026. [Online]. Available: https://www.sigmaaldrich.com/PL/pl/product/roche/colldro?srsltid=AfmBOopqPrNHjxa9Z0RZ9YZLk0GzeBlh8cL2oJ2YSISsKNgJUOWdu8XP

[238] 'Collagenase Manual', Worthington Biochemical Corp. Accessed: Jun. 11, 2026. [Online]. Available: https://www.worthington-biochem.com/products/collagenase/manual

[239] G. Feldmann, J. Penaud-Laurencin, J. Crassous, and J. P. Benhamou, 'Albumin Synthesis by Human Liver Cells: Its Morphological Demonstration', *Gastroenterology*, vol. 63, no. 6, pp. 1036–1048, Dec. 1972, doi: 10.1016/S0016-5085(19)33181-6.

[240] M. Watanabe *et al.*, 'Maintenance of hepatic functions in primary human hepatocytes cultured on xeno-free and chemical defined human recombinant Laminins', *PLoS One*, vol. 11, no. 9, pp. 1–15, 2016, doi: 10.1371/journal.pone.0161383.

[241] M. Kiamehr *et al.*, 'Dedifferentiation of primary hepatocytes is accompanied with reorganization of lipid metabolism indicated by altered molecular lipid and miRNA profiles', *Int. J. Mol. Sci.*, vol. 20, no. 12, Jun. 2019, doi: 10.3390/ijms20122910.

[242] K. E. O'Neill *et al.*, 'Hepatocyte-ductal transdifferentiation is mediated by reciprocal repression of SOX9 and C/EBPα', *Cell. Reprogram.*, vol. 16, no. 5, pp. 314–323, Oct. 2014, doi: 10.1089/cell.2014.0032.

[243] A. Rogue, C. Lambert, C. Spire, N. Claude, and A. Guillouzo, 'Interindividual variability in gene expression profiles in human hepatocytes and comparison with HepaRG cells', *Drug Metabolism and Disposition*, vol. 40, no. 1, pp. 151–158, Jan. 2012, doi: 10.1124/dmd.111.042028.

[244] Z. Peng *et al.*, 'The validation of quality attributes in Primary Human Hepatocytes Standard', *Cell Regeneration*, vol. 14, no. 1, Dec. 2025, doi: 10.1186/s13619-025-00258-6.

[245] R. Wolbold *et al.*, 'Sex is a major determinant of CYP3A4 expression in human liver', *Hepatology*, vol. 38, no. 4, pp. 978–988, 2003, doi: 10.1053/jhep.2003.50393.

[246] M. Schirmer *et al.*, 'Sex-dependent genetic markers of CYP3A4 expression and activity in human liver microsomes', *Pharmacogenomics*, vol. 8, no. 5, pp. 443–453, 2007, doi: 10.2217/14622416.8.5.443.

[247] Y. Zhang *et al.*, 'Transcriptional Profiling of Human Liver Identifies Sex-Biased Genes Associated with Polygenic Dyslipidemia and Coronary Artery Disease', *PLoS One*, vol. 6, no. 8, p. e23506, Aug. 2011, doi: 10.1371/journal.pone.0023506.

[248] Y.-T. Chen, L. Trzoss, D. Yang, and B. Yan, 'Ontogenic expression of human carboxylesterase-2 and cytochrome P450 3A4 in liver and duodenum: Postnatal surge and organ-dependent regulation', *Toxicology*, vol. 330, pp. 55–61, Apr. 2015, doi: 10.1016/j.tox.2015.02.007.

[249] SrikanthC. Nallani, B. Goodwin, ArthurR. Buckley, DonnaJ. Buckley, and PankajB. Desai, 'Differences in the induction of cytochrome P450 3A4 by taxane anticancer drugs, docetaxel and paclitaxel, assessed employing primary human hepatocytes', *Cancer Chemother. Pharmacol.*, vol. 54, no. 3, pp. 219–229, Sep. 2004, doi: 10.1007/s00280-004-0799-9.

[250] S. J. Woolsey, S. E. Mansell, R. B. Kim, R. G. Tirona, and M. D. Beaton, 'CYP3A Activity and Expression in Nonalcoholic Fatty Liver Disease', *Drug Metabolism and Disposition*, vol. 43, no. 10, pp. 1484–1490, Oct. 2015, doi: 10.1124/dmd.115.065979.

[251] R. Jamwal, S. M. de la Monte, K. Ogasawara, S. Adusumalli, B. B. Barlock, and F. Akhlaghi, 'Nonalcoholic Fatty Liver Disease and Diabetes Are Associated with Decreased CYP3A4 Protein Expression and Activity in Human Liver', *Mol. Pharm.*, vol. 15, no. 7, pp. 2621–2632, Jul. 2018, doi: 10.1021/acs.molpharmaceut.8b00159.

[252] S. B. Naraharisetti *et al.*, 'Human Liver Expression of CYP2C8: Gender, Age, and Genotype Effects', *Drug Metabolism and Disposition*, vol. 38, no. 6, pp. 889–893, Jun. 2010, doi: 10.1124/dmd.109.031542.

[253] A. Aljohmani and D. Yildiz, 'Biological sex differences in pharmacokinetics and adverse drug reactions', *Naunyn. Schmiedebergs. Arch. Pharmacol.*, vol. 399, no. 3, pp. 3285–3301, Feb. 2026, doi: 10.1007/s00210-025-04721-8.

[254] J. Liu, Y.-F. Lu, J. C. Corton, and C. D. Klaassen, 'Expression of cytochrome P450 isozyme transcripts and activities in human livers', *Xenobiotica*, vol. 51, no. 3, pp. 279–286, Apr. 2021, doi: 10.1080/00498254.2020.1867929.

[255] C. Rodríguez-Antona, M. T. Donato, E. Pareja, M.-J. Gómez-Lechón, and J. V. Castell, 'Cytochrome P-450 mRNA Expression in Human Liver and Its Relationship with Enzyme Activity', *Arch. Biochem. Biophys.*, vol. 393, no. 2, pp. 308–315, Sep. 2001, doi: 10.1006/abbi.2001.2499.

[256] Y. Zhang, E. V. Laz, and D. J. Waxman, 'Dynamic, Sex-Differential STAT5 and BCL6 Binding to Sex-Biased, Growth Hormone-Regulated Genes in Adult Mouse Liver', *Mol. Cell. Biol.*, vol. 32, no. 4, pp. 880–896, Feb. 2012, doi: 10.1128/MCB.06312-11.

[257] R. U. Rahman *et al.*, 'Single-cell transcriptomics reveals the impact of sex and age in the healthy human liver', *JHEP Reports*, vol. 8, no. 5, p. 101773, May 2026, doi: 10.1016/j.jhepr.2026.101773.

[258] L. Pelletier, S. Rebouissou, D. Vignjevic, P. Bioulac-Sage, and J. Zucman-Rossi, 'HNF1α inhibition triggers epithelial-mesenchymal transition in human liver cancer cell lines', *BMC Cancer*, vol. 11, no. 1, p. 427, Dec. 2011, doi: 10.1186/1471-2407-11-427.

[259] S. Fujino *et al.*, 'HNF1A regulates colorectal cancer progression and drug resistance as a downstream of POU5F1', *Sci. Rep.*, vol. 11, no. 1, p. 10363, May 2021, doi: 10.1038/s41598-021-89126-2.

[260] P. He, Z.-Y. Tang, S.-L. Ye, and B.-B. Liu, 'Relationship between expression of alpha-fetoprotein messenger RNA and some clinical parameters of human hepatocellular carcinoma.', *World J. Gastroenterol.*, vol. 5, no. 2, pp. 111–115, Apr. 1999, doi: 10.3748/wjg.v5.i2.111.

[261] W. Chen, J. Peng, J. Ye, W. Dai, G. Li, and Y. He, 'Aberrant AFP expression characterizes a subset of hepatocellular carcinoma with distinct gene expression patterns and inferior prognosis.', *J. Cancer*, vol. 11, no. 2, pp. 403–413, 2020, doi: 10.7150/jca.31435.

[262] D. Deharde *et al.*, 'Bile canaliculi formation and biliary transport in 3D sandwich-cultured hepatocytes in dependence of the extracellular matrix composition', *Arch. Toxicol.*, vol. 90, no. 10, pp. 2497–2511, Oct. 2016, doi: 10.1007/s00204-016-1758-z.

[263] K. Wrzesinski and S. J. Fey, 'After trypsinisation, 3D spheroids of C3A hepatocytes need 18 days to re-establish similar levels of key physiological functions to those seen in the liver', *Toxicol. Res.*, vol. 2, no. 2, pp. 123–135, 2013, doi: 10.1039/C2TX20060K.

[264] H. Gaskell, P. Sharma, H. E. Colley, C. Murdoch, D. P. Williams, and S. D. Webb, 'Characterization of a functional C3A liver spheroid model', *Toxicol. Res. (Camb).*, vol. 5, no. 4, pp. 1053–1065, 2016, doi: 10.1039/C6TX00101G.

[265] A. Wencel, K. E. Zakrzewska, A. Samluk, B. H. Noszczyk, D. G. Pijanowska, and K. D. Pluta, 'Dried human skin fibroblasts as a new substratum for functional culture of hepatic cells', *Acta Biochim. Pol.*, vol. 64, no. 2, pp. 357–363, Jul. 2017, doi: 10.18388/abp.2016_1481.

[266] I. Miller *et al.*, 'Ki67 is a Graded Rather than a Binary Marker of Proliferation versus Quiescence', *Cell Rep.*, vol. 24, no. 5, pp. 1105-1112.e5, Jul. 2018, doi: 10.1016/j.celrep.2018.06.110.

[267] C. Meyer *et al.*, 'Distinct dedifferentiation processes affect caveolin-1 expression in hepatocytes', *Cell Communication and Signaling*, vol. 11, no. 1, p. 6, Dec. 2013, doi: 10.1186/1478-811X-11-6.

[268] A. Kaimori, J. Potter, J. Kaimori, C. Wang, E. Mezey, and A. Koteish, 'Transforming Growth Factor-β1 Induces an Epithelial-to-Mesenchymal Transition State in Mouse Hepatocytes in Vitro', *Journal of Biological Chemistry*, vol. 282, no. 30, pp. 22089–22101, Jul. 2007, doi: 10.1074/jbc.M700998200.

[269] G. B. Fu *et al.*, 'Expansion and differentiation of human hepatocyte-derived liver progenitor-like cells and their use for the study of hepatotropic pathogens', *Cell Res.*, vol. 29, no. 1, pp. 8–22, Jan. 2019, doi: 10.1038/s41422-018-0103-x.

[270] M. G. Vander Heiden, L. C. Cantley, and C. B. Thompson, 'Understanding the Warburg Effect: The Metabolic Requirements of Cell Proliferation', *Science (1979).*, vol. 324, no. 5930, pp. 1029–1033, May 2009, doi: 10.1126/science.1160809.

[271] D. M. Bissell, G. A. Levine, and M. J. Bissell, 'Glucose metabolism by adult hepatocytes in primary culture and by cell lines from rat liver', *American Journal of Physiology-Cell Physiology*, vol. 234, no. 3, pp. C122–C130, Mar. 1978, doi: 10.1152/ajpcell.1978.234.3.C122.

[272] K. Shiroyama, K. Moriwaki, S. Kusunoki, N. Saeki, and O. Yuge, 'Glucose loading during primary culture has opposite effects on the viability of hepatocytes exposed to potassium cyanide and to iodoacetic acid', *Metabolism*, vol. 50, no. 3, pp. 342–348, Mar. 2001, doi: 10.1053/meta.2001.20204.

[273] M. D. Davidson, K. R. Ballinger, and S. R. Khetani, 'Long-term exposure to abnormal glucose levels alters drug metabolism pathways and insulin sensitivity in primary human hepatocytes', *Sci. Rep.*, vol. 6, no. 1, p. 28178, Jun. 2016, doi: 10.1038/srep28178.

[274] K. J. Dabos *et al.*, 'Comparison of Bioenergetic Activity of Primary Porcine Hepatocytes Cultured in Four Different Media', *Cell Transplant.*, vol. 13, no. 3, pp. 213–229, Apr. 2004, doi: 10.3727/000000004783984007.

[275] K. Weber, D. Ridderskamp, M. Alfert, S. Hoyer, and R. J. Wiesner, 'Cultivation in Glucose-Deprived Medium Stimulates Mitochondrial Biogenesis and Oxidative Metabolism in HepG2 Hepatoma Cells', *Biol. Chem.*, vol. 383, no. 2, pp. 283–290, Feb. 2002, doi: 10.1515/BC.2002.030.

[276] G. Schicht, L. Seidemann, R. Haensel, D. Seehofer, and G. Damm, 'Critical Investigation of the Usability of Hepatoma Cell Lines HepG2 and Huh7 as Models for the Metabolic Representation of Resectable Hepatocellular Carcinoma', *Cancers (Basel).*, vol. 14, no. 17, p. 4227, Aug. 2022, doi: 10.3390/cancers14174227.

[277] G. H. Na, D. G. Kim, Y. H. Kim, J. H. Han, and E. S. Jung, 'Effects of glucose concentration in the medium on rat hepatocyte culture', *Ann. Surg. Treat. Res.*, vol. 87, no. 2, p. 53, 2014, doi: 10.4174/astr.2014.87.2.53.

[278] T. Hayashi *et al.*, 'Excess glucose alone induces hepatocyte damage due to oxidative stress and endoplasmic reticulum stress', *Exp. Cell Res.*, vol. 442, no. 2, p. 114264, Oct. 2024, doi: 10.1016/j.yexcr.2024.114264.

[279] T. Nishikawa *et al.*, 'Normalizing mitochondrial superoxide production blocks three pathways of hyperglycaemic damage', *Nature*, vol. 404, no. 6779, pp. 787–790, Apr. 2000, doi: 10.1038/35008121.

[280] S. Cassim, V.-A. Raymond, P. Lapierre, and M. Bilodeau, 'From in vivo to in vitro: Major metabolic alterations take place in hepatocytes during and following isolation', *PLoS One*, vol. 12, no. 12, p. e0190366, Dec. 2017, doi: 10.1371/journal.pone.0190366.

[281] V. M. Gohil *et al.*, 'Nutrient-sensitized screening for drugs that shift energy metabolism from mitochondrial respiration to glycolysis', *Nat. Biotechnol.*, vol. 28, no. 3, pp. 249–255, Mar. 2010, doi: 10.1038/nbt.1606.

[282] M. Protasoni and J.-W. Taanman, 'Remodelling of the Mitochondrial Bioenergetic Pathways in Human Cultured Fibroblasts with Carbohydrates', *Biology (Basel).*, vol. 12, no. 7, p. 1002, Jul. 2023, doi: 10.3390/biology12071002.

[283] S. Yokota and H. D. Fahimi, 'Immunocytochemical localization of albumin in the secretory apparatus of rat liver parenchymal cells.', *Proceedings of the National Academy of Sciences*, vol. 78, no. 8, pp. 4970–4974, Aug. 1981, doi: 10.1073/pnas.78.8.4970.

[284] E. Fries, L. Gustafsson, and P. A. Peterson, 'Four secretory proteins synthesized by hepatocytes are transported from endoplasmic reticulum to Golgi complex at different rates.', *EMBO J.*, vol. 3, no. 1, pp. 147–152, Jan. 1984, doi: 10.1002/j.1460-2075.1984.tb01775.x.

[285] H. F. Lodish and N. Kong, 'The secretory pathway is normal in dithiothreitol-treated cells, but disulfide-bonded proteins are reduced and reversibly retained in the endoplasmic reticulum.',

Journal of Biological Chemistry, vol. 268, no. 27, pp. 20598–20605, Sep. 1993, doi: 10.1016/S0021-9258(20)80767-4.

[286] C. Barlowe, 'COPII: A membrane coat formed by Sec proteins that drive vesicle budding from the endoplasmic reticulum', *Cell*, vol. 77, no. 6, pp. 895–907, Jun. 1994, doi: 10.1016/0092-8674(94)90138-4.

[287] S. I. Bannykh, T. Rowe, and W. E. Balch, 'The organization of endoplasmic reticulum export complexes', *Journal of Cell Biology*, vol. 135, no. 1, pp. 19–35, 1996, doi: 10.1083/jcb.135.1.19.

[288] T. H. Ward, R. S. Polishchuk, S. Caplan, K. Hirschberg, and J. Lippincott-Schwartz, 'Maintenance of Golgi structure and function depends on the integrity of ER export', *J. Cell Biol.*, vol. 155, no. 4, pp. 557–570, Nov. 2001, doi: 10.1083/jcb.200107045.

[289] R. J. Webb, J. D. Judah, L.-C. Lo, and G. M. H. Thomas, 'Constitutive secretion of serum albumin requires reversible protein tyrosine phosphorylation events in *trans* -Golgi', *American Journal of Physiology-Cell Physiology*, vol. 289, no. 3, pp. C748–C756, Sep. 2005, doi: 10.1152/ajpcell.00019.2005.

[290] E. Ikonen, M. Tagaya, O. Ullrich, C. Montecucco, and K. Simons, 'Different requirements for NSF, SNAP, and Rab proteins in apical and basolateral transport in MDCK cells', *Cell*, vol. 81, no. 4, pp. 571–580, May 1995, doi: 10.1016/0092-8674(95)90078-0.

[291] E. Ikonen, R. G. Parton, F. Lafont, and K. Simons, 'Analysis of the role of p200-containing vesicles in post-Golgi traffic.', *Mol. Biol. Cell*, vol. 7, no. 6, pp. 961–974, Jun. 1996, doi: 10.1091/mbc.7.6.961.

[292] N. B. Cole, N. Sciaky, A. Marotta, J. Song, and J. Lippincott-Schwartz, 'Golgi dispersal during microtubule disruption: regeneration of Golgi stacks at peripheral endoplasmic reticulum exit sites.', *Mol. Biol. Cell*, vol. 7, no. 4, pp. 631–650, Apr. 1996, doi: 10.1091/mbc.7.4.631.

[293] R. Enat, D. M. Jefferson, N. Ruiz-Opazo, Z. Gatmaitan, L. A. Leinwand, and L. M. Reid, 'Hepatocyte proliferation in vitro: its dependence on the use of serum-free hormonally defined medium and substrata of extracellular matrix.', *Proceedings of the National Academy of Sciences*, vol. 81, no. 5, pp. 1411–1415, Mar. 1984, doi: 10.1073/pnas.81.5.1411.

[294] Y. Toba *et al.*, 'Comparison of commercially available media for hepatic differentiation and hepatocyte maintenance', *PLoS One*, vol. 15, no. 2, p. e0229654, Feb. 2020, doi: 10.1371/journal.pone.0229654.

[295] L. Hayflick and P. S. Moorhead, 'The serial cultivation of human diploid cell strains', *Exp. Cell Res.*, vol. 25, no. 3, pp. 585–621, Dec. 1961, doi: 10.1016/0014-4827(61)90192-6.

[296] W. Wagner *et al.*, 'Replicative Senescence of Mesenchymal Stem Cells: A Continuous and Organized Process', *PLoS One*, vol. 3, no. 5, p. e2213, May 2008, doi: 10.1371/journal.pone.0002213.

[297] S. Schäuble *et al.*, 'Quantitative Model of Cell Cycle Arrest and Cellular Senescence in Primary Human Fibroblasts', *PLoS One*, vol. 7, no. 8, p. e42150, Aug. 2012, doi: 10.1371/journal.pone.0042150.

[298] C. Liu, S. Sekine, and K. Ito, 'Assessment of mitochondrial dysfunction-related, drug-induced hepatotoxicity in primary rat hepatocytes', *Toxicol. Appl. Pharmacol.*, vol. 302, pp. 23–30, Jul. 2016, doi: 10.1016/j.taap.2016.04.010.

[299] C. Xiang *et al.*, 'Long-term functional maintenance of primary human hepatocytes in vitro', *Science (1979).*, vol. 364, no. 6438, pp. 399–402, Apr. 2019, doi: 10.1126/science.aau7307.

[300] M. A. Nieto, R. Y.-J. Huang, R. A. Jackson, and J. P. Thiery, 'EMT: 2016', *Cell*, vol. 166, no. 1, pp. 21–45, Jun. 2016, doi: 10.1016/j.cell.2016.06.028.

[301] M. K. Jolly *et al.*, 'Stability of the hybrid epithelial/mesenchymal phenotype', *Oncotarget*, vol. 7, no. 19, pp. 27067–27084, May 2016, doi: 10.18632/oncotarget.8166.

[302] S. Miura *et al.*, 'Hepatocytes differentiate into intestinal epithelial cells through a hybrid epithelial/mesenchymal cell state in culture', *Nat. Commun.*, vol. 15, no. 1, p. 3940, May 2024, doi: 10.1038/s41467-024-47869-2.

[303] H. Xie *et al.*, 'A two-step strategy to expand primary human hepatocytes in vitro with efficient metabolic and regenerative capacities', *Stem Cell Res. Ther.*, vol. 15, no. 1, p. 281, Sep. 2024, doi: 10.1186/s13287-024-03911-0.

[304] S.-Q. Ying *et al.*, 'Hepatocyte-derived tissue extracellular vesicles safeguard liver regeneration and support regenerative therapy', *J. Nanobiotechnology*, vol. 22, no. 1, p. 521, Aug. 2024, doi: 10.1186/s12951-024-02790-0.

[305] F. Alisafaei *et al.*, 'Vimentin is a key regulator of cell mechanosensing through opposite actions on actomyosin and microtubule networks', *Commun. Biol.*, vol. 7, no. 1, p. 658, May 2024, doi: 10.1038/s42003-024-06366-4.

[306] S. Usman *et al.*, 'Vimentin Is at the Heart of Epithelial Mesenchymal Transition (EMT) Mediated Metastasis', *Cancers (Basel).*, vol. 13, no. 19, p. 4985, Oct. 2021, doi: 10.3390/cancers13194985.

[307] S. E. Leggett, A. M. Hruska, M. Guo, and I. Y. Wong, 'The epithelial-mesenchymal transition and the cytoskeleton in bioengineered systems', *Cell Communication and Signaling*, vol. 19, no. 1, p. 32, Mar. 2021, doi: 10.1186/s12964-021-00713-2.

[308] Y. Xing *et al.*, 'Vimentin intermediate filaments facilitate transportation of hepatitis C virus components', *Eur. J. Cell Biol.*, vol. 104, no. 3, p. 151505, Sep. 2025, doi: 10.1016/j.ejcb.2025.151505.

[309] J. W. Grisham, 'A morphologic study of deoxyribonucleic acid synthesis and cell proliferation in regenerating rat liver; autoradiography with thymidine-H3.', *Cancer Res.*, vol. 22, pp. 842–9, Aug. 1962, [Online]. Available: http://www.ncbi.nlm.nih.gov/pubmed/13902009

[310] M. Li *et al.*, 'Study on the activity of the signaling pathways regulating hepatocytes from G0 phase into G1 phase during rat liver regeneration', *Cell. Mol. Biol. Lett.*, vol. 19, no. 2, pp. 181–200, Jan. 2014, doi: 10.2478/s11658-014-0188-2.

[311] Y. Miyaoka, K. Ebato, H. Kato, S. Arakawa, S. Shimizu, and A. Miyajima, 'Hypertrophy and Unconventional Cell Division of Hepatocytes Underlie Liver Regeneration', *Current Biology*, vol. 22, no. 13, pp. 1166–1175, Jul. 2012, doi: 10.1016/j.cub.2012.05.016.

[312] Y. Zou, Q. Bao, S. Kumar, M. Hu, G.-Y. Wang, and G. Dai, 'Four Waves of Hepatocyte Proliferation Linked with Three Waves of Hepatic Fat Accumulation during Partial Hepatectomy-Induced Liver Regeneration', *PLoS One*, vol. 7, no. 2, p. e30675, Feb. 2012, doi: 10.1371/journal.pone.0030675.

[313] E. Cruvinel *et al.*, 'Long-term single-cell passaging of human iPSC fully supports pluripotency and high-efficient trilineage differentiation capacity', *SAGE Open Med.*, vol. 8, Jan. 2020, doi: 10.1177/2050312120966456.

[314] G. Levy *et al.*, 'Long-term culture and expansion of primary human hepatocytes', *Nat. Biotechnol.*, vol. 33, no. 12, pp. 1264–1271, Dec. 2015, doi: 10.1038/nbt.3377.

[315] R. McClelland *et al.*, '*Ex Vivo* Conditions for Self-Replication of Human Hepatic Stem Cells', *Tissue Eng. Part C Methods*, vol. 14, no. 4, pp. 341–351, Dec. 2008, doi: 10.1089/ten.tec.2008.0073.

[316] L. Song, H. Wang, X. Gao, K. Shen, W. Niu, and X. Qin, 'Proliferation and differentiation potential of mouse adult hepatic progenitor cells cultured <italic>in vitro</italic&gt';, *Acta Biochim. Biophys. Sin. (Shanghai).*, vol. 42, no. 2, pp. 122–128, Feb. 2010, doi: 10.1093/abbs/gmp112.

[317] X. Luo *et al.*, 'Directed Differentiation of Adult Liver Derived Mesenchymal Like Stem Cells into Functional Hepatocytes', *Sci. Rep.*, vol. 8, no. 1, p. 2818, Feb. 2018, doi: 10.1038/s41598-018-20304-5.

[318] D. T. Covas *et al.*, 'Multipotent mesenchymal stromal cells obtained from diverse human tissues share functional properties and gene-expression profile with CD146+ perivascular cells and fibroblasts', *Exp. Hematol.*, vol. 36, no. 5, pp. 642–654, May 2008, doi: 10.1016/j.exphem.2007.12.015.

[319] M. B. Herrera *et al.*, 'Isolation and Characterization of a Stem Cell Population from Adult Human Liver', *Stem Cells*, vol. 24, no. 12, pp. 2840–2850, Dec. 2006, doi: 10.1634/stemcells.2006-0114.

[320] S. S. Sekhon, X. Tan, A. Micsenyi, W. C. Bowen, and S. P. S. Monga, 'Fibroblast Growth Factor Enriches the Embryonic Liver Cultures for Hepatic Progenitors', *Am. J. Pathol.*, vol. 164, no. 6, pp. 2229–2240, Jun. 2004, doi: 10.1016/S0002-9440(10)63779-0.

[321] G. Benton, I. Arnaoutova, J. George, H. K. Kleinman, and J. Koblinski, 'Matrigel: From discovery and ECM mimicry to assays and models for cancer research', *Adv. Drug Deliv. Rev.*, vol. 79, pp. 3–18, 2014, doi: 10.1016/j.addr.2014.06.005.

[322] E. A. Aisenbrey and W. L. Murphy, 'Synthetic alternatives to Matrigel', *Nat. Rev. Mater.*, vol. 5, no. 7, pp. 539–551, May 2020, doi: 10.1038/s41578-020-0199-8.

[323] N. Schierbaum, J. Rheinlaender, and T. E. Schäffer, 'Combined atomic force microscopy (AFM) and traction force microscopy (TFM) reveals a correlation between viscoelastic material properties and contractile prestress of living cells', *Soft Matter*, vol. 15, no. 8, pp. 1721–1729, 2019, doi: 10.1039/C8SM01585F.

[324] K. Bhadriraju, M. Yang, S. Alom Ruiz, D. Pirone, J. Tan, and C. S. Chen, 'Activation of ROCK by RhoA is regulated by cell adhesion, shape, and cytoskeletal tension', *Exp. Cell Res.*, vol. 313, no. 16, pp. 3616–3623, Oct. 2007, doi: 10.1016/j.yexcr.2007.07.002.

[325] C. Guillot and T. Lecuit, 'Mechanics of Epithelial Tissue Homeostasis and Morphogenesis', *Science (1979).*, vol. 340, no. 6137, pp. 1185–1189, Jun. 2013, doi: 10.1126/science.1235249.

[326] D. M. Bissell, D. M. Arenson, J. J. Maher, and F. J. Roll, 'Support of cultured hepatocytes by a laminin-rich gel. Evidence for a functionally significant subendothelial matrix in normal rat liver.', *J. Clin. Invest.*, vol. 79, no. 3, pp. 801–12, Mar. 1987, doi: 10.1172/JCI112887.

[327] T. Dohda, Y. Nakamura, M. Kamihira, and S. Iijima, 'Functional role of RhoA in growth regulation of primary hepatocytes.', *J. Biochem.*, vol. 135, no. 5, pp. 631–7, May 2004, doi: 10.1093/jb/mvh076.

[328] A. Hall, 'Rho GTPases and the actin cytoskeleton.', *Science*, vol. 279, no. 5350, pp. 509–14, Jan. 1998, doi: 10.1126/science.279.5350.509.

[329] R. Guo, X. Xu, Y. Lu, and X. Xie, 'Physiological oxygen tension reduces hepatocyte dedifferentiation in in vitro culture.', *Sci. Rep.*, vol. 7, no. 1, p. 5923, Jul. 2017, doi: 10.1038/s41598-017-06433-3.

[330] R. Pagan, I. Martin, M. Llobera, and S. Vilaro, 'Epithelial–Mesenchymal Transition of Cultured Rat Neonatal Hepatocytes Is Differentially Regulated in Response to Epidermal Growth Factor and Dimethyl Sulfoxide', *Hepatology*, vol. 25, no. 3, pp. 598–606, Mar. 1997, doi: 10.1002/hep.510250318.

[331] M. Kimura and M. Ogihara, 'Density-dependent proliferation of adult rat hepatocytes in primary culture induced by epidermal growth factor is potentiated by cAMP-elevating agents', *Eur. J. Pharmacol.*, vol. 324, no. 2–3, pp. 267–276, Apr. 1997, doi: 10.1016/S0014-2999(97)00078-2.

[332] S. Liu, L. Wierød, E. Skarpen, H. Grøsvik, G. Duan, and H. S. Huitfeldt, 'EGF Activates Autocrine TGFα to Induce Prolonged EGF Receptor Signaling and Hepatocyte Proliferation', *Cellular Physiology and Biochemistry*, vol. 32, no. 3, pp. 511–522, 2013, doi: 10.1159/000354454.

[333] O. Oz, E. Iscan, T. Batur, and M. Ozturk, '3D Organoid modelling of hepatoblast-like and mesenchymal-like hepatocellular carcinoma cell lines', *Hepatoma Res.*, vol. 7, 2021, doi: 10.20517/2394-5079.2021.43.

[334] R. Y. Nguyen *et al.*, 'Cytoskeletal dynamics regulates stromal invasion behavior of distinct liver cancer subtypes', *Commun. Biol.*, vol. 5, no. 1, p. 202, Mar. 2022, doi: 10.1038/s42003-022-03121-5.

[335] B. C. Fuchs *et al.*, 'Epithelial-to-Mesenchymal Transition and Integrin-Linked Kinase Mediate Sensitivity to Epidermal Growth Factor Receptor Inhibition in Human Hepatoma Cells', *Cancer Res.*, vol. 68, no. 7, pp. 2391–2399, Apr. 2008, doi: 10.1158/0008-5472.CAN-07-2460.

[336] Z. C. Nwosu *et al.*, 'Liver cancer cell lines distinctly mimic the metabolic gene expression pattern of the corresponding human tumours', *Journal of Experimental & Clinical Cancer Research*, vol. 37, no. 1, p. 211, Dec. 2018, doi: 10.1186/s13046-018-0872-6.

[337] R. Missiaen *et al.*, 'GCN2 inhibition sensitizes arginine-deprived hepatocellular carcinoma cells to senolytic treatment', *Cell Metab.*, vol. 34, no. 8, pp. 1151-1167.e7, Aug. 2022, doi: 10.1016/j.cmet.2022.06.010.

[338] H. H. Chung, M. Mireles, B. J. Kwarta, and T. R. Gaborski, 'Use of porous membranes in tissue barrier and co-culture models', *Lab Chip*, vol. 18, no. 12, pp. 1671–1689, Jun. 2018, doi: 10.1039/C7LC01248A.

[339] F. Mukasheva, L. Adilova, A. Dyussenbinov, B. Yernaimanova, M. Abilev, and D. Akilbekova, 'Optimizing scaffold pore size for tissue engineering: insights across various tissue types', *Front. Bioeng. Biotechnol.*, vol. 12, Nov. 2024, doi: 10.3389/fbioe.2024.1444986.

[340] J. L. Hernandez and K. A. Woodrow, 'Medical Applications of Porous Biomaterials: Features of Porosity and Tissue-Specific Implications for Biocompatibility', *Adv. Healthc. Mater.*, vol. 11, no. 9, pp. 1–50, May 2022, doi: 10.1002/adhm.202102087.

[341] S. Cai, C. Wu, W. Yang, W. Liang, H. Yu, and L. Liu, 'Recent advance in surface modification for regulating cell adhesion and behaviors', *Nanotechnol. Rev.*, vol. 9, no. 1, pp. 971–989, Oct. 2020, doi: 10.1515/ntrev-2020-0076.

[342] J. Wei *et al.*, 'Adhesion of mouse fibroblasts on hexamethyldisiloxane surfaces with wide range of wettability', *J. Biomed. Mater. Res. B Appl. Biomater.*, vol. 81B, no. 1, pp. 66–75, Apr. 2007, doi: 10.1002/jbm.b.30638.

[343] A. Nabe, 'Surface modification of polysulfone ultrafiltration membranes and fouling by BSA solutions', *J. Memb. Sci.*, vol. 133, no. 1, pp. 57–72, Sep. 1997, doi: 10.1016/S0376-7388(97)00073-2.

[344] Y. H. Cho, H. W. Kim, S. Y. Nam, and H. B. Park, 'Fouling-tolerant polysulfone–poly(ethylene oxide) random copolymer ultrafiltration membranes', *J. Memb. Sci.*, vol. 379, no. 1–2, pp. 296–306, Sep. 2011, doi: 10.1016/j.memsci.2011.05.075.

[345] A. Al-Amoudi and R. W. Lovitt, 'Fouling strategies and the cleaning system of NF membranes and factors affecting cleaning efficiency', *J. Memb. Sci.*, vol. 303, no. 1–2, pp. 4–28, 2007, doi: 10.1016/j.memsci.2007.06.002.

[346] M. Jakubowska *et al.*, 'Hollow fiber bioreactor with genetically modified hepatic cells as a model of biologically active function block of the bioartificial liver', *Biocybern. Biomed. Eng.*, vol. 44, no. 1, pp. 9–19, Jan. 2024, doi: 10.1016/j.bbe.2023.11.003.

[347] A. W. Tilles, H. Baskaran, P. Roy, M. L. Yarmush, and M. Toner, 'Effects of oxygenation and flow on the viability and function of rat hepatocytes cocultured in a microchannel flat-plate bioreactor', *Biotechnol. Bioeng.*, vol. 73, no. 5, pp. 379–389, Jun. 2001, doi: 10.1002/bit.1071.

[348] W. J. McCarty, O. B. Usta, and M. L. Yarmush, 'A Microfabricated Platform for Generating Physiologically-Relevant Hepatocyte Zonation', *Sci. Rep.*, vol. 6, no. 1, p. 26868, May 2016, doi: 10.1038/srep26868.

[349] A. A. Palakkan *et al.*, 'Evaluation of Polypropylene Hollow-Fiber Prototype Bioreactor for Bioartificial Liver', *Tissue Eng. Part A*, vol. 19, no. 9–10, pp. 1056–1066, May 2013, doi: 10.1089/ten.tea.2012.0332.

[350] S. F. Abu-Absi *et al.*, 'Characterization of a Hollow Fiber Bioartificial Liver Device', *Artif. Organs*, vol. 29, no. 5, pp. 419–422, May 2005, doi: 10.1111/j.1525-1594.2005.29070.x.

[351] D. Mavri-Damelin, S. Eaton, L. H. Damelin, M. Rees, H. J. F. Hodgson, and C. Selden, 'Ornithine transcarbamylase and arginase I deficiency are responsible for diminished urea cycle function in the human hepatoblastoma cell line HepG2', *Int. J. Biochem. Cell Biol.*, vol. 39, no. 3, pp. 555–564, 2007, doi: 10.1016/j.biocel.2006.10.007.

[352] Y. S. Choi *et al.*, 'Ammonia Removal Using Hepatoma Cells in Mammalian Cell Cultures', *Biotechnol. Prog.*, vol. 16, no. 5, pp. 760–768, Oct. 2000, doi: 10.1021/bp000099d.

[353] S. J. A. C. Peters, H. P. Haagsman, and K. van Norren, 'Arginase release by primary hepatocytes and liver slices results in rapid conversion of arginine to urea in cell culture media', *Toxicology in Vitro*, vol. 22, no. 4, pp. 1094–1098, Jun. 2008, doi: 10.1016/j.tiv.2008.01.016.

[354] Y. Zhang *et al.*, 'A Structure-function Analysis of Hepatocyte Arginase 2 Reveals Mitochondrial Ureahydrolysis as a Determinant of Glucose Oxidation', *Cell. Mol. Gastroenterol. Hepatol.*, vol. 17, no. 5, pp. 801–820, Jan. 2024, doi: 10.1016/j.jcmgh.2024.01.016.

[355] B. Lee, H. Yu, F. Jahoor, W. O'Brien, A. L. Beaudet, and P. Reeds, '*In vivo* urea cycle flux distinguishes and correlates with phenotypic severity in disorders of the urea cycle', *Proceedings of the National Academy of Sciences*, vol. 97, no. 14, pp. 8021–8026, Jul. 2000, doi: 10.1073/pnas.140082197.

List of Figures

Figure 1.1. Liver segments. 16
Figure 1.2. Liver lobules.. 18
Figure 1.3. Liver zonation.. 19
Figure 1.4. Scheme of the urea cycle occurring in a hepatocyte. 20
Figure 1.5. Liver structure at the cellular level. 22
Figure 1.6. Structure of human serum albumin (ALB). 23
Figure 1.7. Structure of Alpha-Fetoprotein (AFP). 25
Figure 1.8. Structure of alpha-1-antitrypsin (A1AT) 26
Figure 1.9. Structure of HNF4α. 28
Figure 1.10. Structure of cytochrome P450 3A4 (CYP3A4).). 29
Figure 1.11. Stages of liver disease progression. 35
Figure 1.12. Bridging therapies in liver failure.. 41
Figure 1.13. Molecular Adsorbent Recirculating System (MARS).. 42
Figure 1.14. Schematic of an extracorporeal liver assist device (ELAD) used as a liver support system. 45
Figure 3.1. Steps in preparing a hollow fiber bioreactor.. 96
Figure 3.2. System for dynamic culture.. 97
Figure 4.1. Distribution of liver cell isolations by sex and cell island formation. 103
Figure 4.2. Distribution of liver cell isolations by donor age group and cell island formation.. 105
Figure 4.3. Distribution of liver cell isolations by type or mixture of digestive enzymes and cell island formation.. 106
Figure 4.4. Representative images showing morphological changes in cell islands obtained from liver tissue specimen H53 [LCI(H53)].. 108
Figure 4.5. Representative images showing changes in the morphology of cell islands from liver sample H72 [LCI(H72)].. 109
Figure 4.6. Representative images showing morphological changes in cell islands isolated from liver tissue specimen H74 [LCI(H74)]. 110
Figure 4.7. Summary of optimal conditions for hepatocyte culture. 111
Figure 4.8. Images of immunocytostained cells producing albumin. 112
Figure 4.9. Cytometric identification of human hepatocytes was performed in the liver isolates. 114
Figure 4.10. Percentage of albumin-positive cells isolated from resected human liver fragments. 115
Figure 4.11. Percentage of alpha-1 antitrypsin (A1AT)-positive cells isolated from resected human liver fragments. 115
Figure 4.12. Percentage of CYP3A4- and HNF4α-positive cells isolated from resected human liver fragments.. 116
Figure 4.13. Albumin secretion measured in cells isolated from liver sample LCI(H72). 118
Figure 4.14. Measurement of albumin secretion in cells isolated from liver sample LCI(H74). 119
Figure 4.15. Expression mRNA levels of *ALB*, *ARG1*, and *CPS1* genes in LTIs.. 121
Figure 4.16. Expression of *CYP3A4*, *CYP2C8*, and *CYP2E1* genes at the transcript level in LTIs.. 125
Figure 4.17. Expression of *HNF4α* and *HNF1α* genes at the mRNA level in LTIs.. 127
Figure 4.18. *AFP* and *VIM* gene expression at the mRNA level in LTIs.. 129
Figure 4.19. Cytometric comparison of the distribution of hHDPCs, C3A, HDFn, and hH_2 cell populations. 130
Figure 4.20. Apical vacuoles (AV) are present between C3A cells.. 131
Figure 4.21. Apical vacuoles in human hepatocytes. 131

Figure 4.22. Comparison of apical vacuole formation in C3A, HDFn, and hHDPCs.. 132
Figure 4.23. Expression of hepatic markers in different cell types. 137
Figure 4.24. Comparison of the Percentage of Antibody-Positive Cells in Liver Isolates and in Liver-Derived Cell Lines at Different Passages.. 139
Figure 4.25. Comparison of metabolic activity among HepG2, HDFn, and hHDPCs determined by the MTT assay 141
Figure 4.26. Average number of live cells and cell viability in HepG2, HDFn, and hHDPCs cultures. 142
Figure 4.27. Albumin secretion by hHDPCs, HepG2, and HDFn cells.. 143
Figure 4.28. Glucose consumption by hHDPCs, HepG2, and HDFn cells.. 145
Figure 4.29. Scheme of experiment for hHDPCs culture in different media.. 146
Figure 4.30. Comparison of cell number, doubling time, and viability across different passages and culture media.. 148
Figure 4.31. Glucose consumption by hHDPCs cultured in different media.. 151
Figure 4.32. Experimental design: effect of HGS on hHDPCs proliferation. 152
Figure 4.33. Average number of live cells and cell viability of hHDPCs at passages +5, +8, and +12 cultured in DMEM (D) or HM (H), with or without HGS supplementation (D+H, H+H). 154
Figure 4.34. Albumin expression across ten passages of hHDPCs. 155
Figure 4.35. Protein expression changes during long-term culture of hHDPCs. 157
Figure 4.36. Western blot analysis of hHDPCs 160
Figure 4.37. Protein expression levels. 162
Figure 4.38. Comparison of cell growth during long-term cultures.. 164
Figure 4.39. Experimental design. 165
Figure 4.40. Changes in cell number and confluency dynamics in long-term cultures. 167
Figure 4.41. Observation of morphological changes and proliferation of liver cell isolates.. 167
Figure 4.42. Morphological changes and proliferation of liver cell isolates. 169
Figure 4.43. Albumin secretion by cells during long-term culture. 170
Figure 4.44. Detection of albumin and proliferation marker in cells after long-term culture.. 171
Figure 4.45. Expression levels of positive and negative MSC markers in consecutive passages of hHDPCs 172
Figure 4.46. Detection of MSC markers in hHDPCs derived from three donors (H37, H65, H72) and analyzed at passages +2, +8, and +11.. 173
Figure 4.47. Expression of positive and negative MSC markers in different cell types (hHDPCs, HDFn, hH_3, C3A, SH-SY5Y, HUVEC). 174
Figure 4.48. Experimental plan for the re-differentiation of hHDPCs into hepatocyte-like cells. 175
Figure 4.49. Morphological changes of hHDPCs at different passages cultured in media with or without growth factor supplementation 177
Figure 4.50. Number of viable cells in hHDPCs cultures during re-differentiation experiments.. 178
Figure 4.51. Schematic representation of the experiment design, stages I and II. 179
Figure 4.52. Morphological changes of cells cultured in expansion medium (EM). 184
Figure 4.53. Albumin production by hHs and hDHes cultured in expansion medium (EM) on collagen-coated surfaces. 185
Figure 4.54. Morphology of hDHes cultured during Stage II on collagen-coated surfaces.. 187
Figure 4.55. Cell growth during the differentiation culture of hDHes at different passages.. 188
Figure 4.56. Albumin production by hDHes cultured in differentiation medium (DM) on collagen-coated surfaces. 189
Figure 4.57. Differences in cell numbers obtained during the 4-day culture of liver cancer cell lines. 190

Figure 4.58. Comparison of cell viability among liver cancer cell lines.. 190
Figure 4.59. Doubling time of liver cancer cell lines.. 191
Figure 4.60. Phenotypic differences between liver cancer cell lines.. 192
Figure 4.61. Metabolic activity of liver cancer cell lines per cell. 192
Figure 4.62. Albumin secretion by liver cancer cell lines. 194
Figure 4.63. Formation of Apical Vacuoles (AVs) by liver cancer cell lines.. 195
Figure 4.64. Comparison of protein and gene expression in liver cancer cell lines.. 198
Figure 4.65. Selected protein production and gene expression in liver cancer cell lines. *8*.. 203
Figure 4.66. Structure of the inner and outer surfaces of a capillary membrane. 204
Figure 4.67. Cross-section of the capillary membrane. 205
Figure 4.68. Contact angle measurement of a water droplet on the surface of a polysulfone capillary membrane.. 206
Figure 4.69. Metabolic activity of C3A_EGFP cells cultured in membrane-conditioned medium or in the presence of polysulfone capillary membranes. 207
Figure 4.70. Cell viability of cells cultured in membrane-conditioned medium or in the presence of polysulfone capillary membranes. 207
Figure 4.71. Albumin secretion by C3A_EGFP cells cultured in membrane-conditioned medium or in the presence of polysulfone capillary membranes. 208
Figure 4.72. Populations of fluorescent beads of different sizes (FSC).. 209
Figure 4.73. Albumin secretion by different cell types under dynamic and static conditions. 211
Figure 4.74. Albumin secretion by HepG2 cell lines under dynamic and static conditions.. 212
Figure 4.75. Albumin secretion during dynamic and static culture of human hepatocytes (hHs). 212
Figure 4.76. Urea production by different cell types under dynamic (Dyn) and static (Stat) culture conditions.. 213
Figure 4.77. Urea production by HepG2 cell lines under dynamic (Dyn) and static (Stat) culture conditions.. 214
Figure 4.78. Urea production by human hepatocytes under dynamic (Dyn) and static (Stat) culture conditions.. 215

List of Supplementary Figures

Supplementary Figure S8.1. Number of live HepG2, hHDPCs, and HDFn cells. 307
Supplementary Figure S8.2. Microscopic comparison of hHDPCs growth at three different passages (+5, +8, +12) cultured in DMEM or HM, with or without HGS supplementation.. 308
Supplementary Figure S8.3. Detection of albumin in hHDPC cells. 309
Supplementary Figure S8.4. Observation of morphological changes and proliferation of different types of cells. 311
Supplementary Figure S8.5. Albumin production by hHs_1 and hDHes cultured in EM on drHDFn_EGF+HGF-coated surfaces.. 312
Supplementary Figure S8.6. Comparison of albumin production between cells cultured on collagen and drHDFn_EGF+HGF surfaces. 313

List of Tabels

Table 1.1. Biological functions of positive and negative MSC markers. 33
Table 2.1. List of the cell lines used during course of experiments. 54
Table 2.2. Types of culture media used during experiments 55
Table 2.3. Basic culture media supplements. 56
Table 2.4. Additional culture media supplements. 56
Table 2.5. List of used digestive enzymes. 57
Table 2.6. Commercial kits used during course of experiments. 57
Table 2.7. Ingredients necessary for buffer or solution preparation 58
Table 2.8. List of antibodies used for FC, WB, IF, ELISA analysis. 59
Table 2.9. List of primers used for RT-qPCR. 61
Table 2.10. Composition of the running buffer. 62
Table 2.11. Composition of the transfer buffer. 63
Table 2.12. Composition of the TBST buffer. 63
Table 2.13. Composition of the mild stripping buffer. 63
Table 2.14. Composition of the strong stripping buffer. 64
Table 2.15. Composition of the resolving gel. 64
Table 2.16. Composition of the stacking gel. 64
Table 2.17. Reagents and equipment for WB analysis 65
Table 2.18. The composition of the wash buffer. 65
Table 2.19. Seeding densities and types of fibroblast variants 68
Table 2.20. Reagents and materials used for the characterization of polysulfone capillary membranes. 69
Table 2.21. Laboratory equipment used in the study. 70
Table 2.22. Materials and consumables used in the study. 71
Table 3.1. Composition of media for the culture of C3A, HepG2, HOS, hHDPCs, hHs, and liver cells. 73
Table 3.2. Medium used for HUVEC culture. 74
Table 3.3. Medium used for SH-SY5Y culture. 74
Table 3.4. Medium used for SNU475, SNU449 cultures. 74
Table 3.5. Compositions of the culture media used for dedifferentiation of hHDPCs into hepatocytes. 74
Table 3.6. The composition of the culture medium used for thawing and initial culture of human hepatocytes. 75
Table 3.7. Composition of the Expansion Medium_1 (EM1) used for culturing cells on a collagen-coated surface. 75
Table 3.8. Composition of the Expansion Medium_1* (EM1*) used for culturing cells on the drHDFn_EGF+HGF growth surface. 76
Table 3.9. Composition of the Expansion Medium_2 (EM2) used after 5 days of culturing cells on a collagen-coated surface. 76
Table 3.10. Composition of the Expansion Medium_2* (EM2*) used after 5 days of culturing cells on the drHDFn_EGF+HGF growth surface. 77
Table 3.11. The composition of the Differentiation Medium (DM) used to generate hepatocyte-like cells. 77
Table 3.12. A compilation of liver samples from patients, from which liver cells were isolated. 80

Table 3.13. A compilation of liver samples from patients, which were used for various experiments without prior cell isolation..... 81
Table 3.14. A compilation of liver samples from patients in the research team's collection. Cell isolation was performed before starting work on this doctoral thesis. 81
Table 3.15. Summary of information on donors of commercially available hepatocytes. 82
Table 4.1. Average values of donor age, isolation yield, liver tissue mass, and cell viability were calculated for 30 hepatocyte donors. 100
Table 4.2. Average values of donor age, liver tissue mass, isolation yield, and cell viability with respect to donor gender, cancer/metastases presence, chemotherapy treatment, or healthy donors.... 101
Table 4.3. Average values of donor age, liver tissue mass, isolation yield, and cell viability, including the ability to form cell islands by donor gender and the impact of chemotherapy on island formation. 102
Table 4.4. Percentage and total number of isolations showing or not showing hepatocyte island formation, by patient sex and age group..... 104
Table 4.5. Percentage and total number of isolations showing or not showing hepatocyte island formation, by patient sex and age group, calculated for each age group..... 105
Table 4.6. Percentage and total number of isolations with or without hepatocyte island formation, by type or mixture of digestive enzyme. 107
Table 4.7. Comparison of size and granularity between hHDPCs, C3A, HDFn, and hHs..... 130
Table 4.8. Comparison of cell number across individual passages under different culture conditions. 184
Table 4.9. Ultrafiltration values (U1, U2) obtained during measurements performed for three independent hollow fiber bioreactors. 209
Table 4.10. Membrane retention values determined for different types of particles..... 210
Table 5.1. Comparison of donor characteristics, isolation yield, cell viability, and isolation methods between the present study and published literature. 218

List of Publications

1. “Colourimetric non-enzymatic determination of urea using an LTCC-based microfluidic system”. E. Remiszewska, K. Malecha, M. Grzeczkowicz, M. Jakubowska, M. Wisniewska, KD Pluta, DG Pijanowska. Sensors and Actuators B. Chem., 2026. IF = 7.7; MEiN points = 200.
2. “Variable expression of hepatic genes in different liver tumor cell lines: conclusions for drug testing”. M.J. Wisniewska, A. Wencel, M. Jakubowska, J.A. Motyl, K. Dudek, B. Burzynska, D.G. Pijanowska and K.D. Pluta. Front. Cell Dev. Biol., 2025, 13:1646602. IF = 4.3; MEiN points = 100; doi: 10.3389/fcell.2025.1646602.
3. “Hollow fiber bioreactor with genetically modified hepatic cells as a model of biologically active function block of the bioartificial liver”. M. Jakubowska, M. Wisniewska, A. Wencel, C. Wojciechowski, M. Gora, K. Dudek, A. Chwojnowski, B. Burzynska, DG. Pijanowska, K.D. Pluta. Biocybernetics and Biomedical Engineering, 2024, 44(1): 9-19. IF = 6.6; MEiN points = 140; doi: 10.1016/j.bbe.2023.11.003.
4. “Cell-based clinical and experimental methods for assisting the function of impaired livers - present and future of liver support systems”. K.D. Pluta, M. Ciezkowska, M. Wisniewska, A.

Wencel, D.G. Pijanowska. Biocybernetics and Biomedical Engineering, 2021, 41(4): 1322-1346. IF = 6.6; MEiN points = 140; doi: 10.1016/j.bbe.2021.06.005.
5. "Effects of genetically modified human skin fibroblasts, stably overexpressing hepatocyte growth factor, on hepatic functions of co-cultured C3A cells". A. Wencel, M. Ciezkowska, M. Wisniewska, K.E. Zakrzewska, D.G. Pijanowska, K.D. Pluta. Biotechnology and Bioengineering, 2021, 118(1): 72-81. IF = 3.6; MEiN points = 100; doi: 10.1002/bit.27551.

Research Projects

1. Participation in the project "Continuous Monitoring System for Drainage Fluids for Assessing Treatment Progress in Patients with Secondary Bacterial Peritonitis", funded by the Medical Research Agency (ABM; 2024/ABM/03/KPO/KPOD.07.07-IW.07-0115/24-00).
2. Participation in the Polish–Italian project "Compartmentalized Membrane Bioreactor as a Platform for Studying Xenobiotic-Induced hEpatotoxicity (CoMBinE)". As part of the collaboration, delivered a seminar entitled *"LDFs as a Potentially New Source of Cells for BAL Applications"* at the Institute on Membrane Technology of the Italian National Research Council (CNR-ITM), Rende, Calabria, Italy (2025).
3. Participation in the project "The Role of Interactions Between Alpha-Synuclein and Sphingosine-1-Phosphate-Dependent Signaling in Experimental Models of Parkinson's Disease: Identification of Novel Therapeutic Targets for Synucleinopathies", funded by the National Science Centre (NCN, SONATINA grant no. UMO-2019/32/C/NZ4/00455).
4. Principal Investigator of an internal research project entitled "Preparation of Biological Material – Isolated Human Hepatocytes for Seeding into a Hollow-Fiber Perfusion Bioreactor", funded by the Nalecz Institute of Biocybernetics and Biomedical Engineering, Polish Academy of Sciences.
5. Participation in the project "Och!DOK Interdisciplinary Doctoral Studies: Development and Application of Bioengineering and Computational Methods in the Prevention, Diagnosis and Treatment of Civilization Diseases", funded by the National Centre for Research and Development (NCBR; POWR.03.02.00-00-I028/17).

Conferences

1. "Characteristics of dedifferentiated human hepatocytes isolated from liver tissues"; M.J. Wisniewska, M. Jakubowska, A. Wencel, D.G. Pijanowska, K.D. Pluta; Joint 20th Nordic-Baltic Conference on Biomedical Engineering and the 24th Polish Conference on Biocybernetics and Biomedical Engineering (NBC 2025 & PCBBE 2025); 2025, Warsaw, Poland; (oral presentation).
2. "Cellular characterization of dedifferentiated human hepatocytes"; M. Wisniewska, M. Jakubowska, A. Wencel, D.G. Pijanowska, K.D. Pluta; XXIII Polish Conference on Biocybernetics and Biomedical Engineering; 2023, Lodz, Poland; (poster).

3. “Dedifferentiated human hepatocytes – cells characterization”; M. Wisniewska, M. Jakubowska, A. Wencel, D.G. Pijanowska, K.D. Pluta; 49th ESAO and IFAO Congress; 2023, Bergamo, Italy; (poster).
4. “Quick and reliable method for estimation of the quality of the liver isolate intended for culturing in the hollow fiber flow bioreactor”, M.J. Wisniewska, M. Jakubowska, A. Wencel, D.G. Pijanowska, K.D. Pluta, 48th Annual ESAO Congress; 2022, Krems, Austria; (poster).
5 „Construction of Hollow Fiber Bioreactors for Hepatic Cell Culture”; M. Wisniewska, M. Jakubowska (Ciezkowska), A. Wencel, D.G. Pijanowska K.D. Pluta. XXII Polish Conference on Biocybernetics and Biomedical Engineering; 2021, Warsaw, Poland; (poster).
6. “Development of the method for isolation of human liver cells“ M.J. Wiśniewska, A. Wencel, D.G. Pijanowska, K.D. Pluta. 1st InterBioMed Young Scientists Forum, Centre for Advanced Materials and Technologies CEZAMAT, Warsaw University of Technology; 2019, Warsaw, Poland; (poster).

Other Scientific Activities

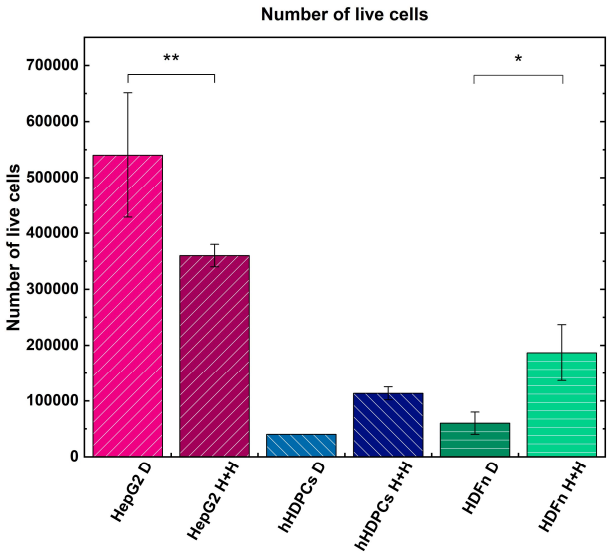
1. Participation in the ESAO Winter School 2021, The Bionic Human: Biomaterials, (Bio)Artificial and Bioengineered Organs, and Cybernetics for the Future of Regenerative Medicine (online), 2021.
2. Participation in Cloud-yESAO 2020 – 1st Digital Conference of the Young ESAO, Developing, Improving & Sharing Knowledge with the World (online), 2020.
3. Participation in the ESAO Winter School 2020, Materials, Surfaces & Cells: Science & Technology for Bioartificial Organs and Tissue Engineering; 2020, Lutherstadt Wittenberg, Germany.

8 Supplementary

8.1 Comparison of hHDPCs, HepG2, and HDFn Cultures

8.1.1 Albumin Secretion and Glucose Consumption

A)

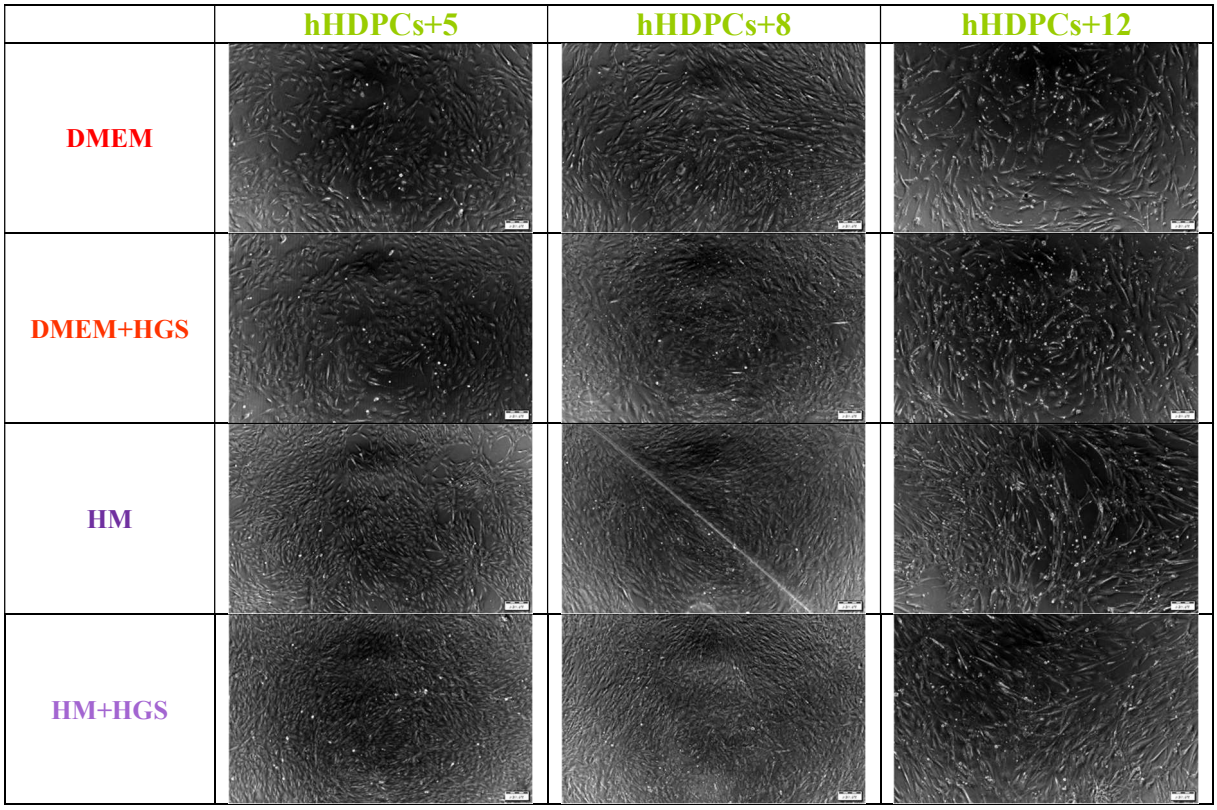


A1)

		HepG2	HepG2	hHDPCs	hHDPCs	HDFn	HDFn
		D	H+H	D	H+H	D	H+H
HepG2	**D**		0.001191	0.000032	0.000066	0.000038	0.000096
HepG2	**H+H**	0.001191		0.000048	0.000185	0.000083	0.001547
hHDPCs	**D**	0.000032	0.000048		0.121863	0.642548	0.006758
hHDPCs	**H+H**	0.000066	0.000185	0.121863		0.228210	0.106380
HDFn	**D**	0.000038	0.000083	0.642548	0.228210		0.013600
HDFn	**H+H**	0.000096	0.001547	0.006758	0.106380	0.013600	

Supplementary Figure S8.1. Number of live HepG2, hHDPCs, and HDFn cells. A) Cells were seeded in 24-well plates at densities of 7×10^4 cells per well for HepG2 and 2.5×10^4 cells per well for hHDPCs and HDFn, with three replicates per cell type. Cultures were maintained in DMEM (D) or HM supplemented with HGS (H+H) for 4 days. **A1)** Statistical significance (p values) for Supplementary Figure S8.1, calculated using ANOVA followed by Duncan's post-hoc test. Results are presented as mean ± SD (n=3). Significance levels: *p<0.05, **p<0.01, ***p<0.001.

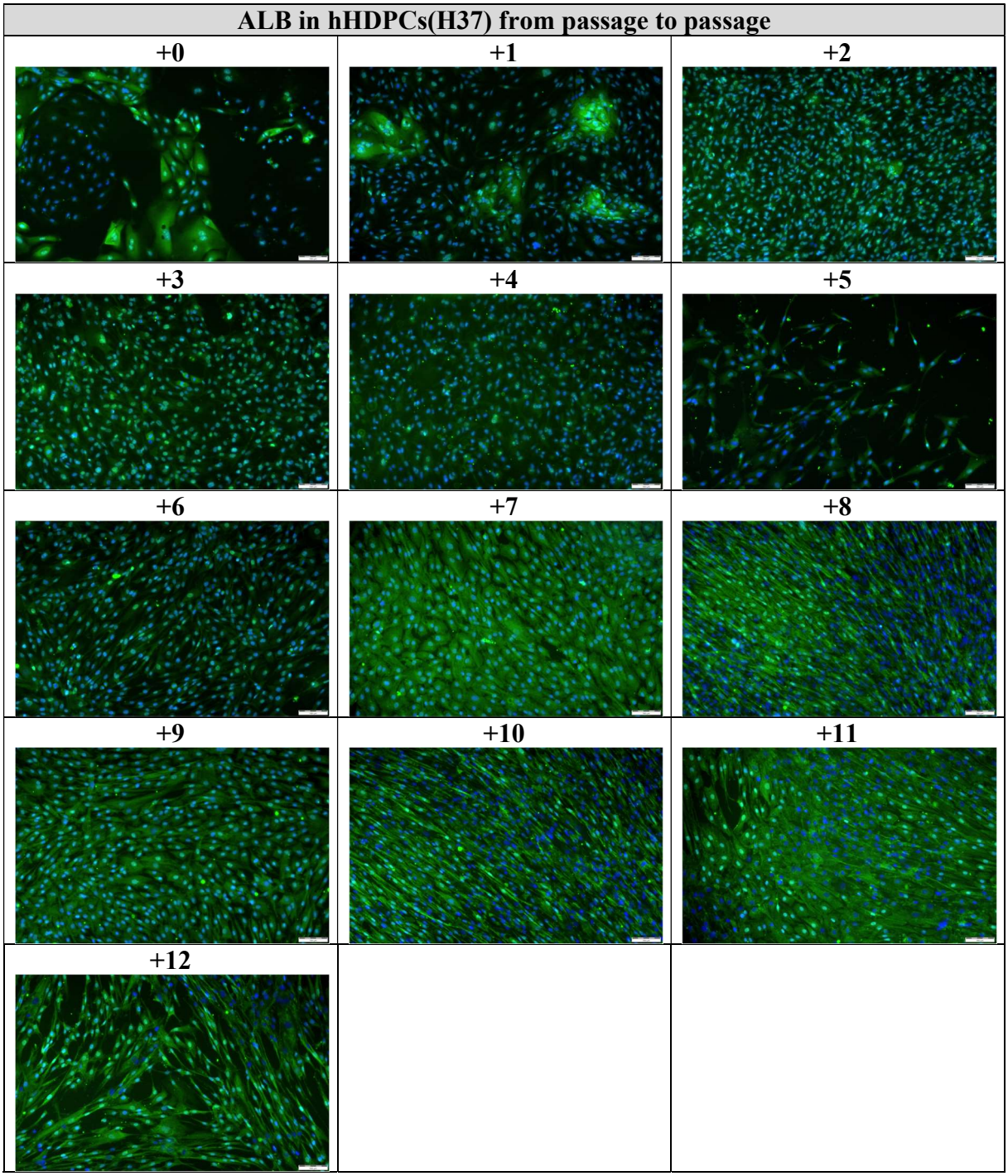
8.2 Effect of Hepatocyte Growth Supplement (HGS) on hHDPCs Proliferation



Supplementary Figure S8.2. Microscopic comparison of hHDPCs growth at three different passages (+5, +8, +12) cultured in DMEM or HM, with or without HGS supplementation. Cells were cultured for 4 days in 24-well plates at a density of 2.5×10^4 cells per well. Microphotographs were taken using an inverted fluorescent microscope Olympus IX-71 (Olympus, Warsaw, Poland) at 4× magnification (scale bar = 200 μm).

8.3 Proteins Fluctuation During hHDPCs Passaging

8.3.1 Albumin Expression Fluctuation – IF

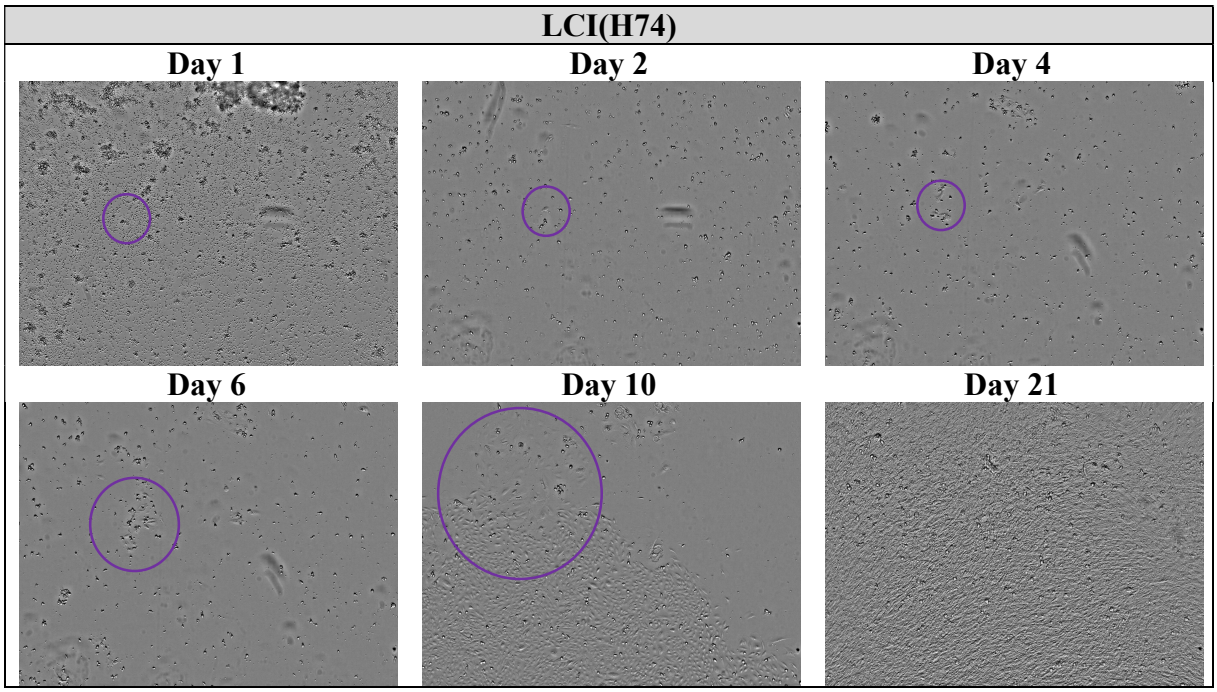


Supplementary Figure S8.3. Detection of albumin in hHDPC cells. hHDPCs were cultured in 24-well plates using HM+HGS medium. For each passage, cells were seeded at a density of 1.5×10^4 cells per well and cultured for 5 days. Passage numbers are indicated above each image with a "+" sign followed by the passage number. After culture, cells were fixed and stained with anti-human albumin antibodies. Albumin-positive cells are shown in green, while cell nuclei are visualized in blue. The nuclei were stained with DAPI. Merged fluorescence images were captured using an IX-71 inverted fluorescence microscope at 10x magnification (scale bar = 100 μm), with identical exposure settings.

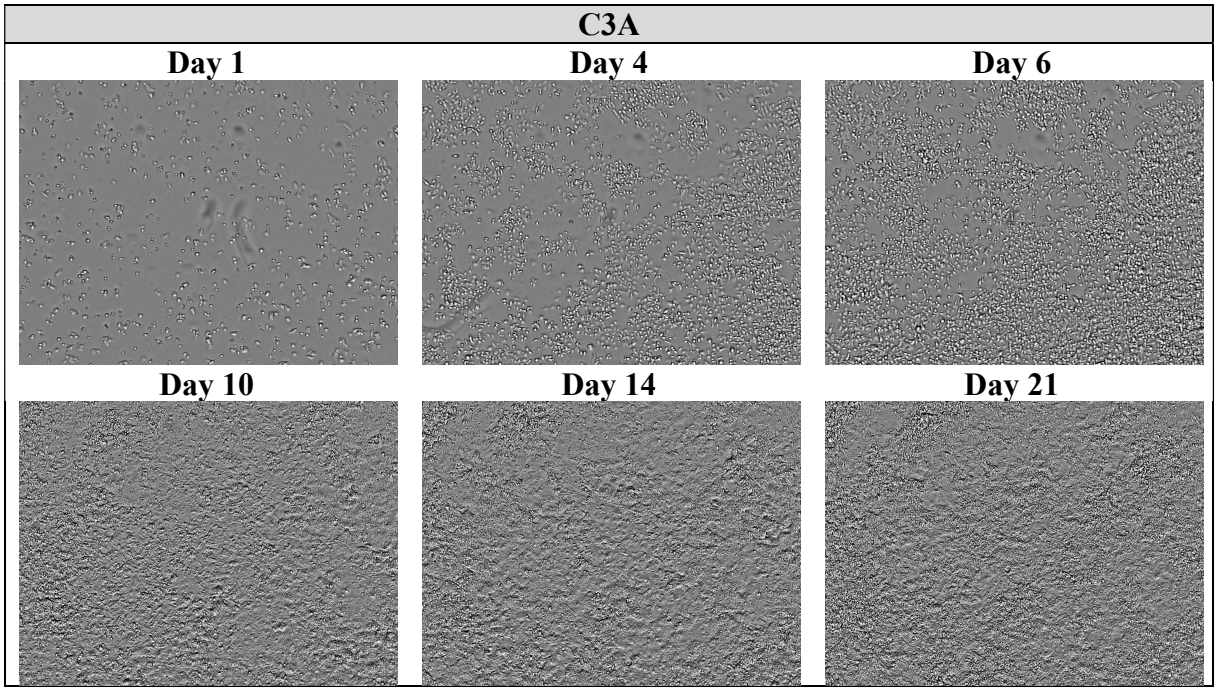
8.4 Long-Term Monitoring of Morphology and Proliferation of hHDPCs

8.4.1 Microscopic Observations

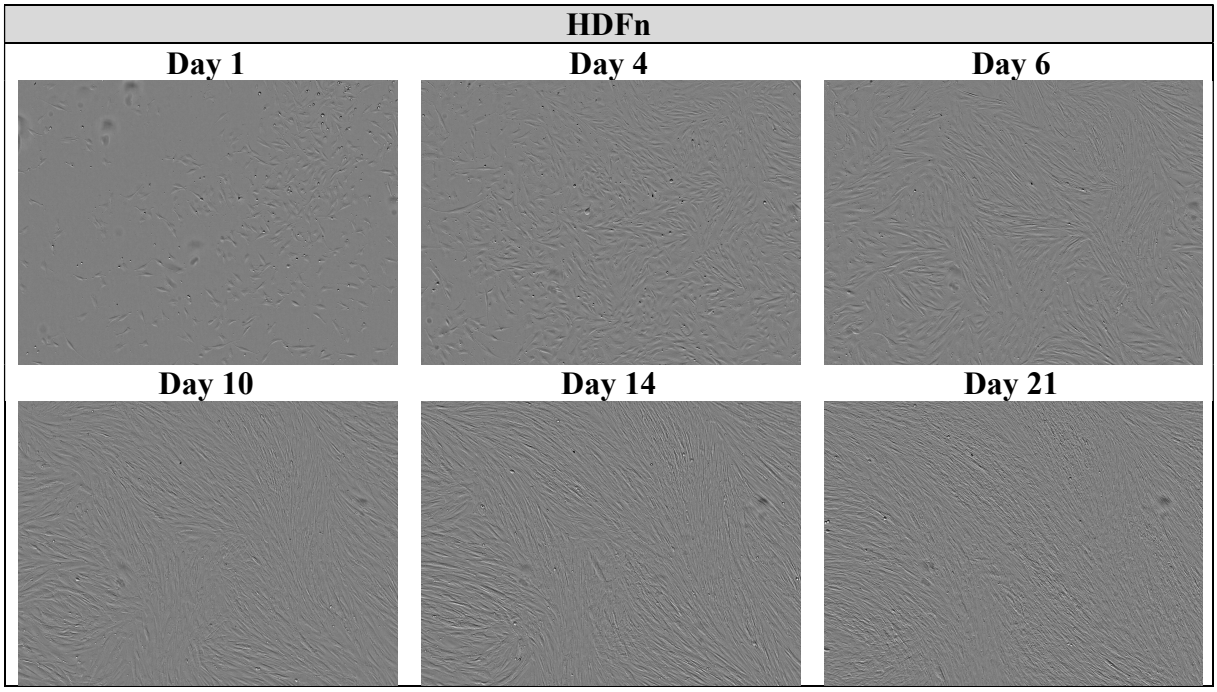
A)



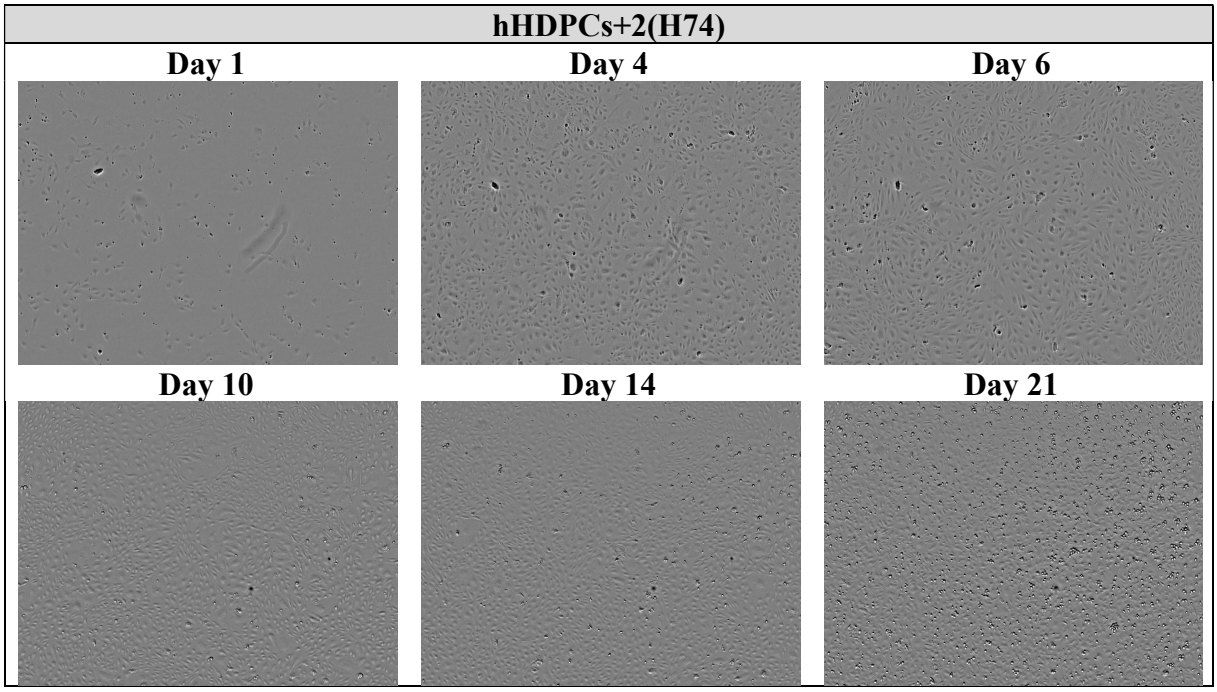
B)



C)



D)

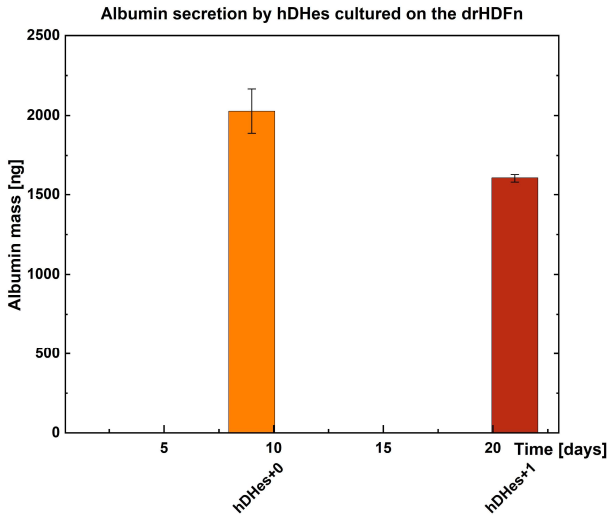


Supplementary Figure S8.4. Observation of morphological changes and proliferation of different types of cells. Micrographs illustrate morphological transformations of the cells during the 21-day culture period. Images were captured using the OLYMPUS Provi CM20 system at 4× magnification. Photographs were taken every 4 hours; however, only selected representative images are presented in the figure. **A)** Images of LCI(H74). The purple circle indicates a hepatocyte island that started to proliferate after several days in culture. **B)** Images of C3A cells. **C)** Images of HDFn cells. **D)** Images of hHDPCs+2(H74).

8.5 Obtaining Human Dedifferentiated Hepatocytes (hDHes) Dividing and Retaining Hepatocyte Functions

8.5.1 Stage I – Proliferating Hepatocytes-Like Cells

A)

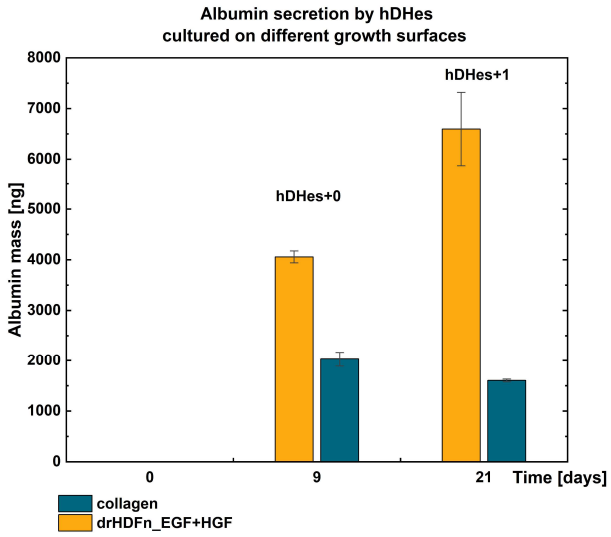


A1)

	hHs_1	hDHes+1
hHs_1		0.051692
hDHes+1	0.051692	

Supplementary Figure S8.5. Albumin production by hHs_1 and hDHes cultured in EM on drHDFn_EGF+HGF-coated surfaces. A) Human hepatocytes (hH_1) were seeded at a density of 3 x 10^5 cells per well on plates coated with dried fibroblasts overexpressing EGF and HGF. After 9 days, one passage (hDHes+1) was performed, and the culture continued for 21 days. Albumin production were measured by ELISA in triplicate (n = 3). **A1)** Statistical significances obtained for Supplementary Figure S8.5. The statistical analysis carried out using one-way analysis of variance (ANOVA) and Duncan pos-hoc test. Results are presented as mean value ± SD, n=3. Level of significance: *p<0.05, **p<0.01, ***p<0.001.

A)



A1)

		hHs_1	hHs_1	hDHes+1	hDHes+1
		collagen	drHDFn	collagen	drHDFn
hHs_1	collagen		0.005756	0.002656	0.003155
hHs_1	drHDFn	0.005756		0.000390	0.320567
hDHes+1	collagen	0.002656	0.000390		0.000280
hDHes+1	drHDFn	0.003155	0.320567	0.000280	

Supplementary Figure S8.6. Comparison of albumin production between cells cultured on collagen and drHDFn_EGF+HGF surfaces. A) For both surface types, cells were seeded at 3 x 10^5 per well. Only the first 21 days of data were compared due to cell death on the dried fibroblast substrate. Albumin secretion levels were measured by ELISA (n = 3). **A1)** Statistical significances obtained for Supplementary Figure S8.6. The statistical analysis carried out using one-way analysis of variance (ANOVA) and Duncan pos-hoc test. Results are presented as mean value ± SD. n=3. Level of significance: *p<0.05, **p<0.01, ***p<0.001.